

Lecture Notes in Mechanical Engineering

Vitalii Ivanov · Justyna Trojanowska ·  
Ivan Pavlenko · Jozef Zajac ·  
Dragan Peraković *Editors*

# Advances in Design, Simulation and Manufacturing III

Proceedings of the 3rd International  
Conference on Design, Simulation,  
Manufacturing: The Innovation Exchange,  
DSMIE-2020, June 9–12, 2020, Kharkiv,  
Ukraine – Volume 1: Manufacturing and  
Materials Engineering

 Springer

# **Lecture Notes in Mechanical Engineering**

## **Series Editors**

Fakher Chaari, National School of Engineers, University of Sfax, Sfax, Tunisia

Mohamed Haddar, National School of Engineers of Sfax (ENIS), Sfax, Tunisia

Young W. Kwon, Department of Manufacturing Engineering and Aerospace Engineering, Graduate School of Engineering and Applied Science, Monterey, CA, USA

Francesco Gherardini, Dipartimento Di Ingegneria, Edificio 25, Università Di Modena E Reggio Emilia, Modena, Modena, Italy

Vitalii Ivanov, Department of Manufacturing Engineering Machine and Tools, Sumy State University, Sumy, Ukraine



**Lecture Notes in Mechanical Engineering (LNME)** publishes the latest developments in Mechanical Engineering - quickly, informally and with high quality. Original research reported in proceedings and post-proceedings represents the core of LNME. Volumes published in LNME embrace all aspects, subfields and new challenges of mechanical engineering. Topics in the series include:

- Engineering Design
- Machinery and Machine Elements
- Mechanical Structures and Stress Analysis
- Automotive Engineering
- Engine Technology
- Aerospace Technology and Astronautics
- Nanotechnology and Microengineering
- Control, Robotics, Mechatronics
- MEMS
- Theoretical and Applied Mechanics
- Dynamical Systems, Control
- Fluid Mechanics
- Engineering Thermodynamics, Heat and Mass Transfer
- Manufacturing
- Precision Engineering, Instrumentation, Measurement
- Materials Engineering
- Tribology and Surface Technology

To submit a proposal or request further information, please contact the Springer Editor of your location:

**China:** Dr. Mengchu Huang at [mengchu.huang@springer.com](mailto:mengchu.huang@springer.com)

**India:** Priya Vyas at [priya.vyas@springer.com](mailto:priya.vyas@springer.com)

**Rest of Asia, Australia, New Zealand:** Swati Meherishi at [swati.meherishi@springer.com](mailto:swati.meherishi@springer.com)

**All other countries:** Dr. Leontina Di Cecco at [Leontina.dicecco@springer.com](mailto:Leontina.dicecco@springer.com)

To submit a proposal for a monograph, please check our Springer Tracts in Mechanical Engineering at <http://www.springer.com/series/11693> or contact [Leontina.dicecco@springer.com](mailto:Leontina.dicecco@springer.com)

**Indexed by SCOPUS. The books of the series are submitted for indexing to Web of Science.**

More information about this series at <http://www.springer.com/series/11236>

Vitalii Ivanov · Justyna Trojanowska ·  
Ivan Pavlenko · Jozef Zajac ·  
Dragan Peraković  
Editors

# Advances in Design, Simulation and Manufacturing III

Proceedings of the 3rd International  
Conference on Design, Simulation,  
Manufacturing: The Innovation Exchange,  
DSMIE-2020, June 9–12, 2020, Kharkiv,  
Ukraine – Volume 1: Manufacturing  
and Materials Engineering

 Springer

*Editors*

Vitalii Ivanov  
Sumy State University  
Sumy, Ukraine

Justyna Trojanowska  
Poznan University of Technology  
Poznan, Poland

Ivan Pavlenko  
Sumy State University  
Sumy, Ukraine

Jozef Zajac  
Technical University of Kosice  
Presov, Slovakia

Dragan Peraković  
University of Zagreb  
Zagreb, Croatia

ISSN 2195-4356

ISSN 2195-4364 (electronic)

Lecture Notes in Mechanical Engineering

ISBN 978-3-030-50793-0

ISBN 978-3-030-50794-7 (eBook)

<https://doi.org/10.1007/978-3-030-50794-7>

© The Editor(s) (if applicable) and The Author(s), under exclusive license  
to Springer Nature Switzerland AG 2020

This work is subject to copyright. All rights are solely and exclusively licensed by the Publisher, whether the whole or part of the material is concerned, specifically the rights of translation, reprinting, reuse of illustrations, recitation, broadcasting, reproduction on microfilms or in any other physical way, and transmission or information storage and retrieval, electronic adaptation, computer software, or by similar or dissimilar methodology now known or hereafter developed.

The use of general descriptive names, registered names, trademarks, service marks, etc. in this publication does not imply, even in the absence of a specific statement, that such names are exempt from the relevant protective laws and regulations and therefore free for general use.

The publisher, the authors and the editors are safe to assume that the advice and information in this book are believed to be true and accurate at the date of publication. Neither the publisher nor the authors or the editors give a warranty, express or implied, with respect to the material contained herein or for any errors or omissions that may have been made. The publisher remains neutral with regard to jurisdictional claims in published maps and institutional affiliations.

This Springer imprint is published by the registered company Springer Nature Switzerland AG  
The registered company address is: Gewerbestrasse 11, 6330 Cham, Switzerland

# Preface

This volume of Lecture Notes in Mechanical Engineering contains selected papers presented at the 3rd International Conference on Design, Simulation, Manufacturing: The Innovation Exchange (DSMIE-2020), held in Kharkiv, Ukraine, on June 9–12, 2020. The conference was organized by the Sumy State University, National Technical University “Kharkiv Polytechnic Institute,” and International Association for Technological Development and Innovations, in partnership with Technical University of Kosice (Slovak Republic), Kielce University of Technology (Poland), University of West Bohemia (Czech Republic), Poznan University of Technology (Poland), and Association for Promoting Innovative Technologies—Innovative FET (Croatia).

DSMIE-2020 is the international forum for fundamental and applied research and industrial applications in engineering. The conference focuses on a broad range of research challenges in the fields of Manufacturing, Materials, Mechanical, and Chemical Engineering, addressing current and future trends in design approaches, simulation techniques, computer-aided systems, software development, ICT tools, and Industry 4.0 strategy implementation for engineering tasks solving. DSMIE-2020 brings together researchers from academic institutions, leading industrial companies, and government laboratories located around the world for promoting and popularization of the scientific fundamentals of manufacturing.

DSMIE-2020 received 161 contributions from 28 countries around the world. After a thorough peer-review process, the Program Committee accepted 93 papers written by authors from 23 countries. Thank you very much to the authors for their contribution. These papers are published in the present book, achieving an acceptance rate of about 58%. Extended versions of selected best papers will be published in scientific journals: *Management and Production Engineering Review* (published by De Gruyter and indexed by ISI/ESCI, Scopus), *Archives of Mechanical Technology and Materials* (Poland), and *Journal of Engineering Sciences* (Ukraine).

We would like to thank members of the Program Committee and invited external reviewers for their efforts and expertise in contributing to reviewing, without which it would be impossible to maintain the high standards of peer-reviewed papers.

Program Committee members and invited external reviewers devoted their time and energy for peer-reviewing manuscripts. Our reviewers come from all over the world and represent 29 countries and affiliated with 63 institutions.

Thank you very much to keynote speakers: Erwin Rauch (Italy), Dagmar Caganova (Slovak Republic), Mateusz Barczewski (Poland), Arun Nagarajah (Germany), Domenico Guida (Italy), Alex Enrich Prast (Sweden) for sharing their knowledge and experience.

The book “Advances in Design, Simulation and Manufacturing III” was organized in two volumes according to the main conference topics: Volume 1—Manufacturing and Materials Engineering and Volume 2—Mechanical and Chemical Engineering. Each volume is devoted to research in design, simulation, and manufacturing in the areas of (1) Manufacturing Engineering, (2) Materials Engineering, (3) Mechanical Engineering, and (4) Chemical Engineering.

This volume consists of five parts. The first part is aimed at the development of CAx technologies for product design. It includes studies in the development of modern trends in manufacturing engineering using the comprehensive mathematical modeling, computer-integrated and control information systems, as well as parameter optimization of machine tools and applications of digital twins. This part also includes studies in the field of ensuring the reliability of technological equipment and advanced training of modern engineers.

The second part includes studies in the field of implementation of smart manufacturing systems and Industry 4.0 strategies. Notably, ways for implementation of artificial neural networks for object recognition and robotics precision applications are presented, as well as state-of-the-art in product-service systems is analyzed. This part also consists of applications for data analysis, multi-agent, and fuzzy predictive models, as well as production planning and time optimization for manufacturing processes at intelligent and self-optimizing enterprises. The possibilities of using 5G, methods for modeling traffic, and operational planning of transportation systems are additionally included in this part.

The third part is devoted to contributing to the field of technological assurance. Mainly, it presents studies, which are aimed at the development of additive manufacturing processes, ensuring the requirements of engineering and functional safety, increasing productivity and improvement of quality of cutting tools using cloud technologies, optimization of technological processes using the damageability and durability models. This part also includes studies, which are aimed at the improvement of accuracy and productivity for the manufacturing process, its optimization, and ensuring technological capabilities.

The fourth part is based on numerical simulation and experimental studies of cutting, milling, grinding, pressing, and profiling processes. Ways for modeling of the thermomechanical processes during the machining of steels, polymers, composites, and wear-resisting coatings are also presented in this part.

The fifth part is aimed at the development and implementation of advanced materials. Particularly, the influence of modifiers and ligatures on the casting parts, and surface hardening of nanocrystalline layers are analyzed. Ways for simulation of properties and elastoplastic behavior of composite and inhomogeneous materials

are studied, as well as scientific and practical fundamentals for obtaining nanostructures, and corrosion-resistant nanocoatings are developed.

We appreciate the partnership with Springer, StrikePlagiarism, EasyChair, and our Sponsors for their essential support during the preparation of DSMIE-2020.

Thank you very much for DSMIE Team. Their involvement and hard work were crucial to the success of the DSMIE-2020 conference.

DSMIE's motto is "Together we can do more for science, technology, engineering, and education."

June 2020

Vitalii Ivanov  
Justyna Trojanowska  
Ivan Pavlenko  
Jozef Zajac  
Dragan Peraković

# Organization

## Steering Committee

### General Chair

Vitalii Ivanov Sumy State University, Ukraine

### Co-chair

Andriy Marchenko National Technical University “Kharkiv Polytechnic Institute,” Ukraine

### Members

Olena Avdieieva National Technical University “Kharkiv Polytechnic Institute,” Ukraine

Yevheniia Basova National Technical University “Kharkiv Polytechnic Institute,” Ukraine

Sergey Dobrotvorskiy National Technical University “Kharkiv Polytechnic Institute,” Ukraine

Oleksandr Gusak Sumy State University, Ukraine

Oleksandr Liaposhchenko Sumy State University, Ukraine

Olena Naboka National Technical University “Kharkiv Polytechnic Institute,” Ukraine

Ivan Pavlenko Sumy State University, Ukraine

Alexander Permyakov National Technical University “Kharkiv Polytechnic Institute,” Ukraine

Oleksandr Usaty National Technical University “Kharkiv Polytechnic Institute,” Ukraine

Vitalii Yepifanov National Technical University “Kharkiv Polytechnic Institute,” Ukraine

## Program Committee (in alphabetical order)

Gabriel Abba	University of Lorraine, France
Jean-Francois Antoine	University of Lorraine, France
Katarzyna Antosz	Rzeszow University of Technology, Poland
Peter Arras	KU Leuven, Belgium
Michal Balog	Technical University of Kosice, Slovak Republic
Shahzad Barghi	University of Western Ontario, Canada
Jozef Bocko	Technical University of Kosice, Slovak Republic
Glen Bright	University of KwaZulu-Natal, South Africa
Sajid Ullah Butt	National University of Sciences and Technology, Pakistan
Dagmar Caganova	Slovak University of Technology, Slovak Republic
Emilia Campean	Technical University of Cluj-Napoca, Romania
Robert Cep	VSB-Technical University of Ostrava, Czech Republic
Vasile George Cioata	Polytechnic University of Timisoara, Romania
Olaf Ciszak	Poznan University of Technology, Poland
Oguz Colak	Eskisehir Technical University, Turkey
Ronnie II Concepcion	University of Perpetual Help System DALTA, Philippines
Marcela Contreras	Autonomous University of Occidente, Mexico
Radu Cotetiu	Technical University of Cluj-Napoca, Romania
Alina Crisan	University of Agricultural Sciences and Veterinary Medicine, Romania
Predrag Dasic	University Union "Nikola Tesla," Serbia
Oleksandr Derevianchenko	Odessa National Polytechnic University, Ukraine
Mihai Dragomir	Technical University of Cluj-Napoca, Romania
Milan Edl	University of West Bohemia, Czech Republic
Mathieu Gautier	University Lyon, France
Renata Gnatowska	Czestochowa University of Technology, Poland
Mihaly Gorbe	John von Neumann University, Germany
Domenico Guida	University of Salerno, Italy
Oleksandr Gusak	Sumy State University, Ukraine
Mikulas Hajduk	Technical University of Kosice, Slovak Republic
Michal Hatala	Technical University of Kosice, Slovak Republic
Siamak Hoseinzadeh	University of Pretoria, South Africa
Ihor Hurey	Lviv Polytechnic National University, Ukraine
Vitalii Ivanov	Sumy State University, Ukraine
Maryna Ivanova	National Technical University "Kharkiv Polytechnic Institute," Ukraine
Bozena Kaczmarska	Kielce University of Technology, Poland
Lydmila Kalafatova	Donetsk National Technical University, Ukraine
Lucia Knapcikova	Technical University of Kosice, Slovak Republic



Oldrych Kodym Peter Krizan	College of Logistics, Czech Republic Slovak University of Technology, Slovak Republic
Jan Krmela	Alexander Dubcek University of Trencin, Slovak Republic
Dmytro Kryvoruchko	Sumy State University, Ukraine
Ivan Kuric	University of Zilina, Slovak Republic
Piotr Kurylo	University of Zielona Gora, Poland
Oleksandr Liaposhchenko	Sumy State University, Ukraine
Slawomir Luszcinski	Kielce University of Technology, Poland
Jose Mendes Machado	University of Minho, Portugal
Arun Mathew	Vellore Institute of Technology, India
Mykola Melnychuk	Lutsk National Technical University, Ukraine
Ronald L. Mersky	Widener University, USA
Ievgen Mochalin	Zhejiang Normal University, China
Marek Ochowiak	Poznan University of Technology, Poland
Daniela Onofrejova	Technical University of Kosice, Slovak Republic
Oleh Onysko	Ivano-Frankivsk National Technical University of Oil and Gas, Ukraine
Vitalii Pasichnyk	National Technical University of Ukraine “KPI named after I. Sikorskyi,” Ukraine
Justyna Patalas-Maliszewska	University of Zielona-Gora, Poland
Ivan Pavlenko	Sumy State University, Ukraine
Dragan Perakovic	University of Zagreb, Croatia
Marco Perisa	University of Zagreb, Croatia
Oleksandr Permiakov	National Technical University “Kharkiv Polytechnic Institute,” Ukraine
Jan Pitel	Technical University of Kosice, Slovak Republic
Grigore Marian Pop	Technical University of Cluj-Napoca, Romania
Oleksandr Povstyanoy	Lutsk National Technical University, Ukraine
Erwin Rauch	Free University of Bolzano, Italy
Michal Rogalewicz	Poznan University of Technology, Poland
Andrii Rogovyi	Kharkiv National Automobile and Highway University, Ukraine
Yiming Rong	Southern University of Science and Technology, China
Saad Nahi Saleh	Tikrit University, Iraq
Michal Sasiadek	University of Zielona Gora, Poland
Vira Shendryk	Sumy State University, Ukraine
Robert Sika	Poznan University of Technology, Poland
Amarjit Singh	National Institute of Technology Hamirpur, India
Lesya Shkitsa	Ivano-Frankivsk National Technical University of Oil and Gas, Ukraine
Vsevolod Sklabinskyi	Sumy State University, Ukraine

Volodymyr Sokolov V.	Dahl East Ukrainian National University, Ukraine
Dusan N. Sormaz	Ohio University, USA
Marcin Sosnowski	Jan Długosz University of Częstochowa, Poland
Michael Storchak	University of Stuttgart, Germany
Vadym Stupnytskyi	Lviv Polytechnic National University
Antoni Swic	Lublin University of Technology, Poland
Yuliia Tarasevych	AGH University of Science and Technology, Poland
Volodymyr Tonkonogyi	Odessa National Polytechnic University, Ukraine
Justyna Trojanowska	Poznan University of Technology, Poland
Michael Tseitlin	National Technical University “Kharkiv Polytechnic Institute,” Ukraine
Lela Turmanidze	Batumi Shota Rustaveli State University, Georgia
Leonid Ulyev	National Technical University “Kharkiv Polytechnic Institute,” Ukraine
Nicolae Ungureanu	Technical University of Cluj-Napoca, Romania
Leonilde Rocha Varela	University of Minho, Portugal
Yana Vasilchenko	Donbass State Engineering Academy, Ukraine
Joachim Venus	Leibniz Institute for Agricultural Engineering and Bioeconomy, Germany
Josef Voldrich	University of West Bohemia, Czech Republic
George-Christopher Vosniakos	National Technical University of Athens, Greece
Djordje Vukelic	University of Novi Sad, Serbia
Christian Willberg	German Aerospace Center, Germany
Jerzy Winczek	Czestochowa University of Technology, Poland
Oleg Zabolotnyi	Lutsk National Technical University, Ukraine
Jozef Zajac	Technical University of Kosice, Slovak Republic
Viliam Zaloga	Sumy State University, Ukraine
Volodymyr Zavalov	National University of Food Technologies, Ukraine
Jan Zdebor	University of West Bohemia, Czech Republic
Lianyu Zheng	Beihang University, China

### **Invited External Reviewers (in alphabetical order)**

Volodymyr Atamanyuk	Lviv Polytechnic National University, Ukraine
Jan Awrejcewicz	Lodz University of Technology, Poland
Jose Manoel Balthazar	Institute of Aeronautics and Space, Brazil
Paulo Jorge Bartolo	University of Manchester, UK
Kristina Berladir	Sumy State University, Ukraine
Vladimira Binasova	University of Zilina, Slovak Republic
Frantisek Botko	Technical University of Kosice, Slovak Republic

Ricardo Branco	University of Coimbra, Portugal
Yelizaveta Chernysh	Sumy State University, Ukraine
Liviu Adrian Crisan	Technical University of Cluj-Napoca, Romania
Asfaw Gezae Daful	Higher College of Technology, UAE
Ivan Dehtiarov	Sumy State University, Ukraine
Yuliia Denysenko	Sumy State University, Ukraine
Tygran Dzuguryan	Maritime University of Szczecin, Poland
Alyona Glushko	National Technical University “Kharkiv Polytechnic Institute,” Ukraine
Prashanth Konda Gokuldoss	Tallinn University of Technology, Estonia
Reza N. Jazar	RMIT University, Australia
Lydmila Kalafatova	Donetsk National Technical University, Ukraine
Nikolaos Karkalos	National Technical University of Athens, Greece
Sergii Khovanskyi	Sumy State University, Ukraine
Kateryna Kostyk	National Technical University “Kharkiv Polytechnic Institute,” Ukraine
Ivan Kozii	Sumy State University, Ukraine
Steffen Georg Kunnen	University of Duisburg-Essen, Germany
Dmytro Levchenko	Innovative Solutions LLC, Ukraine
Svitlana Lugova	JSC Nasosenergomash Sumy, Ukraine
Angelos Markopoulos	National Technical University of Athens, Greece
Anton Okun	National Technical University “Kharkiv Polytechnic Institute,” Ukraine
Ruslan Ostroha	Sumy State University, Ukraine
Emmanouil Papazoglou	National Technical University of Athens, Greece
Paulina Rewers	Poznan University of Technology, Poland
Mariia Saverska	National Technical University “Kharkiv Polytechnic Institute,” Ukraine
Serhii Sharapov	Sumy State University, Ukraine
Malgorzata Sokala	Kielce University of Technology, Poland
Olha Turchyn	National Technical University “Kharkiv Polytechnic Institute,” Ukraine
Tetiana Tykhomyrova	National Technical University “Kharkiv Polytechnic Institute,” Ukraine
Roman Vaskin	Sumy State University, Ukraine
Oleksii Vodka	National Technical University “Kharkiv Polytechnic Institute,” Ukraine
Mykola Yukhymenko	Sumy State University, Ukraine
Tetyana Zhylenko	Sumy State University, Ukraine

**DSMIE Team (in alphabetical order)**

Olena Avdieieva	National Technical University “Kharkiv Polytechnic Institute,” Ukraine
Yevheniia Basova	National Technical University “Kharkiv Polytechnic Institute,” Ukraine
Kristina Berladir	Sumy State University, Ukraine
Maryna Demianenko	Sumy State University, Ukraine
Ludmyla Dobrovolska	National Technical University “Kharkiv Polytechnic Institute,” Ukraine
Vitalii Ivanov	Sumy State University, Ukraine
Maryna Ivanova	National Technical University “Kharkiv Polytechnic Institute,” Ukraine
Kateryna Kostyk	National Technical University “Kharkiv Polytechnic Institute,” Ukraine
Oleksandr Liaposhchenko	Sumy State University, Ukraine
Ivan Pavlenko	Sumy State University, Ukraine
Oleksandr Starynskyi	Sumy State University, Ukraine

# Contents

## CAx Technologies for Product Design

<b>Comparative Analysis of Platforms for Designing a Digital Twin . . . . .</b>	<b>3</b>
Dmytro Adamenko, Steffen Kunnen, and Arun Nagarajah	
<b>Computer-Integrated Design Pistons with the Influence of Casting Defects . . . . .</b>	<b>13</b>
Oleg Akimov, Vitaliy Alyokhin, Kateryna Kostyk, Leonid Saltykov, and Julia Riabets	
<b>Improvement of the Effectiveness of General Engineering Courses Using Trainers . . . . .</b>	<b>23</b>
Mykola Korotun, Yuliia Denysenko, Nina Malovana, and Olena Dutchenko	
<b>Modeling of Spindle Node Dynamics Using the Spectral Analysis Method . . . . .</b>	<b>35</b>
Oleg Krol and Volodymyr Sokolov	
<b>Method of Design of Interference Fit Based on Complex Mathematical Modeling . . . . .</b>	<b>45</b>
Vladimir Nechiporenko, Valentin Salo, Petro Litovchenko, Vladislav Yemanov, and Stanislav Horielyshev	
<b>Design of Conveyor Control Information System Considering Transport Delay . . . . .</b>	<b>55</b>
Oleh Pihnastyi, Georgii Kozhevnikov, and Tetiana Bondarenko	
<b>Fundamentals of CAD Design of Rotary Milling Cutters for Multitooth Products . . . . .</b>	<b>65</b>
Nataliya Ravska, Alexander Klochko, Oleksiy Ivanovskiy, Vyacheslav Vovk, and Valeriya Parnenko	

<b>Design Calculation of Electrohydraulic Servo Drive for Technological Equipment</b> .....	75
Volodymyr Sokolov, Olga Porkuian, Oleg Krol, and Yevhen Baturin	
<b>Parametric Optimization of Technological Layout of Modular Machine Tools</b> .....	85
Ihor Yakovenko, Alexander Permyakov, Olena Naboka, Olga Prihodko, and Yurii Havryliuk	
<b>Smart Manufacturing and Industry 4.0 Strategy</b>	
<b>Methods for Modeling Urban Road Traffic Using Timed Automata</b> ...	97
Camelia Avram, Jose Machado, and Adina Aștilean	
<b>Object Recognition Using Neural Networks for Robotics Precision Application</b> .....	108
Giampiero Celenta and Domenico Guida	
<b>Big Challenges of Small Manufacturing Enterprises in Industry 4.0</b> ...	118
Sergey Dobrotvorskiy, Yevheniia Basova, Ludmila Dobrovolska, Yevgeny Sokol, and Nikolay Kazantsev	
<b>Data Analysis of Readiness Programs of Machine-Building Enterprises</b> .....	128
Bohdan Haidabrus, Serhiy Protsenko, Philipp Rosenberger, and Janis Grabis	
<b>Workplace Optimization Using a Collaborative Robot</b> .....	137
Pavel Kábele and Milan Edl	
<b>Global Trend of Implementation of Industrial Robots Relating to Industry 4.0</b> .....	147
Isak Karabegović, Raul Turmanidze, and Predrag Dašić	
<b>Multi-agent Model of Energy Consumption at the Metallurgical Enterprise</b> .....	156
Sergey Kiyko, Evgeniy Druzhinin, Oleksandr Prokhorov, and Bohdan Haidabrus	
<b>Development and Implementation Possibilities of 5G in Industry 4.0</b> ...	166
Dragan Peraković, Marko Periša, Petra Zorić, and Ivan Cvitić	
<b>Industry 4.0+: The Next Level of Intelligent and Self-optimizing Factories</b> .....	176
Erwin Rauch	
<b>State-of-the-Art in Product-Service System Classification</b> .....	187
Mariusz Salwin and Andrzej Kraslawski	

**Service Costs in Operational Planning of Transportation with Small Batches of Cargo in City** ..... 201  
 Natalya Shramenko, Dmitriy Muzylyov, and Vladyslav Shramenko

**The Methodology of Obtaining Power Consumption Fuzzy Predictive Model for Enterprises** ..... 210  
 Sergii Tymchuk, Sergii Shendryk, Vira Shendryk, Ivan Abramenko, and Anastasiia Kazlauskaite

**Production Planning and Setup Time Optimization: An Industrial Case Study** ..... 220  
 José Pedro Vaz, Leonilde Varela, Bruno Gonçalves, and José Machado

**Technological Assurance**

**Concept Development of a Consistently Traceable Process and System Solution for Ensuring the Requirements of Engineering and Functional Safety** ..... 233  
 Dominik Ehring, Robin Pluhnau, and Arun Nagarajah

**Improvement of the Quality of Cutting Tools States Recognition Using Cloud Technologies** ..... 243  
 Oleksandr Fomin and Oleksandr Derevianchenko

**Adaptive Slicing in the Additive Manufacturing Process Using the Statistical Layered Analysis** ..... 253  
 Yaroslav Garashchenko and Nina Zubkova

**Increasing Productivity of Connecting Rods Machining** ..... 264  
 Vitalii Ivanov, Ivan Dehtiarov, Viliam Zaloga, Illia Kosov, and Volodymyr Savchuk

**Optimization of the Technological Process Based on Analysis of Technological Damageability of Castings** ..... 276  
 Yaroslav Kusi and Vadym Stupnytskyy

**A Probabilistic-Statistical Model of Durability of Parts Under Cyclic Loading** ..... 285  
 Nataliia Lamnauer, Oleksandr Kupriyanov, Anton Skorkin, and Oleg Kondratyuk

**Combined Thermo-Mechanical Techniques for Post-processing of the SLM-Printed Ni-Cr-Fe Alloy Parts** ..... 295  
 Dmytro Lesyk, Silvia Martinez, Oleksii Pedash, Vitaliy Dzhemelinskiy, and Bohdan Mordyuk

**Theoretical Analysis of Conditions for Improving Gear Grinding Accuracy and Productivity** ..... 305  
 Fedir Novikov, Vladimir Polyansky, Igor Riabenkov, Andrii Hutorov, and Oksana Yermolenko

<b>Ensuring the Bending Stiffness of Pre-compressed Cantilever Boring Bars During Fine Boring</b> .....	315
Alexandr Orgiyan, Vladimir Kobelev, Vitalii Ivanov, Anna Balaniuk, and Albakush Aymen	
<b>Improvement of the Accuracy of Grinding by Means of Coolant Supply</b> .....	325
Mykhaylo Stepanov, Maryna Ivanova, Petro Litovchenko, Larysa Ivanova, and Alexey Kotliar	
<b>Optimization of Modular Fixture Setup Time in an Automated Assembly Line</b> .....	336
Hossein Tohidi and Tarek AlGeddawy	
<b>Numerical Simulation and Experimental Studies</b>	
<b>Investigation of Waveforms of Roller Bearing's Working Surfaces on Centerless Grinding Operations</b> .....	349
Vasyl Chalyj, Sergiy Moroz, Vitaliy Ptachenchuk, Valentyn Zablotskyj, and Stanislav Prystupa	
<b>Theoretical and Experimental Studies of Changes in the Workpiece Shape During Narrow Die Indentation</b> .....	361
Vitalii Chukhlib, Evhen Klemeshov, Serhii Gubskiy, Anton Okun, and Nikolay Biba	
<b>A Numerical-Analytical Model of the Temperature Field Distribution During Orthogonal Cutting of Composites</b> .....	371
Gennadii Khavin, Magomedemin Gasanov, Alexander Permyakov, and Viktoria Nevludova	
<b>Simulation of Thin-Walled Parts End Milling with Fluid Jet Support</b> .....	380
Serhii Kononenko, Sergey Dobrotvorskiy, Yevheniia Basova, Ludmila Dobrovolska, and Vitalii Yepifanov	
<b>Research of Thermomechanical Processes When Processing Cylindrical Surfaces with Wear-Resistant Coatings</b> .....	390
Maksym Kunitsyn and Anatoly Usov	
<b>Investigation of the Grinding Process Considering the Increase of the Active Surface of Abrasive Grains</b> .....	401
Maksym Kurin, Serhii Nyshnyk, and Anatolii Dolmatov	
<b>Processing of Parts Under Pulse Loading of a Vibrating Hopper</b> .....	411
Volodymyr Symoniuk, Viktor Denysiuk, and Yurii Lapchenko	
<b>Finite Element Analysis of Profile Grinding Temperature</b> .....	422
Natalia Lishchenko, Vasily Larshin, and Sergey Uminsky	



**Influence of the Thread Profile Accuracy on Contact Pressure in Oil and Gas Pipes Connectors** ..... 432  
 Oleh Onysko, Volodymyr Kopei, Iuliia Medvid, Lolita Pituley, and Tetiana Lukan

**Numerical Simulation of Local Plastic Deformations of a Cylindrical Workpiece of a Steel Wheel Rim** ..... 442  
 Yuliia Salenko, Ruslan Puzyr, Oleksandr Shevchenko, Viktoriia Kulynych, and Oleksandr Pedun

**Peculiarities of Interaction of Micro-roughnesses of Contacting Surfaces at FANT** ..... 452  
 Ihor Shepelenko, Yakiv Nemyrovskyy, Yuri Tsekhanov, Sergii Mahopets, and Oleh Bevz

**The Influence of Milling Parameters on Cutting Forces in High-Speed Milling of Polymer Materials** ..... 462  
 Alper Uysal, Eshreb Dzhemilov, and Ruslan Dzhemalyadinov

**Advanced Materials**

**Influence of Modifiers-Ligatures on the Properties of Cast Aluminum Alloy AK5M2 for the Automotive Industry** ..... 473  
 Kristina Berladir, Tetiana Hovorun, Oleksandr Gusak, Yaroslav Reshetniak, and Djanibek Khudaybergenov

**Influence of Surface Hardened Nanocrystalline Layers on the Resistance of Contact Fatigue Destruction** ..... 483  
 Volodymyr Gurey and Ihor Hurey

**Numerical Simulation of Elasto-Plastic Behavior of Isotropic Composite Materials** ..... 492  
 Anton Karvatskii, Ihor Mikulionok, Serhii Leleka, and Vladyslav Solovei

**Simulation of the Process of Obtaining Nanostructures During Laser Radiation on Materials, Cutting Tools and Parts** ..... 502  
 Gennadiy Kostyuk, Viktor Popov, Mykola Nechyporuk, Oleksandr Tymofyeyev, and Hanna Yevsieienkova

**Strength Properties Control of Mixtures Based on Soluble Glass with Ethereos Solidifiers** ..... 511  
 Olga Ponomarenko, Tatyana Berlizeva, Igor Grimzin, Nataliia Yevtushenko, and Tatiana Lysenko

**Design of New Nanocoatings Based on Hard Alloy** ..... 522  
 Viktor Popov, Gennadiy Kostyuk, Oleksandr Tymofyeyev, Kateryna Kostyk, and Olena Naboka

<b>Structure and Corrosion Resistance of Vacuum-Arc Multi-period CrN/Cu Coatings</b> . . . . .	532
Hanna Postelnyk, Oleg Sobol, Ondrej Chocholaty, and Sergey Knyazev	
<b>Effect of Morphological Features on Dielectric Properties of Plasma Electrolytic Oxidation Coatings on D16T Aluminum Alloy</b> . . . . .	542
Elena Sevidova, Larisa Pupan, Yuriy Gutsalenko, Aleksandr Rudnev, and Oksana Titarenko	
<b>Structural Engineering of Nanocomposite Coatings Based on Tungsten and Titanium Carbides</b> . . . . .	552
Oleg Sobol' and Osman Dur	
<b>Numerical Simulation of the Microstructure of Structural-Inhomogeneous Materials</b> . . . . .	562
Oleg Zabolotnyi, Viktoriya Pasternak, Igor Andrushchak, Nataliia Ilchuk, and Kostiantyn Svirzhevskiy	
<b>Author Index</b> . . . . .	573

# **CAx Technologies for Product Design**



# Comparative Analysis of Platforms for Designing a Digital Twin

Dmytro Adamenko<sup>(✉)</sup> , Steffen Kunnen , and Arun Nagarajah

University Duisburg-Essen, Lotharstr 1, 47057 Duisburg, Germany  
dmytro.adamenko@uni-due.de

**Abstract.** The advancing digitization and related topics such as Industry 4.0 are becoming increasingly important for companies. Digital Twin is one of the most popular terms in the context of Industry 4.0. While not new, this approach has been brought to life with recent technological advances. Digital twins of products should help to analyze their life cycle and optimize development, operation, and service processes. For that, the necessary data must be collected and stored throughout the product life cycle and can also be provided for other tasks. The data is usually available in different formats and at different endpoints. Collection and integration of data into existing information systems are also complicated due to the typically large amount of data and typically manageable only with great effort. The structure and design of the digital twin are currently not standardized. Different are the structures, scope, and design methods. Regardless of building techniques and structure, a digital twin building platform must be defined to bring together models and data from different disciplines and to ensure the benefit of using the digital twin. In the present work, the various platforms that can be used to create a digital twin are examined and compared, since each platform has advantages and disadvantages.

**Keywords:** Digital twin · IoT · Platform

## 1 Introduction

Digitalization in the economy and industry is progressing. The state-of-art industry is often referred to as Industry 4.0. The increased integration of data into value networks, the adaptation of set-up and workflow organizations or the development of data-driven systems and business models for knowledge management are just a few of the challenges companies face in the future. Industry 4.0 comprises intelligent machines, equipment and products that independently exchange information, initiate actions, and individually control each other [1]. The aim is to fundamentally improve industrial processes along the entire product life cycle and manage the increasing complexity.

The driving force behind Industry 4.0 is the Internet. Through the Internet, there is a worldwide network that is possible across corporate or national borders [2]. Industry 4.0 and digitization meanwhile provide countless subject areas that are continually evolving. Thus, new technologies, such as Big Data Analytics, Cyber-Physical Systems, Cloud Computing, and Internet of Things, are being developed rapidly. An essential feature of Industry 4.0 is the information aggregation in engineering and

operation across different projects, plants, and plant operators. With the Internet of Things (IoT), the communication could not be guaranteed.

The IoT framework supports the object-to-object communication and sharing of data through the enhanced connectivity between physical and virtual objects, services and systems. IoT environment is widely used in various industries in achieving automation for multiple purposes. While designing the framework, a network of sensors, real-time processing tools, role-based, and autonomous devices are interpenetrated with each other for real-time collection of object data. A digital twin is one of the leading terms closely linked to the Internet of Things and Industry 4.0.

## 2 Literature Review

### 2.1 Digital Twin Definition

The term digital twin was first introduced in 2010. At that time, the digital twin was described as a model consisting of three main components: the physical object in the real world, a virtual object in the digital world, and connection between the real and virtual objects via data and information [3]. Since the value of a digital twin became clear, it is gaining more and more interest and importance in many companies and industries. Currently, the concept is developed by the world's largest companies. The digital twin has been placed in the top 10 strategic trends for the year and estimated that by 2021, half of all significant industrial groups would use digital twin, increasing their effectiveness by up to 10% [4]. Digital Twin technology is becoming an integral part of the simulation, testing, and operation of different products. This technology shows great potential for increasing the quality of the components and thus the better predictive maintenance and minimization of downtime of machinery and equipment. A digital twin can be used not only for the maintenance, but also for analysis since it can also contain measurement data from internal sensors.

The term digital twin is getting increasingly popular but is still not standardized. However, to conceptualize this technology, both industry and academia have tried to define the term in several different ways. The numerous descriptions of the Digital Twin differ depending on the purpose and scope of each other.

Negri et al. introduce the definition of a digital twin is following: "the virtual and computerized counterpart of a physical system that can be used to simulate it for various purposes, exploiting a real-time synchronization of the sensed data coming from the field" [5].

Tao et al. present a digital twin as a concept of managing and handling data through all phases of the product lifecycle using real-time mirroring of the physical system, connecting data from all phases of the product lifecycle and continuous updating of virtual models [6]. The approach is presented in Fig. 1.

In the newest publications, the digital twin is no longer described with the already mentioned three, but with five dimensions [7]. The data of the digital twin and the service are added as respective dimensions. Figure 2 shows this model in more detail. Thus, PE stands for the physical entity, VE for virtual equipment, SS for services; DD refers to digital twin data, and CN for the connections [7].

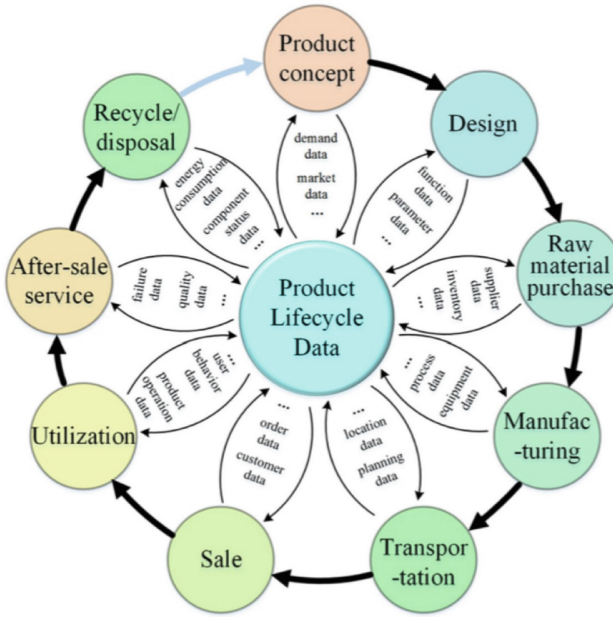


Fig. 1. The stages of the product lifecycle and related data [6].

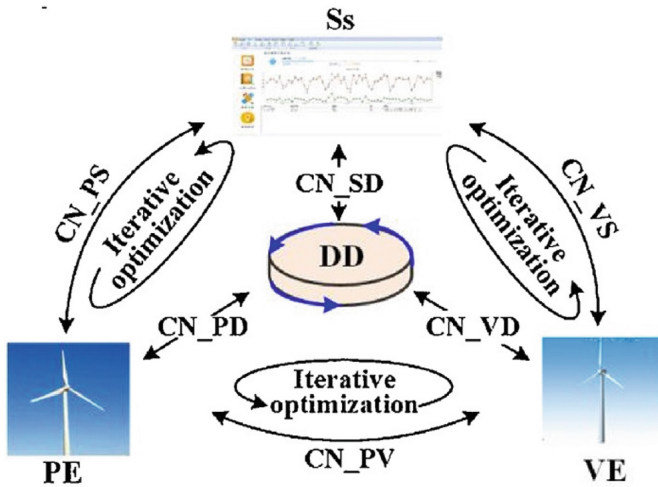


Fig. 2. Dimensions of a digital twin [2].

It is shown that models, data, as well as the connections and services, are the essential components of a digital twin [8]. The data allows the digital twin to operate continuously. In addition to the information collected by sensors, the data also includes values from simulations as well as further knowledge related to the physical object [8].

The connections are needed to enable the interactions of all elements of the digital twin. Services provide the functions and information of the digital twin for the general user in such a way that they can be easily accessed without much prior knowledge [8].

It is also shown that the digital twin is not a single model, but instead consists of a multitude of interrelated models [9]. These are based on current and historical information of the object to be imaged [10]. All relevant data generated during the lifecycle are incorporated into the digital twin and are continuously developed [9].

As shown before, the definitions of digital twins are wide-ranging, vary in different fields, and are sometimes even contradictory. Therefore, it is necessary to present a digital twin in the context of this paper: a virtual image of a real object. This image contains all properties, information, and states of the purpose. The digital twin is not a single model but consists of a multitude of interrelated models, data, and services.

## 2.2 Challenges of Digital Twin

The most important motivation for the realization of the digital twin is the creation of continuous data exchange between the real and virtual objects, as well as the integration of different simulation models in a simulation of the whole system. Thus, the digital twins allow simulating the production, operation, and demolition of an object. Besides, you get the opportunity to replace the real tests with the virtual ones before setting the desired operating mode, evaluating the results, and drawing conclusions for the plant operation.

There are several challenges in creating digital twins. For one thing, data usually comes in different data models that are not directly coupled with each other. Data streams from sensors and documents describing a machine are generally also not in the same format. Furthermore, the synchronization of the physical object and the digital twin over the entire life cycle presents a challenge. Deviations between the real system and the digital image cause, the larger the deviations are, the more the digital twin loses its value. If the discrepancies are too great, the Digital Twin will no longer benefit because the information is no longer reliable.

It is also important to put collected data in a semantic relationship, as many data become more meaningful, the more they are connected to other data. The data should allow statements about the functionality of the physical object underlying the Digital Twin. The more data is collected, and the more it can be integrated into the network, the more accurately the data describes the product and its functionality. Besides, it is important to be able to cover the entire lifecycle management of a product. Data must, therefore, be collected and converted and represent the current status.

Heterogeneous data sets in a uniform format form the basis for digital services. Additionally, relationships between measurement data and data about machine components should be able for modeling to be able to represent complex logical relationships between them.

Ensuring the continuous delivery of data requires an infrastructure that allows real-time interaction between the image and the physical object. This infrastructure includes Internet connectivity and speed, as well as sensors and embedded systems. With the infrastructure, the transmission and processing of the information must be possible in real time. In addition to the infrastructure needed to build and run a digital twin, it will

take time to create the various high-resolution models with existing hardware and software. The costs and effort must, therefore, be contrasted with the benefits of a digital twin. A digital twin must also be customizable. In other words, if something changes in the object itself or in the ambient conditions or operating conditions, these must be easily adaptable in the digital twin. If individual components or systems are replaced during maintenance, this information must be stored in the digital twin and the models must be adapted under the new component [8].

As well as a definition, also the design and data linking methods of digital twins have no standards and vary upon the different use cases and software tools.

### 2.3 Digital Twin Design

Two fundamentally different ways of building up the Digital Twin can be distinguished in existing approaches. One possibility is to create a system model of the physical object. The other option is to build a data structure that organizes and links the sensor data and other information. However, these two possible approaches can be combined into an additional possibility.

The scope of Digital Twins, as well as the design methodology, are not standardized and vary a lot depending on the application case, existing infrastructure, and present software tools.

#### Data-Based Digital Twin

In the data-based approach, the data of the physical object is structured according to specific criteria in a particular platform. A common approach is to sort data by different functionalities or assemblies of the physical object. In this way, a simple structure is created, which makes it possible to gain an overview of the performance of the object quickly. The data can be evaluated and analyzed using algorithms and functions combined with machine learning. In this way, predictive models and models for predictive maintenance are created [2].

The process for creating a data-based digital twin looks similar in the platforms presented. The first step is to make sure that all data needed for models is accessible. For this purpose, a data structure is created that is accessed by the various models and services. In the second step, models, analyses, and functions are created, verified with data, and then provided. The results and data are saved. Thus, the behaviour of the object can be understood over a more extended period based on the data. To generate added value for the end-user and to provide information from the digital twin, applications must be finalized.

A data-based digital twin has the advantage that not all technical information is required for the creation. All that is needed is access to the sensors to analyse them. How the data are structured can be decided by the user himself.

#### System-Based Digital Twin

The system-based digital twin focuses on the actual physical object. The logical links and relationships between the individual components are defined. The system is described using models from different perspectives. Each perspective is one aspect of the system, such as e.g. structure or behavior. For each aspect, a separate partial model



can be created. The sum of all partial models with the cross-aspect links corresponds to the system model.

In building the digital twin, the partial models (such as CAD, CAE, or simulation models) are merged into a system model. Based on the functional, logical, and physical structure of the system model of the wind turbine, a structure is created that defines the relationships between the components of the digital twin. The system model is supplied with the sensor data during operation. Requirements, application scenarios, and product structure information are modeled in specialized software tools using interactive visualizations.

The partial models are fully parameterized and linked to the parameters of the system model so that later operating conditions and object modifications can be simulated, and the system model remains sustainable. The sensor data is imported into the system model by coupling discrete sensor values with the functional relationships of the partial model parameters mapped in the system model. These discrete values can be provided either directly by sensors or indirectly by intermediate dataloggers. The information provided is imported into the system model via an interface. The sensor data serves as an input parameter into the system model, the changed state of which is then recalculated and displayed based on the modeled parameter relationships.

## 2.4 Platforms for Digital Twin

Additional platforms or software components are needed to translate documents and sensor data into an interpretable format and make them usable for the digital twin. These platforms serve as a unified tool for creating and managing Digital Twins. Through such a platform, different companies can create digital twins for their benefit, all of which share a standard format and design features.

IoT platforms serve as a link between the real and the virtual world, connecting the networked devices to the applications that process the data. There are a large number of providers of various IoT platforms. Each platform is different from the other with its own characteristics and focused on a particular industry [2]. In the case of using the IoT-platforms, the digital twin is data-based and has a bottom-up design.

Digital twins can also be designed using commercial simulation tools, such as ANSYS, Maplesim, MATLAB, and SimulationX. These tools support system-based design methods so that in this case, the twin has the top-down design.

## 3 Research Methodology

For analysis of the existing platform, a digital twin of the wind turbine will be constructed in four selected platforms that are suitable for realizing a digital twin. To compare the platforms better with each other, specific characteristics are analyzed. More specifically, the following criteria are considered:

- user interface;
- interfaces;
- data structure;

- platform structure (applications, services, etc.);
- possibilities to create your applications;
- predictive maintenance possibility;
- price Structure;
- expansion options;
- documentation.

The platform for the digital twin of the turbine should include the possibility to link the geometry and simulation models, as well as continuously updating weather and sensor data.

Such platforms as MindSphere (Siemens), ThingWorx (PTC), Predix (GE), and Watson (IBM) as well as simulation tool Matlab (Mathsoft) and SimulationX (ESI) are analyzed. These platforms are most distributed in industrial applications and offer a variety of interfaces with tools and components.

## 4 Results

The digital twins created with the platforms all meet the requirements defined for the digital twin at the beginning. All tested platforms provide sufficient ways to connect sensors or devices to the platform using standard interface protocols as well. Predix and ThingWorx offer the broadest range of ways to connect devices and sensors to the platform, though.

In the basic structure, the platforms differ significantly. While IBM Watson has several major components that can be expanded by add-ons, Predix is based on a service model. ThingWorx has several significant parts, whereas MindSphere offers three basic packages that can be developed as required.

MindSphere and ThingWorx provide a graphical user interface for the settings and configurations of the digital image. These platforms use libraries of building blocks, which can be combined by drag-and-drop operations, which is clear and intuitive.

The Predix user interface also has graphical elements that must be created and configured by the user himself. The devices or analysis functions must be added by programming the platform. Watson's IoT platform combines both options. Settings can be made both by input fields of a graphical user interface but can also be programmed. However, some elements of the platform are created and set up only by using lines of code. Users who have experience in programming and want to create their applications, however, can take full advantage of the possibilities with all platforms. However, the effort for programming is much bigger than the creation of functions and interfaces by dragging and dropping and filling input fields.

All four platforms can develop their applications. The MindSphere platform provides extra tools for development. All four platforms have the option to purchase additional applications through a store [2]. The results of the comparison are presented in Tables 1, 2, 3 and 4.

**Table 1.** Analysis results for GE Predix.

Advantages	Disadvantages
<ul style="list-style-type: none"> <li>• Costs for individual services visible</li> <li>• Catalog with many services</li> <li>• Development environment for own applications</li> </ul>	<ul style="list-style-type: none"> <li>• Price is based on data volumes</li> <li>• No own simulation tools</li> <li>• Unclear structure</li> </ul>

**Table 2.** Analysis results for IBM Watson.

Advantages	Disadvantages
<ul style="list-style-type: none"> <li>• Graphical interface or programming possible</li> <li>• Main components of the platform can be extended via add-ons</li> <li>• Instructions including example code</li> </ul>	<ul style="list-style-type: none"> <li>• Confusing documentation</li> </ul>

**Table 3.** Analysis results for Siemens MindSphere.

Advantages	Disadvantages
<ul style="list-style-type: none"> <li>• Graphical interface</li> <li>• Developer Cockpit for developing your applications</li> <li>• Ability to upload data sets for Predictive Learning</li> <li>• Data exchange with another Siemens software possible</li> </ul>	<ul style="list-style-type: none"> <li>• Pricing structure</li> </ul>

**Table 4.** Analysis results for PTC ThingWorx.

Advantages	Disadvantages
<ul style="list-style-type: none"> <li>• Graphical interface</li> <li>• Intuitive creation of predictive maintenance applications</li> <li>• Data exchange with another PTC software possible</li> <li>• Add-on store</li> </ul>	<ul style="list-style-type: none"> <li>• Pricing structure</li> </ul>

For Predictive Maintenance or Machine Learning, tools are provided on all four platforms. MindSphere and ThingWorx convince with precise applications and easy-to-create models. The ThingWorx platform makes creating predictive models very easy. The model is automatically trained after loading the datasets, and the data is analyzed. MindSphere, on the other hand, needs to upload a certain amount of data to train the model for the analysis.

ThingWorx offers the benefit of extensive documentation with step-by-step instructions and video tutorials that can be used directly in a trial version. MindSphere also has extensive documentation, but video tutorials or step-by-step instructions are not available. For Predix, in addition to detailed but confusing documentation, some step-by-step instructions are offered. The Watson IoT Platform also has extensive documentation that includes some step-by-step instructions. However, this is confusing and not sufficient to understand the individual components of the platform in detail.

The documentation and the provided documentation of the four IoT platforms are most convincing at ThingWorx [2].

Another advantage of ThingWorx is the ability to connect AR applications to the digital twin easily. MindSphere's dominance over the other platforms is the direct feedback loop back to research and development.

In addition to MindSphere, Siemens also offers other software that can be used for the digital twin. In this way, simulations and CAD modeling with software from Siemens can be realized. PTC, like Siemens, also offers simulation tools, but can also integrate third-party software (such as ANSYS) in addition to its own. Predix and Watson IoT platforms rely on third-party software for simulation models. Partnerships have been established to facilitate the integration of these tools [2].

The time required to create a digital twin is the lowest at the ThingWorx platform.

With the two simulation tools MATLAB (Simulink) and SimulationX, the structure of the digital twin is similar. Building upon imported CAD data or with function blocks and existing data sheets, a system model of the object is created. The further development of the model does not differ significantly between the tools. The visualization of the models takes place in both windows in view windows. The operation and display are easier to handle with SimulationX. However, unlike SimulationX, MATLAB has a Machine Learning Toolbox that can be used to build Predictive Maintenance algorithms. The documentation of MATLAB is more detailed compared to SimulationX. Sensor data can be imported in both formats in different data formats [2].

The creation of a system model is more natural to realize due to the more uncomplicated import possibilities of SimulationX with the mentioned advantages. For this reason, SimulationX is selected. Since SimulationX and MATLAB communicate with each other via an interface, functionalities that only MATLAB offers can also be provided for models in SimulationX. The advantages of both tools are combined.

The most detailed DT is achieved by communicating the system models from the simulation tools with the IoT platforms. Simulations can be performed in the system models based on the data sent to the platform. These simulations then return results to the platform that can be used for visualizations or further calculations and analyses. For this level of detailing, the effort is too high and not possible due to the lack of sensor access [2].

## 5 Conclusions

While analyzing and comparing the different platforms for digital twin, both Digital Twin design methods were used. Each of the tested tools showed advantages and disadvantages, so none of them presents a perfect solution. The solution to be chosen depends on specific functions and goals to be realized with the Digital Twin. The programming skills of the person also must be taken into account.

Another critical criterion is access to sensor data or access to the system. If this is not given, it is impossible to generate data-based Digital Twin. For system-based Digital Twin, however, all technical details, including the description of the object in the physical, requirement, and logical levels of the system, are required. Among the tools for the system-based design of the Digital Twin, SimulationX was the most

suitable for the chosen application. Among the platforms for data-based Digital Twin, the best results are shown by ThingWorx.



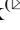



The possibilities and application of the Digital Twin are additionally limited by the infrastructure and software used, including computing power, but with the further development of these technologies, the use of the Digital Twin approached can be extended.

## References

1. Kagermann, H., Wahlster, W., Helbig, J.: Implementing recommendations for project Industry 4.0. Campus, Frankfurt a. M. (2013)
2. Vogt, O.: Selection of a suitable platform for imaging a digital twin. Master thesis, University Duisburg-Essen, Duisburg (2019)
3. Grieves, M.: Digital Twin: Manufacturing Excellence through Virtual Factory Replication. Whitepaper (2014)
4. Gartner: Top 10 Strategic Technology Trends for 2019 (2018)
5. Negri, E., Fumagalli, L., Macchi, M.: A review of the roles of digital twin in CPS-based production systems. *Procedia Manuf.* **11**(June), 939–948 (2017)
6. Tao, F., Cheng, J., Qi, Q., Zhang, M., Zhang, H., Sui, F.: Digital twin-driven product design, manufacturing and service with big data. *Int. J. Adv. Manuf. Technol.* **94**(9–12), 3563–3576 (2018)
7. Tao, F., Zhang, M.: Digital twin driven prognostics and health management for complex equipment. *CIRP Ann. Manuf. Technol.* **67**(1), 169–172 (2018)
8. Tao, F., Zhang, M., Nee, A.: *Digital Twin Driven Smart Manufacturing*. Academic Press, Cambridge (2019)
9. Schleich, B., Anwer, N., Mathieu, L., Wartzack, S.: Shaping the digital twin for design and production engineering. *CIRP Ann.* **66**, 141–144 (2017)
10. Kitain, L.: The New Age of Manufacturing: Digital Twin Technology. <https://www.seebo.com/digital-twin-technology>. Accessed 15 Oct 2019



# Computer-Integrated Design Pistons with the Influence of Casting Defects

Oleg Akimov , Vitaliy Alyokhin , Kateryna Kostyk  ,  
Leonid Saltykov , and Julia Riabets 

National Technical University “Kharkiv Polytechnic Institute”,  
2, Kyrpychova Street, Kharkiv 61002, Ukraine  
eklitus@gmail.com

**Abstract.** In this work, the scientific and practical problem of increase of strength reliability of cast pistons of internal combustion engines taking into account the influence of defects of the casting of gas-shrink character and application of the computer-integrated design is considered. The research aims to create a methodology for determining the locations and sizes of defects in the cast piston with the joint use of computer-integrated modeling and experimental studies in production. For the first time, a method of complex determination of dislocation locations and sizes of gas-shrinkage defects in a cast piston with joint use of computer-integrated modeling and experimental studies in production is proposed and developed. The boundary conditions for calculating the thermal and stress-strain state of the VAZ 21083-1004015 piston in the locations of defects are specified. In this work, the scientific and practical problem of increasing the strength reliability of cast engine pistons is solved, taking into account the influence of casting defects of a gas-shrink nature and using computer-integrated design. Thus, the joint use of the modern computer-integrated design of cast engine pistons with continuous design and technological interaction, which is a powerful tool for the development of new parts and modernization of existing ones, is justified. Also, the paper substantiates the need for the use of systems of engineering modeling of technological processes of production and analysis of the thermal and stress-strain state of cast engine pistons.

**Keywords:** Computer-integrated design · Piston · Engine · 3D model · Casting defect

## 1 Introduction

One of the most important parts for the reliable operation of the engine is the piston while ensuring its strength reliability and the required strength characteristics largely depend on the quality of the structural materials used, the parameters of the production technology. As a rule, in engines with forced ignition of motor transport purpose, pistons made of aluminum alloys are used, which have sufficiently high strength properties and wear resistance in the cast state.

Current trends in the design, production, and operation of internal combustion engines are characterized by a constant increase in power with minimal emissions of toxic components, which leads, in turn, to an increase in thermomechanical loads on individual parts and components of the engine. Shortening the design time of new engines while increasing the requirements for strength reliability has led to the continuous improvement of the design and production technology of individual parts.

In modern engine-building, when designing new internal combustion engines and modernizing existing ones, considerable attention is paid to modern methods of strength calculations of engine components and parts. Special attention is paid to the calculations of resource strength and strength reliability, as they determine the performance of the engine parts as a whole. For strength calculations, a part of a given configuration from a certain structural material is used, but without taking into account technological factors arising in the manufacturing process. The results of such calculations and cyclic strength tests are not accurate enough and require additional research which will take into account the real casting defects in the piston body.

Design and production of internal combustion engine pistons with continuous design and technological interaction is not possible without taking into account the technological aspects of manufacturing, namely casting defects of gas-shrink nature. Such defects are always present in the body of cast pistons of the internal combustion engine made of aluminum alloys, but the effect of the size and location of their dislocation on the strength characteristics has not been studied.

The research aims to create a methodology for determining the locations and sizes of defects in the cast piston with the joint use of computer-integrated modeling and experimental studies in the workplace.

## 2 Literature Review

The review considers the literary sources shows that sufficient attention is given to strength calculations of parts of pistons of diesel engines, in particular the prediction of the heat-stressed state and evaluation thermostatic strength in the field of combustion chambers of the pistons, the calculation of the basic parts of internal combustion engines, etc. Modern methods of calculation of the deflected mode of pistons of internal combustion engines are presented widely in the fundamental works dedicated to the design of internal combustion engines [1–3]. Study of wear characteristics and resistance to fatigue fracture of materials in engine parts represented in the works [4–8].

However, the tasks that researchers and specialists in this field currently have to face are quite complex and require huge costs for experimental implementation. Often, one of the only opportunities for the analysis of the research problem is mathematical or computer-integrated modeling. Preparation of production of pistons is the most important stage, during which the possibility of the capacity of the enterprise is determined, 3D models of pistons are developed, modeling and fine-tuning of the design, production technology, design and technological documentation of the product is produced, as well as bench tests are carried out [9–11]. The computer-integrated design provides a constant and complete interaction of technical departments responsible for the production of quality products and technical documentation.

In modern engine building, according to the principles of design and technological design, the requirements for the reliability of parts are fulfilled at the initial stage of production and are regulated by technical conditions [12, 13]. The reliability of cast engine pistons, subjected to multiple cyclic changes in the load and speed modes of the engine, depends on the resistance to fatigue failure of the material in the various stress nodes of the part. The concept of reliability includes a set of concepts: reliability, durability, maintainability, and persistence. As a measure of trouble-free operation of the piston, the time before the failure (destruction) is used.

The strength reliability of the piston is one of the main aspects of the overall reliability of the engine design. A quantitative indicator of the level of strength reliability is the probability of fatigue failure under operating conditions, the causes of which are associated with insufficient strength. The strength reliability of cast engine pistons depends on the parameters and quality. By definition, the quality of the piston is a set of properties that determine the degree of its suitability for use for its intended purpose. Over time, the quality of the product decreases. The strength reliability of cast engine pistons is defined as an indicator of the state of the structure, providing a high degree of probability of maintaining its integrity and the absence of damage that can provoke destruction.

The reliability of the engine piston, under certain operating conditions, is influenced by the structure of the material. The structure of the material varies and is controlled at the phase transition stages during the cooling of the cast part, as well as during solidification, most of the most important properties of the piston are formed. The strength reliability of the cast pistons of the internal combustion engine and the level of quality is laid and performed at the initial stages of production using computer-integrated design.

A rather complex issue is the availability of reference data obtained experimentally to calculate the endurance limits of real parts and their structural elements. The lack of experimental and calculated data on the stress concentration in the locations of technological defects leads to the fact that the fatigue failure mechanism underlying the method of determining the endurance limit may be in conflict with the actual mechanism of fatigue damage accumulation in the material in a particular case and is a discrepancy between the calculated and experimental results. There is a fairly large number of works devoted to methods for determining the endurance of materials and structural elements, which are based on various hypotheses of fatigue damage accumulation in materials, take into account the various physical processes occurring in materials under cyclic loading, using different design schemes.

Thus, the analysis of modern methods of computer-integrated design of cast engine pistons with continuous design and technological interaction and the use of CALS principles showed that sufficient attention is paid to the formation of casting defects (gas-shrink porosity) in the engine pistons, in particular pistons made of aluminum alloys, but will not affect the assessment of the impact on the strength reliability of their size and characteristic locations.



### 3 Research Methodology

All theoretical aspects are based on the fundamental principles of the theory of internal combustion engines, the theory of machines and mechanisms, the theory of machine parts and modern mathematical tools. Numerical and numerical-analytical methods are applied in the process of design and technological design. In particular, the method of finite differences in three-dimensional volumetric formulation for modeling thermal and hydrodynamic casting processes, the method of finite elements for the analysis of thermomechanical loading of cast parts of the internal combustion engine. Generalization of experimental data and numerical results of calculating the influence of casting defects on the strength characteristics of cast engine pistons was carried out using the method of planning the experiment.

For the simulation of thermal and hydrodynamic processes for the production of cast pistons with an integrated computer system, LVM Flow developed a methodology which determined the boundary conditions of the system casting-form-environment, as well as the refined mathematical model, based on which it was simulated the processes under consideration that are similar to the previously known finite-difference model laid down by the creators of this software package.

In this work, a 3D casting model was developed based on the VAZ 21083-1004015 piston with a technological gating-feeding system. A finite-difference piston model with a gating-feeding system and a metal mold was created using the 3D import module built into LVMFlow.

## 4 Results

### 4.1 Method of Determining the Locations and Sizes of Defects (Gas-Shrink Porosity) in the Cast Piston of the Internal Combustion Engine Using the Computer-Integrated Simulation of Thermal and Hydrodynamic Processes of Production

For the simulation of thermal and hydrodynamic processes of production of cast pistons of internal combustion engines using the integrated computer system, LVM Flow 2.91 developed a technique according to which:

The first stage defines the boundary conditions of the casting-form-environment system and also specifies the mathematical models based on which the modeling of the processes under consideration, which are analogs of the previously known finite-difference models laid down by the creators of this application package, was carried out.

The second stage developed a 3D model of the casting at the base of the piston VAZ 21083-1004015 with the process of the gating-feeding system. During the development and design of the gating and feeding system for casting the piston from aluminum alloys, the following conditions for filling the mold with smelt were observed:

- no swirls in the smelt when filling the form;
- obtaining stable laminar motion;
- avoiding splashing of the smelt in places of transition from thin to thick casting arrays and vice versa.

The third stage was the creation of a finite-difference model of the piston with a gating-feeding system and a metal form with the built-in LVM Flow 3D module imports. The established parameters of the cells are:

- cell size-1.3 mm;
- number of cells-3 563 430 pc.;
- piston casting material-AK12M2MgN GOST 1583-93 (DSTU 2839-94);
- material tooling-Steel 40Cr, grey cast iron 20.

The boundary conditions of heat exchange of the casting-chill system are assigned based on the fact that the forming parts of the chill are coated with a mold paint with a thickness of 0.2 mm and thermal conductivity of  $190 \text{ W/m} \cdot \text{K}$ .

The initial temperature of the mold is  $t = 523 \div 553 \text{ K}$ . The smelt temperature before pouring into the mold is accepted at 983 K. For the orientation of the nature of the phase transitions during cooling, the central rod and the rods forming the holes under the finger have water cooling, with the initial water temperature at 293 K (Fig. 1).

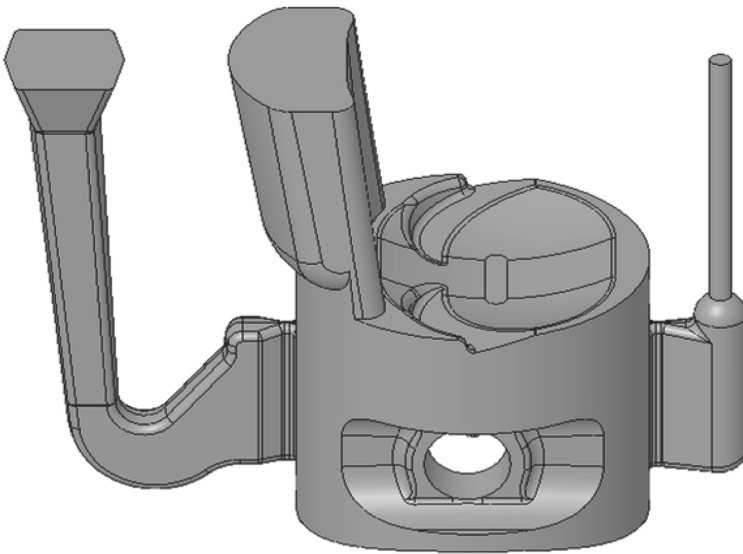


**Fig. 1.** The 3D model of casting piston VAZ 21083-1004015 with gating system.

The analysis of the simulation results revealed the nature of the form filling with smelt (Fig. 2) and the values of the filling rate for each element of the gating system are obtained, namely:

- when moving in the mold riser observed increase in speed to avoid temperature losses at the initial stage of filling; - the movement of the smelt at the entrance to the mold was slight turbulence of the flow and the speed of its movement was 0.4 m/s;
- analysis of the simulation results of filling the mold smelt motion in the casting cavity showed that the speed of its movement was 0.2 m/s. Analysis of the dynamics of the phase transition during cooling of the casting, the coupling zones, crystallizing the latter, allows determining the place of the possible occurrence of gas-shrink defects. The conclusion is based on the analysis of the dislocation of gas-shrink defects expressed in the LVM Flow by the Niyama criterion. It is used to predict microporosity and shrinkage porosity large enough to be detected by radiographic testing. The Niyama criterion is defined as [14]:

$$\text{Niyama} = \frac{G}{\sqrt{\dot{T}}}, \quad (1)$$

where  $G$  is the temperature gradient in K/mm,  $\dot{T}$  is the cooling rate in K/s.

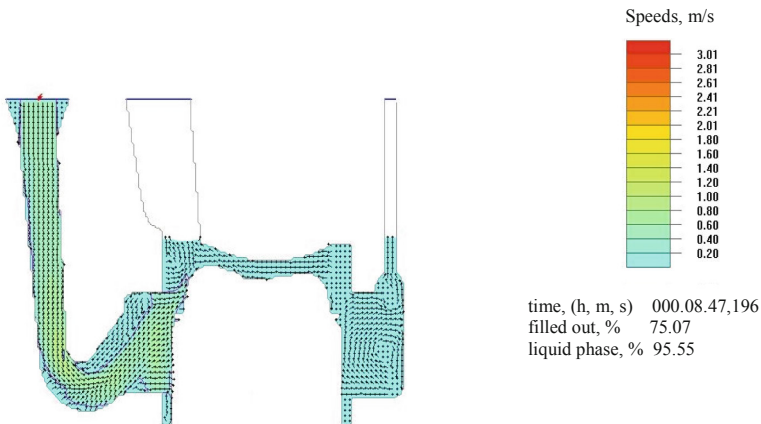


**Fig. 2.** General view of form-filling by the smelt.

Places of dislocation of defects, according to this criterion, are presented in Fig. 3.

Analysis of the simulation results according to the Niyama criterion showed that the most susceptible to the formation of gas-shrink porosity are arrays of the boss throughout the area around the finger hole, the bottom of the piston under the combustion chamber and the transition zone from the piston body to the bottom, inside the piston part. Based on the results of computer-integrated modeling of thermal and hydrodynamic processes of the casting of internal combustion engine pistons, it was assumed that the defects of gas-shrink nature can be fatigue failure concentrators in the structural elements of the part, and therefore can affect the strength reliability during operation.

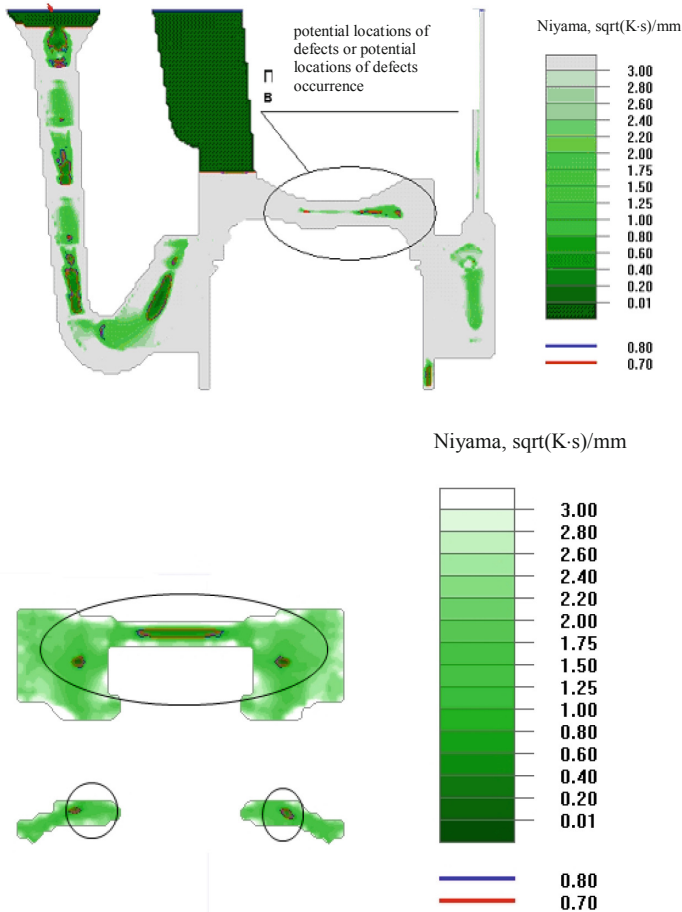


**Fig. 3.** Locations of shrinkage defects according to the criterion of Niyama.

#### 4.2 Experimental Determination of Places and Sizes of Defects (Gas-Shrink Porosity) in a Cast Piston of an Internal Combustion Engine in Real Production

The results of the studies allowed to form the boundary and initial conditions for modeling the stress-strain state of the piston in the places of formation of gas-shrink porosity.

Experimental studies of cast pistons of internal combustion engines in production conditions are necessary to confirm the results of computer-integrated modeling: locations, sizes of emerging technological defects, debugging of the production process. As a result of the disassembly of the pilot batch, the results were obtained, in which a summary was made concerning only the gas-shrink porosity and without taking into account the defects associated with the technical side of the production

process itself (gaps, nicks, slag inclusions on the surface of the machined part). Images gas-shrink defects in different arrays of the piston parts VAZ 21083-1004015 were also obtained (Fig. 4).

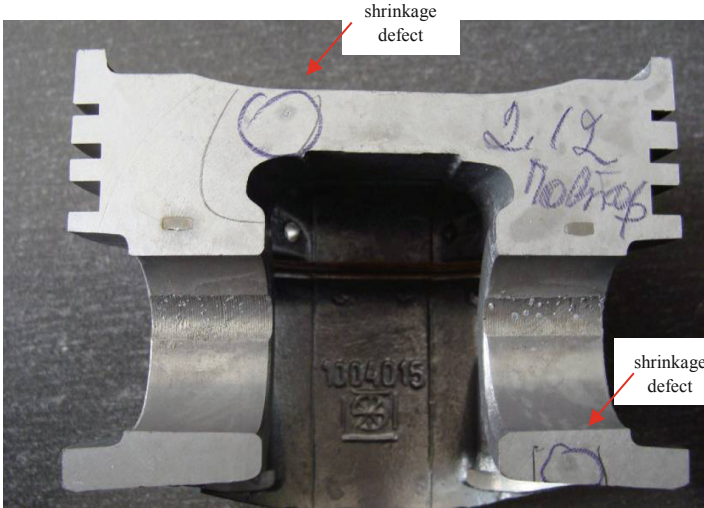


**Fig. 4.** The location of the shrinkage defects in a body cast piston.

Figure 4 shows a general view of the piston dissected along the axis of the finger holes with gas-shrink defects (gas-shrink porosity) in its body.

Locations and sizes gas shrink defects identified in the experimental studies confirm the results of the computer-integrated simulation. The joint solution of the problems of computer-integrated modeling and experimental research in the production allowed predicting the formation of gas-shrink defects in the production of engine pistons.

## 5 Conclusion

In this paper, the scientific and practical problem of improving the strength reliability of cast pistons of internal combustion engines, taking into account the influence of casting defects of gas-shrink nature and the use of computer-integrated design.

Thus, the joint use of the modern computer-integrated design of cast pistons of internal combustion engines with continuous design and technological interaction, which is a powerful tool for the development of new parts and modernization of existing ones, as well as the need for the use of engineering modeling of technological processes of production and analysis of the thermal and stress-strain state of the cast.

For the first time, the method of complex determination of locations and sizes of gas-shrink defects in a cast piston with joint use of computer-integrated modeling and experimental researches on production is offered and developed. The boundary

conditions for the calculation of the thermal and stress-strain state of the piston VAZ 21083-1004015 in the places of dislocation of defects are specified.

According to the method of determining the locations and sizes of defects in the cast engine piston, the process of crystallization of the piston was modeled and investigated in the form, identified the location of defects in various parts of the part, which were confirmed by the results of experimental studies.

Based on the obtained results, recommendations were formulated for the introduction of gas-shrink defects in the 3D model of the piston and the boundary conditions were adjusted to calculate the thermal and stress-strain state, as well as for the subsequent analysis of the effect of defects on the strength reliability of the cast piston of the internal combustion engine.

**Acknowledgments.** We thank Professor of the Department of aircraft engine design at the National Aerospace University named after N.Ye. Zhukovsky “KhAI”, D.Sc., Professor Oleksandr V. Bilohub and Vice-rector of National Technical University “Kharkiv Polytechnic Institute” D.Sc., Professor Andriy P. Marchenko for theoretical and technical help.

## References

1. Chetvertakov, V.A.: Calculating variable deformation of piston engine cases. In: Soviet Shipbuilding [USSR], vol. 2, pp. 1–6 (1987)
2. Chigrinova, N.M., Kuznechik, O.O., Chigrinov, V.E., Presnyakov, G.A., Chigrinov, V.V.: Influence of heat-shielding coatings formed by means of anodic micro-arc oxidation on the service life characteristics of piston engines. *Powder Metall. Met. Ceram.* **44**(5–6), 304–307 (2005)
3. Shevchenko, Y.N., Savchenko, V.G.: Three-dimensional problems of thermoviscoplasticity: focus on Ukrainian research. *Int. Appl. Mech.* **52**(3), 217–271 (2016)
4. Carvalho, O., Buciumeanu, M., Madeira, S., Soares, D., Silva, F.S., Miranda, G.: Optimization of AlSi–CNTs functionally graded material composites for engine piston rings. *Mater. Des.* **80**, 163–173 (2015)
5. Ye, H.: An overview of the development of Al-Si-alloy based material for engine applications. *J. Mater. Eng. Perform.* **12**(3), 288–297 (2003)
6. Becker, E.P.: Trends in tribological materials and engine technology. *Tribol. Int.* **37**(7), 569–575 (2004)
7. Seifi, M., Salem, A., Beuth, J., Harrysson, O., Lewandowski, J.J.: Overview of materials qualification needs for metal additive manufacturing. *JOM* **68**(3), 747–764 (2016)
8. Zhang, J.H., Chen, M.: Assessing the impact of China’s vehicle emission standards on diesel engine remanufacturing. *J. Clean. Prod.* **107**, 177–184 (2015)
9. Sharma, R.S., Singhal, I., Gupta, S.: Innovative training framework for additive manufacturing ecosystem to accelerate adoption of three-dimensional printing technologies. *3D Print. Addit. Manuf.* **5**(2), 170–179 (2018)
10. Harries, S., Abt, C., Brenner, M.: Upfront CAD-parametric modeling techniques for shape optimization. In: *Advances in Evolutionary and Deterministic Methods for Design, Optimization and Control in Engineering and Sciences*, vol. 48, pp. 191–211 (2019)
11. Murthy, B.S., Howard, T.J.: Product maturation guide—a digital simulation outcome. *Procedia CIRP* **43**, 82–87 (2016)

12. Dhahad, H.A., Alawee, W.H., Marchenko, A., Klets, D., Akimov, O.: Evaluation of power indicators of the automobile engine. *Int. J. Eng. Technol.* **7**(4.3), 130–134 (2018)
13. Akimov, O., Soloshenko, V., Kostyk, K.: Computer-integrated design of cast parts on the criterion of performance on the example of the turbine wheel turbocharger. In: *CEUR Workshop Proceedings*, vol. 2353, pp. 324–338 (2019)
14. Carlson, K.D., Beckermann, C.: Prediction of shrinkage pore volume fraction using a dimensionless Niyama criterion. *Metall. Mater. Trans. A* **40**(1), 163–175 (2009)



# Improvement of the Effectiveness of General Engineering Courses Using Trainers

Mykola Korotun , Yuliia Denysenko , Nina Malovana,  
and Olena Dutchenko 

Sumy State University, 2, Rymkogo-Korsakova St., Sumy 40007, Ukraine  
uapogor@gmail.com

**Abstract.** This article runs about the principles of developing and using trainers to enhance students' educational and learning activities while studying engineering. The authors analyzed modern works of the development, implementation, and improvement of the use of trainers. Based on a generalization of the experience of such developments, a methodological approach was provided, based on the properties and functions of actions when using trainers, principles of visual modeling, sign and symbolic activity. The algorithm for the development of trainers in higher educational establishments is also recommended. At the same time, the requirements for the development of trainers were considered, taking into account the primary and secondary characteristics of actions, such as the form of the action, the measure of its generality, as well as the awareness and reasonableness of the actions. In addition, the authors provide a scheme to improve the sign and symbolic activity during the development and use of trainers in the study of engineering disciplines. The given methodological approach to the design of trainers is the possibility of a scientifically-based solution to the problem of the formation of the most general principles of activity for students and the ability to independently develop the whole system of scientific knowledge based on them.

**Keywords:** Trainer · Methodological approach · Simulator · Interchangeability

## 1 Introduction

One of the contradictions in modern higher education is that even though today's students use a computer, audiovisual (video) and other equipment widely, even that they met the basics of technical expertise in physics classes, and some cases in the workshops based on labor skills, where students learn about the elements of drawing, general technical disciplines at the University are perceived with difficulty. These difficulties relate not only to the fact that students are unfamiliar with it or not sufficiently aware of the elements of technique, but because they find it difficult to accept new concepts, which at first glance do not have anything complicated to the ordinary perception of new knowledge. However, the teachers of engineering disciplines notice these problems at the initial meetings with junior students who learn general engineering disciplines.



Besides that, none of the students receive all the knowledge provided in any environment: lectures, textbooks, and others. Nevertheless, the more students are actively engaged with the material, the better the material is absorbed [1].

Despite different forms, methods, and technical means, adequate to modern aims of preparation of specialists of higher engineering qualification used in studying general engineering disciplines, there is a constant lack of scientific developments in the field of intensification of methodological developments to increase the efficiency of perception of the material of technology by students themselves. Despite the fact that the considerable possibilities of realization of didactic information materials and the use of communication technologies, lecture notes, tutorials, methodological developments are still the main information sources.

They are used for the independent study of the material in any form of study: full-time, distance learning, etc. It should also be noted that modern textbooks in general technical disciplines are not much different from textbooks written in the previous century. This certainly has its explanation in that elementary concept relating to mechanical engineering as well as elements of machine parts remain, and are likely to remain virtually unchanged for the indefinite period of humanity's existence. Nevertheless, in our view, the use of modern information technology can make a significant "coloring" in the information space of general engineering disciplines. Their full function is not to use trainers.

Therefore, the study aims to determine the effectiveness of the use of intelligent computer trainers for cognitive activity in the study of general engineering disciplines.

## 2 Literature Review

The main tasks of the educational process management, in addition to improving the effectiveness of learning and skills is also its optimization, aimed at further development of creative abilities, in constant search for new and on this basis to generate new ideas. To do this, educational institutions should provide their staff with the right tools and technologies to provide their personnel with the opportunity to obtain an extraordinary experience [2].

In teaching practice, there are the following stages of management learning and cognitive activity: a learning object management, development management program of the educational and cognitive activity, implementation of programs, monitor learning, making adjustments in programs, and educational activities. The basics of the psychological and pedagogical theory of educational activity management were embedded in the theory of the gradual formation of educational and cognitive activities [3].

With the traditional and collective means of education, today, the issues of the further search for improvement in the management of educational and cognitive activity have not lost their relevance, since new pedagogical technologies, so-called "flexible", that allow approaching individual abilities as much as possible for each student and organizing individual training and its control in terms of collective learning. They make special training processes managed, individually differentiated, with a high level of personal training and productive training [4].

Different types of learning opportunities are provided by different parts of the brain that process information differently. These different learning opportunities can be activated using communication in a variety of information formats [5, 6]. One of the most effective tools for the modern engineer is using augmented [7, 8] and virtual reality [9] technologies.

In recent years, multimedia examples have been used to improve students' learning. It was found that the test results were improved after the inclusion of the multimedia systems module. On the other hand, studies show that some students believe that such examples were not useful in preparing for the exam. Thus, N. Hubing et al. [10] believe that effective multimedia modules require periodic review based on feedback and students' learning, as well as updates based on new stimulating technology.

Modern computer technology (multimedia) allows creating dialog tutorials and trainers that include computer animation, audio, and video. At a minimum, it will enhance the sense of reality when working with the trainer and open up new opportunities in the learning process.

W. Honekamp [11] recommended a classification-hierarchy of trainers, where the lower level is occupied by computer training/teaching programs and trainers, and the higher level is trainers for simulation of reality (simulation) in the military, medicine, aviation, etc. For example, military trainers include CAX, CTC, TES. Thanks to them, a person practices the operations that are as real as possible, in fact only dealing with their electronic counterpart. However, such systems are different from trainers in greater detail, the complexity of development, and complexity of use (the use of some trainers requires sufficient training). Thus, M. Petty et al. describe the variability of detail and the level of aggregation from the level of the military mission to the level of engineering training [12]. Recent scientific developments, such as [11–13], address some of the issues of developing, implementing, and improving the use of such simulators.

Interactive teaching tools in engineering on computers or smartphones improve students' analytical abilities and coordinate educational activities [14–16]. For example, P. Hernandez et al. [14] their experience in implementing an interactive course for studying the injection molding process was shared. The course includes interactive product graphical window, rheological simulation video, process description and interactive graphic window of mold.

However, the analysis of the sources showed a lack of information on the methodological approaches to the development of trainers used by students studying general engineering disciplines.

Generally, the use of training simulators is a set of interrelated actions. According to N. Talizina [3], the action is a holistic system of elements. These elements provide three basic functions: orientational, executive, and control-corrective. The central function is indicative. It is this function that is used when using simulators. The executive function when using simulators is least used because it is related only to the ability to work with the software on which the simulator is based. The control-correcting function is also applied indirectly, and it is in the fact that the user of the simulator either independently, or under the guidance and supervision of the teacher evaluates their assimilation of a particular section of the subject, and depending on such assessment, continues or stops using the simulator. From the point of view [3], the

executive function is the least effective and should even be excluded from the learning process because it only forms mechanical skills and does not capture the attention of the learning process.

But this approach of analyzing actions when using trainers, cannot be agreed, because simulators just make it possible through mechanical repetition of a particular concept, schema, and the ratio can be accelerated by visual memory of learning of the material being studied. In this case, the simulator replaces the routine cross-over of several times of schemes or rewrites of formulas and definitions, as is always suggested or recommended for use in the educational process. That is, the executive function of training actions when using trainers only increases the efficiency of studying subjects of general engineering disciplines.

### 3 Research Methodology

Based on the generalization of the experience of scientists involved in the development of new educational technologies in higher education, it is possible to present the simulation process in the creation of simulators for general engineering disciplines as a set of interrelated elements, Fig. 1. In the view of the authors, modeling cannot be performed unless you have the educational elements (definitions, the issues, the discipline structure, the requirements for the result, that is, the knowledge and competencies that a future Bachelor of Engineering should possess.

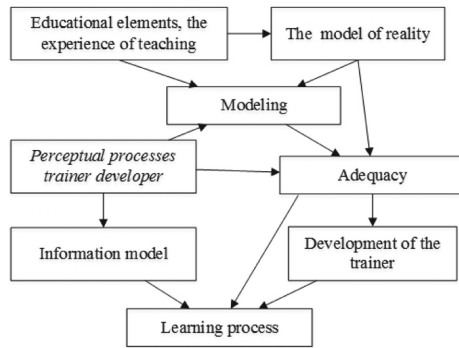
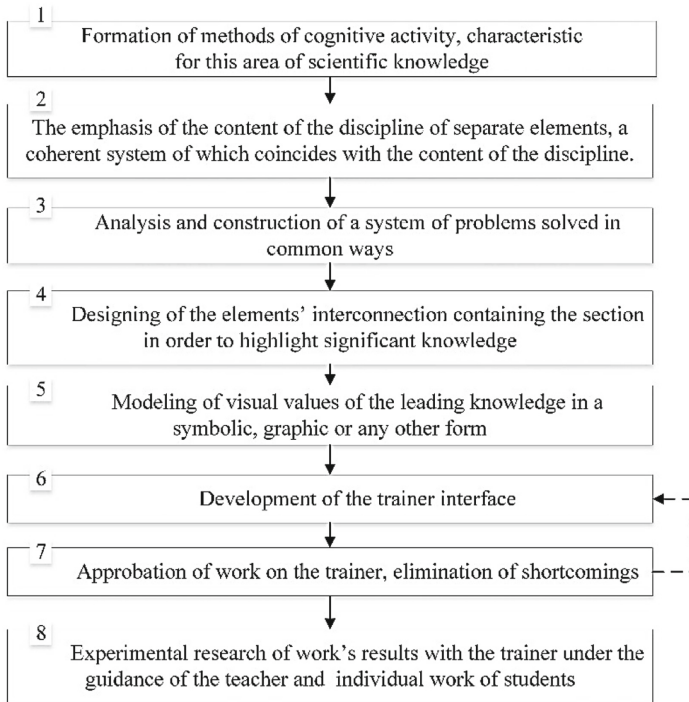


Fig. 1. Modeling process when creating trainers.

Teaching experience and capabilities (information technology skills) and the conditions for creating simulators are also relevant, as is the imaginative representation of reality, such as a real representation of landings with a gap, tension, transients, and their use in various fields of technology. The simulation process itself involves the inclusion of a perceptual (visualized) form of actions of the simulator developer, which is related to the abstract representation of information models previously made possible for other phenomena, for another physical nature, but associatively which can be used to adequately design the trainer of general technical disciplines. The developed trainer is

tested for the adequacy of the developed discipline in the training process for the purpose of diagnostics for the final results and adjustments to improve the results. Considering these elements, it is possible to represent the simulation process when creating trainers for general engineering disciplines in the form of an algorithm, Fig. 2.



**Fig. 2.** The algorithm for developing trainers for engineering disciplines.

In addition, when developing trainers according to this algorithm, the requirement of quality assurance and action properties must be taken into account. Primary properties include the form of action, the measure of its generality, deployment, assimilation, and independence. All these parameters must be met by trainers when studying engineering disciplines.

Yes, in the form of action, the trainers should not reproduce static material (diagram, drawing from a textbook), and show them in dynamics, just as the teacher interprets this on a blackboard, pencil on paper, but even better, even more effectively, with greater accuracy than can be done with a pencil on paper.

The original form of action can be either material or materialized, that is when materialized action acts as a material object, the model not the material object itself. When studying engineering disciplines, it is possible to use both forms of action, for example, when studying a micrometer, its materialized object in the simulator can be presented in two variants: in 2D (i.e., it is presented as a drawing with explanations and

animation of the principle of operation) and as a more realistic object in 3D, visually physically matched to a real photo and video object. However, there is a significant difference in actions with materialized objects.

Materialized photo and video objects are unmanageable, which significantly restricts the use of such objects in simulators without significantly developed action scenarios in such cases. This disadvantage does not have materialized objects made in 3D that provide at least an animation of the actions of the materialized object, which makes it possible to widely use them in simulators of engineering disciplines. When choosing the initial form of action in the trainer, it is important to evaluate and compare the efficiency of the material and materialized forms, and for the materialized form it is also the efficiency of the types of materialization. In some cases, especially for the students with visual thinking, individual circuits in trainers can be performed without complicated materialization, that is, presented in a perceptual form.

The measure of generalization of actions is another basic concept that should be used in the development of the trainer, and the ability to measure it during learning of the training material. It is experimentally established that the generalization is carried out according to the properties coming to the indicative basis of activity. Other characteristics are not seen as significant for action. In the case of trainers in the discipline “Interchangeability, standardization, and technical measurements” (hereinafter ISTM), when designing planting schemes, the basic basis of activity lies in a clear conception of the terms “shaft and hole” and these concepts are in turn related to the details of the machines, so and with their geometric interpretation in the plane of the drawing.

The mental form of action is the final one in the way of transformation of the action from external to internal, that is, if the trainer uses either material or materialized forms of action, depending on what structural elements of the developed actions and what materialized in the first place depends on the result mental form of action, i.e. perception, assimilation, memorization, abstract presentation of educational material.

Secondary action properties are a consequence of the formed primary properties. The strength of actions depends not only on the number of repetitions of actions on the trainer but also on whether all the forms (materialized, others) on the way to the mental have been passed or whether they have been generalized.

Awareness in developing a simulator creation technique is contained in the ability to justify, argue that the trainer is correct depends on the quality of the action, and this is possible when looking at the development of actions from the outside.

Secondary action properties are a consequence of the formed primary properties. The strength of actions depends not only on the number of repetitions of actions on the trainer but also on whether all the forms (materialized, others) on the way to the mental have passed or whether they have been generalized.

Awareness in developing a simulator creation technique is contained in the ability to justify, argue that the simulator is correct, depends on the quality of the action, and this is possible when looking at the development of actions from the outside.

Reasonableness of actions shows the degree to which they are adequate to the conditions under which they are fulfilled, that is, to what extent are the essential conditions that are guided by creating a methodology for the trainer. This determines that the reasonableness of actions on the simulator is determined by the content of its orienting basis. It is possible to achieve the necessary degree of reasonableness by

correctly selecting the conditions that the simulator developer should rely on. It can be done by controlling the process of assimilation of the material, that is, through control. Thus, when developing a methodology for creating simulators, it is necessary to highlight and take into account not only the types of actions but also to show and justify the indicators against which they should be created.

Types of models that are a sign and symbolic and are used in visual modeling can be attributed such as: logical, relational, semantic, productive, and frame [13]. Logical models use alphanumeric symbolism, which is the most common in general technical disciplines. A striking example is the discipline of ISTM, where the alphanumeric symbolism is widely used. For logical models, it is possible to use graphs, where vertices define the learning elements (concepts, theorems), and edges represent the relationships between the elements. Despite the brightness of graphs, in information trainers their use is limited.

Relational models are usually tables, such as tables of major deviations, tables of tolerances and landings, generally, tables are widely used in standardization, and an auxiliary (reference) material they can be used in the development of simulators. Semantic models are associated with the definition of the symbolism of signs (symbols, images), that is, the requirements for semantic models correlate with the requirements for sign symbolic activity, and are therefore offered for the use in the development of information simulators.

Production of the model record of the procedure of actions of the user of the simulator, for example, to move the tolerance of the shaft on its main deviation to create the layout of tolerance zones of shaft and hole defined landing. The most striking example of frame-based models is the field of tolerances and fits ISTM, where units of knowledge are placed in “frames” – the “framework” that carry symbolic information about the state of the object in the design, analysis, research, and, of course, be reflected in the trainers with ISTM, although such training elements of other engineering disciplines may be reflected in the development of information equipment. Thus, the use of frame models for training meets the knowledge requirements, where it receives the activity work on the trainer, the connection with theory and practice, structure and names of the frames provide the internal interpretation of the knowledge placed into frames.

In the development of intelligent trainers, visual modeling technologies (Fig. 3) are used, which allows stimulating the level of motivation to acquire new knowledge in engineering disciplines. The development of trainers does not involve the use of research functions but is intended as a means of assimilation of theoretical material, that is, by the type of symbols and symbolic activity, it is the schematization, since individual simulators (especially from ISTM) most often have schemes of placement of tolerance zones and landings.

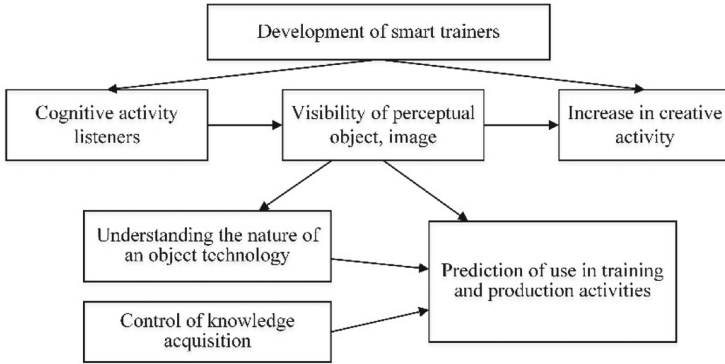


**Fig. 3.** The scheme of improvement of symbolic and symbolic activity during the development and use of trainers the study of engineering disciplines.

### 4 Results

Trainers should be considered as an interactive training facility designed to consolidate knowledge, acquire skills and control knowledge in the study of Interchangeability, Standardization and Technical Measurement. The trainers are intended for the best assimilation of the material both at independent work and in the presence of the teacher. The benefits of simulators are that you can repeat the proposed tasks any number of times, which allows you to better, faster and easier learn the basic concepts of the theory of interchangeability of machine parts.

The example of the trainer interface is shown in Fig. 4.

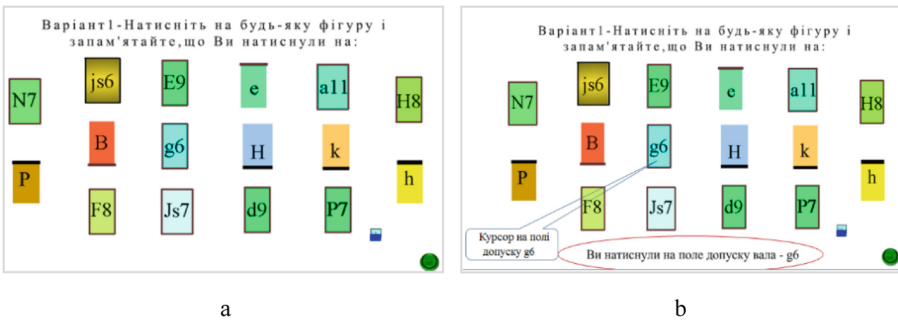


**Fig. 4.** The interface of the trainer “Concept of Tolerance Zone” (a - the input of the trainer; b - the trainer state).

The above-shown trainer presents 16 objects (figures) of the ISTM, which include tolerance zones and major deviations. Examples of tolerance zones are given for both shafts and holes. The basic deviations are also given for both shafts and holes. To increase the training effect, objects (figures) are presented in three variants. You can switch between the options at the bottom of the right corner of the slide. Clicking on any object at the bottom of the slide shows an answer that you need to study and remember. In this example in Fig. 3, the answer is: “You have pressed the shaft tolerance zone g6!”. In the following trainer (Fig. 5), 8 zones of tolerances of openings A8–H8 are used. Above the zero line, the locations of the major deviations are shown. The explanatory text for the trainer is as follows: move the hole tolerance zone with the cursor and position them correctly on the basic deviations when correctly. In this case, the main deviations are the lower ones, i.e. the tolerance zone must be placed on them.

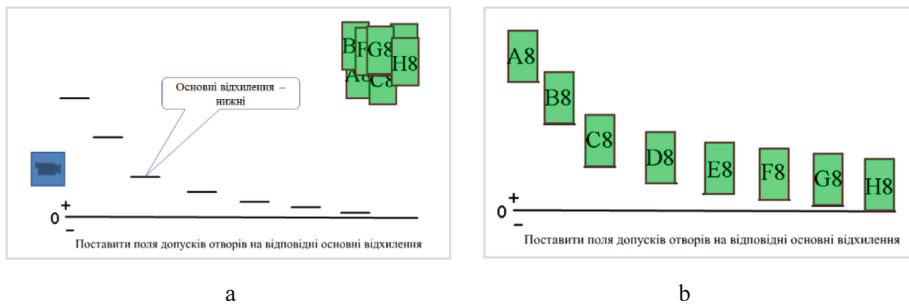


**Fig. 5.** The trainer Interface “Location of Hole Tolerance Zones” (a - the input of the trainer; b - the trainer state).

Exiting trainer mode returns the training tolerance zone to its original position. The correct training position is shown on the slide after the slide of the trainer.

In the trainer, 4 basic deviations of openings and 4 basic deviations of shafts are presented (Fig. 6). Above and below the zero line, the locations of the major deviations are shown. In this case, some of the fundamental deviations are upper, some are lower, and the deviations J and j are symmetrically positioned at the zero line. The locations of the main deviations are provided for self-training. There are no major deviations in the trainer under the guidance of the teacher. One can switch from the self-training to the teacher-controlled work by clicking on the button in the lower right corner of the slide.



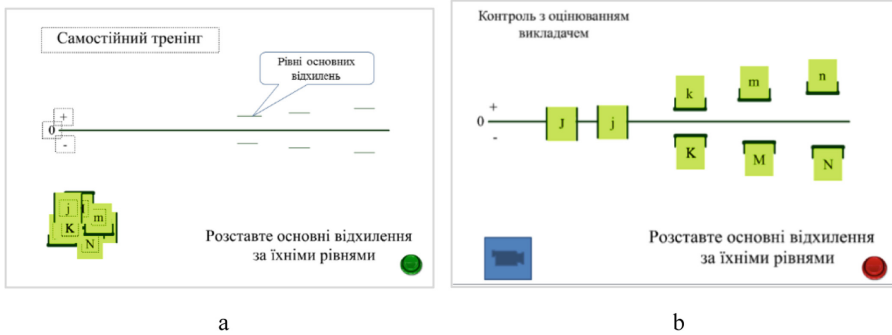


**Fig. 6.** The trainer interface “Shaft and Hole Tolerance Zone” (a - the input of the trainer; b - the trainer state).

The most successful assimilation is when the action performed by the listeners coincides with the visual material that coincides with the actions leading to the awareness of the object of assimilation. This is the result observed when using the proposed trainers because when using the first trainer tolerance zone must be drawn and signed in different letters, which takes time and ability to draw fields. In this case, the number of repetitions without a simulator is limited by the time of drawing and reflection on the recording of relevant symbolic symbols. The trainer greatly facilitates the perception of the training material without restrictions on the number of repetitions and the variety of materials offered. Such a trainer is effectively used in the section where the tolerance zones begin to be studied. The basic deviation trainer also has the advantage that even the simplest thing, such as the risk of a fundamental deviation relative to the zero line, is not always immediately fully understood by the trainees, and even more so ignored by them for repetition in connection with seemingly elementary things for their repetition by graphical means.

## 5 Conclusions

Today’s students, despite their extensive knowledge of computer technology, are not sufficiently familiar with the elements of mechanical engineering in the study of general engineering disciplines and have difficulty in it.

The analysis of information sources showed that the issues of the further search for improvement in the management of educational and cognitive activity have not lost their relevance, due to the introduction of new pedagogical technologies that allow to approach as much as possible the individual abilities of each listener and organize their individualization and adjustments.

One of the sources of increasing motivational and educational-cognitive activity is the development and implementation of information trainers, which use both materialized and perceptual (visualized) forms of action, i.e. information trainers add special attention to the study of general engineering disciplines.

The proposed methodological approach to the design of the structure and content of trainers is a real opportunity to come to a scientifically based solution to the problem of formation of the most general principles and concepts of technology for students and on their basis the ability to independently build a complete system of scientific knowledge (go beyond the acquired information).

Developed and presented as an example of information trainers used in the study of general engineering discipline ISTM, the introduction of which has increased the motivational, educational and cognitive activity.

For further research, it is planned to develop a functional model of the intellectual trainers based on the use of graphic and animated software products and to check its adequacy in terms of both collective and individual (distance) learning tools, and make necessary adjustments in its development. In addition, it is planned to study the issue of performance evaluation on the trainer.

## References

1. What's A Learning Simulation? TeachThought Staff, Technology (2017). <https://www.teachthought.com/technology/6-important-questions-answered-about-learning-simulations/>. Accessed 05 Oct 2019
2. Harness Digital to Modernize Higher Education. ECampusNews. <https://www.ecampusnews.com/resource-library/harness-digital-to-modernize-higher-education-3/>. Accessed 05 Oct 2019
3. Talyzina, N.: Knowledge Management. Moskow State University, Moskow (1984). (in Russian)
4. Gurye, L., Kirsanov, A., Kondratyev, V., Yarmakeev, I.: Integrative Foundations of the Innovative Educational Process in Higher Professional School: Monograph. WINITI, Moskow (2006). (in Russian)
5. Buckley, D.: In pursuit of the learning paradigm: coupling faculty transformation and institutional change. *EDUCAUSE Rev.* **37**(1), 29–38 (2002)
6. Panina, E.A., Stash, S.M.: Using of interactive learning tools in the educational process. *Sci. Alm.* 228–231 (2015). <https://doi.org/10.17117/na.2015.01.228>. (in Russian)
7. Ivanov, V., Pavlenko, I., Trojanowska, J., Zuban, Y., Samokhvalov, D., Bun, P.: Using the augmented reality for training engineering students. In: Bruzzone, A.G., et al. (eds.) *Proceedings of the 4th International Conference of the Virtual and Augmented Reality in Education, VARE 2018*, pp. 57–64 (2018)
8. Ivanov, V., Pavlenko, I., Liaposhchenko, O., Gusak, O., Pavlenko, V.: Determination of contact points between workpiece and fixture elements as a tool for augmented reality in fixture design. *Wirel. Netw.* (2019). <https://doi.org/10.1007/s11276-019-02026-2>
9. Bun, P., Trojanowska, J., Ivanov, V., Pavlenko, I.: The use of virtual reality training application to increase the effectiveness of workshops in the field of lean manufacturing. In: Bruzzone, A.G., et al. (eds.) *Proceedings of the 4th International Conference of the Virtual and Augmented Reality in Education, VARE 2018*, pp. 65–71 (2018)
10. Hubing, N., Oglesby, D., Philpot, T., Yellamraju, V., Hall, R., Flori, R.: Interactive learning tools: animating statics. In: *American Society for Engineering Education Annual Conference & Exposition 2002, Session 2368*, American Society for Engineering Education (2002)
11. Honekamp, W.: Simulation as a training aid. Hamburg Academy of Police, Hamburg (2003)
12. Sokolowski, J., Tolk, A., Petty, M.: Introduction to DoD/Military Simulations. Modeling Analysis and Simulation Center, Old Dominion University, Virginia (2002)

13. Santos, I., Dam, P., Arantes, P., Raposo, A., Soares, L.: Simulation training in oil platforms, pp. 47–53. Springer, Cham (2016)
14. Hernandez, P., Taboada, S., Suarez, L., Marrero, M.D, Ortega, F., Benitez, A.: Interactive learning tool in product development for injection moulding. In: The Manufacturing Engineering Society International Conference, MESIC 2015, pp. 197–204. Procedia Engineering (2016)
15. Meegahapola, L., Thilakarathne, C.: Dynamic learner-assisted interactive learning tools for power systems engineering courses. *IEEE Trans. Educ.* **62**(2), 149–156 (2019). <https://doi.org/10.1109/TE.2018.2889621>
16. Salmerón-Manzano, E., Alcayde, A., Montoya, F., Novas N., García-Salvador, R., Garrido-Cárdenas, J., Martínez-Lao, J., Zapata-Sierra, A., Fernández-Ros, M., Soler-Ortiz, M., Gázquez Parra, J., Manzano-Agugliaro, F.: Smartphone as an interactive learning tool: assessment of the use in university teaching. In: 10th International Conference on Education and New Learning Technologies, Palma, Spain, 2–4 July 2018 (2018)



# Modeling of Spindle Node Dynamics Using the Spectral Analysis Method

Oleg Krol<sup>(✉)</sup>  and Volodymyr Sokolov 

Volodymyr Dahl East Ukrainian National University, 59-a Central Pr.,  
Severodonetsk 93400, Ukraine  
krolos@i.ua

**Abstract.** The article discusses the study of the elastic system dynamics for spindle assembly of drilling-milling-boring machining center type. A three-dimensional model of the spindle assembly on rolling bearings is built. A constructive and design diagram of the spindle assembly and a system of forces acting in the process of milling workpieces are formed. The statement on the polyharmonic nature of the input power effect change during the milling process is substantiated. The phenomenon of modeling disturbing effects by superimposing a “white noise” type random component in the MatLab software environment is investigated. The synthesized input signal and its spectral density using the method of Fast Fourier Transform in a Signal Processing environment are obtained. The concept of the spectral windows for increasing the information content of the obtained dynamic characteristics and reducing the variance of frequency estimates is analyzed. The selection of the best spectral window is carried out, with the help of which the distortion of spectral estimates is minimized.

**Keywords:** Spindle node · Frequency response data · Spectral windows

## 1 Introduction

In the range of metal-cutting equipment, the share of high-speed machines and machining centers with advanced technological capabilities is constantly increasing. In contrast to specialized machines, the design of machining centers (MC) is formed both by a set of specific aggregates for high-speed machining and by the principle of their construction – without “hard” kinematic connections between their aggregates [1–3].

Spindle nodes (SpN) of the machining centers are complex mechanical systems consisting of various types of elastic elements, combined into a single design of the machine forming unit and which is the object of modeling and research. Between the input and output data, there are quantitative relationships that determine the complex SpN mathematical model, the study of which can be carried out in the environment of various computer-aided design systems.

A study of the effectiveness of the forming components functioning for metal-cutting equipment according to the criteria of rigidity and vibration resistance is carried out in various integrated CAD systems, in which it is necessary to connect 3D modeling systems of the forming components with design calculation modules for structural

rigidity and vibration resistance. They particularly impact the greatest influence on the accuracy and quality of the products. This is especially important for modern machine tools designed for finishing machining of precision parts. The share of such machines in the population of machine-building enterprises is increasing, which indicates the relevance of methods for assessing vibration resistance. Such a situation from the methodological viewpoint necessitates the parallel use of three-dimensional modeling with parameterization [4, 5] and research methods in the field of vibration resistance of the machine-forming nodes of the machine and its instrumental equipment.

## 2 Literature Review

The issues of the dynamic quality of metal-cutting machines elastic systems are presented in a wide range of studies. In [6, 7], an analysis of the dynamics of functioning is implemented based on the matrix method of initial parameters by constructing frequency formulary of forming units (FU) – analytical models describing the dependence of the output characteristics of the FU elastic units (tool and workpiece movements) at a variable input load. Based on these models, the express procedure is being developed to determine the stability limits, both the functioning of the machine and the cutting process.

In [8], questions of studying the resonance modes of carrier system oscillations for heavy multi-purpose machine model MSP6401 are considered. The presence of general resonance modes in the operating frequency range from 10 to 100 Hz, when loading a variable by the value of the cutting force, is shown. The impact of force on the spindle from the side of the end mill is carried out according to a harmonic law. Based on modal analysis, eight general-resonance modes are obtained, three of which are in a narrow range of 31–37 Hz. However, the law of change of the input signal of force and its effect on the dynamics of the machine in the work is not specified.

The rigidity of the machine's main components affects the accuracy of machining parts in a wide range of sizes. A new approach based on dynamic characteristics (including dynamic correspondence) is used in [9]. The authors propose a procedure for plotting the Stability Lobe Diagram (SLD method) to evaluate the stability of the cutting process on heavy lathes. This method operates with a multi-frequency model based on Chebyshev polynomials. This opens up opportunities for determining the limiting values of the cutting conditions maximizing the productivity of the shaping process. Based on the lobe graphs, the asymmetry of the milling machine design is estimated to increase the dynamic stability in a certain range of stiffness parameters:  $(5.6\text{--}6.0) \cdot 10^6$ , N/mm, presented in [10].

The dynamics of the milling machine is the subject of work [11, 12]. The authors focus on the influence of the layout, taking into account the configuration of the axes, in particular the axis of high-speed spindle rotation and fast feed of the workpiece. Traditionally, a workpieces and milling tools critical influence on the dynamics of the machine properties is noted. The advantage of this work is the creation of a database system, including a variety of layouts and configurations of the axes. The structure of such structured databases contains separate sections in which the main properties of the forming units are presented: spindles with cutters and rotary tables with workpieces. In

such structures for presenting information, a place has been found through 3D models of the main formative nodes of the machine, analytical models, and arrays of experimental data. At the same time, it is not clear from the text of the article how information about random components of input signals (cutting forces) is presented in the databases and how the analytical processing of random components of impacts on machine nodes is carried out.

The paper [13] is devoted to the construction of a 3D model of the spindle assembly of a turning group CNC machine and its study by the finite element method in CAD environment SOLIDWORKS and CAE ANSYS software [13]. The authors use a 10-node model based on the rod formalization with three degrees of freedom in each node of the rod. The study of dynamic characteristics on the spectrum consists of 5 natural frequencies and the corresponding forms of vibration. A feature of the work is the procedure for predicting the processing of this product outside the resonance zone, taking into account the changing load. This makes it possible to obtain an estimate of the stiffness index when bending stresses dominate. However, the authors note the need to simplify the original 3D model (removing chamfers and small holes and other structural elements) in the process of converting 3D file formats between SOLIDWORKS and ANSYS. It should also be noted that in the machines of the milling group the dimension of the working area increases, which increases the complexity of the research procedure due to the variety of tooling and the composition of technological operations.

The analysis of the above works shows the importance of determining dynamic characteristics within the entire working area of the machine, presented in the form of solid models taking into account experimental data. In turn, the efficiency of the analytical apparatus is directly related to the choice of representing the random component in the laws of change in cutting forces as an elastic system input signal to the machine using the methods of spectral analysis and the fast Fourier transform.

### **3 Research Methodology**

#### **3.1 Formulation of the Problem**

Developing a comprehensive procedure for assessing frequency response data of a spindle nodes for drilling-milling-boring machining centers based on an analysis of the flexibility balance and vibration modes of forming unit using spectral analysis toolkit.

#### **3.2 Construction of the 3D Model and Design Diagram of Spindle Node**

The modern computer-aided design system allows implementing the technology of collective end-to-end 3D design of products for various purposes [14–16]. With its help, the designer can carry out the whole range of necessary work from the initial three-dimensional preparation of his idea and detailed modeling of the final product to the study of the effectiveness of the design according to the criteria of rigidity and vibration resistance.

Based on the developed solid-state models of individual parts in the KOMPAS-3D environment a 3D model of the spindle node's design was created using the specialized software application "Shafts and 3D mechanical transmissions" (Fig. 1).

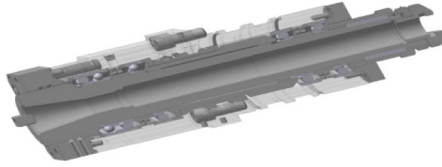


**Fig. 1.** A three-dimensional model of the machining center spindle node.

Let's consider the spindle assembly of the machining center MC200VF4, which is a two-support structure (Fig. 2) mounted on two rolling bearings:

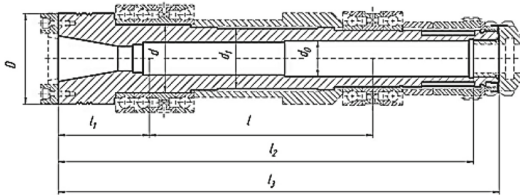


**Fig. 2.** Scheme of the spindle node.

This design of the spindle assembly can be represented as a beam of constant cross-section on two hinged supports. At the same time, rolling bearings have finite stiffness and their action in the design scheme can be conditionally replaced by springs. The bearings are considered (Fig. 2): the front support in the form of a triplex is a set of three angular contact bearings 2-46113 installed according to the Tandem-X scheme with a preload in the form of two bushings of different heights [17–19].

### 3.3 Analysis of the Elastic System Dynamics for MC Spindle

An analysis of the balance of flexibility and vibration modes of the main nodes of the drilling-milling-boring machining centers showed that the most intense vibrations are characteristic of the main forming unit: spindle-arbor-tool. Milling as an operation with intermittent cutting is characterized by a large range of force and disturbing influences that occur during processing, including the probabilistic component.

In the studies and design of metal-cutting machines [20–22], the spectral components were often not taken into account when creating models of the elastic system dynamics for machines. To analyze random processes during machining, numerical methods based on the spectral analysis apparatus and Fast Fourier Transform methods (FFT) can be effectively used [23–25].

Consider the elastic system of a milling-drilling-boring machining center in the form of a linear system with many degrees of freedom. The system includes a number of concentrated and distributed elements with corresponding inertial, elastic, and dissipative characteristics [26–28].

Preliminary experiments on the base model of the MC200VF4 machining center [29, 30] made it possible to evaluate the movement of the tool and workpiece mounted on the turntable under the influence of the nodes weight and forces  $P_{x,y,z}$ . Evaluation layout option suggested an unfavorable nodes arrangement of the machine carrier system – the spindle in the most distant position; and the workpiece in the lowest position.

For the experiment on a comprehensive rigidity assessment of the machine-forming nodes, the technological operation of surface milling in the ZOY plane, reflecting the flexibility of the nodes in all directions and at different points in the workspace was selected. This would provide an opportunity to obtain an objective assessment of the compliance effect on the processing accuracy. The spatial layout of the forming units involves moving the support from the upper to the lowermost position along the Z-axis and the movement of the table from the far left to the far right position. The material of the processed housing part is cast iron; tool - end mill, material of the cutting part WK6 (WC = 94%; Co = 6%), cutter diameter  $d_c = 100$  m, number of teeth  $z = 8$ , milling width  $B = 50$  mm; cutting conditions: cutting depth  $d = 1$  mm; feed  $f = 30$  mm/min; velocity  $v = 160$  m/min.

To assess the influence of the elastic system parameters on the level of dynamic compliance, it is necessary to build vibration modes at those natural frequencies that are characterized by a relatively high level of the tools and the workpiece vibration. An analysis of the experimental amplitude-frequency characteristics showed that the low-frequency oscillations  $f_i$  (Hz) are of most interest:  $f_i = \{20.4; 28.4\}$  [5, 8].

At the indicated frequencies, the vibration modes of the carrier system, the numerical values of the displacements for the tool and the workpiece (Table 1) were calculated. They are based on the numerical values of the linear (mm) and angular displacements ( $\mu\text{m}/\text{mm}$ ) along the corresponding axes  $\{X, Y, Z; \varphi_z\}$  during cantilever loading (forces  $P_j$  are applied at the end of the spindle):  $P_z = -164.0$  N;  $P_y = P_x = 164.0$  N.

As it is known [23], the frequency response of a system is defined as the Fourier transforms  $Y(f)$  of the system reaction (in this case, the displacement  $y(t)$ ) on the impulse action of the force  $P_0(t)$ .

In the process of cutting, a change in forces is quite complex. In particular, we can consider the effect of build-up forming on the effect of “delayed” forces with increasing thickness of the shear layer. Such nonlinear physical effects during spectral analysis are taken into account by introducing a random component of the “white noise” type [24].

The presence of two base frequencies with a maximum level of oscillation:  $\{f_1 = 20.4$  Hz;  $f_2 = 28.4$  Hz $\}$  determines the shape of the input force action  $P_f(t)$  in the form of a polyharmonic signal:  $P_j = P_1 \sin \omega_1 t + P_2 \sin \omega_2 t$ . Here  $P_1$  and  $P_2$  are the amplitudes of harmonic oscillations at frequencies of 20.4 Hz and 28.4 Hz. The oscillation frequencies of the spindle elastic system under consideration can be determined through a certain frequency  $\omega$ , with  $\omega_1 = 5 \cdot \omega$ ;  $\omega_2 = 7 \cdot \omega$  and the sum



**Table 1.** The experimental value of displacements

Node	Direction	Frequency, Hz	
		20.4	28.4
Tool	<b>X</b>	-0.021	0.0063 mm
	<b>Z</b>	-0.018	0.028 mm
	<b>Y</b>	-0.027	-0.0036 mm
	$\varphi_z$	$0.35 \cdot 10^{-5}$	$-0.53 \cdot 10^{-5}$ $\mu\text{m}/\text{mm}$
Workpiece	<b>X</b>	-0.031	-0.0057 mm
	<b>Z</b>	-0.1	-0.021 mm
	<b>Y</b>	-0.11	-0.036 mm
	$\varphi_z$	$0.12 \cdot 10^{-3}$	$-0.56 \cdot 10^{-4}$ $\mu\text{m}/\text{mm}$

will be a periodic function with a period of  $2\pi/\omega = \pi/2$ . In this case, the waveform is written as (1):

$$P_j(t) = 198 \sin \omega_1 t + 101 \sin \omega_2 t. \quad (1)$$

The superposition of a random component of the “white noise” type (the *rand(t)* command in the MatLab system) [25] with zero mean and “unit dispersion” allows forming a combined (synthesized) signal that reflects the ratio of the action of the cutting force and the corresponding spindle displacement:  $Z_j(t) = P_j(t) + 2 \text{rand}(t)$ . Taking into account the random component, the spectral density  $P_{yy}(i\omega)$  of the signal  $P_j(t)$  is calculated: with the number of samples  $N = 256$  (256-point FFT), the FFT of the signal  $y_j(t)$  can be implemented using the MatLab command “fft”:

$\bar{Z}_o(i\omega) = \text{fft}(y_j(t), 256)$ . For the first 128 points (the other 128 points are symmetrical) of the  $P_{yy}(i\omega)$  spectrum, a graphical representation is performed using the commands:  $f = 1000 \cdot (0:127)/256$ ;  $\text{plot}(f, P_{yy}(i\omega) (1:128))$ .

Figure 3 shows a plot of the synthesized signal  $Z_i(t)$  (Fig. 3a) and a plot of spectral density (Fig. 3b). A clear separation of the two harmonics was achieved by reducing the sampling rate and filtering of high-frequency noise components. The obtained frequency characteristics of the input parameters allow us to proceed to the problem of elastic-deformation description in a random setting.

As a result of the discrete Fourier transform, the current spectrum  $A(j\omega, T)$  of the signal  $\bar{y}_j(j\omega)$  is obtained. The limitation of the observation interval is accompanied by a distortion of the spectrum modeled by a rectangular weight function (rectangular window)  $u(t)$ , with the Fourier transform of a rectangular function  $|U(f)|$  [24].

The transition to the finite interval  $T$  leads to the convolution of the Fourier transform of the initial signal  $\xi(t)$  of infinite length with a function of the form  $\text{sinc}(x) = (\sin(x))/x$ , where  $x = \omega T/2$ , as a result of which the calculated spectrum of the signal

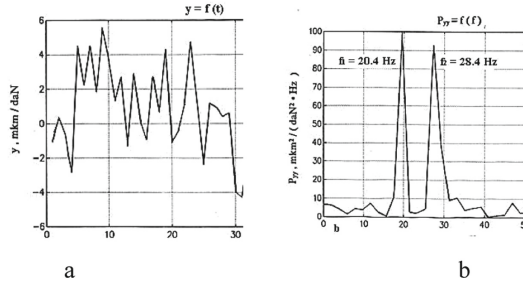


**Fig. 3.** The output signal of the elastic system: a – graph of the synthesized  $Z_i(t)$ ; b – spectral density function  $P_{yy}(i\omega)$ .

$\xi(t)$  turns out to be distorted (spectral splatter). Analysis of this signal over a limited interval gives (2) the current spectrum  $A_1(j\omega)$ :

$$A_1(j\omega) = \frac{\xi^2}{4} \left[ \frac{\sin[T(\omega + \omega_0)/2]}{T(\omega + \omega_0)/2} + \frac{\sin[T(\omega - \omega_0)/2]}{T(\omega - \omega_0)/2} \right]. \tag{2}$$

The MatLab environment implements the calculation and construction of the main spectral windows to analyze and evaluate the dynamic characteristics of the spindle node and improve the quality of its frequency characteristics. The spectrum graph using a rectangular spectral window is shown in Fig. 4.

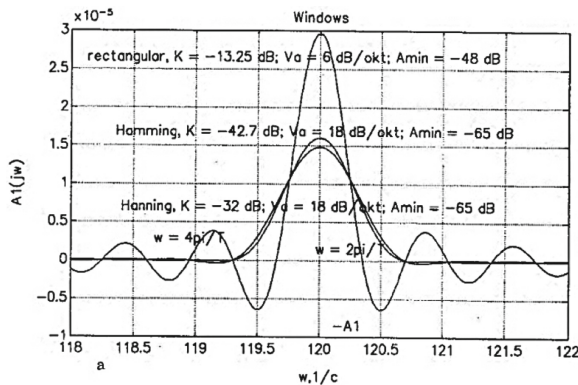


**Fig. 4.** Spectral windows of the current spectrum.

The calculations showed that the level value (greatest) of the side lobes is  $K = 0.217$ , and the intensity of the decrease inside maximums is  $V_0 = 6$  dB per octave. The maximums of the side lobes slowly decrease to the level  $A_{min} = 0.004$  (or to  $-48$  dB) at a frequency equal to half the sampling frequency.

Using the spectral analysis apparatus to assess the dynamic quality of the spindle node of the MC allows effectively reducing the redundancy of the processed information and increase the information content of the obtained spectral characteristics.

## 4 Results

At the same time, as practice shows, large lateral function maxima are observed for a rectangular spectral window, which leads to a large leakage of energy from frequencies different from those located at the points  $\omega = \omega_0$ , which leads to a decrease in the information content of the obtained estimates. In case of the presence of the side lobes with localization at the points  $\omega = -\omega_0$ , it becomes possible to obtain erroneous statistical estimates of spectral characteristics. The main reason for this is the appearance on the graph of the first two lobes of the maximum values of the spectrum, which are 1/5 of the main lobe maximum. For decreasing energy leakage to the side lobes, it is necessary to use more complex weight functions, such as windows: Hanning, Hamming, Kaiser, etc.

The accuracy of the results obtained for those natural frequencies, which are characterized by a high level of relative fluctuations of the tool and the workpiece, allows identifying the most dangerous cutting conditions from the standpoint of the quality of the processed surface. Thus, the use of the Hamming spectral window allows estimating the level of energy leakage in the Eigen frequency zone and leads to a decrease in dispersions to 7.5% and in the maximum level of side lobes to 42.7 dB. This leads to an increase in the information content of the obtained estimates. The proposed tools for assessing the level of the oscillatory process can be recommended for other types of machining with a multi-blade tool (various types of milling, drilling, etc.) under polyharmonic loading.

The use of Hamming and Hanning spectral windows reduces the variance of the spectral estimate. For the case of dividing the total observation length, the signal  $T$  changes into 10 segments ( $T_p = 0.1T$ ), the dispersion ratio (without window/with window) is  $(3/4T)/T_p$ , i.e. decreases to 7.5% of the variance of the estimate corresponding to the sample (not smoothed) spectrum. To increase the adequacy while limiting the observation time of a random process simulating the oscillations of the spindle node under consideration, four weight functions (windows) associated with the spreading of the spectrum were used. Based on a quantitative analysis of the width of the main lobe and the levels of the side lobes, a Hamming spectral window was selected. It is characterized by a smaller width of the main lobe of the frequency response and a decrease in the maximum level of the side lobes of the spectrum.

## 5 Conclusion

Based on the studies, a comprehensive procedure has been developed to study the dynamic quality of a two-support spindle node of the drilling-milling-boring machining center type. A three-dimensional model of the spindle unit was built using the specialized application "Shafts and mechanical transmissions". Experimental research of

the forming nodes vibration for the machining center MC200VF4 at low frequencies is carried out. In practice, the proposed models and algorithms for evaluating the frequency characteristics in the form of MatLab programs will allow express assessment of the dynamic quality of the machine for various conditions of the milling process (a type of milling cutter, processing scheme, and spatial position of the forming units) on the scale of the entire processing workspace. The practical implementation of the proposed results can be presented in the form of a software package based on the Discrete Fourier transform and spectral windows in the Signal Processing environment with adaptation to changing processing conditions. This will make it possible to influence the accuracy and quality of manufactured products by identifying the most dangerous areas of the processing workspace, controlling the change in cutting conditions to reduce vibration levels and identify resonant frequencies in the case of the polyharmonic nature of the loading of the forming machine parts. The analysis of the various spectral windows' effectiveness in the environment "Signal Processing" is implemented.






## References

1. Avramova, T.M., Bushuev, V.V., Gilova, L.Ya.: Handbook on Metal-Cutting Machine Tools. Mechanical Engineering, Moscow (2012)
2. Khomyakov, S., Kochinev, N., Sabirov, F.: Simulation and experimental study of the dynamics for spindle nodes characteristics. *Izvestiya of TSU* **3**, 251–258 (2011)
3. Push, A.V., Zverev, I.A.: Spindle Nodes. Designing and Research. Stankin, Moscow (2000)
4. Krol, O., Sokolov, V.: Modelling of spindle nodes for machining centers. *J. Phys. Conf. Ser.* **1084**, 012007 (2018)
5. Krol, O., Sokolov, V.: Modeling carrier system dynamics for metal-cutting machines. In: International Russian Automation Conference (RusAutoCon) 2018, Sochi, pp. 1–5. IEEE (2018)
6. Popov, V.A., Loktev, V.A.: Dynamics of Machines. Technique, Kiev (1975)
7. Khanov, A.M., Kobityansky, A.E., Shafranov, A.V.: The study of the dynamics of spindle assemblies of machines based on mathematical modeling. *Bull. Perm State Tech. Univ. Eng.* **14**(2), 27–33 (2012)
8. Vasilevich, Yu., Dovnar, S., Shumsky, I.: Modal analysis of the carrier system. *Sci. Life* **4**, 14–24 (2014)
9. Urbikain, G., Campa, F., Zulaika, J.: Preventing chatter vibration in heavy-duty turning operations in large horizontal lathes. *Sound Vib.* **340**, 317–321 (2015)
10. Türkeş, E.: Chatter stability analysis approach for stability analysis of rotating machinery vibrations. *J. Eng. Sci.* **3**, 1–17 (2017)
11. Brecher, C., Fey, M., Daniel, M.: Modeling of position-, tool- and workpiece-dependent milling machine dynamics. *High Speed Mach.* **2**, 15–25 (2016)
12. Brecher, C., Bäumlner, S., Daniels, M.: Prediction of dynamics of modified machine tool by experimental substructuring. In: Proceedings of the IMAC, pp. 297–305 (2014)
13. Kong, J., Cheng, X.: Modal analysis of CNC lathe's spindle based on finite element. *Adv. Eng. Res. (AER)* **148**, 318–321 (2017)
14. Krol, O., Sokolov, V.: Parametric modeling of gear cutting tools. In: Gapinski, B., et al. (eds.) *Advances in Manufacturing II 2019. LNME*, vol. 4, pp. 3–11. Springer, Cham (2019)

15. Ivanov, V., Dehtiarov, I., Pavlenko, I., Kosov, M., Hatala, M.: Technological assurance and features of fork-type parts machining. In: Ivanov, V., et al. (eds.) *Advances in Design, Simulation and Manufacturing II, DSMIE 2019. LNME*, pp. 114–125. Springer, Cham (2020). [https://doi.org/10.1007/978-3-030-22365-6\\_12](https://doi.org/10.1007/978-3-030-22365-6_12)
16. Liaposhchenko, O., Pavlenko, I., Monkova, K., Demianenko, M., Starynskiy, O.: Numerical simulation of aeroelastic interaction between gas-liquid flow and deformable elements in modular separation devices. In: Ivanov, V., et al. (eds.) *Advances in Design, Simulation and Manufacturing II, DSMIE 2019. LNME*, pp. 765–774. Springer, Cham (2020). [https://doi.org/10.1007/978-3-030-22365-6\\_76](https://doi.org/10.1007/978-3-030-22365-6_76)
17. Pronikov, A.S.: *Design of metal-cutting machine tools and machine systems. Mechanical Engineering*, Moscow (1995)
18. Chermensky, O., Fedotov, N.: *Rolling bearings. Mechanical Engineering*, Moscow (2003)
19. Balmont, V.B.: *Calculations of High-Speed Spindle Units. VNIITEMR*, Moscow (1987)
20. Vasilkov, D.V., Weitz, V.L., Shirladze, A.G.: *Electromechanical Drives of Metalworking Machines. Calculation and Design: Textbook. Polytechnic*, St. Petersburg (2011)
21. Strutinsky, V.B.: *Mathematical Modeling of Processes and Systems of Mechanics: A Textbook. ZhITI, Zhytomyr* (2001)
22. Strutinsky, V.B., Melnychuk, P.P.: *Mathematical Modeling of Metal-Cutting Machines: Monograph. ZhITI, Zhytomyr* (2002)
23. Bendat, J., Pirsol, A.: *Applied Analysis of Random Data. Mir*, Moscow (1989)
24. Solodovnikov, A., Spivakovsky, A.: *Fundamentals of the Theory and Methods for Spectral Information Processing. LSU, Leningrad* (1986)
25. *MATLAB: User's Guided for MS-DOS Personal Computers. The Math Works, Jnk.* (1989)
26. Stentsel, Y., Porkuiian, O., Litvinov, K., Sotnikova, T.: Studying additional measurement errors for control tools using an integral functional method. *East.-Eur. J. Enterp. Technol.* **3** (5(99)), 36–43 (2019)
27. Sokolov, V., Krol, O., Stepanova, O.: Choice of correcting link for electrohydraulic servo drive of technological equipment. In: Ivanov, V., et al. (eds.) *Advances in Design, Simulation and Manufacturing II, DSMIE 2019. LNME*, pp. 702–710. Springer, Cham (2020)
28. Gasanov, M., Kotliar, A., Basova, Y., Ivanova, M., Panamariova, O.: Increasing of lathe equipment efficiency by application of gang-tool holder. In: Gapiński, B., Szostak, M., Ivanov, V. (eds.) *Advances in Manufacturing II, MANUFACTURING 2019. LNME*, vol. 4, pp. 114–125. Springer, Cham (2019)
29. Krol, O., Sokolov, V.: Parametric modeling of transverse layout for machine tool gearboxes. In: Gapiński, B., et al. (eds.) *Advances in Manufacturing II. LNME*, vol. 4, pp. 122–130. Springer, Cham (2019)
30. Krol, O., Sokolov, V.: 3D modelling of angular spindle's head for machining centre. *J. Phys. Conf. Ser.* **1278**, 012002 (2018)



# Method of Design of Interference Fit Based on Complex Mathematical Modeling

Vladimir Nechiporenko<sup>(✉)</sup> , Valentin Salo , Petro Litovchenko ,  
Vladislav Yemanov , and Stanislav Horielyshev 

National Academy of the National Guard of Ukraine,  
3, Zakhysnykiv Ukrayiny Sq., Kharkiv 61001, Ukraine  
69nevlani@gmail.com

**Abstract.** The work presents the solution of the urgent problem for creating effective means of computer-aided design of rational fits with the interference fit for connecting machine elements during the assembly. As a result of the study, theoretical principles, methods, and software for the automated design of interference fit are developed. The structure of functional relationships between the restrictions on the ranges of values of the initial parameters for calculating fits and the parameters that meet the loading conditions taking into account the operational, strength and technological requirements for them are obtained. Research of tightened bandage joints is carried out, based on which, a model of the fit area in the form of an  $n$ -parametric geometric image was constructed, which parameters are the interference, specific pressure in the joint, and its geometric dimensions. Based on the analysis of the results of computational experiments, an algorithm is proposed for constructing a geometric interpretation of the model in two-dimensional and three-dimensional coordinate systems. To improve the program for the automated calculation of interference fit, an effective methodology is developed for the analytical description of the area of existence of suitable fits using the mathematical apparatus of the theory of  $R$ -functions. The research results allow increasing the productivity and quality of the design of interference fits, as well as recommend methodological and software tools for integration into CAE/CAD/CAM.

**Keywords:** Specific pressure · Diameter and length of fit · Probabilistic tolerance interference · Area of existence · Constraint factors · Mathematical apparatus of the theory of  $R$ -functions

## 1 Introduction

The technical level and competitiveness of machines are ensured at the stages of their design, production, and modernization. One of the most common methods of joining machine elements during the assembly is the interference fit on a smooth surface, which accounts for up to 35% of the total number of all types of joints in modern engineering. The strength, reliability, and durability of the entire joint and individual parts entirely depend on the proper selection of such fits. During the assembly, the actual interference fit is affected by a random factor (dispersion of the dimensions of the

parts within the tolerance), which makes it difficult to predict the strength of the joint. When calculating fits, most often several design solutions satisfy loading conditions but do not take into account the totality of operational requirements. When designing fits, an urgent and practically significant scientific problem is the search for the most rational design solution from a finite set of permissible ones. In this regard, there is a need to create an effective method for computer-aided design of joints based on complex mathematical modeling for the area of existence of interference fit parameters.

## 2 Literature Review

Many scientific papers are devoted to theoretical and experimental studies of the strength in an interference fit. Recently, the finite element method (FEM) has been used to calculate and predict the strength of the interference fit. This approach allows evaluating the strength of the joint surface without predicting the guaranteed strength for the batch of products, as well as the possible level of load at which the destruction of the joint. Thus, in [1], based on the FEM, the influence of the shape geometry error on the fit of interference fit for a cylindrical joint is determined. In [2], for various methods of processing joined surfaces, the issue of the strength of the axis of wheel pairs of rail vehicles with an axial displacement of the wheel joint is considered. Studies have shown that during the thermal assembly of polished parts, an increase in strength by 2–2.5 times is observed compared to the mechanical pressing.

The bearing capacity of joints with a guaranteed interference fit can be increased if the fit surface is modified by making it with annular grooves of shallow depth commensurate with the interference fit [3, 4].

Hybrid joints, including adhesive joints and interference fit, are widely used. The strength of such a joint allows for the transfer of significant axial forces. In [5], the issues of increasing the strength of friction joints due to the glue of a special composition between the contacting surfaces of the parts are considered. Moreover, the joint can withstand a load of up to 120 MPa. In [6], the influence of the assembly method on the strength of hybrid joints is considered, and the design and optimization of butt adhesive joints in lightweight constructions were performed in [7], which took into account the ratio between the inner and outer diameters, the yield strength of the sleeve, and the friction coefficient between the mating parts.

There is currently no clear theory for joining plastic parts, although an interference fit is often used to assemble them. In [8], the influence of surface morphology and the degree of influence of interference on the forces of pressing and unpressing in the joint was considered, and in [9], the influence of the parameters of the inner profile of the hub during its molding by the extrusion by a shaft is studied. One of the ways to increase the strength in tightened joints is considered in [10], where a new method for restoring machine parts is proposed and the stress state of parts made from powder metal compositions is evaluated. From the analysis of various issues of increasing the bearing capacity of interference fit [1–10], it follows that each of the proposed methods is either energy-intensive or requires significant funds.

When designing technical products with fits, it is necessary to use IT technologies. There is a wide range of application packages based on which various technical

problems are solved. In [11], the joints of parts are calculated in the WinMachine AWP system using the AWP Joint block. The program calculates the maximum allowable interference, after which all possible fits from the specified range are selected. However, at the same time, a clear decision-making methodology is not formulated when choosing the final fit option with an interference fit from the list of alternative ones.

The analysis of scientific publications shows that a reasonable choice of the final design solution from a finite set of admissible is a difficult task for the designer of the interference fit and is still relevant, as well as a practically significant problem. Therefore, this work aims to create a system of effective tools for the automated design of interference fits based on complex modeling of the area of their existence.

### 3 Research Methodology

In the developed new system approach to systematize the factors of constraints on the fit parameters, the structure of the functional relationship of the initial calculation parameters with the group of constraints on the input parameters of fits – sets  $a$ ,  $b$ ,  $c$ ,  $d$ . The creation of a system of constraints at the stage of the formation of an array of source data allows discarding their impossible and insignificant combinations.

For the accepted limitations, the systematization of stress, operational, and technological factors is presented in Fig. 1, in which the group of constraint factors  $a$  determines the type of fit smooth surface;  $b$  – a type of joint;  $c$  – a list of possible combinations of materials covering and covered surfaces;  $d$  – the method of assembling the joint.

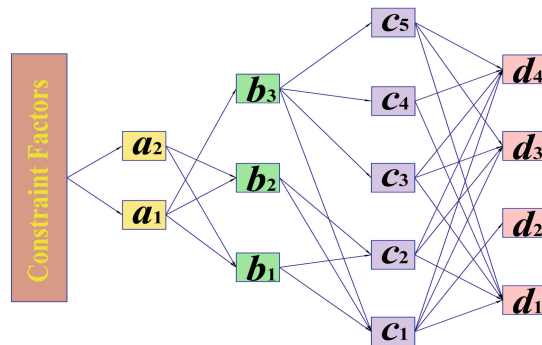


Fig. 1. The relationship between constraint factors.

Elements of sets (subsets):  $a_1$  and  $a_2$  – cylindrical and conical surfaces;  $b_1$  – shaft-hub;  $b_2$  – shaft-hub with a key;  $b_3$  – hub–ring gear (bandage);  $c_1$  – steel–steel;  $c_2$  – steel–cast iron;  $c_3$  – steel–bronze (brass);  $c_4$  – cast iron–bronze (brass);  $c_5$  – cast iron–steel;  $d_1$  – mechanical fitting;  $d_2$  – hydropressing;  $d_3$  and  $d_4$  – heating of the covering and cooling of the covered parts. From Fig. 1 it follows that for cylindrical joints there are no constraints either on the factor of a combination of the materials or on the



method of producing the joint (except hydropressing, which is used only for the combination of steel-to-steel materials), that is:

$$\left. \begin{array}{l} a_1 \in b_1 \in c_2 \notin d_2; a_1 \in b_1 \in c_3 \notin d_2; \\ a_1 \in b_1 \in c_4 \notin d_2; a_1 \in b_1 \in c_5 \notin d_2. \end{array} \right\} \quad (1)$$

The use of mechanical assembly methods is regulated by limiting the actual interference fit, that is, with  $N_o \leq [N_o]$  ( $N_o$  and  $[N_o]$  – the actual and allowable relative interference). In this case, the constraints  $c_1 \notin d_1 \notin d_2, c_2 \notin d_1 \notin d_2, c_3 \notin d_1 \notin d_2, c_4 \notin d_1 \notin d_2$  occurs at  $N_o > [N_o]$ . Function (1) can't be obtained in the form of a specific mathematical dependence but is a set of many constraints that are imposed on the load, technological and operational parameters of the designed fits.

The final number of possible combinations of constraints is obtained by discarding those for which the solution to the problem is impossible or irrational. When manually calculating and choosing fits, the designer intuitively adheres to most of these constraints, but even with the many branches of the computing process, an experienced designer is not able to choose the most rational continuation of the calculation at each of its stages.

To solve this problem, the authors develop theoretical principles and a methodology implemented in the Interference Fit computer program, in which the whole complex of logical operations and the implementation of the functional relationships of the given parameters with a variety of fits corresponding to the load and operation conditions are implemented. Further modernization of the Interference Fit program is associated with the implementation of strength calculations of critical elements of modern structures [12–14].

## 4 Results

### 4.1 A Mathematical Model of the Area of Existence of the Interference Fit and the Selection of a Rational Design Solution

In the typical calculation of the interference fit, the following tasks are solved:

- based on the initial data and additional strength, operational, technological or other requirements for the joint, fit parameters are set to meet these requirements;
- a calculation is performed, as a result of which several fit options are obtained that correspond to the calculation conditions – a finite set  $m$  of acceptable design solutions, from which one is selected.

For a reasonable search for the final design solution, it is necessary to introduce an additional set of fit parameters, by which it is possible to choose the most rational fit option. Therefore, the next step in improving the methodology is the creation of a mathematical model of the area of existence of suitable interference fit (AESIF), corresponding to the specified operating conditions. Based on numerical and analytical studies, the construction of an  $n$ -parametric image (Fig. 2) in a three-dimensional coordinate system is carried out.

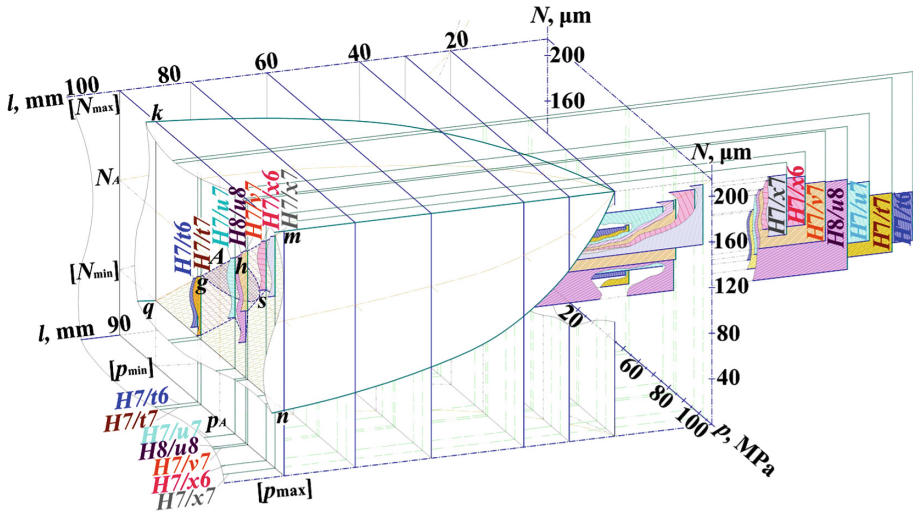


Fig. 2. The research results of the volumetric model of the retaining connection with discrete values of the fit length and a constant value of the fit diameter.

In this case, the user needs to set the  $n$ -th number of criteria that significantly increase the probability of choosing the most rational option for the final design solution. As criteria for AESIF determination, the spatial model parameters are as a function – interference (limiting maximum  $[N_{\max}]$  and minimum  $[N_{\min}]$ , probabilistic  $N_{i\max}$ ,  $N_{i\min}$  and actual  $N_i$ ), and as arguments – specific contact pressure on the working surfaces of the fit parts (limiting minimum  $[p_{\min}]$  and maximum  $[p_{\max}]$ , as well as the actual  $p_i$  for the  $i$ -th fit) and its geometrical parameters – diameter  $d$ , working length  $l$  and heating temperature of the covering  $t_2$  (or cooling of the covered  $t_1$ ) part using the thermal assembly method.

#### 4.2 The Choice of a Rational Interference Fit Based on a Two-Parameter Mathematical Model

After analyzing the calculation results, a three-dimensional  $n$ -parametric model constructed in the  $l, p, N$  coordinates at a fixed value of the joint diameter ( $d = 85$  mm) is obtained by superimposing planar AESIF figures on the specified spatial image in a discrete section. It is formed by the secant plane  $l_k$  (for a discrete value of the working length  $l$ ) in the coordinate system  $pN$  with the function  $N = f(p)$ .

To check the correctness of the obtained mathematical model, the joint of the ring gear with the wheel hub is investigated at the values of the initial parameters: axial force  $F_a = 1500$  N; torque  $T = 2000$  N · m; the diameter of the inner surface of the covered part  $d_1 = 50$  mm; conventional outer diameter of the covering part  $d_2 = 130$  mm; material of the covered part – Steel 45X; material of the covering part – Steel 50; fit diameter  $d = 85$  mm; working fit length  $l = 90$  mm. After a series of calculations for the obtained suitable fits in the area of their existence, a function graph is constructed (Fig. 3) for the discrete section  $l_k$ .

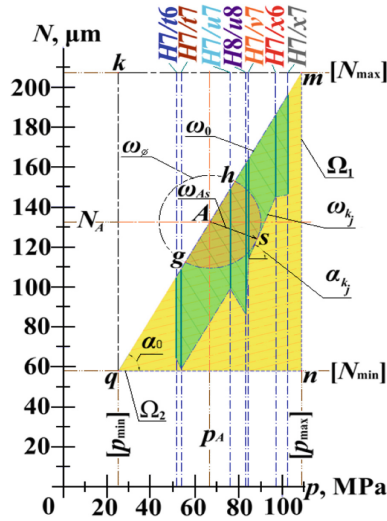


**Fig. 3.** Areas of the existence of suitable interference fit with a constant diameter value and a discrete length value.

By the method of complete interchangeability, all standard fittings are suitable if the actual specific pressure and the interference in the  $i$ -th fit correspond to the condition:  $[p_{\min}] \leq p_i \leq [p_{\max}]$  and  $[N_{\min}] \leq N_i \leq [N_{\max}]$ . In the  $pN$  coordinate system, such AESIF boundaries are a  $kmnq$  rectangle with a center of symmetry at point  $A$  for given conditions.

The set of probabilistic tolerances of suitable standard fits (finite set  $m$ ) is in the triangle  $mnq$  (lower half of the  $kmnq$  rectangle). From this set, one should choose a rational design solution located inside the AESIF boundaries in the  $k$ -th coordinate plane  $pN$  of the model. For a reasonable choice of a rational fit, the authors decide to circle the boundaries of the probabilistic tolerances of the set  $m$ . When connecting the points of the largest and smallest values of the probabilistic tolerances of the interference by segments, a polygon is formed. Thereby, a narrower area of a finite set of a suitable interference fit (AFSSIF), as an AESIF subset, is obtained.

At the next stage, in the  $k$ -th coordinate plane  $pN$ , the localized reliable zone of a suitable interference fit (LRZSIF) located inside the AFSSIF is studied in more detail, which significantly narrows the search for a rational design solution. In this case, the  $i$ -th fit should be chosen inside within the above zone, as the final design decision. The designer has the right to change this decision at his discretion.

The authors studied various forms of LRZSIF (rectangular, ellipsoidal and circular). In this case, the circular shape with the center at the point  $A$  ( $p_i \rightarrow p_A, N_i \rightarrow N_A$ ) of the  $kmnq$  rectangle AESIF turned out to be the most effective. Since AFSSIF is located in the  $mnq$  triangle AESIF, the LRZSIF has a semicircular shape bounded by the arc  $gsh$ .

The point  $s$  of the semicircle  $gsh$  should be the shortest point of contact to the nearest segment of the minimum values of the probability interference of the AFSSIF

figure from the center of symmetry of the point  $A$  of the AESIF and determine the minimum value of the radius  $R = As$  of the arc  $gsh$  of the LRZSIF.

The analysis of the results shows that the standard fit will be the most rational, in which part of the length of the probability tolerance segment will be the longest inside the  $gsh$  zone. In this case, the number of alternative fits from the set  $m$  that fall into the specified zone is significantly reduced, and there is a real chance for choosing a single design solution.

### 4.3 An Analytical Presentation of the Mathematical Model of the $pN$ Area of the Existence of Fit

It is established that using the graphical-analytical method with the construction of a flat model of AESIF, it is not possible to uniquely formalize the process of choosing a rational design solution, which necessitates an analytical description of AESIF. At the next stage of the study, the problem of the analytical description of the permissible boundaries of the values of rational solutions – AESIF, as well as AFSSIF and LRZSIF, having a hierarchical structure, was solved.

First, the description is made for the parameters which values form a geometric flat image in the  $k$ -th coordinate plane  $pN$  of the two-parameter model. To describe this model, the mathematical apparatus of the theory of  $R$ -functions is used [15–20].

The equation of the shape of the flat area of the AESIF  $\Omega_\Delta$  (in the triangle  $mnq$ ) is analytically defined as the intersection of sets:

$$\left. \begin{aligned} \Omega_\Delta &= (\Omega_1 \wedge_0 \Omega_2) \wedge_0 \omega_0; \quad \Omega_1 = (([p_{\max}] - [p_{\min}])/2)^2 - (p - p_A)^2; \\ \Omega_2 &= (([N_{\max}] - [N_{\min}])/2)^2 - (N - N_A)^2; \quad p_A = p - ([p_{\max}] - [p_{\min}])/2; \\ N_A &= N - ([N_{\max}] - [N_{\min}])/2; \quad \omega_0 = p - \frac{[p_{\max}] - [p_{\min}]}{[N_{\max}] - [N_{\min}]} N + \frac{[p_{\max}] - [p_{\min}]}{2}, \end{aligned} \right\} \quad (2)$$

where  $\wedge_0$  – the symbol of the  $R$ -conjunction, which means the intersection of sets;  $(p, N)$  – coordinates of the specific pressure  $p$  (MPa) and interference  $N$  ( $\mu\text{m}$ );  $[p_{\min}]$ ,  $[p_{\max}]$  and  $[N_{\min}]$ ,  $[N_{\max}]$  – the boundaries of permissible values of specific pressures and interference, respectively;  $(p_A, N_A)$  – the actual coordinates of the center of symmetry (point  $A$ ) of the rectangle  $kmnq$  AESIF in the given  $k$ -th section;  $\Omega_1$  – set of permissible values fit in the form of a vertical strip (for the allowable specific pressure  $[p_{\min}]$  and  $[p_{\max}]$ );  $\Omega_2$  – set of acceptable fit values in the form of a horizontal strip (for the permissible interference  $[N_{\min}]$  and  $[N_{\max}]$ );  $\omega_0$  – set representing the diagonal  $mq$ , included in the sets  $\Omega_1$  and  $\Omega_2$  of the rectangle  $kmnq$ .

According to the theory of  $R$ -functions [15], the circle equation, which is limited to a part of a circular shape LRZSIF, has the analytical form:

$$\omega_\otimes = \left( N_s - N_A + (p_s - p_A) \frac{P_{i+1} - P_i}{N_{(i+1)\min} - N_{i\min}} \right)^2 - (p - p_A)^2 - (N - N_A)^2, \quad (3)$$

where  $N_{i\min}$ ,  $N_{(i+1)\min}$  – respectively, the coordinates of the points of the lower boundaries (minimum values) of the tolerances of probability interference for the corresponding standard fits of AFSSIF with specific actual pressures  $p_i$  and  $p_{i+1}$ ;  $p_s$  and  $N_s$  – the coordinates of the shortest point  $s$  of touching the segment between the points of the lower tolerances of the probability interference from  $N_{i\min}$  to  $N_{(i+1)\min}$  (from point A) and a semicircle with an arc  $gsh$ :

$$p_s = \frac{\left(N_A + \frac{p_A(p_{i+1}-p_i)}{N_{(i+1)\min}-N_{i\min}} - \frac{N_{i\min}p_{i+1}-N_{(i+1)\min}p_i}{p_{i+1}-p_i}\right) \left(\frac{N_{(i+1)\min}-N_{i\min}}{p_{i+1}-p_i}\right)}{1 + \left(\frac{N_{(i+1)\min}-N_{i\min}}{p_{i+1}-p_i}\right)^2}; \quad (4)$$

$$N_s = \frac{\frac{N_{i\min}p_{i+1}-N_{(i+1)\min}p_i}{p_{i+1}-p_i} + \left(\frac{N_{(i+1)\min}-N_{i\min}}{p_{i+1}-p_i}\right)^2}{1 + \left(\frac{N_{(i+1)\min}-N_{i\min}}{p_{i+1}-p_i}\right)^2}. \quad (5)$$

The equation for the semicircular truncated ( $mq$  diagonal) LRZSIF is as follows:

$$\omega_{gsh} = \omega_0 \wedge_0 \omega_{\otimes}. \quad (6)$$

The analytical descriptions of AFSSIF are carried out using the mathematical apparatus of  $R$ -functions [15] in the same way.

## 5 Conclusions

1. The concept and theoretical basis for calculating the interference fit are developed based on the main operational, strength, and technological requirements for them. A technique and a program Interference Fit for automated calculation of interference fit are created.
2. Based on the mathematical apparatus of the theory of  $R$ -functions, a method for determining the analytical model of the area of existence of rational fits is proposed, which made it possible to significantly increase the level of formalization of the solution to the problem and improve the program for the automated calculation of fits.
3. An extensive graphic material of numerical calculations has been obtained, which is of interest to the engineering practice when choosing rational fits. An analysis of the results confirms the effectiveness of using the proposed method for computer-aided design of machine parts joints based on complex mathematical modeling of the area of existence of interference fit parameters.
4. The developed methodological and software tools can improve the quality and productivity of design and can be integrated into CAE/CAD/CAM systems.





## References

1. Kupriyanov, A.V.: The strength of the connection with an interference fit in the presence of an error in the geometry of the form. *Bull. KhNTU* **3**(54), 145–150 (2015). (in Ukrainian)
2. Malitsky, I.F., Chernyatina, E.V.: The influence of roughness and processing methods on the strength of the interference fit. *Eng. Ser. Eng. Technol.* **13**, 149–153 (2014). (in Ukrainian)
3. Ryazantseva, I.L., Dyundik, O.S.: The interference fit of increased bearing capacity. *Dyn. Syst. Mech. Mach.* **6**(1), 109–113 (2018). (in Russian)
4. Malitsky, I.F., Yaroslavova, A.B.: Quality joints with guaranteed fit of parts with insufficient rigidity. *Eastern-Eur. J. Enterp. Technol.* **3,2**(15), 33–36 (2005)
5. Mengel, R., Häberle, J., Schlimmer, M.: Mechanical properties of hub shaft joints adhesively bonded and cured under hydrostatic pressure. *Int. J. Adhes. Adhes.* **27**(7), 568–573 (2007)
6. Croccolo, D., Agostinis, M., Mauri, P.: Influence of the assembly process on the shear strength of shaft–hub hybrid joints. *Int. J. Adhes. Adhes.* **44**, 174–179 (2013)
7. Croccolo, D., Agostinis, M., Vincenzi, N.: Design and optimization of shaft–hub hybrid joints for lightweight structures: analytical definition of normalizing parameters. *Int. J. Mech. Sci.* **56**(1), 77–85 (2012)
8. Bottini, L., Boschetto, A.: Interference fit of material extrusion parts. *Add. Manuf.* **25**, 335–346 (2019)
9. Dörr, F., Funk, M., Liewald, M., Binz, H., Köstlmeier, R.: Influence of internal hub profile on joining process of shaft-hub-connection by lateral extrusion. *Procedia Eng.* **81**, 1988–1993 (2014)
10. Skoblo, T., Ribalko, I., Sidashenko, A., Tikhonov, A., Naumenko, A.: Assessment of thermal stresses during restoration using a new surfacing method. *MOTROL. Comm. Motorization Energetics Agric.* **15**(7), 17–25 (2013)
11. Karataev, O.R., Khamidullina, D.A., Tyurin, A.N.: Tightened bandages and calculations in the APM Joint module. *Bull. Kazan Technol. Univ. Eng.* **17**(23), 317–319 (2014). (in Russian)
12. Stepanov, M., Ivanova, L., Litovchenko, P., Ivanova, M., Basova, Y.: Determination of parameters of cylindrical grinding with additional intermediate dressing. In: *Advances in Design, Simulation and Manufacturing II: DSMIE 2019 Conference Proceedings, LNME*, pp. 330–340 (2019)
13. Salo, V., Rakivnenko, V., Nechiporenko, V., Kirichenko, A., Horielyshev, S., Onopreichuk, D., Stefanov, V.: Calculation of stress concentrations in orthotropic cylindrical shells with holes on the basis of a variational method. *Eastern-Eur. J. Enterp. Technol.* **3,7**(99), 11–17 (2019)
14. Salo, V.A., Nechiporenko, V.M.: Research of durability of the elastic cylindrical structure affected by the local loading. *Collect. Sci. Works NANGU* **2**, 76–82 (2017). (in Ukrainian)
15. Rvachev, V.L., Krupa, L.V., Sklepus, N.G., Uchishvili, L.A.: The method of *R*-functions in problems of bending and vibrations of complex shape. *Scientific Thought, Kharkiv* (1973). (in Ukrainian)
16. Nechiporenko, V.M., Salo, V.A., Litovchenko, P.I., Kovbaska, B.V., Verkhorubov, D.O.: Using of the theory of *R*-functions for producing a rational interference fit. *Collect. Sci. Works NANGU* **2**, 72–76 (2016). (in Ukrainian)
17. Awrejcewicz, J., Kurpa, L., Shmatko, T.: Investigating geometrically nonlinear vibrations of laminated shallow shells with layers of variable thickness via the *R*-functions theory. *Compos. Struct.* **125**, 575–585 (2015)

18. Balestrino, A., Caiti, A., Crisostomi, E., Grammatico, S.: Stabilizability of linear differential inclusions via  $R$ -functions. *IFAC Proc.* **43**(14), 1092–1097 (2010)
19. Pokras, V., Rvachev, M.: Application of the  $R$ -functions method to viscoplastic analysis in metal forming. *J. Mater. Process. Technol.* **60**(1–4), 493–500 (1996)
20. Varvak, M.: Ellipsoidal/radial basis functions neural networks enhanced with the Rvachev function method in application problems. *Eng. Appl. Artif. Intell.* **38**, 111–121 (2014)



# Design of Conveyor Control Information System Considering Transport Delay

Oleh Pihnastyi<sup>1</sup> , Georgii Kozhevnikov<sup>1</sup>  ,  
and Tetiana Bondarenko<sup>2</sup> 

<sup>1</sup> National Technical University “KpPI”, 2, Kyrpychova St.,  
Kharkiv 61002, Ukraine

kozhevnikov.gk@gmail.com

<sup>2</sup> Ukrainian Engineering-Pedagogics Academy,  
16, Universitetskaya St., Kharkiv 61003, Ukraine

**Abstract.** In this paper, the design method of optimal control for the conveyor-based transport system, when the quality criterion contains a variable delay in the controls, has been considered. The task of optimal control has been set and the Hamiltonian of the system has been written taking into account the delay in the controls. In the design of optimal control by the flow parameters of the transport system, a control object model containing partial differential equations was used. The mechanism that forms a variable value of the transport delay in the flow parameters of the transport system has been shown. Two characteristic modes of the conveyor system functioning are considered as follows: a transient state, when the value of the linear density at the transport system output is determined by the initial distribution of material along the transport route, and a steady-state state, when the value of the linear density at the transport system output is determined through the values of the movement speed of the conveyor belt and the intensity of the material at the conveyor section input. Equations that make it possible to calculate the controls of the flow parameters of the transport system for which the Hamiltonian of the system satisfies the Hamilton–Jacobi equation have been provided. Controls of the flow parameters are synthesized for the case when the phase coordinate does not reach the limits. It is shown that for the synthesis of controls, it is necessary to predict the magnitude of the output flow from the transport system.

**Keywords:** Production line · PDE-model of the production · Transition period · Optimal control · Differential constraints · Accumulating bunker · Distributed system

## 1 Introduction

The conveyor-based transport systems are widely used in enterprises with a flow-line conveyer method of production [1], mining [2–6], and for servicing traffic flows in seaports [7, 8]. Such a prevalence of conveyor-based transport at leading world enterprises is due to the low unit cost of transportation of a unit mass load [9, 10]. The use of this mode of transport is especially important in conditions when both the freight flow through the transport system and the length of the transport route are constantly



increasing [11–13]. The conveyor production method is the easiest way to organize a flow-line production. This simplicity is due to the following feature: all elements that are on the conveyor belt within the conveyor section move at the same speed equal to the speed of the conveyor belt. The carrying capacity control of the conveyor-based transport system comes down to controlling the intensity of the material entering the conveyor section input [14, 15] or controlling the speed of the conveyor belt [2, 6, 10, 16, 34]. The transported material is accumulated on the conveyor belt or in accumulating bunkers located at the input and output of sections. To avoid damage to the conveyor belt, the specific linear density of the material on the conveyor belt is restricted by the maximum permissible value [10, 17]. The power of the drive motors of the conveyor section limits the total amount of material that can be on the belt [17]. An additional constraint is a capacity of accumulating bunkers for storing the material [14, 15]. These limitations have a significant impact on the complexity of designing the transfer conveyor control systems. Moreover, the transfer conveyor is a distributed system. Due to this, the linear density of the material at the conveyor section output is determined through the value of the linear density at the conveyor section input with a variable transport delay [19, 20]. The existence of variable transport delays for transport systems of great length is particularly important [21–23]. The reason for the variable transport delay is a change in the speed of the conveyor belt, for example, as a result of the functioning of the belt speed control systems [17, 18, 24]. This requires the construction of intelligent control systems for the flow parameters of the transport system, taking into account the value of the variable transport delay. The relevance of this problem determined the purpose of this work: constructing a methodology for designing the control algorithms of the conveyor-based transport system in the case of a variable transport delay.

## 2 Literature Review

Among the common models of the control object used to design the control algorithms of the conveyor-based transport system, it is worth mentioning the models using the Finite Element Method (FEM) [3, 25–27], the Finite Difference Method (FDM) [21], and the Discrete Element Method (DEM) [5, 28]. The Discrete Element Method used by Cundall in 1971 to solve rock mechanics problems can be considered as a generalization of the Finite Element Method (FEM). These methods belong to the family of numerical methods intended for calculating a continuous medium; they are demanding on computing resources, which limits the dimension of the model and requires the appropriate qualifications of the model developer. They allow obtaining only an approximate solution to the problem for specific values of the flow parameters for given initial and boundary conditions of the transport system. It is advisable to use them in the absence of analytical models of the transport system. The use of models applying FEM, FDM, DEM methods for designing algorithms for controlling the flow parameters of the transport system is associated with significant computational difficulties and requires significant time spending, often exceeding the time allotted for decision making. The following classes of models, which are based on averaged balance sheet equations of a state of flow parameters [6] and equations of system dynamics [14], can

be used to design control algorithms for steady-state operation modes. Since each of the models does not take into account the momentary change in the belt speed and the uneven distribution of the material along the transport route, it is difficult to use them without significant improvement to design the control algorithms taking into account the transport delay. The use of artificial intelligence models based on the multiple regression equations [29, 30] and neural network equations [27, 31, 32] requires a significant amount of test data, which is difficult to obtain for non-stationary modes of operation of the conveyor-based transport system. Thus, the construction of highly efficient control algorithms that would allow taking into account the variable transport delay in flow parameters is associated with the development and further improvement of the analytical models of the conveyor-based transport systems. Such an analytical model for a conveyor-based transport system was obtained in [19] and received a further improvement in [23, 24, 33]. One of the main results provided in [19] is that an analytical dependence that determines the linear density of the material  $\theta_0(\tau, \xi)$  along the transport route at an arbitrary point of time  $\tau$  and an arbitrary point  $\xi$  is obtained:

$$\theta_0(\tau, \xi) = (H(\xi) - H(\xi - G(\tau))) \frac{\gamma(G^{-1}(G(\tau) - \xi))}{g(G^{-1}(G(\tau) - \xi))} + H(\xi - G(\tau))\psi(\xi - G(\tau)) \quad (1)$$

$$G(\tau) = \int_0^\tau g(\alpha) d\alpha,$$

where dimensionless variables:

$$\tau = \frac{t}{T_d}, \quad \xi = \frac{S}{S_d}, \quad \delta(\xi) = S_d \delta(S) \quad (2)$$

$$\theta_0(\tau, \xi) = \frac{[\chi]_0(t, S)}{[\chi]_{0\max}}, \quad \psi(\xi) = \frac{\Psi(S)}{[\chi]_{0\max}}, \quad n_0(\tau) = \frac{N_0(t)}{S_d[\chi]_{0\max}},$$

$$\vartheta(\tau) = \sigma(t) \frac{T_d}{S_d[\chi]_{0\max}}, \quad \gamma(\tau) = \lambda(t) \frac{T_d}{S_d[\chi]_{0\max}},$$

$$\vartheta_{in}(\tau) = \sigma_{in}(t) \frac{T_d}{S_d[\chi]_{0\max}}, \quad g(\tau) = a(t) \frac{T_d}{S_d}.$$

are expressed in terms of the following dimensional quantities:  $[\chi]_0(t, S)$  – the linear density of the material at an arbitrary point in time  $t$  in the technological position of the conveyor line, characterized by the coordinate  $S \in [0, S_d]$ , where  $S_d$  – the total length of the transport route; composition  $\delta(S)\lambda(t)$  determines the place of input of the material ( $S = 0$ ) with intensity  $\lambda(t)$  (where  $\delta(S)$  – delta Dirac function); the function  $N_0(t)$  characterizes the amount of material in the storage hopper with capacity  $N_b$  at a time  $t$ ;  $[\chi]_0(0, S) = H(S)\Psi(S)$  – the density of the material along the transport route at the initial time  $t = 0$ ;  $[\chi]_{0\max}$  – maximum allowable linear density value; material flow at

the input to the storage hopper  $\sigma_{in}(t)$  and the flow  $\sigma(t)$  at the output of the transport system are set; material comes from the hopper to the input of the conveyor line with adjustable intensity; linear density  $[\chi]_0(0, S)$  and material flow  $[\chi]_1(t, S)$  at an arbitrary time moment are interconnected by the value of the speed of movement of the conveyor belt  $a = a(t)$

$$[\chi]_1(t, S) = a(t)[\chi]_0(t, S); \quad (3)$$

$T_d$  – the characteristic time it takes for the material to travel the transportation route;  
 $H(S)$  – Heaviside step function

$$H(S) = \begin{cases} 0, & S < 0, \\ 1, & S \geq 0, \end{cases} \quad S \in [0; S_d]. \quad (4)$$

Equation solution

$$G(\tau_{tr}) - 1 = 0 \quad (5)$$

allows calculating the duration of the transition period when the linear density of the material at the exit from the transport system is determined through the distribution of the material  $\psi(\xi)$  at the initial time. The density of the material  $\theta_0(\tau, 1)$  at the output from the conveyor section can be expressed in terms of the value of the intensity  $\lambda(t)$  and speed of the conveyor belt

$$\theta_0(\tau, 1) = \begin{cases} \frac{\gamma(\tau - \Delta\tau_1)}{g((\tau - \Delta\tau_1))}, & G(\tau_{tr}) - 1 \geq 0; \\ \psi(1 - G(\tau)), & G(\tau_{tr}) - 1 < 0; \end{cases} \quad \tau_1 = G^{-1}(G(\tau) - 1), \quad (6)$$

$$\theta_1(\tau, 1) = g(\tau)\theta_0(\tau, 1), \quad \Delta\tau_1 = \Delta\tau_1(\tau) = \tau - \tau_1,$$

where  $\Delta\tau_1$  is the amount of transport delay. Expressions (1)–(6) allow constructing an analytical model of the transport system taking into account the transport delay  $\Delta\tau_1(\tau)$ , which will be used in the present work for the synthesis of optimal control algorithms.

### 3 Research Methodology

Consider the task of optimal control of the main conveyor line with an input storage hopper (Fig. 1). When designing the optimal control of the conveyor line parameters, the quality criterion should be used [1, 4]

$$J = \int_0^{\tau_k} F d\tau \rightarrow \min, \quad F = \frac{1}{2}(\theta_1(\tau, 1) - \vartheta(\tau))^2 \quad (7)$$

The control of the material output flow is carried out by controlling the intensity of material input  $\gamma(\tau) = u_\gamma(\tau)$  and regulating the speed of the conveyor belt  $g(\tau) = u_g(\tau)$  which allows presenting the integrand for the quality criterion in the form

$$F = \begin{cases} \frac{1}{2} \left( \frac{u_\gamma(\tau - \Delta\tau_1)}{u_g(\tau - \Delta\tau_1)} u_g(\tau) - \vartheta(\tau) \right)^2, & \tau \geq \tau_{tr}; \\ \frac{1}{2} (\psi(1 - G(\tau)) u_g(\tau) - \vartheta(\tau))^2, & \tau < \tau_{tr}. \end{cases} \quad (8)$$

The optimal controls  $u_\gamma(\tau)$  and  $u_g(\tau)$  leading to the minimum functional (7) for differential constraints, is defined

$$\frac{dn_0(t)}{dt} = \vartheta_{in}(\tau) - u_\gamma(\tau), \quad n_0(0) = n_{00} \quad (9)$$

constraint on the maximum permissible value of linear density

$$0 \leq \theta_0(\tau, \xi) \leq 1,$$

storage hopper capacity

$$0 \leq n_0(\tau) \leq n_b,$$

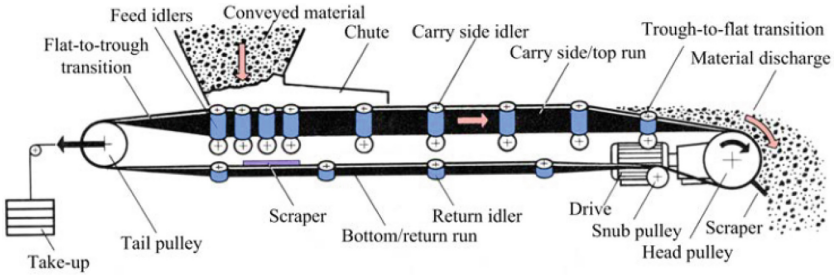


**Fig. 1.** Schematic diagram of the main conveyor line [35].

control constraints

$$u_{\gamma\min} \leq u_\gamma(\tau) \leq u_{\gamma\max}, \quad u_{g\min} \leq u_g(\tau) \leq u_{g\max},$$

From the definition of the quality criterion it follows

$$\frac{dJ}{d\tau} = F.$$

On the other hand, considering the quality functional as a function of time and phase coordinates  $q_i$

$$\frac{dJ}{d\tau} = \frac{\partial J}{\partial \tau} + \sum_i \frac{\partial J}{\partial q_i} \frac{dq_i}{d\tau} = \frac{\partial J}{\partial \tau} + \sum_i \psi_i \frac{dq_i}{d\tau}, \quad \psi_i = \frac{\partial J}{\partial q_i},$$

and combining the last two expressions, it should be

$$F = \frac{\partial J}{\partial \tau} + \sum_i \psi_i \frac{dq_i}{d\tau}$$

where  $\psi_i$  are the conjugate functions of the system under consideration. Taking into mind the definition for the Hamilton function

$$H = -F + \sum_i \psi_i \frac{dq_i}{d\tau},$$

the Hamilton-Jacobi equation should be

$$0 = \frac{\partial J}{\partial \tau} + H. \quad (10)$$

Thus, it is required to find such controls  $u_\gamma(\tau)$  and  $u_g(\tau)$ , for which the quality criterion  $J(u_\gamma(\tau), u_g(\tau), u_g(\tau - \Delta\tau_1))$  satisfies the Hamilton-Jacobi Eq. (10). Such controls will provide a minimum quality criterion (7) with the integrand (8). For other controls that do not satisfy equality (10), the quality criterion will have a value that is above the minimum.

## 4 Results

Let's consider the construction of optimal controls for the case when only the quality criterion of the transport system contains a delay in control. Since the differential constraint (9) does not contain delay in the phase coordinates and the controls, the Hamiltonian should be represented as follows

$$H = -\frac{1}{2} (\psi(1 - G(\tau)) u_g(\tau) - \vartheta(\tau))^2 + \psi_1 (\vartheta_{in}(\tau) - u_\gamma(\tau)), \quad \tau < \tau_{tr}$$

$$H = -\frac{1}{2} \left( \frac{u_\gamma(\tau - \Delta\tau_1)}{u_g(\tau - \Delta\tau_1)} u_g(\tau) - \vartheta(\tau) \right)^2 + \psi_1 (\vartheta_{in}(\tau) - u_\gamma(\tau)), \quad \tau \geq \tau_{tr}.$$

The optimal control of the transport system in the interval is determined by the system of equations of the system in the form

$$\frac{\partial H}{\partial u_g(\tau)} = -(\psi(1 - G(\tau))u_g(\tau) - \vartheta(\tau)) \left( \psi(1 - G(\tau)) + \frac{d\psi(1 - G(\tau))}{du_g(\tau)} u_g(\tau) \right) = 0. \quad (11)$$

Since the Hamiltonian of the system in question is linear in the control over the interval  $\tau < \tau_{lr}$ , the Hamilton function relatively  $u_\gamma(\tau)$  reaches the maximum value at the ends of the control  $u_\gamma(\tau)$ . Taking in addition to equality (11) the optimal control  $u_g$  is determined from the equalities

$$u_g(\tau) = \frac{\vartheta(\tau)}{\psi(1 - G(\tau))} \text{ or } u_g(\tau) = \frac{C_g}{\psi(1 - G(\tau))},$$

where  $C_g = C_g(\tau)$  is an integration constant. Similarly, the optimal control of the transport system on the interval  $\tau \geq \tau_{lr}$  should be determined:

$$\frac{\partial H}{\partial u_g} = -\left(\frac{u_{\gamma 1}}{u_{g 1}} u_g - \vartheta(\tau)\right) \frac{\partial}{\partial u_g} \left(\frac{u_{\gamma 1}}{u_{g 1}} u_g\right) = 0, \quad \tau_1 = \tau - \Delta\tau_1, \quad \tau_2 = \tau + \Delta\tau_1, \quad \tau \geq \tau_{lr},$$

$$\frac{\partial H}{\partial u_\gamma} = -\left(\frac{u_\gamma}{u_g} u_g(\tau_2) - \vartheta(\tau_2)\right) \frac{\partial}{\partial u_\gamma} \left(\frac{u_\gamma}{u_g} u_g(\tau_2)\right) - \psi_1(\tau_2) \frac{\partial u_\gamma(\tau_2)}{\partial u_\gamma} = 0,$$

$$u_\gamma = u_\gamma(\tau), \quad u_g = u_g(\tau), \quad u_{\gamma 1} = u_\gamma(\tau_1), \quad u_{g 1} = u_g(\tau_1),$$

$$u_{\gamma 2} = u_\gamma(\tau_2), \quad u_{g 2} = u_g(\tau_2), \quad \vartheta = \vartheta(\tau), \quad \vartheta_2 = \vartheta(\tau_2).$$

From the first equation, it follows

$$u_g = \vartheta \frac{u_{g 1}}{u_{\gamma 1}} \text{ or } \frac{u_{\gamma 1}}{u_{g 1}} + u_g \frac{\partial}{\partial u_g} \left(\frac{u_{\gamma 1}}{u_{g 1}}\right) = 0. \quad (12)$$

From the second equation, it follows

$$u_\gamma = \psi_1(\tau_2) \frac{\dot{u}_{\gamma 2}}{\dot{u}_\gamma} \left(\frac{u_g}{u_{g 2}}\right)^3 + \vartheta_2 \frac{u_g}{u_{g 2}}, \quad 1 = G(\tau_2) - G(\tau). \quad (13)$$

where

$$\frac{\partial u_{\gamma 2}}{\partial u_\gamma} = \frac{\dot{u}_{\gamma 2}}{\dot{u}_\gamma} \frac{d\tau_2}{d\tau} = \frac{\dot{u}_{\gamma 2}}{\dot{u}_\gamma} \frac{u_g}{u_{g 2}}, \quad 0 = \frac{dG(\tau_2)}{d\tau_2} \frac{d\tau_2}{d\tau} - \frac{dG(\tau)}{d\tau}, \quad \frac{d\tau_2}{d\tau} = \frac{u_g}{u_{g 2}}.$$

The second equalities from (12) by the method of separation of variables should be integrated and such equations should be obtained

$$z = \frac{u_{\gamma 1}}{u_{g 1}}, \quad \frac{\partial z}{z} = -\frac{\partial u_g}{u_g}, \quad \frac{u_{\gamma 1}}{u_{g 1}} u_g = C_g,$$

where the integration constant  $C_g$  is independent of control  $u_g$ . Since the controls  $u_\gamma$  and  $u_g$  are arbitrary, it follows that  $u_g(\tau) = u_g(\tau_1)$ . The case of an equality of controls  $u_g(\tau) = u_g(\tau_1)$  is considered in detail in [36].

Let's consider in detail the option when the restrictions associated with the capacity of the storage hopper  $0 \leq n_0(\tau) \leq n_b$  are not achieved. Then the conjugate function  $\psi_1(\tau)$  can be determined from the equation

$$\frac{d\psi_1(\tau)}{d\tau} = -\frac{\partial H}{\partial n_0} = 0, \quad \psi_1(\tau_k) = 0.$$

The boundary condition  $\psi_1(\tau_k) = 0$  is presented since no boundary conditions are specified for the phase coordinates  $n_0(\tau_k)$ . The solution of the equation for the adjoint function allows us to determine the controls in the following form

$$u_g = \vartheta \frac{u_{g1}}{u_{\gamma 1}}, \quad u_{g\min} \leq u_g(\tau) \leq u_{g\max}, \quad (14)$$

$$u_\gamma = \vartheta_2 \frac{u_g}{u_{g2}}, \quad u_{\gamma\min} \leq u_\gamma(\tau) \leq u_{\gamma\max}. \quad (15)$$

The speed of the belt  $u_g(\tau)$  at the current time  $\tau$  is set by the value of speed at time  $u_g(\tau - \Delta\tau_1)$  and intensity  $u_\gamma(\tau - \Delta\tau_1)$  at the time  $(\tau - \Delta\tau_1)$ . The quality criterion takes a minimum value if equality (14) holds. The choice of control  $u_\gamma(\tau)$  should be such that control  $u_g(\tau + \Delta\tau_1)$  at the moment  $(\tau + \Delta\tau_1)$  ensures equality (14). This imposes constraints on the choice of control  $u_\gamma(\tau)$ . From (15) it follows

$$u_{g\min} \leq \vartheta_2 \frac{u_g}{u_{\gamma}} \leq u_{g\max}, \quad \Rightarrow \quad \frac{u_g \vartheta_2}{u_{g\max}} \leq u_\gamma \leq \frac{u_g \vartheta_2}{u_{g\min}}. \quad (16)$$

The control  $u_\gamma(\tau)$  corresponds to the control  $u_g(\tau + \Delta\tau_1)$  at the moment  $(\tau + \Delta\tau_1)$  from Eq. (14).

## 5 Conclusions

The main result of this work is that the methodology for designing the optimal control of the transport system for the case when the quality functional contains delays in the control of the flow parameters has been provided. Using the developed optimal control technique, the flow parameters of the conveyor-based transport system have been synthesized taking into account the transport delay. The influence of the initial distribution of the material along the transport route on the program for controlling the output flow from the transport system has been shown. A program for combined control of the flow parameters of the transport system has been defined. The next step

in the development of the issue discussed in the paper is the development of a control system design method that would enable taking into account limitations on the phase coordinates and transport delay in phase coordinates.

## References






1. Pihnastyi, O.: *Statistical Theory of Control Systems of the Flow Production*. LAP LAMBERT Academic Publishing, Beau Bassin (2018)
2. Bebic, M., Ristic, L.: Speed controlled belt conveyors: drives and mechanical considerations. *Adv. Electr. Comput. Eng.* **18**(1), 51–60 (2018)
3. He, D., Pang, Y., Lodewijks, G., Liu, X.: Healthy speed control of belt conveyors on conveying bulk materials. *Powder Technol.* **327**, 408–419 (2018)
4. Zhang, S., Xia, X.: Modeling and energy efficiency optimization of belt conveyors. *Appl. Energy* **88**(9), 3061–3071 (2011)
5. Yang, G.: Dynamics analysis and modeling of rubber belt in large mine belt conveyors. *Sens. Transducers* **181**(10), 210–218 (2014)
6. Reutov, A.: Simulation of load traffic and steeped speed control of conveyor. In: *IOP Conference Series: Earth and Environmental*, vol. 87, p. 082041 (2017)
7. Kuptsov, N.: The study of the actual dimensions of bulk carriers for the technological design of seaports. *Bull. State Univ. Sea River Fleet Admiral S.O. Makarov* **2**(42), 323–336 (2017). <https://doi.org/10.21821/2309-5180-2017-9-2-323-336>
8. Dafnomilis, I., Duinkerken, M., Junginger, G., Lodewijks, M., Schott, D.: Optimalequipment deployment for biomass terminal operations. *Transport. Res. Part E: Logist. Transp. Rev.* **115**, 147–163 (2018)
9. Hiltermann, J., Lodewijks, G., Schott, D., Rijsenbrij, J., Dekkers, J., Pang, Y.: A methodology to predict power savings of troughed belt conveyors by speed control. *Part. Sci. Technol.* **29**(1), 14–27 (2011)
10. DIN 22101:2002-08. Continuous conveyors. Belt conveyors for loose bulk materials. Basics for calculation and dimensioning. – Normenausschuss Bergbau (FABERG) im DIN Deutsches Institut für Normung e.v. Normenausschuss Maschinenbau (NAM), p. 51 (2002)
11. Alspaugh, M.: Latest developments in belt conveyor technology. In: *MINExpo 2004*, New York, Las Vegas, NV, USA (2004)
12. Kung, W.: *The Henderson Coarse Ore Conveying System. A Review of Commissioning, Start-up, and Operation*, Bulk Material Handling by Belt Conveyor 5, Society for Mining, Metallurgy and Exploration, Inc. (2004)
13. Siemens. Innovative solutions for the mining industry. <https://new.siemens.com/global/en/markets/mining-industry.html>. Accessed 12 Oct 2019
14. Wolstenholm, E.: Designing and assessing the benefits of control policies for conveyor belt systems in underground mines. *Dynamica* **6**(2), 25–35 (1980)
15. Marais, J., Pelzer, R.: Analysing DSM opportunities on mine conveyor systems. In: *Industrial and Commercial Use of Energy Conference*, pp. 28–30 (2008)
16. Antoniuk, J.: Energy-saving belt conveyors installed in polish collieries. *Transp. Prob.* **5**(4), 5–14 (2010)
17. Lauhoff, H.: Speed control on belt conveyors – does it really save energy? *Bulk Solids Handl. Publ.* **25**(6), 368–377 (2005)
18. Semenchenko, A., Stadnik, M., Belitsky, P., Semenchenko, D., Stepanenko, O.: The impact of an uneven loading of a belt conveyor on the loading of drive motors and energy consumption in transportation. *Eastern-Eur. J. Enterp. Technol.* **4**(1)(82), 42–51 (2016)



19. Pihnastyi, O., Khodusov, V.: Model of conveyer with the regulable speed. *Bull. South Ural State Univ. Ser. Math. Model. Program. Comput. Softw. (Bull. SUSUMMCS)* **10**(4), 64–77 (2017)
20. Cornet, J.: Head and Tail Controls in Long Overland Conveyors. *Bulk Mater. Handl. Conveyor Belt* **4**, 55–67 (2015)
21. Mathaba, T., Xia, X.: A parametric energy model for energy management of long belt conveyors. *Energies* **8**(12), 13590–13608 (2015)
22. Karolewski, B., Ligocki, P.: Modelling of long belt conveyors. *Maint. Reliab.* **16**(2), 179–187 (2014)
23. Pihnastyi, O., Khodusov, V.: Model of a composite magistral conveyor line. In: *IEEE International Conference on System analysis & Intelligent computing (SAIC 2018)*, Kyiv, Ukraine (2018)
24. Pihnastyi, O., Khodusov, V.: Optimal control problem for a conveyor-type production line. *Cybern. Syst. Anal.* **54**(5), 744–753 (2018)
25. He, D., Pang, Y., Lodewijks, G.: Belt conveyor dynamics in transient operation for speed control. *Int. J. Civil Environ. Struct. Constr. Archit. Eng.* **10**(7), 865–870 (2016)
26. He, D., Pang, Y., Lodewijks, G., Liu, X.: Determination of acceleration for belt conveyor speed control in transient operation. *Int. J. Eng. Technol.* **8**(3), 206–211 (2016)
27. Xi, P., Song, Y.: Application research on BP neural network PID control of the belt conveyor. *JDIM* **9**, 266–270 (2011)
28. Fan, F., Liu, Ju., Parteli, E., Poschel, Th.: Vertical motion of particles in vibration-induced granular capillarity. In: *Powders and Grains 2017 – 8th International Conference on Micromechanics on Granular Media*, Montpellier, France, vol. 140 (2017)
29. Andrejiova, M., Marasova, D.: Using the classical linear regression model in analysis of the dependences of conveyor belt life. *Acta Montanist. Slovaca* **18**(2), 77–84 (2013)
30. Grincova, A., Marasova, D.: Experimental research and mathematical modelling as an effective tool of assessing failure of conveyor belts. *Maint. Reliab.* **16**(2), 229–235 (2014)
31. Noack, R., Arloth, J.: From digital prototype to Hybrid Twin™ New potentials in the dynamic simulation of belt conveyors. *Aufbereitungs-Technik/Mineral Process.* **59**(04), 47–55 (2018)
32. Xinglei, L., Hongbin, Yu.: The design and application of control system based on the BP neural network. In: *Proceedings of the 3rd International Conference on Mechanical Engineering and Intelligent Systems (ICMEIS 2015)*, pp. 789–793 (2015)
33. Pihnastyi, O., Khodusov, V.: Calculation of the parameters of the composite conveyor line with a constant speed of movement of subjects of labour. *Sci. Bull. National Mining Univ.* **4** (166), 138–146 (2018)
34. Halepoto, I., Shaikh, M., Chowdhry, B.: Design and implementation of intelligent energy efficient conveyor system model based on variable speed drive control and physical modeling. *Control Phys. Model. Int. J. Control Autom.* **9**(6), 379–388 (2016)
35. *Conveyorbeltguide Engineering: Conveyor components.* <http://conveyorbeltguide.com/engineering.html>. Accessed 09 Sept 2019
36. Pihnastyi, O., Khodusov, V.: The optimal control problem for output material flow on conveyor belt with input accumulating bunker. *Bull. South Ural State Univ. Ser. Math. Model. Program. Comput. Softw.* **12**(2), 67–81 (2019)



# Fundamentals of CAD Design of Rotary Milling Cutters for Multitooth Products

Nataliya Ravska<sup>1</sup> , Alexander Klochko<sup>2</sup> ,  
Oleksiy Ivanovskiy<sup>1</sup> , Vyacheslav Vovk<sup>1</sup> ,  
and Valeriya Parnenko<sup>1</sup> 

<sup>1</sup> National Technical University of Ukraine “Igor Sikorsky Kyiv Polytechnic Institute”, 37, Peremohy Avenue, Kiev 03056, Ukraine  
art@artograph.com.ua

<sup>2</sup> National Technical University “Kharkiv Polytechnic Institute”,  
2, Kyrpychova Street, Kharkiv 61002, Ukraine

**Abstract.** The studies presented in the article are aimed at developing the basics of ensuring the creation of CAD systems for disk run-in milling cutters for machining multitooth products regardless of profile. The development of this tool is based on its design methodology, which is based on the theory of shaping and design of cutting tools. Based on the analysis of the methods of processing multitooth products, the prospects of processing multitooth products with round disc milling cutters are substantiated. In this work, the problem of determining the cutting edges with the perpendicular and inclined axes of the tool and product is solved. The smallest design diameter of a disk run-in mill is determined. The design of the run-in mills, which provides the manufacture of chip grooves between the teeth of the product, is considered. The development of the design of the disk run-in mills included determining the diameter, taking into account regrinding. The geometric parameters of cutters are established. Based on the developed methodology for creating a CAD system for disk rolling mills, an automated system for designing disk rolling mills has been created. The operation study of milling cutters designed using this system confirmed the high accuracy of the products and prospects of their application. It is shown that the development of CAD systems for such mills significantly reduces the design and technological preparation of the production of multitooth products by disk rolling mills.

**Keywords:** Circular milling cutters · Multitooth products · Cutting tools · Step accuracy

## 1 Introduction

Toothed products of various shapes of the tooth profile (straight, shaped) are widely used in products of various industries.

The main methods for processing multitooth products [1] and the methods that implement them [2], equipment [3], tools [4], and kinematic schemes [5] are considered in [6, 7]. All the existing methods have their advantages and disadvantages, the

appropriateness of which in the manufacture of multitooth products joints is determined by the production conditions.

One of the progressive methods for the formation of teeth of various profile shapes is their cutting with circular run-in milling cutters.

Such cutters are designed based on a multi-start “globoid” source worm with the tooth surface of a product [7]. When turning the original worm into a cutting tool, one tooth or a group of cutter teeth is formed on each of its turns, which allows you to create circular cutters that work by the rolling method [8].

The movement kinematics of such a tool is reduced to the rotation of a workpiece and the rotation of a tool kinematically associated with it. Such disk rolling milling cutters can be designed both for the products formation of the same tooth profile with a uniform arrangement of their circumference and for cutting individual groups of teeth [9] that differ in profile [10] and angular steps. In the first case, when a cutter is rotated by one tooth, a workpiece is also rotated by one tooth. In the second case, a teeth group is cut in one revolution of a cutter. Cutting kinematics with this tool also includes the feed movement along the part axis, which leads to the sliding of its surface by itself. In this case, the movement of a treated surface relative to the tool will be an instant screw movement [8], where the contact of the “globoid” worm with the side surface of the workpiece tooth occurs along the line (characteristics).

This position allows you to design geometrically accurate circular milling cutters with straight and shaped cutting edges, in a certain way oriented relative to the tool body.

The advantages of such cutters are their manufacturability, ability to equipped with hard alloy and superhard materials, regrinding simplicity, ability to process products with undercutting and control high accuracy in the step of machined parts, which is mainly determined by the equipment accuracy.

A separate cutter is required for the processing of multitooth products with circular milling cutters for each of the tooth profile.

The theoretical foundations for the design of such cutters are considered only for the processing of multi-tooth products with a straight tooth profile [11].

This inhibits their use for processing teeth of various profiles, in particular, shaped. This problem can be solved by creating a computer-aided design (CAD) system for circular milling cutters. Therefore, the basis development of its creation is relevant.

The purpose of the work is to develop, within the framework of a general methodology for the design of circular milling cutters, the basis of CAD design of such mills for processing any tooth profile of multitooth products with a given unevenness of their location.

## 2 Literature Review

Toothed products are processed by copying [1], running in mesh [7] and touching methods [8] (by passing the contour on CNC machines [12]).

The copying methods are that the profile or projection of the tool profile coincides with all its points with the groove profile of the multitooth products. Processing, in this

case, is carried out on conventional universal machines using a dividing head or special dividing devices [13].

By copying, multitooth products can be manufactured with single-angle or two-angle cutters [8].

Using the copying method, the teeth of both a curved and a straight profile are made using grinding wheels [14]. The advantage is high surface quality and shortened production cycle, the disadvantage is the high cost of a grinding wheel.

When processing multitooth products according to the copying method, as a result of the periodic division process, the tooth pitch error is accumulated, which is unacceptable with a large number of teeth. The time spent on cutting the next tooth reduces processing performance. This happens when processing products with a small pitch and a large number of teeth.

Processing multitooth products using running in mesh [15] provides high performance, the ability to automate the processing process, and the accuracy of products obtained [16].

The running-in mesh can be used to process multitooth products with worm cutters. The advantages of the worm cutter include the fact that it is not a permanent installation tool and during operation can move along its axis during wear, which significantly increases the overall tool life.

The disadvantages of worm cutters include the fact that it is impossible to process a tooth with a positive rake angle.

To process multitooth products with a large number of teeth and positive rake angles prof. Sakharov G.N (речення не закінчене, не вистачає дієслова). Worm cutters have been developed [1], which profile the tooth cavity along a transition curve or use a modification of the relative movements of a worm cutter and a workpiece. However, it must be borne in mind that the tooth tip of such a worm cutter wears out intensively, which reduces tool life and machining accuracy. The introduction of motion modification during processing accordingly complicates the machine kinematics.

This disadvantage is deprived of constant-time worm cutters operating by the break-in method, which are designed to obtain a straight-line profile of the product without transition curves [17].

However, the disadvantage of milling machines of a permanent installation is the design complexity and it does not also allow movement on the mandrel and require a certain installation relative to a workpiece being processed, which complicates the operation of this tool [18].

A special constructive variety of such mills is a special milling machine of a permanent installation.

In [9], the method was proposed for cutting ratchet wheels with a disk-shaped rolling mill with the mutual rolling movement of a wheel and a mill. However, this method does not solve the issues of processing multitooth products of various profiles with a variable pitch.

In [14], the method was developed for shaping a curved tooth profile of cutting saws with grinding wheels on special CNC machines.

Making teeth from various saws in this way requires not only special CNC machines but high tool costs.

Other existing methods of processing multitooth products are plasma cutting, in which the cutting tool is a gas jet converted into a plasma by an electric arc [7].

One of the main advantages of plasma cutting is processing speed, productivity, and high precision.

But during plasma cutting of sheet material, the material is melted, which requires further sharpening of a cutting part, removal of large allowances.

The advantages of laser cutting include, first of all, the high quality of the obtained blanks [19], and software optimization of sheet cutting significantly saves tool steel [20]. However, laser cutting requires expensive equipment and significant energy costs.

### 3 Research Methodology

The use of modern CAD systems [21, 22] concerning the design object and analysis are universal systems [23, 24]. Their “universality”, on the one hand, determines the wide distribution of these systems [25, 26], and on the other hand, does not allow obtaining the maximum effect from the automation of design work [27].

CAD of disk grinding mills refers to specialized systems and is based on a common methodology for their design.

The general methodology for the design of disk milling cutters that we are considering provides the development of basic principles for constructing an automated system [28], which ensures the processing of multitooth products regardless of the shape of tooth profile and the unevenness of their location along the step [29].

In a general case, the design methodology, including the disk turning-milling cutters, is based on the basic principles of the theory of shaping.

Circular milling cutters are designed based on the initial tool surface with linear contact with the tooth surface of a workpiece [8].

The initial tool surface is defined as the envelope to successive positions of the tooth surface of a product when it moves relative to the tool during processing.

Then, the cutting edge of a cutter is determined as the intersection line of the original tool surface and the front surface.

The determination of the initial tool surface formed under the formative movements of the product and the tool is the most difficult stage of profiling. Therefore, we find the initial tool surface and take for the cutting edge the characteristic, which is the contact line of the original tool surface and the tooth surface at a certain selected moment. This greatly simplifies the problem solution.

In this case, the tool axis and the workpiece are intersecting straight lines.

Characteristics, i.e. the shape of the cutting edges, depending on the shape of the profile of the product teeth. They can be straight and curved lines. The shape of the cutting edges of a disk rolling mill is determined by the coordinates of their points.

Thus, to determine the coordinates of the cutting edges points, first of all, the shape of the tooth profile of the workpiece must be known. The teeth shape can have a symmetrical and asymmetric profile. In addition to the tooth profile of the product, product diameter, as well as profile angle for each tooth profile and angular pitch of each tooth must be known.

Toothed products can be manufactured with the help of uniform and variable pitch. An example of multitooth products is cutting saws with a variable pitch in a group.

The sequence of calculating the coordinates of the point for the cutting edges of the run-in mill in the coordinate system associated with the mill  $X_f Y_f Z_f$  is calculated in the sequence shown in Fig. 1. The methodology for their determination with a perpendicular and inclined installation of the cutter axis with respect to the product axis for a symmetrical [11] and asymmetric tooth profile of the product is given in [14].

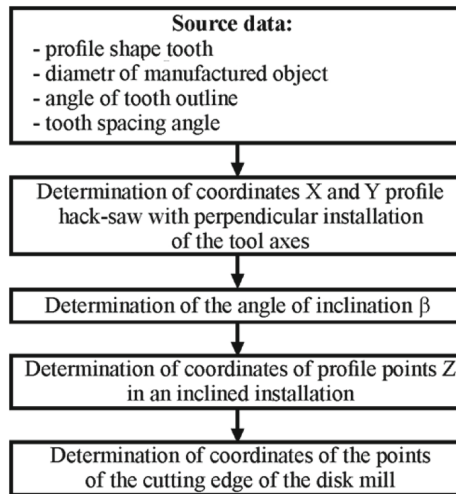


Fig. 1. The sequence of determining the cutting edges points of the rolling mill teeth.

In Fig. 1 the general case of inclined installation at an angle of the cutter axis relative to the product axis is considered.

When  $\beta = 0$ , the coordinates of the cutter cutting edges are considered when it is perpendicular to its installation relative to the workpiece.

Along with determining the shape of cutting edges, the task is to ensure the manufacture of multitooth products by a disk rolling mill without penetration of the cutting edge into the product body.

In this case, the second condition of shaping will be maintained.

When installing the axis of the disk rolling mill perpendicular to the product axis in the cavity, the appearance of transition curves [8]. Processing without transient curves will be in the case when adjacent sections of the original tool surface are in contact with each other or are separated from each other at a certain distance, then the characteristics at the boundary of the section will not break and join at a point whose coordinates will determine the processing without transition curves.

When analyzing the shaping of multitooth products, the problem of determining transition surfaces is also considered when installing the axis of a disk rolling mill perpendicular to the product axis. Based on the solution of this problem, the transitions radii can also be determined with an inclined installation of the cutter at an angle of

inclination  $\beta_i < \beta$ , at which processing without transition surfaces is carried out. This allows you to control the size of the rounding radius in the allowable or specified values.

The next step in the construction of CAD disk milling cutters for processing multitooth products is to consider the general methodology for resolving issues related to the design of this tool.

The design of rotary milling cutters is characterized by two groups of parameters, the first group of which is calculated according to the dependencies obtained based on the theory of shaping of gear products by milling cutters, the second - according to the recommendations of regulatory documents and scientific sources.

When developing the design of the disk rolling milling cutters, the primary task is to determine their outer diameters that most satisfy the operating conditions of this tool, i.e. determination of the outer diameter of the cutter with regrind. Its definition is based on the estimated minimum diameter.

The determination of the outer diameter of the disk rolling mill is carried out for its largest tooth. The methodology for its determination is as follows:

1. The minimum design diameter of the run-in mill is determined;
2. The outer diameter is determined to take into account regrinding;
3. The method of setting the axis of the run-in mill relative to the workpiece axis is determined. Depending on the permissible or given radii of the transition curves, the possibility of installing a cutter perpendicular to the workpiece axis is determined;
4. When installing the axis of the run-in mill to the saw axis, the outer diameter of the mill is determined;
5. If it is impossible to process with a perpendicular installation, use an inclined installation.

After determining the outer diameter of the milling cutters, the structural parameters are calculated for the dependencies obtained based on the provisions of the theory of shaping. Then, parameters are selected depending on the cutting part parameters.

The geometrical parameters recommended for processing certain multitooth products that correspond to geometrical parameters in the tool system do not fully reflect the actual picture of the parameter values during the cutting process. During the tool operation, the geometric parameters along with its cutting edge change and depend on the shape of their front, rear surfaces and movements carried out during the processing of the tool relative to the workpiece [29].

The methodology for determining the values of geometric parameters along the cutting edge is given in [29].

An analysis of their change shows that with an increase in the length of the cutting edges, the range of angles changes. With a decrease in the outer diameter of the cutter, the range of their change decreases and can take negative values. When machining multitooth products with rotary cutters, the change in the front  $\gamma$  and rear  $\alpha$  angles along the cutting edges is exactly the opposite.

Based on this analysis, the geometric parameters in the tool system are determined, which are put down in on the drawings. The verification of the general methodology for the development of CAD software for rotary milling cutters for the processing of multitooth products is considered on the example of computer-aided design of circular milling cutters for processing cutting saws with a variable pitch in the group.

### 4 Results

The methodology result is the development of CAD for the processing of multitooth products, regardless of the profile and variable arrangement of steps. It is a variable  $\Delta$ . Due to this, we built a CAD structural diagram for processing pieces of the saw with variable progress in the group and the angle of inclination of the front plane relative to the vertical with respect to the axis perpendicular (Fig. 2).

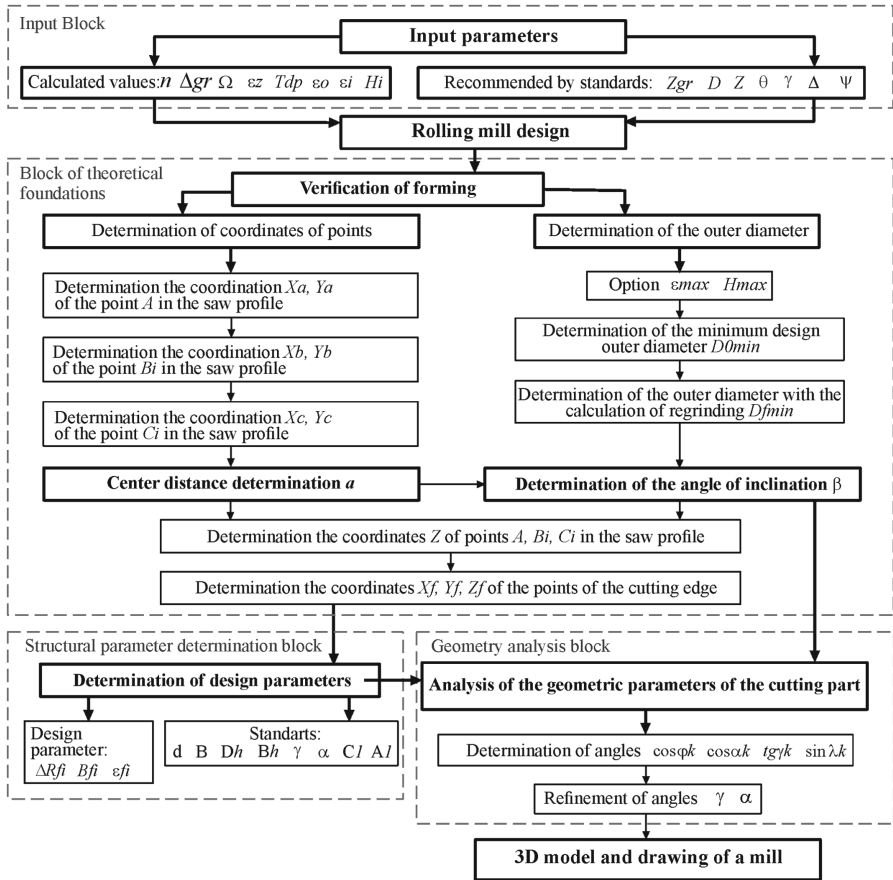


Fig. 2. Structural diagram of CAD disk grinding milling cutters with variable pitch.

Computer-aided design using a CAD structural diagram is shown in Fig. 2. A program for calculating the structural parameters of the cutter with a variable pitch using a CAD system using the Visual Basic language [30] has been developed. The SolidWorks program [31] created a parametric model of a rolling mill (Fig. 3).



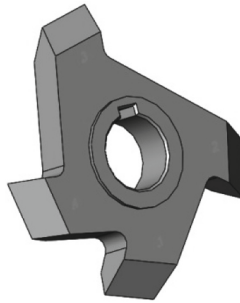
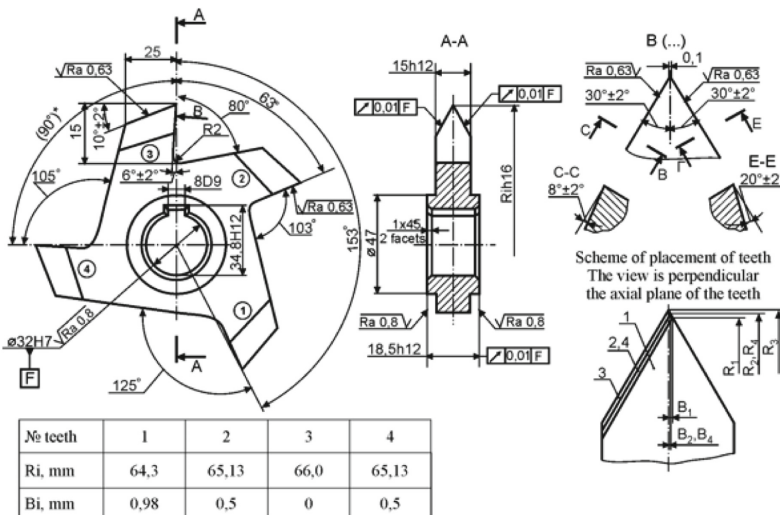


Fig. 3. 3D model of the run-in mill.

After entering the input parameters, the program performs preliminary calculations, the results of which are displayed in the text box of the window. The result of the program is the construction of a 3D model of the rolling cutter for processing a given cutting saw with a variable pitch and its drawings.

Based on the constructed 3D model of the run-in mill, a cutter drawing is created in the SolidWorks program [32].

As a result of computer-aided design, the design for a circular milling cutter for machining a fine-tooth cutting saw with tooth irregularity in the group  $\Delta = 30\%$  and the number of teeth  $Z_{gr} = 4$  has been developed. The drawing of a rolling mill is shown in Fig. 4.



Scheme of teeth placement

Fig. 4. Disk run-in mill  $Z_0 = 4$ .

According to this drawing, a milling cutter is made and tested. As a result of industrial tests, which included cutting a  $\varnothing 215$  mm saw with  $Z = 96$ , which was carried out on a gear hobbing machine.

As a result of the tests, the error in the step of the cut by disk milling cutters is 2–3 times smaller than the permissible, and the radius of the chip grooves meets the specified standard.

## 5 Conclusions

Using the basic principles of the theory of surface shaping and designing cutting tools, the general methodology for designing disk milling cutters for the manufacture of multitooth products has been developed.

Using this methodology allows us to build CAD systems of such a tool with any tooth profile and their variable arrangement, which is their basis. Studies on the development of CAD milling tools on the example of the manufacture of cutting saws with a variable pitch showed high accuracy of the products both in the tooth profile of the product and in the step.

The CAD milling cutter developed on this basis significantly reduces the time for design and technological preparation of production.





## References

1. Sakharov, G.: Break-in tools. Engineering, Moscow (1983). [in Russian]
2. Stupnitsky, V., Gritsay, I., Slipchuk, A.: Possession and progressive methods of forming details. Navalny pos\_bnik, Lviv Polytechnic, Lviv (2012). [in Russian]
3. Shepeleva, G.: Theory of shaping and contact of moving bodies. Stankin, Moscow (1999). [in Russian]
4. Chryssoulouris, G.: Laser Machining Theory and Practice. Springer, New York (2013)
5. Nee, J.G.: Fundamentals of Tool Design. Society of Manufacturing Engineers Dearborn, Michigan (2010)
6. [http://www.ctmag.com/news/articles/fundamentals\\_industrial-sawing](http://www.ctmag.com/news/articles/fundamentals_industrial-sawing). Accessed 06 Sept 2018
7. Stephenson, D., Agapiou, J.: Metal Cutting Theory and Practice. CRC Press, United States (2016)
8. Rodin, P.: Fundamentals of surface shaping by cutting. High school, Head Publishing House, Kyiv (1977). [in Russian]
9. Rodin, P., Odintsova, A.: Disc shaped cutters for cutting ratchet wheels by rolling. In: Topical problems in the field of mechanical engineering, radio electronics, automation and computer engineering, thermal power engineering and industrial technology, Kiev. pp. 7–8 (1988). [in Russian]
10. Ravska, N., Parnenko, V., Rodin, R.: Cutting method of circular saws with variable pitch. Patent for cinnamon, model UA 104229, Publish 25 January 2016 (2016). [in Ukrainian]
11. Parnenko, V.: Calculation of the parameters for disc saws that use method of running for toolmaking with uneven tooth pitch. Bull. Nat. Tech. Univ. Ukraine “KPI” **72**, 152–156 (2014). [in Russian]

12. <http://metalurg.su/preimushhestva-i-nedostatki-plazmennoj-rezki.html>. Accessed 18 Jan 2018
13. Ravska, N., Rodin, P., Nikolaenko, T., Melnichuk, P.: The basics of shaping on top with mechanical testing. View SKD-Druk, Kyiv (2013). [in Ukrainian]
14. Ravskaya, N., Lorokh, R.: The law of motion of the grinding wheel when machining the teeth of cutting saws. *Sat. Cutting tools Technol. Syst.* **51**, 84–87 (1997). [in Russian]
15. Odintsova, A., Malamed, E.: Permanent milling cutter for ratchet wheel processing. *Technol. Organ. Prod.* **4**, 28–30 (1984). [in Russian]
16. Pankratov, Yu.: *Profiling Rolling Tools*. Polytechnic Service, St. Petersburg (2010)
17. Rodin, P., Odintsova, A.: Profile of a mill of a permanent installation for machining gear products on gear hobbing machines. *Cutting Tool* **33**, 62–64 (1985). [in Russian]
18. Rodin, P., Odintsova, A., Olifirenko, M.: The method of cutting ratchet wheels and a circular angle mill for its implementation. C.A. No. 1373501, no. 6 (1988). [in Russian]
19. Salenko, O., Zagirnyak, M., Fomovska, O., Dotsenko, V., Schetin, V.: Processes and possession of a laser cutting. Monograph, Kharkov - Madrid (2013). [in Russian]
20. Golovko, L., Luk'yanenko, S.: *Laser technology and computer modeling*. Vistka, Kyiv (2009). [in Russian]
21. Grechishnikov, V., Kirsanov, G.: *Automated design of metal cutting tools*. Mosstankin, Moscow (1984). [in Russian]
22. Petukhov, A.: *Systems of computer-aided design of technological processes*. Tutorial. Gomel state technical University of P.O. Sukhoi, Belarus (2011). [in Russian]
23. Tandon, P.: *Cutting Tool Geometry: 3D Perspective: Computer Aided Geometric Design of Cutting Tools*. LAP LAMBERT Academic Publishing, Latvia (2011). [in Russian]
24. Srinivas, J.: *CAD/CAM: Principles and Applications*. Oxford University Press, United Kingdom (2016)
25. Ravska, N.S.: Research of the multi-tooth instruments for Recreation 3D Projects. *Herald of the DSEA* **2**(33), 54–59 (2014). [in Ukrainian]
26. Vikram, S.: *Fundamentals Of Computer Aided Manufacturing*. S.k. Kataria & Sons, Delhi (2011)
27. Lechovitser, V., Balushok, K., Lipsky, E.: Development of the specialized system “Toothpicking”. *Technol. Syst.* **3**(5), 74–77 (2000). [in Russian]
28. Pankratov, Yu.: *CAD cutting tools*. Lan, Moscow (2013). [in Russian]
29. Ravska, N.: Fundamentals of kinematic theory of geometrical parameters in the part of the instrument. *Reliab. Tools Optim. Technol. Syst.* **24**, 9–18 (2009). [in Russian]
30. Zibirov, V.: *Visual Basic 2010 with examples*. BHV-Petersburg, Petersburg (2010). [in Russian]
31. Alyamovsky, A.: *SolidWorks Simulation. Engineering analysis for professionals: tasks, methods, recommendations*. DMK Press, Moscow (2015). [in Russian]
32. Alyamovsky, A.: *SolidWorks Simulation. How to solve practical problems*. BHV-Petersburg, Petersburg (2012). [in Russian]



# Design Calculation of Electrohydraulic Servo Drive for Technological Equipment

Volodymyr Sokolov<sup>(✉)</sup> , Olga Porkuian , Oleg Krol ,  
and Yevhen Baturin 

Volodymyr Dahl East Ukrainian National University, 59-a, Pr. Central,  
Severodonetsk 93400, Ukraine  
sokolov.snu.edu@gmail.com

**Abstract.** The engineering method for design calculation of electrohydraulic servo drive with throttle regulation is proposed. The method is adapted on drives of technological equipment, in particular, equipment for mechanical processing of materials. The engineering method allows determining the main parameters and choosing elements and devices of the drive, to predict its static and dynamic characteristics. As the input data are considered: maximum loading; maximum tracking speed without load; maximum tracking error (or allowable tracking error at maximum speed); piston stroke; reduced mass of moving parts. The method includes the following main stages: construction of the drive settlement scheme, choice of the working fluid and the nominal working pressure; calculation of the constructive parameters and choice of the hydraulic cylinder; choice of the electrohydraulic amplifier; definition of the feedback parameters, determining the drive quality factor and calculation the transfer coefficient of the electronic block; evaluation of the drive static characteristics, calculation of the speed and load characteristics; construction of the drive linear model, stability assessment; research of the drive dynamic characteristics and the control quality, drive correction. The example of the design calculation of the electrohydraulic servo drive for technological equipment is presented. For calculations used the MATLAB application package.

**Keywords:** Engineering method · Static characteristics · Dynamic characteristics · Transient process

## 1 Introduction

The modern technologies for mechanical processing of materials impose ever-increasing requirements on the technical and functional characteristics of technological equipment drives [1–5]. The quality of the products obtained largely depends on the possibility of implementing the optimal laws of movement of the working bodies, the accuracy of controlling their movements and the stability of speeds under variable load conditions.

The achievement of arbitrary kinematics of the working body, the possibility of program implementation of the optimal laws of its movement is provided by the use of automatic electrohydraulic drives [6–10] and, in particular, electrohydraulic servo

drives (EHSD) with throttle regulation in the technological equipment with power up to 8 kW. The creation of high-performance EHSD for technological equipment requires engineering methods for design calculation, allowing to evaluate the main parameters and to choose elements and devices of drive, to predict its static and dynamic characteristics.

## 2 Literature Review

Individual methods and design procedures of automatic electrohydraulic drives for various technological equipment for mechanical processing, in particular, equipment for processing materials by pressure, metal-cutting machines, and systems, equipment for tool production, etc., are widely presented in the literature [11–15].

At the same time, there are no generally accepted engineering methods for the design calculation of EHSD for technological equipment. The existing methods are not universal, are focused on different classes of equipment, use different input data, apply different calculation methods and, as a consequence, have different calculation results.

The series of papers by the authors [16–20] devoted to the development of automatic drives for technological equipment, mathematical modeling, and research of their static and dynamic characteristics, correction of control quality, allow us to propose a unified engineering method for design calculation of EHSD.

The work purpose is to develop an engineering method for the design calculation of EHD with throttle regulation for technological equipment, allowing to evaluate the main parameters and to choose elements and devices of the drive, to predict its static and dynamic characteristics.

## 3 Research Methodology

### 3.1 Construction of the Drive Settlement Scheme, Choice of the Working Fluid and the Nominal Working Pressure

The above analysis of the literature indicates that to determine the main parameters and choose elements and devices of the EHSD with throttle control, the following values should be taken as input data:  $R_{max}$  – maximum loading (force);  $V_{max}$  – maximum tracking speed without load;  $\varepsilon_{max}$  – maximum tracking error (or allowable tracking error at maximum speed);  $H$  – piston stroke;  $m$  – a reduced mass of moving parts.

Then the design calculation can be carried out in the following order.

The settlement scheme reflects the main elements and devices of the EHSD, indicates the relationships between them. EHSD is designed to reproduce with a given accuracy the working body of the control signal, which changes arbitrarily. Drive has electrical input control signal  $U$  and electrical feedback in the form of voltage  $U_{fb}$ . The principle of EGSP operation consists in the continuous comparison of the input signal with a displacement of the output link and regulation of the flow of working fluid supplied to the hydraulic cylinder, depending on the error of the specified values, which is determined by the error signal  $U_e = U - U_{fb}$ .

The basis can be taken as the scheme presented in the authors' papers [9, 21] and shown in Fig. 1. The settlement scheme indicates HC – hydraulic cylinder; EHA – electrohydraulic amplifier, including electromechanical transducer (EMT) and the hydraulic amplifier (HA); the FB – feedback gauge, EB – electronic block. The following main variables of the EHSD are marked on the scheme:  $U$  – input (control) voltage;  $U_{fb}$  – FB voltage;  $y, V$  – displacement and speed of the piston;  $p_{ps}, p_d$  – the pressure of pump station and drain.

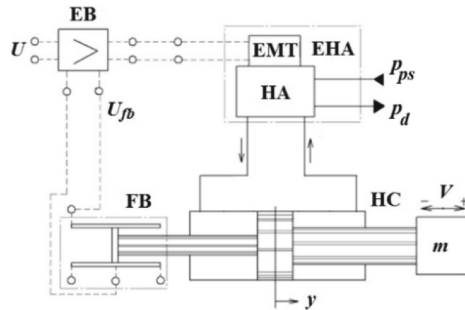


Fig. 1. The settlement scheme of the EHSD.

The working fluid is chosen based on technical requirements for technological equipment, or recommendations contained in the technical data of the main hydraulic devices [22–24]. The nominal working pressure  $p_{nom}$  is taken according to the capabilities of series-produced hydraulic units for technological equipment. The  $p_{nom}$  value is set from the standard series, *MPa*: ... 4; 6,3; 10; 12,5; 16; 20; 25; 32; 40 ...

### 3.2 Calculation of the Constructive Parameters and Choice of the HC

The effective HC area is estimated

$$F = (1, 3 \dots 1, 5) \frac{R_{max}}{P_{nom}}. \tag{1}$$

The diameter of the piston  $D$  is determined by the value  $F$ . For HC with the double-sided rod, it is necessary to consider the ratio of the diameter of the rod  $d_r$  and piston.

The estimated piston diameter  $D$  and rods diameter are rounded to standard values. Usually, if the discrepancy between the calculated piston diameter  $D$  and the smaller standard exceeds 5%, then a greater value is taken.

According to the parameters  $p_{nom}, D, d_r$  and the stroke of the piston  $H$ , a series-produced HC is chosen from catalogs or reference books. In the absence of an appropriate series-produced engine, a technical assignment for the development of original HC is drawn up.

In further calculations, the corrected effective HC area is taken.

### 3.3 Choice of the EHA

The EHA choice is also made through catalogs or reference books. The maximum working pressure  $p_{max}$  of the EHA must be greater than or equal to the nominal working pressure  $p_{nom}$  for a drive, i.e.  $p_{max} \geq p_{nom}$ . The EHA flow rate at differential pressure  $\Delta p_{EHA}$ , which is specified in the technical data, must satisfy the condition

$$Q_{EHA} \geq (1, 1 \dots 1, 2) FV_{max} \sqrt{\frac{\Delta p_{EHA}}{P_{ap}}}, \quad (2)$$

where  $p_{ap} = p_{ps} - p_d$  – pressure applied (pressure difference  $p_{ps}$  and  $p_d$  in EHA lines, see Fig. 1).

At the stage of design, the calculation is recommended to take  $p_{ap} = (0.75 - 0.85) p_{nom}$ . For the chosen EHA, the gain coefficient by flow rate for the unloaded drive is estimated,  $m^3/(s A)$ ,

$$K_{Qi} = \frac{Q_{EHA}}{i_{nom}} \sqrt{\frac{P_{ap}}{\Delta p_{EHA}}}, \quad (3)$$

where  $i_{nom}$  – nominal control current.

### 3.4 Definition of the FB Parameters, Determining the Drive Quality Factor and Calculation the EB Transfer Coefficient

In most cases, the FB for the EHSD under consideration is formed using linear displacement sensors. To determine the FB transfer coefficient, the “zero” displacement ( $y = 0$ ) of the drive output unit is considered to correspond to the average piston position, and the maximum displacement is  $\pm H/2$  and corresponds to the maximum output voltage of the linear displacement sensor. This voltage value at the design calculation stage is conveniently set equal to the maximum value of the control signal  $\pm U_{max}$ , which, in turn, can be taken equal to the maximum input voltage for the EHA. Then the FB transfer coefficient is defined as,  $V/m$ ,

$$k_{fb} = \frac{2U_{max}}{H}. \quad (4)$$

The drive quality factor  $D_{EHSD}$  is the system open-loop gain and is assigned according to the accuracy requirements of the EHSD,  $1/s$ ,

$$D_{EHSD} \geq (1, 05 \dots 1, 1) V_{max} / \varepsilon_{max}. \quad (5)$$

The  $D_{EHSD}$  value is used to determine the EB transfer coefficient,  $1/\Omega$ ,

$$k_{eb} = \frac{D_{ESHDF}}{k_{Qi} k_{fb}}. \quad (6)$$

### 3.5 Evaluation of the Drive Static Characteristics, Calculation of the Speed and Load Characteristics

The static characteristics of the EHSD are the dependencies connecting the speed of the output unit  $V$ , the loading  $R$ , and the error signal  $U_\varepsilon$ . It is recommended to build the speed  $V(U_\varepsilon)$  and load  $V(R)$  characteristics according to the following approximate dependence

$$V = U_\varepsilon \frac{D_{EHSD}}{k_{eb}} \sqrt{1 - \frac{R}{p_{ap}F} \text{sign} U_\varepsilon}. \quad (7)$$

The speed characteristic is obtained at  $R = 0$  in the range  $-k_{fb}\varepsilon_{max} \leq U_\varepsilon \leq k_{fb}\varepsilon_{max}$ , the calculation of the load characteristic is performed at  $U_\varepsilon = \pm k_{fb}\varepsilon_{max}$  in the range  $-p_{ab}F \leq U_\varepsilon \leq p_{ab}F$ .

### 3.6 Construction of the Drive Linear Model, Stability Assessment

Parameters estimation of the linear model is performed according to the structural scheme of the control signal transfer, which is shown in Fig. 2 (here  $s$  – Laplace variable).

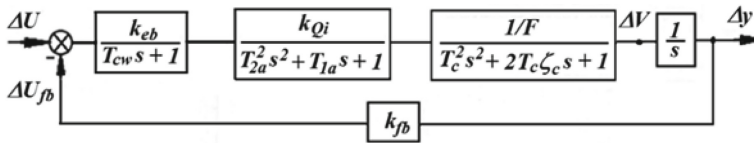


Fig. 2. The structural scheme of the control signal transfer.

On the structural scheme:  $T_{cw}$  – time constant of the control winding

$$T_{cw} = L_c/R_e, \quad (8)$$

where  $L_c$  – inductance of the control winding;  $R_e$  – active resistance of the electrical circuit EB-EHT;

$T_{2a}$ ,  $T_{1a}$  – time constants of the EHA, which are defined on frequencies  $\nu_1$ ,  $\nu_2$  of phase shift on 450 and 900°, the values of which are presented in the EHA passport data:

$$T_{2a} = \frac{1}{2\pi\nu_2}; T_{1a} = \frac{1}{2\pi\nu_1} - \frac{2\pi\nu_1}{(2\pi\nu_2)^2}. \quad (9)$$

The hydromechanical time constant of the HC



$$T_c = \sqrt{\frac{mH}{4E_cF}}, \quad (10)$$

where  $E_c$  – reduced elastic modulus of the HC.

For design calculation, it is recommended to take

$$E_c = (0.85-0.95) E_f, \quad (11)$$

where  $E_f$  – elastic modulus of the working fluid that is chosen [21, 25].

The coefficient of relative damping of the HC taken approximately from the range

$$\zeta_c = 0, 2 \dots 0, 5. \quad (12)$$

According to the structural scheme (Fig. 2), the transfer function of the EHSD according to the control signal is

$$W(s) = \frac{k_{yu}}{a^6s + a^5 + a_4s^4 + a_3s^3 + a_2s^2 + a_1s + 1}, \quad (13)$$

where  $k_{yu}$  - transfer coefficient of the EHSD,  $m/V$ ,

$$k_{yu} = 1/k_{fb}; \quad (14)$$

$$\begin{aligned} a_1 &= \frac{1}{D_{EHSD}}; \quad a_2 = \frac{T_{cw} + T_{1a} + 2T_c\zeta_c}{D_{EHSD}}; \\ a_3 &= \frac{T_{cw}T_{1a} + 2T_c\zeta_cT_{cw} + T_{2a}^2 + 2T_c\zeta_cT_{1a} + T_c^2}{D_{EHSD}}; \\ a_4 &= \frac{T_{2a}^2T_{cw} + 2T_c\zeta_cT_{cw}T_{1a} + T_c^2T_{cw} + 2T_c\zeta_cT_{2a}^2 + T_{1a}T_c^2}{D_{EHSD}}; \\ a_5 &= \frac{2T_{2a}^2T_cT_{cw}\zeta_c + T_c^2T_{cw}T_{1a} + T_{2a}^2T_c^2}{D_{EHSD}}; \quad a_6 = \frac{T_{2a}^2T_c^2T_{cw}}{D_{EHSD}}. \end{aligned} \quad (15)$$

Stability can be assessed using various methods [26–28], in particular, using the Hurwitz criterion. For the 6th order system with a transfer function (13), it is required for positive coefficients  $a_1 \dots a_6$  to fulfill the inequalities (16)

$$\begin{cases} a_4a_5 > a_3a_6; \\ (a_4a_5 - a_3a_6)(a_2a_3 - a_1a_4) > (a_2a_5 - a_1a_6)^2. \end{cases} \quad (16)$$

In the case of an unstable system, it is necessary to perform the EHSD correction, as will be discussed below.

### 3.7 Research of the Drive Dynamic Characteristics and the Control Quality, Drive Correction

The calculation of the transition process and frequency characteristics is performed. The assessment of the regulation quality is carried out, conclusions on the need for correction of EHSD are made. It is recommended to perform calculations in the MATLAB application package environment or the Simulink subsystem [29, 30].

The issue of choosing a correcting link for improving the regulation quality of EHSD for technological equipment is considered in detail in the authors' paper [9]. The serial installation of a real proportional-differential link in the EMT circuit is quite effective.

$$W_c = \frac{Ts + k}{T_{in}s + 1}, \quad (17)$$

where  $T$ ,  $k$  – time constant and transfer coefficient of the correcting link;  $T_{in}$  – time constant characterizing the inertia of the correcting link.

## 4 Results

We will show an example of the EHSD design calculation for special technological equipment for the processing of materials by pressure for the following input data: the maximum force  $R_{max} = 160$  kN; the maximum tracking speed without load  $V_{max} = 0,05$  m/s; the maximum tracking error  $\varepsilon_{max} = 0,005$  m; the piston stroke  $H = 0,5$  m; the reduced mass of moving parts  $m = 500$  kg.

We use the settlement scheme shown in Fig. 1. We choose hydraulic oil IGP-30 as a working fluid [16]. We accept the nominal working pressure  $P_{nom} = 32$  MPa.

We estimate the effective HC area  $F = 0,007$  m<sup>2</sup>. The value  $F$  determines the diameter of the piston. For the HC with double-sided rod and the ratio of rod and piston diameters  $d_r/D = 1/2$  we get  $D = 0,109$  m.

We choose the hydraulic cylinder HC125.63-02 ( $D = 125$  mm,  $d_r = 63$  mm) [16]. In further calculations, we use the corrected effective HC area  $F = 0,0091$  m<sup>2</sup>.

We accept  $P_{ap} = 22,6$  MPa. We focus on the RP type of EHA [16], for which  $\Delta P_{EHA} = 32$  MPa. The flow rate of EHA must be  $Q_{EHA} \geq 6,23 \cdot 10^{-3}$  m<sup>3</sup>/s = 37,4 l/min.

We choose the EHA - throttling direction control hydraulic valve - RP10, for which  $\Delta P_{EHA} = 32$  Mpa,  $Q_{EHA} = 50$  l/min,  $i_{nom} = 850$  mA,  $v_1 = 80$  Hz,  $v_2 = 125$  Hz,  $L_c = 1,0$  H,  $R_e = 100$   $\Omega$ . For the chosen EHA, we estimate the gain coefficient by flow rate  $K_{Qi} = 0,516 \cdot 10^{-3}$  m<sup>3</sup>/(s A).

We accept  $U_{max} = 10$  V. Then the FB transfer coefficient  $k_{fb} = 40$  V/m, drive quality factor  $D_{EHSD} = 10,7$  s<sup>-1</sup>, the EB transfer coefficient  $k_{eb} = 1,754$   $\Omega^{-1}$ .

We have the following static characteristic of thee EHSD

$$V = 0,2675U_\varepsilon \sqrt{1 - \frac{R}{2,057 \cdot 10^5} \text{sign}U_\varepsilon} \text{ m/s}. \quad (18)$$

The speed and load characteristics are shown in Fig. 3.

We perform estimation of the parameters of the linear model: the time constant of the control winding  $T_{cw} = 0,01$  s; the time constants of the EHA  $T_{1a} = 0,0011$  s,  $T_{2a} = 1,27 \cdot 10^{-3}$  s; the hydromechanical time constant of the HC  $T_c = 2,62 \cdot 10^{-3}$  s; the coefficient of relative damping of the HC  $\zeta_c = 0,25$ ; the transfer coefficient of the EHSD  $k_{yu} = 0,025$  m/V.

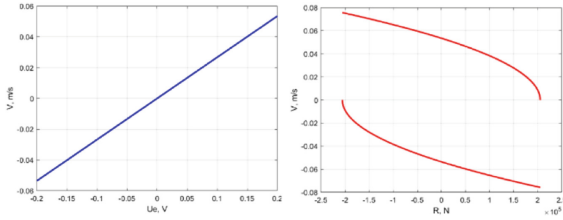


Fig. 3. The speed and load characteristics.

We have the coefficients of the transfer function:  $a_1 = 0,0934$ ;  $a_2 = 0,0011$ ;  $a_3 = 3,26 \cdot 10^{-6}$ ;  $a_4 = 1,03 \cdot 10^{-8}$ ;  $a_5 = 1,05 \cdot 10^{-11}$ ;  $a_6 = 1,04 \cdot 10^{-14}$ . The system is stable.

The transient and amplitude-phase characteristics are shown in Fig. 4. The block diagram for modeling the dynamic characteristics of the EHSD under consideration with a correcting link in the Simulink environment is shown in Fig. 5.

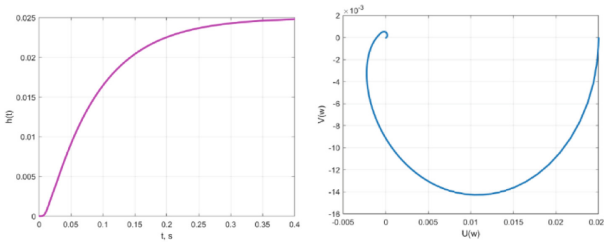


Fig. 4. The transient and amplitude-phase characteristics.

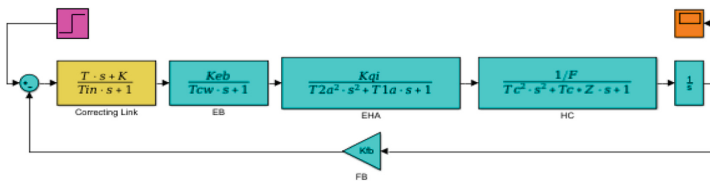


Fig. 5. The block diagram for modeling the dynamic characteristics of the EHSD with the correcting link in the Simulink environment of the MATLAB package.

### 5 Conclusions

Thus, the engineering method for design calculation of EHSD with throttle regulation was developed. The method is adapted on drives of technological equipment, in particular, equipment for mechanical processing of materials. The engineering method allows determinate the main parameters and chooses elements and devices of the drive,

to predict its static and dynamic characteristics. The input data are considered as follows: maximum loading (force); maximum tracking speed without load; maximum tracking error (or allowable tracking error at maximum speed); piston stroke; reduced mass of moving parts. The used approaches allow increasing the reliability of the design calculation.

The method includes the following main stages: construction of the drive settlement scheme, choice of the working fluid and the nominal working pressure; calculation of the constructive parameters and choice of the HC; choice of the EHA; definition of the FB parameters, determining the drive quality factor and calculation the EB transfer coefficient; evaluation of the drive static characteristics, calculation of the speed and load characteristics; construction of the drive linear model, stability assessment; research of the drive dynamic characteristics and the control quality, drive correction.

The example of the EHSD design calculation for special technological equipment with the maximum force 160 kN and maximum tracking speed without load 0,05 m/s is given. The results of calculations the drive static and dynamic characteristics in the environment of the MATLAB application package are presented.






## References

1. Navrotsky, K.: Theory and Designing Hydro- and Pneumodrives. Machinery Engineering, Moscow (1991)
2. Karpus, V., Ivanov, V., Dehtiarov, I., Zajac, J., Kurochkina, V.: Technological assurance of complex parts manufacturing. In: Ivanov, V., et al. (eds.) Advances in Design, Simulation and Manufacturing. DSMIE 2018. LNME, pp. 51–61. Springer, Cham (2019)
3. Sokolov, V., Krol, O., Stepanova, O.: Automatic control system for electrohydraulic drive of production equipment. In: 2018 International Russian Automation Conference (RusAuto-Con). IEEE (2018)
4. Fesenko, A., Basova, Y., Ivanov, V., Ivanova, M., Yevsiukova, F., Gasanov, M.: Increasing of equipment efficiency by intensification of technological processes. Periodica Polytechnica Mech. Eng. **63**(1), 67–73 (2019)
5. Fedorovich, V., Mitsyk, A.: Mathematical simulation of kinematics of vibrating boiling granular medium at treatment in the oscillating reservoir. Key Eng. Mater. **581**, 456–461 (2014)
6. Rydberg, K.-E.: Hydraulic Servo Systems: Dynamic Properties and Control. Linköping University Electronic Press, Linköping (2016)
7. Sveshnikov, V.: Hydrodrives in modern mechanical engineering. Hydraul. Pneum. **28**, 10–16 (2007)
8. Pavlenko, I., Simonovskiy, V., Demianenko, M.: Dynamic analysis of centrifugal machines rotors supported on ball bearings by combined application of 3D and beam finite element models. J. Phys. Conf. Ser.: Mater. Sci. Eng. **233**, 012053 (2017)
9. Sokolov, V., Krol, O., Stepanova, O.: Choice of correcting link for electrohydraulic servo drive of technological equipment. In: Ivanov, V., et al. (eds.) Advances in Design, Simulation and Manufacturing. DSMIE 2019. LNME, pp. 702–710. Springer, Cham (2020)
10. Pavlenko, I., Trojanowska, J., Ivanov, V., Liaposhchenko, O.: Scientific and methodological approach for the identification of mathematical models of mechanical systems by using artificial neural networks. In: Machado, J., Soares, F., Veiga, G. (eds.) Innovation, Engineering and Entrepreneurship. HELIX 2018. LNEE, vol. 505, pp. 299–306 (2019)

11. Popov, D.: Dynamics and Regulation Hydro- and Pneumatic Systems. Machinery Engineering, Moscow (1987)
12. Sokolov, V.: Transfer functions for shearing stress in nonstationary fluid friction. In: Radionov, A., et al. (eds.) Proceedings of the 5th International Conference on Industrial Engineering (ICIE 2019). ICIE 2019. LNME, vol. 1, pp. 707–715. Springer, Cham (2020)
13. Rasskazova, Y., Stepanova, O., Azarenko, N.: Perfection of Electrohydraulic Drives of Machine-Building Equipment. VDEUNU, Severodonetsk (2016)
14. Krol, O., Sokolov, V.: Parametric modeling of gear cutting tools. In: Garpiński, B., Szostak, M., Ivanov, V. (eds.) Advances in Manufacturing II. Lecture Notes in Mechanical Engineering, vol. 4, pp. 3–11. Springer, Cham (2019)
15. Kreyenin, G., Krivts, I.: Hydraulic and Pneumatic Drives of Industrial Robots and Automatic Manipulators. Machinery Engineering, Moscow (1993)
16. Sveshnikov, V.: Hydrodrives of Tools. Machinery Engineering, Moscow (2008)
17. Popov, D.: Non-stationary Hydromechanical Processes. Machinery Engineering, Moscow (1982)
18. Pavlenko, I.: Static and dynamic analysis of the closing rotor balancing device of the multistage centrifugal pump. Appl. Mech. Mater. **630**, 248–254 (2014)
19. Abrahamova, T., Bushuyev, V., Gilova, L.: Metal-cutting Machine Tools. Machinery Engineering, Moscow (2012)
20. Kovalenko, A., et al.: Basics of Volume Hydraulic Drive of Building and Road Machines. DonSABA, Lugansk (1999)
21. Sokolov, V., Krol, O., Stepanova, O.: Nonlinear simulation of electrohydraulic drive for technological equipment. J. Phys: Conf. Ser. **1278**, 012003 (2019)
22. Popov, D.: Mechanics of Hydro- and Pneumodrives. MSTU, Moscow (2005)
23. Rogovyi, A., Khovanskyy, A.: Application of the similarity theory for vortex chamber superchargers. J. Phys. Conf. Ser.: Mater. Sci. Eng. **233**, 012011 (2017)
24. Rogovyi, A.: Energy performances of the vortex chamber supercharger. Energy **163**, 52–60 (2018)
25. Sokolov, V.: Diffusion of circular source in the channels of ventilation systems. In: Fujita, H., et al. (eds.) Advances in Engineering Research and Application. ICERA 2018. LNNS, vol. 63, pp. 278–283. Springer, Cham (2019)
26. Kim, D.: Theory of Automatic Control, vol. 1. Linear systems. Fizmathlit, Moscow (2003)
27. Pupkov, K., Egupov, N.: Methods of Classical and Modern Theory for Automation Control, vol. 3. Synthesis of Controllers for Automation Control Systems. MSTU, Moscow (2004)
28. Lurie, B., Enright, P.: Classical Automation Control Methods. BHV-Petersburg, Saint-Petersburg (2004)
29. Nuruzzaman, M.: Modeling and Simulating in Simulink for Engineers and Scientists. Author-House, Bloomington (2004)
30. Tewari, A.: Modern Control Design with MATLAB and Simulink. Wiley, Weinheim (2002)



# Parametric Optimization of Technological Layout of Modular Machine Tools

Ihor Yakovenko<sup>1</sup> , Alexander Permyakov<sup>1</sup> , Olena Naboka<sup>1</sup> ,  
Olga Prihodko<sup>2</sup> , and Yurii Havryliuk<sup>1</sup> 

<sup>1</sup> National Technical University “Kharkiv Polytechnic Institute”,  
2, Kyrpychova St., Kharkiv 61002, Ukraine  
igor.dych59@gmail.com

<sup>2</sup> Belgorod State Technological University named after V.G. Shukhov,  
46, Kostyukova St., Belgorod 308012, Russian Federation

**Abstract.** The article describes issues of structural-parametric optimization in the process of synthesis of structures of technological layouts with multi-tool machining on equipment built on the concept of modular design. In the research process, the existing practice of designing this equipment class and statistical studies of previously released machine tools were used. The paper proposes a methodology for calculating the cutting conditions of individual tools during multi-tool machining for various options for replacing the tool during operation and taking into account the probabilistic nature of tool life at a given mean time between failures, what allows providing a specified output cycle of the product with minimal costs associated with the operation of the cutting tool and minimize other components of the technological cost of processing. The proposed methodology is useful both in the design of the new machine tools and in the modernization of previously made machines, built on the concept of modular design.

**Keywords:** Modular equipment · Tool setup · Multi-tool machining · Tool life · Cutting conditions · Mean time between failures

## 1 Introduction

Packaged equipment, designed on a modular approach based on unified units and elements, has a complex structure of the technological layout, which allows providing high productivity and low cost due to a significant concentration of operations.

Modern mechanical engineering pays quite close attention to reduce the technological cost of production. One of the important factors affecting the technological cost is the operating costs of the cutting tool, which amounts from 15% to 25% in serial and large-scale machine-building manufacturing. The solution to this problem is especially relevant for multi-tool setups when the processing of surfaces with different sizes and forms is carried out by various groups of standardized and special combined cutting tools jointed into one tool block.

Automation of designing specialized packaged equipment which use a large number of diverse cutting tools with its lifetime parameters puts forward the

requirement of formalizing the process and developing a mathematical model for calculating the processing modes of each cutting tool (including each step of combined cutting tool) based on belonging to a specific element of the technological layout. The design process is complicated by the need to comply with the cycle time of product release with the mandatory ensuring of quality parameters. In general, the design problem can be formulated as follows: developing a mathematical model of parametric optimization of cutting conditions while implementing the technological layout of packaged equipment, which provides the most effective machining option from the viewpoint of the objective function, provided that the specified qualitative and quantitative characteristics of the processing object are realized.

## 2 Literature Review

The issues of parametric optimization of machine tools designed on modular principles were considered in a number of articles [1–16].

The paper [1] describes a procedure of calculating the machining conditions for milling operations according to minimum production cost as the objective function. Optimum values of machining conditions for each pass are determined based on the objective function criteria by circular direction search method developed specifically for this purpose.

The paper [2] describes the development and utilization of an optimization system, which determines optimum machining parameters for milling operations. An objective function based on maximum profit in milling operation has been used.

Issues of optimization of the machining modes for machine tools by the criterion of the maximum productivity rate for multi-tool machining processes on a lathe are considered [3]. However, in all these works, issues of hole-making operations with combined tools and tool blocks are ignored.

Optimization of multi-tool cutting conditions on machine tools and automated lines for turning using the criterion of maximum productivity is considered [4, 5].

Specifically, in paper Levin's and [4] the problem appeared for the optimization of cutting modes when designing manufacturing processes for batch processing on multiple position machines with multispindle heads has been considered. Work was concentrated on the understanding that batches can contain parts of several types. However, in that case, the tools of each spindle head employed for different parts can differ as authors have noted. It was pointed out that each tool can perform different manufacturing operations for different parts but with the same cutting modes. The key results of work [4] were a complex optimization problem formulated in terms of a geometric program. Then, a novel decomposition approach was suggested. The authors claimed that the proposed techniques reduce the search for an approximate solution of this problem to a finite sequence of easier convex and linear programming sub-problems which can be efficiently solved by known methods.

The authors of the work [5] looked for solutions to multi-tool machining processes of simultaneous action that are highly important for the manufacturing industry. In work, mathematical models for the productivity rate of a machine tool for the multi-tool and single-cutter machining processes with changes in the cutting speed have been

formulated. The equations presented in the paper included basic parameters of machining processes, machining time, the cutting speed, reliability attributes of mechanisms, and cutters of a machine tool. The authors claimed that the equations of the productivity rate with single and multi-tool machining processes of simultaneous action, which were presented in research [5], enable finding of the optimal cutting speed for each cutter. The maximum productivity rate was suggested to achieve through the minimization of the machining time, optimization of the failure rates of the cutters, and optimization of their cutting speeds for multi-tooling processes. Some of the major results emerging from the paper are formulated equations for productivity rate, allowing the prediction of more authentic results and which should allow used in preparing economically effective multi-tool manufacturing processes of work parts.

However, the issues of minimum technological cost under the condition of fulfilling the desired productivity were also not considered.

Work [6] was devoted to the study of rational cutting conditions for group machining of identical parts on multi-position multi-tool equipment. A mathematical model for minimizing technological costs while maintaining kinematic relationships between spindle speeds in one spindle box was proposed. However, the possibility of changing the kinematic relationships at the design stage was not taken into account.

The parametric optimization was used for the design of a flexible fixture through the proper choice of parameters of the fixture elements; as a result, the reserves for fixture optimization were revealed, and possible variants of the fixtures were proposed [7, 8].

In earlier works, such as [9], the questions of optimization of cutting conditions when machining with multi-cutting tool blocks, and in [10, 11] questions of optimization of cutting speed linked to the probabilistic nature of tool durability while ensuring a desirable mean time to failure of the cutting tool were considered in detail. However, the issues concerning the calculation of the optimal parameters of cutting conditions when machining with tool blocks consisting of end cutting tools have not been fully studied. This especially applies to the consideration of factors that are determined by the structural layout of the tool block (cutting length of the tool, the length of the machining pass of the tool block, the required output cycle time, etc.), when assigning cutting parameters for each tool.

Synthesis of technological layouts of packaged equipment, taking into account multi-position multi-tool machining with a high concentration of technological impact on the workpiece, was considered in the [12]. However, the optimization of processing parameters was not touched on, although against the background of a wide variety of used cutting tools and the variation in the duration of technological transitions, for such a complex system as a modular machine tool, an additional reduction in machining costs can be achieved by optimizing cutting conditions.

Thus, the purpose of this article is to identify and study factors affecting the parameters of the machining process using combined tools and multi-tool blocks in the implementing the technological layout of packaged equipment, as well as the development of a mathematical model for calculating the optimal cutting conditions for each tool, taking into account requirements of specified machining quality and output cycle time of the manufactured part.



### 3 Research Methodology

In general, the operating costs of the cutting tool  $C_{ti}$  are mainly related to its sharpening, setup, and equipment idle time during tool replacement.

Analysis of factors affecting operating costs indicated that they depend both on the structure of the tool setup (parameters associated with the length of the machining pass of the tool block, cutting length, the complexity of tool setup, time of tool setup and change, etc.), and on the machining parameters (cutting speed or revolution rate and path velocity of the tool block). The tool block path velocity is determined by the need to synchronize operations and ensure the necessary output cycle time  $\tau$ , and on the other hand, affects the parameters of the cutting conditions and, consequently, to the durability  $T_i$  of each tool of the block. Therefore, if we cannot vary the value of output cycle time since this provides the required production program, then, it's possible to minimize operation costs by optimizing the parameters of the cutting conditions by varying the durability of each specific tool.

Currently, there are several basic methods of tool replacement: failure replacement, scheduled replacement, mixed replacement. The most progressive is the scheduled replacement of the tool, which, however, is used only in 15% of the cases of servicing multi-tool setups. With this approach, the tool set-up is usually done outside the machine tool, and its replacement is carried out by the setup person, serving several machines. Moreover, the replacement is carried out during the technological or lunch break. Then, the item of expenses related to equipment downtime due to tool replacement is excluded from the operating costs of the tool, since machining at this time is not performed under the production schedule. In other words, it is possible to replace the tool by a setup person without the participation of the main worker on schedule, corresponding to the time of the planned equipment pause during the production cycle (technological or lunch break, the start of a new shift, etc.).

The output cycle of the product is determined by the necessary production program and therefore is taken as the initial constant when performing parametric calculations of the tool parameters, which must necessarily provide the required technical characteristics of the processing object and the specified time.

It has been established that the cutting speed has a much greater influence on tool life than feed, therefore, it is advisable to optimize tool life and operating costs by varying the cutting speed (speed) of the tool at the maximum allowable feed rate [9, 10]. However, the dependences "cutting speed - tool durability" have a "hump-shaped" character, therefore, in mass and large-scale production, when machining on modular machine tools and automated lines, it is necessary to check the possibility of processing at low cutting conditions without deterioration of the tool life index [10]. In other words, for each machining option, there is a minimum permissible value of the cutting speed (revolution rate), at which the change of tool life from cutting speed corresponds to the classical dependence. This allows estimating the minimum minute feed of the tool block and the rotation rate of each tool, providing the specified output cycle. In this case, the calendar durability of the cutting tool can be described by the dependence

$$T_i = \frac{T_{pi} \cdot T_{bi} \cdot n_{bi}^{\mu_i}}{(T_{pi} - T_{bi}) \cdot \bar{n}_{\min i}^{\mu_i} + T_{bi} \cdot n_{bi}^{\mu_i}} \cdot \frac{\tau}{t_{pi}} \cdot K_{st}, \quad (1)$$

where  $T_i$  - calendar durability of  $i$ -th tool, min;  $T_{pi}$  - the maximum permissible value of durability of  $i$ -th tool for the considered machining condition, min;  $T_{bi}$  - the basic value of the durability of the  $i$ -th tool, for which the normative machining condition were determined, min;  $t_{pi}$  - cutting time of the  $i$ -th tool, min;  $K_{st}$  - coefficient taking into account the probability of failure of the tool before the estimated time between failures by tool life;  $n_{bi}$  - the revolution rate of the  $i$ -th tool, corresponding to the basic value of the durability, rpm;  $\bar{n}_{\min i}$  - the calculated revolution rate of the  $i$ -th tool, which provides the specified output cycle, rpm;  $\tau$  - output cycle of the detail, min;  $\mu_i$  - exponent in the dependence of the “cutting speed - tool durability” for basic values of cutting conditions for a specific method of machining.

The probability distribution of tool life in most cases obeys the law of normal distribution, and the coefficient of variation of tool life under normal conditions does not exceed 35%. When machining in the normative ranges of cutting speed and a given probability of no-failure operation  $\gamma = 95\%$ , the coefficient taking into account the probability of failure of the tool before the estimated time between failures by tool life for steel  $K_{st} = 0.85 \dots 0.8$  min and for cast iron  $K_{st} = 0.93 \dots 0.88$  min [10].

## 4 Results

An analysis of the dependence of the operating cost of the tool on its durability for specific tools and tool setup variants showed that the function is monotonically decreasing and, in the case of tool replacement for failures, it is continuous, and for the case of a scheduled replacement of tool it is piecewise-continuous (Fig. 1).

If it is possible to organize the tool replacement on a fixed schedule at points in time  $\{T_{01}, T_{02}, \dots, T_{0m}\}$  for each tool of setup there are many boundary values of durability  $T_{bi} = \{t_{bim} | m = 1 \dots M\}$ , forming the range  $[T_{0m}, t_{bim}]$ , for which the possibility of assigning a more rational value of tool durability is compared to the calculated one. If for the considered tool with  $T_i$  durability there is a range such as

$$T_{0m} \leq T_i < t_{bim}, \quad (2)$$

then it is advisable to replace the tool on a fixed schedule, as in this case, the tool costs correspond to the durability of the scheduled replacement, or

$$C_u = C_{[T_{0m}]} = \text{const when } T_i \rightarrow T_{0m}, \quad (3)$$

and therefore it is possible to optimize the cutting conditions to values, when  $T_i \approx T_{0m}$  (for example, increase cutting speed to ensure durability  $T_{0m}$  while reducing the feed per revolution of the tool), which allows reducing some operation costs of the consumer that to a greater extent depend on the tool feed, at a fixed cost associated with its operation.

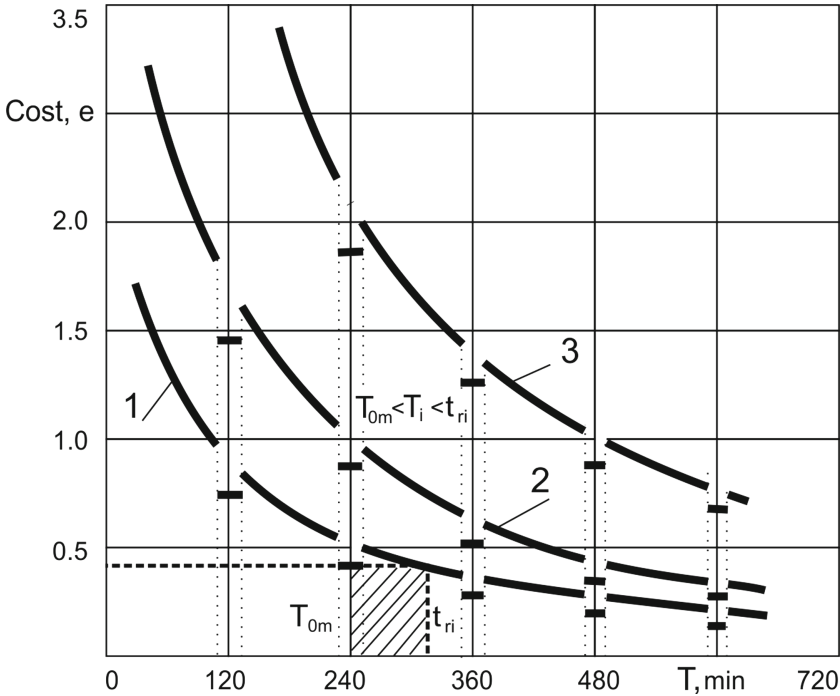


**Fig. 1.** Tool operation costs, depending on its durability in multi-tool processing on a modular machine tool: 1 - drill; 2 - countersink; 3 - reamer.

The operational shutdown schedule of the equipment may differ from the values given in Fig. 1 and can be conformed to the accepted working chart at a particular plant. With a large number of tool groups in the tool block, it is advisable to use different schedules for each group; however, the development of such schedules should be carried out during the operations planning, taking into account the work schedule of other production sections.

In the cases when condition (2) is not satisfied for any range, and also when it is not possible to organize a planned tool replacement, it is more economical to use the entire resource of the tool and replace it in case of failure. Then it is advisable to assign the minimum allowable cutting conditions based on technological, organizational and technical boundary conditions and given productivity.

The value of  $t_{bim}$  and, therefore, the interval  $[T_{0m}, t_{bim}]$  are determined by the share of costs associated with the downtime of the equipment when replacing the tool, and, first of all, depend on the cost of equipment and factors affecting the duration of the direct replacement of tools (such as the design of cartridges, accessibility to the installation zone of the cartridge, the need for additional time to ensure the withdrawal of the tool from the processing zone in the presence of a conductor sleeve, etc.).

This approach allows not only to develop the most rational processing option using tool blocks for an existing tool replacement organization at the enterprise but also to

offer the most effective tool replacement method for a specific processing option, which will further reduce operating costs.

In the case of a planned preventive tool change according to a fixed schedule, it is necessary to select the nearest lower value from the preferred row of values  $T_{0m}$ . Considering the percentage of the cutting time of the  $i$ -th tool in the total operating time of the tool block, it is possible to determine the revolution rate of each  $i$ -th tool based on the equation

$$\tilde{n}_i^{\mu i} - \frac{T_{pi} \cdot T_{bi} \cdot n_{bi}^{\mu i} \cdot \tau \cdot S_i}{(T_{pi} - T_{bi}) \cdot T_{0m} \cdot L_i} \cdot \tilde{n}_i + \frac{T_{bi} \cdot n_{bi}^{\mu i}}{(T_{pi} - T_{bi})} = 0, \quad (4)$$

where  $\tilde{n}_i$  - the calculated revolution rate of the  $i$ -th tool, which provides the specified reliability, rpm;  $S_i$  - feed rate of the  $i$ -th tool, mm/rev;  $L_i$  - cutting length for the  $i$ -th tool, mm.

For tools that do not limit machining, it is necessary to compare the obtained value of the tool revolution rate with the minimum acceptable value for these cutting conditions. The minimum allowable value of cutting speed (revolution rate) is determined for specific machining conditions under which the dependence of the “cutting speed - tool durability” is downward (or the admissible minimum cutting speed conventionally corresponds to the “hump” of the function). In the case when the received value is less than the boundary  $[n]_{\min}$ , the boundary value of the rotational speed is assigned to the tool and the feed value for this tool is adjusted

$$\text{if } \tilde{n}_i < [n]_{\min} \text{ then } S'_i = S_i \cdot \frac{\tilde{n}_i}{[n]_{\min}}; \tilde{n}_i = [n]_{\min}, \quad (5)$$

where  $[n]_{\min}$  - minimum permissible revolution rate of the  $i$ -th tool, rpm;  $S'_i$  - the feed of the  $i$ -th tool, adjusted for the accepted revolution rate, mm/rev. Obtained, from the viewpoint of operating costs, the values of the optimal revolution rates make it possible to determine the final feed values  $S_i$  of the  $i$ -th tool. The corrected feed values in many cases are less than the values obtained at the stages of preliminary calculations, provided that they get within the specified boundaries when metal removal is possible, i.e. machining by cutting.

If the value  $S'_i$  is less than the minimum permissible value, then it is necessary either to change the cutting pass time of the tool block and recalculate the cutting conditions of all tools of the block

$$\text{if } S'_i < [S]_{\min} \text{ then } t_{cp} = t_{cp} \cdot \frac{S'_i}{[S]_{\min}}; S'_i = [S]_{\min}, \quad (6)$$

where  $[S]_{\min}$  - the minimum permissible feed of the  $i$ -th tool, mm/rev;  $t_{cp}$  - the cutting pass time of the tool block corrected for the minimum allowable feed, min.

In those cases, when the calculated characteristics of the speed and feed are less than the corresponding boundary values, it is necessary to change the structure of the association of surfaces for machining using the tool block and completely recount the parameters of all tool blocks.

This approach allows more efficient use of cutting tools, reduce the impact of power factors in the cutting zone (increase the rigidity of the “machine tool - fixture - workpiece - cutting tool” system, extend the lifetime of power units), reduce the cost of electricity, and possibly other items of the technological cost of processing (subject to the rest of the limiting factors).

## 5 Conclusions

For various options of structures of tool blocks of technological layouts of modular machine tools, a quantitative relationship has been established between the parameters of the cutting process, the output cycle of the product and the durability of the cutting tool with various methods of replacing the tool.

A methodology has been developed for determining the parameters of the cutting process when machining parts using tool blocks, based on an analysis of the objective function, which uses the technological cost of processing and, in particular, the costs associated with the operation of the tool.

The proposed methodology for calculating the parameters of the cutting process serves as the basis for a mathematical model for creating a computer-aided design system for the structure and parameters of tool blocks when machining with end-cutting tools in the face of rigid requirements for the product manufacturing cycle and the use of progressive tool block maintenance systems.

This allowed creating a parametric synthesis methodology for the most rational version of the general technological layout of the modular machine tools, taking into account both structural and parametric characteristics of tool blocks, as well as the possibility of their optimization in each specific case. This methodology can be used both in the design of new equipment and in the modernization of previously made machines, built on the concept of modular design.

## References

1. Cakir, M.C., Gürarda, A.: Optimization of machining conditions for multi-tool milling operations. *Int. J. Prod. Res.* **38**(15), 3537–3552 (2000)
2. Baskar, N., Asokan, P., Prabhakaran, G., et al.: Optimization of machining parameters for milling operations using non-conventional methods. *Int. J. Adv. Manuf. Technol.* **25**(11–12), 1078–1088 (2005)
3. Ahmed Alwaise, A.M., Usubamatov, R., Zain, Z.M.: Optimization of multi-tool machining process. *Aust. J. Basic Appl. Sci.* **5**(9), 2111–2119 (2011)
4. Levin, G., Rozin, B., Dolgui, A.: Optimization of multi-tool cutting modes in multi-item batch manufacturing system. In: 7th IFAC Conference on Manufacturing Modelling, Management, and Control (MIM 2013), vol. 46, no. 9, pp. 766–771. IFAC Proceedings Volumes, Saint Petersburg, Russian Federation (2013)
5. Usubamatov, R., Zain, Z.M., Sin, T.C., Kapaeva, S.: Optimization of multi-tool machining processes with simultaneous action. *Int. J. Adv. Manuf. Technol.* **82**(5–8), 1227–1239 (2016)

6. Levin, G.M., Rozin, B.M., Steblinskaya, O.I.: Optimization of dynamically variable cutting modes of batch processing on multi-position multi-tool equipment. *Informatics* **4**, 91–99 (2014). (in Russian)
7. Ivanov, V., Dehtiarov, I., Pavlenko, I., et al.: Parametric optimization of fixtures for multiaxis machining of parts. In: Hamrol, A., Kujawinska, A., Barraza, M. (eds.) *Advances in Manufacturing II, Vol 2 – Production Engineering and Management. Lecture Notes in Mechanical Engineering*, pp. 335–347. Springer, Cham (2019). [https://doi.org/10.1007/978-3-030-18789-7\\_28](https://doi.org/10.1007/978-3-030-18789-7_28)
8. Karpus, V.E., Ivanov, V.A.: Universal-composite adjustable machine-tool attachments. *Russ. Eng. Res.* **28**(11), 1077–1083 (2008)
9. Gilman, A.M., Gostev, G.V., Egorov, Y., et al.: *Computer-Aided Design of Optimal Settings for Metal-Cutting Machine Tools*, 1st edn. Mashinostroenie, Moscow (1984). (in Russian)
10. Danilenko, B.D.: Some issues of rationing cutting conditions. In: *University Proceedings. Mechanical Engineering*, vol. 6, p. 352. Mashinostroenie, Moscow (2004). (In Russian)
11. Igumnov, B.N.: *Calculation of Optimal Cutting Conditions for Machine Tools and Automatic Lines*, 1st edn. Mashinostroenie, Moscow (1974). (in Russian)
12. Timofeev, Yu.V., Yakovenko, I.E., Permyakov, A.A., et al.: Optimization synthesis of instrumental adjustments during multi-transition processing on special equipment. *Collect. "Cutt. Tools"* **49**, 26–31 (1994). (in Russian)
13. Rai, J.K., Brand, D., Slama, M., Xirouchakis, P.: Optimal selection of cutting parameters in multi-tool milling operations using a genetic algorithm. *Int. J. Prod. Res.* **49**(10), 3045–3068 (2011)
14. Levin, G., Rozin, B., Dolgui, A.: Optimization of multi-tool cutting modes for batch manufacturing in large series machining environment. In: *14th IFAC Symposium on Information Control Problems in Manufacturing (INCOM 2012)*, vol. 45, no. 6 part 1, pp. 444–448. IFAC Proceedings Volumes, Bucharest, Romania (2012)
15. Gasanov, M., Kotliar, A., Basova, Y., Ivanova, M., Panamariova, O.: Increasing of lathe equipment efficiency by application of gang-tool holde. In: Hamrol, A., Grabowska, M., Maletic, D., Woll, R. (eds.) *MANUFACTURING 2019. LNCS*, vol. 3, pp. 133–144. Springer, Cham (2019)
16. Kotliar, A., Basova, Y., Ivanova, M., Gasanov, M., Sazhniev, I.: Technological assurance of machining accuracy of crankshaft. In: Diering, M., Wieczorowski, M., Brown, C. (eds.) *MANUFACTURING 2019. LNCS*, vol. 5, pp. 37–51. Springer, Cham (2019)

# **Smart Manufacturing and Industry 4.0 Strategy**



# Methods for Modeling Urban Road Traffic Using Timed Automata

Camelia Avram<sup>1</sup>(✉), Jose Machado<sup>2</sup>, and Adina Aștilean<sup>1</sup>

<sup>1</sup> Technical University of Cluj Napoca,  
28, Strada Memorandumului, 400114 Cluj Napoca, Romania  
camelia.avram@aut.utcluj.ro

<sup>2</sup> Universidade do Minho, Campus de Azurém, 4800-058 Guimarães, Portugal

**Abstract.** Among the whole range of resources for a good economic and social life of a country, the transport system performs a key role. The efficiency of the country's street network will be central for further developments or will determine its stagnation. With the continuous increase in the number of vehicles and the effect of urbanization, traffic-roads are suffering different solicitations and utilizations for which they were not prepared, sized and projected. Due to the extreme importance of traffic-roads, research must be initialized to reduce the effects of traffic-jams in the streets, size the optimal number of traffic-lanes, and the information about the real-time traffic conditions needs to be implemented in Global Position Systems. The real-time data integration, flexibility, and the extensibility of the models and computational costs were other important aspects considered during the process of developing the models. The proposed TCA-Traffic Cellular Automata-model has appropriate results in the urban traffic theory. The results obtained in different scenarios were simulated and formally verified in the simulation/formal verification environment UPPAAL.

**Keywords:** Traffic control · Timed automata model · Computer simulation · Formal verification

## 1 Introduction

Over the last years, special attention has been given to the modelling of traffic congestion and jams, these becoming ubiquitous daily events for most residents of large cities. The fluctuations in the average speed affect the scheduled time of the trip, lead to excessive fuel consumption at low speeds and, implicitly, to excessive CO<sub>2</sub> emissions. Due to the high density of traffic, there is an increased probability of collisions and accidents even if the speed is not high. In the nearest future, because of the permanent increase in the population and, consequently, the number of vehicles, a rapid worsening of the situation is expected to occur in the conditions in which the development of an infrastructure that could solve the congestion problem will be a long process. The usage of public and alternative means of transport together with adequate scheduling of work for different categories of inhabitants, as well as the implementation of intelligent control systems, could partially solve the problem [1].



Real situations which could lead to oversaturated traffic conditions should be highlighted to predict and prevent such events and to ensure efficient traffic management. For these purposes, a comprehensive analysis of common and/or specific circumstances and factors generating traffic congestion in a multitude of cities of different countries is needed, a lot of recent and older studies being accomplished in this direction.

In previous studies, a considerable variety of models was proposed to capture realistic conditions of urban road traffic, several relevant results being presented in [2–5]. The system’s complexity, its functionalities, and particular restrictions, the specific entities and speeds are only some of the most important factors that were taken into account in different modelling cases. The integration of real-time data, the flexibility, and the extensibility of the models, as well as the computational costs, were other important aspects considered during the process of developing the models.

Noting that congestion is an inevitable consequence of urban motorized areas, in [6], Sole-Ribalta et al. highlight the necessity to model and understand the congestion phenomena, and propose a model to predict the behavior of networks after the onset of congestion.

In [7], Kesting and Treiber investigate the possible contributions of reaction time, update time and adaptation time to instabilities of traffic flow, and consider the finite velocity adaptation time as a source of string instabilities leading to oscillating congested traffic.

An approach with the advantage of using easily accessible inputs is presented in [8]. The authors calculate the travel time on each segment of a route, and, using these results and the free flow time, determine the predicted travel time to identify eventual congestion.

Considering that congestion is determined by both micro-level and macro-level factors, the authors of [9] carried out a comprehensive review of the existing practices regarding the identification of traffic congestion in different countries, identification of the congestion measurement metrics, congestion measurement methodologies and inconsistencies, finally suggesting a range of features for a measure of congestion.

Even if the multitude of studies contributed to certain progress in this research direction, in most cases, the capacity of many proposed models to describe and analyze traffic behavior in complex networks is tested insufficiently, the consequence is the inability of the system to reflect specific situations.

Motivated by the above considerations and using an approach proposed in [10], the present paper brings a contribution to identify the causes and characteristics of traffic congestion in some points of interest of a crowded city. The proposed formal verification is based on a two-layered modelling technique using timed automata and the UPPAAL environment, as a model-checker adapted to verify the system behavior [11].

## 2 Literature Review

### 2.1 Cellular Automata

A cellular automaton (CA) is a mathematical model for dynamic systems that evolves via discrete steps. It is appropriate to natural model systems that can be described as a massive collection of simple objects interacting locally with each other. Cellular automata provide a basic model for complex systems that are generated by a simplistic set of rules [12].

CA consists of a finite and regular grid of cells; each one can have a finite number of states, ranging according to the deterministic rules that include the states of neighborhood cells. The grid can be any finite number of dimensions. Time is also discretized and the state of a cell at the time  $t$  is a function of the state at the time  $t-1$  from a finite number of cells in its neighborhood. This neighborhood corresponds to a particular selection of adjacent cells (which may include the cell itself). All cells progress according to the same updating rule based on the values of their neighboring cells. Each time the rules are applied to the entire grid, a new generation is produced [13].

Cellular automata have been (or could be) applied in an extensive range of computing areas, such as mathematics, physics, theoretical biology and microstructure modelling [14]. Cellular automata are commonly used in models of traffic flow and pedestrians, fluids (gases or liquids), the evolution of cells or viruses such as HIV, image processing and random number generation [12].

CA offer many advantages over standard computing architecture such as:

- *Implementation*: CA requires very few wires;
- *Scalability*: It is easy to upgrade a CA by adding other cells;
- *Robustness*: CA continues to perform even when a cell is faulty because the local connectivity property helps to contain the error [15].

### Road layout and the physical environment

When the cellular automaton analogy is applied to vehicular road traffic flows, the physical environment of the system represents the road the vehicles are driving on. In a classic single-lane setup for traffic cellular automata, the layout consists of a one-dimensional grid. Each cell can either be empty or occupied by exactly one vehicle (single-cell models). Another possibility is to allow a vehicle to occupy several consecutive cells (multi-cell models) [16].

An example of the time-space dynamics of TCA is represented in Fig. 1, where two consecutive vehicles “ $i$ ” and “ $j$ ” are driving on a 1D grid. A typical discretization scheme assumes  $\Delta t = 1$  s and  $\Delta x = 7.5$  m corresponding to speed increments of  $\Delta v = \Delta x / \Delta t = 27$  km/h. The spatial discretization corresponds to the average length that a vehicle occupies in a traffic-jam. (In this context, its width is not considered). The temporal discretization is based on a typical driver’s reaction time [17].

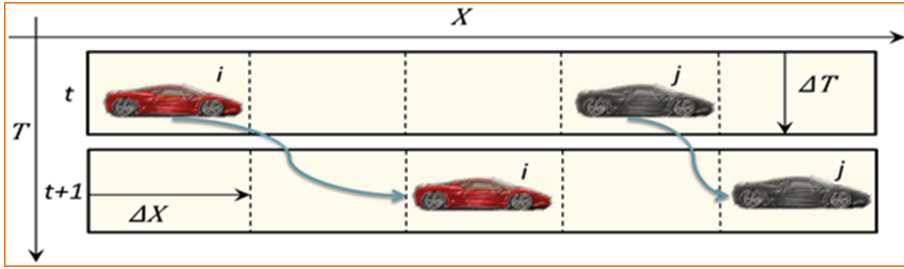


Fig. 1. The time-space dynamics of TCA.

### Vehicle movements and the set of rules

The circulation of individual vehicles in traffic flow is described by a set of rules that reflects the car-following and lane-changing behavior, evolving in time and space. This set of rules included in TCA is consecutively applied to all vehicles in parallel. The system's state is changed through synchronous position updates of all vehicles: for each vehicle, the new speed is calculated, after its position is updated according to its new speed, and, finally, a possible lane-change maneuver is considered. It is furthermore assumed that a driver does not react to events between consecutive time iterations.

For single traffic-lane models, it is assumed that vehicles act as anisotropic particles, i.e., they only respond to frontal stimuli. The car-following stimuli are the states of the direct frontal neighborhood of each vehicle. The radius of this neighborhood should be large enough so that vehicles can move without collisions. Typically, this radius is equal to the maximum speed that a vehicle can achieve, expressed in cells per time step [18].

## 2.2 Timed Automata

An automaton is a device that recognizes a determinate language, having states which represent situations of a system [19]. If the number of states is finite, the automaton is called finite, in the other case is termed infinite.

To include time variables, in [20], the theory of the finite automata was changed and the concept of timed automata was developed. In this context, the time was modelled discretely. A timed automaton is a finite automaton with a finite set of time values.

During a run of a timed automaton, clock values increase all at the same speed, along with the transitions of the automaton. The clocks can be reset to zero (independently of each other) in the transition of the automaton, keeping the time elapsed since the last reset.

Timed automata can be used to model and analyse the timing behavior of computer systems, i.e., real-time systems or networks. Methods for checking both safety and liveness properties have been developed and intensively studied.

### 2.3 Selection of Timed Automata

A large number of formalisms can be used to model timed systems. Timed automata were adopted as the modelling formalism for modelling due to two main reasons: first, the study of the proposed traffic-system proposed needs to take time into account; and, second, it is the input formalism of the UPPAAL model-checker [21].

The extension of timed automata implemented in UPPAAL allows a more detailed modular modelling, because it is a formalism with a low modelling capacity, hence it can generate basic models. Moreover, it is a software available for free, which can be simulated and formally verified in the same environment, without having to convert models between simulation and formal verification being UPPAAL, which well adapted to the formal verification of timed systems.

## 3 Research Methodology

### 3.1 Road Traffic Modeling Issues

The formalism adopted for modelling the systems considered is Timed Automata (TA). Also, because the UPPAAL simulation and verification environment will be used for performing the simulation and formal verification analysis techniques, those models were edited using the editor of this software tool.

In this section, the model presented in [10] is used with some updates (regarding the size of the map, performances and feature optimization).

### 3.2 High Complexity Models

If applied to models with a high level of complexity or large traffic-scenarios, the basic models previously proposed in the literature cannot be easily changeable or reused due to various limitations.

To solve these limitations, models based in matrices were created to model the traffic-environment. A matrix is a compact data structure that can be easily extendable and can function as a map of street cells.

The matrices implemented in these models to model the road traffic environment have the following features:

- Each line corresponds to an independent traffic lane of a street.
- The value present in column number one corresponds to the number of cells that each street has.
- The following columns are fulfilled with empty street cells or traffic elements.

Due to UPPAAL's limitations, it is not possible to create vectors or arrays with different sizes and some of the values present in this matrix have no significance.

One of the key aspects of creating good traffic road models is to define in a precise and unambiguous way the streets that will be studied with all relevant information for correct vehicular circulation.

The case study considered in the simulation is a small group of roads in the downtown city of Cluj-Napoca, Romania, containing the maximum traffic-elements that a street can have.

This section details the physical environment of the simulation, describing the street (number, direction, and length of traffic-lanes), the location of crosswalks, bus stations, and tram stations, railways where the tram moves, the intersections between streets, and the operational mode of traffic lights for road, rail and pedestrian traffic.

In Fig. 2 is presented the street network considered for this simulation. The total network length is approx. 4000 m and this simulation contains eighteen crosswalks, eight intersections, thirty eight traffic-lanes for automobiles and 26 lines of buses, and two pathways for tram movement, ten traffic-lights for drivers and ten traffic-lights for pedestrians, eight bus stops and two tram stops, as well as two parking areas.

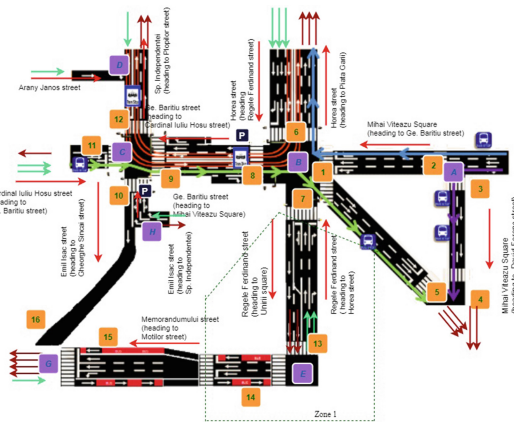


**Fig. 2.** The simulated map – first scenario.

Three simulation scenarios were considered: in the first one, the map is as it is presented into the figure, in the second one dedicated bus lanes were added (by transforming the regular lanes into public transportation only, Fig. 3) and the third one (using Fig. 3) is considered using different schedules for public transportation (the first with a bus coming every 10 min, and the second one with a bus coming every 5 min). The “Zone 1” from Fig. 2 is modified and is presented in Fig. 3. Each street is described based on the model described in [10]. To implement the considered map, 80 traffic-lanes, 580 automobiles, 38 buses, and 18 trams were declared. After, the traffic elements and the predefined routes for buses and trams were implemented. The time needed to travel between intersections 6 and 15 by car increases (a lower value is in the first scenario where no dedicated bus lanes are implemented), for public transportation the time decreases thank to the use of a dedicated bus lane and implementing a more frequent schedule to add comfort for travelers.

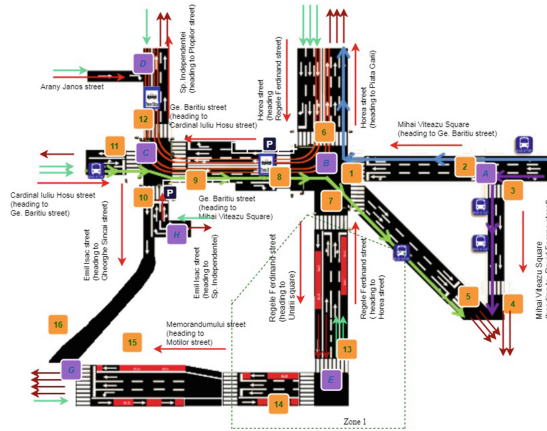


**Fig. 3.** The simulated map – second scenario.

## 4 Results

All simulations were done in the version of UPPAAL 4.1.18 (rev.5444), Academic and non-commercial use. The options used in all simulations and verifications were the following:

Search order: depth first; because it is a search strategy that will search all the possible ways, and not only the fast path.

State Space Reduction: Conservative; which reduces the number of states to be searched, and consumes less memory when a large system is simulated.

State Space Representation: DBM; is the fastest way to get the reachable state, but increases the memory used.

Diagnostic Trace: None;

Extrapolation: Automatic;

Hash table size: 16 MB; because it reduces the memory consumption.

The computer used in all the simulation and validation queries has the following hardware features: Intel Core i7, processor 3940 which means 8 processors 3.7 GHz each, 16 GB of memory and the storage memory of a hard drive with the 7200 speed.

### Formal verification of the model

In what follows it is enough to know that, in the UPPAAL version the logic,  $A$  is the universal quantifier on paths (for any path . . .),  $E$  is the specific quantifier on paths (there is a path. . .),  $\square$  the universal quantifier over states in a path (for any state ...) and,  $\langle \rangle$  the specific quantifier over states in a path (there is a state...). The tables below briefly present the used validation queries, all were run for each automobile, bus or tram (Tables 1, 2, 3, 4 and 5). A java program was created to generate a file with queries to be validated into UPPAAL.

**Table 1.** Testing for each automobile if the time needed to pass each street is between the minimum and maximum value allocated.

Description	Properties	Result
	Greater than a minimum value	
Test the value of the time for each automobile on street 0.	E[] forall (i : idA) automobile(i).time_per_street(0) > 0.5 * indexSC[0][0]	Yes
	E <> forall (i : idA) automobile(i).time_per_street(0) > 0.5 * indexSC[0][0]	Yes
...		

Testing the above properties for each vehicle in part (automobiles in Table 2, buses in Table 3 and trams in Table 4).

Testing if the time needed to pass a cell is smaller or greater than a predefined value, or is in a fixed interval, in Table 5.

**Table 2.** Automobiles.

Description	Properties	Result
	Greater than a minimum value	
Test the value of the time for automobile (0) on street (0)	E[] automobile(0).time_per_street(0) > 0.5 * indexSC[0][0]	Yes
	E <> automobile(0).time_per_street(0) > 0.5 * indexSC[0][0]	Yes
	E[] automobile(0).time_per_street(0) < 27 * indexSC[0][0]	Yes
	E <> automobile(0).time_per_street(0) < 27 * indexSC[0][0]	Yes
	E[] (automobile(0).time_per_street(0) > 0.5 * indexSC[0][0]) && (automobile(i).time_per_street(0) < 27 * indexSC[0][0])	Yes
	E <> (automobile(0).time_per_street(0) > 0.5 * indexSC[0][0]) && (automobile(0).time_per_street(0) < 27 * indexSC[0][0])	Yes
...		

**Table 3.** Buses.

Description	Properties	Result
	Greater than a minimum value	
Test the value of the time for a bus (0) on street (0)	E[] bus(0).time_per_street(0) > 0.5 * indexSC[0][0]	Yes
	E <> bus(0).time_per_street(0) > 0.5 * indexSC[0][0]	Yes
	E[] bus(0).time_per_street(0) < 27 * indexSC[0][0]	Yes
	E <> bus(0).time_per_street(0) < 27 * indexSC[0][0]	Yes
	E[(bus(0).time_per_street(0) > 0.5 * indexSC[0][0]) && (bus(i).time_per_street(0) < 27 * indexSC[0][0])]	Yes
	E <> (bus(0).time_per_street(0) > 0.5 * indexSC[0][0]) && (bus(0).time_per_street(0) < 27 * indexSC[0][0])	Yes
...		

**Table 4.** Tram.

Description	Properties	Result
	Greater than a minimum value	
Test the value of the time for the tram (0) on street (0)	E[] tram(0).time_per_street(0) > 0.5 * indexSC[0][0]	Yes
	E <> tram(0).time_per_street(0) > 0.5 * indexSC[0][0]	Yes
	E[] tram(0).time_per_street(0) < 27 * indexSC[0][0]	Yes
	E <> tram(0).time_per_street(0) < 27 * indexSC[0][0]	Yes
	E[(tram(0).time_per_street(0) > 0.5 * indexSC[0][0]) && (tram(i).time_per_street(0) < 27 * indexSC[0][0])]	Yes
	E <> (tram(0).time_per_street(0) > 0.5 * indexSC[0][0]) && (tram(0).time_per_street(0) < 27 * indexSC[0][0])	Yes
...		

**Table 5.** The time needed to pass a cell.

Description	Properties	Result
	Greater than a minimum value	
Testing the time needed for automobile 0 to pass a cell in a street	E[] automobile(0).time_per_cellA[0] < 27	Yes
	E[] automobile(0).time_per_cellA[0] > 1/2	Yes
	E[] ((automobile(0).time_per_cellA[0] > 1/2) && (automobile(0).time_per_cellA[0] < 27))	Yes
...		



## 5 Conclusions

The cellular automata allow observing different phenomena, manage to dissect its components in individual variables, and to understand how local changes affect the whole grid of cells.

The main goal of this work was to create a systematic approach for a complex urban traffic scenario, and the structure implemented has the potential to be further developed. This systematic approach can be extendable in an easy and unlimited way, the only limitation being the computational power available. This versatility is reached with the compact environment that the matrices provide, and the elementary modules implemented for modelling all the traffic-elements and possible interactions in the traffic scenario.

In the context of formal verification, this model presents all possible scenarios that can occur, even the ones that are physically impossible, and the results presented are in order of the maximum level of permissiveness.

## References

1. Ahmed, A.H.: A review of adaptive intelligent traffic control systems. *J. Res. Bus. Soc. Sci.* **1**(1), 14–23 (2018)
2. Tian, Z., Jia, L., Dong, H., Su, F., Zhang, Z.: Analysis of urban road traffic network based on complex network. *Procedia Eng.* **137**, 537–546 (2016)
3. Zambrano-Martinez, J.L., Calafate, C.T., Soler, D., Cano, J.C., Manzoni, P.: Modeling and characterization of traffic flows in urban environments. *Sensors (Basel)* **18**(7) (2018)
4. Mardiyati, R., Ismail, N., Faroqi, A.: Review of microscopic model for traffic flow. *ARPN J. Eng. Appl. Sci.* **9**(10), 1794–1800 (2014)
5. Rahman, M., Chowdhury, M., Xie, Y., He, Y.: Review of microscopic lane-changing models and future research opportunities. *IEEE Trans. Intell. Transp. Syst.* **14**(4), 1942–1956 (2013)
6. Sole-Ribalta, A., Gomez, S., Arenas, A.: A model to identify urban traffic congestion hotspots in complex networks. *R. Soc. Open Sci.* **3**(10) (2016)
7. Kesting, A., Treiber, M.: How reaction time, update time, and adaptation time influence the stability of traffic flow. *Comput. Aided Civil Infrastruct. Eng.* **23**(2), 125–137 (2008)
8. Jain, S., Jain, S.S., Jain, G.: Traffic congestion modelling based on origin and destination. *Procedia Eng. Elsevier* **187**, 442–450 (2017)
9. Rao, A.M., Rao, K.R.: Measuring urban traffic congestion – a review. *Int. J. Traffic Transp. Eng.* **2**(4), 286–305 (2012)
10. Valente, E., Avram, C., Machado, J., Astilean, A.: An innovative approach for modelling urban road traffic using timed automata and formal methods. *J. Adv. Transp.* (2018)
11. Behrmann, G., David, A., Larsen, K.G.: A tutorial on uppaal, in formal methods for the design of real-time systems. *Lecture Notes in Computer Science*, vol. 3185, pp. 200–236. Springer (2004)
12. Fidel Román, F.A.: *Autómata celular*. Universidad Cesar Vallejo, Peru (2019)
13. de Almeida, C.M., Vieira Monteiro, A.M., Câmara, G., Soares-Filho, B.S., Cerqueira, G.C., Pennachin, C.L., Batty, M.: *Empiricism and Stochastics in Cellular Automaton Modeling of Urban Land Use Dynamics*. Centre for Advanced Spatial Analysis London, UK (2003)
14. Eppstein, D.: *Growth and Decay in Life-Like Cellular Automata*. In: Adamatzky, A. (ed.) *Game of Life Cellular Automata*. Springer, London (2010)

15. Lemont, B.K., Seybold, P.G., Cheng, C.K.: Modeling of Chemical Systems using Cellular Automata. Published in Springer VIII (175) (2005)
16. Nagel, K.: Particle hopping models and traffic flow theory. *Phys. Rev.* **53**(5), 4655–4672 (1996)
17. Nagel, K., Schreckenberg, M.: A cellular automaton model for freeway traffic. *J. de Physique I, France* **2**, 2221–2229 (1992)
18. Maerivoet, S., Moor, B.D.: Transportation planning and traffic flow models. *Phys. Rep.* **419** (1), 1–64 (2005)
19. Montgomery, E.: *Introdução aos Sistemas de Eventos Discretos e à Teoria de Controle Supervisório*, Alta Books (2005)
20. Alur, R., Dill, D.L.: A theory of Timed Automata. *Theoret. Comput. Sci.* **126**, 183–235 (1994)
21. Behrmann, G., David, A., Larsen, K.G.: A tutorial on UPPAAL. In: *Proceedings of the 4th International School on Formal Methods for the Design of Computer, Communication, and Software Systems (SFM-RT 2004)* (2004)



# Object Recognition Using Neural Networks for Robotics Precision Application

Giampiero Celenta<sup>1</sup>(✉) and Domenico Guida<sup>2</sup>

<sup>1</sup> MEID4 Academic Spin-Off of the University of Salerno,  
Via Giovanni Paolo II, 132, 84084 Fisciano, SA, Italy  
giampiero.celenta@libero.it

<sup>2</sup> Department of Industrial Engineering, University of Salerno,  
Via Giovanni Paolo II, 132, 84084 Fisciano, SA, Italy

**Abstract.** The fourth industrial revolution is based on the fusion of different technologies and, in particular, between machines and information, and encourages companies to integrate new tools in their production processes to improve working conditions and increase productivity and production quality of companies. The future of production, therefore, depends on increasingly intelligent machinery through the use of digital systems. Intelligent machines and systems are the key elements for future integrated infrastructures based on human-machine interaction and information sharing. This sharing requires the implementation of shared languages that allow different systems to dialogue in a simple way. With this in mind, the ability of machines or systems to learn new operations through the use of algorithms based on neural networks allows us to have increasingly flexible machines capable of replicating the learning processes of human beings. Such self-learning techniques will allow developing a new class of machines capable of revolutionizing our companies.

**Keywords:** Object detection · Learning systems · Unmanned vehicles · Feed-forward controllers · Ultrasonic sensors

## 1 Introduction

The fourth industrial revolution is the process that will lead to fully automated and interconnected industrial production [1, 2]. In this context, the new digital technologies will have a profound impact in the four development fields: the first is the use of data, computing power and connectivity, and is declined in big data, open data, Internet of Things, machine-to-machine and cloud computing for the centralization of information and its conservation [3, 4]. The second is analytics: once the data is collected, we need to derive its value [5]. Today, only 1% of the data collected is used by companies, which could instead obtain advantages from “machine learning”, i.e. from machines that improve their performance by “learning” from the data gradually collected and analyzed [6]. The third direction of development is the interaction between man and machine, which involves the increasingly widespread “touch” interfaces and augmented reality [7, 8]. Finally, there is a whole sector that deals with the transition from digital to “real”, including additive manufacturing, 3D printing, robotics,

communications, machine-to-machine interactions and new technologies for storing and using energy in a targeted way, rationalizing costs and optimizing performance [9]. In this context, the use of open-source design [9, 10] and simulation software [11, 12] is constantly expanding thanks to many benefits such as the development that often happens ahead of others in terms of technologies, stable and secure solutions [13]. Another non-trivial aspect is the cost of a project based on open source software that is overall advantageous compared to proprietary software [14, 15]. Every open-source product can be the result of the work of tens, hundreds or thousands of developers across the world [16]. Each point is treated by a specialist and the implementation of old and new technologies is very rapid [17, 18].

## 2 Literature Review

It will always be available and updated by the developer community, unlike commercial software whose life is linked to the manufacturer's commercial choices [19, 20]. A good example of new technologies is the development of new open-source software that allows testing new designs and architectures for robots in simulation, reducing development time and costs for new systems [21]. In the field of robotics, the new middleware ROS (Robot Operating System), is the new open-source tool for robotic applications [22]. Most of the users are found in research laboratories but, in recent years, the adoption of ROS has been gradually moving to the commercial sectors, in particular to industrial robots and service robots, such as domestic robots [23]. This environment, as an operating system, works mainly as a messaging structure and has many already made libraries to manage sensors and actuators to get data from the surrounding, to use such data purposely and to control actuators to interact with the environment [24]. Robotics capabilities such as autonomous navigation or motion planning in mobile robots or manipulators are already integrated methods in ROS [25]. SLAM (Simultaneous Localization and Mapping) and AMCL (Adaptive Monte Carlo Localization), are already implemented in the Navigation stack and MoveIt package and are highly configurable through fine-tuning parameters, ready to use capabilities for almost any robotics implementation [25]. Such characteristics have been already used in Neural Network projects, basically using the communication structure of a classical ROS implementation as an integrator [26]. A good dynamic model is critical for the development of optimal control systems [27]. Most multibody software allows us to create models from CAD files, thus allowing to obtain very detailed models based on which control laws can be designed [28]. The Applied Mechanics group of the Department of Industrial Engineering of the University of Salerno has long used the 3D design software Solidworks for creating detailed rigid multibody models for the proprietary SimScape environment and the open-source Gazebo environment [29]. On the other hand, the use of low-cost electronic components makes it possible to obtain good models using identification techniques, based on which optimal control laws can be designed [30]. As for most of the multibody software, Gazebo also creates detailed robots by using CAD files in the XML or DAE format [31]. Most multibody simulation software considers systems made up of rigid bodies, but it is possible to study the behavior of flexible multibody systems by using ANCF techniques [32, 33]. The idea is

to design retrofitting devices for vehicles already present on the market for making autonomous agricultural machines [34]. In this case, our goal will be to retrofit a petrol engine tracked vehicle for precision agriculture applications in vineyards [35]. The vehicle must be able to recognize the support poles and vine plants inside the vineyard and must be able to navigate within the rows, analyzing the shape of the vineyard, the number of poles and plants, the vegetative state of the vines, etc. [36, 37]. In this paper, we report the investigation activity on the use of ultrasonic sensors and artificial intelligence techniques to identify objects [38]. In Sect. 2, we describe the test-rig used for our preliminary experimental activity and the inverse dynamics analysis conducted on a multibody model of the UGV for evaluating the feed-forward voltage needed for the desired trajectory [39]. In the same section, we report the training process of the neural network for object detection, while Sect. 3 reports the result of the activities carried out by the robot [40]. In the final section, we present our conclusions.

### 3 Research Methodology

The rover used for this activity is an Unmanned Ground Vehicle or UGV, a small differential drive robot used for testing new control methods and Identification techniques [41]. The UGV is driven by two EMG30, 12 V DC motors fully equipped with encoders and a 30:1 reduction gearbox. The motors are connected to an MD25, a dual motor driver, that, through the use of a PWM signal, allows the onboard controller to actuate the robot. On the rear, a tilting wheel allows the robot to move limiting slippage of the driving wheels. The chassis of the vehicle is made of methyl methacrylate. All onboard devices are powered by a 12 V – 7 Ah lead-acid rechargeable battery. The onboard controller installed on the vehicles is an Arduino Galileo, microcontroller board based on the Intel Quark SoC X1000 Application Processor, a 32-bit Intel Pentium-class system on a chip. The processor is a 400 MHz 32-bit Intel Pentium processor with 512 Kbytes of embedded SRAM [42]. It is designed to support shields that operate at either 3.3 V or 5 V and has 14 digital I/O pins, 6 of which can be used as PWM outputs. In Fig. 1, we reported the retrofitted tracked vehicle and a navigation scheme of the activities that the retrofitted vehicle will have to perform inside the vineyard [43].

The robot must be able to advance avoiding the obstacles constituted by the support poles and the vine plants and navigate within the rows. A scheme of the possible trajectories is reported in Fig. 1(a). The tracked vehicle is a tracked dumper Mini-transporter Tekna TT350 (see Fig. 1(b)) equipped with two rubber tracks driven by a 2 HP 4 Strokes petrol engine. The system is also provided with a safety lever, two levers for the distribution of torque to the sprockets and the accelerator. On the vehicle, there is a hydraulic system with mineral oil kept under pressure by a pump actuated by a 12 V electric motor [44]. For the retrofitting activity, we decided to remove the dumper bucket and to use the hydraulic system for controlling the machine. All the control levers that are actuated by steel cables have been properly connected to the solenoid group to steer the machine using PWM (pulse-width modulation) signals. The voltage supplied by the Arduino microcontroller individual I/O ports is 5 V. For this reason, it was necessary to design and build in our laboratory a power board to actuate the hydraulic actuators. The microcontroller used for controlling the machine is an Arduino

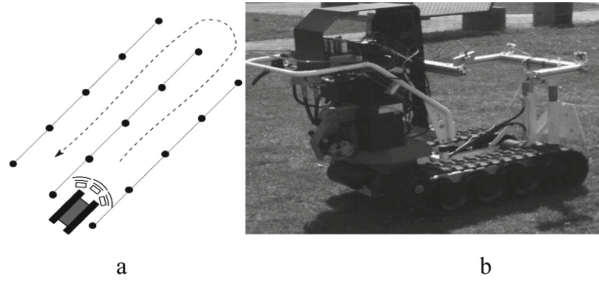


**Fig. 1.** Retrofitted tracked vehicle and navigation scheme for the vineyard.

Galileo with an SoC X1000 Application Processor, a 32-bit Intel Pentium-class system on a chip. It is designed to support shields that operate at either 3.3 V or 5 V and has 14 digital I/O pins, 6 of which can be used as PWM outputs. The processor is a 400 MHz 32-bit Intel Pentium processor with 512 Kbytes of embedded SRAM. For detecting obstacle proximity, sensors have been installed to stop the tracked vehicle in case of danger. In particular, ultrasonic low-cost sensors capable of detecting obstacles from 1 cm up to 4 m will be used. For this reason, we decided to investigate the use of ultrasonic sensors for object recognition [45].

Accurate modelling takes time, but it allows to make the cinematic and dynamic study that derives from it more effective. 3D models obtained by using appropriate design software, allow defining, in a very accurate way, the properties of mass and geometry, to evaluate the inertial forces and torques of the bodies and the feed-forward control laws for desired trajectories [46]. For this analysis, SolidWorks software was used, which allowed reproducing the real vehicle in a 3D environment [47].

The multibody model is made by importing the geometry into the calculation software Matlab-Simulink, as reported in Fig. 2(a). To do so, it is necessary to install the SimMechanics plugin whose task is to connect the 3D design software to the Matlab software. Once the trajectory and the desired law of motion have been decided, it is possible to calculate the equivalent inertia of the whole vehicle. We have therefore developed a model of the EMG30 engine considering both the electric and the mechanical dynamics. The model is reported in Fig. 2(b). The purpose was to find the low voltage for the engines according to the chosen laws of motion. From the simulation carried out, we found that, for the speed values requested by the robot, the relationship between the input voltage and output speed can be considered constant.

The hypothesis made for the numerical simulation is a pure rolling condition for the driving wheels [48].

The second goal of this research is motivated by two desires: to obtain a better understanding of the human brain, and to develop computers that can deal with abstract and poorly defined problems [49]. Generally, a network is formed by three layers called the input layers, the hidden layer, and the output layer. Each layer consists of one or more nodes represented by the small circles in the diagram, while the arrows between the nodes indicate the information flows between the layers. Input layer nodes are also called passive nodes because they do not change input data, but they receive and duplicate data for their multiple outputs, as for the hidden layers, as for the output

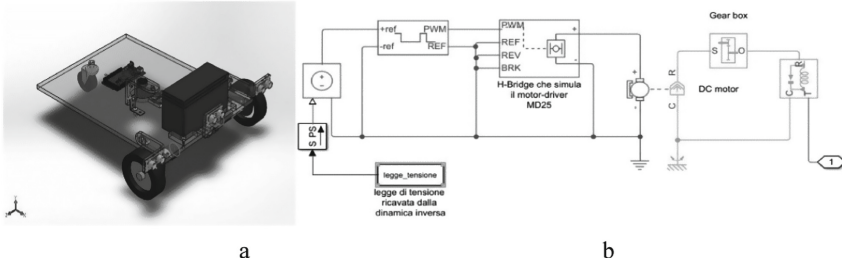


**Fig. 2.** The multibody model and the electro-mechanical model of the actuator.

layers which are both active nodes. For this activity, we decided to use the ultrasonic sensors installed on the front of the vehicle for object recognition.

The SRF05 sensor has a claimed detection distance range that goes from 2 cm–450 cm with a precision of 2 mm. The ultrasonic sensor detects the echo by listening for the returning wavefronts. This echo has an attack/decay envelope, which means it builds up to a peak and then fades away. Depending on which wavefront is the 1st to be strong enough to be detected, which could be the 1st, 2nd or even 3rd, the results can vary widely.

The first part of the study involved acquiring the data measured by the ultrasonic sensors. The objects that the rover must be able to recognize are the cone, the cube, and the wall. To allow the robot to recognize such objects from any angle, measurements were obtained by randomly shifting the relative position of the three objects, with respect to the four ultrasonic sensors (see Fig. 3). In total, 5000 measurements were made to provide a reliable network. As a result, output units are made up of column vectors.

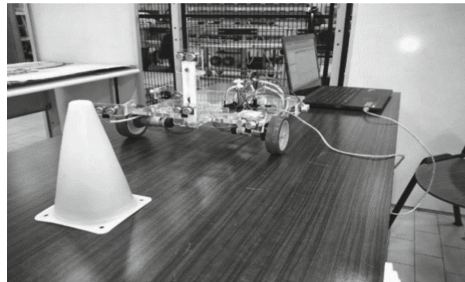


**Fig. 3.** The data acquisition process for the cone geometry.

Therefore, for the cone, we will have the vector  $h_{\theta}(x) \approx [1\ 0\ 0\ 0]^T$ , for the cube the vector  $h_{\theta}(x) \approx [0\ 1\ 0\ 0]^T$  and for the wall the vector  $h_{\theta}(x) \approx [0\ 0\ 1\ 0]^T$ . So, given the training set  $\{(x^{(1)}, y^{(1)}), (x^{(2)}, y^{(2)}), \dots, (x^{(m)}, y^{(m)})\}$ , we used the Matlab neural network tool to design, train and display the neural network to be loaded later on the on-board controller. Machine learning typically works with three large randomly

sampled data sets. The largest one should be the training set. Such data teaches the net how to weigh different features, assigning coefficients to minimize training errors. Such coefficients, known as meta-data, are contained into vectors. Compared to the totality of the data acquired by the ultrasonic sensors, we divided them into three classes as reported in Table 1. The network that we used for the object detection problem is a two-layer feed-forward network, with a sigmoid transfer function both in the hidden layer and in the output layer. The number of neurons in the hidden layer is set to 500. The number of neurons in the output layer is set to four since it is the number of elements of the target vector.

**Table 1.** Data distribution for neural network training

Total data	5000 samples
Training set	3500 samples
Validation set	1250 samples
Testing set	1250 samples

## 4 Results

Figure 4 shows the comparison between a straight and a curvilinear desired trajectory with the actual trajectories followed by the rover during the experimental activities.

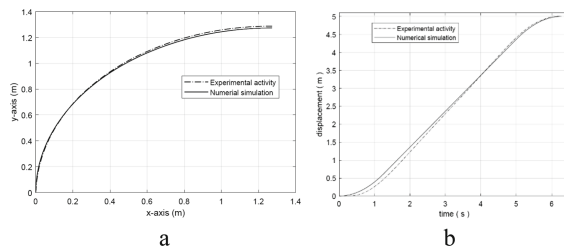


**Fig. 4.** Comparison of trajectories of the numerical model with the real system: a) curvilinear trajectory, b) linear trajectory.

Low advancing speeds were used to replicate the same condition during the experimental activity. As it is possible to notice, in Fig. 4(a) and in Fig. 4(b) the feed-forward laws allow the UGV to follow the desired trajectories. Obviously, in the case of the rover, the experimental tests were conducted in the laboratory on a rigid plane. The case of the tracked vehicle that will operate on a deformable terrain will be different. In that case, it will be necessary to take into account the deformation of the land according to the laws of the Terramechanics.

Within this activity, the aim was to test the effectiveness and practicality of using neural network-based algorithms to identify obstacles by using low-cost ultrasonic sensors. By analyzing the confusion matrix, reported in Fig. 5, we understand that in



1299 cases the cone was detected correctly, corresponding to 39.4% of cases. In 800 cases, equal to 24.2%, the cube was detected correctly, while in 600 cases the wall was detected correctly, corresponding to 18.2% of total cases. 400 wall scans were incorrectly classified as a cube, corresponding to 12.1% of all acquisitions.

		1	2	3	
Output Class	1	1299 39.4%	0 0.0%	0 0.0%	100% 0.0%
	2	0 0.0%	800 24.2%	400 12.1%	66.7% 33.3%
	3	1 0.0%	200 6.1%	600 18.2%	74.9% 25.1%
		99.9% 0.1%	80.0% 20.0%	60.0% 40.0%	81.8% 18.2%
		1	2	3	Target Class

Fig. 5. Confusion matrix.

Similarly, in 200 cases the cube is incorrectly classified as a wall. Finally, from the confusion matrix, we understand that the cone is correctly recognized in 100% of cases. Out of 1200 cube predictions, 66,7% of them are correct and, for the wall, 74,9% of 801 wall predictions are correct. To increase the accuracy of the network, we can choose to use multiple layers or use multiple sensors (sensor fusion techniques) to better identify the differences between the geometries analyzed.

## 5 Conclusions

This paper is aimed at the evaluation of the use of low-cost ultrasonic sensors for navigation application and to test the use of neural networks for the identification of objects. A small UGV was used to test the potential of such techniques. A multibody model of the UGV was created using the Solidworks and Matlab calculation software. In particular, in the Simulink environment, a model of the EMG30 engine was developed to evaluate the voltage required for predetermined motion laws, taking into account the robot’s inertia. Subsequently, ultrasonic sensors SRF05 were tested for detecting objects. The data collected by the four sensors on the front of the robot has been used for training the neural network to recognize a cone, a cube, and flat walls. To test the effectiveness of the neural network, an exploration and recognition activity was conducted. The procedures described in this work will be implemented on the retrofitted tracked vehicle for precision agriculture applications.

## References





1. Vega, J., Cañas, J.M.: Open vision system for low-cost robotics education. *Electronics* **8**(11), 1295 (2019)
2. Pappalardo, C.M., Patel, M.D., Tinsley, B., Shabana, A.A.: Contact force control in multibody pantograph/catenary systems. *Proc. Inst. Mech. Eng. Part K: J. Multi-body Dyn.* **230**, 307–328 (2016)
3. Lages, W.F.: Parametric identification of the dynamics of mobile robots and its application to the tuning of controllers in ROS (2017). <https://doi.org/10.1007/978-3-319-54927-96>
4. Dewi, C., Chen, R.-C.: Decision making based on IoT data collection for precision agriculture. *Stud. Comput. Intell.* **830**, 31–42 (2020)
5. Pappalardo, C.M., Patel, M., Tinsley, B., Shabana, A.A.: Pantograph/catenary contact force control. In: *ASME 2015 International Design Engineering Technical Conferences and Computers and Information in Engineering Conference*. American Society of Mechanical Engineers Digital Collection, Boston, Massachusetts, USA, 2–5 August, pp. 1–11 (2015)
6. Iticha, B., Takele, C.: Digital soil mapping for site-specific management of soils. *Geoderma* **351**, 85–91 (2019)
7. Meghanathan, N., Skelton, G.W.: Risk notification message dissemination protocol for energy efficient broadcast in vehicular ad hoc networks. *IAENG Int. J. Comput. Sci.* **37**(1), 1–10 (2010)
8. Uslu, E., Akmak, F., Altunta, N., Marangoz, S., Amasyal, M.F., Yavuz, S.: An architecture for multi-robot localization and mapping in the Gazebo/robot operating system simulation environment. *Simulation* **93**(9), 771–780 (2017)
9. Darweesh, H., Takeuchi, E., Takeda, K., Ninomiya, Y., Sujiwo, A., Morales, L.Y., Kato, S.: Open source integrated planner for autonomous navigation in highly dynamic environments. *J. Robot. Mechatron.* **29**(4), 668–684 (2017)
10. Prieto, S.A., Adán, A., Vázquez, A.S., Quintana, B.: Passing through open/closed doors: a solution for 3D scanning robots. *Sensors* **19**(21), 4740 (2019)
11. Portugal, D., Araújo, A., Couceiro, M.S.: A guide for 3D mapping with low-cost sensors using ROS. *Stud. Comput. Intell.* **831**, 3–23 (2020)
12. Shaqura, M., Shamma, J.S.: A multicopter design software tool for automated generation of simulation and visualization models. *Lect. Notes Electr. Eng.* **495**, 451–474 (2020)
13. Post, M.A., Bianco, A., Yan, X.T.: Autonomous navigation with open software platform for field robots. *Lect. Notes Electr. Eng.* **495**, 425–450 (2020)
14. Vithalani, S., Soni, S., Rajpura, P.: Autonomous navigation using monocular ORB SLAM2. *Lect. Notes Electr. Eng.* **618**, 59–68 (2020)
15. Wang, T., Guan, X.: Research on obstacle avoidance of mobile robot based on multi-sensor fusion. *Adv. Intell. Syst. Comput.* **928**, 760–770 (2020)
16. Pappalardo, C.M., Wang, T., Shabana, A.A.: Development of ANCF tetrahedral finite elements for the nonlinear dynamics of flexible structures. *Nonlinear Dyn.* **89**, 2905–2932 (2017)
17. Steckenrider, J.J., Furukawa, T.: Multi-dimensional belief fusion of multi-Gaussian structures. *Inf. Fusion* **57**, 71–88 (2020)
18. Silano, G., Iannelli, L.: CrazyS: a software-in-the-loop simulation platform for the Crazyflie 2.0 nano-quadcopter. *Stud. Comput. Intell.* **831**, 81–115 (2020)
19. Alvarado Vázquez, B.P.E., Matía, F.: A tour-guide robot: moving towards interaction with humans. *Eng. Appl. Artif. Intell.* **88**, 103356 (2020)
20. Vилlecco, F.: On the evaluation of errors in the virtual design of mechanical systems. *Machines* **6**, 36 (2018)

21. Formato, A., Ianniello, D., Romano, R., Pellegrino, A., Vilecco, F.: Design and development of a new press for Grape Marc. *Machines* **7**, 51 (2019)
22. Formato, G., Romano, R., Formato, A., Sorvari, J., Koironen, T., Pellegrino, A., Vilecco, F.: Fluid-structure interaction modeling applied to peristaltic pump flow simulations. *Machines* **7**, 50 (2019)
23. Formato, A., Ianniello, D., Pellegrino, A., Vilecco, F.: Vibration-based experimental identification of the elastic moduli using plate specimens of the olive tree. *Machines* **7**, 46 (2019)
24. Sena, P., Attianese, P., Pappalardo, M., Vilecco, F.: FIDELITY: fuzzy inferential diagnostic engine for on-line support to physicians. In: Proceedings of the 4th International Conference on the Development of Biomedical Engineering in Vietnam, Ho Chi Minh City, Vietnam, 8–10 January 2012, pp. 396–400 (2012)
25. Sena, P., D’Amore, M., Pappalardo, M., Pellegrino, A., Fiorentino, A., Vilecco, F.: Studying the influence of cognitive load on driver’s performances by a fuzzy analysis of lane keeping in a drive simulation. *IFAC Proc.* **46**, 151–156 (2013)
26. Sena, P., Attianese, P., Carbone, F., Pellegrino, A., Pinto, A., Vilecco, F.: A fuzzy model to interpret data of drive performances from patients with sleep deprivation. *Comput. Math. Methods Med.* **2012**, 868410 (2012)
27. Zhang, Y., Li, Z., Gao, J., Hong, J., Vilecco, F., Li, Y.: A method for designing assembly tolerance networks of mechanical assemblies. *Math. Probl. Eng.* **2012**, 513958 (2012)
28. Vilecco, F., Pellegrino, A.: Evaluation of uncertainties in the design process of complex mechanical systems. *Entropy* **19**, 475 (2017)
29. Colucci, F., De Simone, M.C., Guida, D.: TLD design and development for vibration mitigation in structures. *Lect. Notes Netw. Syst.* **76**, 59–72 (2020)
30. Guida, R., De Simone, M.C., Dašić, P., Guida, D.: Modeling techniques for kinematic analysis of a six-axis robotic arm. *IOP Conf. Ser.: Mater. Sci. Eng.* **568**(1), 012115 (2019)
31. Rivera, Z.B., De Simone, M.C., Guida, D.: Unmanned ground vehicle modelling in Gazebo/ROS-based environments. *Machines* **7**(2), 42 (2019)
32. De Simone, M.C., Rivera, Z.B., Guida, D.: Obstacle avoidance system for unmanned ground vehicles by using ultrasonic sensors. *Machines* **6**, 18 (2018)
33. Concilio, A., De Simone, M.C., Rivera, Z.B., Guida, D.: A new semi-active suspension system for racing vehicles. *FME Trans.* **45**, 578–584 (2017)
34. Naviglio, D., Formato, A., Scaglione, G., Montesano, D., Pellegrino, A., Vilecco, F., Gallo, M.: Study of the grape cryo-maceration process at different temperatures. *Foods* **7**, 107 (2018)
35. Martinez, J.L., Moràn, M., Morales, J., Rein, A.J., Zafra, M.: Field navigation using fuzzy elevation maps built with local 3D laser scans. *Appl. Sci.* **8**(3), 397 (2018)
36. Pappalardo, C.M.: A natural absolute coordinate formulation for the kinematic and dynamic analysis of rigid multibody systems. *Nonlinear Dyn.* **81**, 1841–1869 (2015)
37. De Simone, M.C., Guida, D.: Identification and control of a unmanned ground vehicle by using Arduino. *UPB Sci. Bull. Ser. D* **80**, 141–154 (2018)
38. Patel, M.D., Pappalardo, C.M., Wang, G., Shabana, A.A.: Integration of geometry and small and large deformation analysis for vehicle modelling: chassis, and airless and pneumatic tyre flexibility. *Int. J. Veh. Perform.* **5**, 90–127 (2019)
39. De Simone, M.C., Guida, D.: Control design for an under-actuated UAV model. *FME Trans.* **46**, 443–452 (2018)
40. Kulkarni, S., Pappalardo, C.M., Shabana, A.A.: Pantograph/catenary contact formulations. *J. Vib. Acoust.* **139**, 011010 (2017)
41. Pappalardo, C.M., Yu, Z., Zhang, X., Shabana, A.A.: Rational ANCF thin plate finite element. *J. Comput. Nonlinear Dyn.* **11**, 051009 (2016)

42. Słomiany, M., Dąbek, P., Trojnacki, M.: Motion planning and control of social mobile robot – part 1. Robot hardware architecture and description of navigation system. *Adv. Intell. Syst. Comput.* **920**, 513–523 (2020)
43. De Simone, M.C., Guida, D.: Modal coupling in presence of dry friction. *Machines* **6**(1), 8 (2018)
44. Pappalardo, C.M., Zhang, Z., Shabana, A.A.: Use of independent volume parameters in the development of new large displacement ANCF triangular plate/shell elements. *Nonlinear Dyn.* **91**, 2171–2202 (2018)
45. De Simone, M.C., Rivera, Z.B., Guida, D.: Finite element analysis on squeal-noise in railway applications. *FME Trans.* **46**, 93–100 (2018)
46. Quatrano, A., De Simone, M.C., Rivera, Z.B., Guida, D.: Development and implementation of a control system for a retrofitted CNC machine by using Arduino. *FME Trans.* **45**, 565–571 (2017)
47. Pappalardo, C.M., Wang, T., Shabana, A.A.: On the formulation of the planar ANCF triangular finite elements. *Nonlinear Dyn.* **89**, 1019–1045 (2017)
48. Li, H., Lei, Z., Zhang, N.: UAV target location based on multi-sensor fusion. *Lect. Notes Electr. Eng.* **594**, 637–644 (2020)
49. Pappalardo, C.M., Wallin, M., Shabana, A.A.: A new ANCF/CRBF fully parameterized plate finite element. *J. Comput. Nonlinear Dyn.* **12**, 031008 (2017)



# Big Challenges of Small Manufacturing Enterprises in Industry 4.0

Sergey Dobrotvorskiy<sup>1</sup> , Yevheniia Basova<sup>1</sup> ,  
Ludmila Dobrovolska<sup>1</sup> , Yevgeny Sokol<sup>1</sup>,  
and Nikolay Kazantsev<sup>2</sup> 

<sup>1</sup> National Technical University “Kharkiv Polytechnic Institute”,  
2, Kyrpychova St., Kharkiv 61002, Ukraine  
e. v. basova. khpi@gmail.com

<sup>2</sup> Alliance Manchester Business School, Booth St W, Manchester M15 6PB, UK

**Abstract.** In the paper, the problems of small manufacturing enterprises, which limit the pace of their development in the face of the current trend in the development of digital technologies were considered. The analysis of information solutions of world leaders involved in the development of Industry 4.0 in the field of open application development is presented. The development trends of Industry 4.0 for small enterprises are described. As a greater homogenization of information technology and software in various small manufacturing enterprises, it is proposed to use the approach developed in JavaMach Cluster, which based on a modular ERP system. A userfriendly interface that allows access to the internal databases of such manufactures is presented to create more homogeneous information technology and software for small machinery manufacturing enterprises. Justified assessment of the effectiveness of the graphical interface connected to the databases of small machinery manufacturing enterprises. The issues related to the formation of unified information flows in the workspace of the modern sector of the economy of small manufacturing enterprises. The basic principles of creating and using non-dissonant databases of such enterprises in the formation of virtual companies are identified. Using the example of an included in the ERP-system module of rolled metal choice, we demonstrated a way to solve the problems of small machinery manufacturing enterprises under the development of Industry 4.0.

**Keywords:** Virtual company · Modular ERP-system · Pre-production engineering · Interface · Database · JavaMach Cluster

## 1 Introduction

The Industry 4.0 concept has a set of modern technologies for the industry (Internet of Things, Big Data, robotics, virtual reality, and much more), the use of which is aimed at creating a new generation of manufacture systems [1]. As of today, companies still solve the problems associated with creating the basic conditions for Industry 4.0. Consequently, the path of development starts with the digitalization. Although digitalization itself is not part of Industry 4.0, information and connectedness are essential

requirements for its implementation. These two initial stages are followed by four other stages with the development of the characteristics necessary for Industry 4.0. Informatization is the first stage on the path of development, as it represents the basis for digitalization. At the stage of connectedness, interrelated elements replace the separate penetration of information technologies. At the third stage - the visualization stage, a digital model of the company is formed. The integration of PLM, ERP and MES systems provides a comprehensive picture that allows seeing the current state of affairs [2, 3]. The integration of CAD, CAE, CAM, CAPP systems is presented in the research of the developing CAFD system [4]. Also, modular approaches and applications can help create a single source of reliable data. The next stage helps the company understand why certain events occur and use this information to gain the necessary knowledge by analyzing the root causes [5–9].

In the new Industry 4.0 paradigm, computer systems should be more integrated and connected than at present. It means that for all areas of the business from the manufacture and the supply chain to the final consumer, full integration and coherence will be required. This coherence should offer the best service and quality throughout the product value chain. This integration should also cover different departments of the company’s internal architecture to induce greater unity, which can bring significant value to the business. At modern enterprises, hierarchical information infrastructures are treated with the strictest. At the top levels is the enterprise resource planning system (ERP) and product life management system (PLM), below which are manufacturing execution systems and directly production departments (MES (manufacturing execution system) and NC/PLC (numerical controller/programmable logic controller)), CRM (Customer Relationship Management), PDM (Product Data Management), CAPP (Computer-Aided Process Planning), CAE (computer-aided engineering), CAM (computer-aided manufacturing), CAD (computer-aided design/drafting), and in the lowest are sensor systems and peripheral equipment of the company facilities. The leading system integration has traditionally occurred in the horizontal direction, not vertically. A modern look at the development of Industry 4.0 requires enhanced integration both vertically and inter-level integration both in single machinery manufacturing enterprise and between different machinery manufacturing enterprises to be able to quickly concerted efforts to implement orders. From the above, Fig. 1 could be deduced.

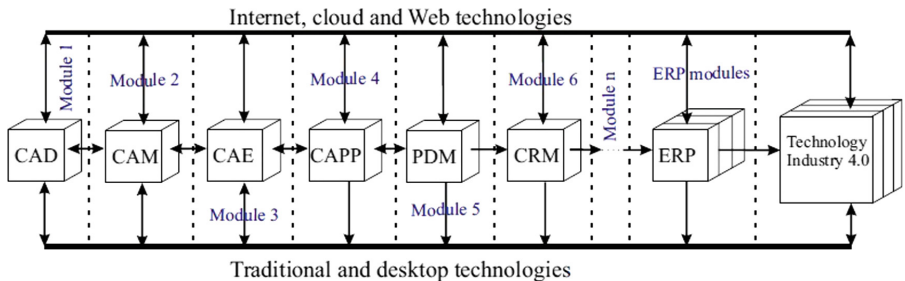


**Fig. 1.** Interaction of the internal structure of a small machinery manufacturing enterprise with technologies of Industry 4.0.

It can be seen that horizontal integration is the central line, which consists of simple, free, open-source programs (applications). Moreover, vertical integration is carried out on the modularization concept, where each module interacts with Industry 4.0 technologies and traditional technologies (for example, CAD module has the following structure: in the center is FreeCAD, the cloud component is OnShape, the traditional component is SolidWork).

The central problem of implementing the Industry 4.0 concept for a small machinery manufacturing enterprise is the digitize all stages of manufactures production (CAD/CAM/CAE/CAPP), management (PDM, PLM), marketing and customer relationship management (CRM), overall coordination (ERP) and full product life cycle (PLC) with a single information and software platform.

The objective of this research is to analyze problems in IT and software services in small machinery manufacturing enterprises, which prevents transition towards Industry 4.0 and to discuss possible ways of solving them.

## 2 Literature Review

In terms of integration raising of small machinery manufacturing enterprises with Industry 4.0 and enhance vertical integration between these small enterprises in establishing partnerships, the following problems exist in the area of data and software [10]: difficulties with real-time data exchange; use of semi-structured data transfer formats; use of information systems without standardized data transfer interfaces; use of various information systems; lack of standards and user-interfaces for communication; information asymmetry; the lack of data on the benefits of networking; the lack of information on advanced technologies (Industry 4.0). However, the cost of such integration is critical for small machinery manufacturing enterprises., It can be reduced through the use of open and free information management and software.

From an analysis of the current state of the issue, we determined that at present, world leaders involved in the development of Industry 4.0 tend to develop open applications for small enterprises too.

One of the leading developers in the field of IoT (Internet of Things) is the Predix Platform - the cloud platform as a service (PaaS) for the industrial Internet from General Electric [11]. Predix is built on Cloud Foundry, which is, an open-source platform implementation that helps lower development costs. Cloud Foundry supports the software life cycle from initial development through every step from testing to implementation. Since the Predix platform connects machines, data, people, and other assets, it uses advanced technology for distributed computing, Big Data analysis, the asset management database, and the interaction between computers. The platform provides a broad spectrum of industrial microservices that available to enable enterprises to improve productivity.

Another successful platform is SAP [12]. Especially for small and medium-sized enterprises ERP S/4 HANA or SAP Business One solutions have been developed. By default, five sections are predefined in SAP Business ONE: the main page, finance, sales, purchases, services. Unfortunately, the program is not open.

However, the success of individual companies and platforms cannot solve the common problems of Industry 4.0. Currently, there comes an understanding of the have to follow the path of open information and software technologies and creating synergies among many companies (such as small manufacturing enterprises), as the tasks of Industry 4.0 are very complex.

Bosch argues that as Industry 4.0 moves from potential to reality, it is clear that no company or manufacturing organization (especially the small and medium-sized) can't do this alone [13]. Industry 4.0 solutions are highly dependent on the ability to involve both a technical and organizational point of view throughout the segmented value chains that bring together providers and manufacturers. Open standards are critical to the realization of manufactures' common interests. Industry 4.0 marks the beginning of the end for a proprietary web interface. Bosch Rexroth strongly supports international standards. Industry 4.0 also crosses the scope of existing technologies, and one of the most striking examples is Bosch's Open Core Engineering technology, which builds the bridge between automation and information technology.

It is very promising is the project that started recently from German Machine Tool Builders - Umati [14]. This project involves creating a connection and ensuring a seamless language for machines, systems, and software, simple, fast and secure the exchange of data, which are essential to take advantage of digitalization on the manufacturing. (OPC UA standard).

An important step is also the creator of the establishment of the European SmartFactory network - EU EWIV [15].

However, with the rapid advancement of Industry 4.0 by large companies, behind them have left many deficiencies, especially for small manufacturing enterprises that have to be filled. Some companies, including us, are considering this approach. Examples of successful solutions, in our view, are ANT CMMS and DIGICOR.

Company [16] bridges the gaps between ERP-system and other business systems. ANT CMMS provides a comprehensive overview of all maintenance, including: scheduled and upcoming maintenance, manufacturing plan, replacements, etc. For more efficient work, it is possible to create a personalized view with concrete management actions, such as switching, troubleshooting, calibration, maintenance, saving, predictive maintenance. In parallel with the software/hardware solutions, the company is developing a specification for integrating the developed system with existing systems such as ERP. The advantage is the availability of a unitary, integrated, sectoral policy software solution MES and ERP – IQMS' manufacturing software.

The complete existing problems of cooperative issues of small manufacturing enterprises for solving manufacturing problems were traced when creating an open tender Internet platform DIGICOR [17], which is designed for improved integration of small machinery manufacturing enterprises modeled on virtual interim companies.

The implementation approach based on artificial neural networks [18], deep-learning [19], augmented reality [20, 21], and virtual reality [22] to the solutions for Industry 4.0 has the first-priority significance.

One can use the approach developed in JavaMach Cluster [23] when information technology and software are developed based on Java and Java technologies as a greater homogenization of information management and software in various small machinery manufacturing enterprises.



### 3 Research Methodology

Our innovative teams have developed several applications for improving the business of small machinery manufacturing enterprises that combine the flexibility of spreadsheets with the traceability and stringent expected from an integrated business system.

From the analysis of a huge number of tasks in the engineering process of virtual manufacture, the choice of workpiece and tool is highlighted to the fore. A justified and optimal choice of the rolled steel already at this stage lays the formation of the competitive cost of the finished product. This will reveal the fundamentals of enabling for the formation of flexible virtual manufacturing, depending on the initial client's prerequisites and the capabilities of the executors.

At the first stage of ensuring the formation of the facilities of flexible virtual manufacturing, small machinery manufacturing enterprises are faced with the problem of integrating real-time data exchange interfaces. Consequently, it raises the issue of competitiveness of small manufacturing enterprises in the market that arises due to the inability to work in an interface that can connect to the databases of such small manufacturing enterprises. As a solution to this problem, we have created a clear graphical user interface. According to the concept of a modular ERP system presented earlier [23], Java tools were used to implement the user interface, namely, the NetBeans IDE software environment with JDK applications. To simplify the process of implementing the user interface, Java Swing libraries were used. The reasons for choosing JavaSwing are a rich set of interface primitives; the appearance that is configured to various platforms (look and feel); separate model-view architecture; native HTML support.

The presented graphical user interface can connect to databases of small machinery manufacturing enterprises. However, there is a danger of encountering the problem of information asymmetry due to the work of small machinery manufacturing enterprises with different information systems, or the problem of information closure by sources due to problems of industrial espionage, which makes it impossible to check the delivered information quality, etc. immediately.

To solve such problems and to increase the degree of cooperation of small machinery manufacturing enterprises in the formation of virtual companies, we needed to identify the main conditions for the pre-production engineering for the execution of the order at its planning stage. The role of analysis and the optimal choice of material, its processing method, type of metal-cutting equipment and tools have been identified, which, in turn, became the main idea for the development of databases (modules) connected to the developed user interface.

At the stage of developing a database as an embedded unit of modular ERP system [23], we faced the task of preparing and structuring data for inclusion in a future flexible database. It is important to note that in the developed databases, the properties of each material, the characteristics of equipment and tools must be edited locally by the user. At the next stage of database development, we had to structure the data for correct and understandable display in the developed users' interface.

As an example, in this work, a database of a rolled metal product range connected to a developed user interface is presented. The proposed solution covered information on the type of structural section, the name of the assortment standard, rolled steel size, and accuracy tolerance of rolled steel. It is worth noting that for the formation of the structure of virtual companies from many small industries, it is crucial to provide timely and accurate information about tolerances on the basic dimensions of the rolled steel, which affects the final decision on the choice of rolled steel and, as a result, on the formation of the final cost of the manufactured product. Thus, for each of the selected parameters in the database (where we highlighted “document name”, “processing type” and “section shape” as the main data), a special column is highlighted, since this facilitates work with the data and allow them to implement calculate and search methods not only by name but also by properties. For example, using the proposed users’ interface and the database connected to it, the end-user, when choosing the stage executor, will be able to implement a section shape search system based on the choice of standard, which will entail the need of choice for processing type. Thus, the employer has an idea of the real final cost of the future product already at the stage of planning the structure of a virtual company, and, accordingly, its competitiveness.

## 4 Result

For developing more homogeneous informational support and software, the following graphical user interface was created (Fig. 2).

The main function of such interface is the prompt referral to databases with the request of a user who does not have special education in the area of information technology and does not have high qualifications. At the same time, the user can analyze many variants offered by potential elements of a virtual company (small machinery manufacturing enterprises) and choose the optimal one that provides the best solution.

To this end, such interface requires connecting to a large number of databases (Fig. 2) of small machinery manufacturing enterprises. The enterprises should have a homogeneous information structure, information support, software, and join efforts in achieving their development s through effective cooperation of small machinery manufacturing enterprises.

One of the main results of this work is the presentation of one module’s structure of the modular ERP system - the rolled steel selection module (Fig. 3). To ensure the competitiveness of a small machinery manufacturing enterprise in the formation of a virtual company, it is necessary to have not only a homogeneous database structure but also a homogeneous structure of communication links and services offered. So, when forming the assortment (rolled steel) database, we took into account tables of accuracy classes, sizes (in which data on simple and complex assortment forms are stored), sub-sizes, process tolerances. The relationship is organized by creating sequential database table relationships. When adding a new table to the structure, a new entity was created, which includes information about all previous. Such a relationship allowed us to make

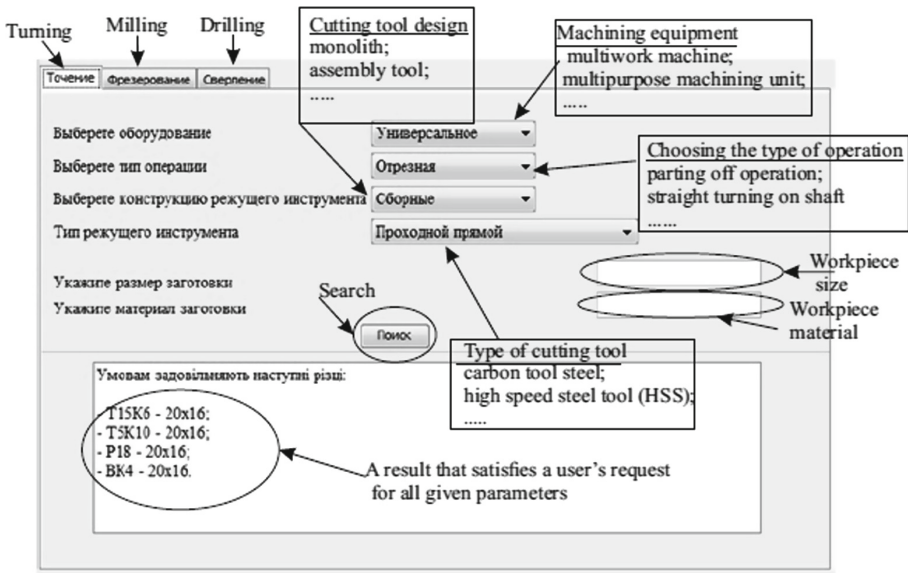


**Fig. 2.** Visualization of graphical user interfaces for the formation of a flexible structure of a virtual company.

the database as simple as possible, since when adding a new table, the number of join tables, and with them, the complexity of the database, increase in arithmetic progression. Also, in addition to creating the database structure and for standard work with it, the task of correctly organizing the process of recording and obtaining information was solved at work.

Note that for the connection of the main tables, it is necessary to add the corresponding identifiers of the main entities to the connection table. Already at this stage, the manual filling of the tables is too long. Also, there is susceptible to errors due to the human factor. In total, to record only one size, consisting of two sub-sizes, it is necessary to create six relates and write ten links to identifiers. It makes a recording of only one size extremely difficult, and recording of all sizes containing a standard is time-consuming and virtually impossible without errors.

The obvious solution of this problem was to automate the filling of tables and their relationships. For this, the necessary services were created at the server level using stored procedures. Such procedures are a set of SQL commands that are compiled and stored on the server. This decision made the database relatively universal for use by various programs since a client needs a minimal amount of information to communicate with the server. Besides, when using a remote server, minimizing the amount of information for communication can reduce the amount of traffic transmitted to speed up the program's performance and, most importantly, would help to reduce the chance of crashes and errors.

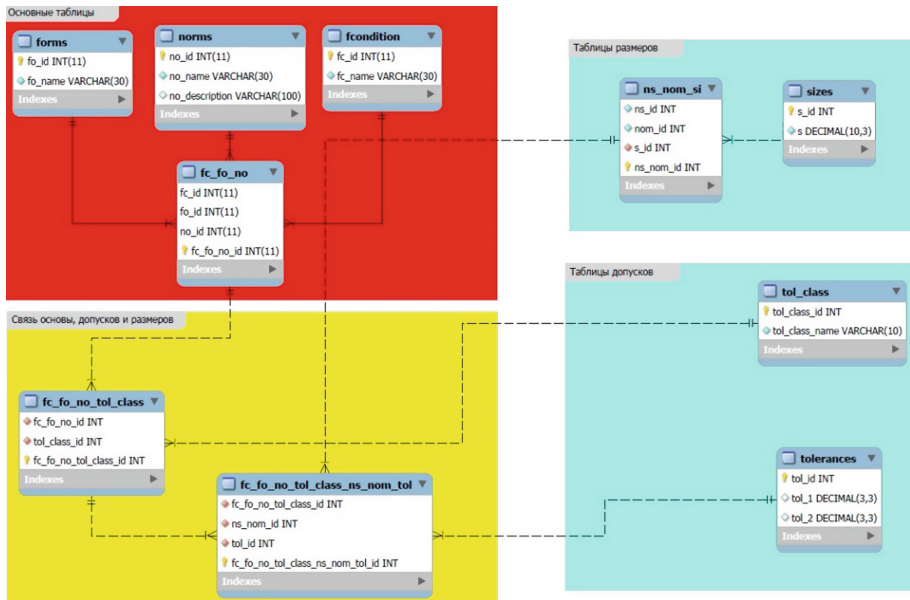


**Fig. 3.** The structure of the database selection of assortment (rolled steel).

Thus Fig. 3 shows a graph of communication technologies when solving a request sent through the users' interface. We use technology to receive information from the user.

Further data received from the user falls into the layer of business logic where we process the request. Then, according to the request, the program searches for the necessary information in the database. It passes it back to the business logic that changes the program interface at the same time and displays the required data.

In this program, it was decided to use a non-direct connection of business logic programs with a database, and to use a layer of intermediary, this level of abstraction allows us not to think about exactly how we need to send queries to the database. The important advantage of this framework is that we do not need to know SQL to work with the database server.

## 5 Conclusion

Industry 4.0 is still a lot of large companies. The role of small ones (as small machinery manufacturing enterprises) is still ahead. The new tasks of leading companies are to solve the problems associated with the creation of basic conditions for Industry 4.0. Accordingly, the development path starts with digitalization, and the basic requirements for its implementation are informatization and connectedness, visibility and permeability. The methodology for creating a single digital space, which integrates the stages of digitalization, informatization has been developed. It connected tasks within the framework of the concept of I. 4.0, which we call Free digital space for I. 4.0

(FGS2I4.0). One of the main goals of FGS2I4.0 was to search for the possibility of integrating PLM, ERP, CRM, which was made possible through the development of modular applications by small interdisciplinary teams based on Java MachCluster.

Hundreds of companies currently represent various kinds of services. Company research was not our goal, but analysis of Industry 4.0 development trends for small machinery manufacturing enterprises.

As a result of our teamwork, a user-friendly interface was created to allow accessing internal databases of small manufacturing enterprises. This interface enables creating more uniform information support and software, which in the conditions of development of small manufacturing enterprises will reduce financial and time costs in the formation of virtual companies.

Working with such a user's interface does not require high qualifications and special education in the areas of information technology by users.

## References

1. Smit, J., Kreutzer, S., Moeller, C., Carlberg, M.: Industry 4.0. Document No. IP/A/ITRE/2015-02. 1st end. European Parliament, Brussels (2016)
2. Pozdneev, B., Tolok, A., Ovchinnikov, P., Kupriyanenko, I., Levchenko, A., Sharovатов, V.: Digital transformation of learning processes and the development of competencies in the virtual machine-building enterprise environment. In: 5th International Scientific and Practical Conference on Virtual Simulation, Prototyping and Industrial Design 2018, 012008. IOP Publishing, Tambov State Technical University, Russian Federation (2019)
3. Trabesinger, S., Pichler, R., Schall, D., Gfrerer, R.: Connectivity as a prior challenge in establishing CPPS on basis of heterogeneous IT-software environments. In: 9th Conference on Learning Factories, CLF 2019, vol. 31, pp. 370–376. Procedia Manufacturing, Braunschweig (2019)
4. Ivanov, V., Vashchenko, S., Rong, Y.: Information support of the computer-aided fixture design system. In: Proceeding of 12th International Conference on ICT in Education, Research and Industrial Applications, ICTERI 2016, vol. 1614, pp. 73–86. CEUR-WS, Ukraine (2016)
5. Schuh, G., Potente, T., Thomas, C., Hauptvogel, A.: Steigerung der Kollaborationsproduktivität durch cyberphysische Systeme. In: Bauernhansl, T., ten Hompel, M., Vogel Heuser, B. (eds.) Industrie 4.0 in Produktion, Automatisierung und Logistik, Wiesbaden, pp. 277–296. Springer, Fachmedien (2014)
6. Afshari, L., Gibson, P.: How to increase organizational commitment through transactional leadership. *Leader. Organ. Dev. J.* **37**(4), 507–519 (2016)
7. Hadian Nasab, A., Afshari, L.: Authentic leadership and employee performance: mediating role of organizational commitment. *Leader. Organ. Dev. J.* **40**(5), 548–560 (2019)
8. Moones, E., Vosgien, T., Kermad, L., Dafaoui, E.M., El Mhamedi, A., Figay, N.: PLM standards modelling for enterprise interoperability: A manufacturing case study for ERP and mes systems integration based on ISA-95. In: Sinderen, V/van, Chapurlat, V. (eds.) 6th International IFIP Working Conference on Enterprise Interoperability, IWEI 2015, Lecture Notes in Business Information Processing, Nimes, France, vol. 213, pp. 157–170 (2015)
9. Schwab, K., Davis, N., Nadella, S.: Shaping the Fourth Industrial Revolution. 1st end. World Economic Forum, Switzerland (2018)

10. Kazantsev, N., Pishchulov, G., Mehandjiev, N., Sampaio, P., Zolkiewski, J.: Problems of cooperation between suppliers in industry 4.0: analysis of the aviation industry. In: Tsenzaryk, M., Arenkov, I. (eds.) *The First International Conference "Business Management in the Digital Economy"* 2018, pp. 171–177. Saint Petersburg State University, St. Petersburg (2018). [in Russian]
11. Predix Developer Network. <https://www.predix.io/>. Accessed 21 Sept 2019
12. Verjüngtes Führungsteam stellt Weichen für die Zukunft. <https://www.sap.com/germany/index.html>. Accessed 01 Oct 2019
13. Rexroth. A Bosch Company. <https://www.boschrexroth.com/en/xc/trends-and-topics/industry-4-0/connected-industry-1>. Accessed 03 Oct 2019
14. VDM. <https://vdw.de/en/technology-and-standardisation/umati-universal-machine-tool-interface/>. Accessed 03 Oct 2019
15. SmartFactory. <https://smartfactory.de/smartfactoryeu-befindet-sich-in-gruendung-2/>. Accessed 03 Dec 2019
16. ANT. <https://antsolutions.eu/en/>. Accessed 04 Dec 2019
17. DIGICOR. Decentralised Agile Coordination Across Supply Chains. <https://www.digicor-project.eu/>. Accessed 04 Oct 2019
18. Pavlenko, I., Trojanowska, J., Ivanov, V., Liaposhchenko, O.: Parameter identification of hydro-mechanical processes using artificial intelligence systems. *Int. J. Mechatron. Appl. Mech.* **2019**(5), 19–26 (2019)
19. Kuric, I., Kandra, M., Klarák, J., Ivanov, V., Więcek, D.: Visual product inspection based on deep learning methods. In: Tonkonogyi V. et al. (eds) *Advanced Manufacturing Processes. InterPartner-2019. Lecture Notes in Mechanical Engineering*, pp. 148–156. Springer, Cham (2020). [https://doi.org/10.1007/978-3-030-40724-7\\_15](https://doi.org/10.1007/978-3-030-40724-7_15)
20. Ivanov, V., Pavlenko, I., Trojanowska, J., Zuban, Y., Samokhvalov, D., Bun, P.: Using the augmented reality for training engineering students. In: Bruzzone A.G. et al. (eds.) *Proceedings of the 4th International Conference of the Virtual and Augmented Reality in Education, VARE 2018*, pp. 57–64 (2018)
21. Ivanov, V., Pavlenko, I., Liaposhchenko, O., Gusak, O., Pavlenko, V.: Determination of contact points between workpiece and fixture elements as a tool for augmented reality in fixture design. *Wirel. Netw.* (2019). <https://doi.org/10.1007/s11276-019-02026-2>
22. Bun, P., Trojanowska, J., Ivanov, V., Pavlenko, I. The use of virtual reality training application to increase the effectiveness of workshops in the field of lean manufacturing. In: Bruzzone A.G. et al. (eds.) *Proc. of the 4th Int. Conf. of the Virtual and Augmented Reality in Education, VARE 2018*, pp. 65–71 (2018)
23. Edl M., Dobrotvorskiy S., Gnuchykh S., Dobrovol'ska L., Sokol E., Hamrol A., Dostatni E.: The role of "JavaMach Cluster" in Industry 4.0. In: Knapčiková, L., Perakovič, D., Balog, M., Periša, M. (eds.) *3rd EAI International Conference on Management of Manufacturing Systems. EAI, Croatia* (2018). <https://doi.org/10.4108/eai.6-11-2018.2279655>



# Data Analysis of Readiness Programs of Machine-Building Enterprises

Bohdan Haidabrus<sup>1</sup>(✉), Serhiy Protsenko<sup>1</sup>, Philipp Rosenberger<sup>2</sup>,  
and Janis Grabis<sup>3</sup>

<sup>1</sup> Sumy State University, 2, Rymyskogo-Korsakova Street, Sumy 40007, Ukraine  
haidabrus@gmail.com

<sup>2</sup> University of Applied Sciences, 226, Favoritenstrasse, 1100 Vienna, Austria

<sup>3</sup> Riga Technical University, 1, Kalku Street, Riga 1658, Latvia

**Abstract.** One of the important aspects of providing the high level of the enterprises IT-readiness at machine-building enterprises is using the data science approach. By using data analysis, we mean the ability of the enterprises' experts to increase using data by the most effective appliance of modern data science algorithms. In our research, the analysis has been carried out and the proposed approach can be used in real practice to evaluate the implementation of program projects to boost IT readiness. For example, at the initial stage, when the project is just starting and we do not know the real values of features, we can assign to modifications the average value for each, and then when the project arrives the real value of modification, we can calculate the target and track the dynamics of the assessment, the quality of the program projects to boost IT-readiness of machine-building enterprises. Thus, an important question is the compliance of the enterprise to the necessary level of IT-readiness which is directly connected with data analysis.

**Keywords:** Data science · Project management · IT-readiness · Program management · Machine learning

## 1 Introduction

The analysis has been carried out and the proposed approach can be used in real practice to evaluate the implementation of projects, for example, at the initial stage, when the project is just beginning and we do not know the real values of features, we can assign to modifications the average value for each, and then when the project arrives the real value of modification, we can calculate the target and track the dynamics of the assessment, the quality of the project of the in-program to boost IT-readiness of machine-building enterprises.

The comprehension of the IT-readiness level at each workplace separately for each type of security will make it possible to calculate the integral indicator of IT-readiness for the workplace, which is proposed to be determined using expert analysis (weighting factors). Expert analysis is the procedure for obtaining an assessment of a problem based on the group opinion of specialists.

## 2 Literature Review

Under the content organization of the IT-readiness improvement, it is necessary to understand what structural units and types of support need the appropriate measures to be carried out. The size of the mismatch between the current and planned state of the company's IT-readiness should be considered up-stream. The magnitude of the mismatch can be defined by comparing the current and planned status, for this their evaluation has to be performed [6].

It is proposed to determine the current state of the company's IT-readiness downwards, beginning with from each workplace and according to the hierarchy of structural and functional elements, ending with the enterprise as a whole. In other words, it is necessary to determine the level of IT readiness at each workplace separately for each type of security:

$$\left\{ R_i^{meth}, R_i^{ling}, R_i^{math}, R_i^{prog}, R_i^{tech}, R_i^{inf}, R_i^{org} \right\} \quad (1)$$

where  $R_i$ – i-th the workplace.

The collective idea is more accurate compared to the individual opinion of each specialist. Through the use of expert judgment, it is usually assumed that the opinion of a group of experts is more credible rather than the opinion of an individual expert [7, 8].

The requirements include: the distribution of assessments that are received from experts should be "smooth"; two group scores provided by two identical subgroups chosen randomly should be close.

The assessment procedure consists of several stages: setting the goal of the study; the choice of a research form; preparation of information materials, questionnaire forms and moderator of the procedure; the selection of experts; examination; statistical analysis of the results; preparation of a report on the results of expert evaluation.

The information to determine the priority of projects within the framework of the model for the formation of the IT-readiness improvement programme was based on the processing of the results of an expert assessment of change peculiarities.

To obtain weighting factors of significance by type of collateral, it is recommended to involve leading specialists of the machine-building enterprise as experts. In particular, these may be heads or leading specialists of such divisions: production directorate, personnel, quality, finance, economic programmes, and complete facilities, technical directorate, logistics department and chief engineer service [15].

## 3 Research Methodology

To reduce the subjectivity of the assessment, it is proposed to attract at least two representatives from each direction. Experts will be asked to assign a significant factor to each type of collateral for each workplace. Therefore, the level of IT-readiness of  $R_i$  the workplace will be next to:



$$R_i = \sum_{j=1}^7 W_j \cdot R_i^j \tag{2}$$

where  $W_j$  – the weighting factor of  $j$ -th type of support.

Similarly, the current level of IT readiness is defined by departments and the enterprise as a whole (see Fig. 1).

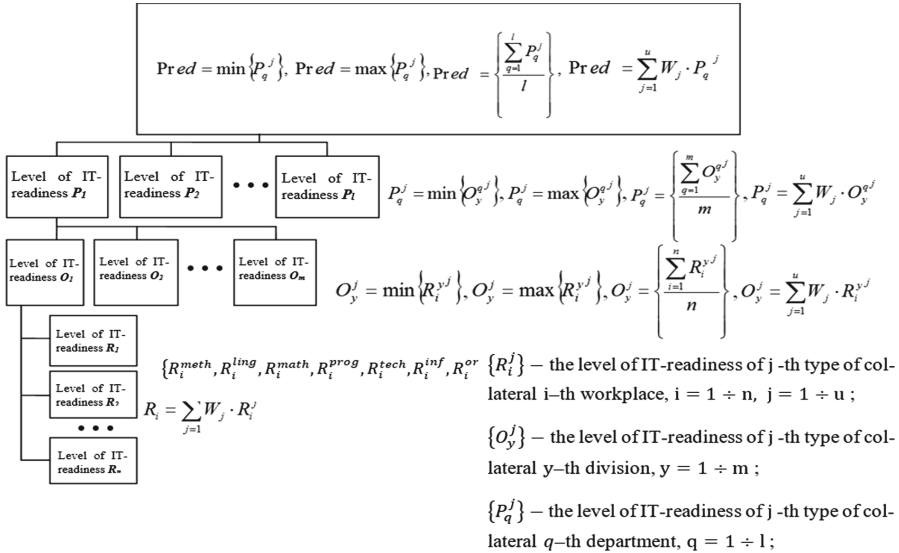


**Fig. 1.** Model for assessing the current and planned status of IT-readiness.

To determine the current IT-readiness level of departments, divisions, and the entire enterprise, the decision maker is up to choose one of the assessment options: minimax (the level of IT-readiness is determined by the highest and lowest values), average (the level of IT-readiness is determined by the highest and lowest values) and expert (the level of IT readiness is determined taking into account the weight of the type of security). Therefore, the level of IT readiness ( $\{O_y^j\}$ ) <sub>$y$</sub>  –of the department of  $j$ -th type of collateral will be next to:

$$O_y^i = \min \{R_i^{y,j}\}, \text{ or } O_y^i = \max \{R_i^{y,j}\} \tag{3}$$

$$\text{or } O_y^i = \left\{ \frac{\sum_{i=1}^n R_i^{y,j}}{n} \right\}, \text{ or } O_y^i = \sum_{j=1}^u W_j \cdot R_i^{y,j} \tag{4}$$

where  $R_i^{y_j}$  – the level of IT-readiness of  $j$  – th type of collateral  $i$  – th workplace, which is stored in  $y$  – th department;  $n$  – the number of attendant’s place in the department.

The proposed state of IT-readiness of the enterprise is proposed to determine “downwards”, whereas the existing portfolio of projects dictates the general level of IT-readiness. The selection of the most rational variant of the planned state is carried out by taking into account such additional restrictions as uniform loading of workplaces, integration of work in the field, etc.

The planned level of IT-readiness will provide the given efficiency on each element of the organizational structure, which will allow fulfilling the order portfolio at the required time.

Consider the process of managing the programme to increase IT-readiness at the PE enterprise as a set of projects by types of support:

$$\theta = \{\theta_1, \theta_2, \theta_3, \dots, \theta_n\} \quad (5)$$

where  $\theta_n$  – projects by types of support.

To implement the project  $\theta_n$  it is necessary to carry out the management action:

$$F^j = \{f_i^j\}, j = \overline{1, n_i} \quad (6)$$

Each action is characterized by the following magnitudes:

$$f = R, N, P, C, S, I, \quad (7)$$

where  $f$  – the action on the organization of an information support system;  $R$  - the regulations for the implementation of the action;  $N$  – the quantitative measure of action (implies the number of processed documents, the amount of input information, etc.);  $P$  – the action performer;  $C$  – the costs necessary to complete the action;  $S$  – the need for resources;  $I$  – the condition for performing actions.

The implementation of the IT-readiness improvement programme is based on such a structured SIP that will provide access to the necessary information in the shortest time span and with the least costs.

The structure of the programme for improving the IT-readiness of PE enterprises should be determined by functional dependencies in the information environment of projects. The task of constructing the rational content of projects by types of support is formed in such a way that, proceeding from the necessary management actions in the projects, it is imperative to figure such a programme for increasing IT-readiness. For which:

$$\sum_{i=1}^n \sum_{j=1}^{n_i} C(f_j^i) \rightarrow \min, \quad (8)$$

where  $C(f_j^i)$  – implementation costs  $f_j^i$  under restrictions:

$$\sum; \Phi; t(f_j^i) \leq t_{\max}(f_j^i); I, \quad (9)$$

where  $\sum$  – structural elements of the enterprise;  $\Phi$  – functional elements of the enterprise;  $t(f_j^i) \leq t_{\max}(f_j^i)$  – allowable function implementation time  $f_j^i$ .

The limitations of the goal function of the IT-readiness improvement programme is the structural and functional elements of the PE enterprise that provide a certain level of costs for the implementation of project management actions, as well as the time and managerial and technological conditions for the implementation of these actions.

Along the same lines it is necessary to take into account that, within the framework of the implementation of the project by support types, actions can be unified and specialized. Unified actions are described by current business processes and are carried out by the existing structural elements of the enterprise, and to perform specialized ones, the creation of separate structures is required specifically for the implementation of a specific project by type of support.

## 4 Results

In our research, we have a dataset consisting of 33 assessments of the IT-readiness state. The use of complex models with a large number of parameters (artificial neural networks) is not advisable. It is more advisable to use approaches of a different regularization plan, such as linear regression of L1 or L2 regulation. In our case, L1 has the advantage that regularization during the training of the model takes away weight with not important modifications. This leads to a decrease in the dimensionality of space and improves the accuracy and stability of the model, and also significantly reduces the likelihood of retraining Linear Regression with L2 Regularization (Ridge Regression) [14].

The results of the prediction of the Lasso model [16] (linear regression with L1 regularization) can be seen from the Fig. 2, Lasso is often gives inaccuracy, and the determination coefficient  $r^2$  has a generally low value  $r^2\_score = 0.33$ .

The result of Lasso regression analysis leads us to the idea that it is possible to predict a specific target value that is rather a difficult task for such a small dataset to assess the level of IT-readiness we are dealing with Curse of dimensionality. In this case, it is better to turn our target estimates into three classes, for example, 0–3 (low level of IT-readiness projects), 4–7 (medium level of IT-readiness projects), 8–10 (high level of IT-readiness projects) and go from the regression task to the task of three-class classification.

It is also advisable to try to analyze our dataset using unsupervised learning methods, such as PCA, t-SNE or Isomap. This will allow seeing the possibility of dividing the value of the target into separate independent classes. Figure 2 shows the result of the t-SNE algorithm (a similar result was obtained using the PCA and Isomap algorithms).

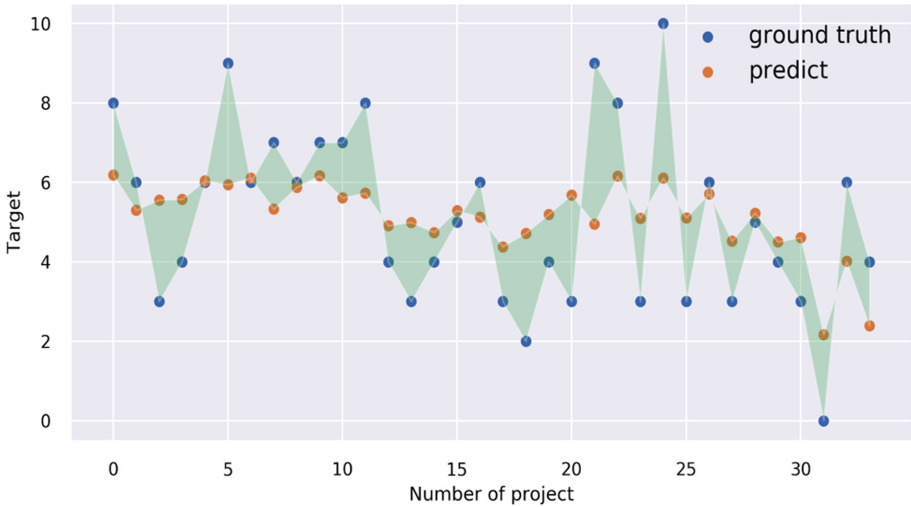


**Fig. 2.** Comparison of the real target (ground truth) with the prediction of linear regression with L1 regularization of Lasso.

The main idea of the t-SNE algorithm is to preserve the distances between individual points in a multidimensional space and to design these distances to a two-dimensional space, that is, if we have points from the same class in a multidimensional space, then they should be near in a two-dimensional image, and points from different classes must be removed from each other. As we can see from Fig. 2, the t-SNE algorithm failed to cluster our data well and separate one target class from another one.

On small datasets, it is generally better to use Bayesian statistics-based algorithms, in particular Automatic Relevance Determination (ARD) or Bayesian Ridge Regression [17, 18]. ARD is more prone to zeroing weights with the unimportant fit, and for each weight (coefficient) a posterior estimation of variance is derived, and then weights (coefficients) with a small dispersion (minimum variance) are reset [15]. The result of the algorithm is shown in Fig. 3.

The operation of the Automatic Relevance Determination algorithm [19] (see Fig. 4) is much better than Lasso and t-SNE and can already be applied in real production, the determination coefficient  $r^2$  has the value  $r^2_{\text{score}} = 0.9$ , which is convenient, therefore, it emphasizes the fact that our model has relevant data.

Automatic Relevance Determination. Using models that are not prone to retraining, such as Random Forest (with not large values  $\text{max\_depth}$  - the depth of the tree) also gives good results but worse than Automatic Relevance Determination.

We also see possible ways to improve the result in the use of synthetic methods for generating additional data, for example, SMOTE (Synthetic Minority Oversampling Technique) and combining the predictions of several models and/or the same model with different hyperparameters, which will lead to a significant reduction in variance and enhance the generalization of our predictions. (Combining the prediction of several models or the same model with different values of hyperparameters reduces variance and enhances generalization.)

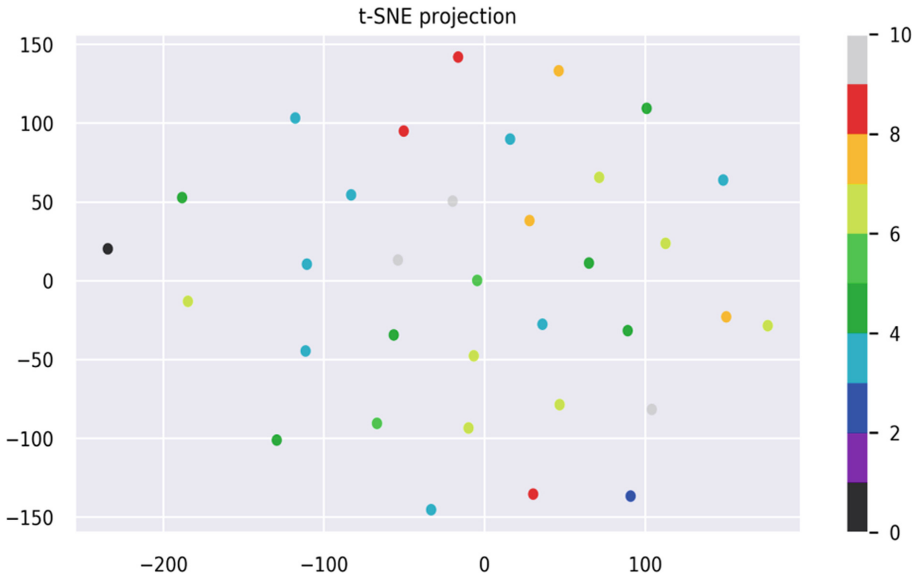


Fig. 3. The result of the t-SNE algorithm.

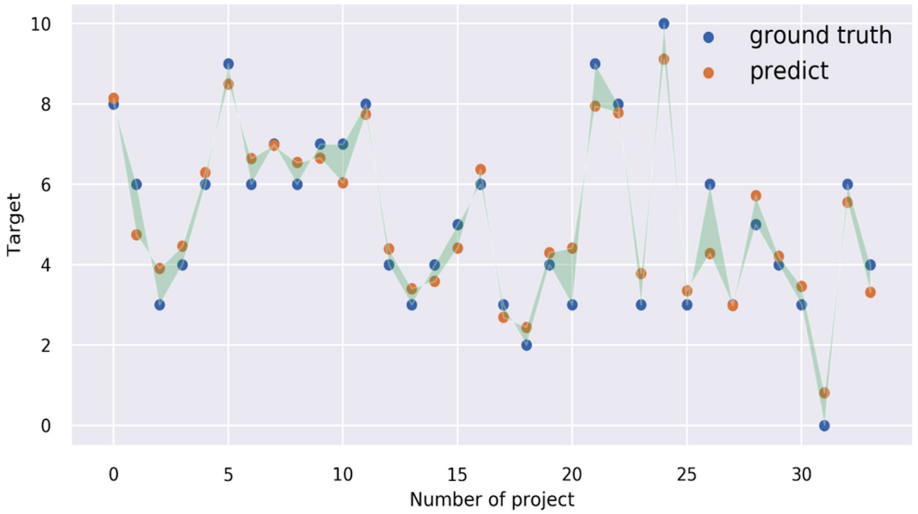


Fig. 4. Comparison of real Target (ground truth) with the prediction by Automatic Relevance Determination algorithm.

## 5 Conclusions

In this research, working with a small dataset and a relatively large number of modifications of boosting IT-readiness parameters, it is necessary to carefully select machine learning algorithms, since it is likely to get overfitting models and a false predicate on new data. The use of traditional linear models with regularization gives a satisfactory result, but in this case, it is better to move from the regression problem to the multiclass classification problem, for example, into three classes. Using algorithms based on Bayesian statistics, Automatic Relevance Determination, in particular, gives the best result in our case for programs to boost IT-readiness. Possible ways to improve the quality of models is to use synthetic approaches to generate additional data, such as SMOTE (Synthetic Minority Oversampling Technique) and combine the prediction of several models.


## References

1. Akintoye, A.S., MacLeod, M.J.: Risk analysis and management in construction. *Int. J. Project Manage.* **15**(1), 31–38 (1997)
2. Labuschagne, C., Brent, A.C.: Sustainable project life cycle management: the need to integrate life cycles in the manufacturing sector. *Int. J. Project Manage.* **23**(2), 159–168 (2005)
3. Miller, R., Lessard, D.: Understanding and managing risks in large engineering projects. *Int. J. Project Manage.* **19**(8), 437–443 (2001)
4. Tick, J., Kovács, Z.: P-graph based workflow synthesis. In: 12th International Conference on Intelligent Engineering Systems - Proceedings, INES, 4481303, pp. 249–253 (2008)
5. Zhang, X.: Win-win concession period determination methodology. *J. Constr. Eng. Manag.* **135**, 550–558 (2009). [https://doi.org/10.1061/\(ASCE\)CO.1943-7862.0000243](https://doi.org/10.1061/(ASCE)CO.1943-7862.0000243)
6. Chenarani, A., Druzhinin, E.A., Kritskiy, D.N.: Simulating the impact of activity uncertainties and risk combinations in R&D projects. *J. Eng. Sci. Technol. Rev.* **10**(4), 1–9 (2017)
7. Kiyko, S.G., Druzhinin, E.A., Koba, S.A., Haidabrus, B.V.: A mathematical background for information technology of project's processes integration taking into account risk factors. *J. Metall. Min. Ind.* **6**(3), 66–77 (2014)
8. Nilsson, L., Elg, M., Bergman, B.: Managing ideas for the development of new products. *Int. J. Technol. Manage.* **24**(5–6), 498–513 (2002)
9. Lanstrand, J., Elg, M.: Non-human resistance in changes towards lean. *J. Organ. Change Manag.* **25**(6), 853–866 (2012)
10. Bushuyev, S., Friedrich Wagner, R.: IPMA Delta and IPMA Organisational Competence Baseline (OCB): new approaches in the field of project management maturity. *Int. J. Manag. Projects Bus.* **7**(2), 302–310 (2014)
11. Chandra, C., Grabis, J.: Configurable supply chain: framework, methodology and application. *Int. J. Manuf. Technol. Manage.* **17**(1–2), 5–22 (2009)
12. Chandra, C., Grabis, J.: Information technology support for integrated supply chain modeling. *J. Hum. Syst. Manag.* **27**(1), 3–13 (2008)

13. Bushuyev, S.D., Bushuyev, D.A., Rogozina, V.B., Mikhieieva, O.V.: Convergence of knowledge in project management. In: Proceedings of the 2015 IEEE 8th International Conference on Intelligent Data Acquisition and Advanced Computing Systems: Technology and Applications, IDAACS, vol. 2 (2015)
14. Wu, A., Koyejo, O., Pillow, J.: Dependent relevance determination for smooth and structured sparse regression. *J. Mach. Learn. Res.* **20**(89), 1–43 (2019)
15. Tick, J.: Business Process based initial modeling at software development. In: SAMI - IEEE 11th International Symposium on Applied Machine Intelligence and Informatics, Proceedings, 6480962, pp. 141–144 (2013)
16. Xu, T., Sun, J., Bi, J.: Longitudinal LASSO: jointly learning features and temporal contingency for outcome prediction. In: Proceedings of the 21th ACM SIGKDD International Conference on Knowledge Discovery and Data Mining. ACM (2015)
17. Drugowitsch, J.: Variational Bayesian inference for linear and logistic regression. arXiv preprint [arXiv:1310.5438](https://arxiv.org/abs/1310.5438). arxiv.org (2013)
18. Piironen, J., Aki Vehtari, A.: Projection predictive model selection for Gaussian processes. In: IEEE 26th International Workshop on Machine Learning for Signal Processing (MLSP) (2016)
19. Rivera, R., Burnaev, E.: Forecasting of commercial sales with large scale Gaussian Processes. arXiv preprint [arXiv:1709.05548](https://arxiv.org/abs/1709.05548), adsabs.harvard.edu (2017)
20. Kritsky, D.N., Druzhinin, E.A., Pogudina, O.K., Kritskaya, O.S.: Decision making by the analysis of project risks based on the FMEA method. In: IEEE 13th International Scientific and Technical Conference on Computer Sciences and Information Technologies, CSIT 2018-Proceedings, pp. 187–190 (2018)



# Workplace Optimization Using a Collaborative Robot

Pavel Kábele and Milan Edl<sup>(✉)</sup> 

University of West Bohemia, 22, Univerzitní St., Pilsen 326 00, Czech Republic  
edl@kpv.zcu.cz

**Abstract.** The study describes increasing the productivity of the production process using robotization. The application of robots in the manufacturing process and logistics requires a very thorough analysis and knowledge of manufacturing processes. The theoretical part describes the knowledge gained from the scientific literature concerning the robotization and technical standards of the Czech Republic. In the practical part there is an analysis of the current situation – i.e. defining a selected production line and selected workplaces on these lines, especially in terms of activities. The activities performed at these sites and their duration are crucial for determining the suitability of the site for implementing the robot. In the next chapter, the workplaces are evaluated in terms of activities that can be transferred from the operator to the robot to determine which percentage replacement of the operator is feasible. Thus, the selection of suitable activities (processes) for automation will be made at the workplace. The technical solution of the implementation is also proposed for the selected workplace. To achieve a successful application of the collaborative robot into the production process, it was necessary to change the location of the workplace, including electrical and air distribution, investment in a new conveyor and laser gauges. The new layout was based on saving space and saving human influence in the production process. The whole study shows a systematic approach to the introduction of the above-described issue.

**Keywords:** Operation · Robot · Layout · Production cycle · Analysis · Rationalization · Process · Improvement

## 1 Introduction

Due to the ever-increasing pressure to improve productivity and production quality, there is a growing interest in the use of automatic production equipment. Another reason is, for example, increasing the competitiveness of companies and keeping them on the financial market. Automation leads to changes in production, technology, and overall logistics processes, not only in engineering but also in other sectors. Manipulators and robots are increasingly gaining ground in various industries in the automation of both whole processes and individual process operations. Improvement of efficiency, quality and labor productivity cannot be ensured without modernization, reconstruction and automation of production facilities.



This publication analyzes the current process in the workplace. The assignment of the project was to apply a collaborative robot to a workplace involved 2 workers. The aim was economic savings. The main requirement was an economic return within a maximum of two years. For a successful application, it was necessary to change the production layout of the workplace.

## 2 Literature Review

Without perfect knowledge of production operations, it is not possible to interfere with production processes [1].

The process is a general term for the gradual flow of events, states, activities or work. In the real world, there are several types of processes, so the term process is used in practice in different meanings [1, 2].

The production process is essentially the sum of all processes in the transformation of materials and raw materials with the participation of labor and means of production into a product. The production process has two interconnected components - technological and working processes [3, 6]. One possible way of analyzing a manufacturing process performed by a worker is described in Porter's reference. He uses the Basic MOST methodology to obtain concrete real data with those further worked to rationalize the process [4, 10, 14].

In his book, Porter defines the application of the robot to the manufacturing process as a step that eliminates the human aspect and the possibility of creating manufacturing errors.

The official definition of a robot, invented by the International Organization for Standardization of Robot Definitions, is according to ISO 8373 as follows [4, 5, 7]: by standard, an industrial robot is an automatically controlled, reprogrammable multi-purpose manipulator, programmable in three or more axes, which can be either fixed or mobile, for use in industrial automation [5, 8]. Industrial robots and manipulators are manipulation mechanisms that can be divided and described by function, design, application possibilities, degree of autonomy, control level, etc.

In addition to the basic classification and classification according to the concept, we can further specify the different types of industrial robots and manipulators according to the individual characteristics, which further the whole group branches into subgroups from the simplest single-purpose feed manipulators to cognitive robots, equipped with the ability of perception and a certain "rational thinking" [4, 5, 8].

Programmable manipulators - are controlled by a programming device.

Design, drive, and function are independent of the machine being operated [6].

Handling abilities - grasping and moving objects, various assembly operations, adjusting objects, handling auxiliary objects such as tools [8].

### 3 Research Methodology

If we want to regulate, evaluate and measure processes, we must measure their performance. An important thing to measure performance is to first determine the measurement points. Both outputs and process inputs must then be measured. The determination of the measuring points depends on the required surveyed indicators and methods of analysis. The number of measurement points must correspond to the possibility of variability during the process. When measuring only inputs and outputs, it would never be possible to identify the causes of deviations from requirements that may arise at any point in the process. Automation, among other things, allows ensuring greater safety, health, comfort and well-being of people at work because it deprives workers hard, health, and life-threatening or fatigue work [10, 15].

The process is effective if its output reaches planned and required parameters, both qualitative and quantitative. On the other hand, the process is effective if all the required and planned parameters achieve the added value that the internal or external customer appreciates. Considering the Pareto principle on process efficiency, it can be said that a process is optimally effective if 80% of the result is obtained at 20% of the input effort [2, 15].

According to [15], the process can be evaluated in two ways:

1. Evaluation of processes in terms of performance (efficiency, process efficiency).
2. Evaluation of processes in terms of variability (process variability due to internal and external influences).

Electromagnetic compatibility (EMC) is another thing that needs to be addressed in terms of safety during implementation. The design and construction of the robot must avoid dangerous movements or situations due to the expected effects of electromagnetic disturbance (EMI), radio frequency disturbance (RFI) and electrostatic discharge (ESD) [7].

When a robot is implemented on site, EMC measurements must be made, and safe values must be achieved. In addition, when implementing a robot on a line that is somehow connected to the robot by software, for example, an EMC measurement for the entire system (robot + line) must be performed. Implementing a robot is, therefore, a very complex legislative issue and it is important to realize which applications robot will be used with, what tools it will work with, etc. It is therefore advisable to carry out a thorough analysis of the workplace where the robot will work and all processes, operations, and activities that robots will perform [7, 12].

Since the aim of the work is to design a suitable robot for implementation in the workplace, it is necessary to obtain the necessary information about the safety requirements that are imposed on it and that are set by certain regulations. Although the robot is constructed and its maximum potential will only be used to work side by side with people in direct contact, it was necessary to find an appropriate regulation that sets out the rules allowing it. Regulations mean directives, laws, decrees, standards, etc.

The collaboration between humans and robots has been described by the authors of EN ISO 10218-1 and EN ISO 10218-2 standards. Already in these standards the requirements of operational cooperation (4 basic principles) of humans and robots are defined [7, 12].

- Principle 1 - Safety monitored stop - see article 5.10.2 in EN ISO 10218-1 and article 5.11.5.2 in EN ISO 10218-2.
- Principle 2 - Manual guidance - see article 5.10.3 in EN ISO 10218-1 and article 5.11.5.3 in EN ISO 10218-2.
- Principle 3 - Speed and position monitoring - see article 5.10.4 in EN ISO 10218-1 and article 5.11.5.4 in EN ISO 10218-2 [11].

### 3.1 Measurement

Based on production observations, analysis of production videos and acquired files from the company, it was possible to describe all activities performed on the lines. A table has been created for each selected workplace, listing all activities performed by two operators. Each activity is assigned a duration. The duration of each activity in the tables was obtained by the arithmetic mean of several values of the duration of the activity, which were obtained from the analysis of video recordings.

MOST is a sensitive method. This feature is very effective in evaluating alternative methods of performing operations with respect to time and cost. The MOST analysis is, therefore, more economical and less demanding compared to other methods. For example, the following general motion sequence model illustrates:

$$A_6B_6G_3A_{10}B_0P_3A_0 \dots \dots \dots 280 \text{ TMU} \tag{1}$$

Movement of a heavy (10 kg) object from the pallet lying on the ground to the workbench with bending (B6) and walking (A6, A10). High index values indicate that this work is ineffective and ergonomically unacceptable (especially during frequent repetitions) and therefore a rationalization of the workplace is required. The movement of the object will be more effective with less fatigue after installing the roller conveyor to the workbench:

$$A_3B_0G_3M_6X_0I_0A_0 \dots \dots \dots 120 \text{ TMU} \tag{2}$$

The fact that MOST is a sensitive method greatly increases its value as a means of measuring labor productivity.

In what situations can the MOST method be used? As manual work usually involves rotating some cycles from one to the next, the MOST method can produce, with its statistically determined times, total times comparable to much more detailed methods for most manual operations. Therefore, the MOST method is suitable for any manual work that involves changing from one cycle to the next regardless of the length of the cycle. Basic MOST should not be used in situations where there is a short cycle (usually within 10 s) and is repeated periodically for a period [3, 13, 15].

### 3.2 Description of Analyzed Workplace

Two operators work in the workplace because of the handling of a heavy object. The start of the operation is the turning of the air conditioning unit which weighs 20 kg. Then the worker presses a button that is connected to the information system. It transmits information about the position of the unit on the production line. The signal is transferred to a printer that prints four nameplates. These labels are removed by the operator number 2 and glued to the cardboard box. After sticking the labels, the scanner reads the production label, which sends a finished status signal. This finished unit leaves for other workplaces.

Figure 1 shows the original state of the workplace with two workers.

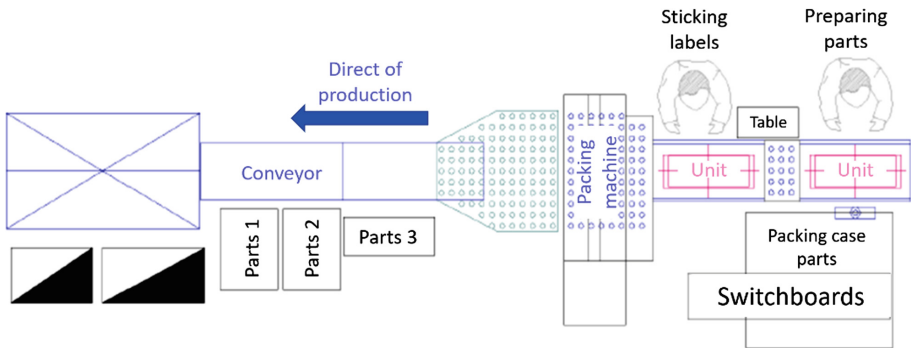


Fig. 1. Layout before.

The main task of the successful project was to install a robot to replace both workers. At the same time, the line clock is not disturbed. When installing the robot, it is necessary to think over how the robot recognizes the position where to stick the nameplate. The internal rule of the company is the return of the rationalization measure within a maximum of 2 years.

### 3.3 Time Measurement

Among the most used methods of time measurement in companies are chronometric. In practice, the application of these methods often fails to observe basic statistical principles and the time standard is determined based on one measurement.

Operation analysis consists of a series of sequential models describing the movement of objects operating. The total time of the complete MOST analysis is given by summing the times calculated from each sequence. The resulting operating time can be left in TMUs or converted to hours, minutes, and seconds. It's worth emphasizing that this time reflects pure work content at 100% performance. The final form of the time standard will include time allowances that include PRD: personal time (P = Personal), rest and exhaustion (R = rest) and unavoidable time loss (D = Delays). Therefore, if the normal time TMU = 1 h and the expected time addition of PRD is 15%, then the final time standard will be 1.15 h [1, 16].

In general, the aim is to replace the process of gluing production and packaging labels to packaged units. See Fig. 1. During monitoring and analysis of the process, problems were recorded that prevented the robot from being impelled. This procedure must always be followed when applying a new type of device.

Table 2 describes the problem. All these problems must be solved before the application of the robot.

**Table 1.** Summary D5 line.

	XF6											
OP1	A	1	B	0	G	3	A	1	B	0	P	3
OP2	A	1	B	2	G	1	A	1	B	0	P	0
OP3	A	0	B	0	G	0	A	1	B	0	P	1
OP4	A	2	B	0	G	1	A	1	B	1	P	0
OP5	A	1	B	0	G	1	A	1	B	0	P	1
Summary	310 TMU											

*Note: To comply with the internal regulations, the values in Table 1 are changed and the table is used only for information on the procedure of the analysis of operations to determine the exact tact of the workplace. The exact description of the workflow must not be published.*

**Table 2.** Mapping problem for the application of robotization.

No.	Problem
1	Some units are not approaching the strapping position
2	Some cables are laid on the ground in front of the strapping machine
3	The robot switches to a unit overrun error when the safety bar is violated
4	The strapping machine is connected to the same socket circuit as the robot
5	If the tape runs out in the strapping machine, no monitoring message appears
6	Some PC labels are not stuck on their entire surface
7	Labels do not unwind correctly from the printer

### 3.4 Mapping of Production Workplace

Another procedure was to create a model in a graphics program. The created model of the workplace serves as a point of reference when changing the layout. Moving individual parts of the production line changes the complete layout. It is always necessary to check how much space there is in the given part of the line for moving boxes and shelves. During the move, it was very difficult to deal with the electrical wiring. Eventually, they had to be completely changed.

In the case of the final design, we work with the created part of the layout and try to place it in the layout of the entire hall. This analysis was performed in VisTable 2019, which can identify material flows.

Figure 2 shows a model of the workplace before the application of robotization. The original layout of the workplace was 15 m<sup>2</sup>. This made it very difficult to load the material and move around the workplace. Workers at this workplace were forced to walk for material up to 3.5 m from their workplace. Creating the model was a clear impetus to the application of the robot, which would replace the workers.

When selecting the robot, mainly parameters such as the size of the serviced space by the robot and the load-carrying capacity of the robot needed for blade handling were considered. The speed and accuracy of today's robots are so high that when selecting a robot for a workstation where  $\pm 1$  mm accuracy is required, all types of robots considered meet the requirements. The glued manufacture labels which have specific codes are then automatically read by another machine. If the deflection is  $> 1$  mm, the production code is not read, and the production line is stopped.

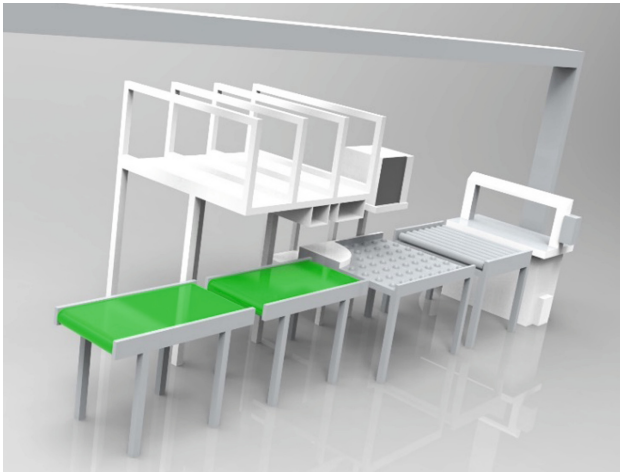


**Fig. 2.** Model of the old workplace.

### 3.5 Selection of a Suitable Robot Type

When solving the robotics design of the workplace for gluing production labels, the requirements of the contracting company were followed. For robotized workplaces, it is important to know the component used in the workplace. The goal is to make the robot to be able to grasp the labels from the printer and stick them to the exact ones on the wrapped unit. These locations are checked with a laser reading the exact position according to the checkpoint. It was difficult to establish this checkpoint because the workplace produces different types and shapes of products. Catching the labels has been solved by using suction cups that attach the label to the non-sticky portion and place the sticky portion on the box. These suction cups were manufactured internally using 3D printing. Figure 3 shows the final solution for the robot.



**Fig. 3.** Final robot application.

The robot was selected based on cooperation with the supplier company. The type of robot was chosen to suit the length of its arm and also to keep the operation costs low. The frame construction had to be designed to maintain the weight of the robot.

## 4 Results

The whole study is based on the topic of the dissertation. Specifically, the methodology of the procedure for the successful application of robotic equipment was used. First, the original workplace was mapped. The layout of the workplace was drawn into a simulation program and the current state was modeled. The assembly process of the workers was very accurately mapped by the MOST methodology, which taught the default value, which symbolized the target speed of the robot speed.

In parallel to the time analysis, there was an analysis of the robot selection, where the main factors were speed efficiency and, of course, cost. The main condition for changing the process and the investments required for this is to guarantee a payback period of 2 years. It is a question of a lifetime whether the robot will not be broken in the process and will not disrupt the production process.

The requirement for workplace robotization was also based on the knowledge that workers indirectly adhere to the production cycle. In the early hours, there was a situation where the workers worked very quickly and then waited for the previous workplace. In the afternoon, these workers did not manage to suffer due to fatigue and exhaustion. The result of this finding confirmed also by the MOST analysis was that workers do not work with even power. The applied robot does the same job as it describes the workflow for employees. However internal data is forbidden to publish.

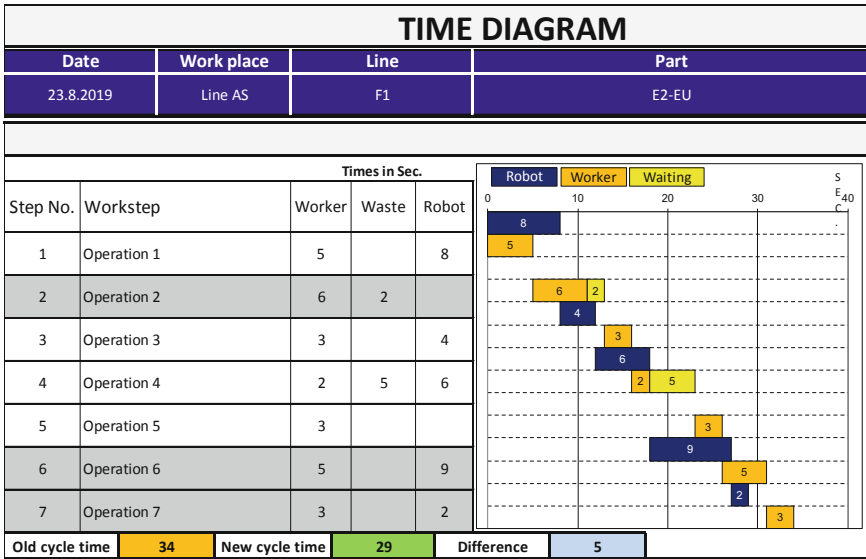


Fig. 4. Picture of process analysis.

## 5 Conclusion

In every project, there is always the most important part of the process analysis. The number of analyses performed depends on the complexity of the process, but nowhere is exactly given how many analyzes are needed. Based on a practical study, the methodology for the implantation of a robotic solution could be described as follows:

*Analysis of layout ► Time analysis of the current process ► Application of 5S methodology ► Analysis of performed tasks ► Time analysis of the new process ► Selection of a suitable robot type ► Economy calculation ► New layout design ► Robot application ► Creating standards TPM*

The company’s goal was to replace 2 workers by the robot. The price of the two workers was 900,000 CZK/year. The robot cost 1.5 million CZK. Costs of layout reconstruction and robot installation 200,000 CZK. Operating costs 200 000 CZK/year. Acceleration of production and a 16% reduction in scrap yields a profit of 130,000 CZK/year. The profit from saving space is 10 000 CZK/year. The return of the robot is, therefore:

$$16 * 900000/12 + 200000 + 16 * 2000000/12 - 16 * 130000/12 - 16 * 10000/12 = \text{Robot cost}$$

(3)



This was accomplished. The total investment will be a return within 16 months. At the same time, the layout of the workplace was saved from 15 m<sup>2</sup> to 9 m<sup>2</sup>. In the time analysis, 5 s were saved. This accelerated production and at the same time automated it. Figure 4 shows a comparison of the original and the new time analysis and compare the timing of the robot and the two workers.



**Acknowledgment.** This paper was supported by the Internal Grant Agency of the University of West Bohemia, project No. SGS-2012-063 - “Integrated design of manufacturing system as metaproduct with a multidisciplinary approach and with using elements of virtual reality.” This paper was created with the subsidy of the project CZ.1.05/2.1.00/03.0093 “RTI - Regional Technological Institute” carried out with the support of the Ministry of Education, Youth and Sports.

## References

1. Masin, I., Vytlačil, M.: *New Ways to Higher Productivity - Industrial Engineering Methods*, 1st edn. Institute of Industrial Engineering, Liberec (2000). (in Czech)
2. Edl, M., Kudrna, J.: *Methods of Industrial Engineering*. SmartMotion, Pilsen (2013). (in Czech)
3. Kosturiak, J., Gregor, M., et al.: *How to Increase Company Productivity*. InForm, Zilina (2002). (in Slovak)
4. Ghosh, B.K., Xi, N., Tarn, T.-J.: *Control in Robotics and Automation: Sensor-Based Integration*. Academic Press, San Diego (1999)
5. Appleton, E., Williams, D.J.: *Industrial Robot Applications*. Wiley, New York (1987)
6. Kolibal, Z., Knoflíček, R.: *Morphological analysis of the construction of industrial robots*. Viena, Editions of scientific and professional literature, Košice (2000). (in Slovak)
7. ČSN EN ISO 10218-1 Robots and robotic devices - Safety requirements for industrial robots - Part 1: Technical Standardization, Metrology and State Testing (2012)
8. Skarupra, J.: *Industrial Robots and Manipulators*. VŠB - Technical University, Ostrava (2008). (in Czech)
9. Nof, S.Y.: *Handbook of Industrial Robotics*, 2nd edn. Wiley, New York (1999)
10. ISO/TS 15066 Robots and robotics devices - Collaborative robots. ISO (2016)
11. Porter, M.E.: *Competitive Strategy: Methods for Analysis of Industry and Competitors*. Victoria Publishing, Prague (1994). (in Czech)
12. EN ISO 10218-2 Robots and robotic devices - Safety requirements for industrial robots - Part 2: Robot systems and integration. Prague: Office for Technical Standardization, Metrology and State Testing (2011). (in Czech)
13. Schulte, C.: *Logistics*. Victoria Publishing, Prague (1994)
14. Tomek, G., Vavrova, V.: *Production and Purchasing Management*. Grada Publishing, Prague (2007). (in Czech)
15. Jurova, M.: *Production and Logistics Processes in Business*. Grada Publishing, Prague (2016). (in Czech)
16. Kabele, P., Edl, M.: *Increasing the efficiency of the production process due to using methods of industrial engineering*. In: Ivanov, V., et al. (eds.) *Advances in Design, Simulation and Manufacturing II*. DSMIE-2019. Lecture Notes in Mechanical Engineering, pp. 126–137. Springer, Cham (2020). [https://doi.org/10.1007/978-3-030-22365-6\\_13](https://doi.org/10.1007/978-3-030-22365-6_13)



# Global Trend of Implementation of Industrial Robots Relating to Industry 4.0

Isak Karabegović<sup>1</sup>, Raul Turmanidze<sup>2</sup> , and Predrag Dašić<sup>3,4</sup> 

<sup>1</sup> University of Bihać, 2/2, Pape Ivana Pavla II Street, 77000 Bihać, Bosnia and Herzegovina

<sup>2</sup> Georgian Technical University (GTU), 77, Merab Kostava Street, 0101 Tbilisi, Georgia

<sup>3</sup> High Technical Mechanical School of Professional Studies, 19, Radoja Krstića Street, 37240 Trstenik, Serbia  
dasicp58@gmail.com

<sup>4</sup> SaTCIP Publisher Ltd., 101, Tržni Centar Pijaca Street, 36210 Vrnjačka Banja, Serbia

**Abstract.** Industry 4.0 is a vision of advanced industrial manufacturing, and one of the foundations it relies on is robotic technology, that is, the implementation of industrial and service robots. Industrial robots have been implemented in all industries in the World in the automation and modernization of production processes. So far, the first generation of industrial robots is still being implemented, which need to be separated from workers for workers' safety. In the last two years, the development of robotic technology has contributed to the implementation of second-generation industrial robots, collaborative robots, into production processes. The paper presents an analysis of the implementation of industrial robots over the last ten years in the World, at the continents of Asia/Australia, Europe, and America, as well as in various industries. The analysis of the implementation of industrial robots in fifteen top countries in the World for 2018 was made, as well as a comparative analysis of the application of traditional industrial robots and collaborative robots in 2017 and 2018 forecasts for the implementation of industrial robots implementation by 2022 have been made.

**Keywords:** Production · Robot · Automation · Collaborative robot · Industry 4.0

## 1 Introduction

WEF named changes occurring in industry and environment in the World - The World Economic Forum (held in Davos in 2016), the fourth industrial revolution, and the first appeared under the name "Industry 4.0" in 2011 at the Hanover Fair in Germany. Prof. Dr. Klaus Schwab published a book called *The Fourth Industrial Revolution* at the World Economic Forum, Geneva Switzerland, 2016. Industry 4.0 is a vision of advanced industrial production that is already being implemented today by using new technologies in the automation of production processes, the exchange, and processing of data. One of the foundations of Industry 4.0 is robotics, that is, industrial robots.

© The Editor(s) (if applicable) and The Author(s), under exclusive license to Springer Nature Switzerland AG 2020

V. Ivanov et al. (Eds.): DSMIE 2020, LNME, pp. 147–155, 2020.

[https://doi.org/10.1007/978-3-030-50794-7\\_15](https://doi.org/10.1007/978-3-030-50794-7_15)

Within the fourth industrial revolution, a new value chain is being formed that relies primarily on Cyber-Physical-Systems (CPS), which is also the other name for the Internet of Things, and its associated service, most commonly implemented in Cloud Computing (CC) [1–6]. Discussion and analysis of the fourth industrial revolution aim to increase awareness of the inclusiveness and speed of the technological revolution and its multiple impacts. It is necessary to create a framework for thinking about “Industry 4.0” that outlines key questions and highlights possible answers; in other words, a platform for achieving public-private collaboration and partnerships on emerging issues related to the technological revolution needs to be provided. Among other technologies, robotic technology and its implementation in all segments of society is one of the cornerstones of automation and modernization of production processes, and thus of Industry 4.0. The development of robotic technology, aided by other emerging technologies, is leading to the development and implementation of second-generation industrial robots - collaborative robots. An analysis of the implementation of industrial robots in production processes in the World and the prediction of their application, as well as the representation of collaborative robots, have been done.

## 2 Literature Review

Industrial robots started to be applied for the first time in the 1960s in industrial manufacturing processes. The development of all technologies, primarily computer, sensor, and information and communication technologies, contributes to the development of robotic technology, and the evolution of robotic technology is shown in Fig. 1.

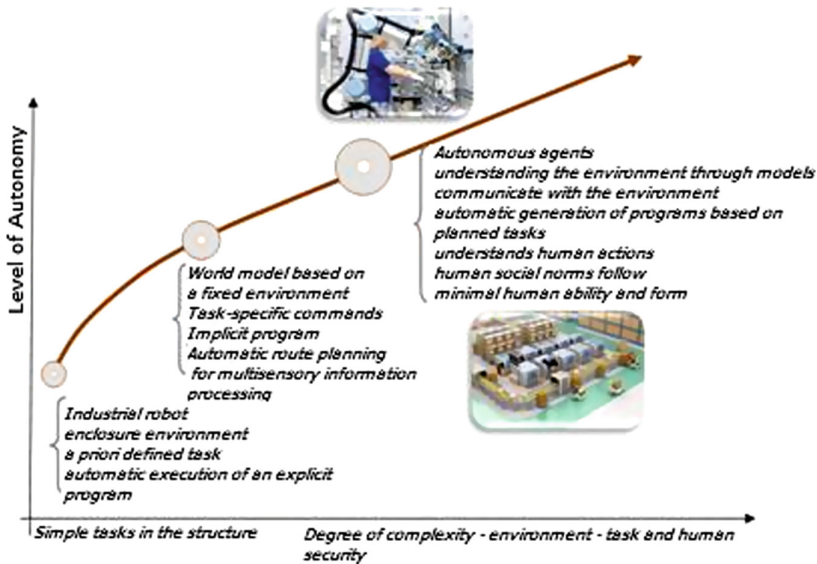


Fig. 1. Development of robotic technology in the World - evolution

At the outset, industrial robots were installed in production processes so that the workspace of an industrial robot had to be separated from the fence from workers in the manufacturing process to ensure that the robot would not injure them. The task of each robot was defined, and the program was automatically executed. The very development and implementation of the aforementioned technologies in robotic technology lead to automatic path planning; the model is based on real data about the robot environment, the commands become specific to each task, and we have the processing of multi-sensory information as well as implicit programs [6, 7]. The evolution and advancement of industrial robots into second-generation collaborative robots (COBOs) occurs, communicating with the environment, understanding the environment through models, automatically generating a program based on planned tasks, understanding human actions, and following human social norms, as Fig. 2 shows.

The development of robotic technology can also be represented through revolutionary solutions in robotic technology in Fig. 2. The first robotic revolution is considered the introduction of industrial robots in the process of automation of industries. The second revolutionary advancement or the second robotic revolution can be considered when the robot became sensitive and safe to work with humans. The third robotic revolution is considered with the introduction of mobile robots in manufacturing processes and mobile manipulators, and the last fourth robotic revolution comes with intelligent robots and robotic systems [8–10].

The advantages of implementing second-generation industrial robots and collaborative robots into production processes (Fig. 2) are enormous, to name just a few:

- simple and straightforward handling tasks characterize them;
- significantly improved performance, when dividing operations between workers and robots;
- the possibility of different levels of automation in the production process, so that tasks can be partially automated in cases where complete automation is too complex or not economical;
- robots play a significant role in Industry 4.0, which connects the real-life factory to virtual reality, which opens up greater prospects for deployment in global manufacturing;
- non-ergonomic workstations can be significantly improved with collaborative robots, where we must keep in mind that worker safety is an absolute prerequisite,
- increasing product diversity and reducing the product lifecycle requires flexible automation, which results in increased use of collaborative robots.

When using second-generation industrial robots (collaborative robots), companies have the following motives: reducing operating costs, reducing capital costs, improving product quality and consistency, improving work quality for workers while respecting health and safety rules, increasing production rates, increasing product manufacturing flexibility, and saving space. It is to be expected that in the future, the trend for the use of collaborative robots is growing.

### 3 Research Methodology

We have obtained statistics on the implementation of industrial and service robots from the International Federation of Robotics (IFR), the UN Economic Commission for Europe (UNECE) and the Organization for Economic Co-operation and Development (OECD) [11–16]. The annual and total application of industrial robots worldwide in all branches of industry is shown in Fig. 2 [11–14, 16].

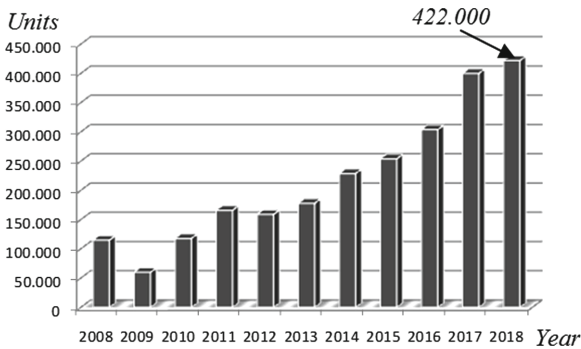


**Fig. 2.** Implementation of industrial robots in all production processes in the World for the period 2008–2018

Based on Fig. 2, we can conclude that the trend of industrial robot implementation in the last ten years in all production processes is growing year by year, which leads us to the fact that an increasing number of production processes are being automated and modernized. The smallest implementation of industrial robots in 2009 was about 60,000 units of robots, and the cause of such a small application is the global economic and industrial crisis.

The number of industrial robots implemented in 2018 has reached a value of approximately 422,000 robot units. To get a real picture of the implementation of industrial robots in the World, an analysis was made on the continents Asia/Australia, Europe, and America (while on the continent Africa there is a minimal implementation of industrial robots and that is why we did not analyze it), which is shown in Fig. 3. The trend in the implementation of industrial robots is the largest on the continent Asia/Australia, and we can say that it unfolds in the last ten years in an exponential function, and every year the difference of application with the other two continents Europe and America is increasing. In the previous 2018, around 283,000 robot units have been implemented in Asia/Australia. It can be concluded that the trend of implementation in Europe and America is going in the direction with a slight increase each year and a slight increase in application in Europe compared to America. In Europe, the implementation reached a value of about 76,000 robot units in 2018, while in the same year in America, it reached a value of about 55,000 robot units. The overall trend of industrial robot implementation in Asia/Australia, Europe, and America is shown in Fig. 4.

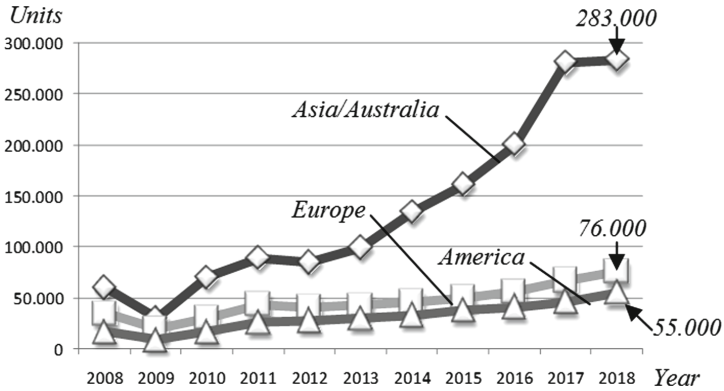


**Fig. 3.** Implementation of industrial robots on an annual basis in all manufacturing processes in Asia/Australia, Europe, and America for the period 2008–2018

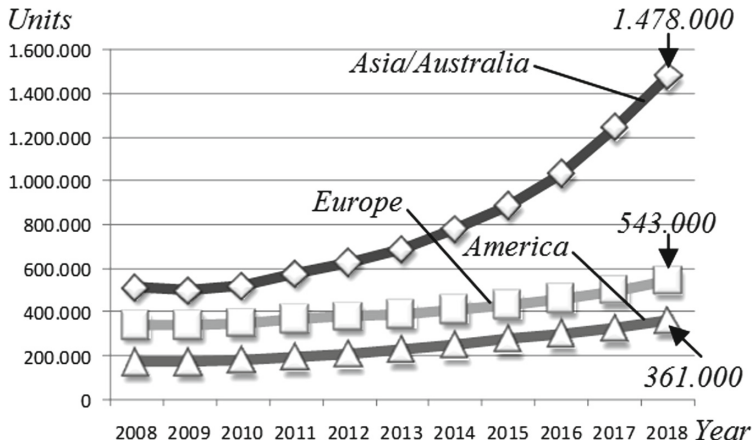


**Fig. 4.** Total implementation of industrial robots on an annual basis in all manufacturing processes in Asia/Australia, Europe, and America for the period 2008–2018

We conclude that the overall trend of industrial robot implementation on the analyzed continents is almost identical to the annual industrial robot implementation. The most significant application trend is in Asia/Australia and is growing exponentially so that in 2018 it reached the value of about 1.478 million units of robots, while the trend of implementation in Europe and America is moving in the direction. However, the trend of application in Europe is higher than in America. In Europe, the trend reached a value of about 543.000 robot units in 2018, while in the same year in America, it reached a value of about 361.000 robot units. To get a real picture of why the trends of industrial robot implementation across continents are like this, an analysis of the implementation of industrial robots in 2018 for fifteen top countries in the World is made and shown in Fig. 5 [11].

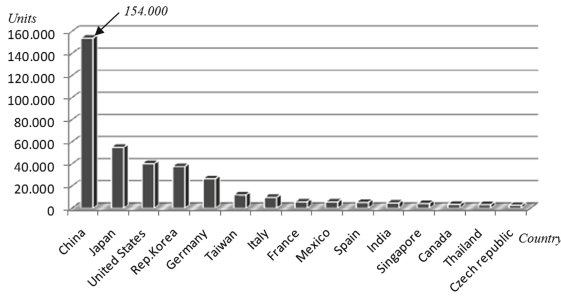


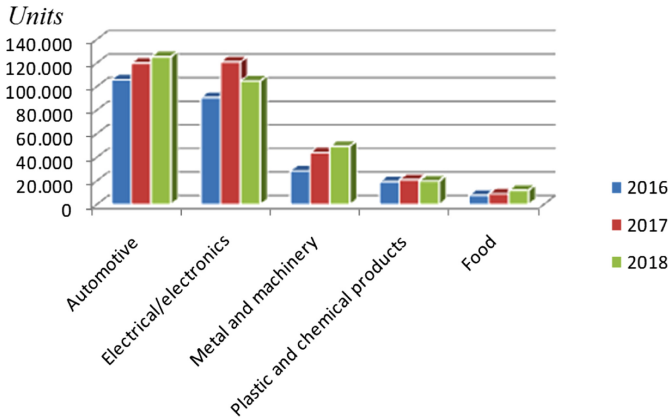
Fig. 5. Implementation of industrial robots in fifteen top countries in the World for 2018

## 4 Results and Discussion

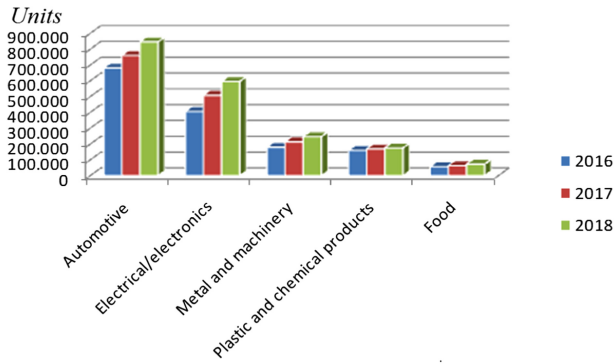
The explanation of the big difference in the implementation of industrial robots in Asia/Australia compared to Europe and America is given by the graph in Fig. 6. where we see that the implementation of industrial robots in the first six countries in 2018, four are located in Asia, namely: China, Japan, Republic of Korea, and Taiwan. China has been ranked first in the World for the implementation of industrial robots for the last six years [9, 10], and the reason for such a trend is the adoption of China’s development strategy called “Made in China 2025”, where it wants to become a technologically most developed country in the World by 2025. Of the total implementation of industrial robots, it is interesting to see the trend of distribution across industries in the World, and such an implementation trend is shown in Fig. 6.

As the trends in the implementation of industrial robots in various industries for 2016–2018 show on an annual and overall level, the automotive industry is in the first place in which about 30–40% of all industrial robots are implemented, the second is the electrical/electronics industry with about 20–30% of all industrial robots, followed by the metal, plastics and chemical industries, and finally, the food industry, which ranks the lowest by industrial robots implementation. The trend of implementation of industrial robots based on Fig. 6. we can see that it is growing year by year both on an annual and on an overall level. In the last two years, collaborative robots have been implemented in production processes, and the trend of implementation is shown in Fig. 7.

Based on the graph shown in Fig. 7, we conclude that the implementation of collaborative robots is small relative to traditional industrial robots. In 2017, 389.000 units of traditional industrial robots were implemented, and 11.000 units were collaborative robots, representing 2.89% of the total implemented robots in the World. In 2018, the implementation of collaborative robots in the World had increased to 3.32% of the total industrial robots implemented. In the coming period, the predictions are that the implementation of collaborative robots will continue to increase globally, thanks to Industry 4.0, which requires flexible automation, rapid change in the production of other products, higher quality, faster production, and cheaper product. and all of the above can be ensured through the implementation of collaborative robots.



a



b

**Fig. 6.** The implementation of industrial robots in the automotive, electrical/electronics, metals and machinery, plastics and chemical products and food industries of the World in period 2016, 2017 and 2018 (a - annual implementation; b - total implementation of industrial robots) [11].

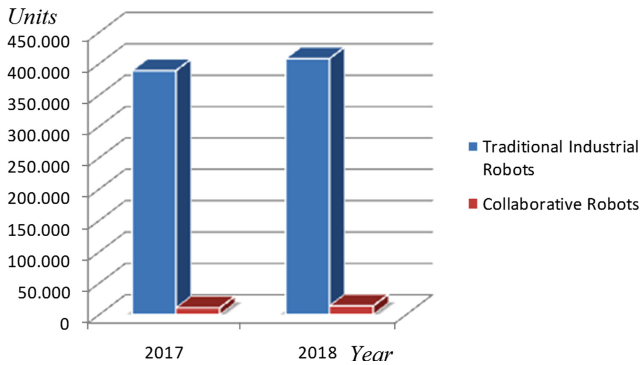


**Fig. 7.** Comparative analysis of traditional industrial robots and collaborative robots in 2017 and 2018 [11]



Based on the graphs shown in Fig. 8, we conclude that the trend of implementation of industrial robots in the World is growing every year, and the forecasts are that it will continue in the next period so that in 2022, the implementation of about 584.000 units of robots is expected. this trend of implementation is expected for several reasons, e.g. global competition in the market, implementation of industry 4.0, reduced product life, flexible automation, declining product prices, and development of new technologies.

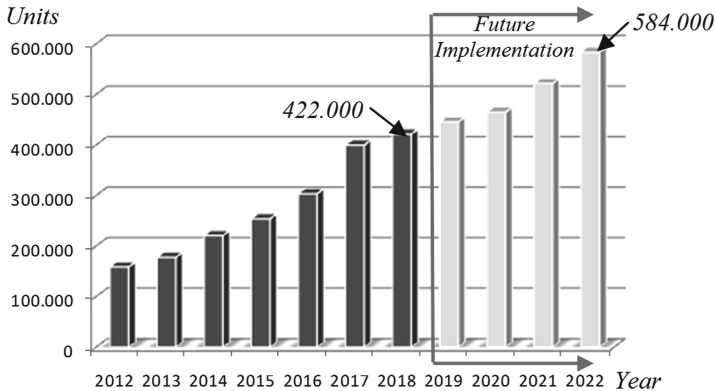


**Fig. 8.** Predictions of industrial robot implementation in all production processes in the World by 2022 [11].

## 5 Conclusion




The fourth industrial revolution is already present in all industries, from manufacturing to selling finished products. The introduction of technologies that form the basis of the fourth industrial revolution “Industry 4.0” as an example of robotic technology and industrial and service robots alters the processes and technologies, as well as the organization of production and sales. With the application of “Industry 4.0”, that is, the implementation of second-generation industrial robots in the production processes of all branches of industry, the linear production process is transformed into a network production process, that is, with all the aforementioned technology, into a closed-loop production process, where we have complete information on the production of the product at all times. By using a large number of smart sensors in the production process, at any given time, we have information about manufacturing devices and machines on which to decide when to replace devices and machines or have permanent maintenance. The implementation of second-generation industrial robots turns rigid automation into flexible automation, and every year the number of implemented industrial and service robots in the industry and all segments of the environment is increasing. This trend will continue in the future, as mentioned in our paper. In the coming years, the number of collaborative robots implemented in manufacturing processes in the industry will continue to increase.

## References

1. Schwab, K.: The Fourth Industrial Revolution. World Economic Forum, Geneva (2017)
2. Beaupre, M.: Collaborative robot technology and applications. In: International Collaborative Robots, Workshop, Columbia, USA (2015)
3. Bunse, B., Kagermann, H., Wahlster, W.: Smart Manufacturing for the Future. Germany Trade & Invest, Berlin (2017)
4. Ecker, C.: Advantages and challenges for small manufactures. In: International Collaborative Robots, Workshop, Columbia, USA (2015)
5. Meniere, Y., Rudyk, I., Valdes, J.: Patents and the Fourth Industrial Revolution. European patent Office, Munich (2017)
6. Ostrgaard, E.: Collaborative robot technology and applications. In: International Collaborative Robots, Workshop, Columbia, USA (2015)
7. Karabegović, E., Karabegović, I., Husak, E.: Collaborative robots innovate automation in metal and car industry in the world. *J. Sci. Eng. Res.* **6**(8), 136–145 (2019)
8. Karabegović, I., Karabegović, E., Mahmić, M., Husak, E.: Implementation of industry 4.0 and industrial robots in production processes. *Lecture Notes in Networks and Systems*, vol. 76, pp. 96–102 (2020)
9. Karabegović, I., Husak, E.: Industry 4.0 based on industrial and service robots with application in China. *J. Mob. Veh.* **44**(4), 59–71 (2018)
10. Karabegović, I.: The Role of industrial and service robots in fourth industrial revolution with focus on China. *J. Eng. Architect.* **5**(2), 110–117 (2017). <https://doi.org/10.15640/jea.v5n2a9>
11. World Robotics 2018: The International Federation of Robotics, Statistical Department, Frankfurt am Main, Germany (2018)
12. World Robotics 2015: The International Federation of Robotics, Statistical Department, Frankfurt am Main, Germany (2015)
13. World Robotics 2011: The International Federation of Robotics, Statistical Department, Frankfurt am Main, Germany (2011)
14. World Robotics 2010: The International Federation of Robotics, Statistical Department, Frankfurt am Main, Germany (2010)
15. Anandan, T.M.: collaborative robotics puts people first, Contributing Editor, Robotic Industries Association (RIA), Ann Arbor, Michigan, USA (2018)
16. Karabegović, I., Turmanidze, R., Dašić, P.: Robotics and automation as a foundation of fourth industrial revolution – industry 4.0. In: Tonkonogyi V. et al. (eds.) *Advanced Manufacturing Processes. InterPartner-2019. Lecture Notes in Mechanical Engineering*, pp. 128–136. Springer, Cham (2020). [https://doi.org/10.1007/978-3-030-40724-7\\_13](https://doi.org/10.1007/978-3-030-40724-7_13)



# Multi-agent Model of Energy Consumption at the Metallurgical Enterprise

Sergey Kiyko<sup>1</sup>, Evgeniy Druzhinin<sup>2</sup> , Oleksandr Prokhorov<sup>2</sup>,  
and Bohdan Haidabrus<sup>3</sup>  

<sup>1</sup> PJSC “Electrometallurgical works “Dniprospetsstal” named after A.M. Kuzmin, 81, Yuzhnoe Shosse, Zaporizhzhya 69008, Ukraine

<sup>2</sup> National Aerospace University “Kharkiv Aviation Institute”, 17, Chkalova St., Kharkiv 61070, Ukraine

<sup>3</sup> Sumy State University, 2, Rymkogo-Korsakova St., Sumy 40007, Ukraine  
haidabrus@gmail.com

**Abstract.** An agent-based simulation model has been developed for analyzing the energy management processes of a metallurgical enterprise when implementing a portfolio of energy-saving projects. The overall goal of improving energy efficiency at the enterprise is realized through the management of a portfolio of energy-saving projects that are aimed at performing the following tasks: optimizing the energy balance; minimization of natural gas consumption; optimization of energy efficiency, etc. The features of the informational interaction of agents in a multi-agent system are disclosed, due to mechanisms related to decentralized multi-project planning, including the resolution of resource conflicts when performing tasks, the search for the most optimal resources, which ensure that the work will be carried out on the most favorable conditions. Thus, the article is devoted to solving the complex problem of analyzing the energy management processes of a metallurgical enterprise when implementing a portfolio of energy-saving projects.

**Keywords:** Portfolio of energy-saving projects · Project feasibility · Risk · Resource allocation · Agent model · Metallurgical enterprise

## 1 Introduction

The formation of a science-based energy conservation strategy plays a significant role for metallurgical enterprises in meeting their goals of saving energy resources, reducing emissions, minimizing costs and increasing efficiency and competitiveness.

Evaluating and selecting projects for energy-saving measures to be implemented, objectively assessing the share of each energy resource in the total flow, determining the energy intensity of individual production, workshop, entire enterprise, and adjusting the strategic direction in energy management will allow the existence of an energy consumption model at the enterprise. To implement optimal management of energy flows, a method that uses a multi-agent approach is proposed, it consists of forming a community of agents for energy consumption, energy conversion, energy production and the purchase of electricity on the external market.

## 2 Literature Review

Hybrid Petri nets are used [1] for modeling and analysis of metallurgical processes. The dynamic flow of materials and real-time changes of each technological state in the metallurgical process are visually modeled with the application of this model. The problem of modeling the production and consumption of electricity in hybrid power systems is considered [2]. Calculation of optimal quantity and parameters of the components for generating renewable energy, depending on the projected demand for its consumption, is possible because of modeling. Logistics control of the resources flow in energy-saving projects in metallurgical industry is presented in the research [3].

A multi-agent approach to project portfolio management is considered [4, 5]. The author gives the system architecture of the agent model, the goals of functioning and features of the software implementation of various agents. However, the models of agent behavior in solving portfolio management problems remained outside the scope of the presentation. The method of mathematical programming and the model of dynamic mathematical optimization were used to establish excess gas in the optimal distribution among buffer consumers and dispatching steam production is considered in [6, 7]. In [8, 9] authors present the results of the optimization of electricity costs at metallurgical enterprises, provides basic information about the development of the simulation model and the stage of optimization. Multi-agent technologies have significant advantages in terms of constructing autonomous, adaptive, with the possibility of the auction and coordinated interaction of their elements modeling systems, which makes them the preferred approach for solving the problem of decentralized multi-project planning [11–13].

We developed an agent model for managing the distribution of energy resources, which is based on the interaction of suppliers' agents, consumption agents, production agents and transformation agents performing a search for correspondence of the available energy resources or the external energy market in the factory "market".

## 3 Research Methodology

Agent modeling assumes that the model includes many agents interacting with each other and with the external environment – information (software) elements that have their own goals and objectives, internal state and rules of behavior. One of the most important tasks in agent-based modeling of streaming energy consumption processes in the system under consideration is the formation of many alternative options for the consumption and production of energy resources. Such a model is necessary for the operational management of the processes of distribution and consumption of electricity in in-plant and in-workshop networks, as well as for monitoring the operating modes of the main energy-intensive technological equipment.

In this case, the simplest option for organizing a multi-agent community in solving problems of managing the distribution of energy resources can be based on the interaction of suppliers' agents, consumption agents, production agents and transformation agents that search for correspondence of available energy resources or the external energy market in the in-house "market" (Fig. 1).



When forming an agent-based representation of a simulation model, it is necessary to proceed from the selection of elements with individual behavior.

All purchased or produced energy resources are sold at a transfer rate to an Energy Distribution Agent, all consumed energy resources are purchased from an energy distribution agent at a transfer rate. At the same time, energy consumption agents issue a forecast of consumption for a certain perspective to the energy distribution agent. With a lack of resources from them, they buy them from an energy distribution agent. Energy consumption agents are divided by type of energy resource consumed: active and reactive electricity, thermal energy, fuel. For example, for each electricity consumption agent, the following parameters are set: power, rated line current, brand, section and length of the line cable, the specific resistance of the wire, number of automatic machines for power receivers, number of magnetic starters for power receivers, line load factor. Thus, the electrical characteristics of each section are formed. An energy distribution agent records applications in its database monitor limits and accepts them, in accordance with the state of resources, current energy balance, and acceptable risks. Here, the current state is determined, within the framework of which a shortage or excess of energy resources for a certain period is revealed. Consequently, there is either the use of available energy resources or the sale of energy resources or the purchase of energy resources. It turns out that the market is "a day ahead" - it works based on the exchange on which the indicative price of energy is determined, which all participants are guided by when concluding agreements and submit their applications today for tomorrow. The transfer of resources to energy consumption agents is carried out according to certain priorities, the purpose of which is to solve the problem of combining the achievement of target goals in terms of efficiency and profitability. An energy distribution agent may also refuse to allocate resources if there is a discrepancy with the amount of the application, there is currently a shortage or the established limits are exceeded. Verified applications are accepted. Accepted transfer transactions are involved in further calculations during modeling, rejected transactions can be finalized by agents (change in the number of energy resources, term and other attributes of the transaction) or deletion. After receiving a response from the agents about the operation, the energy distribution agent also records the actual energy costs.

If the limit is exceeded, a conflict arises, which must be resolved: either increase the limit, or reject the application, or revise the energy balance and, therefore, redistribute energy resources, taking them from other agents (groups).

An energy distribution agent performs a regulatory function in setting transfer prices for electricity and heat; its main task is to regulate the energy balance structure. The system of prices and tariffs for energy resources should stimulate a reduction in producer costs and economical consumption of energy by consumers. An energy distribution agent also interacts with a purchasing agent to cover energy shortages.

The formation of such an internal energy market creates an environment for the formation of various tariff offers for consumers, including the dependence on their distinctive load schedule (for instance, depending on the time of the day). The key mechanism of agent interaction is negotiations concerning the conclusion of domestic transfer deals for attracting/using resources between the agents of energy consumption, supply, production, and distribution.

An important feature of the model proposed is also the association of agents in question in groups by direction. Criteria for the selection of individual groups of agents in the model are the implementation of a set of interrelated and similar services and operations that make up a unified technological chain; the presence of its market activity; the presence of a body governing and coordinating activities. It is expected that various groups of agents will be distinguished based on the operations performed (electric steel, rolling, roasting, refining, heat treatment, and others), effective service by types of clients (corporate order, state order, investment order), and according to the territorial principle. Generally, an agent can belong to several groups. For each formed group, a coordinating agent is generated (Electrical steel, Rolling, Heating, etc.). The multidimensional and detailed distribution of energy consumption indicators within the framework of such a structure makes it possible to evaluate efficiency and influence individual structural divisions, business directions and products.

Each agent in the model is assigned its list of indicators, monitoring of which may point out the approach or emergence of undesirable (risks) situations. Exceeding the established limits by the values of indicators is the basis for the activation of various mechanisms and situational scenarios. Thus, when the voltage drops below the established value, the balancing mechanism is automatically turned on to maintain it. Also, there are occurrences of losses. In this case, *Indicators Agents* are generated in the system - their number corresponds to possible solutions to the situation, each of which tries to carry out its task in parallel, realizing the generated scenario independently of the others and not knowing about their existence. That is, calculations are carried out simultaneously for all alternative strategies and scenarios. Meanwhile, the strategies can be adjusted in the course of the calculations. Each agent of supply, production or consumption should be responsible for its imbalance, that is, deviations from the schedule of production or consumption. By concluding bilateral contracts or by purchasing energy resources in the domestic or foreign market a day in advance, energy suppliers and energy consumers commit themselves to ensure their consumption and production at certain hours at an appropriate level. In this case, they are considered to be parties responsible for the balance personally (or included on a contractual basis in a certain balancing group of agents).

It is not that simple to provide absolute correspondence to contracts in practice. For example, the weather conditions can worsen, which will lead to the increased demand for electricity for consumers in real-time or an unexpected failure in the operation of the transformer can happen, etc.

Within the established agent model, the meta level's function of management of energy efficiency is reflected in the adjustment of controlling parameters, influencing the agents' behavior in the process of informational interaction (increasing/decreasing production, spending cuts, etc.) The vector of controlling actions includes the adjustment of limits of energy consumption; eliminating losses of energy resources; utilization or sale of energy generated in the main production, etc.

Next, we will examine the mechanisms for selecting energy-efficient projects for our agent model in detail. Moreover, it is possible to use two types of energy-economic models - elementary and integrated. The Elementary model displays the technical and economic features of one energy-saving process, which belongs to one of the sub-systems of the enterprise. Integrated allows you to coordinate the basic characteristics

of elementary projects that belong to various subsystems of the enterprise (for example, for a heating system, this is the heating and electric power of machines and equipment, diameters of central heating pipes, etc.).

So, for a heating system the cost of fuel equivalent saving is one of the aspects of energy efficiency – this is achieved by switching from one implementation scheme to another, provided that, for example, the power and thermal power for the consumer are equal. To assess the relationship between the state of the enterprise, the profitability of heat generation and the prices of fuel and energy resources, the following ratio is proposed:

$$1 + R = r \cdot (\eta_k^{br} - q_{tr\ loss}) / (k \cdot (1 + r_e \cdot (q_{sn} + q_n))), \quad (1)$$

where  $r = c/c_f$ , ( $c$  – is the cost of heat,  $c_f$  – is the cost of fuel,  $c_e$  – is the cost of electricity);  $\eta_k^{br}$  – the energy efficiency of the heating unit;  $q_{tr\ loss}$  – heat losses;  $q_n$  – electricity losses; and  $q_{sn}$  – energy transportation costs;  $k$  – coefficient of additional costs associated with the generation of thermal energy.

Based on this, the possibility of connecting energy consumption agents to the centralized heat supply of an energy distribution agent is modeled. The value of annual fuel equivalent savings is used as a criterion for energy efficiency:

$$\Delta B = \Delta b_E - (b_{eltr} \cdot b_e \cdot b_{fch}) \cdot Q > 0 \quad (2)$$

where  $\Delta b_E$  – is the specific fuel equivalent savings;  $b_{eltr}$  – specific loss of electricity during transportation of energy;  $b_e$  – specific loss of fuel equivalent in electricity generation after connecting the consumer;  $b_{fch}$  – refers to the specific loss of fuel equivalent associated with the compensation of heat loss;  $Q$  – heat production per year.

The capacity setting of the base  $Q_b$  and peak  $Q_p$  loads of heat sources are implemented using the criterion of minimizing the total costs:

$$Z = k_b Q_b + k_p Q_p + n \left( \frac{E_b c_b a_b}{\eta_b} + \frac{E_p c_p a_p}{\eta_p} \right) \rightarrow \min, \quad (3)$$

where  $k_b$  and  $k_p$  are the specific capital costs of the base load and peak heat sources;  $E_b$  and  $E_p$  – the amount of thermal energy per year;  $c_b$  and  $c_p$  indicate the price of the primary energy source in the state of the base load and peak;  $\eta_b$  and  $\eta_p$  are the conversion factors of the primary energy source used for heat production;  $a_b$  and  $a_p$  – additional cost factors in the base load and peak states, which show the relationship between total operating costs and energy costs incurred in the production of thermal energy;  $n$  is the period of implementation of the energy-saving project. The power ratio of  $Q_b$  and  $Q_p$  is determined by the temperature limits of the atmospheric air. If the temperature is above this level, a heat source with a base load carries a heat load; if below the limit level, both the base load and the peak heat sources carry a heat load.

The model justifies the use of combined heat sources with a base load and peak. The heat source of the base load is characterized by high energy efficiency and large



initial capital costs, while the source of the peak heat shows relatively low energy efficiency and moderate initial capital costs.

Mathematically, the task of energy savings determined by the formula:

$$EP = e_1x_1 + e_2x_2 + \dots + e_ix_i + e_nx_n \rightarrow \max, \quad (4)$$

where  $EP$  – total savings resulting from the implementation of energy-efficient projects;  $x_i$  – savings from the project  $i$ ;  $e_i$  – annual savings, resulting from the corresponding project.

The set of feasible alternative solutions is generated by the following control systems in the form of inequalities:

$$\begin{aligned} kx_1 + k_2x_2 + \dots + k_ix_i + k_nx_n &\leq K, \\ x_1 &\leq X_1, x_2 \leq X_2, \dots, x_i \leq X_i, x_n \leq X_n \\ x_1 &\geq 0, x_2 \geq 0, \dots, x_i \geq 0, x_n \geq 0 \end{aligned} \quad (5)$$

where  $k_i$  – specific costs incurred in the result of the implementation of the project;  $x_i$  – the maximum possible effect of the project;  $k$  – the number of available resources to use to implement all the projects under consideration.

The formula describes the objective function as the total savings received from the implementation of projects. These inequalities are obvious inherent conditions that are associated with financial constraints and restrictions on the effect of each project.

The considered task makes sense when:

$$kx_1 + k_2x_2 + \dots + k_ix_i + k_nx_n > K \quad (6)$$

This inequality means that the amount of available resources is less than the number of resources needed to implement all projects in full.

To expand the range of selection criteria for energy-efficient projects, the above objective function can be represented as a comprehensive criterion of utility:

$$P = \frac{e_1k_1}{T_{1av}} + \frac{e_2k_2}{T_{2av}} + \dots + \frac{e_nk_n}{T_{nav}} \rightarrow \max, \quad (7)$$

where  $T_{nav}$  – the middle rank of the project  $i$  based on the criterion  $p$ .

$$T_{iav} = (T_{i1} + T_{i2} + \dots + T_{ia} + \dots + T_{ip})/p, \quad (8)$$

where  $T_{ia}$  – the rank of the project  $i$  based on the criterion  $\alpha$ .

Along with the payback period, a comprehensive criterion of utility allows us to take into account other portfolio project effects using expert methods, for example, improving energy security, etc.

Thus, some of the mechanisms of the agent simulation model for analyzing the energy management processes of a metallurgical enterprise during the implementation of portfolio energy-saving projects were considered.

## 4 Results

The multi-agent model was developed in the Anylogic simulation environment. The developed models allow us to identify, to analyze and to choose the promising energy-saving projects to choose among them the most viable one. We managed to optimize the portfolio and this allowed us to focus on the most desirable goals. Approbation of the developed models and computer means in PJSC Dniprospsststal proved that the effective management of energy efficiency based on the program and portfolio project management is possible.

In the period from 2016 to 2018, the company introduced energy conservation measures, which are presented in Table 1. In total, it was planned to reduce the consumption of natural gas by 1% and heat energy by 1.2% using these measures. Using the model, an assessment was made whether the targeted use of energy resources is being implemented after the implementation of projects and measures for saving energy.

**Table 1.** Inventory of energy-saving portfolio projects.

Energy-saving project	Cost thou., UAH	Total savings, thou., t/s fuel	Cost of savings, thou., UAH
The implementation of a reducing device at the input of steam No. 3	350	0,1845	1225
Thermotechnical adjustment of the overlay of the thermal furnace of the rolling workshop	440	0,0360	220
Thermotechnical adjustment of the overlay of the heating wells of the rolling workshop	270	0,0220	135
Thermotechnical adjustment of the overlay of HELIOS installations of the calibration workshop	290	0,0244	145
Thermotechnical adjustment of chamber furnaces	315	0,028	157,5
The implementation of innovative fibrous materials for lining the glide tubes of a small-section rolling mill furnace	560	0,097	1225

The change in the efficiency of electric energy consumption as a result of the implementation of energy-saving measures was calculated. As a fragment, Fig. 2 shows a graph of the accumulated amounts of actual energy consumption for one of the months and the target energy consumption obtained as a result of modeling.

As can be seen from the figure, the enterprise reduced fuel consumption as a result of energy-saving measures. Despite the fact that the enterprise has not reached the target level of energy efficiency, the forecast error in modeling energy consumption for a metallurgical enterprise is at a satisfactory level.

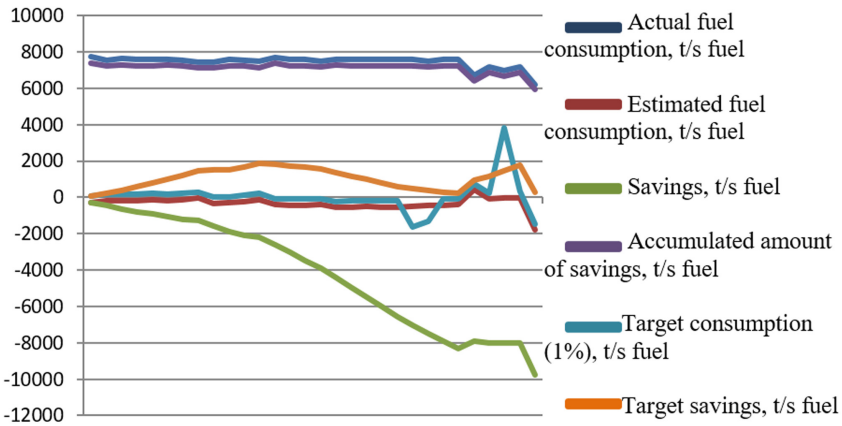


**Fig. 2.** Comparison of results of modeling and actual fuel consumption.

The consumption of electricity by the enterprise in 2017 has made 421168.0 thousand kWh (Fig. 3). Due to the implementation of the energy-saving program in 2017, the enterprise saved 1.7 million kWh and 350 thousand m<sup>3</sup> of gaseous fuel. In comparison with 2011 electricity consumption on steel-melting production has decreased by 30%. Also, the share of costs of the electricity for steel-melting production has decreased from 71% in 2011 up to 67.8% in 2017.

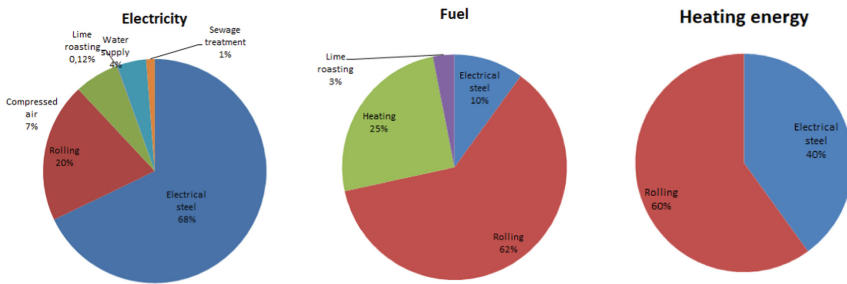


**Fig. 3.** The balance of energy consumption in PJSC Dniprospsststal in 2017.

## 5 Conclusions

Thus, an agent-based simulation model has been developed for analyzing the energy management processes of a metallurgical enterprise while implementing portfolio energy-saving projects. The advantages of the multi-agent approach are the ability to build autonomous, adaptive, with the possibility of the auction and coordinated interaction of the elements of modeling systems, which makes them the preferred approach for solving the problem of decentralized multi-project planning of the portfolio energy-saving projects.




Using this model allows analyzing projects consistently to identify the possibility of their implementation at the enterprise, to coordinate project implementation plans and enterprise plans at various planning levels. The proposed approach has distinctive features: integration of strategic decisions (accept or reject new projects) and operational aspects (resource allocation); flexible resource management.

## References

1. Yujuan, R., Bao, H.: Modeling and simulation of metallurgical process based on hybrid Petri net. In: IOP Conference Series: Materials Science and Engineering, p. 157 (2016)
2. Shcherbakov, M.V., Nabiullin, A.S., Kamaev, V.A.: Multiagent system for modeling the production and consumption of electricity in hybrid power systems. Eng. Bull. Don **20**(2), 217–221 (2012)
3. Kiyko, S., Druzhinin, E., Prokhorov, O., Ivanov, V., Haidabrus, B., Grabis, J.: Logistics control of the resources flow in energy-saving projects: case study for metallurgical industry. Acta Logist. **7**(1), 49–60 (2020). <https://doi.org/10.22306/al.v7i1.159>
4. Zhou, L.: Multi-agent based project portfolio management approach. In: Proceedings of the International Symposium on Intelligent Information Systems and Applications, pp. 240–243 (2009)
5. Martin, J., Elg, M., Wallo, A., Kock, H.: Four facets of learning in performance measurement. Int. J. Prod. Perform. Manag. **67**(9), 1608–1624 (2018)
6. Liu, J., Cai, J.: Optimization model based on electric power generation in steel industry. Math. Prob. Eng. **23**(2) (2014)
7. Ali, M.S., Agalya, R., Shekher, V., Joo, Y.H.: Non-fragile sampled data control for stabilization of non-linear multi-agent system with additive time varying delays, Markovian jump and uncertain parameters. Nonlinear Anal.: Hybrid Syst. **36**, 100830 (2020)
8. Krysanov, V., Danilov, A., Burkovsky, V., Gusev, P., Gusev, K.: Optimization of energy consumption of the enterprise using simulation modeling. In: Proceedings of 14th International Conference on Electromechanics and Robotics “Zavalishin’s Readings”, pp. 707–715 (2019)
9. Nilsson, L., Elg, M., Bergman, B.: Managing ideas for the development of new products. Int. J. Technol. Manag. **24**(5–6), 498–513 (2002)
10. Prokhorov, A.V.: Model of dynamic management of resources of agents’ distributed interaction. Systems of management, navigation and communication: collection of research papers, Poltava national technical Yirii Kondratiuk university, No. 1 (37), pp. 93–97 (2016)
11. Saraeian, S., Shirazi, B., Motameni, H.: Optimal autonomous architecture for uncertain processes management. Inf. Sci. **501**, 84–99 (2019)
12. Chandra, C., Grabis, J.: Information technology support for integrated supply chain modeling. Hum. Syst. Manag. **27**(1), 3–13 (2008)
13. Grabis, J., Kampars, J.: Design of capability delivery adjustments. Lecture Notes in Business Information Processing, vol. 249, pp. 52–62 (2016)



# Development and Implementation Possibilities of 5G in Industry 4.0

Dragan Peraković<sup>(✉)</sup> , Marko Periša , Petra Zorić ,  
and Ivan Cvitić 

University of Zagreb, 4, Vukelićeva, Zagreb 10000, Croatia  
dragan.perakovic@fpz.hr

**Abstract.** The Industry 4.0 environment combines innovative information and communication technologies with Internet and physical systems, enabling advanced wireless communications and the Internet of Things services. Such digital and wireless transformation has the potential to drive economic growth in manufacturing using 5G technology. A key component of this potential lies in the collaboration between stakeholders in the manufacturing and mobile ecosystems industries who have acted in parallel in the past. In the future, the 5G technology will have a major impact on industry and mobility and will enable manufacturers to complete end-to-end automation with the virtual deployment of new product lines or the entire factory. Directly contributing to the social and economic development, 5G will be the technology that will enable growth and transformation in the Industry 4.0. This paper aims to show the impact that 5G can have on improving manufacturing processes in a smart factory environment and how it can respond to its increasing requirements. It will also outline the technical challenges that the manufacturing industry may meet when implementing this technology. Accordingly, an overview of the state of implementation of the 5G technology and a future development plan of Industry 4.0 in Europe will be given.

**Keywords:** Information and communication technology · Cellular networks · Industrial revolution · Smart manufacturing

## 1 Introduction

Digital transformation is becoming a key driver of rapid change in the world. Its potential is reflected in the fact that it has the potential to significantly improve the lives of customers while providing new opportunities for creating and collecting value for businesses. The telecommunications industry is at the top of that transformation as an industry that is witnessing major changes in its market environment, but also as a key driver of digitization in the world. The investment of the telecommunications industry in technology and interoperability has fostered a shift in information flow through the global economy.

Digitization, with the development of information and communication technologies (ICT), has become important for the creation of the concept of Industry 4.0 (I4.0). This concept refers to the fourth industrial revolution, and the term I4.0 itself is originally

taken from Germany [1]. Apart from Europe, there are also major changes in the manufacturing sectors in the US and China, so I4.0 can be said to have become a global phenomenon.

The development of industry throughout history (Fig. 1) has been driven by the expansion of technologies, primarily ICT, which began during the third industrial revolution. Within this generation of industrial development, comes the appearance of automation which leads to mass production. Automation is one of the main pillars of the current industrial revolution [2].

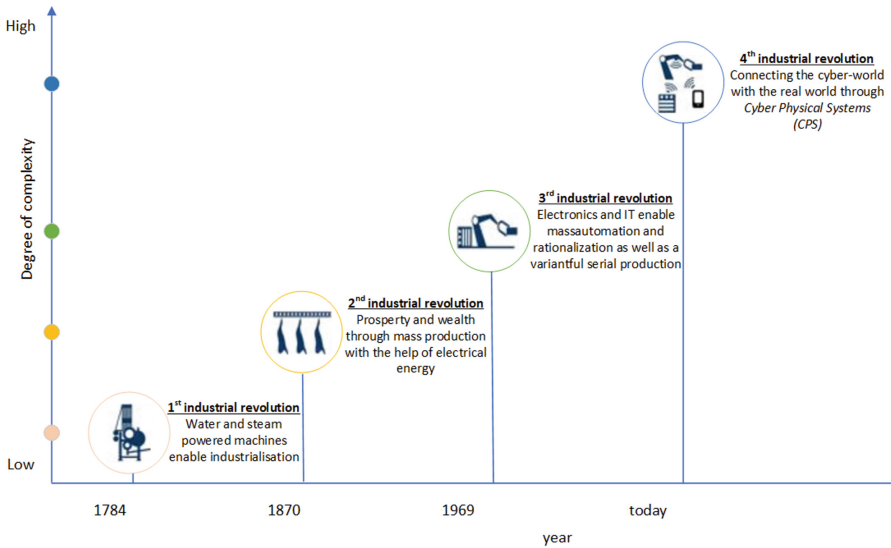


Fig. 1. The evolution of industrial revolutions [3].

The focus of I4.0 is not on industrial work as in previous industrial revolutions, but on IT systems, robotics, automation environment, and efficiency. Production process automation with digitization and constant data exchange creates a set of interconnected devices of different technologies and stakeholders, which enables advanced wireless communications and the Internet of Things (IoT) services. The major challenge of I4.0 is to achieve interoperability, which requires the fulfillment of specific principles that guarantee a complete process of accuracy and efficiency [4].

## 2 Literature Review

According to research [5], the market for I4.0 products and services is expected to grow to \$310 billion by 2023. This forecast is based on the state of I4.0 adoption in the manufacturing vertical and the analysis of two different technology subsets in the I4.0 market: related industry development blocks and other supported I4.0 technologies.

The I4.0 enabled ICT, and therefore the smart factory is communication technologies, IoT, Internet of Services (IoS) and Wireless Sensor Network (WSN) [6–8].

IoT is the most represented ICT in I4.0 [4, 9]. It enables the connection of things from environments such as machines, workers, customers, or products to deliver real-time information. It is important to mention that IoT is constantly and rapidly evolving with the new proposed technology while exceeding into the new application domain with the currently available technology [10]. I4.0 integrates IoT and its related services into industrial manufacturing, providing vertical and horizontal integration across the entire value chain and all layers of automation. The 2017 Gartner forecasts refer to how the number of connected IoT devices in I4.0 will reach 20.4 billion in 2020 [11]. One of the challenges for the manufacturing industry is the smart factory, which is thriving because of IoT development and automation [12]. The smart factory is an integrated and flexible production system that learns and adapts to new requirements using a continuous flow of data from connected production and operating systems [13]. The I4.0 environment is characterized by a transition from traditional automation to a fully integrated system without human intervention. The ability to adapt and obtain real-time information makes a smart factory more efficient and proactive [14, 15].

After the appearance of the 1<sup>st</sup> generation or 1G in 1980, digital wireless communication systems are progressing every 10 years [16]. Some of the many requirements that the current mobile wireless technologies (3G and 4G) need to accomplish, but do not have the ability to, are related to high-speed rate, high coverage, low latency, a large number of connected devices, high reliability and high level of security. 5G, on the other hand, plays a key role in accelerating production in the current industry, as well as in facilitating future services in the industry of the future. Its architecture enables dynamic programming to provide separate layers for different applications, thus creating new business use cases [17]. 5G features are related to data transfer speed (10 Gb/s) and latency (<1 ms) that support real-time applications. It brings reliability, latency, scalability, architecture, and services to the smart factory environment [18]. The number of 5G networks in the world is constantly increasing. According to [5], 321 telecommunications operators in 103 countries invest in 5G. This refers to testing or trials in the 5G network, network implementation, licensing, and service launch.

5G will provide better flexibility and quality of service (QoS) through network slicing. This term refers to a means of creating logically separate unique use case virtual networks using the same physical network [19, 20]. However, the focus in 5G is on the machine-type device to device (D2D) communication and IoT. The network architecture will provide ultra-reliable low delay communication for D2D communication [21]. Given D2D communication in the smart factory production environment, there is a need for good spectral resource management and an interference management system to ensure high communication reliability. The implementation of IoT applications is challenging due to a large number of devices, limited resources and heterogeneous environments [10]. In addition to the technical challenges that the 5G technology faces, the impact of this technology on the environment and human health has been the subject of research [22].

The manufacturing industry has only recently started implementing many industrial wireline communication protocols with IEEE 802.1 Ethernet with Time Sensitive Networking (TSN) extensions. The 3rd Generation Partnership Project (3GPP) has set a

5G standard for wireless technology deployment in the industry. Such convergence on TSN and Ethernet will help integrate fixed and wireless industrial business communication [23]. Although the final requirements for 5G have still not been completed, the International Telecommunication Union (ITU) radio communications sector (ITU-R) has identified three typical scenarios for the future evolution of 5G in a smart factory: Enhanced Mobile Broadband (eMBB), Massive machine type communication (mMTC) and Ultra-reliable and low latency communication (URLLC) [11, 24]. Designing the URLLC scenario represents the biggest challenge [25]. Paper [26] represents new solutions for the physical layer of URLLC communication for 5G.

Network operators in the value chain must partner with other stakeholders that provide sensors, applications, and integrated services to ensure a reliable communication infrastructure. For this reason, it is necessary to establish new business models that are oriented on ecosystems [27, 28]. Machine-controlled robots, sensors, and logistics enable manufacturers to achieve large increases in productivity. The 5G technology will enable the growth and transformation of I4.0 and thus directly contribute to social and economic development [18]. In parallel with continuous investments and improvements in mobile technology globally for the public network, providers of communications services have identified the industry as an addressable market segment for providing services on the 5G non-public network (NPN) [29]. Although 5G has not yet been implemented in all countries of the world, numerous researches are turning to newer technology than 5G, respectively the 6G technology. The authors in [30] present the expected applications that have certain requirements as well as possible technologies for 6G communication. Papers [31] and [32] discuss the possible technologies to provide the basis for 6G systems as well as potential use cases, one of which is related to the manufacturing industry. Machine type communication in 6G has also been the subject of research [33].

According to the above-mentioned, this paper is aimed at providing information on how 5G can improve manufacturing processes in a smart factory environment as well as respond to its increasing requirements in terms of reliability, latency, scalability, architecture, and services.

### 3 Research Methodology

Numerous scientific methods have been used to demonstrate the development and implementation of 5G in the I4.0 environment, but also for future predictions. The historical method was used to show the chronology of I4.0 development as well as mobile wireless technologies. The inductive method is used for the application of an inductive way of concluding in which, based on individual facts and cognition, new facts and general conclusions of the paper were realized. Given the many types of induction, in this paper, the authors used incomplete, predictive and analogical induction. Incomplete induction was used to create conclusions based on a smaller limited number of individual occurrences that apply to other facts. Predicative induction is used to predict future occurrences and happenings, while analogical induction was used to make conclusions by analogy whereby the conclusion was based on various use cases investigated in a systematic analysis of scientific and professional



literature. The authors also used a deductive method to derive new statements from one or more of the investigated statements that arise from previous statements.

The abstract method separated the irrelevant and emphasized important elements and conclusions of this paper’s research area, while the generalization method has made individual terms more general. The classification method divided the knowledge gained from the analysis of scientific and professional literature into logical entities, and conclusions were established regarding the capabilities that 5G provides in the I4.0 environment, i.e. smart factory, to identify the impact that 5G has on the technologies in I4.0. The comparative method is used to compare research on the technical characteristics of 5G obtained by analysis to provide an overview of the possibilities that 5G implementation can bring into a smart factory environment.

Figure 2 illustrates the process of a systematic method of analyzing the scientific and professional literature used in this paper. The authors have studied over 150 scientific and professional papers from scientific databases such as Springer, Science Direct, IEEE Xplore. Google Scholar was also used to find related publications on ICT and smart manufacturing in the business field. The scientific and professional literature search was based on the same keywords such as I4.0, smart manufacturing, ICT in I4.0, cellular networks, and 5G.

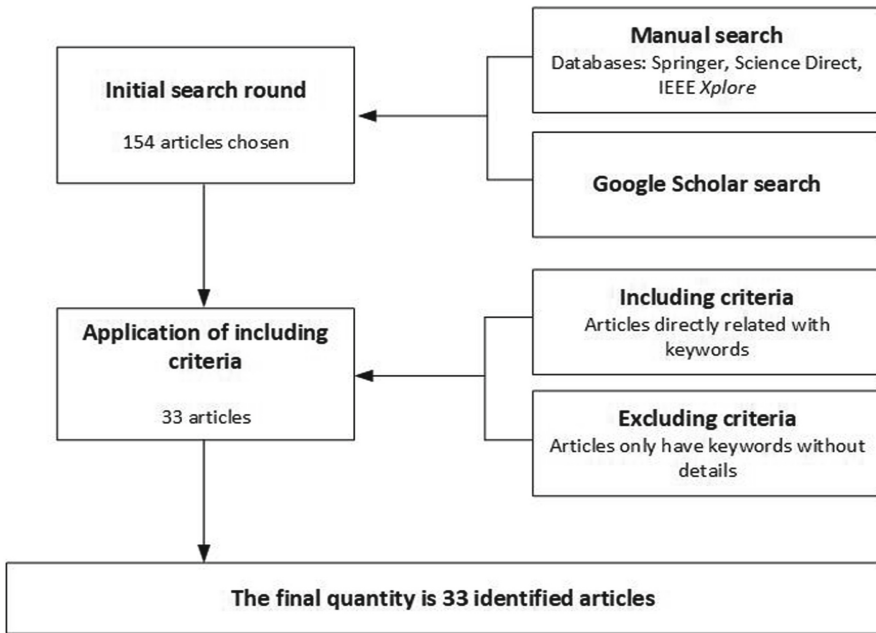


Fig. 2. Literature selecting.

The synthesis method connected separated elements, processes and relationships into a unique complex where its parts are interconnected. Accordingly, from the total number of papers, using the synthesis method of the results obtained by this search,

most relevant scientific and professional papers that have at least 2 of 5 searched keywords were selected.

## 4 Results

With the above-explained methodology, the paper presents the following results. EU Public-Private Partnership (5G-PPP) is a joint initiative between the ICT industry in Europe and the European Commission for reviewing and creating the next generation of communication networks and services to provide ultra-fast connectivity and real-time service delivery. The initiative was launched in 2013 and, thanks to it, Europe is at the forefront of the current phase of exploring 5G implementation compared to other regions. In 2016, the European Commission announced a 5G Action Plan for Europe to step up the efforts to deploy 5G infrastructure and services in the Digital Single Market by 2020. To achieve investment in 5G infrastructure, certain measures have been proposed, concerning the commercial implementation and provision of the frequency band for 5G. The Action Plan and the new European Electronic Communications Code are aimed at boosting industry competitiveness in the digital single market.

Finland is one of the first countries in the world that has issued licenses for the 3.5 GHz spectrum to enable the construction of 5G networks. European countries that have so far issued 5G operating licenses among operators and their profit are shown in Table 1. Other countries are currently in the process of participating or planning to launch the 5G spectrum auction by the end of 2019 and in 2020.

**Table 1.** Countries that released 5G operational licenses among mobile network operators on auctions.

Country	Spectrum bands	Total paid by operators
Austria	390 MHz from 3.4–3.8 GHz	€1.88 million
Finland	3.410–3.800 MHz	€77 million
Germany	2 GHz and 3.6 GHz	\$6.1 billion
Italy	75 MHz in the 700 MHz, 200 MHz at 3.6–3.8 GHz and 1 GHz in the 26.5–27.5 GHz	\$7.6 billion
Latvia	50 MHz block at 3550–3600 MHz	€6.53 million
Romania	700 MHz, 800 MHz, 1500 MHz, 2600 MHz and 3400–3800 MHz	€500 million
Spain	3.6–3.8 GHz	\$507 million
Switzerland	700 MHz, 1.4 GHz, 2.6 GHz, and 3.5 GHz	€338 million
UK	3.4 GHz and 2.3 GHz	£1.4 billion

It is important to mention that there are some obstacles to the full implementation of a 5G network in Europe. One of the major obstacles is market fragmentation. For this reason, some operators are hesitant about making major investments in next-generation technology.

5G has the potential to provide wireless connectivity for a wide range of use cases and applications in I4.0. The potential that 5G implementation can bring to industrial production is recognized in the scientific and research world as well as in the industry itself. The biggest indicator of the above-mentioned is in financial investments so far. Before 5G implementation in the industrial area, operators need to consider their business relationship to the market size. A common and important item missing from most business plans is the distribution of the Potential Available Market (PAM), Total Addressable Market (TAM), Served/Serviceable Available Market (SAM) and Serviceable & Obtainable Market (SOM). Their identification requires market research that will bring information about operators' product and market potential that can be reached with 5G implementation.

The paper presents the requirements of a smart factory and how 5G can respond to them, as can be seen in Table 2. Latency is one of the most important parameters of a smart factory. In a smart factory where a 5G network is implemented, the latency will

**Table 2.** Smart factory requirements and 5G characteristics that meet the requirements.

Parameter	Requirement/Description	5G response to smart factory requirements
Reliability	Improved coverage and efficiency for IoT devices and users	Ultra-high reliability, 99.999% of packets
Latency	1 ms or less	1–10 ms
Connection density	Supporting extreme density of IoT devices, minimum of 100 devices/m <sup>2</sup>	1 thousand–1 million devices/m <sup>2</sup>
Mobility	Seamless mobility for reliable operation and ubiquitous connectivity	Mobility performance can be enhanced through multi-connectivity
Battery lifetime	Long battery lifetime to support billions of low power and low-cost IoT devices	Up to 10 years
Availability	Communication service availability 24/7/365	99.999% of the time
Access	Broadband access in dense areas	Indoor ultra-high broadband access
Security	Improved security strategy to improve the security on the whole network End-to-end protection mechanism, protection of identity and location privacy	Strong E2E security, mutual authentication between device and network
Data connection	Faster data connections between machine communication	10–100 times faster
Data rate	Higher data rate than today for real-time communication	Peak data rates of 20 Gb/s in the downlink and 10 Gb/s in the uplink
QoS	Traffic classification and prioritization	Flexible QoS framework that can support traffic flows

not only be lower but also more predictable. This means that processes with time-critical events can rely on data transmission using 5G to communicate with other processes that also have time-critical events. Another important parameter is the availability of a communication service, given the number of connected devices in a smart factory environment. Also, a faster data connection is expected between connected devices than it is today, with 5G allowing 10–100 times faster connectivity than current mobile networks. Related to the security of production data that is exchanged between connected devices, 5G provides powerful end-to-end (E2E) security.

Combining wireless sensors and the 5G technology achieves data collection from production lines and their transfer to the cloud for easy monitoring and control. Also, 5G enables real-time communication between logistics and products, humans and robots. In terms of business potential, I4.0 is one of the main users of 5G technology. The main role of 5G networks in I4.0 is to contribute to the future IoT generation by connecting billions of intelligent things that create a real future and massive IoT.

During the implementation of 5G in its environment, the manufacturing industry needs to establish a reliable radio network in a closed environment. This applies to new innovative technologies and approaches. Also, spectrum availability is one of the challenges, since public networks operating in the same spectrum can cause interference to the wireless signals that the manufacturing process relies on. For this reason, there is a need to provide services on 5G NPNs in a smart factory environment.

## 5 Conclusion

ICTs are responsible for developing the digital transformation that forms the backbone of I4.0, while IoT is the most represented ICT in I4.0. Some of the many requirements that the communication technology needs to fulfill for the smooth operation of a smart factory are the high-speed transmission, high coverage, low latency, many connected devices, high reliability, and high security. 5G technology can meet these requirements. Its data rate and latency features support real-time communication between logistics and products, humans and robots.

The massive growth in 5G implementation is part of the European Commission's action plan aimed at boosting industry competitiveness in the digital single market. One of the primary interests is 5G NPN in production scenarios. However, the above-mentioned still includes a wide range of use cases with an appropriate variety of network configurations. In the long run, there may be a decline in the various communication technologies currently in use. This would significantly reduce the number of relevant industrial connectivity solutions. There are several challenges related to transforming a company's business towards 5G, however, developing business models is one of the biggest challenges. Companies in Europe will be able to deliver industrial ecosystems in a safer and faster way with the help of 5G while providing sustainable value for all stakeholders. In the future, 5G is likely to become the standard wireless technology of choice as it can enable direct and seamless wireless communication from the smart factory to the cloud.

## References

1. Ślusarczyk, B.: Industry 4.0 – are we ready? *Polish J. Manag. Stud.* **17**, 232–248 (2018)
2. Oztemel, E., Gursev, S.: Literature review of Industry 4.0 and related technologies. *J. Intell. Manuf.* **31**(1), 127–182 (2018)
3. Dense air: Next Generation Private Mobile Networks for Industry 4.0. <https://www.theiet.org/media/2597/dense-air.pdf>. Accessed 10 Nov 2019
4. Lu, Y.: Industry 4.0: a survey on technologies, applications and open research issues. *J. Ind. Inf. Integr.* **6**, 1–10 (2017)
5. 5G Networks and Devices: a Global Snapshot (2019)
6. Peraković, D., Periša, M., Zorić, P.: Challenges and issues of ICT in Industry 4.0. In: Ivanov, V., et al. (eds.) *Advances in Design, Simulation and Manufacturing II. DSMIE-2019. Lecture Notes in Mechanical Engineering*, pp. 259–269. Springer, Cham (2020). [https://doi.org/10.1007/978-3-030-22365-6\\_26](https://doi.org/10.1007/978-3-030-22365-6_26)
7. Peraković, D., Periša, M., Zorić, P.: Identification of the relevant parameters for modeling the ecosystem elements in Industry 4.0. In: Knapcikova, L., Balog, M., Perakovic, D., and Periša, M. (eds.) *4th EAI International Conference on Management of Manufacturing Systems*, p. 362. Springer, Cham (2020)
8. Periša, M., Kuljanić, T.M., Cvitić, I., Kolarovszki, P.: Conceptual model for informing user with innovative smart wearable device in Industry 4.0. *Wirel. Netw.* **25**, 1–12 (2019)
9. Pisching, M.A., Junqueira, F., Filho, D.J.D.S., Miyagi, P.E.: An architecture based on IoT and CPS to organize and locate services. In: *IEEE International Conference on Emerging Technologies and Factory Automation, ETFA, 2016-Novem*, pp. 1–4 (2016)
10. Li, S., Xu, L.Da, Zhao, S.: 5G internet of things: a survey. *J. Ind. Inf. Integr.* **10**, 1–9 (2018)
11. Cheng, J., Chen, W., Tao, F., Lin, C.L.: Industrial IoT in 5G environment towards smart manufacturing. *J. Ind. Inf. Integr.* **10**, 10–19 (2018)
12. Ericsson: *The 5G business potential second edition* (2017)
13. Bunse, B., Kagermann, H., Wahlster, W.: *Industrie 4.0, Smart Manufacturing for the Future. Report* (2014)
14. Temesvári, Z.M., Maros, D., Kádár, P.: Review of mobile communication and the 5G in manufacturing. *Procedia Manuf.* **32**, 600–612 (2019)
15. Peraković, D., Periša, M., Cvitić, I.: Analysis of the possible application of assistive technology in the concept of Industry 4.0. In: Radojičić, V., Bojović, N., Marković, D., Marković, G. (eds.) *The Thirty-Sixth Symposium on Novel Technologies in Postal and Telecommunication Traffic - PosTel 2018*, pp. 175–184. Pekograf d.o.o., Belgrade, Republic of Serbia (2018)
16. 1G, 2G, 3G, 4G - The Evolution of Wireless Generations. <https://support.chinavasion.com/index.php?Knowledgebase/Article/View/284/42/1g-2g-3g-4g—the-evolution-of-wireless-generations>. Accessed 8 Nov 2019
17. Karrenbauer, M., Ludwig, S., Buhr, H., Klessig, H., Bernardy, A., Wu, H., Pallasch, C., Fellan, A., Hoffmann, N., Seelmann, V., Taghouti, M., Wunderlich, S., Tercero Lozano, P., Hoell, A., Stimming, C., Patel, D., Seetaraman, S., Bender, S., Eberhardt, E., Schildknecht, T., Herfs, W., Storms, S., Stich, V., Niebert, N., Schotten, H.D., Fitzek, F.H.P.: Future industrial networking: from use cases to wireless technologies to a flexible system architecture. *at - Automatisierungstechnik* **67**, 526–544 (2019)
18. Rao, S.K., Prasad, R.: Impact of 5G technologies on Industry 4.0. *Wirel. Pers. Commun.* **100**, 145–159 (2018)
19. Walia, J.S., Hämmäinen, H., Kilkki, K., Yrjölä, S.: 5G network slicing strategies for a smart factory. *Comput. Ind.* **111**, 108–120 (2019)

20. Taleb, T., Afolabi, I., Bagaa, M.: Orchestrating 5G network slices to support industrial internet and to shape next-generation smart factories. *IEEE Netw.* **33**, 146–154 (2019)
21. Jovović, I., Husnjak, S., Forenbacher, I., Maček, S.: Innovative application of 5G and blockchain technology in Industry 4.0. *EAI Endorsed Trans. Ind. Netw. Intell. Syst.* **6**, 157122 (2019)
22. Di Ciaula, A.: Towards 5G communication systems: are there health implications? *Int. J. Hyg. Environ. Health* **221**, 367–375 (2018)
23. Zielinski, E., Schulz-Zander, J., Zimmermann, M., Schellenberger, C., Ramirez, A., Zeiger, F., Mormul, M., Hetzelt, F., Beierle, F., Klaus, H., Ruckstuhl, H., Artemenko, A.: Secure real-time communication and computing infrastructure for Industry 4.0 — challenges and opportunities. In: 2019 International Conference on Networked Systems (NetSys), pp. 1–6 (2019)
24. Lien, S.-Y., Hung, S.-C., Deng, D.-J., Wang, Y.J.: Efficient ultra-reliable and low latency communications and massive machine-type communications in 5G new radio. In: *GLOBECOM 2017 - 2017 IEEE Global Communications Conference*, pp. 1–7. IEEE (2017)
25. Siddiqi, M.A., Yu, H., Joung, J.: 5G ultra-reliable low-latency communication implementation challenges and operational issues with IoT devices. *Electronics* **8**, 981 (2019)
26. Ji, H., Kim, W., Shim, B.: New radio technologies for ultra reliable and low latency communications. In: *TENCON 2018 - 2018 IEEE Region 10 Conference*, pp. 1620–1623. IEEE (2018)
27. Lema, M.A., Laya, A., Mahmoodi, T., Cuevas, M., Sachs, J., Markendahl, J., Dohler, M.: Business case and technology analysis for 5G low latency applications. *IEEE Access* **5**, 1 (2017)
28. Peraković, D., Periša, M., Sente, R.E.: Information and communication technologies within Industry 4.0 concept. In: Ivanov, V., et al. (ed.) *Advances in Design, Simulation and Manufacturing. DSMIE-2018. Lecture Notes in Mechanical Engineering*, pp. 127–134. Springer, Cham (2019). [https://doi.org/10.1007/978-3-319-93587-4\\_14](https://doi.org/10.1007/978-3-319-93587-4_14)
29. 5G-ACIA: 5G for Connected Industries and Automation (White Paper - Second Edition). Frankfurt am Main, Germany (2018)
30. Chowdhury, M.Z., Ahmed, S., Jang, Y.M.: 6G Wireless Communication Systems: Applications, Requirements, Technologies, Challenges, and Research Directions. *arXiv. abs/1909.1* (2019)
31. Giordani, M., Polese, M., Mezzavilla, M., Rangan, S., Zorzi, M.: Towards 6G networks: use cases and technologies. *IEEE Commun. Mag.* **58**, 1–7 (2019)
32. Tariq, F., Khandaker, M., Wong, K.-K., Imran, M., Bennis, M., Debbah, M.: A Speculative Study on 6G, pp. 1–8 (2019)
33. Mahmood, N.H., Alves, H., López, O.A., Shehab, M., Osorio, D.P.M., Latva-aho, M.: Six Key Enablers for Machine Type Communication in 6G, pp. 1–14 (2019)



# Industry 4.0+: The Next Level of Intelligent and Self-optimizing Factories

Erwin Rauch <sup>(✉)</sup> 

Free University of Bolzano, 1, Universitätsplatz, 39100 Bolzano, Italy  
erwin.rauch@unibz.it

**Abstract.** For almost a decade now, production science has been dealing with Industry 4.0. In recent years, a large number of technological innovations have been developed and introduced into practice, enabling the implementation of smart and connected manufacturing systems. Over the next years, researchers and practitioners will face new challenges in Industry 4.0 to achieve the original vision of an intelligent and self-optimizing factory. We are currently at a crossroads between the first level of Industry 4.0, which was characterized by technologically driven innovations, and a future level of Industry 4.0+, which will be based on data-driven innovation. This article introduces these two phases of Industry 4.0 and gives a direction of research trends with growing attention in manufacturing science and practice. In the context of Industry 4.0+, two research directions, in particular, are expected to generate groundbreaking changes in production and its environment. This is, on the one hand, the introduction of Artificial Intelligence into manufacturing and on the other hand the use of nature as inspiration in the form of Biological Transformation.

**Keywords:** Industry 4.0 · Industry 5.0 · Society 5.0 · Intelligent manufacturing · Self-optimization · Artificial intelligence · Biological transformation

## 1 Introduction

Digital technologies are increasingly changing society. In the production sector, the term ‘Industry 4.0’ (I4.0) in particular introduced a new era of digitally networked production almost 10 years ago. The basic idea of Industry 4.0 was to be able to unfold the advantages through comprehensive connectivity on the shop floor as well as, by connecting products, machines, employees with the production system and with all those involved in the value chain, thereby minimizing information disruptions and the resulting inefficiencies by smart factories. To manage interconnected systems between physical assets and computational capabilities so-called cyber-physical systems (CPS) were introduced as transformative technologies leveraging the interconnectivity of machines. Since the proclamation of Industry 4.0 in 2011 at the Hannover Fair [1], a lot has happened in this direction. While Industry 4.0 was mainly limited to Germany in the first few years, almost all European countries have now launched Industry 4.0 initiatives. A look at scientific databases such as Scopus shows that since 2017 a large number of international publications have been added. Most of the larger companies

have already started initiatives and pilot projects to introduce new technologies related to Industry 4.0 in production as well as logistics. Many of the small and medium-sized companies (SME) do not yet have such a smart and connected manufacturing system, but will be able to achieve this goal in the medium-term as results from research are already transferred into broader industrial practice [2].

The next groundbreaking level to be achieved, are intelligent and self-optimizing manufacturing systems. While a smart factory can be understood as a manufacturing system, which is capable to apply previously acquired knowledge an intelligent factory may be seen as a factory, which can autonomously acquire new knowledge and apply it for self-optimization purposes. To achieve this goal the results from the first era of Industry 4.0 play, an important role as connectivity and modern technologies are a prerequisite for the next level of Industry 4.0 called 'Industry 4.0+' in this article. Currently, several authors are speaking also about Industry 5.0 [3, 4] although it might be seen more like the second level of Industry 4.0 with a final vision of an intelligent and self-learning and self-optimizing factory. Based on the results of the first level, production resources can collect a large amount of high-quality data using sensors, vertical and horizontal data integration guarantees seamless data exchanges, a large amount of big data can be stored and managed via cloud technologies and be processed into more structured data with big data technologies. The next level of Industry 4.0+ is aimed at taking advantage of this data creating intelligent and self-optimizing factories, whereby we are already still far away from this vision. It is important to look for new and innovative solutions to how this new level of data quantity and quality can be utilized in companies for self-monitoring and intelligent self-optimization of the manufacturing system. Artificial intelligence (AI) and biological transformation in manufacturing may open up completely new possibilities in this direction. Although the theoretical basis of AI and approaches of bio-inspired manufacturing existed already years ago, now is the right time to take full advantage of these concepts as large amounts of data are available in factories and computational capabilities increased significantly in the last years.

This article introduces the concept of implementing Industry 4.0 on two levels, a first technology-driven level, and a second data-driven level. In this visionary look in the future, the author gives an outlook on how to achieve the vision of intelligent and self-optimizing factories of the future with Industry 4.0+. To reach this vision researchers and practitioners will need to deal with artificial intelligence and the concept of biological transformation, which will most probably dominate research in manufacturing in the next decade.

## **2 Literature Review**

### **2.1 Industry 4.0 – The Fourth Industrial Revolution**

Industry 4.0 is the umbrella term for the Fourth Industrial Revolution, which has particularly occupied scientists in production engineering over the past almost 10 years. The term was presented for the first time at the Hannover Messe 2011 by German scientists (Acatech - National Academy of Science and Engineering), who wanted to



sensitize the public and policymaker to a new high-tech strategy for Germany. In the following two years, a working group was set up in Germany to develop recommendations for the implementation of Industry 4.0. In 2013, the final report “Recommendations for implementing the strategic initiative INDUSTRIE 4.0” was presented to the public [1].

In the following years, mainly from 2014 to 2016, most of the European countries launched national initiatives and funding programs to roll out Industry 4.0. To name just a few, these are the “Piano Nazionale di Industria 4.0” in Italy [5], “Smart Industry - a strategy for new industrialization for Sweden” in Sweden [6], “Industrie 4.0 Österreich” in Austria [7] or “Industria Conectada 4.0” in Spain [8].

According to a keyword search for “Industry 4.0” (selecting only non-European countries) mainly since 2017, Industry 4.0 has also achieved significant status as a term on an international level. Especially in Asia, the term Industry 4.0 is widespread. Thailand with the initiative “Thailand 4.0” [9] or “Made in India” [10] can be mentioned here as an example. In the North American region (USA and Canada) the concepts of Industry 4.0 are often known under the terms “Internet of Things” (IoT), Smart Manufacturing or Intelligent Manufacturing [11].

If we look back to the beginnings of Industry 4.0, what were the challenging goals for this new Fourth Industrial Revolution back then? The final report of Kagermann et al. [1] may be used as one of the first documents on Industry 4.0. Industry 4.0 is the Fourth Industrial Revolution after three previous revolutions. After mechanization at the end of the 18th century (1st Industrial Revolution) and electrification at the beginning of the 20th century (2nd Industrial Revolution), computer technology, electronics, and automation were introduced at the beginning of the 1970s (3rd Industrial Revolution). The Fourth Industrial Revolution is characterized by the aim to connect machines, people, products, and the entire value network by vertical and horizontal data integration to create smart and connected factories. According to [1] “smart factories constitute a key feature of Industry 4.0 being capable of managing complexity, being less prone to disruption and able to manufacture goods more efficiently”.

In the widest vision of Industry 4.0, smart factories become intelligent factories. They will lead to the emergence of dynamic, real-time optimized, self-organizing manufacturing systems with production facilities that are autonomous, capable of controlling themselves in response to different situations, self-configuring, self-regulating, self-aware and self-optimizing [1, 12]. In such intelligent factories, employees will be freed up from having to perform routine tasks, enabling them to focus on creative, value-added activities. They will thus retain a key role, particularly in terms of supervision and quality assurance [1]. A smart factory enables rapid and flexible adaptation or reconfigurability through connected machines able to get data as well as to offer information to other elements in the manufacturing system (e.g. people, products). Intelligent factories can think, learn, remember and in a given moment share that amount of knowledge, or react in certain situations [13]. Intelligent manufacturing systems are highly automated at the manufacturing level and are self-repairing, self-optimizing and self-configuring by taking advantage of AI and neural networks technology [14].

## 2.2 Industry 5.0 – Is this the Next Industrial Revolution?

After about 10 years of industry 4.0 and ever shorter innovation cycles in a highly dynamic environment, many scientists are naturally asking and looking for the next big hype in production science. For this reason, in some studies, a Fifth Industrial Revolution has already been heralded (Industry 5.0) while other works and national programs introduce the term Society 5.0. In the following, we will have a more detailed look at these terms.

Looking for the keyword “Industry 5.0” the first listed work in Scopus from Sachsenmeier has been published in 2016 and introduces Bionics (the imitation or abstraction of the “inventions of nature) as the next disruptive revolution in the industry [15]. Other works like Özdemir and Hekim published in 2018 [3] or Pathak et al. in 2019 [16] bring in AI and therefore intelligent cyber-physical systems as the next game changer in the industrial field. The fifth revolution is described in [16] as a cyber-physical system comprising people, AI and the physical system of enterprises well connected through high-speed internet and in particular the application of collaborative robots (cobots) in manufacturing. Also in [4] Industry 5.0 is explained as the concept, where robots are intertwined with the human brain and work as a collaborator instead of a competitor. In [17] the authors address also fast decision-making processes as well as a mass customize based platform collaboration to be part of a new industrial environment where firms are involving their customers more closely. If we now evaluate all these definitions of Industry 5.0 as a new industrial revolution, it becomes relatively quickly clear, that these are topics and goals which were already discussed years before in Industry 4.0 and which, due to the latest progress (e.g. in AI), are moving within reach. To answer the question posed in the title of this section: no, these issues do not in any way herald a new groundbreaking and all-changing industrial revolution.

## 2.3 Society 5.0 – An Extension of Industry 4.0 or a New Revolution?

An interesting development in this regard is the rise of the term ‘Society 5.0’ in Japan. The Society 5.0 (SuperSmart Society) was introduced in 2016 by Japan’s most important business federation (Keidanren) and being strongly promoted by Council for Science, Technology, and Innovation; Cabinet Office, Government of Japan [18, 19]. Society 5.0 is not limited only to manufacturing, but it solves social problems with the help of advanced IT technologies, IoT, robots, AI and augmented reality (AR). These technologies are actively used in people’s common life, at work, in healthcare and other spheres of activity for the benefit and convenience of every single person [20]. In [21] and [22] the different social (and not industrial) revolutions are explained as follows.

- Society 1.0 means hunting and gathering,
- Society 2.0 is the agricultural society,
- Society 3.0 is the industrial society,
- Society 4.0 is the information society,
- Society 5.0 is the ‘super smart society’.

This leads us to become more familiar with the concept of the Industrial Revolution. How is an industrial revolution characterized and what elements make a period an industrial revolution? According to [1] an industrial revolution brings a radical transformation of the world in which we live and work. In the last industrial revolutions, the radical transformation was mainly characterized by a change from “manual labor” towards “brainwork” and therefore a significant impact on industrial work and our social life. Following [23] and as stated by Joseph Schumpeter such revolutions can be seen as “create destruction” in which old industries died and new ones were born. Very often so-called disruptive technologies accelerated or extended such kind of revolution [23]. Friedrich Engels in ‘The Condition of the Working Class in England’ [24] in 1844 spoke of “an industrial revolution, a revolution which at the same time changed the whole of civil society”. Therefore what is currently understood by the term Society 5.0 is nothing completely new compared to Industry 4.0, but can be seen as a more far-reaching extension to people’s life, as it envisions a complete change in our society and population.

### 3 Research Methodology

In this research, we analyze the focus of the last years of research on Industry 4.0 as well as future trends and main topics to be addressed in the next years. Thus, we introduce the concept of a two-step implementation of Industry 4.0. Figure 1 shows the classic picture of the four industrial revolutions with the extension of Industry 4.0 by the next level of Industry 4.0+. The first level aims at achieving a smart and connected factory, while the next and future level of Industry 4.0 aims to achieve an intelligent and self-optimizing factory. The first level of Industry 4.0 is characterized by technology-driven innovation, which is also the prerequisite for the next level. The second level of Industry 4.0 is characterized by data and intelligence-driven innovation.

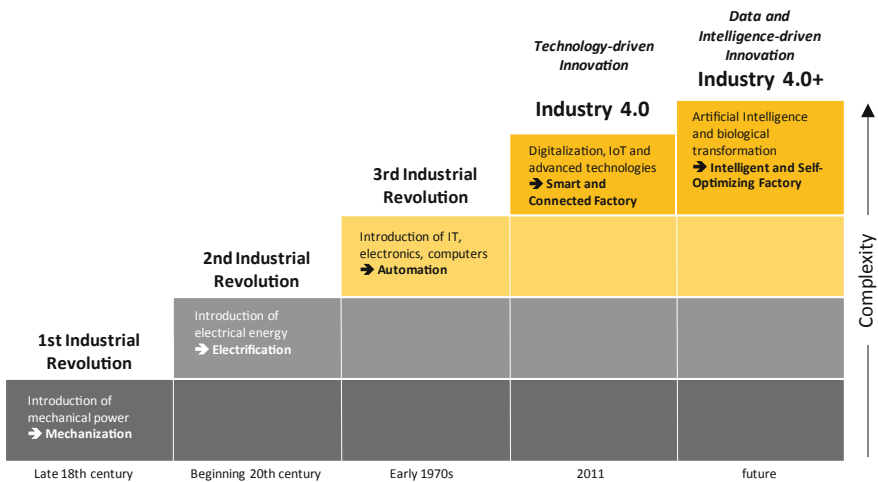


**Fig. 1.** Industry 4.0+: intelligent and self-optimizing factories as the next level in manufacturing.

## 4 Results

### 4.1 The First Level of Industry 4.0: Technology-Driven Innovation

In recent years, the main goal has been to create smart and connected factories that can also collect and process in real-time large amounts of data related to the product and manufacturing system (also known as ‘Digital Shadow’) to efficiently produce personalized and mass customized products (with the target ‘lot size 1’). This data can be used to create a digital twin as a prerequisite for a cyber-physical production system (CPPS) [25].

Various works are dealing with technologies of Industry 4.0 [26]. In recent years the categorization into the nine key technologies [27] shown in Table 1 has established itself and is used as a basis for many national Industry 4.0 programs. Table 1 shows the fundamental benefits that these technologies enable.

The first level of Industry 4.0 was mainly technology-driven to create the prerequisites for the next level of Industry 4.0. All these technologies have fundamentally contributed to the creation, storage, protection, exchange, processing, “simple” analysis and visualization of information or data, as well as to give people in the manufacturing system the opportunity to interact with the virtual world.

**Table 1.** The main benefit of Industry 4.0 technologies [27] in the first level of Industry 4.0.

No.	I4.0 technology	Description	Main benefit
1	Autonomous robots	Collaborative robots that are easy to program and interconnected with the manufacturing system	Human-machine collaboration
2	Additive manufacturing	Produce small batch sizes of complex customized products on demand in geographically decentralized manufacturing units	Produce customized products on demand
3	Virtual and Augmented Reality (VR/AR)	Provide workers with real-time information to improve their work or decision making as well as for virtual training or interaction	Visualization of data and interaction
4	Simulation	Simulation systems to mirror in real-time the physical world in a virtual model for testing, optimization, and interaction	Processing of data and interaction
5	Horizontal and vertical data integration	Data integration along the value chain (horizontal) and from the enterprise level to the machine level (vertical)	Exchange and visualization of data
6	Industrial Internet of Things	Integration of field devices and sensors for increasing multidirectional communication, interoperability, and decentralized control	Gathering, exchange, and visualization of data

(continued)

**Table 1.** (continued)

No.	I4.0 technology	Description	Main benefit
7	Cloud	Storage and management of a large amount of data on open sharing platforms to achieve short reaction times and thus enabling data-driven services	Storage and management of data
8	Cybersecurity	Protect manufacturing systems from cyber-attacks through secure, reliable communications as well as sophisticated identity and access management	Protection of data
9	Big data and analytics	Collection and comprehensive evaluation of production and enterprise data	“Simple” processing and analysis of data

## 4.2 The Second Level of Industry 4.0: Data and Intelligence Driven Innovation

While in the first level of Industry 4.0 we were mainly concerned with the technologies with which we could generate a higher quality of data and handle larger amounts of data, the second level of Industry 4.0 will be far more data and intelligence-driven. In the coming years, the goal will be to fully realize the Industry 4.0 vision by equipping our manufacturing systems with intelligence using nature as an inspiration and profit from the latest advances in AI. This will make it possible to create future intelligent and self-optimizing factories, as announced in the first vision of Industry 4.0 [1].

**Artificial Intelligence in Manufacturing.** AI is currently on everyone’s lips and is expected to dominate production research over the next years. We can differentiate in AI the following three terms: artificial intelligence, machine learning (ML) and deep learning (DL). In general deep learning is a subset of machine learning, and machine learning is a subset of artificial intelligence [28].

AI is a branch of computer science and defined to be the science and engineering of making intelligent machines. In AI a computer system can perform tasks that normally require human intelligence, such as visual perception, speech recognition, decision-making, and translation between languages [29]. ML as a subset of AI is empowering computer systems with the ability to “learn”. ML intends to enable machines to learn by themselves using the provided data and make accurate predictions. DL is a subset of machine learning and the next evolution of ML. DL algorithms are roughly inspired by the information processing patterns found in the human brain. It refers to the number of layers in a neural network making it able to process also unstructured data compared to machine learning techniques where features for classification need to be provided manually [28, 29].

An intelligent and self-optimizing manufacturing system can be realized by using AI (including ML and with increasing amount and complexity of data especially DL). Possibilities for the application of AI in manufacturing are expected in automated or assisted engineering design, manufacturing system reconfiguration, production planning, predictive maintenance, quality inspection as well as in supply chain management [30]. The introduction of AI in manufacturing enables manufacturing systems to become self-aware, self-comparing, self-predicting, self-optimizing and thus also more resilient as traditional manufacturing systems [12].

**Biological Transformation – Nature as Inspiration.** Resilience is also one of the central characteristics of many biological systems. From a biological point of view, resilience is a property that enables a system to maintain its functions against internal and external disturbances [31]. Increasing technical capabilities in information processing and computer capacities have enabled a growing understanding of biological processes in our environment in recent years. It is to be expected that biology and information technology will grow closer together in the future. Therefore, biological transformation is also seen as a parallel process to digital transformation [32]. According to [33], biological transformation can be transferred in three levels to industrial production:

- Bio-inspired manufacturing: involves the imitation or transfer of phenomena from nature to complex technical problems.
- Bio-integrated manufacturing means the integration of technological and biological processes into industrial value-added processes.
- Bio-intelligent manufacturing: as the combination of technical, informatics and biological systems creating robust and self-sufficient value creation systems.

This results in completely new potentials in the use of nature as a source of inspiration by not only imitating biological effects but by intelligently transferring principles from nature to various fields of application, such as manufacturing. This can be seen as a process that interacts symbiotically with digital transformation. While the first two levels of biological transformation mentioned above have already been applied in the past and present, the third level represents a groundbreaking innovation that will be able to fully unfold its full potential shortly based on the latest Industry 4.0 technologies and enhanced by the progress in AI.

## 5 Conclusions

This article shows that Industry 4.0 can be structured on two levels. The first level of Industry 4.0 was determined by technology-driven innovations, which serve as prerequisites and enablers for the creation, management, and processing of data. The next years will be characterized by the next data and intelligence-driven level of Industry 4.0 (Industry 4.0+) to achieve the vision of an intelligent and self-optimizing factory of the future. The paper shows that mainly two future directions will dominate research in this

area: (i) AI to transform data into autonomous intelligence and biological transformation to learn from nature in how to deal with complex problems. In addition, the term Industry 4.0+ is discussed concerning other terms such as Industry 5.0 and Society 5.0. The detailed analysis shows that the current Industry 5.0 definitions are only the next level of Industry 4.0, which is referred to as Industry 4.0+ in this article. Concerning the term Society 5.0, it was shown that this term is based on other social revolutions and is merely an extension of Industry 4.0 to social life. A visionary outlook into the research landscape of the coming years is given to stimulate further research activities in AI and biological transformation. Further, the implementation of technologies from both the first phase and the second phase of Industry 4.0 requires the development and consolidation of appropriate standards.

### Acknowledgment.



This project has received funding from the European Union's Horizon 2020 research and innovation program under the Marie Skłodowska-Curie grant agreement No 734713 (SME 4.0 – Industry 4.0 for SMEs).

### References

1. Kagermann, H., Helbig, J., Hellinger, A., Wahlster, W.: Recommendations for implementing the strategic initiative INDUSTRIE 4.0: securing the future of German manufacturing industry. Final report of the Industrie 4.0 Working Group. Forschungsunion im Stifterverband für die Deutsche Wirtschaft e.V., Berlin (2013)
2. Rauch, E., Vickery A.R., Brown, C., Matt, D.T.: SME requirements and guidelines for the design of smart and highly adaptable manufacturing systems. In: Matt, D.T., Modrak, V., Zsifkovits, H. (eds.) *Industry 4.0 for SMEs Challenges, Opportunities and Requirements*. Palgrave Macmillan, Basingstoke (2019, in press). <https://doi.org/10.1007/978-3-030-25425-4>
3. Özdemir, V., Hekim, N.: Birth of industry 5.0: making sense of big data with artificial intelligence, “the internet of things” and next-generation technology policy. *Omics: J. Integr. Biol.* **22**(1), 65–76 (2018)
4. Nahavandi, S.: Industry 5.0—a human-centric solution. *Sustainability* **11**(16), 4371 (2019)
5. MISE. Presentato il Piano nazionale Industria 4.0. <https://www.mise.gov.it/index.php/it/peri-media/comunicati-stampa/2035187-il-ministro-dello-sviluppo-economico-carlo-calenda-illustra-il-piano-nazionale-industria-4-0>. Accessed 21 Nov 2019
6. Government Offices of Sweden. Smart Industry - a strategy for new industrialization for Sweden. [https://www.government.se/498615/contentassets/3be3b6421c034b038dae4a7ad75f2f54/nist\\_statsformat\\_160420\\_eng\\_webb.pdf](https://www.government.se/498615/contentassets/3be3b6421c034b038dae4a7ad75f2f54/nist_statsformat_160420_eng_webb.pdf). Accessed 21 Nov 2019
7. Verein Industrie 4.0 Österreich. Industrie 4.0 Österreich. <https://plattformindustrie40.at/>. Accessed 21 Nov 2019
8. Gobierno de España. Industria Conectada 4.0. <https://www.industriaconectada40.gob.es/Paginas/index.aspx>. Accessed 21 Nov 2019
9. ThaiEmbDC. Thailand 4.0. <https://thaiembdc.org/thailand-4-0-2/>. Accessed 21 Nov 2019


10. DIPP Government India. Towards Smart Manufacturing: Industry 4.0 and India. <http://www.makeinindia.com/article/-/v/towards-smart-manufacturing-industry-4-0-and-india>. Accessed 21 Nov 2019
11. Manufacturing USA. Manufacturing USA. <https://www.manufacturingusa.com/institutes>. Accessed 21 Nov 2019
12. Lee, J., Davari, H., Singh, J., Pandhare, V.: Industrial artificial intelligence for industry 4.0-based manufacturing systems. *Manuf. Lett.* **18**, 20–23 (2018)
13. Hozdić, E.: Smart factory for industry 4.0: a review. *Int. J. Mod. Manuf. Technol.* **7**(1), 28–35 (2015)
14. Juhás, P., Molnár, K.: Key components of the architecture of cyber-physical manufacturing systems. *Industry 4.0* **2**(5), 205–207 (2017)
15. Sachsenmeier, P.: Industry 5.0—the relevance and implications of bionics and synthetic biology. *Engineering* **2**(2), 225–229 (2016)
16. Pathak, P., Pal, P.R., Shrivastava, M., Ora, P.: Fifth revolution: applied AI & human intelligence with cyber physical systems. *Int. J. Eng. Adv. Technol.* **8**(3), 23–27 (2019)
17. Mihardjo, L.W.W., Sasmoko, Alamsyah, F., Elidjen: Boosting the firm transformation in industry 5.0: experience-agility innovation model. *Int. J. Recent Technol. Eng.* **8**(2), 735–742 (2019)
18. Nirmala, J.: Super Smart Society: Society 5.0. <https://www.roboticstomorrow.com/article/2016/09/super-smart-society-society-50/8739>. Accessed 22 Nov 2019
19. Skobelev, P.O., Borovik, S.Y.: On the way from Industry 4.0 to Industry 5.0: from digital manufacturing to digital society. *Industry 4.0* **2**(6), 307–311 (2017)
20. Cebit. Society 5.0: Japan’s digitization. <http://www.cebit.de/en/news-trends/news/society-5-0-japans-digitization-779>. Accessed 11 Dec 2017
21. Salgues, B.: Society 5.0: Industry of the Future, Technologies, Methods and Tools. Wiley, Hoboken (2018)
22. Unesco. Japan pushing ahead with Society 5.0 to overcome chronic social challenges. <https://en.unesco.org/news/japan-pushing-ahead-society-50-overcome-chronic-social-challenges>. Accessed 23 Nov 2019
23. Senge, P.M., Carstedt, G., Porter, P.L.: Next industrial revolution. *MIT Sloan Manag. Rev.* **42**(2), 24–38 (2001)
24. Engels, F.: The condition of the working class in England. In: *The Sociology and Politics of Health*, pp. 22–27. Routledge, Abingdon (2005)
25. Uhlemann, T.H.J., Lehmann, C., Steinhilper, R.: The digital twin: realizing the cyber-physical production system for industry 4.0. *Procedia CIRP* **61**, 335–340 (2017)
26. Dalenogare, L.S., Benitez, G.B., Ayala, N.F., Frank, A.G.: The expected contribution of industry 4.0 technologies for industrial performance. *Int. J. Prod. Econ.* **204**, 383–394 (2018)
27. Rößmann, M., Lorenz, M., Gerbert, P., Waldner, M., Justus, J., Engel, P., Harnisch, M.: Industry 4.0: the future of productivity and growth in manufacturing industries. *Boston Consult. Group* **9**(1), 54–89 (2015)
28. Garbade, M.J.: Clearing the Confusion: AI vs Machine Learning vs Deep Learning Differences. <https://towardsdatascience.com/clearing-the-confusion-ai-vs-machine-learning-vs-deep-learning-differences-fce69b21d5eb>. Accessed 28 Oct 2019
29. SkyMind. Artificial Intelligence (AI) vs. Machine Learning vs. Deep Learning. <https://skymind.ai/wiki/ai-vs-machine-learning-vs-deep-learning>. Accessed 28 Oct 2019
30. Rauch, E., Matt, D.T.: Artificial intelligence in design: a look into the future of AD. In: Suh, N.S., Cavique, M., Foley, J. (eds.) *Design Engineering and Science*. Springer, Berlin (2020)



31. Van Brussel, H., Valckenaers, P.: Design of holonic manufacturing systems. *J. Mach. Eng.* **17**(3), 5–23 (2017)
32. Dieckhoff, P., Möhlmann, R., van Ackeren, J.: *Biologische Transformation und Bioökonomie*. White Paper. Fraunhofer Verlag, Munich (2018)
33. Mieke, R., Bauernhansl, T., Schwarz, O., Traube, A., Lorenzoni, A., Waltersmann, L., Full, J., Horbelt, J., Sauer, A.: The biological transformation of the manufacturing industry—envisioning biointelligent value adding. *Procedia CIRP* **72**, 739–743 (2018)



# State-of-the-Art in Product-Service System Classification

Mariusz Salwin<sup>1</sup>  and Andrzej Kraslawski<sup>2,3</sup> 

<sup>1</sup> Warsaw University of Technology, 85, Narbutta Street, Warsaw, Poland  
mariusz.salwin@onet.pl

<sup>2</sup> Lappeenranta University of Technology, P.O. Box 20, 53581  
Lappeenranta, Finland

<sup>3</sup> Lodz University of Technology, 213, Wólczajska Street, Łódź 90-001, Poland

**Abstract.** The Product-Service System (PSS) is an integrated combination of products and services. This concept includes a service-based competitive strategy, environmental sustainability and the basis for distinguishing itself from competitors offering cheaper products. The adoption of PSS involves focusing on selling the functionality of the product instead of selling the products. The important element of PSS is classification, i.e. the systematic division of PSS into classes according to a defined principle. The literature on the classification of PSS is very narrow and it does not sufficiently address the possibilities and categories that can be distinguished. The typologies developed have not captured the wealth of classes of PSS so far. The paper presents a comprehensive analysis of the PSS classification. In addition, the paper systematically reviews the literature on the PSS classification published over the last 18 years. Its main objective is to identify the main aspects of the PSS classification, the common features to the various classifications and their limitations. By researching the available classifications, we hope to make it easier for businesses to develop new PSS-based offers and to adapt their business models to specific types of PSS. This publication deals with and analyses 10 classifications of PSS.

**Keywords:** Product-Service System · Product-Service System classification · Product-Service System typology · Product-Service System continuum · Servitisation continuum

## 1 Introduction

Product Service Systems are particular cases of servitization. The concept emerged in Scandinavia in the late 1990s [1]. For the first time, the term “Product-Service System” was used in the report Product Service Systems, Ecological and Economic Basics in 1999 [1]. The definition of PSS proposed in this report says: ‘A product service-system is a system of products, services, networks of “players” and supporting infrastructure that continuously strives to be competitive, satisfies customer needs and have a lower environmental impact than traditional business models’ [1]. In the following years, the term was gaining in importance and evolved [2–5].

PSS emerged because traditional manufacturing companies wanted to be able to cope with the changing market forces and realized that by linking services with products they might guarantee higher profits for themselves than by offering products only [6]. In the face of shrinking markets and increased commoditization of their products, these companies perceived rendering services as a new path to higher profits and growth [7, 8]. Increasingly more often they draw attention to possibilities it may produce. This, in turn, links with additional benefits because by using services to meet the needs instead of owning products we reduce demand for materials and energy [9].

PSS is a valuable concept for manufacturers from highly developed countries. The manufacturing industry is experiencing deep changes globally. Traditional manufacturers face growing challenges posed by countries with low costs of labor. However, in highly developed countries the will to retain profitable manufacturing capacity remains strong because manufacturing directly supports exports, service-based economy, and supplements scientific and technical base. This is why manufacturers are encouraged to apply solutions based on the PSS model, which may help them enhance competitiveness and deliver new value to customers [10, 11].

The classification of PSS is an important area of research in PSS that is still not sufficiently analyzed. The main objective of the classification is to break down according to specific rules and principles. The basis for classification is the introduction of clear and logical distribution criteria based on the typical and unique characteristics of the PSS. Such features include product ownership, functionality, environmental impact and the main revenue generating mechanism [12–14]. The PSS classification provides means by which specific events can be compared and understood. The available classifications show that between pure product sales and service provision there are a number of different PSS options where products and services are combined to varying degrees [13, 15]. The transformation from the manufacturing company to the service company and related issues is also taken into account [8, 16–18].

The paper is structured as follows: the first part is the introduction; the next part contains the literature analysis of the existing classifications of PSS; the third part presents the research methodology; the next part contains results; the last part is the conclusions.

## 2 Literature Review

This section reviews the classification of PSS proposed in the literature. The first step of the analysis shows what the available classifications are aimed at and what they are focused on, and the compilation of their number of citations is made (Table 1).

Table 1. Table captions should be placed above the tables.

Authors and years	Number of citations		Product-Service System classifications (Categorization PSS)	Focus								
	Google Scholar	Research Gate										
Mathieu, 2001 [17]	738	439	1. Organizational intensity (X-axis) 1.1. Tactic 1.2. Strategic 1.3. Cultural 2. Service specificity (Y-axis) 2.1. Customer Services 2.2. Product Services 2.3. Service as a Product	Focusing on the nature of the offer, how service maneuvers are organized, the strength and dimension of their impact on the company								
Mont, 2002 [22]	2030	1226	1. Products/services/combinations/substitutions 2. Services, at the point of sale 3. Different concepts of product use: 3.1. Use oriented 3.2. Result oriented 4. Maintenance services 5. Revalorisation services	Focusing on the main elements of a PSS that can serve as a common reference data for research and design of PSS								
Oliva and Kallenberg, 2003 [8]	2559	1550	<table border="1"> <tr> <td>Product-oriented services</td> <td>End-user's process-oriented services</td> </tr> <tr> <td>Transaction-based services</td> <td>Professional services</td> </tr> <tr> <td>Relationship-based services</td> <td>Operational services</td> </tr> <tr> <td>Maintenance services</td> <td></td> </tr> </table>	Product-oriented services	End-user's process-oriented services	Transaction-based services	Professional services	Relationship-based services	Operational services	Maintenance services		Describing the process of transforming a manufacturing company into a more service-oriented one. In their deliberations, the authors particularly took into account the services accompanying durable, durable products, usually necessary to maintain their functionality during their life cycle
Product-oriented services	End-user's process-oriented services											
Transaction-based services	Professional services											
Relationship-based services	Operational services											
Maintenance services												
Tukker, 2004 [13]	1806	1152	1. Product-oriented 1.1. Product related 1.2. Advice and consultancy 2. Use-oriented 2.1. Product lease 2.2. Product renting/sharing 2.3. Product pooling 3. Result-oriented 3.1. Activity management 3.2. Pay per service unit 3.3. Functional result	It is a classification according to a range of values determined based on a product or service. It is connected with the ease of their implementation and at the same time with the complexity of the system								

(continued)

Table 1. (continued)

Authors and years	Number of citations Google Scholar	Research Gate	Product-Service System classifications (Categorization PSS)	Focus
Uchihira and collaborators, 2007, 2008 [18, 23]	17	7	<ol style="list-style-type: none"> <li>1. Adjustment Expansion               <ol style="list-style-type: none"> <li>1.1. Consulting</li> <li>1.2. Customizing</li> <li>1.3. Downtime and Risk Reduction</li> </ol> </li> <li>2. Commitment Expansion               <ol style="list-style-type: none"> <li>2.1. Financial Risk Reduction</li> <li>2.2. Social Risk Reduction</li> <li>2.3. Operational Efficiency</li> </ol> </li> <li>3. Territory Expansion               <ol style="list-style-type: none"> <li>3.1. Seamless Services</li> <li>3.2. Rich Content</li> </ol> </li> </ol>	Focusing on ways of expanding production activities, emphasizing the importance of contacts and customer relations
Neely, 2008 [12]	1204	790	<ol style="list-style-type: none"> <li>1. Integration-oriented</li> <li>2. Product-oriented</li> <li>3. Service-oriented</li> <li>4. Use-oriented</li> <li>5. Result-oriented</li> </ol>	Focusing on a fuller presentation of the scope of service strategies implemented by the company
Martinez and collaborators, 2010 [16]	484	315	<ol style="list-style-type: none"> <li>1. Interaction mainly transactional; some addition of peripheral services</li> <li>2. Product + service delivery</li> <li>3. Customization of product and service</li> <li>4. Product + service co-designed; total solutions</li> </ol>	Focusing on the analysis of the customer-supplier interface
Fan and Zhang, 2010 [24]	14	7	<ol style="list-style-type: none"> <li>1. Product-oriented</li> <li>2. Application-oriented</li> <li>3. Result-oriented</li> <li>4. Integrated-oriented</li> <li>5. Service-oriented</li> </ol>	Scope of the strategy of services provided by manufacturing companies
Clayton and collaborators, 2012 [15]	64		<ol style="list-style-type: none"> <li>1. Integration-oriented</li> <li>2. Product-oriented</li> <li>3. Service-oriented</li> <li>4. Use-oriented</li> <li>5. Result-oriented</li> </ol>	Understanding how to create product and service offers
Van Ostaeyen and collaborators, 2013 [14]	101	84	<ol style="list-style-type: none"> <li>1. Input-based</li> <li>2. Availability based</li> <li>3. Usage-based</li> <li>4. Performance-based</li> <li>4.1. Solution-oriented</li> <li>4.2. Effect-oriented</li> <li>4.3. Demand-oriented</li> </ol>	Focusing on the performance orientation of the dominant revenue mechanism of the PSS and the level of integration of the elements of the PSS

The classification proposed by Mathieu [17] is based on two dimensions. The first is Service specificity (Customer Services, Product Services, Service as a Product), and the second is Organizational intensity (Tactic, Strategic, Cultural). It introduces the concept that service has the potential to be more than just an offer or a product service. The classification uses the term service maneuvers. Service specificity is partly derived from the logic of service classification and focuses on the nature of the offer. It refers to the type of content of a production service maneuver (Customer Services, Product Services, Service as a Product). The second dimension, Service specificity, focus on the way service maneuvers are organized, the strength and dimension of their impact on the company. The first dimension is the domain of the offer, takes a market view and focuses on delivering value to customers in an efficient way. On the other hand, Organizational intensity implies positions that an organization can take, it concerns the internal point of view. There is a correlation between these dimensions, namely the greater the intensity of the service maneuver, the greater the specificity of the service in general. The forces shaping these dimensions are also different. In the first dimension, the organization only has to make a plan, make a decision, while in the context of Organizational intensity it has to create a plan. The company introduces customer service or the product as the service or the organization creates tactical or cultural maneuvers [17].

The classification developed by Mont [22] provides a list of the main elements of PSS that can serve as a common reference date for PSS research and design. The author divides the PSS into five main categories based on the combination of a product with services at different stages of the life cycle of the product and covering different concepts for the use of the product [22].

Oliva and Kallenberg [8] are the authors of another approach to distinguishing between types of PSS systems. They described the process of transforming a manufacturing company into a more service-oriented company. In their conceptions, they considered primarily the services associated with durable products, typically necessary to maintain their functionality throughout their life cycle (e.g. installation, repair, improvement, decommissioning). The authors have introduced here the terms product installed base (product IB) and services installed base (services IB) (a range of services related to a product or process required by an end-user throughout the life of a product to function effectively in the context of its operating process). Focusing on the unique attributes of services IB enables a new classification of the opportunities in the services market that are needed to compete. The developed classification has two dimensions of organizational transformation. The first one concerns the change in the understanding of customer interaction from transaction-based to relationship-based. The second dimension of the transformation concerns the type of services provided and the values delivered, from product-oriented to end-user process-oriented [8].

The classification developed by Tukker [13] distinguishes three main types of PSS (product-oriented, use-oriented, result-oriented), which are divided into eight categories (product-related, advice and consultancy, product lease, product renting/sharing, product pooling; activity management, pay per service unit, functional result) distinguished according to the range of values determined based on the product or service. Moving from the first to the last of these types of PSS, dependence on the product as the main component of the PSS decreases and customer needs are formulated more

abstractly. In each case, the supplier has little more freedom to satisfy the actual needs of the customer. However, abstract requirements are often difficult to render into specific (qualitative) performance indicators, which make it difficult for suppliers to determine what they have to offer, and for customers to know whether they have what they are asking for [13].

A different approach to PSS classification was developed by Uchihira and collaborators [18, 23] focusing on how to develop contacts with customers. A Customer Expansion Model was presented that includes three types of expansion: adjustment expansion, commitment expansion, and territory expansion. These types of expansions can provide added value to services such as better product quality, customer protection, and product convenience. These three types of expansion are divided into more detail, detailing eight elementary patterns of service functions (consulting, customizing, downtime and risk reduction; financial risk reduction, social risk reduction, operational efficiency; seamless services, rich content) [18, 23].

Neely [12] has developed further PSS classification based on the Tukker [13] classification. The author, conducting his research, concluded that an extension of the PSS classification system is required to fully reflect the range of servicing strategies implemented by companies. Neely [12], using criteria similar to those of Tukker [13] for the traditional PSS (product-oriented, user-oriented result-oriented), added two new PSS types: integration oriented and service-oriented. PSS integration oriented is created when a company tries to add services downstream and introduce vertical integration. PSS service-oriented is when a company adds services to products by integrating these services into the product itself [12].

Another classification in the form of servitisation continuum closely related to PSS was developed by Martinez and collaborators [16]. Servitisation was defined as a strategic innovation of the organization's capabilities and processes, to start delivering value by selling integrated product and service offers. Martinez and collaborators [16] combined the challenges with the position in the servitisation continuum that the organization wants to achieve. Four criteria were distinguished to assess the level of servitisation of the organization. Low levels of servitisation can be achieved with relatively small changes, while deep levels of servitisation require wider interactions between suppliers and customers, so the challenges facing the company are more serious and need to be more supported in all of these aspects [16].

Another developed classification was created based on the Tukker [13] and Neely [12] classifications. The authors have added the Product-Service System application-oriented to the well-known PSS types. The classification takes into account the dimension of the market environment when formulating the strategy. The aim is to adapt the Product-Service System to the market forces that companies face. It allows companies to adopt the right PSS strategy to gain a competitive advantage [24].

Based on Neely [12] classification, Clayton and collaborators [15] have incorporated five types of PSS into a continuum from pure product to service. The aim is to help create a product and service offering. The author points out that in the classification the company is not able to offer only PSS user-oriented or result-oriented [15].

Van Ostaeen and collaborators [14] distinguished four main types of PSS. This classification categorizes PSS types according to two distinguishing features: the efficiency orientation of the dominant revenue mechanism and the degree of integration

between the elements of the product and service. This classification makes it possible to convey the specific characteristics defining PSSs: which products and services are included in the offer, which of them are integrated and which are their revenue mechanisms. It attaches great importance to the concept of function in PSSs [14].

In the next stage of the analysis, we focused on the analysis of features important for the Product-Service System (Table 2), which are regularly repeated in the literature [1, 2, 10]. Such presentation helps to capture them precisely and show which of them are taken into account in particular PSS classifications.

Among 19 analyzed factors, 14 occur in the classification developed by Martinez and collaborators [16]. This author was the only one who took into account the time scale. Only Tukker [13] considered the environmental impact of PSSs in his classification. This aspect was not taken into account as a criterion for any other classification. Each classification takes into account material and intangible assets relevant to the PSS, as well as social aspects.

The next step in the analysis was to focus on the structure of the PSS classification. This analysis will allow us to capture the similarities and differences and gaps in the classifications available (Table 3).

It is noteworthy that certain types of PSS in the classifications have a different name and relate to the same name. Martinez and collaborators [16], whose classification is very close to Neely [12] despite its other names and additional aspects related to the issues of transformation of the enterprise, can be given as an example. Most of the classifications developed include three types of PSS, product-oriented, use-oriented, result-oriented, each of which also covers the transition from a pure product to pure service. It should be emphasized here that individual types are not described precisely, they are only signals without explaining how the product is combined with the service and to what extent this integration takes place. In the part of the classification, apart from these three types, the aspects related to the strategy and transformation of the enterprise and expansion can be identified.

The analyzed PSS classifications can be divided into two main groups (Table 4). The first is the classification in which important attention is paid to classifying the offer possibilities, i.e. showing that there are a number of possibilities offered by a PSS to an enterprise between the pure sale of products and the provision of services. The second group concerns classifications that pay attention to the transformation of an enterprise, i.e. the transition from a product manufacturer to a service provider.

It should be stressed that the classifications available in the literature are intended for enterprises of different sizes operating in different branches of the economy.

## 3 Research Methodology

### 3.1 Research Aim

The paper is aimed at the identification and analysis of the existing knowledge on the Product-Service System classifications by highlighting the main features of available PSS classifications, their similarities, and their limitations.



Table 2. Product-Service System classifications analysis

Attributes	Authors										Total
	Mathieu [17]	Mont [22]	Oliva and Kallenberg [8]	Tukker [13]	Uchihira and collaborators [18, 23]	Neely [12]	Martinez and collaborators [16]	Fan and Zhang [24]	Clayton and collaborators [15]	Van Ostaeyen and collaborators [14]	
1. Ownership				+		+		+	+	+	6
2. Tangible	+	+	+	+	+	+		+	+	+	10
3. Intangible	+	+	+	+	+	+		+	+	+	10
4. Function											2
5. Distinguishing features		+		+		+		+	+	+	6
6. Comparison of specific events		+		+		+		+	+	+	7
7. The dimension of the market environment	+							+			2
8. Transformation of a company	+		+		+	+		+			6
9. Product life cycle						+			+	+	4
10. Customer relationship					+	+					2
11. Innovation						+					1
12. Change of organizational culture	+		+		+	+					5
13. Role of the manufacturer/supplier	+	+	+	+	+	+		+	+	+	10
14. Element integration level	+	+	+	+	+	+		+	+	+	9
15. Economic aspect	+			+						+	3
16. Environmental aspect				+							1
17. Social aspect	+	+	+	+	+	+		+	+	+	10
18. Time scale						+					1
19. Company strategy	+		+			+					3
Total	10	7	8	10	7	12	14	10	9	12	

Table 3. Structure of the PSS classification

Authors	Mathieu [17]	Mont [22]	Oliva and Kallenberg [8]	Tukker [13]	Uchihira and collaborators [18, 23]	Neely [12]	Martinez and collaborators [16]	Fan and Zhang [24]	Clayton and collaborators [15]	Van Ostaeyen and collaborators [14]
Integration-oriented		+	+			+			+	
Product-oriented	+	+	+	+	+	+	+	+	+	
Application-oriented							+	+		
Service-oriented		+				+	+	+		
Use-oriented		+		+		+	+	+		+
Result-oriented		+		+		+	+	+		+
Input-based										+
Availability based										+
Organizational intensity	+									
Service specificity	+									
Transaction-based services			+							
Aspects related to the enterprise transformation process	+		+		+		+			
Adjustment expansion					+					
Commitment expansion					+					
Territory expansion					+					

**Table 4.** Product-Service System classification group

Group 1	Group 2
Mont [22]	Mathieu [17]
Tukker [13]	Oliva and Kallenberg [8]
Neely [12]	Uchihira and collaborators [18, 23]
Fan and Zhang [24]	Martinez and collaborators [16]
Clayton and collaborators [15]	
Van Ostaeeyen and collaborators [14]	

In the paper we formulated the following research questions:

- What is the state-of-the-art in the classification of PSS?
- What are the main limitations available in the literature of PSS classification?

The analysis carried out in this article also provides suggestions for possible future directions for research on the development of the PSS typology. By exploring existing classifications, we hope to help capture the wealth and business opportunities of PSS.

### 3.2 Systematic Review

The methodology adopted in this paper is the systematic review of the literature [19]. It was chosen for using a scientific and transparent process aimed at minimizing prejudice through a detailed search for works published in the literature [20]. The authors used suggestions from Tranfield and collaborators and took the following steps [21]:

1. Planning the review. In this paper, the authors focus on the classification of PSS and their analysis, which is the main objective of this paper. It was decided to search only for those articles which use the terms “Product-Service System classification” and “Servitisation continuum” or indicate them as synonyms.
2. Conducting the review. The authors searched (in the title, abstract and keywords) for the terms “Product-Service System classification” and “Servitisation continuum” or their synonyms in databases such as EBSCOhost, Emerald, IEEE Xplore Digital Library, Ingenta, Insight, ProQuest, Science Direct, Scopus, Springer Link, Taylor & Francis Online, Web of Science, Wilma and Google Scholar. The databases used in the review are a tool to search for sources of electronic literature, particularly useful for works published after 1995 with a wide range of topics and journals.
3. Reporting and dissemination. In this phase, the available classifications of PSS were examined in detail. According to the guidelines, we received 450 articles covering the period 2001 to 2019. The choice based on title and summary leads to a limited set of 10 articles in which 10 PSS classifications were found.

## 4 Results

Based on the literature review, it is possible to identify a research gap in the available PSS classifications to focus further efforts on filling this gap. The biggest gaps in the PSS classification are:

- None of the methodologies classifications mention the Canvas Business Model, especially the areas in which they will be taken into account in the transformation from product manufacturer to the service provider.
- None of the available classifications took into account quality criteria related to solutions delivered to the customer.
- Little emphasis was also placed on sustainability issues. These aspects were signaled in some, however, when creating any classification, these criteria were not taken into account. Therefore, none of the typologies presented included the classification in terms of environmental, economic/financial as well as social performance in the proposed PSS-based solutions.
- The available classifications do not combine the variability of the PSS offer with the change in the structure and culture of the organization caused by the transition from producer to service provider.
- The available typologies are not able to capture the full complexity and capabilities of PSS. The classifications are not able to capture the differences and nuances that exist in practice between the different variants of PSS.
- Most classifications do not take into account market conditions and the environment. Market forces (demand, supply and competition characteristics) which companies face and which allow them to adopt the right strategy are ignored in the classifications.
- Insufficient characterization and reference to PSS user-oriented, PSS result-oriented, and PSS performance-based practices is an important issue. These are general descriptions that do not take into account product-specific parameters, strategies implemented by companies, market requirements and business practice.
- While creating the classification, the mechanisms concerning the company's revenues and customer costs are omitted.

## 5 Conclusions

The research discussed in this paper has been undertaken to identify the main weaknesses in the classification of PSSs and their limitations.

When analyzing the different typologies of PSSs proposed in the literature, some similarities and differences can be identified. Some classifications have been derived from others by developing or modifying them, some divisions are repeated by different authors, but are presented in a different context, while others represent a completely different approach to PSSs. One of the main common features is the orientation towards a product or a service, an aspect that is hidden under different names in each classification.

In the literature, we have identified 10 PSS classifications, 6 of which relate to the offer opportunities offered by PSS to enterprises and 4 to the transformation of enterprises from product manufacturers to service providers. Based on the literature, examples and available case studies, the classifications are not capable of capturing the diversity of PSSs, are not very detailed, and are not always able to meet the objectives and tasks that are set and set by the market. This is a very incomplete presentation of the types of systems that a manufacturer can create and offer on the market. The low level of detail in their description can make the transition from product manufacturer to service provider very difficult. The classifications presented in the first group are distinguished according to the range of values determined based on the product or service, i.e. they lead from a pure product to pure service. In the second group, they are distinguished according to the transformation of the manufacturing company into a more service-oriented company (strategy, cultural changes). Regardless of the group to which they have been qualified, the PSS classifications focus on the tangible value of the product, the intangible value of the service, the level of integration of these elements, the ownership of the product and the role of the producer/supplier. Subsequent types of PSS are presented in the available classifications in a very general way, only specifying who owns the ownership of the product in each of them. An important feature of the classification is their flexibility and universality, which allows them to be used in enterprises of different sizes and industries.

In addition, the analysis provides a solid basis for the development of new PSS classifications that will be able to capture the richness of the PSS offer and how the enterprise is transformed. It shows what improvements need to be made and what aspects need to be considered when developing a classification to fully reflect the scope of a PSS.

The analysis shows that the subject matter of the PSS classification is still evolving and that there is a need for a new, more accurate classification reflecting business practice in the PSS area. The analysis is the starting point for developing a new method to fill the gaps in the PSS classification.

## References

1. Goedkoop, M., van Haler, C., te Riele, H., Rommers, P.: Product Service-Systems, ecological and economic basics (1999)
2. Brandstotter, M., Haberl, M., Knoth, R., Kopacek, B., Kopacek, P.: IT on demand - towards an environmental conscious service system for Vienna (AT). In: 2003 EcoDesign 3rd International Symposium on Environmentally Conscious Design and Inverse Manufacturing, Tokyo, Japan, pp. 799–802. IEEE (2003). <https://doi.org/10.1109/ECODIM.2003.1322776>
3. Centenera, J., Hasan, M.: Sustainable Product-Service System. *Int. Bus. Res.* **7**, 62–71 (2014). <https://doi.org/10.5539/ibr.v7n7p62>
4. Manzini, E., Vezzoli, C.: A strategic design approach to develop sustainable product service systems: examples taken from the ‘environmentally friendly innovation’ Italian prize. *J. Clean. Prod.* **11**, 851–857 (2003). [https://doi.org/10.1016/S0959-6526\(02\)00153-1](https://doi.org/10.1016/S0959-6526(02)00153-1)
5. Mont, O.K.: Product-Service Systems Final Report. Swedish Environmental Protection Agency, Stockholm (2000)

6. Sawhney, M., Balasubramanian, S., Krishnan, V.V.: Creating growth with services: in a world of commoditized products, companies are turning to service offerings for growth. The key to success involves redefining markets in terms of customer activities and outcomes, not products and services. *MIT Sloan Manag. Rev.* **45**, 34–44 (2004)
7. Bates, K., Bates, H., Johnston, R.: Linking service to profit: the business case for service excellence. *Int. J. Serv. Ind. Manag.* **14**, 173–183 (2003). <https://doi.org/10.1108/09564230310474147>
8. Oliva, R., Kallenberg, R.: Managing the transition from products to services. *Int. J. Serv. Ind. Manag.* **14**, 160–172 (2003). <https://doi.org/10.1108/09564230310474138>
9. Toepfer, K.: The role of Product Service Systems in a sustainable society. United Nations Environment Programme Division of Technology. Industry and Economics, pp. 1–6 (2002)
10. Baines, T.S., ET AL. Irving, P., Johnson, M., Kingston, J., Lockett, H., Martinez, V., Michele, P., Tranfield, D., Walton, I.M., Wilson, H.: State-of-the-art in product-service systems. *Proc. Inst. Mech. Eng. Part B J. Eng. Manuf.* **221**, 1543–1552 (2007). <https://doi.org/10.1243/09544054JEM858>
11. Hewitt, P.: The government's manufacturing strategy, secretary of state for trade and industry. *Westminster* **4**, 1–60 (2002)
12. Neely, A.: Exploring the financial consequences of the servitization of manufacturing. *Oper. Manag. Res.* **1**, 103–118 (2008). <https://doi.org/10.1007/s12063-009-0015-5>
13. Tukker, A.: Eight types of product–service system: eight ways to sustainability? Experiences from SusProNet. *Bus. Strat. Env.* **13**, 246–260 (2004). <https://doi.org/10.1002/bse.414>
14. Van Ostaeyen, J., Van Horenbeek, A., Pintelon, L., Duflou, J.R.: A refined typology of product–service systems based on functional hierarchy modeling. *J. Clean. Prod.* **51**, 261–276 (2013). <https://doi.org/10.1016/j.jclepro.2013.01.036>
15. Clayton, R.J., Backhouse, C.J., Dani, S.: Evaluating existing approaches to product-service system design: a comparison with industrial practice. *J. Manuf. Technol. Manag.* **23**, 272–298 (2012). <https://doi.org/10.1108/17410381211217371>
16. Martinez, V., Bastl, M., Kingston, J., Evans, S.: Challenges in transforming manufacturing organisations into product-service providers. *J. Manuf. Technol. Manag.* **21**, 449–469 (2010). <https://doi.org/10.1108/17410381011046571>
17. Mathieu, V.: Service strategies within the manufacturing sector: benefits, costs and partnership. *Int. J. Serv. Ind. Manag.* **12**, 451–475 (2001). <https://doi.org/10.1108/EUM000000006093>
18. Uchihira, N., Kyoya, Y., Kim, S.K., Maeda, K., Ozawa, M., Ishii, K.: Analysis and design methodology for recognizing opportunities and difficulties for product-based services. *J. Inf. Process.* **16**, 13–26 (2008). <https://doi.org/10.2197/ipsjip.16.13>
19. Pittaway, L., Robertson, M., Munir, K., Denyer, D., Neely, A.: Networking and innovation: a systematic review of the evidence: networking and innovation: a systematic review of the evidence. *Int. J. Manag. Rev.* **5–6**, 137–168 (2004). <https://doi.org/10.1111/j.1460-8545.2004.00101.x>
20. Annarelli, A., Battistella, C., Nonino, F.: Product service system: a conceptual framework from a systematic review. *J. Clean. Prod.* **139**, 1011–1032 (2016). <https://doi.org/10.1016/j.jclepro.2016.08.061>
21. Tranfield, D., Denyer, D., Smart, P.: Towards a methodology for developing evidence-informed management knowledge by means of systematic review. *Br. J. Manag.* **14**, 207–222 (2003). <https://doi.org/10.1111/1467-8551.00375>
22. Mont, O.K.: Clarifying the concept of product–service system. *J. Clean. Prod.* **10**, 237–245 (2002). [https://doi.org/10.1016/S0959-6526\(01\)00039-7](https://doi.org/10.1016/S0959-6526(01)00039-7)

23. Uchihira, N., Kyoya, Y., Kim, S.K., Maeda, K., Ozawa, M., Ishii, K.: Analysis and design methodology for recognizing opportunities and difficulties for product-based services. In: PICMET 2007 - 2007 Portland International Conference on Management of Engineering & Technology, Portland, OR, USA, pp. 2755–2762. IEEE (2007). <https://doi.org/10.1109/PICMET.2007.4349613>
24. Fan, X., Zhang, H.: Aligning product-service systems with market forces: a theoretical framework. In: 2010 International Conference on Service Sciences, Hangzhou, China, pp. 110–114. IEEE (2010). <https://doi.org/10.1109/ICSS.2010.59>



# Service Costs in Operational Planning of Transportation with Small Batches of Cargo in City

Natalya Shramenko<sup>1,2</sup> , Dmitriy Muzylyov<sup>1</sup> ,  
and Vladyslav Shramenko<sup>1,3</sup> 

<sup>1</sup> Kharkiv Petro Vasylenko National Technical University of Agriculture,  
44, Alchevskyyh St., Kharkiv 61002, Ukraine

nshramenko@gmail.com

<sup>2</sup> Ukrainian State University of Railway Transport, 7, Feierbakh Sq.,  
Kharkiv 61050, Ukraine

<sup>3</sup> V. N. Karazin Kharkiv National University, 4, Svobody Sq.,  
Kharkiv 61022, Ukraine

**Abstract.** The research considers organization peculiarities of cargo transportation by small batches in city routes. At the same time, there is a tendency to reduce shipment sizes, a large number of customers, regularity, and deliveries frequency. A large amount of input information, numerical evaluation of the efficiency criterion, and selection of an intelligent technology from alternatives set are required to decide on the choice of transport service technology for cargo owners according to the development of Industry 4.0 at operational work planning of the transport enterprise. Simulation has been used to determine the effect of process parameters of agricultural cargo distribution in small batches on customer service costs. Simulation experiments were carried out with the help of created software. The total daily cost of shipping small-batch cargo is proposed as a criterion for the service efficiency of cargo owners on delivery routes. It considers the cost of freight transportation and the cost of idle vehicles time under uploads and unloads. A regression model describing the dependence of the total daily expenses for the discharge of small-batch cargoes on the technological parameters: the nominal load capacity of trucks, number of customers, and average sizes of delivery was obtained. It is proposed to use the obtained regression model by carriers when organizing small cargo batches transportation in cities. This will make it possible to choose a rational technology when servicing cargo owners on delivery routes in order to reduce the cost of transporting agricultural goods in small batches.

**Keywords:** Delivery routes · Vehicle load capacity · Small-batch cargoes · Process parameters · Costs



## 1 Introduction

There is a tendency to reduce deliveries size [1] and an increase in the share of small-batch cargo in total volumes of delivery at city routes in the current market conditions [2].

A feature of cargo transportation with small batches is many consumers in the territory of settlements, as well as an extensive product range, for which the delivery is carried out from different producers. The population needs a constant supply of various resources and goods and requires the delivery of equipment, materials, industrial goods, and other resources in small batches. This connects with limited consumption. The accumulation and storage of such products are costly. This is especially true for the transportation of agricultural goods.

It is necessary to find new scientific and practical solutions, methods, and models to optimize the transport process [3], considering that the organization level of cargo transportation with small batches is not sufficient enough [4]. This decision will help to reduce the operation resources of trucks and improve the quality services of transportation.

## 2 Literature Review

It is necessary to consider holistic, integrated transport [5] and technological systems [6] and optimization models formation for their analysis [7] according to solving of organization problems in rational interaction processes of production, logistics and consumption systems with transport processes [8] and interaction between certain kinds of transport. This provides greater overall efficiency compared to the total efficiency of elements taken separately [9].

Studies [10] reflect the impact of road transport parameters on the logistics system operation and propose an essential structure for determining groups of shortcomings in interrelation with a system of technical and operational characteristics of motor vehicles [11] during transport services of cargo flows. The situations analysis of appeared shortcomings groups within the framework of several transport operation characteristics (time, load capacity, velocity) shows that deterioration of technical and operational characteristics of transport operation leads to reduction of service quality [12], reduction of vehicles productivity, increase of transportation costs [13].

Recently, the attention of scientists has been attracted to the tasks of managing the supply of agricultural goods by road transport in conditions of non-stationary demand [14]. At the same time, it is crucial to predict demand during the operational period to improve transport service quality, and resources use [15]. The conducted studies prove the feasibility of using new information and communication technologies and simulation to make the correct decision on the choice of a rational option of cargo delivery [16] to minimize the costs of logistics companies [17]. The implementation of new information and communication technologies in Industry 4.0 [18] is characterized by its

ability to make decisions independently and independently [19] and is driven by the development of smart technologies [20] and the Internet of Things [21].

According to this, the task of determining the impact of technological parameters on the total costs associated with the distribution of these goods to consumers arises in the operational planning of the agricultural cargo supply process.

However, most methods of organizing transport services for cargo owners on delivery routes do not take into account consumers' requirements according to the conditions of their service [22, 23].

It has been found that in the development of the concept of transport services for consumers, more attention was paid to the satisfaction of the carrier's requirements, and the interests of shippers and consignees in the time of goods export (import) are sidelined [24] or remain entirely unaccounted for, which indicates a deterioration in transport services quality [25].

Exact methods do not allow creating optimal routes for many clients [26]. As a rule, routine tasks for motor vehicles are carried out using 'branches and borders' [27], which, with a large number of delivery points, cause significant calculation errors [28, 29]. Most straightforward and efficient methods are heuristic [30], which allow us to find the right solutions [31] quickly, but at the same time, they are not guaranteed to find the optimal solution.

Previous researches have shown that the creation of an optimal cargo delivery scheme was based not on increasing the specific weight of cargo mileage but on reducing the total distance [32].

Analysis of theoretical approaches and practical experience [33] shows that existing methods and models of planning and organization of delivery routes [34], especially for a large client's number, do not take into account consumers requirements for the cargo delivery time and do not provide for the choice of rational load capacity of the car.

### 3 Research Methodology

#### 3.1 Purpose and Task Setting

The study object is the process of supplying agricultural goods in small batches by city routes.

The study subject is the organization technology of delivery routes when supplying agricultural cargoes in small batches by city routes.

The research purpose is to determine the technological parameters influence of shipping agricultural cargoes by small batches on the costs of servicing consumers at delivery routes for choosing a rational technology.

The following objectives must be solved to achieve this goal:

- choose an efficiency criterion to find a rational load capacity and model of trucks for operation on delivery routes;
- simulate the delivery process of agricultural cargoes by small batches;

- determine the dependence of total daily costs of servicing cargo owners from technological parameters of supplying agricultural cargoes by small batches.

### 3.2 A Criterion for the Efficiency of Servicing Consumers on Distribution Routes

Shortcomings in the design of city delivery routes were revealed as an analysis result of agricultural cargo transportation technology by small batches:

- non-optimal routes are formed with a large number of serviced cargo owners. This leads to additional time consumption, deterioration of technical and economical vehicles parameters during operation;
- does not consider the consumer's requirements for vehicle arrival time under uploading, which leads to deterioration of service quality, company image, client outflow;
- The suitability of use trucks with rational load capacity is not analyzed on delivery routes. As a result, the high transportation cost, need to attract additional rolling stock, availability of unserved consumers;
- interests of consumers are fully satisfied in the case of just-in-time transport of goods, but the carrier gets the high time and financial costs, as the productivity of the rolling stock is reduced and the number of vehicles required for transport increases, leading to the application of higher tariffs and therefore affecting the competitiveness of enterprises;
- The expected total costs are not analyzed from small transportation batches, which leads to the use of inappropriate technology for delivery routes design.

The study was carried out for the farm, which carries out daily deliveries of agricultural goods in small batches to many consumers. At the same time, it is necessary to take into account the requirements of consumers regarding the time of cargo supply, provided that the cost of agricultural cargo delivery is minimized.

Processing large amounts of input information, numerical evaluation of the efficiency criterion and choosing a rational technology from alternatives set are required in order to decide on the choice of transport service technology for cargo owners with the Industry 4.0 development at operational planning of transport enterprise business.

'Grey box model' shows a generated structural diagram of the research object (Fig. 1).

Input parameters:  $q_{capj}$  – nominal load capacity j-th truck brand used at the delivery routes,  $\tau$ ;  $N$  – quantity of consumers, units;  $\bar{q}$  – average batch size, tons.

An output parameter is daily costs for the delivery of agricultural cargo by small batches at city routes –  $B_{total}$ , UAH/daily.

External factors:  $P_{auto}$  – acquisition cost of trucks, UAH;  $P_{fuel}$  – cost one gallon of fuel, UAH/l;  $t_{up}^{1t}$  – loading time 1 ton of cargo, hour;  $t_{un}^{1t}$  – unloading time 1 ton of cargo, hour;  $t_i$  – consumer requirements regarding the time of cargo supply, hours.

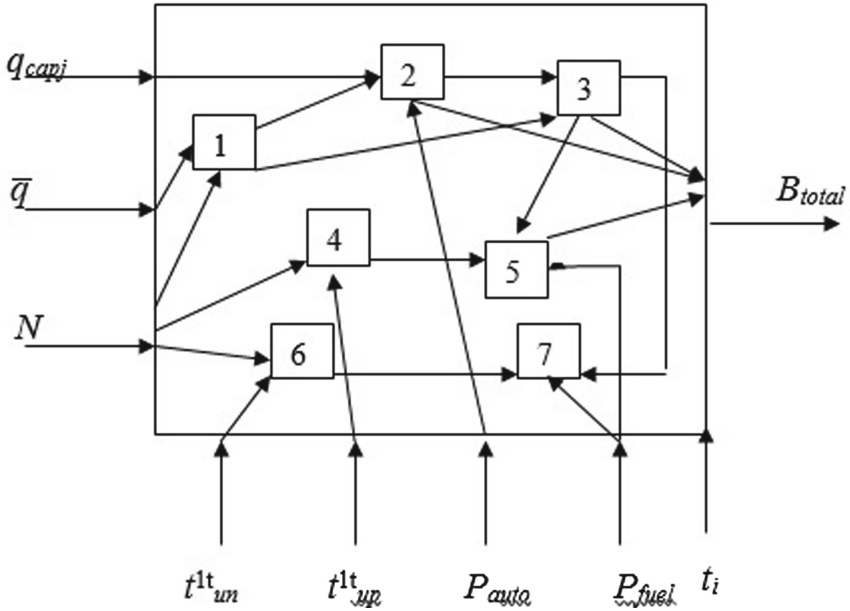


**Fig. 1.** A cybernetic model of cargo delivery process in city routes: 1 - the processing of consumer requests; 2 - a selection of truck brand for operation on delivery routes; 3 - design of cargo transportation routes; 4 - loading of the vehicle at the supplier; 5 - cargo transportation to i-th consumer; 6 - unloading of cargo at the i-th consumer; 7 - return of empty rolling stock from the last unloading place to the supplier's enterprise.

Total daily costs for the discharge of small-batch cargoes are proposed as a criterion for the efficiency of servicing consumers on distribution routes taking into account the operating costs for the delivery activity and the costs for the maintenance of vehicles:

$$C_{total} = f(L_{total}, C_{var}, C_{const}, V_{op}, t_{up}^{lt}, t_{un}^{lt}, q_{capj}, C_{hour}^{up/un}, \bar{q}, N) \rightarrow \min, \quad (1)$$

where  $L_{total}$  – Total mileage length of vehicles on delivery routes, km/day;  $C_{var}$  – variable costs per 1 km of mileage, e.u./km;  $C_{const}$  – constant costs per 1 km of mileage, e.u./km;  $V_{op}$  – operating velocity of vehicle, km/hour;  $t_{up}^{lt}$  – loading time 1 ton of cargo, hour;  $t_{un}^{lt}$  – unloading time 1 ton of cargo, hour;  $q_{capj}$  – nominal load capacity j-th truck brand used at the delivery routes, tons;  $C_{hour}^{up/un}$  – cost of trucks downtime under uploading (unloading), e.u./hour;  $\bar{q}$  – average batch size, tons,  $\tau$ ;  $N$  – the quantity of consumers, units.

Simulation experiments were carried out with the help of designed software. The distinctive feature of the software is rational delivery routes design during goods transportation by small batches at the city routes for a large number of customers. The program field accidentally generates customer and terminal locations, as well as transportation volumes and delivery time of cargo to customers (Fig. 2).

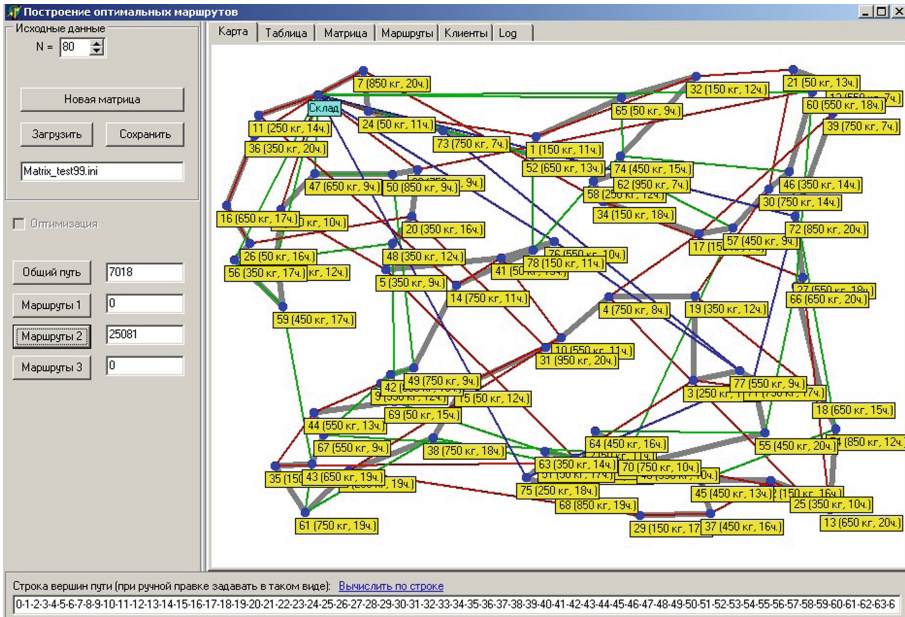


Fig. 2. Software interface “Formation of rational delivery routes”.

Imitation approach is chosen for simulation of the research subject since the overwhelming number of transport process parameters during transportation small-batch cargoes at city routes are random variables.

### 4 Results

It is necessary to determine the interval for changing batches sizes to be ordered by the customers while simulating the operation of vehicles on delivery routes. For this purpose, statistics were collected on the supply size for small-batch freights and data of 1-ton cargo uploading and unloading duration.

A Plackett-Burman experiment plan has been developed for the simulation experiment. Such intervals of input factors variation are considered: vehicle load capacity - [3; 6] t; number of consumers - [10; 100] unit; average batches size is [0.241; 0,741]. The number of series in the experiment was determined to be 90. The number of experiments in the series is justified based on the normal distribution of the numerical value of total daily costs for small-batch cargoes supply. It was found that a sufficient number of experiments in each series vary from 5 to 98 (at a confidence level of 95%) based on calculation results. One hundred cases of the experiment were conducted in each series to ensure the significance of the results.

Transportation of agricultural goods in small batches is most often carried out by onboard trucks with awning and vans with a load capacity of 3 to 6 tons. 14 alternative brands of automobiles were considered, for each of which a set of technical and

economic characteristics was collected: load capacity, linear fuel consumption rates, prices of trucks, and others. The next vehicles were chosen for research as a comparison result of linear fuel consumption rates and truck prices considering their minimal values: Foton BJ 1049, Hyundai HD-72, and KamAZ 4308-6064-79 (C3).

Routes have been formed, total trucks mileage on these routes has been determined and total daily costs for the supply of agricultural goods have been calculated as a result of the simulation cargo small batches distribution. The design of delivery routes was carried out for customer service conditions of 'by periods of the day'. This technology partially considering consumer's requirements regarding the supply time of goods.

A regression model was obtained based on the results of the simulation experiment. This model accurately describes the dependence of the total daily costs for small-batch cargoes distribution from a nominal load capacity of trucks operating on delivery routes, the number of customers, as well as the average batch size supply.

The results of the analysis for many hypotheses put forward about dependence type show that the most adequate (determining factor is 0.9106) is the following dependency type:

$$B_3 = 0,5978 \cdot N^2 - 12,9844 \cdot q_{cap}^2 + 4783,3061 \cdot \bar{q}^2, \quad (2)$$

The function range of definition:  $N \in [18; 100]$ ,  $q_{cap} \in [3; 6]$ ,  $\bar{q} \in [0,241; 0,741]$ .

The results of the regression analysis indicate that the following technological parameters have a significant impact on the costs of servicing cargo owners: quantity of consumers, average batch size, and the nominal load capacity of trucks.

Thus, the parameter  $N$  has the greatest impact on the cost of servicing cargo owners on delivery routes according to the obtained dependence (2). It describes the number of customers served, as well as the supply volume. At the same time, the load capacity of trucks operating on a delivery route is essential.

Carriers can use the study results during the organization of small-batch cargo delivery in cities. This will allow choosing a rational technology when servicing cargo owners on delivery routes in conditions of minimal total daily costs.

## 5 Conclusions

As an analysis result of the organization of agricultural goods supply by small batches in cities, several shortcomings have been identified. It has been found that most of the existing models of the transport process do not consider the interests of shippers and consignees during the delivery time of the goods, and therefore the quality of transport services is deteriorated.

The total daily cost of shipping agricultural cargo by small batches is proposed as a criterion of service efficiency of cargo owners on delivery routes.

A regression model was obtained based on the results of the simulation experiment. This model accurately describes the dependence of the total daily costs for small-batch cargoes distribution from a nominal load capacity of trucks operating on delivery routes, the number of customers, as well as the average batch size supply.

Directions of further research: determination of rational load capacity of trucks for operation on delivery routes depending on customer's number and the average supply volume; design reasonable structure of rolling stock fleet; creating differentiated tariffs for goods transportation and flexible tariff policy of carriers aimed at the complete satisfaction of cargo owner's requirements.

## References






1. Vasyanin, V., Ushakova, L.: Vehicle routing problems with delivery and collection of small-lot cargo in the internal service areas of trunk nodes of hierarchical transport network. *Math. Model. Econ.* **3–4**, 102–131 (2016)
2. Ovsyannikova, G., Shoshin, D.: The organization of road transport of small consignments at a dairy plant. *Young Sci.* **11**, 87–90 (2014)
3. Tolebayeva, A., Vitvitskiy, E.: Operational planning improvement of enterprises goods' carriage by small shipments in the cities. *Bull. Sib. State Automob. Highway Acad.* **1(59)**, 77–87 (2018)
4. Lipanov, V., Kichkaylo, S.: Modeling and improvement of the algorithm formation for the optimized transport routes. *Coll. Sci. Works Kharkiv Univ. Air Forces* **2(35)**, 105–109 (2013)
5. Shramenko, N., Shramenko, V.: Mathematical model of the logistics chain for the delivery of bulk cargo by rail transport. *Sci. Bull. Natl. Min. Univ.* **5(167)**, 136–141 (2018)
6. Shramenko, N.: The methodological aspect of the study feasibility of intermodal technology of cargo delivery in international traffic. *Sci. Bull. Natl. Min. Univ.* **4(160)**, 145–150 (2017)
7. Bosov, A., Khalipova, N.: Formation of separate optimization models for the analysis of transportation-logistics systems. *East.-Eur. J. Enterp. Technol. Control Process.* **3(87)**, 11–20 (2017)
8. Shramenko, N., Shramenko, V.: Optimization of technological specifications and methodology of estimating the efficiency of the bulk cargoes delivery process. *Sci. Bull. Natl. Min. Univ.* **3**, 146–151 (2019)
9. Shramenko, N.: Methodology for evaluation of synergy effect in terminal cargo delivery system. *Actual Probl. Econ.* **8(182)**, 439–444 (2016)
10. Goryainov, A.: Isolation of diagnostic parameters in groups of indicators of transport performance. *Sci. Bull. KNTUA* **136**, 265–271 (2013)
11. Goryainov, A.: Groups of deficiencies and symptoms when transporting freight flows. *Tech. Serv. Agric. For. Transp. Complexes* **4**, 16–22 (2016)
12. Shramenko, N.: Effect of process-dependent parameters of the handling-and-storage facility operation on the cargo handling cost. *East.-Eur. J. Enterp. Technol.* **5/3(77)**, 43–47 (2015)
13. Shramenko, N.: Evaluation of the effectiveness of piggyback traffic in the context of creating transport and logistics clusters. *Sci. Bull. Natl. Min. Univ.* **6(162)**, 151–155 (2017)
14. Kotsiuk, M.: Investigation of the process of storage and sale of perishable products. *Bull. NTU* **31**, 275–284 (2015)
15. Shramenko, N., Muzylyov, D.: Forecasting of overloading volumes in transport systems based on the fuzzy-neural model. In: Ivanov, V. (ed.) *Advances in Design, Simulation and Manufacturing II, DSMIE 2019, LNME*, pp. 311–320. Springer, Cham (2020). [https://doi.org/10.1007/978-3-030-22365-6\\_31](https://doi.org/10.1007/978-3-030-22365-6_31)
16. Shramenko, N., Pavlenko, O., Muzylyov, D.: Computer modeling and intelligent systems. In: Subbotin, S. (ed.) *CMIS-2019, CEUR Workshop Proceedings*, vol. 2353, pp. 935–949 (2019)

17. Alekseev, S.: Prospects for the implementation and use of innovative intelligent technologies in modern transport systems. *Int. J. Open Inf. Technol.* **6**(6), 38–43 (2018)
18. Alcácer, V., Cruz-Machado, V.: Scanning the Industry 4.0: a literature review on technologies for manufacturing systems. *Eng. Sci. Technol. Int. J.* **22**(3), 899–919 (2019)
19. Tarasov, I.: Industry 4.0: concept & development. *Bus. Strateg.* **6**(50), 57–63 (2018)
20. Bawa, M., Caganova, D., Szilva, I., Spirkova, D.: Importance of Internet of Things and big data in building smart city and what would be its challenges. In: Leon-Garcia, A., et al. (eds.) *Smart City 360°. Smart City 360 2016, Smart City 360 2015. Lecture Notes of the Institute for Computer Sciences, Social Informatics and Telecommunications Engineering*, vol. 166. Springer, Cham (2015)
21. Dovgal, V., Dovgal, D.: Internet of Things: concept, applications and tasks. *Bull. Adygey State Univ.* **1**(216), 129–135 (2018)
22. Prokofieva, O.: Development of a methodology for optimizing delivery routes. Unpublished Ph.D. thesis, ISTU, Irkutsk, Russia Federation (2004)
23. Podshivalova, K.: Improving the efficiency of transportation of small-lot cargo by road. Unpublished Ph.D. thesis, VSTU, Volgograd, Russia Federation (2007)
24. Vasiliev, S.: Development of a methodology for the transportation of small-lot cargo by road, taking into account probabilistic factors. Unpublished Ph.D. thesis, St. Petersburg, Russia Federation (2009)
25. Filippov, D.: Managing and optimizing the process of forming routes for the supply of consumer goods in distribution centers. Unpublished Ph.D. thesis, State University of Management, Moscow, Russia Federation (2012)
26. Nikonorov, V.: Mathematical methods for solving the problem of small-batch traffic routing. *Sci. Tech. Statements St. Petersburg State Polytech. Univ. Econ.* **6**(137), 222–226 (2011)
27. Kostyuk, Yu.: Effective implementation of the algorithm for solving the task of the courier company using the Verwey and Boundaries method. *Appl. Discrete Math.* **2**(20), 78–90 (2013)
28. Zhestkova, S.: The use of the “branches and borders” method in solving problems of transport routing. *World Transp. Technol. Mach.* **1**, 94–100 (2012)
29. Kotov, V., Zhestkova, S.: Determination of radial routes for the carriage of goods by road transport. *Bull. Orenburg State Univ.* **4**(179), 72–76 (2015)
30. Luchko, M., Fateev, M.: Improvement of transport services for combined and delivery routes in the supply chain. *Bull. V. Dal East-Ukr. Natl. Univ.* **4**(146(2)), 120–126 (2010)
31. Samuilov, V., Petrov, A., Zubarev, A.: Comparative analysis of heuristic methods for routing urban transport. *Urals Transp.* **4**(35), 12–16 (2012)
32. Rogatkin, A., Zakharkina, M.: Vehicle routing optimization: heuristics algorithms and practice of logistics management. *Bull. Mosc. Int. Acad.* **1**, 124–134 (2016)
33. Polyakov, A., Galuschak, A., Galuschak, D., Grabenko, M.: Technique of the choice of the rolling stock, route and schedule of transportation of goods. *Sci. Works Vinnitsa Natl. Tech. Univ.* **3**, 1–10 (2011)
34. Krasnikova, D., Rakhmankulova, R.: Organization specifics for delivery by motor transport on assembled and distributive routes. *Sci. Methodical Electron. J. “Concept”* **13**, 4081–4085 (2015)





# The Methodology of Obtaining Power Consumption Fuzzy Predictive Model for Enterprises

Sergii Tymchuk<sup>1</sup> , Sergii Shendryk<sup>2</sup> , Vira Shendryk<sup>2</sup> ,  
Ivan Abramenko<sup>1</sup> , and Anastasiia Kazlauskaite<sup>2</sup> 

<sup>1</sup> Kharkiv Petro Vasilenko National Technical University of Agriculture,  
19, Rizdviana St., Kharkiv 61052, Ukraine

<sup>2</sup> Sumy State University, 2, Rymaskogo-Korsakova St., Sumy 40007, Ukraine  
v.shendryk@cs.sumdu.edu.ua

**Abstract.** The Industry 4.0 concept involves the use of intelligent technology to improve the production processes, such as using centralized management at the system level, which leads to faster and more flexible energy management. Thus, large and small industrial and utility companies need to create a system for predicting electricity consumption. This paper is devoted to the development of a methodology for obtaining a power consumption predictive model based on the use of fuzzy regression analysis. The proposed technique of forming a fuzzy predictive model, considering the weekly and annual cycles, made it possible to simply form a kind of prediction schedule of daily electricity consumption of any complexity. A criterion applied considers both the degree of estimates closeness to the raw data and the degree of fuzziness. The predicting model provides an opportunity to obtain a daily electricity consumption schedule for any day of the month of the year, as well as a short-term daily prediction. The testing results and study of the proposed method effectiveness are presented.

**Keywords:** Power consumption · Prediction · Fuzzy regression analysis · Prediction error

## 1 Introduction

At present, there is a tendency to introduce the Industry 4.0 concept into manufacturing and production processes. This approach involves the use of intelligent technology to improve production processes. Industry 4.0 solutions increase efficiency, productivity, and environmental sustainability. Energy consumption's management plays a crucial role in Industry 4.0 as a whole. Stringent environmental regulations and rising energy costs require increased energy efficiency. Therefore, the importance of technological innovation to save energy increases [1], especially using centralized management at the system level, which leads to faster and more flexible energy management [2, 3] based on the choice of an appropriate operating mode taking into account real-time and long-term predicted energy consumption data. In today's energy market, large and small industrial and utility companies need to create a system for predicting electricity

consumption, which minimizes the deviation of consumption of power from the declared on the market for the day ahead. It is known that electricity consumption by consumers is random and depends on many changing factors (e.g., consumer load, and environmental conditions). Methods based on deterministic and probabilistic-statistical methods are used to solve these problems. Today the most common method is regression analysis.

In some cases, for some reason, the information on electricity consumption may not be sufficient, or it may be interval or unclear. Thus the use of traditional methods of estimating and predictive power consumption becomes very difficult. Therefore, the task of constructing predictive power models is related to solving the uncertainty of the source information. One way to solve uncertainty is to build predictive models using fuzzy regression analysis, which is based on the theory of possibilities and fuzzy set theory, as opposed to conventional regression analysis based on probability theory.

## 2 Literature Review

To this date, several fuzzy regression construction methods have been developed that can be used to construct predictive power models.

First of all, it is a fuzzy regression analysis based on the minimum fuzzy criterion. In [4, 5], its application is theoretically substantiated. This criterion does not consider the internal structure of the fuzzy data being processed. When this is insignificant, a fuzzy interval regression is used, in particular, when solving predictive energy problems [6, 7] or describing the output [8, 9]. For a more accurate prediction of power consumption, it is necessary to know not only the interval but also the structure of the fuzzy value in the interval.

Second, it is a fuzzy regression analysis combined with the least-squares method (FLSRA). It appears in two variants: FLSRA by the criterion of minimum fuzziness [4, 10] and FLSRA by the criterion of maximum compatibility [4, 11]. The following disadvantage characterizes the first variant: the higher the degree of reliability, the higher the fuzziness of the regression model. The disadvantage of the second variant can be noted as follows: firstly, the higher the desired compatibility between the data and the model, the fuzzier the scattering, secondly, the centerline equation differs from the ordinary FLSRA – the regression equation, and thirdly, the unpopularity due to the excessive complexity of calculations.

Several papers are devoted to methods of determining regression coefficients. The simplest way to found regression coefficients is in linear models [12, 13], and the approach to solving this problem for small sets of fuzzy initial data is also interesting [14]. It uses the knowledge of FLSRAs as well as linear programming methods. For nonlinear models, nonlinear programming methods are used, described in general in [15] and even evolutionary algorithms [16]. In the context of the power prediction task, all of these methods can be applied. The main difficulty is agreeing on two different criteria: maximum data and model compatibility and minimal model fuzziness. A successful solution to this problem is proposed in [17].

It is necessary to obtain and investigate regression dependence for long-term and short-term prediction of power consumption by the enterprise. The initial data are the

results of measurements of electricity consumption by the equipment of the Automated Information-Measuring System of Commercial Electricity Metering (ASCEM) of enterprise for the previous year. The prediction dependence should allow receiving a daily schedule of electricity consumption for any day of the month of the next year, as well as an operational prediction for the next day.

### 3 Research Methodology

#### 3.1 Method of Forming Fuzzy Predictive Regression Model of Power Consumption Terms

Electricity is a cyclical process. Moreover, the characteristics of each cycle depend on several external and internal factors. Internal factors include such forms, which are difficult to formalize in general as the number of units of load, the schedule of days off and holidays. Exteriors include seasonality and climatic characteristics. There are several other factors associated with emergencies that are generally carried out beyond the prediction task. Cycles can be divided by their length into daily, weekly, monthly, annual. Depending on the predictive goals, the model should describe any of these cycles. The degree of consideration of external and internal factors depends on the predicting cycle for which the model is being developed. The longer the cycle, the more factors to consider. Based on the materials produced, we can also conclude that the longer the predicting cycle, the higher the predictive error. The model developed for the prediction for the year considers the most significant number of factors but has the maximum error for the daily prediction. However, the model developed for the daily prediction has minimal error in the prediction for the day, but its error is excessively large for the prediction for the month or year ahead because the number of factors considered in it is limited.

#### 3.2 Formation of Predictive Type Depending on the Day

The type of predicting dependence is determined based on the analysis of the initial data. It should be noted that the process of determining the optimal type of regression function is not formalized. And the traditionally applied polynomial approach, justified in interpolation problems, is often futile for predictive tasks. Analyzing the daily schedules of electricity consumption, we can draw the following conclusion: electricity consumption during the day can be divided into periods of morning, evening peaks, and background consumption. Since the graphs of power consumption clearly show peaks during the day, it is rational to predict the predictive function, not in the form of a polynomial, but the form of a superposition of the Gaussian curves for the peaks of consumption (peak) and direct for background consumption (bg). The process of electricity consumption has some uncertainty. Therefore, the predictive model is fuzzy. Instantaneous power consumption is approximated by a fuzzy triangular number, which is described by the tuple  $W = \langle W^{mod}, W^{min}, W^{max} \rangle$ . Accordingly, the daily cycle of power consumption can be described by the function of the form:

$$\begin{aligned}
 W(t) &= \langle W^{\text{mod}}(t), W^{\text{min}}(t), W^{\text{max}}(t) \rangle, \\
 W^{\text{mod}}(t) &= W_{\text{bg}}^{\text{mod}}(t) + W_{1\text{peak}}^{\text{mod}}(t) + W_{2\text{peak}}^{\text{mod}}(t), \\
 W^{\text{min}}(t) &= W_{\text{bg}}^{\text{min}}(t) + W_{1\text{peak}}^{\text{min}}(t) + W_{2\text{peak}}^{\text{min}}(t), \\
 W^{\text{max}}(t) &= W_{\text{bg}}^{\text{max}}(t) + W_{1\text{peak}}^{\text{max}}(t) + W_{2\text{peak}}^{\text{max}}(t),
 \end{aligned} \tag{1}$$

where  $t$  is the current time during the day.

A general graphical view of the fuzzy predictive model is shown in Fig. 1.

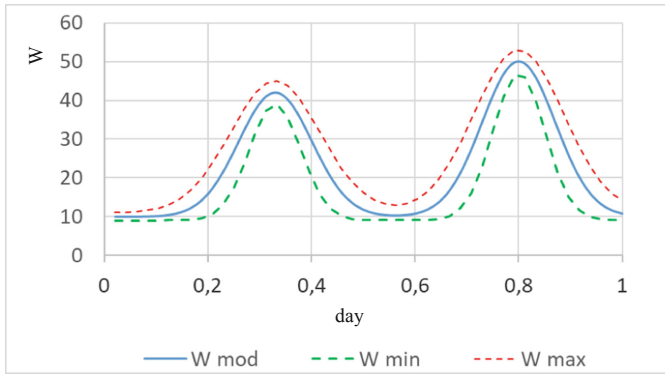


**Fig. 1.** Illustration for building a fuzzy predictive model of electricity consumption during the day.

The components of expressions (1) have the following functional form:

$$\begin{aligned}
 W_{\text{bg}}^{\text{mod}}(t) &= a_1 t + a_2; \quad W_{\text{bg}}^{\text{min}}(t) = b_1 t + b_2; \quad W_{\text{bg}}^{\text{max}}(t) = c_1 t + c_2; \\
 W_{1\text{peak}}^{\text{mod}}(t) &= a_3 \cdot \exp(-(t-a_4)^2/a_5); \quad W_{1\text{peak}}^{\text{min}}(t) = b_3 \cdot \exp(-(t-b_4)^2/b_5); \\
 W_{1\text{peak}}^{\text{max}}(t) &= c_3 \cdot \exp(-(t-c_4)^2/c_5) \\
 W_{2\text{peak}}^{\text{mod}}(t) &= a_6 \cdot \exp(-(t-a_7)^2/a_8); \quad W_{2\text{peak}}^{\text{min}}(t) = b_6 \cdot \exp(-(t-b_7)^2/b_8); \\
 W_{1\text{peak}}^{\text{max}}(t) &= c_6 \cdot \exp(-(t-c_7)^2/c_8)
 \end{aligned} \tag{2}$$

### 3.3 Consideration in the Predictive Dependence of Weekly and Annual Cycles

Information on weekly and annual cycles in the integral form is contained in the coefficients  $a_1$ – $a_8$ ,  $b_1$ – $b_8$ ,  $c_1$ – $c_8$ . To determine these dependencies, it's necessary to include the day of the week and the week of the year in the fuzzy regression analysis.

It should be noted that weekly and exceptionally annual cycles are more related to seasonal external oscillations, which are nonlinear in nature. However, based on the preliminary analysis, it is determined that the second-degree polynomial models are optimal in this case. That is, it is suggested to consider the weekly cycles in the following form:

$$\begin{aligned}
 a_i &= a_{i1}d_n^2 + a_{i2}d_n + a_{i3}, \\
 b_i &= b_{i1}d_n^2 + b_{i2}d_n + b_{i3}, \\
 c_i &= c_{i1}d_n^2 + c_{i2}d_n + c_{i3}, \\
 i &= \overline{1, 8},
 \end{aligned}
 \tag{3}$$

where  $d_n$  is the day number of the week.

In turn, the coefficients obtained in (3) depend on the number of the week of the year in the following form:

$$\begin{aligned}
 a_{ij} &= a_{ij1}n^2 + a_{ij2}n + a_{ij3}, \\
 b_{ij} &= b_{ij1}n^2 + b_{ij2}n + b_{ij3}, \\
 c_{ij} &= c_{ij1}n^2 + c_{ij2}n + c_{ij3}, \\
 i &= \overline{1, 8}, j = \overline{1, 3},
 \end{aligned}
 \tag{4}$$

where  $n$  is the number of the week.

Substituting (4) into (3) and further into (2), daily predictive dependencies for any day of the year, taking into account both the daily, weekly, and annual cycles of electricity consumption, is obtained. The predictive model is written using matrix algebra. To do this, we introduce the following notation:

$$\begin{aligned}
 a_i &= D^T \times A_i \times N; \quad b_i = D^T \times B_i \times N; \quad c_i = D^T \times C_i \times N; \\
 i &= \overline{1, 8},
 \end{aligned}
 \tag{5}$$

where  $A_i, B_i, C_i$  are regression coefficient matrixes.

$$\begin{aligned}
 A_i &= \left\| \begin{matrix} a_{i11} & a_{i12} & a_{i13} \\ a_{i21} & a_{i22} & a_{i23} \\ a_{i31} & a_{i32} & a_{i33} \end{matrix} \right\|; \quad B_i = \left\| \begin{matrix} b_{i11} & b_{i12} & b_{i13} \\ b_{i21} & b_{i22} & b_{i23} \\ b_{i31} & b_{i32} & b_{i33} \end{matrix} \right\|; \quad C_i = \left\| \begin{matrix} c_{i11} & c_{i12} & c_{i13} \\ c_{i21} & c_{i22} & c_{i23} \\ c_{i31} & c_{i32} & c_{i33} \end{matrix} \right\| \\
 N &= \left\| \begin{matrix} n^2 \\ n^1 \\ n^0 \end{matrix} \right\| - \text{vector of the numbers of the week of the year.}
 \end{aligned}$$

$$D = \left\| \begin{matrix} d_n^2 \\ d_n^1 \\ d_n^0 \end{matrix} \right\| - \text{vector of day number week degrees.}$$

Thus, the process of constructing the type of dependencies for the prediction of power consumption with all cycles is completed.

The coefficients (5) calculated in this way are substituted in (2) and further, in (1), general kind of fuzzy predictive model of electricity consumption, which considers daily, weekly, and annual cycles, is received.

The regression coefficients, which are elements of the matrix  $A_i, B_i, C_i$  in expression (5), are determined as a result of applying a fuzzy regression analysis on the data set for electricity consumption per year. The ASCEM records the experimental data, usually with a period of 30 min. Therefore, when looking for regression coefficients, time is sampled with the specified step. Then the expressions for the criteria for finding the values of the regression coefficients, as proposed in [14], provide that for the  $k$ -th day of the year there are  $m$  discrete values for time, take the form:

$$\begin{aligned} S_k &= \frac{1}{m} \sum_{i=1}^m (W_{ki}^{\max} - W_{ki}^{\min}) / W_{eki} + \frac{1}{m} \sum_{i=1}^m (1 - \mu_W(W_{eki})), \\ \mu_W(W_{eki}) &= \max \left( 0, \min \left( \frac{W_{eki} - W_{kji}^{\min}}{W_{ki}^{\text{mod}} - W_{ki}^{\min}}, \frac{W_{ki}^{\max} - W_{eki}}{W_{ki}^{\max} - W_{ki}^{\text{mod}}} \right) \right), \\ S &= \frac{1}{365} \sum_{k=1}^{365} S_k \rightarrow \min. \end{aligned} \tag{6}$$

As a result, the values of the regression coefficients are obtained. This operation is performed once at the end of the year.

### 3.4 Formation of Fuzzy Regression Model of Power Consumption for Short-Term Prediction

As noted above, dependencies (5) are the starting point for forming a short-term prediction. In addition to the current time, they also contain the day of the week and the number of the week of the year as arguments. For a short-term prediction on a given date, it is necessary to clarify the dependences (5) on the data obtained by the ASCEM recently.

For clarification, there is no need to search again for all elements of the  $A_i, B_i, C_i$  matrices. If the statement, that expressions (5) qualitatively describe the dependences of electricity consumption on the number of the week in the year, the number of the week, the current time of day, is accepted and the basis for such approval is the results of data processing for the year, then quantify the dependencies (5) based on operational power consumption data can be selected by selecting permanent dependency members. That is necessary to find:

$$a_{233}, a_{333}, a_{633} \quad b_{233}, b_{333}, b_{633} \quad c_{233}, c_{333}, c_{633} : S \rightarrow \min. \tag{7}$$

Criterion  $S$  is defined by expression (6).

Accordingly, sophisticated methods are unnecessary to solve this problem. It is sufficient to implement the dichotomy procedure for coefficients (7).

### 4 Results

The study includes the development of a long-term predictive dependence on the results of the processing of electricity consumption for the previous year, the correction of this model for the short-term prediction, and the evaluation of its quality on a sample of raw data not participated in the development of the long-term model.

Data for electricity consumption of one of the small enterprises for 2013 was processed according to the above method. To find out how large the correction sample, it should be explored three options. The first option: daily correction for the same day of the previous week is taken as the corrective sample. The short-term predictive model was developed by adjusting the long-term model for dates from 20/01 to 26/12 in 10-day increments. The results were averaged. The result was the following qualitative indicators for the short-term predictive model: the average coincidence of 0.322008, average fuzzy of 1.283895, averaged MAPE = 32.81878. Meanwhile, when applying the long-term predictive model, the average degree of coincidence is 0.592667, the average degree of fuzziness is 3.216254, the average MAPE = 29.99075. That is, with this variant of correction, the short-term model produces worse quality indicators than the long-term one except for the medium degree of fuzziness (see Fig. 2).

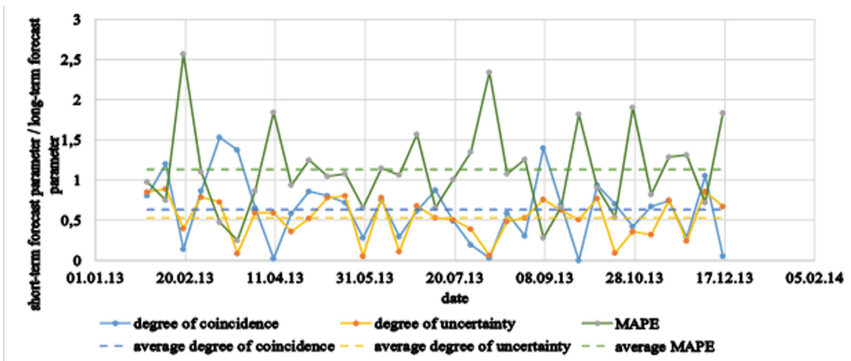


Fig. 2. Relative characteristics of the short-term prediction when correcting the long-term model based on the data of one day last week.

The second option: daily correction of the three previous days is taken as the corrective sample. The short-term predictive model was also developed by adjusting the long-term model for dates from 20/01 to 26/12 in 10-day increments. The results were averaged. The result was the following qualitative indicators for the short-term predictive model: the average coincidence of 0.515338, average fuzzy of 2.541996, averaged MAPE = 31.19147. With this correction option, the short-term model again produces poorer quality scores than the long-term one, except for the average degree of fuzziness (see Fig. 3), but the indicators are better than the first option indicators.

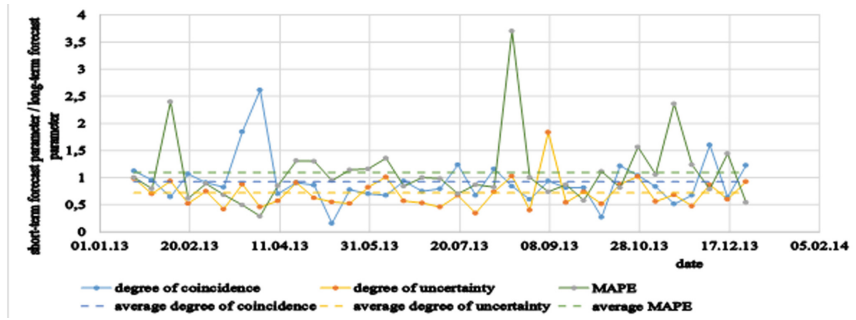


Fig. 3. Relative characteristics of the short-term prediction when correcting the long-term model based on the data of the previous three days.

The third option: daily correction of the seven previous days is taken as the corrective sample. The short-term predictive model was also developed by adjusting the long-term model for dates from 20/01 to 26/12 in 10-day increments. The results were averaged. The result was the following qualitative indicators for the short-term predictive model: the average coincidence of 0.558486, the average degree of fuzzy 2.202243, averaged MAPE = 26.40401. In this version of the correction, the short-term model gives better quality indicators than the long-term and the medium degree of fuzziness and the MAPE (see Fig. 4). The slight decrease in the degree of coincidence is explained by the significant decrease in the degree of fuzziness since these parameters contradict each other, and it is impossible to improve both at the same time.

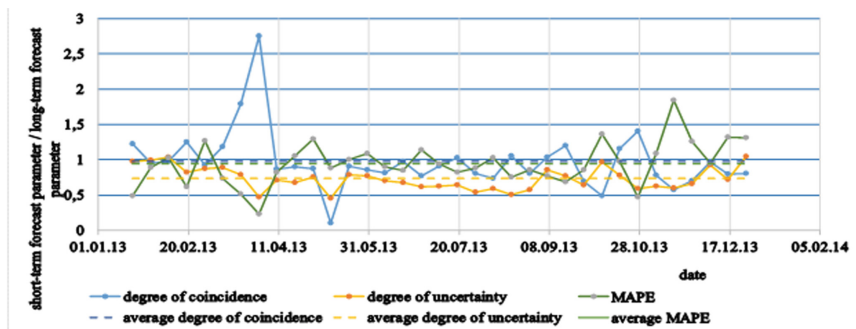


Fig. 4. Relative characteristics of short-term prediction when correcting long-term models based on previous week's data.

Thus, the corrective sample should be constructed based on the power consumption data of the seven days immediately adjacent to the predicting date.

The predictive properties of the developed model were tested on the 5 months, which were not considered when constructing the long-term predictive model.

Daily correction of the seven previous days was selected as the corrective sample. The short-term predictive model was also developed by adjusting the long-term model developed using previous year data on dates from 15/01 to 25/05 in 10-day increments. The results were averaged. The result was the following qualitative indicators for the



short-term predictive model: the average coincidence of 0.5662, average fuzzy of 1.839911, averaged MAPE = 18.51306. The long-term predictive model showed the following qualitative indicators: the average coincidence of 0.472266, average fuzziness of 2.67646, average MAPE = 27.90493.

The short-term model gives better quality indicators than the long-term in all parameters (see Fig. 5). By the way, the new data set and the long-term model showed better performance. This indicates a more stable and predictable operation of the company compared to the previous year.

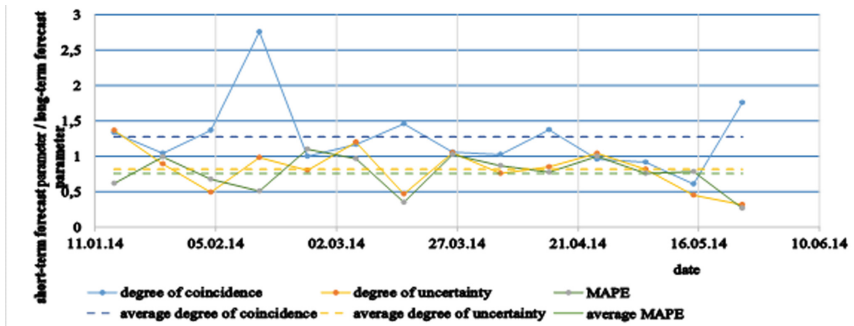


Fig. 5. Relative characteristics of the short-term prediction for the correction of the long-term model based on the previous week's data in the sample of next year's data.

The results show that in case of insignificant changes in the technological process of the enterprise, the developed method of adapting once obtained long-term predictive models to short-term prediction is effective. Moreover, for 2014 data, the predictive model is even more efficient than the sample for which the model was developed. This indicates that for the enterprise, the type of long-term predictive model is well developed and may not change annually, but can be used to adapt to short-term predictions over many years.

## 5 Conclusions

The proposed technique of forming a fuzzy predictive model in the form of a superposition of a linear and two Gaussian functions, taking into account the weekly and annual cycles, made it possible to simply form a kind of prediction schedule of daily electricity consumption of any complexity.





The conducted research of the developed method of construction of the model of long-term prediction and short-term prediction based on an adaptation of long-term predictive models showed that the quality of short-term predicting according to the degree of coincidence, degree of fuzziness and medium-modulus relative error during data sampling is quite stable. The degree of compatibility increased on average by 0.09, the degree of fuzziness decreased by 0.8, and the MAPE decreased by 9.4% compared with the long-term predictive model. The results obtained confirm the effectiveness of the proposed method.

## References

1. Shendryk, V., Boiko, O., Parfenenko, Y., Shendryk, S., Tymchuk, S.: Handbook of Research on Industrial Advancement in Scientific Knowledge. Decision Making for Energy Management in Smart Grid. IGI-Global, USA (2019). <https://doi.org/10.4018/978-1-5225-7152-0.ch014>
2. Jafari, M., Malekjamshidi, Z., Lu, D.D.-C., Zhu, J.: Development of a fuzzy-logic-based energy management system for a multiport multioperation mode residential smart microgrid. *IEEE Trans. Power Electron.* **34**(4), 3283–3301 (2019). <https://doi.org/10.1109/TPEL.2018.2850852>
3. Arcos-Aviles, D., Julio Pascual, J., Marroyo, L., Sanchis, P., Guinjoan, F.: Fuzzy logic-based energy management system design for residential grid-connected microgrids. *IEEE Trans. Smart Grid* **9**(2), 530–543 (2018). <https://doi.org/10.1109/TSG.2016.2555245>
4. Chang, Y.H.O., Ayyub Bilal, M.: Fuzzy regression methods - a comparative assessment. *Fuzzy Sets Syst.* **119**(2), 187–203 (2001). [https://doi.org/10.1016/S0165-0114\(99\)00091-3](https://doi.org/10.1016/S0165-0114(99)00091-3)
5. Tarantsev, A.: The principles of constructing regression models with initial data with a fuzzy description. *Automat. Telemekh.* **11**, 215–220 (1997)
6. Manusov, V., Mogilenko, A.: Methods for estimating electricity losses in the face of uncertainty. *Electricity* **3**, 2–8 (2003)
7. Tau Lee, H., Hua Chen, S.: Fuzzy regression model with fuzzy input and output data for manpower forecasting. *Fuzzy Sets Syst.* **119**(2), 201–213 (2001). [https://doi.org/10.1016/S0165-0114\(98\)00382-0](https://doi.org/10.1016/S0165-0114(98)00382-0)
8. Yu, J.-R., Tzeng, G.-H., Li, H.-L.: General fuzzy piecewise regression analysis with automatic change-point detection. *Fuzzy Sets Syst.* **119**(2), 247–257 (2001). [https://doi.org/10.1016/S0165-0114\(98\)00384-4](https://doi.org/10.1016/S0165-0114(98)00384-4)
9. Chen, Y.-S.: Outliers detection and confidence interval modification in fuzzy regression. *Fuzzy Sets Syst.* **119**(2), 259–272 (2001). [https://doi.org/10.1016/S0165-0114\(99\)00049-4](https://doi.org/10.1016/S0165-0114(99)00049-4)
10. Wang, H.-F., Tsauro, R.-C.: Insight of a fuzzy regression model. *Fuzzy Sets Syst.* **112**(3), 355–369 (2000). [https://doi.org/10.1016/S0165-0114\(97\)00375-8](https://doi.org/10.1016/S0165-0114(97)00375-8)
11. Celmins, A.: Least squares model fitting to fuzzy vector data. *Fuzzy Sets Syst.* **22**, 245–269 (1987). [https://doi.org/10.1016/0165-0114\(87\)90070-4](https://doi.org/10.1016/0165-0114(87)90070-4)
12. Yen, K.K., Ghoshray, S., Roig, G.: A linear regression model using triangular fuzzy number coefficients. *Fuzzy Sets Syst.* **106**, 167–177 (1999). [https://doi.org/10.1016/S0165-0114\(97\)00269-8](https://doi.org/10.1016/S0165-0114(97)00269-8)
13. Soliman, S.A., Rahman, M.H.A., El-Hawary, M.E.: Application of fuzzy linear regression algorithm to power system voltage measurements. *Electr. Power Syst. Res.* **42**, 195–200 (2000). [https://doi.org/10.1016/S0378-7796\(96\)01205-9](https://doi.org/10.1016/S0378-7796(96)01205-9)
14. Seraya, O.V., Demin, D.A.: Linear regression analysis of a small sample of fuzzy input data. *J. Automat. Inf. Sci.* **44**(7), 34–48 (2012). <https://doi.org/10.1615/jautomatinfscien.v44.i7.40>
15. Raskin, L.G., Seraya, O.V.: *Fuzzy Mathematics*. Parus, Kharkov (2008)
16. Buckley, J.J., Feuring, T.: Linear and non-linear fuzzy regression: Evolutionary algorithm solutions. *Fuzzy Sets Syst.* **112**(3), 381–394 (2000). [https://doi.org/10.1016/S0165-0114\(98\)00154-7](https://doi.org/10.1016/S0165-0114(98)00154-7)
17. Tymchuk, S., Katyukha, I.: Development of regression coefficient selection quality criterion in power consumption forecasting problems. *East. Eur. J. Enterpr. Technol.* **5**/8(71), 16–20 (2014)



# Production Planning and Setup Time Optimization: An Industrial Case Study

José Pedro Vaz , Leonilde Varela , Bruno Gonçalves ,  
and José Machado 

University of Minho, Campus de Azurém, 4804–533 Guimarães, Portugal  
jmachado@dem.uminho.pt

**Abstract.** Production activity control approaches, methods, and mechanisms have been widely applied over the last decades, and continue to be of utmost importance nowadays, within the context of the currently fast-growing Industry 4.0 era. In this paper, a Simio-based simulation model is proposed and its application in a printing factory is illustrated. The main aim of this work consists of providing general production planning improvements in the considered factory, with a special focus on the reduction of setup time. The proposed model is based on several distinct production activity control mechanisms, for instance, the CONWIP and the Routing Group mechanisms from Simio, which did enable to reach good improvements regarding a set of performance measures considered, including machines' setup time reduction, along with the maximization of the percentage of products delivered on time. Future work is also planned to be carried out to improve other kinds of performance measures, and by using other types of production activity control mechanisms, to be further applied in other industrial companies and sectors.

**Keywords:** Production planning and control · Optimization · Simulation · Scheduling · Setup

## 1 Introduction

Production planning and control (PPC) plays a crucial role in Companies [1], and one of its utmost concerns falls within optimization problems [2, 3].

An efficient PPC system enables information to be obtained and also efficiently manages material flows, the efficient use of people and equipment, coordination between the organization's internal activities with those of its suppliers, and also communication with its customers, according to market needs [1, 4, 5].

In short, a PPC system provides managers with support for decision making and operations management.

In this paper, a simulation model for production planning and setup optimization is presented, and its application to a printing company is further illustrated through a case study.

The application of the proposed simulation model in the printing company intends to enable a critical analysis to validate a new productive method for the company.

To obtain a viable solution for the company, different Production Activity Control (PAC) methods were used to test which one could bring more income to the company. Two working days were considered and simulated. Also, their modes of production (according to the production control mechanisms) were changed to obtain results. According to the analysis of the results obtained, the CONWIP mechanism enabled to reach a higher performance compared to the Routing Group and Real Cases approaches in the company. Within the CONWIP mechanism, the “Largest Value First” showed superiority over the “Short Value First” and “First In First Out” dispatching rules, by enabling to obtain more products, with the same high-quality standards in a shorter period. According to the results obtained, the application of this new procedure in the Company can help to increase and improve production, as it aims to reduce costs in a given planned time horizon and without using any additional competitive advantages, for instance, regarding quality requisites.

This paper is organized as follows. Section 2 presents some general insights about production activity control, to briefly describe the main PAC approaches and mechanisms used in this work. Section 3 describes the industrial case study approached, and the proposed Simio-based simulation model developed. Section 4 refers to the analysis of the main results obtained. Finally, in Sect. 5, the main conclusions are outlined, along with some future work directions.

## 2 Literature Review

Production Activity Control focuses on several distinct management functions, and one of its main and also more studied ones is production scheduling [6]. Moreover, it is also generally noticeable that PAC, for instance, its production scheduling function shows a tendency, over the last decades, to be approached as a combinatorial problem to be solved by using exact and heuristic mathematical techniques [1, 2, 4, 6]. Although, and also with an increasing tendency, PAC, and more specifically production scheduling, are being studied through alternative approaches, including a variety of approximation algorithms and techniques [3, 7], the simulation technique [8–10] is gaining considerable visibility and affirmation, and experiencing a particular increase in the current Industry 4.0 context.

### 2.1 Production Activity Control Approaches and Mechanisms

A wide range of PAC approaches and mechanisms exists, based on quite different production paradigms and aiming at different objectives, through the evaluation of a varying set of performance measures. Some of the very well-known PAC mechanisms are the following:

#### **Toyota Kanban System (TKS)**

The Toyota Kanban System (TKS) is a PAC mechanism based on pull production and aiming to eliminate waste [11]. TKS’s premise is that the material will not be produced or moved until there is something or someone able to notify that need. For this reason, a Kanban system is used. A Kanban system is a subsystem of TKS and enables to control

the waiting levels in a production system. When a queue reaches its default maximum level, there is a need to launch an order to stop the production.

### **CONstant Work-In-Process (CONWIP)**

The CONWIP control system was introduced in 1990 as an attempt to introduce a more flexible pull system than TKS [12]. In a pull system, production is based on actual demand. Therefore, production just occurs if there is a request for a product by the end customer - make-to-order production. This pull variant is known for its ease of implementation.

CONWIP can be applied in diverse production environments and, as a rule, is based on a card system that is linked to a particular job, being used so that no job can enter the system without the associated production authorization card [13].

## **3 Research Methodology**

The basis of any scientific and engineering approach is modelling. Operational research models consist, according to [14], in a mathematical formulation that seeks to portray the real situation as well as possible, either in order to make better decisions or even just to better understand it [14, 15]. The same approach is addressed by simulation models, which were used in this work to represent the real contexts into computational software in order to generate different real scenarios to make better decisions. The simulation technique is also capable of modelling the real context uncertainty which provides a high degree of confidence when making a decision.

Like any model, a simulation model implicitly incorporates decision variables, parameters, and constraints. The objective function may or may not be modelled in the main model. This allows a much higher level of flexibility when analysing the system behaviour.

By crossing simulation and mathematical models, it is possible to obtain the optimal solution (mathematical models) and then test it with simulation to anticipate the behaviour of the system. As simulation models are capable of modelling system uncertainty (and usually the mathematical models cannot), the iterative application of both models usually leads to a confident feasible solution.

This chapter describes analyses and test changes to the production system of the company's printing section. These changes focus on the application of several rules for production activity control. The main objectives are to minimize the total production time and reduce delayed deliveries.

Therefore, a SIMIO software-based model [16] was developed (Fig. 1) to trustworthily represent the printing section of the company. Several production activity control mechanisms were implemented in order to test different scenarios and identify a more efficient method for the company.

This model was developed in simulation software, namely, SIMIO™. Figure 2 illustrates the model that represents the printing section. This model represents the conceptual modelling of the printing section. Each workstation (KBA\_1, KBA\_2, KBA\_3, KBA\_4) represents a different printing machine.

In this model, the entities that flow in the simulation model are the production orders. These orders were imported directly from an Excel file, which contains all relevant information. A total of 64 product families were considered for this model. When a production order arrives at the workstation, 2 tasks are performed: the preparation (setup time, if needed) and the processing time. In this sense, all the setup and processing times were defined for all product families.

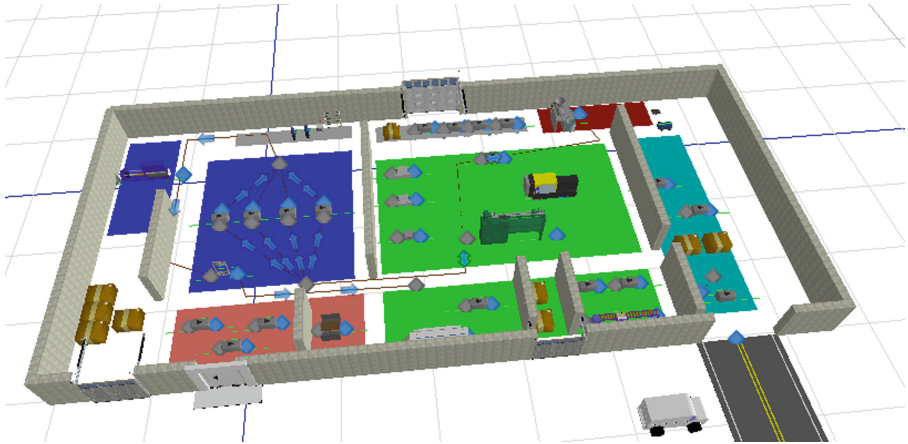


Fig. 1. Company layout representation (In SIMIO™).

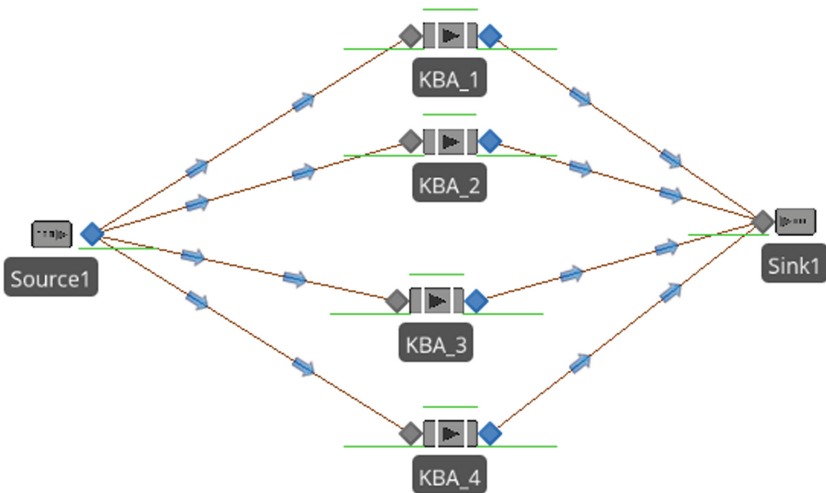


Fig. 2. Norprint production environment modelled on SIMIO™ software.

To add additional and needed modelling logic to the SIMIO simulation model, several processes were created in order to compute the key performance indicators needed to assess system behaviour (for example, total production time, and a number of products delivered on time).

The implemented production control mechanisms were defined for different control stages of the production run. At the scheduling stage, two approaches were modelled, the FIFO and CONWIP approaches. At the sequencing stage, 4 methods were implemented: FIFO (the first order arriving at the workstation is the first order processed), the highest value of processing time (in Simio modelling the LVF – largest value first – is used to model this behaviour), the smallest value of production time (in Simio modelling the LVF – largest value first – is used to model this behaviour), and the Routing Group (a proprietary mechanism from Simio to allocate entities to workstations).

Along with the 4 printing machines production layout, a secondary layout was developed to test a context in which the printing section of the company would have 3 printing machines (instead of 4). This scenario aims to assess the feasibility of the 3 machines production layout, as during the project the possibility of selling one of the printing machines was revealed.

For all the alternative scenarios tested, the key performance indicators assessed were the time in the system and the percentage of product deliveries made on time.

## 4 Results

After analysing and validating the simulation model, two different scenarios were simulated. All tests were simulated applying 100 replications for each run, which confers statistical meaning to the results, guaranteeing a confidence interval level greater than 95%. The scenarios represent real case studies that the printing section had to tackle in two different days, such as:

- Real Case 1 – April 3 and 4, 2018;
- Real Case 2 – May 24 and 25, 2018.

### 4.1 Real Case 1

All the relevant information about the production process regarding the real case 1 is presented in Table 1.

The printing section deals with these orders and achieved a percentage of products delivered on time of around 35%. A simulation model representing the production control mechanisms of the real case scenario was used to validate the model. After running the simulation model, the results obtained were a percentage of 38,8% of products delivered on time and a total production time of 18,5 h. These values corroborate the simulation model's validity.

Thus, the next steps involve the implementation of different production control mechanisms to seek better solutions for the printing section.

**Table 1.** Real case 1 data (time in hours).

Order	Order ID	Family	Release date	Setup time	Production time	Total time	Family class
Obras Pioneiras	1	Part20	0	0,87	6,41	7,27	4
Everlux	2	Part38	0	0,28	7,41	7,70	6
Miguel D'atte	3	Part35	0	0,83	7,59	8,43	3
A Nona Vítima	4	Part1	0	0,25	6,70	6,95	1
O Livro das Decisões	5	Part17	0	0,25	6,41	6,66	1
Catálogo Galvão	6	Part56	0	0,87	7,29	8,15	8
Golden Generation	7	Part48	0	0,87	23,76	24,62	8
Belmiro dos Santos	8	Part23	0	0,83	6,48	7,31	7
Sinalux	9	Part54	0	0,28	6,95	7,24	6
Conselhos para ler	10	Part52	0	0,28	7,76	8,04	6

### Routing Group

The Routing Group method considers the state of the queue of a workstation and also its remaining production capacity to allocate orders to workstations. This means that for the real case studies, by applying the Routing Group mechanism, each time a product is available to start production, the model compares all queues and remaining production capacity of all workstations and allocate product production to the workstation with more availability. This mechanism was implemented for the 4 printing machines layout and the 3 printing machines layout. For each scenario, the ranking rule for the products (meaning, the rule to define priority to start processing) was defined by the production time of each product and by the FIFO rule, which means 3 different scenarios for each layout applying the routing group mechanism. The results of the simulation are presented in Table 2.

As expected, in terms of total time in production, the scenarios with 4 printing machines' performance were better than in the scenarios with 3 printing machines. However, in terms of the percentage of products delivered on time, not all scenarios with 4 printing machines perform better than the scenarios with 3 printing machines. The scenario with 3 machines and the highest production time performs better than the scenario with 4 machines and the smallest production time regarding the percentage of products delivered on time. The scenario that performs better is the one with 4 machines and the highest production time with a percentage of products delivered on time of 56%. It means that giving priority to orders with high production times will lead to better production performance. Globally, every scenario performed better (or at least the same) than the real printing section production in real case 1.



**Table 2.** Results of the Routing Group mechanism for real case 1.

Scenario		Results	
Layout	Ranking rule	Total time in production	% of on-time deliveries
4 machines	FIFO	17.31	48.8
4 machines	Highest production time	17.24	56.0
4 machines	Smallest production time	17.31	44.8
3 machines	FIFO	22.27	35.9
3 machines	Highest production time	23.05	45.5
3 machines	Smallest production time	18.13	35.9

**CONWIP**

In this section, the same scenarios are simulated by changing the production control mechanism to CONWIP. The results of the simulation are presented in Table 3.

By applying the CONWIP mechanism it is possible to observe that the differences between scenarios of 3 and 4 machines are not as noticeable as with the application of the routing group method. There is a scenario with 4 machines that performed worse than all the scenarios with 3 machines. Regarding the percentage of products delivered on time, all the scenarios with 4 machines performed better than the scenarios with 3 machines. Again, the scenario with better performance is the one with 4 printing machines and with the ranking rule as the highest production time. This scenario achieves 56, 02% in terms of the percentage of products delivered on time.

**Table 3.** Results of the CONWIP mechanism for real case 1.

Scenario		Results	
Layout	Ranking rule	Total time in production	% of on-time deliveries
4 machines	FIFO	17.18	44.8
4 machines	Highest production time	17.17	56.0
4 machines	Smallest production time	21.33	42.2
3 machines	FIFO	18.30	35.9
3 machines	Highest production time	17.47	38.7
3 machines	Smallest production time	18.05	35.9

Comparing both mechanisms (routing group and CONWIP), it is not possible to unequivocally highlight the best mechanism. It is possible to verify a slightly better performance of the CONWIP mechanism in terms of reducing the total time in production, and it is possible to verify a slightly better performance of the routing group mechanism in terms of the percentage of products delivered on time.

## 4.2 Real Case 2

This case study is important to prove the robustness of the simulation model, as the typology of orders is different from the ones simulated in real case 1. All the relevant information about the production process regarding the real case 1 is presented in Table 4. The real results that the printing section obtained on the 24th and 25th of May, regarding the percentage of products delivered on time, was around 35%.

Next, the same control mechanisms are applied to seek a better performance for the printing section.

**Table 4.** Real case data 2 (time in hours).

Order	Order ID	Family	Setup time	Production time	Total time	Family class
Galeria Militar	1	Part40	0,87	7,75	8,61	8
Banda Desenhada	2	Part29	0,25	22,46	22,71	5
LaForcade	3	Part23	0,83	6,48	7,31	7
Fotogaleria Estação Coimbra	4	Part48	0,87	23,76	24,62	8
Atelier Digital	5	Part5	0,25	6,76	7,01	5
Na Massa do Sangue	6	Part17	0,25	6,41	6,66	1
A Garrafa Mágica	7	Part1	0,25	6,70	6,95	1
Material Escolar	8	Part29	0,25	22,46	22,71	5
Cerâmica	9	Part24	0,87	6,48	7,35	8
Jerusalém	10	Part34	0,28	7,32	7,60	2
Primeiro Tratado Pedagógico	11	Part33	0,25	7,30	7,55	1
O Ano da Morte de Ricardo Reis	12	Part9	0,25	22,71	22,96	1
Paula Rego	13	Part9	0,25	22,71	22,96	1

## Routing Group

The same type of scenarios was simulated with the routing group control mechanism. The results obtained are presented in Table 5.

**Table 5.** Results of the Routing Group mechanism for real case 2.

Scenario		Results	
Layout	Ranking rule	Total time in production	% of on-time deliveries
4 machines	FIFO	27.89	39.0
4 machines	Highest production time	29.30	46.8
4 machines	Smallest production time	27.89	39.0
3 machines	FIFO	32.11	37.9
3 machines	Highest production time	37.22	58.1
3 machines	Smallest production time	29.30	32.5

As expected, generally, the scenarios with 4 printing machines perform better in terms of total time in production. In terms of the percentage of products delivered on time, the scenarios with 3 machines perform worse except for the scenario with 3 machines and the highest production time, which is the best scenario of all, with 58.1% of products delivered on time. Again, globally, regarding the percentage of products delivered on time, all scenarios performed better than the printing section real production except for the scenario with 3 machines and the smallest production time with 32.5% (worse than the 35% of the real case).

**CONWIP**

In this section, the same scenarios are simulated by changing the production control mechanism to CONWIP. The results of the simulation are presented in Table 6.

By applying the CONWIP mechanism it is possible to observe that, generally, in terms of total time in production, the scenarios with 4 machines perform better than the scenarios with 3 machines. Moreover, comparing to the routing group mechanism, the CONWIP mechanism performed better in all scenarios considering the total time in production. Regarding the percentage of products delivered on time, all scenarios with 3 and 4 machines performed worse with CONWIP than the respective scenarios with the routing group, except for the scenario with 4 machines and the highest production time that performs better and is the best scenario of all. This scenario achieves 68, 03% in terms of the percentage of products delivered on time, which represents almost the double amount of products delivered on time.

**Table 6.** Results of the CONWIP mechanism for real case 2.

Scenario		Results	
Layout	Ranking rule	Total time in production	% of on-time deliveries
4 machines	FIFO	24.67	37.6
4 machines	Highest production time	27.57	68.0
4 machines	Smallest production time	23.46	33.4
3 machines	FIFO	29.01	35.9
3 machines	Highest production time	35.02	45.8
3 machines	Smallest production time	27.50	29.5

Comparing both mechanisms (routing group and CONWIP), no mechanism stands out in terms of global performance. Nevertheless, the mechanism that presents more consistency in delivering the best scenario is the CONWIP. In both real case studies, the CONWIP mechanism presented the best scenario (in real case 1 tied with the routing group). Additionally, considering the clients’ point of view, the most important indicator is the percentage of products delivered on time, which corroborates the selection of the CONWIP mechanism (merged with the highest production time ranking rule) as the best mechanism for the production control of the printing section.

## 5 Conclusion

Throughout the development of this project, it was possible to realize that the proposed simulation model for supporting production activity control at a printing company showed improvements compared to those used at the company. Therefore, the use of the proposed simulation model enables us to reach general benefits, not just in terms of improved production efficiency, but also and consequently, through an increased level of customer satisfaction. Through this project, it was possible to achieve better production performance, for instance, regarding total setup time reduction.

Two different real case studies were simulated in a total of 24 generated and analysed scenarios. All scenarios ran 100 replications, which confer statistical significance to the results (over 95% confidence). The routing group mechanism (property of Simio) and the CONWIP mechanism were simulated for both real case studies and, although no mechanism has stood out in terms of global performance, the CONWIP mechanism demonstrated more consistency in delivering better results. The best scenario, considering the percentage of products delivered on time (the most important performance indicator from the clients' point of view) was achieved by the application of the CONWIP mechanism with the highest production time as a ranking rule, achieving a percentage of 68.0%.

In the prospects, it is suggested to apply the developed Simio-based simulation model to other industrial environments and sectors, along with the implementation of sensitivity analysis of the model, in order to further test the effect of variations of any of the production activity control mechanisms and underlying variables used. Additionally, and to make the model increasingly reliable, it would be interesting to introduce two more variants of the model, by integrating: a production failure/interruption factor of the machines; add work orders with urgent priority; and also, consider the percentage of utilization of the machines in the workspace.

**Acknowledgment.** This work has been supported by FCT – Fundação para a Ciência e Tecnologia within the Project Scope: UID/CEC/00319/2019.

## References

1. Brucker, P.: Scheduling algorithms. *J. Oper. Res. Soc.* **50**, 774 (1999)
2. Varela, M., Ribeiro, R.: Evaluation of simulated annealing to solve fuzzy optimization problems. *J. Int. Fuzzy Syst.* **14**(2), 59–71 (2003)
3. Reddy, M., Ratnam, C., Agrawal, R., Varela, M., Sharma, I., Manupati, V.: Investigation of reconfiguration effect on makespan with social network method for flexible job shop scheduling problem. *Comput. Ind. Eng.* **110**, 231–241 (2017)
4. Pinedo, M.: Scheduling, vol. 29. Springer, New York (2012)
5. Gallagher, J.: *Information Systems: A Manager's Guide to Harnessing Technology*. University of Minnesota Libraries Publishing, Minneapolis (2015)
6. Browne, J.: Production activity control - a key aspect of production control. *Int. J. Prod. Res.* **26**(3), 415–427 (1988)
7. Williamson, D., Shmoys, D.: *The Design of Approximation Algorithms*. Cambridge University Press, Cambridge (2011)

8. Mason, S., Hill, R., Mönch, L., Rose, O., Carlo, M.: Proceedings of the 2008 Winter Simulation Conference (2008)
9. Kelton, W.: Simulation with ARENA. McGraw-hill, New York (2002)
10. Kelton, W., Smith, J., Sturrock, D., Verbraeck, A.: Simio & Simulation: Modeling, Analysis, Applications. Learning Solutions, Chennai (2011)
11. Sugimori, Y., Kusunoki, K., Cho, F., Uchikawa, S.: Toyota production system and kanban system materialization of just-in-time and respect-for-human system. *Int. J. Prod. Res.* **15**(6), 553–564 (1977)
12. Spearman, M., Woodruff, D., Hopp, W.: CONWIP: a pull alternative to kanban. *Int. J. Prod. Res.* **28**(5), 879–894 (1990)
13. Framinan, J., Gonzalez, P., Ruiz-Usano, R.: The CONWIP production control system: review and research issues. *Prod. Planning Control* **14**(3), 255–265 (2003)
14. Winston, W., Jeffrey, B.: Operations Research: Applications and Algorithms. Thomson/Brooks/Cole, California (2004)
15. Varela, M., Trojanowska, J., Carmo-Silva, S., Costa, N., Machado, J.: Comparative simulation study of production scheduling in the hybrid and the parallel flow. *Manage. Prod. Eng. Rev.* **8**(2), 69–80 (2017)
16. Simio, LLC: About Simio | Simio (2018). <https://www.simio.com/about-simio/>

# **Technological Assurance**



# Concept Development of a Consistently Traceable Process and System Solution for Ensuring the Requirements of Engineering and Functional Safety

Dominik Ehring<sup>(✉)</sup> , Robin Pluhnau , and Arun Nagarajah

University Duisburg-Essen, IPE-PEP, 1, Lotharstr., 47057 Duisburg, Germany  
dominik.ehring@uni-due.de

**Abstract.** In times of digital transformation and the growing degree of automation and connectivity of machines, the product complexity increases. Due to the growing risk of misapplication, the early and consistent consideration of Functional Safety is becoming increasingly important with a growing share of electrical-electronical functions. How does the consideration of the reduction of dangers and risks in concept development could be improved by requirements engineering? The aim of this paper is not the expansion of theoretical understanding, instead, it focuses on important aspects of industrial implementation. Unlike theory, Functional Safety is not an integral part of the Requirements Engineering methodology in the evaluated company of the agricultural engineering sector. There are two separate approaches so that continuous traceability in the process is very difficult to ensure. If changes in requirements occur during the development process, which affects safety-relevant functions, the effects on Functional Safety may be ignored. This fact isn't limited to the evaluated agricultural company, instead of this, it represents a cross-company and cross-industry problem. The project objective is the development of a concept for the integration of Functional Safety in the methodology of Requirements Engineering. To examine the research question if Model-Based Systems Engineering is a suitable approach for combining Requirements Engineering and Functional Safety, the RFLP structure is built on the example of a tire pressure control system. As a result, determined requirements, such as “bidirectional traceability”, “cross-disciplinary, function-oriented approach”, “possibility of linking requirements and architectures”, “reusability” and “possibility of clustering” are validated.

**Keywords:** Model-Based Systems Engineering · Bidirectional traceability · RFLP

## 1 Introduction

Faulty systems lead to increased safety risk and present potential hazards for humans and machines. One result of the digital transformation and the associated growing degree of automation and connectivity of machines are increasing product requirements, especially concerning the guarantee of Functional Safety (Löw et al. 2010).

© The Editor(s) (if applicable) and The Author(s), under exclusive license to Springer Nature Switzerland AG 2020

V. Ivanov et al. (Eds.): DSMIE 2020, LNME, pp. 233–242, 2020.

[https://doi.org/10.1007/978-3-030-50794-7\\_23](https://doi.org/10.1007/978-3-030-50794-7_23)

Unlike theory, Requirements Engineering (RE) and Functional Safety are often two separate approaches in entrepreneurial practice (Mhenni et al. 2014). In this context, the frequently used keywords, such as “consistency”, “completeness”, “clustering”, “reusability” and “traceability” are only empty phrases, if for example changes in requirements do not reveal any effects on safety or security.

The described problem is not limited to the analysis of agricultural machinery manufactures but represents a cross-industry phenomenon. Generally, the activities of Functional Safety are characterized by manual, time and labor-intensive steps. Mhenni et al. (2014) show the common problems of Functional Safety in product development. In general, the activities of Functional Safety are characterized by the use of incompatible tools, informal documents and often time decoupled implementation to the design. As a result, early consideration of Functional Safety is nearly impossible, because fundamental design decisions have already been made (Mhenni et al. 2014). Mhenni et al. (2014) also mention the problem of inconsistency between the system model and the results of the safety analysis. The reason for this is the parallel development of the architecture, while a transferred development status is checked by the Functional Safety steering team. There is no automatic safety-related update to the architecture changes (Mhenni et al. 2014).

The importance of Functional Safety grows with increasing product complexity in the context of a higher electrical-electronical (E/E) function percentage in machines. This means that, in addition to the number of functions, their dependencies, the requirements for certifications increase, as well as control over the entire system through autonomous system decisions (Burton/Habermann 2012).

In principle, Functional Safety must be guaranteed across different disciplines (E/E, mechanics, hydraulics, Software). As a result, a safety requirement can be implemented, for example, both by a mechanical component and by a software function (Hoogenboom/Graser 2019). In the context of product development, Model-Based Systems Engineering (MBSE) is currently one of the most popular and most discussed approaches in theory and practice (Madni/Purohit 2019). Therefore, this research examines to what extent MBSE can meet the analyzed requirements. In other words, it will be determined if the potential weaknesses that become apparent during a process analysis can be eliminated by applying the MBSE approach.

The use of an MBSE approach in the product development of a manufacturer of agricultural machinery could seem strange if the prejudices of a strongly mechanized industry predominate in people’s minds. However, agricultural engineering often plays a pioneering role in vehicle and aerospace industries (Hartl 2017). Today’s agricultural machinery is characterized by a high degree of automation, a double-digit number of control units and complex interaction of systems. The terms “smart farming” and “precision farming” characterize the current development in the field of agricultural machinery technology (Hartl 2017). In the era of digitalization and changing challenges, Functional Safety must also be guaranteed across machine allocations in the sense of connected systems.



## 2 Literature Review

### 2.1 Requirements Engineering and Functional Safety

Requirements Engineering is the “disciplined, systematic procedure for the determination, documentation, analysis, testing, coordination, and administration of requirements under customer-oriented, technical and economic targets. The aim of RE is to develop qualitatively good - not perfect - requirements and to manage them in risk and quality-oriented manner during implementation. Systematic RE makes the difference between a successful product and a collection of irrelevant functions” (Ebert 2019, p. 33). It can be perceived as a link between customers, operations, sales, marketing, product management, project management and research and development (Ebert 2019; Herrmann et al. 2013). The need for a systematic requirements engineering approach in order to control costs and quality both now and in the future can be deduced from the increasing number of object code commands in software systems. For example, automotive software included around 250.000 object code commands in the 1990s and this number increased to over one billion object code commands in 2018 (Ebert 2019).

### 2.2 Functional Safety

“Functional Safety is given when each specific safety function is executed and the degree of fulfillment required for each safety function is achieved” (Ebert 2019, p.91). Functional Safety is both legally required by the product liability act and described by normative specifications (Martinus 2004).

Standards can be differentiated between “process” and “functionality” requirements. For example, they require analysis and tests (Hazard and Risk Analysis (HARA), Fault Tree Analysis (FTA), Failure Mode and Effects Analysis (FMEA)) as well as the guarantee of quality concerning traceability, repeatability, and intentionality. It is not uncommon for Functional Safety to be perceived as an extended workload in the company due to additional requirements for development and its documentation obligation, especially from a certain safety rating (Agricultural Performance Level (AgPL)). This means that the higher the safety function must be safeguarded in order to achieve the appropriately evaluated performance level, the more complex is its testing and documentation. The reasons for this are the effects on system design (architecture) and potential redundancy (Schlosser/Gerstl 2019). Theoretically, Functional Safety is an integral part of RE and is a part of the analysis and test step. Safety requirements can only be determined in the context of a system and can be refined in reliability requirements at the component level. Traceability of safety requirements is problematic in business practice between different levels and designs. Changes and their effects are to be traced in documents. Functional Safety is to be assigned to the quality requirements, whereby they extend the functional requirements (Ebert 2019).

### 2.3 Model-Based Systems Engineering

Model-Based Systems Engineering is the interdisciplinary description of a system based on a model. According to a uniform notation, the model is comprehensible across all business units, so that there is less room for interpretation for an erroneous development. The system model contains both the system requirements and system architecture and behavior. The classical systems engineering, which allows a model-based, but domain-specific development, is extended in the MBSE by the possibility of interdisciplinary system development. This means that the subject-specific models, such as E/E, software, mechanics and hydraulic architecture, are not substituted but extended by a so-called meta-model. This meta-model is only fed by higher-level parameters that are classified as relevant for all disciplines. The function-oriented approach MBSE allows the overall concept of the system to be developed and overlooked across disciplines so that it can be checked for conformity, among other things. This makes dependencies and interfaces of the individual domains visible. MBSE aims to represent the mode of action and behavior of the mechatronic system, but the system model can also be used for other purposes such as requirements management. In the context of increasing product complexity and global networking, this approach enables document-centric development to be replaced by model-based development, while promoting higher-level exchange within the project. MBSE can master complexity, promote interdisciplinary communication and optimize problem understanding (TwoPillars 2018; Muggeo/Pfenning 2015; Kleiner/Husung 2016).

## 3 Research Methodology

The methodological approach to gain knowledge is divided into six main activities (cf. Fig. 1). The literature research on the topics of “Requirements Engineering” and “Functional Safety” is started in order to build up a theoretical grasp in these scientific disciplines. It follows the current state analysis of RE and Functional Safety in the evaluated company, whereby the respective processes, methods, and tools are evaluated. Based on the analysis of internal manuals, training documents and templates a comprehensive process graphic of Functional Safety is developed. The self-created Visio-graphic serves as a discussion basis for the expert interviews. In the third step, possible differences between theory and practice are revealed by comparing the findings from the analysis with the literary state of the art. By presenting the interim results to a steering committee, an awareness of the problem and a need for action is created. Requirements are collected for a target process for the integration of Functional Safety into the methodology of RE by conducting workshops with three different product companies. The workshops are prepared in a target-oriented way so that, after a brief visualization of the current process and presentation of possible theoretical approaches to solutions, the participants are brought up to a level of knowledge and provided with sources of inspiration for potential process changes. In the course of this, investigation techniques such as “brainstorming” and “writing user stories” are used to identify process and system weaknesses and to describe requirements for a target process. In the fifth step, an RFLP structure is created on a Product Lifecycle Management

(PLM) platform using a tire pressure control system as an example. In the sixth and last step of this research, an approach from the literature is applied to the problem. MBSE is used to integrate Functional Safety into the methodology of RE and to meet the requirements of the workshops. In addition to the elaboration of requirements are served by MBSE, it is also emphasized which requirements cannot be fulfilled.

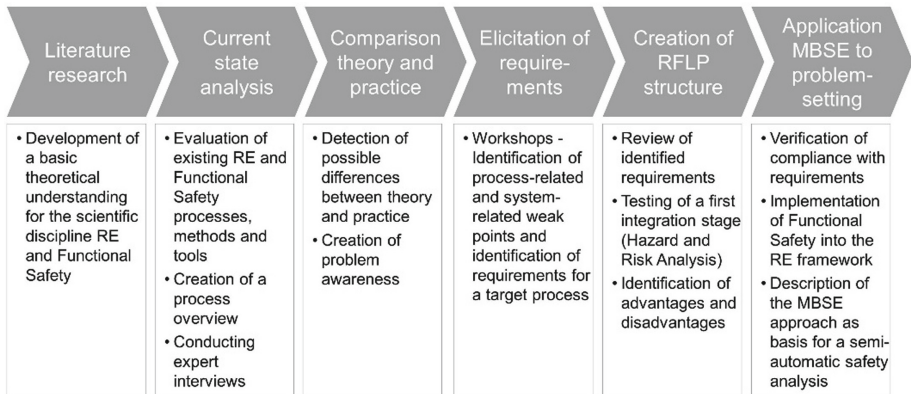


Fig. 1. Methodology.

## 4 Results

Theoretically, Functional Safety is an integral part of RE. At the evaluated enterprise, RE and Functional Safety are currently two separate approaches without integration (cf. Fig. 2). On the one hand, there is the RE framework with an associated layer concept and the 6-step cycle, which is supported by a RE-tool. On the other hand, there is the “construct” of Functional Safety with the process- and system-related weak points and an opaque toolchain. There is a lack of consistent process traceability between the RE and Functional Safety approach. In addition, the methodologies are documented completely separately.

The analysis leads to an identification of manifold problems. Sometimes there is a temporal decoupling in the development of a function, i.e. only the function is developed, without consideration of safety-relevant issues. In the current process, there is further no guarantee for the completeness of the documentation in the event of a change. The reason for this is the manual maintenance of Excel and Word files in a document-centered workflow manner. Moreover, the company has not a uniform communication and document filing. There is no bidirectional traceability. This means that it is not possible to see what effects requirement changes have or where a requirement originates. This point is of great importance in the context of normative and legal requirements as well as product quality. Furthermore, no linking of (safety-) requirements and architecture artifacts are possible. Neither the release documentation is supported, nor is there systematic reuse of already existing artifacts.

The identified weak points of the evaluated agricultural company, coincide with the problems described in the literature, such as an overload of manual, document-centric transfer work, an unmanageable tool-chain with incompatibilities, (isolated) temporal decoupling of Functional Safety and design decisions, inconsistent document storage and an isolated, domain-specific approach to technical architectures (Mhenni et al. 2014). Furthermore, problems arise from differences between the product companies concerning different working methods (agile, classical), role definitions as well as the selection and number of methods of safety analysis.

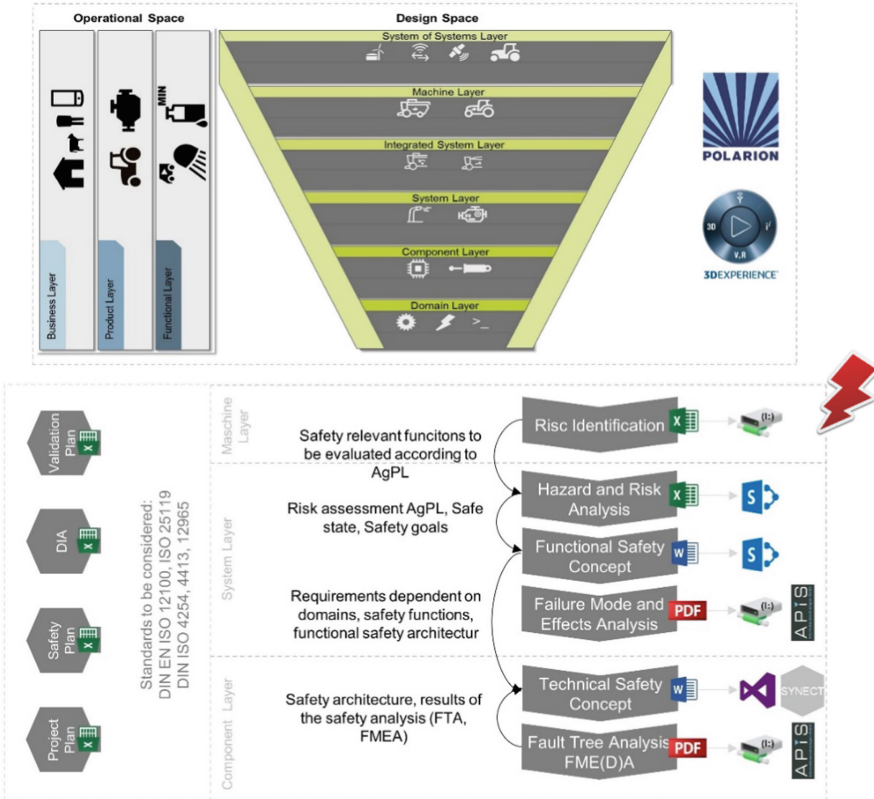


Fig. 2. Need for Functional Safety to be integrated into RE methodology.

Figure 3 shows the integration of Functional Safety into the methodology of Requirements Engineering by applying the MBSE approach from the literature. The existing V-model of the agricultural company retains the layer concept and the 6-step cycle, whereby the individual sub-processes of the Functional Safety “risk identification”, “hazard and risk analysis”, “creation of the functional safety concept” and “creation of the technical safety concept” are integrated into the methodology by the safety analysis (FTA/FMEA). Model-Based Systems Engineering provides the link

between RE and Functional Safety by offering a cross-disciplinary approach, continuous traceability and the possibility of linking requirements and architectures. This enables the effects on safety to be seen when requirements are changed, even with increasing product complexity.

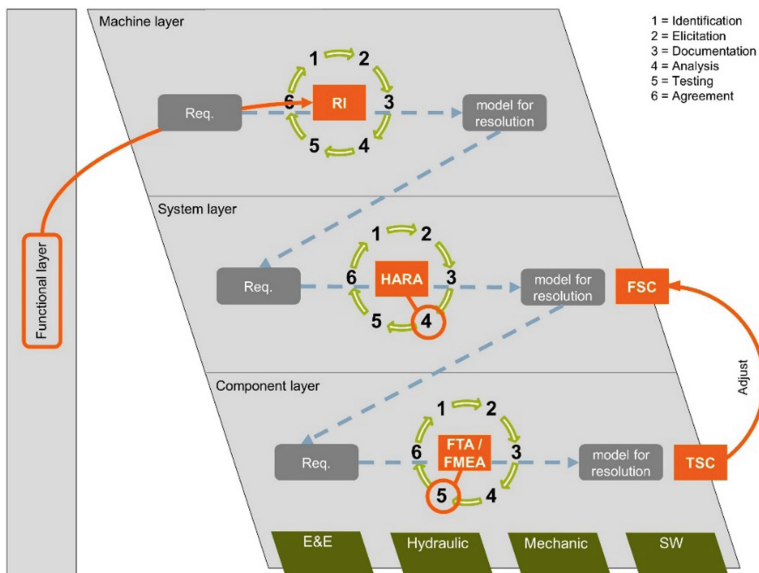
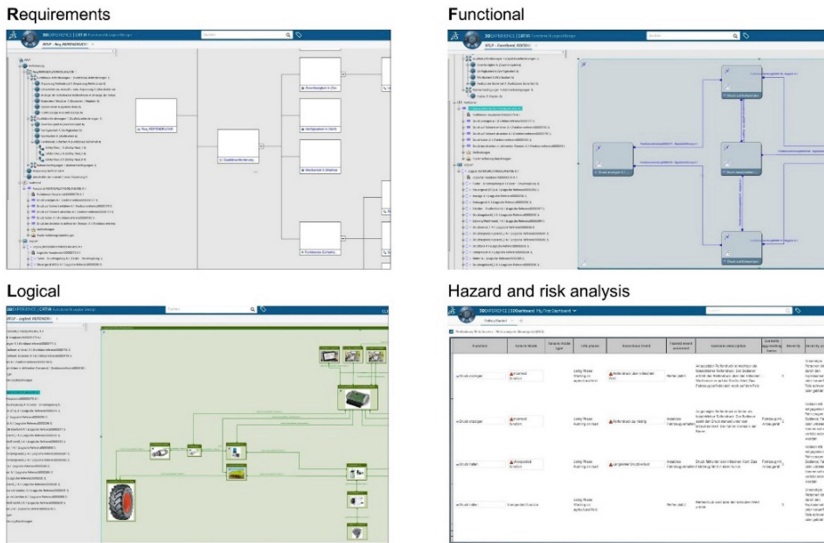


Fig. 3. Integration of Functional Safety into the RE&M framework by using MBSE.

Figure 3 shows a simplified framework, at which point of the Requirements Engineering and Management (RE&M), the Functional Safety must be considered. At the machine level, the risk identification is performed with the help of the solution-neutral functional description of the “Functional Layer”. The safety-relevant functions to be evaluated according to AgPL are analyzed in the HARA at the system level, in the context of the 6-step cycle in “step 4” of the analysis. The results of the HARA represent the safety goals with the corresponding classification according to AgPL and safe states. The safety functions are derived from the safety goals. On their basis, a rough safety architecture is designed. This extends the functional concept by the components which are to guarantee the system safety.

The functional (safety) concept serves as input for the requirements at the component level. After the technically detailed domain-specific architectures have been modeled, the components of the safety-critical path are determined with the aid of the functional safety concept and the safety analysis is carried out with the aid of the technical architectures. In accordance with the 6-step cycle of the RE, it is verified in the “step 5 - testing” using FTA and/or FME(D)A whether the safety objectives are met. If not, measures are defined and must be adapted both in the technical safety concept and in the functional safety concept. This requires a new safety analysis in

order to check the effect of the measure. If all safety objectives are achieved, the overall function can be developed with the technical safety concept and the cross-disciplinary system model for improved communication and understanding (cf. Fig. 3).



**Fig. 4.** RFLP (e.g. tire pressure control system).

For the evaluation of the Model-Based Systems Engineering approach, as a possibility of merging RE and Functional Safety, the structure of an RFLP structure is build. For this purpose, an example of a tire pressure control system is modelled with related “requirements”. Additionally, a functional structure is defined and a cross-disciplinary system model is created on the logical level.

The requirements are divided into functional requirements, such as “switching between manual and automatic adjustment of the tire pressure”, quality requirements and boundary conditions. Further, the quality requirements are divided into “reliability”, “maintainability”, “functional safety” and “information safety”. The logical structure in Fig. 4 shows the system model, where the domain-specific components of the tire pressure control system, such as the “control unit”, the “compressor” and “pressure sensor” are connected to each other. This makes the overall concept including interfaces and information flows visible. Both the higher-level models and the requirements are linked with individual elements. The physical level of the RFLP structure is not considered in this research. Instead of this, a hazard and risk analysis are evaluated in the PLM platform. In order to test the first implementation of a customized HARA template, a data model must be available. The tire pressure control system is used here. The linked functions of the “logical reference” can be loaded into the HARA template. The benefit of platform-integrated HARA lies not only in its simpler handling but above all in its consistent traceability. In this way, the determined safety goals can be linked to associated functional requirements and/or predefined functions. If the

function changes, its effect on safety is immediately apparent. In addition to the automatic calculation of the AgPL, the HARA template also makes use of reusability. Thus, once generated hazard events or scenarios, error modes and other artifacts can be used without redundant work.

The modeling and analysis of the RFLP structure show that it is possible to integrate Functional Safety into the RE methodology via the MBSE approach. Here it can be stated that only a fully integrated platform solution with consideration of all Functional Safety sub-processes (RI, HARA, FSC, TSC, safety analysis) makes sense in order to ensure consistency. Independently of RE and Functional Safety, the MBSE approach must be applied company-wide and taken into account in development activities, since RFLP data cannot be generated and maintained for the safety discipline alone. As essential requirements, the analysis states “bidirectional traceability”, “reusability”, “clustering and assignment of requirements and functions”, “possibility of linking requirements and architectural elements”, as well as “discipline-overlapping, function-oriented approach”. MBSE covers those essential requirements. Beyond this, Munk et al. (2019) and Mhenni et al. (2014) explain that the MBSE approach offers the potential to increase efficiency by being the basis for a (semi-)automatic safety analysis.

## 5 Conclusion

The original question, whether Model-Based Systems Engineering is a suitable approach for the fulfillment of the determined requirements for the integration of the Functional Safety into the methodology of the RE, can be affirmed. The extended validation of MBSE as a possible solution was based on the creation of an RFLP structure using the example of a tire pressure control system. Functional Safety as an integral component of RE means in detail a method extension of the existing RE&M framework of the evaluated agricultural company.

It should be noted that the introduction of MBSE could meet with resistance from corporate policy, as a company-wide changeover would require considerable time and cost. However, the evolution of product development shows that innovations are always accompanied by initial skepticism and uncertainty. However, in order to remain competitive in the long term in times of digital transformation, the effort required to integrate Functional Safety into the RE methodology associated with the introduction of the MBSE approach is worthwhile.

## References

- Burton, S., Habermann, A.: Automotive systems engineering und functional safety: the way forward. ERTS2012(11) (2012). <https://businessdocbox.com/Logistics/80201397-Automotive-systems-engineering-und-functional-safety-the-way-forward.html>. Accessed 08 May 2019
- Ebert, C.: Systematisches Requirements Engineering: Anforderungen ermitteln, dokumentieren, analysieren und verwalten, 6th edn. dpunkt.verlag GmbH, Heidelberg (2019)
- Hartl, U.: Branchenanalyse Landtechnik – Entwicklungstrends und Herausforderungen. In: Forschungsförderung Working Paper, vol. 52, pp. 2509 – 2359. Hans Böckle Stiftung, Düsseldorf (2017)





- Herrmann, A., Knauss, E., Fahney, R., Gartung, T., Glunde, J., Hoffmann, A., Valentini, U.: Requirements Engineering und Projektmanagement. In: Weißbach, R., Herrmann, A., Knauss, E., (eds.) Springer, Heidelberg (2013)
- Hoogenboom, P., Graser, F.: Zertifizierung: Ein Ansatz für ein modernes funktionales Sicherheitskonzept. In: *embedded-software.engineer – Fachwissen für Professionals* (2019). <https://www.embedded-software-engineering.de/zertifizierung-ein-ansatz-fuer-ein-modernes-funktionales-sicherheitskonzept-a-582582/>. Accessed 02 May 2019
- Kleiner, S., Husung, S.: Model Based Systems Engineering: Prinzipien, Anwendung, Beispiele, Erfahrung und Nutzen aus Praxissicht. In: Schulze, S.-O., Tschirmer, C., Kaffenberger, R., Ackva, S. (eds.) *Tag des Systems Engineering 2016*, pp. 13–22. Carl Hanser Verlag, München (2016)
- Löw, P., Pabst, R., Petry, E.: Funktionale Sicherheit in der Praxis, 1st edn. dpunkt.verlag GmbH, Heidelberg (2010)
- Madni, A.M., Purohit, S.: Economic analysis of model-based systems engineering. *Systems* **7**(1), 12 (2019)
- Martinus, M.: Funktionale Sicherheit von mechatronischen Systemen bei mobilen Arbeitsmaschinen (Doctoral dissertation), Technische Universität München (2004)
- Mhenni, F., Nguyen, N., Choley, J.Y.: Automatic fault tree generation from SysML system models. In: *IEEE/ASME International Conference on Advanced Intelligent Mechatronics 2014*, pp. 715–720. IEEE, New York (2014)
- Muggeo, C., Pfening, M.: Die Rolle von MBSE und PLM im Industrial Internet. In: Schulze, S.-O., Muggeo, C. (eds.) *Tag des Systems Engineering 2015*, pp. 279–287. Carl Hanser Verlag, München (2016)
- Munk, P., Nordmann, A., Thaden, E., Amarnath, R., Schweizer, M., Burton, S., Gerstl, S.: Wie Sicherheit von Modellbasierter Entwicklung profitiert. In: *embedded-software.engineer – Fachwissen für Software-Professionals* (2019). <https://www.embedded-software-engineering.de/wie-sicherheit-von-modell-basierter-entwicklung-profitiert-a-816522/>. Accessed 12 Apr 2019
- Rupp, C.: Requirements-Engineering und -Management: Aus der Praxis von klassisch bis agil, 6th edn. Carl Hanser Verlag, München (2014)
- Schlosser, J., Gerstl, S.: Functional Safety Software Engineering: Problemfälle Prozess & Qualität. In: *embedded-software.engineer – Fachwissen für Professionals* (2019). <https://www.embedded-software-engineering.de/problemfaelle-prozess-qualitaet-a-807220/>. Accessed 04 Apr 2019
- TwoPillars: Systems Engineering – What is MBSE? (2019). <https://www.two-pillars.de/what-is-mbse/>. Accessed 22 Jul 2019





# Improvement of the Quality of Cutting Tools States Recognition Using Cloud Technologies

Oleksandr Fomin <sup>(✉)</sup>  and Oleksandr Derevianchenko 

Odessa National Polytechnic University, 1, Shevchenko Ave., Odessa 65044,  
Ukraine  
fomin@opu.ua

**Abstract.** The work considers improving the quality of constructing large-scale diagnostic models in technical diagnostics systems by developing a software architecture for high-performance computing in the form of a web service using cloud-based machine learning technologies. The obtained results are brought to practical realization in the form of tools of the automated system of technical diagnostics of cutting tools with the diagnostic parameters of large dimensions. A method has been developed for building information models of cutting tool states based on indirect measurements using test pulse effects on a cutting system in the form of loads with impacts and recording system responses, based on which information models are built in the form of multidimensional transition functions. The methods of forming test pulse loads of the cutting system by successive insertion of the cutting tool into the workpiece with different cutting depths, with variable feed, and with variable cutting duration are considered. The computational experiment demonstrates the advantages of information models in the form of multidimensional transition functions for modeling nonlinear dynamic systems in problems of diagnosing the states of cutting tools. It has been established that multiclass cutting tools state recognition can be used as an effective technology of automated technical diagnostics systems.

**Keywords:** Tool laboratory · States recognition · Cloud ML

## 1 Introduction

Applied technical diagnostics (TD) problems for complex objects are becoming widespread, especially with a strong interest on the part of smart manufacturing and industry 4.0. Often, such objects are described by large-scale models, the causes of which are the object's complexity and the lack of study of the processes occurring in them, as well as increasing objects speed, the presence of many disturbing influences and environmental interferences.

Simultaneously, taking into account the maximum number of characteristics of diagnosis objects (DO), automated systems of TD (ASTD) provide the high accuracy of diagnosis, but a large amount of diagnostic information reduces the speed of setting up ASTD.

Building a reliable diagnostic model is one of the most difficult problems. There are two ways to reduce diagnostic models [1]. The first is to construct a diagnostic space

based on orthogonal transformations to weaken the statistical relationships between model parameters and to increase the diagnostic value of these parameters [2]. These methods require a large amount of prior data, therefore, they are oriented towards the operation of ODs in certain modes of operation. Expanding the scope of application, operating in a wide range of external conditions leads to an increase in the prior uncertainty of object data, and therefore, to reduce the accuracy of diagnosis. Another way is the selection of diagnostic features using combinatorial analysis for information optimization of diagnostic models by the criterion of maximum accuracy of diagnosis at the learning stage. The main disadvantage of this approach is the need for large computing power when solving large-scale problems.

With the development of cloud technologies, the disadvantages of breeding diagnostic features have become less significant [3]. The advent of cloud managed services [4] makes the direction of diagnostic feature selection an effective tool in the construction of ASTD. These provisions determine the relevance of the development of diagnostic models of large objects in TD systems based on the selection of diagnostic features, using cloud-based machine learning (ML Cloud) technology, which provides high reliability and prompt diagnosis of objects.

**Research Purpose.** The purpose of this research is to create techniques for improving the quality of cutting tools states recognition in TD systems of smart manufacturing and industry 4.0 by developing a software architecture for high-performance computing using ML Cloud.

## 2 Literature Review

Metalworking processes in modern manufacturing are characterized by a continuous increase of cutting processes intensity. This leads to an intensification of the processes of cutting tools (CT) working surfaces wear.

Manufactures of the “Industry 4.0” level are sold on FMM (flexible manufacturing modules) with limited participation of operators. Most of the functions of monitoring, diagnosing and predicting the CT resource are transferred to the corresponding automatic intelligent systems, as an operator is not able to make decisions at the speed that is now required to cutting part (CP) states recognition and prevent sudden or gradual failure of instruments.

The main factors of the CT state’s recognition quality are now the speed and accuracy of assessing the degree of cutting part operability.

Before being recommended for work on the machine tools, CT should be thoroughly studied in the laboratory – with the accumulation of relevant statistics and the formation of automatic classifiers. First of all, this applies to tools made of new materials; data sets on properties and recommended operating modes may appear in the reference literature with a delay. The need for creating a system of operational links between factories (their metalworking shops) and research instrumental laboratories (which are absent in many factories) is obvious. The authors see the solution to this problem in the use of “cloud technologies”. Let us analyze the relevant literature.

In the context of the modern industrial technologies development at the “Industry 4.0” level, “cloud technologies” for data processing are widely used [5–10].

Factory operations have shifted from labor-based to semi-automatic and fully automatic and may even become unmanned in the future [5]. Indicated that factory conditions can be monitored from a distance and the machines can be remotely controlled. The attempt in their study is a step toward cloud-based manufacturing.

The factory shall allow the setup and evaluation of any preferred factory layout. One major challenge is the design of the strategy for communication between the factory modules and the identification of adequate communication technologies [6].

Learning Factories, widely using Internet technologies, have shown to be effective for developing theoretical and practical knowledge in a real production environment [7]. Communication is some of the most recurrent ones associated with a knowledge of the engineering sciences.

Industry 4.0 refers to the importance and the ruling capacity of cloud technologies in various areas [8]. Cloud computing is playing an important role in data collections, and of modern computing technology.

Cloud manufacturing as a new manufacturing paradigm has been attracted to a large amount of research interest [9, 10]. Many papers have been published, that presented the overall research status of cloud manufacturing.

The analysis of publications showed the need to use cloud technologies to ensure the diagnosis of cutting tools in modern FMM. They are complex systems that operate with limited operator involvement. That is why much attention is paid to the creation of modules for diagnosing the states of the main subsystems and machine elements and predicting the probability of their failures. A large number of FMM downtimes are caused by gradual or sudden failures of CT. Therefore, the need to create systems for CT state recognition in machine tools is obvious.

However, this is preceded by lengthy laboratory studies of the features of the wear of the CT, the assessment of the state dynamics of the cutting part, the choice of the optimal geometry of the CP and the optimal cutting conditions.

New instrumental materials are constantly improved and created, data on which are not always available in the reference literature.

Therefore, in the structure of instrumentation in the large factories, a special instrumental laboratory with appropriate test benches was always necessary.

At the same time, under the conditions of Industry 4.0, the possibilities of the modern Internet open up the prospect of creating central tool laboratories that can serve metalworking enterprises of a similar profile (with machines of the same name or similar in type, close ranges of grades of processed materials, types of CT sources, etc.). Extensive databases are formed here with a statistical generalization of test results and data processing.

A similar direction was considered in the above works [5–10] and, in particular, in the author’s publication [11]. The creation of integrated intelligent production requires the creation of intelligent systems for diagnosing the conditions of CT [12]. The following can be quickly transferred to the databases of modern CNC machine tools:

- sets of decision rules for online - diagnosing the state classes of a particular tool,
- data on the need for correction of processing modes “according to state” of CT;

- data on the need for tool presetting,
- data on the forecast of the residual resource and the CT change in a precautionary state;
- other data worked out during laboratory tests.

Machine-tool and laboratory systems for the diagnosis and forecasting of sources have become intelligent.

There is an exchange of data in both directions: factory - central laboratory and laboratory – factory. We turn to the consideration of automated systems for monitoring the CT state. They can be divided into direct [13–15] and indirect [16–21].

The advantage of direct control systems equipped with STV is that they form extensive information on the gradual shape changes of the cutting part of CT and its geometry, on the displacement of the vertex of the RS in the machine coordinate system, etc. To ensure the high quality of production processes in modern metal-cutting machines, the method of direct monitoring of the condition of the cutting tool wearing using vision systems is used [13–15].

Some results of research in machine vision, as a key technology, essential in connecting the manufacturing processes with the digital twin of the manufacturing architecture, are presented in [13]. Designing a system, that uses machine vision in combination with deep learning algorithms. The machine vision method to develop an on-machine turning tool insert condition monitoring system - for tool condition monitoring in the cutting processes of CNC machines, is discussed in [14]. The system can identify fractures, built-up edge, chipping, and flank wear of cutting tools.

The processing of images sequence of wear zones of tools coming from the system of technical vision (STV), requires a very significant expenditure of time and computational resources on preliminary data processing to increase their quality, contours and textures selection of wearing zones [15]. Based on the processed images, information models are formed and classifiers are built.

Known indirect methods of the CT control and diagnostics [16–21] are based on measurements of torque, cutting power, components of cutting forces, acoustic emission, dimensions and roughness of the machined surface of the part, etc.

Systems of direct monitoring of the state of CT sources equipped with STV cannot be used in a closed casing processing zone (especially with the active use of lubricating and cooling media). The exception is systems that provide an assessment of the CT state in a special control position of the tool magazine [11].

The specific state of cutting tools CP is recorded by both types of sensors: indirect sensors - during processing, systems with STV - immediately after its interruption. Under the conditions of finishing and precision processing (with small cutting forces, vibrations, levels of the acoustic signal), their accuracy is not high enough. Therefore, it seems appropriate to use combined systems for monitoring the CT states.

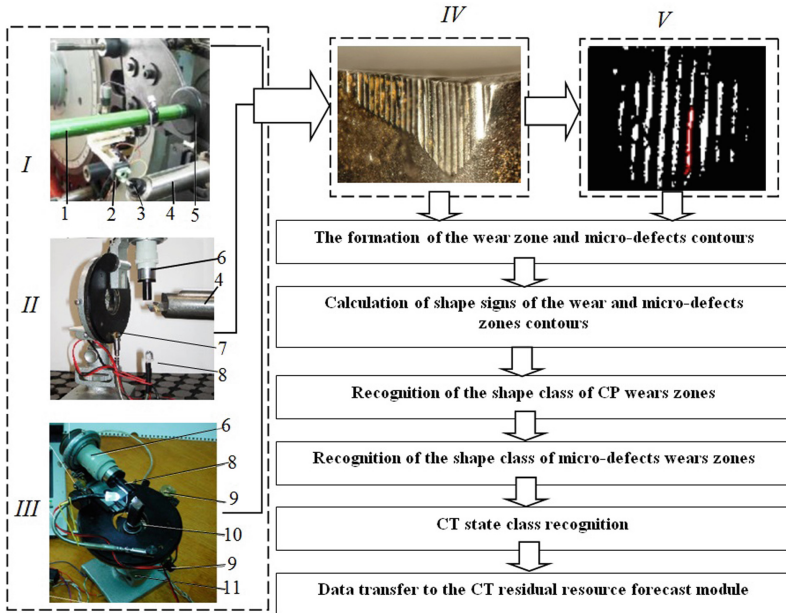


**Fig. 1.** Schematic representation of CT state recognition processes (according to the results of CP laboratory monitoring with the STV use). 1 - stand for mounting the device for moving the digital camera in three directions; 2 - digital camera with a backlight system; 3 - controlled boring tool; 4 - boring bar; 5 - the magnetic base of the rack 1; 6 - digital camera; 7 - remotely controlled camera rotation device; 8 - backlight system; 9 - table rotation mechanism with CT; 10 - CT; 11 - control system housing.

### 3 Research Methodology

The schematic representation of CT state recognition processes (according to the results of CP monitoring with the STV use) in the special instrumental laboratory is shown in Fig. 1.

Micro – defects of CP wear zones include traces of concentrated wear (Fig. 1, positions IV, V), holes along the boundaries of the cut layer, micro cracks, zones of adhesive tearing, and others. They are insignificant under the conditions of roughing and semi-finishing, but they are the causes of CT failures under the conditions of finishing and precision processing. CP's indirect monitoring systems, as a rule, cannot detect them.

Let's move on to the consideration of the corresponding Internet structure using modern cloud technology.

This structure must be able to transmit the results of laboratory research and testing of new tools, recommendations for the modes of their use, decision rules for recognizing their conditions and other - for the factory's machine tools (consumers).

The main stages of the CT state classifiers formation (based on comprehensive studies in the instrumental laboratory (Fig. 1)) are shown in Fig. 2.

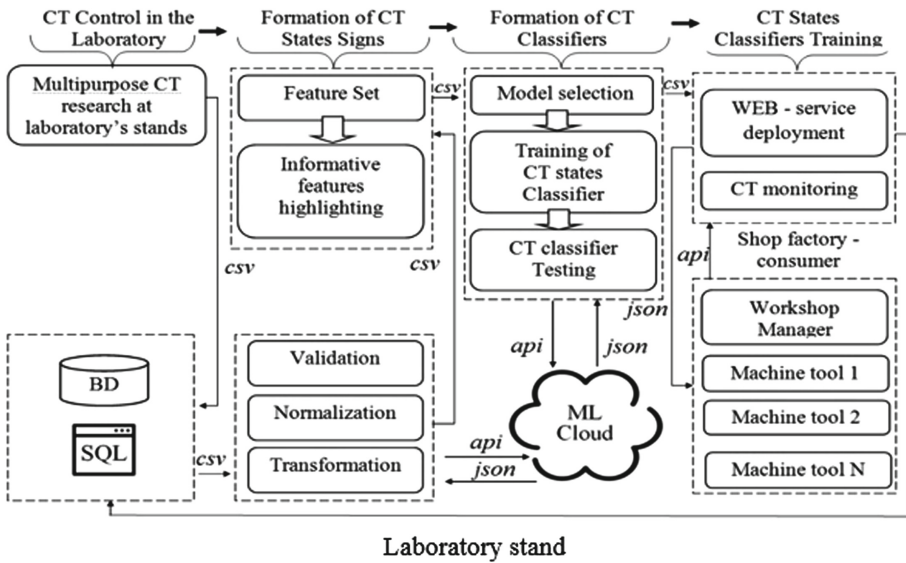


**Fig. 2.** The architecture of decision-making processes for CT states recognizing (and connections of the central instrumental laboratory with the workshops of the consumer plants using the WEB service) with ML Cloud technologies.

Let's clarify the contents of the operations "validation - normalization - data transformation". They analyze the obtained data, check their correction and make the necessary changes, after which informative signs of CP states are extracted.

An enlarged diagram - the structure of service processes by the central instrumental laboratory of many consumers - is shown in Fig. 3.

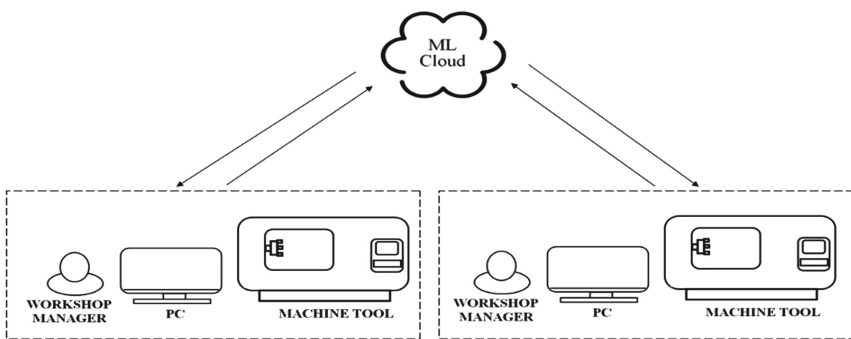


**Fig. 3.** The general structure of the servicing processes of the central instrumental laboratory for many consumers.

The main advantages of using the defined architecture of high-performance computing in the tasks of diagnosis are to increase the reliability and timeliness of diagnosing objects of large size in the absence of powerful hardware resources and mathematical support.

### 4 Results

The application of the developed principles of diagnosis is limited by the lack of effective tools for the functioning of the ASTD. The development of problem-oriented software in the field of control and diagnostics of various cutting tools in modern manufacturing is an urgent problem.

ASTD design tasks based on multidimensional training samples require large time resources and cloud machine learning technologies must be used to accelerate the design process.

Well-known ML Cloud platforms offer similar training and forecasting services. These platforms have similar structural solutions, thus offering a software architecture for high-performance computing using ML Cloud as a basic part of large-scale ASTD objects.

Next, the problem of diagnosing 4 states of a cutting tool in a training sample of 247 measurements of the contours of the cutting tool wear on 8 features is considered:

A fragment of the training sample of 247 measurements on 8 grounds loaded into the Microsoft Azure ML Cloud is presented in Fig. 4.

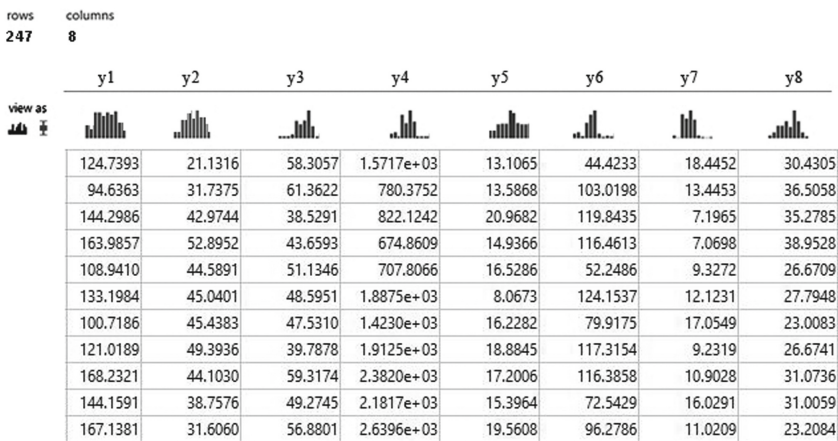


**Fig. 4.** Training sample fragment for multiclass cutting tools states recognition in ML Cloud platform Microsoft Azure.

The common model of multiclass cutting tools states recognition based on ML Cloud platform Microsoft Azure is presented in Fig. 5.

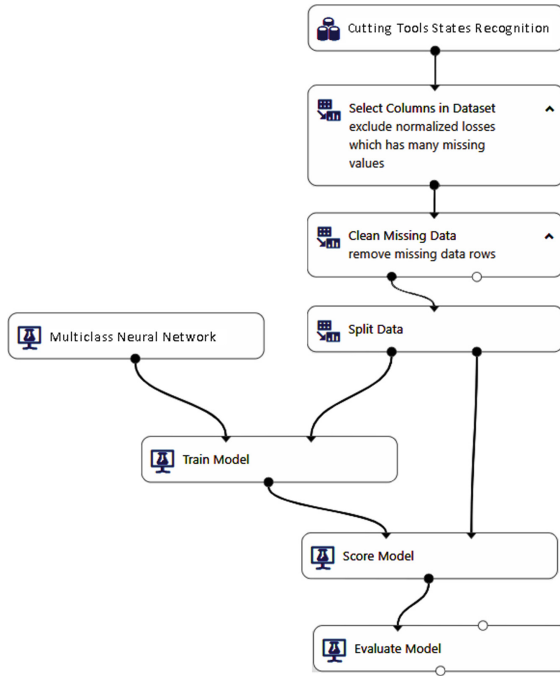


**Fig. 5.** The common model of multiclass cutting tools states recognition based on ML Cloud platform Microsoft Azure.

Results of multiclass cutting tools model machine learning based on ML Cloud platform Microsoft Azure is presented in Fig. 6.

Metrics	
Mean Absolute Error	0.240062
Root Mean Squared Error	0.284372
Relative Absolute Error	0.354608
Relative Squared Error	0.12545
Coefficient of Determination	0.87455

**Fig. 6.** Results of multiclass cutting tools model machine learning based on ML Cloud platform Microsoft Azure.

```

    {"datetime": "2019-10-15-11:08:52",
      "title": "UNIVERSAL MILLING GRADE",
      "partnumber": "ACU2500",
      "tool": {
        "y1": "113", "y2": "31",
        "y3": "39", "y4": "951",
        "y5": "14", "y6": "79",
        "y7": "13", "y8": "23"}
  }
  
```

**Fig. 7.** A message example with the parameters of the diagnosed tool sent to the webservice is given below.

```

    {"datetime": "2019-10-15-11:08:53",
      "title": "UNIVERSAL MILLING GRADE",
      "partnumber": "ACU2500",
      "tool": {
        "class": "3",
        "probability": "0.89382"}
  }
  
```

**Fig. 8.** An example response message from a web server is given below.



The interaction of the client and the web server in the REST API architecture is required for the HTTP protocol. Additional information (models, parameters, control values) will be transferred in JSON format. A message example with the parameters of the diagnosed tool sent to the webserver is given in Fig. 7. An example response message from a web server is given in Fig. 8.

## 5 Conclusions

The presented results allow creating techniques for improving the quality of cutting tools states recognition in TD systems of smart manufacturing and Industry 4.0 by developing a software architecture for high-performance computing using ML Cloud.

The proposed approach provides indicators of the quality of RI states recognition that are 1.2–3% higher than the results obtained by the authors earlier on the same machine in laboratory conditions (using maximum likelihood methods, stochastic approximation, neural networks, and hybrid methods [12]).

At the same time, the obvious advantage of using “cloud technology” is the possibility of using a central tool laboratory to solve the problems of diagnosing CT states on various machines of many factories.

This provides the following benefits when working with distributed data. There are sets of decision rules building for online - diagnosing the state classes of a particular tool; data on the need for correction of processing modes “according to state” of CT; data on the need for tool adjustment; data on the forecast of the residual resource and the moment of the CT change in a precautionary state; other data, worked out during laboratory tests.

Due to this, significant savings are achieved in the corresponding production resources, and, first of all, time and financial.

A computational experiment confirms the advantages of using cloud technologies for cutting tools states recognition in modern manufacturing.

## References

1. Fomin, O., Ruban, O., Derevyanchenko, O.: An approach to the construction of a nonlinear dynamic model process cutting for diagnosis condition of tools. *Appl. Asp. Inf. Technol.* **2**(2), 115–126 (2019)
2. Fainzilberg, L.S.: *Mathematical methods for assessing the utility of diagnostic features.* «Osvita Ukraine», Kiyv (2010)
3. Fomin, O.O.: Formation of a diagnostic features space on the basis of cross sections of Volterra kernels. *Math. Comput. Modeling. Tech. Sci.* **17**, 141–150 (2018)
4. Kalnauz, D., Speranskiy, V.: Productivity estimation of serverless computing. *Appl. Asp. Inf. Technol.* **1**(2), 20–28 (2019)
5. Chen, T.-C.T.: Cloud intelligence in manufacturing. *J. Intell. Manuf.* **5**(28), 1057–1059 (2017)
6. Mukku, V.D., Lang, S., Reggelin, T.: Integration of LiFi technology in an industry 4.0 learning factory. *Procedia Manuf.* **31**, 232–238 (2019). In: 9th Conference on Learning Factories, pp. 232–238. Braunschweig, Germany (2019)

7. Baena, F., Guarin, A., Mora, J., Sauza, J., Retat, S.: Learning factory: the path to industry 4.0. *Procedia Manuf.* **9**, 73–80 (2017)
8. Malladi, A., Potluri, S.: A study on technologies in cloud-based design and manufacturing. *Int. J. Mech. Prod. Eng. Res. Dev.* **6**(8), 187–192 (2018)
9. Liu, Y., Wang, L., Vincent Wang, X.: Cloud manufacturing: latest advancements and future trends. *Procedia Manuf.* **25**, 62–73 (2018). In: 8th Swedish Production Symposium, pp. 62–73, Waterfront Convention Centre Stockholm, Sweden (2018)
10. Newman, S.T., Nassehi, A., Xu, X.W., Rosso, R.S.U., Wang, L., Yusof, Y., et al.: Strategic advantages of interoperability for global manufacturing using CNC technology. *Robot. Comput. Integr. Manuf.* **24**(6), 699–708 (2008)
11. Derevyanchenko, O.G., Krinitsin, D.A.: *Intelligent System for Diagnosing Failures and Predicting the Life of Cutting Tools*. Astroprint, Odesa (2012). (in Russian)
12. Derevyanchenko, O.G., Pavlenko, V.D., Fomin, O.O., Bovnegra, L.V., Pavlenko, S.V.: *Intelligent System of Cutting Tools States Recognition*. Astroprint, Odesa (2013). (in Russian)
13. Deac, G.C., Deac, C.N., Popa, C.L., Ghinea, M., Cotet, C.E.: Machine vision in manufacturing processes and the digital twin of manufacturing architectures. In: *Annals of DAAAM and Proceedings of the International DAAAM Symposium*, Vienna, Austria, pp. 733–736 (2017)
14. Sun, W.-H., Yeh, S.-S.: Using the machine vision method to develop an on-machine insert condition monitoring system for computer numerical control turning machine tools. *Materials* **11**(10), 2–17 (2018)
15. Rifai, A.P., Fukuda, R., Aoyama, H.: Image based identification of cutting tools in turning-milling machines. *Jpn. Soc. Precis. Eng.* **2**(85), 159–166 (2019)
16. Kumar, P., Chauhan, S.R., Pruncu, C.I., Gupta, M.K., Pimenov, D.Y., Mia, M., Gill, H.S.: Influence of different grades of CBN inserts on cutting force and surface roughness of AISI H13 die tool steel during hard turning operation. *Materials* **1**(12), 177 (2019)
17. Chungchoo, C., Saini, D.: On-line tool wear estimation in CNC turning operations using fuzzy neural network model. *Int. J. Mach. Tools Manuf* **1**(42), 29–40 (2019)
18. Lu, Z., Ma, P., Xiao, J., Wang, M., Tang, X.: On-line monitoring of tool wear conditions in machining processes based on machine tool data. *Zhongguo Jixie Gongcheng China Mech. Eng.* **2**(30), 220–225 (2019)
19. Liang, S.Y., Hecker, R.L., Landers, R.G.: Machining process monitoring and control: the state-of-the-art. *J. Manuf. Sci. Eng. Trans. ASME* **2**(126), 297–310 (2004)
20. Xie, Z., Li, J., Lu, Y.: Feature selection and a method to improve the performance of tool condition monitoring. *Int. J. Adv. Manuf. Technol.* **9–12**(100), 3197–3206 (2019)
21. Zhang, X., Tsang, W.-M., Yamazaki, K., Mori, M.: A study on automatic on-machine inspection system for 3D modeling and measurement of cutting tools. *J. Intell. Manuf.* **1**(24), 71–86 (2013)



# Adaptive Slicing in the Additive Manufacturing Process Using the Statistical Layered Analysis

Yaroslav Garashchenko  and Nina Zubkova 

National Technical University “Kharkiv Polytechnic Institute”,  
2, Kyrpychova St., Kharkiv 61002, Ukraine  
zubkova.nina@gmail.com

**Abstract.** The results of the study on the capabilities of adaptive slicing the original 3D model at layered product shaping are presented. The proposed method of adaptive slicing the 3D model allows increasing the process effectiveness and regulates the accuracy of manufacturing products by setting the building step for each lowering of the working platform of additive technologies installation. The building step is selected, taking into account the density of distribution of angles between the building direction vector and the product surface normals that are in the current layer. The developed algorithm for adaptive slicing the 3D model provides for balanced truncation of the distribution, which further reduces the building time compared to existing slicing strategies with variable steps. Evaluation of the effectiveness of adaptive slicing was carried out based on the comparative analysis of the number of layers and the predicted deviations from the regular surface shape as applied to 3D models of industrial products. Improve the effectiveness of the proposed adaptive slicing with an increase in the geometric complexity of the product is revealed.

**Keywords:** Technological preparation · Variable step · Building time · Accuracy of shaping

## 1 Introduction

One of the main problems in preparing a product for materialization by additive manufacturing is slicing the original 3D model [1]. The solution of this problem quite significantly determines the effectiveness of the use of additive manufacturing. The number of layers affects the product building time. The accuracy of shaping when considering the resulting product in a cutting plane going through the  $O_z$  coordinate axis (the building direction) is mainly determined by the thickness of the layers and the surface orientation [2].

The usual slicing strategy is carried out at the set constant building step, i.e. with the same thickness of all layers. This approach does not take into account the features of product geometry. Therefore it leads to a decrease in the accuracy of the resulting surfaces or manufacturing performance. Adaptive strategies based on the use of a

variable building step are developed to eliminate the drawback mentioned above [3, 4]. A variable building step is determined to take into account a set criterion based on the analysis of the surface of the 3D model in the current layer.

## 2 Literature Review

In [5], a comparative analysis of the known methods of adaptive dissection of 3D-models of products based on building time, volume error, and visual assessment of surface quality was performed.

Improvement of adaptive dissection is carried out by step-by-step correction concerning the surfaces parallel to  $XY$  plane [6], indicating heterogeneous requirements  $R_a$  for product surfaces [7]. In [3], an adaptive strategy is proposed based on tree-type cluster analysis ( $k$ -d Tree) with the determination of deviations from the regular shape and volume error.

The variable building step  $h_i$  with adaptive slicing is determined to take into account the following characteristics: protrusion height or cavity depth formed on the product surface as a result of a step effect [3, 8, 9]; the relative difference in the area of adjacent sections [10]; surface roughness parameter  $R_a$  [11]; the arithmetic mean error of the dissected surface [12], considering as the error, the minimum of the two components of the deviation of the product surfaces from the CAD model – vertical or horizontal; volume error in product [13]; the structure of octree about the distribution of material [14].

In the process of evaluating the characteristics of the resulting surface, its profile is considered in the form of steps [3] or radius sections [15].

There are data on the physical and mechanical properties of products obtained using adaptive slicing the 3D model [16]. On the example of FDM technology, there is an insignificant decrease in the tensile strength of test parts (less than 7%) in comparison with their building according to the strategy with a constant step equal to the minimum allowable value.

The main problem is that in actual works with the adaptive cutting of 3D-models, the building step is selected based on the limit values of the chosen parameter characterizing the manufacturing error or surface quality. This problem can be entirely or partly eliminated by taking into account the nature of the distribution of the chosen parameter values. Regardless of the parameter chosen as a criterion, it will depend on the step and the angle between the building direction vector and the normals of the surfaces  $\varphi_{NZ}$ , that fall into the cutting plane of the layer. Therefore, this problem should be considered based on the density distribution of the angles according to their relative area.

The paper considers a scientific hypothesis that the efficiency of adaptive dissection of a 3D model can be increased by using the statistical analysis of the distribution of angles  $\varphi_{NZ}$  taking into account the relative surface area since this will allow determining the building step scientifically to ensure the set accuracy and reduce building time.

The paper aims at studying the capabilities of adaptive dissection of the initial 3D product model based on the statistical analysis of the distribution of angles between the building direction vector and surface normals  $\varphi_{NZ}$  to ensure the set accuracy of shaping with the minimum building time.

### 3 Research Methodology

Implementation of adaptive slicing the initial triangulated 3D-model of the product was carried out as a part of the technological preparation system for materializing complex products using additive manufacturing developed at the Department of Integrated Engineering Technologies of NTU “Kharkiv Polytechnic Institute”. This system allows evaluating the manufacturability of the design and the effectiveness of solving the problems of technological preparation based on the statistical analysis of the studied features of polygonal, voxel and layered 3D models of the product. To solve the problem mentioned above, a subsystem of statistical layered analysis has been developed. The screen form of the subsystem is shown in Fig. 1.

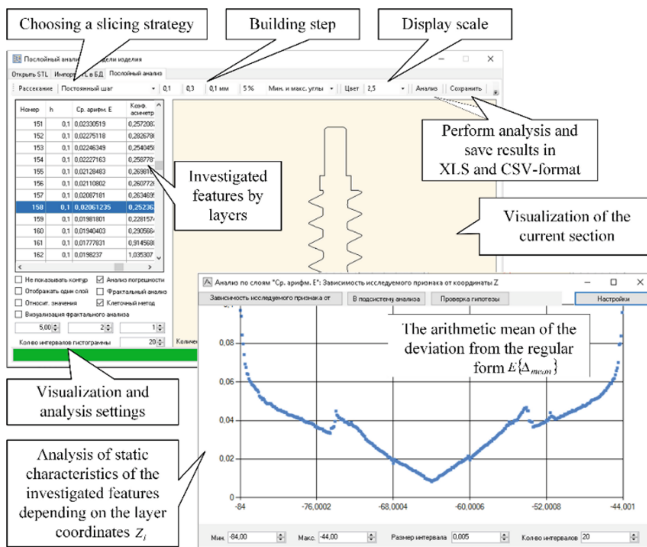


Fig. 1. The subsystem of the layered analysis 3D model of the product.

The transition from the initial triangulation 3D-model of product to the set of layers was carried out according to the procedures developed taking into account the existing works [7] that implement strategies with a constant and variable building step. When performing the dissection procedure at the first stage, a list of coordinates of  $Z_{Ci}$  layers

is created. The second stage includes defining the outlines for each layer. The list of  $Z_{Ci}$  coordinates is formed according to the following dependence

$$Z_{Ci} = Z_{Ci} + h_i, Z_{Ci} \in [Z_{min}, Z_{max}], \quad (1)$$

where  $Z_{min}, Z_{max}$  – the minimum and maximum coordinates of the vertices of the triangulation 3D model;  $h_i$  – building step, for a strategy with a constant step  $h_i = const$ , for an adaptive strategy  $h_i \in [h_{min}, h_{max}]$ ;  $h_{min}, h_{max}$  – minimum and maximum values of the range of building steps allowed by the equipment used and the original material for the resulting product.

As a rule, in the methods of adaptive dissection of a 3D model, the building step  $h_i$  is set taking into account the set limit  $\Delta_{Limit}$  on surface shape deviations (maximum permissible error in shaping) [17]:

$$h_i = \Delta_{Limit} / \cos \varphi_{NZmin}, \quad (2)$$

where  $\varphi_{NZmin}$  – is the minimum angle of an inclination concerning the Z-axis of the normal of the faces that fall into the current layer.

The problem of adaptive slicing of the 3D model of a complex product includes resolving the following issues: the need in taking into account the entire surface of the model, fallen between the planes that determine the current and next layer; uneven angular distribution of surface area  $\varphi_{NZ}$ .

The first problem arises due to the initial uncertainty of the current step  $h_i$ . In the proposed method of adaptive slicing of a 3D model, this problem is solved by initially dissecting the 3D model from the current plane coordinate to the plane determined by the largest allowable value of  $h_{max}$  with the step equal to the discreteness of setting the coordinates of the location of the layer along  $Z_i$  axis.

The second problem is connected with the materialization of 3D models of industrial products with complex geometry. The consequence of both issues is an unreasonable setting of the building step based on incomplete information about the surface, which is formed by the current layer. Because of the existing uneven angle distribution  $\varphi_{NZ}$  of surface area for complex products, the building step set according to the known dependence (2) is understated. In practice, taking into account surfaces with normals having a minimum deviation from Z-axis (building directions) may be excessive if their relative area is less than  $5 \div 20\%$ . This circumstance can be taken into account by relative area truncating the distribution density  $\varphi_{NZ}$  in the current layer by a permissible value. The permissible truncation value must be set from the condition of minimal influence on the resulting quality indicators and product surface accuracy. Such truncation will increase the angle  $\varphi_{NZmin}$  and, therefore, taking into account dependence (2), it will increase the permissible value of the building step  $h_i$ . As a result, it becomes possible to minimize the number of layers and therefore, the building time by increasing  $h_i$  and ensuring in practice the specified limit deviation of the surface shape.

Some examples of angle distributions  $\varphi_{NZ}$  for the surfaces falling into the  $i$ -th layer are shown in Fig. 2. The example given in Fig. 2a refers to unsuitable cases because it does not allow to change the threshold value  $\varphi_{NZmin}$ , necessary for calculating the

current building step  $h_i$  from dependence (2) substantially. An example of angle  $\varphi_{NZ}$  distribution that allows truncation to be performed more efficiently (to change the limit values of the angle  $\varphi_{NZ}$  substantially) is shown in Fig. 2b. This type of distribution is one of the most common among the layers of construction for complex geometry products. For this example (Fig. 3b), when the distribution density  $\varphi_{NZ}$  is area truncated by 5%, it is possible to reduce the range of values  $\Delta\varphi_{NZ}$  by 4 times and choose the angle  $\varphi_{NZmin} \approx 58^\circ$  instead of  $\varphi_{NZmin} \approx 46^\circ$ . In this case, taking into account dependence (2), step  $h_i$  will be chosen equal to 0.19 mm instead of 0.14 mm (at the maximum permissible deviation from the regular surface shape  $\Delta_{Limit} = 0.1$  mm). However, with such a significant increase in the building step for a particular  $i$ -th layer, 5% of the resulting product surface is ignored. Such ignoring does not lead to a noticeable increase in the arithmetic mean of deviations from the regular shape (statistics of deviations for specific 3D models of products is given below).

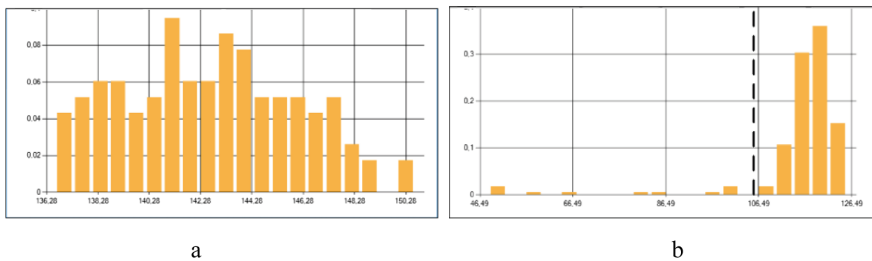


**Fig. 2.** Angle distribution options  $\varphi_{NZ}$  for the surfaces in the layer: a) without the possibility of a significant change in the angle  $\varphi_{NZmin}$ ; b) with the possibility of enough reduction in the range  $\varphi_{NZ}$  when truncating 5% of the area (probability of being outside the confidence range – 0.05).

## 4 Results

The study of the capabilities of the proposed adaptive dissection of the 3D model was carried out by determining the number of layers using test models of simple and complex products shown in Fig. 3.

The dissection of test models was carried out according to strategies with a constant and variable building step to provide comparative analysis.

The strategy with a constant step was carried out at  $h_i = 0.06$  mm. The strategy with a variable step was performed at  $\{h_i\}_{min} = 0.06$  mm,  $\{h_i\}_{max} = 0.20$  mm and acceptable (maximum) surface formation error  $\Delta_{Limit} = 0.06$  and 0.1 mm. The selected range of building steps is recommended for Ultimaker 3D-printers with the simultaneous use of AA 0.4 mm extruder. The proposed adaptive dissection strategy was carried out at 0 ÷ 20% truncation of the distribution of angles  $\varphi_{NZ}$ . The calculation results are given in Table 1.

Comparative analysis of the number of dissection layers for specific 3D-models (Table 1) shows the advantage of variable step strategies over constant step ones. This advantage is common for variable step strategies, regardless of the approach chosen in

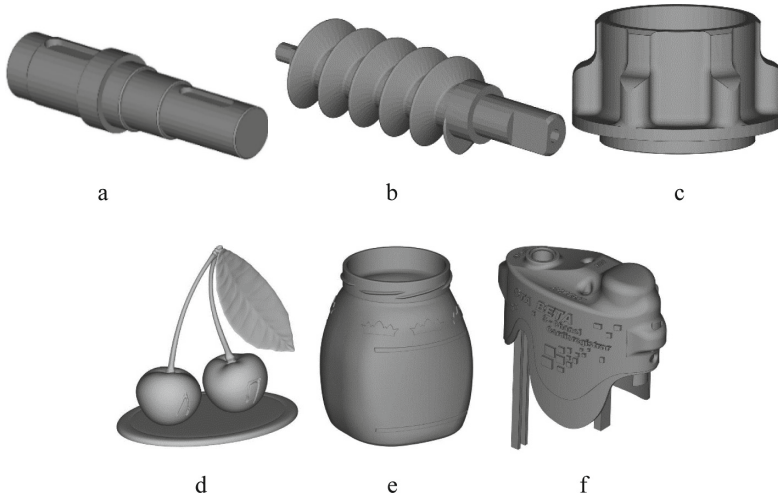


**Fig. 3.** Test 3D models: a) shaft; b) auger; c) case; d) souvenir; e) container; f) lid.

**Table 1.** The results of slicing test models of industrial products by the number of layers.

Model (overall dimensions, mm)	Constant step, $h_i = 0.06$ mm	Variable trimming step $\Delta\phi_{NZ}$ , %				
		0	5	10	15	20
Number of layers, $N_L$						
The permissible deviation from the regular surface shape $\Delta_{L\text{limit}} = 0.06$ mm						
Shaft (60 × 216 × 60)	1000	717	716	715	713	708
Auger (40 × 40 × 144)	667	576	530	456	407	392
Case (210 × 210 × 125)	2084	949	921	898	876	853
Souvenir (73 × 51 × 70)	1169	873	736	695	670	649
Container (102 × 94 × 125)	2092	969	901	874	858	829
Lid (84 × 101 × 43)	721	676	610	592	577	565
The permissible deviation from the regular surface shape $\Delta_{L\text{limit}} = 0.1$ mm						
Shaft (60 × 216 × 60)	1000	456	454	452	450	448
Auger (40 × 40 × 144)	667	338	317	281	257	249
Case (210 × 210 × 125)	2084	729	720	709	703	696
Souvenir (73 × 51 × 70)	1169	525	455	441	434	427
Container (102 × 94 × 125)	2092	734	704	693	688	679
Lid (84 × 101 × 43)	721	406	370	358	351	344

determining the building step. Adaptive slicing performed at  $\Delta\phi_{NZ} = 0\%$  made it possible to reduce the number of layers by 43.7–65.0% concerning the slicing with constant step  $h_i = 0.06$  mm for the considered 3D test models. The truncation of the



distribution density of angles  $\varphi_{NZ}$  made it possible to further reduce the building layer's number for all the considered 3D-models. When truncated by 5% – by 48.7–66.3% (concerning dissection at  $\Delta\varphi_{NZ} = 0\%$  by 0.4–13.3%). When truncated by 10% – by 50.3–66.9% (concerning the slicing of 3D models at  $\Delta\varphi_{NZ} = 0\%$  by 0.9–16.9%). The results of model calculations using 3D models of products differing in the geometric complexity of surfaces revealed a tendency. On the example of the shaft model, there are no significant differences between the options for cross-section with variable step. This difference in the number of  $N_L$  layers increases with the geometric complexity of the products. The data obtained (Table 1) allow us to conclude that the strategy is effective with truncating the distribution of the angle  $\varphi_{NZ}$  for products that are quite complex in geometry. In this study, such 3D-models of the lid, souvenir and screw are presented (in order of increasing efficiency, as shown in Fig. 4).

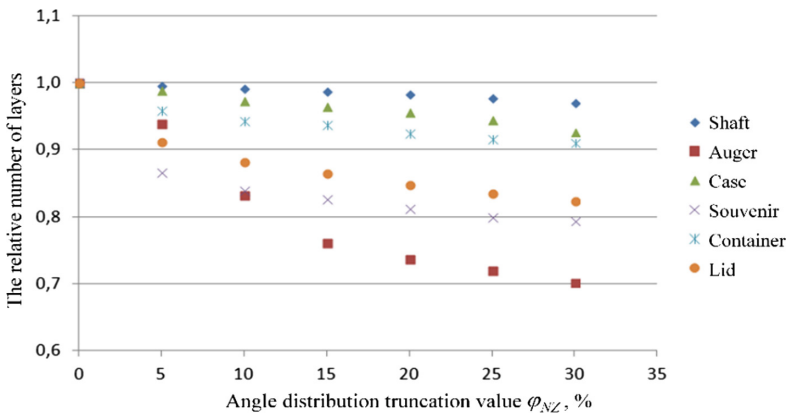


**Fig. 4.** Correlation of the relative number of layers for building test 3D models from the value of truncation of the angle distribution  $\varphi_{NZ}$ .

For methodological reasons, the capabilities of the developed 3D-model dissection strategy were evaluated based on the comparison with the adaptive slicing capabilities offered in Ultimaker Cura (free software) on 3D test models (see Fig. 3).

In the study of adaptive slicing in Ultimaker Cura, various combinations of the following parameters were considered: adaptive layers minimum variation (range of the building steps),  $R_h = 0.14$  mm; adaptive layers variation step size (difference in  $h_i$  for adjacent layers),  $\Delta h_i \in [0.01, 0.10]$  mm; adaptive layers threshold (probability of setting  $h_i$  of a smaller value),  $p_h \in [50, 300]$ .

Table 2 shows the data obtained as a result of dissecting test 3D-models (see Fig. 3) using strategies with constant and variable building steps.

**Table 2.** The results of slicing 3D-models in Ultimaker Cura.

Model (overall dimensions, mm)	Constant step, $h_i = 0.06$ mm		Variable step	
	Number of layers $N_L$	Build time $t_b$ , h	Number of layers $N_L$	Build time $t_b$ , h
Shaft (60 × 216 × 60)	996	47.22	433 ÷ 624	31.1 ÷ 37.1
Auger (40 × 40 × 144)	663	20.23	307 ÷ 472	13.5 ÷ 17.1
Case (210 × 210 × 125)	2080	132.32	694 ÷ 759	58.2 ÷ 62.3
Souvenir (73 × 51 × 70)	1165	12.13	457 ÷ 666	6.7 ÷ 8.1
Container (102 × 94 × 125)	2088	80.77	701 ÷ 823	36.3 ÷ 41.9
Lid (84 × 101 × 43)	717	31.77	399 ÷ 645	21.8 ÷ 29.3

The analysis of the data obtained (Table 2) revealed a certain advantage of the proposed adaptive slicing with truncation  $\varphi_{NZ}$  over that used in Ultimaker Cura as applied to some 3D-models of products that are characterized by complex surface geometry. The adaptive slicing method used in [17] (corresponds to the developed method at  $\Delta\varphi_{NZ} = 0$ ) is inferior in the number of layers for all models. Still, in the case of the lid, the difference is insignificant (less than 2%). As far as the lid model is concerned, it is possible to obtain a smaller number of building layers all over the considered range of values  $\Delta\varphi_{NZ} \in [0, 30]\%$ . The shaft model does not allow to obtain an advantage for the developed adaptive slicing, regardless of the set value  $\Delta\varphi_{NZ}$ . Adaptive slicing at  $\Delta\varphi_{NZ} \geq 5\%$  allows us to get closer in the number of layers and even get lower values for the models of augers, souvenirs, and containers. For the case model, it is possible only at  $\Delta\varphi_{NZ} \geq 20\%$ .

The use of adaptive slicing guarantees the set quality level and accuracy of the obtained product surfaces. Therefore, the layered estimation of deviations from the regular shape  $\Delta_S$  was also performed according to the arithmetic mean value  $\overline{\Delta_S}$ . The protrusion height or the trench depth formed on the surface as a result of the stepwise effect was taken as the predicted deviations from the regular shape [17].

Statistical analysis of the results of the layered calculation of deviations from the regular shape  $\overline{\Delta_S}$  for various variants of slicing some test 3D models using Box Whiskers span diagrams is presented in Fig. 5 (distribution diagrams  $\overline{\Delta_S}$  to compare strategies with a constant building step  $h_i = \{0.06, 0.10, 0.15, 0.20\}$  mm, a variable step at  $\Delta\varphi_{NZ} \in [5, 20]\%$  and the set restriction  $\Delta_{Limit} = 0.1$  mm).

For most 3D-models, slicing with a variable step does not result in significant differences, i.e. the truncation value  $\Delta\varphi_{NZ}$  does not strongly affect the distribution  $\overline{\Delta_S}$ . The resulting distribution  $\overline{\Delta_S}$  for variable step dissections corresponds approximately to the dissection with a constant building step  $h_i \in [0.10, 0.15]$  mm. This can be explained by the set limit value  $\Delta_{Limit} = 0.1$  mm as the most characteristic for  $h_i \in [0.10, 0.15]$  mm.

For 3D-models of a screw, a souvenir and a container the choice of dissection parameters has the most significant influence on the distribution of values  $\overline{\Delta}_S$  that is quite expected since for these models it was possible to reduce most significantly the number of layers and thus reduce the time for their production.

According to the results of the study, the following conditions for the rational use of the proposed adaptive dissection of a 3D-model have been formulated: a product containing a sufficiently large number of surfaces with complex geometry or with a rather broad range of angle distribution between the surface normals and the Z-axis (the building direction); selection of the truncation value  $\Delta\varphi_{NZ} \in [0, 0.2]$  taking into account the allowable increase in local deviation from the regular shape; possibility to reduce distribution truncation value  $\Delta\varphi_{NZ}$  for more complex geometry products.

The developed algorithm of 3D model adaptive slicing is based on the statistical analysis of the distribution of angles between the Z-axis and surface normal  $\varphi_{NZ}$ . The revealed range of rational distribution truncation  $\Delta\varphi_{NZ}$  makes it possible to reduce further building time by  $0.7 \div 30.1\%$  in comparison with the existing strategies of variable dissection [17]. The approach proposed also allows us to evaluate the effectiveness of adaptive slicing with sufficient reliability. It can be assumed based on the increasing efficiency of the proposed adaptive slicing with an increase in the geometric complexity of the product, that its use for a group of products placed on the installation platform will provide a more significant decrease in the building layers number.

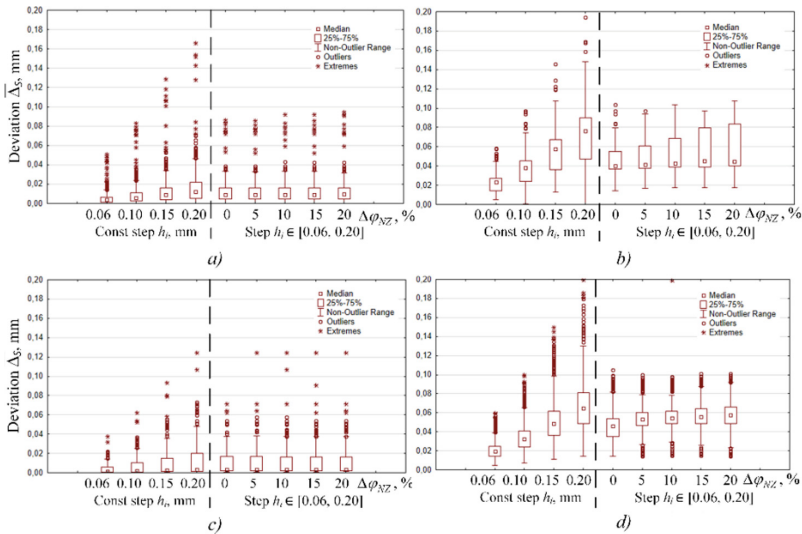


**Fig. 5.** Statistical analysis of the arithmetic mean deviation from the correct shape of the surface  $\Delta_S$ : a) shaft; b) auger; c) case; d) souvenir.

## 5 Conclusions

Statistical analysis of the angles distribution between the Z-axis and the normals of the surfaces, that fall into the section of the layer, which takes into account relative area of the surfaces, makes it possible to scientifically determine the building step to ensure the set accuracy and reduce the product building time using the adaptive slicing 3D model.

An insignificant reduction in the distribution of angles between the Z-axis and surface normals  $\Delta\varphi_{NZ} \in [5, 20]\%$  allows reducing their building time by  $0.7 \div 30.1\%$  for 3D-models of complex products.

The results of the work create the prerequisites for a comprehensive solution to the tasks of technological preparation of additive manufacturing. Further research should be directed to the joint solution of such tasks as rational orientation and placement in the installation working space with the formation of a layered model by adaptive slicing.

## References

1. Zhang, Y., Bernard, A.: AM feature and knowledge based process planning for additive manufacturing in multiple parts production context. In: Proceedings of 25th Annual International Solid Freeform Fabrication Symposium, pp. 1259–1276 (2014)
2. Byun, H.S., Lee, K.H.: Determination of optimal build direction in rapid prototyping with variable slicing. *Int. J. Adv. Manuf. Technol.* **28**, 307–313 (2006)
3. Panhalkar, N., Paul, R., Anand, S.: Increasing part accuracy in additive manufacturing processes using a k-d tree based clustered adaptive layering. *J. Manuf. Sci. Eng.* **136**(6), 061017 (2014)
4. Nadiyapara, H.H., Pande, S.: A review of variable slicing in fused deposition modeling. *J. Inst. Eng. (India) Ser. C* **98**(3), 387–393 (2016)
5. Wang, W., Chao, H., Tong, J., Yang, Z., Tong, X., Li, H., Liu, L.: Saliency-preserving slicing optimization for effective 3D printing. *Comput. Graph. Forum* **34**(6), 148–160 (2015)
6. Sabourin, E., Houser, S.A., Bohn, J.H.: Adaptive slicing using stepwise uniform refinement. *Rapid Prototyp. J.* **2**(4), 20–26 (1996)
7. Cormier, D., Unnanon, K., Sanni, E.: Specifying non-uniform cusp heights as a potential for adaptive slicing. *Rapid Prototyp. J.* **6**(3), 204–211 (2000)
8. Gupta, V., Bajpai, V., Tandon, P.: Slice generation and data retrieval algorithm for rapid manufacturing of heterogeneous objects. *Comput.-Aided Des. Appl.* **11**(3), 255–262 (2013)
9. Mohan Pandey, P., Venkata Reddy, N., Dhande, S.G.: Slicing procedures in layered manufacturing: a review. *Rapid Prototyp. J.* **9**(5), 274–288 (2003)
10. Pan, X.D., Chen, K., Zhang, Z.Y., Chen, D.F., Li, T.T.: Adaptive slicing algorithm based on STL model. *Appl. Mech. Mater.* **288**, 241–245 (2013)
11. Singhal, S.K., Jain, P.K., Pandey, P.M.: Adaptive slicing for SLS prototyping. *Comput.-Aided Des. Appl.* **5**(1), 412–423 (2013)
12. Sikder, S., Barari, A., Kishawy, H.A.: Control of NURBS-based surface error factor using a manufacturing cost optimization in rapid prototyping process. *IFAC Proc. Vol.* **46**(9), 1560–1565 (2013)

13. Taufik, M., Jain, P.K.: Volumetric error control in layered manufacturing. In: The Proceedings of ASME 2014 International Design Engineering Technical Conferences & Computers and Information in Engineering Conference (IDETC/CIE 2014), Buffalo, New York, USA, 17–20 August (2014). V004T06A017 (10 pages)
14. Siraskar, N., Paul, R., Anand, S.: Adaptive slicing in additive manufacturing process using a modified boundary octree data structure. *J. Manuf. Sci. Eng.* **137**(1), 011007 (2014)
15. Boschetto, A., Giordano, V., Veniali, F.: 3D roughness profile model in fused deposition modelling. *Rapid Prototyp. J.* **19**(4), 240–252 (2013)
16. Li, H., Wang, T., Sun, J., Yu, Z.: The adaptive slicing algorithm and its impact on the mechanical property and surface roughness of freeform extrusion parts. *Virtual Phys. Prototyp.* **11**(1), 27–39 (2016)
17. Abdurajimov, L.: Adaptive slicing of product 3D-model in technology of rapid prototyping and manufacturing. *Scientific Notes of the Crimean Engineering and Pedagogical University. Technical Science, SC CEPU, Simferopol*, no. 18, pp. 15–20 (2009). (in Ukrainian)



# Increasing Productivity of Connecting Rods Machining

Vitalii Ivanov<sup>(✉)</sup> , Ivan Dehtiarov , Viliam Zaloga, Illia Kosov,  
and Volodymyr Savchuk

Sumy State University, 2, Rynskogo-Korsakova St., Sumy 40007, Ukraine  
ivanov@tmvi.sumdu.edu.ua

**Abstract.** The paper is dedicated to the increase of the efficiency of multi-product manufacturing. The experience in designing the manufacturing processes of manufacturing machining parts, such as connecting rods, is analyzed. A progressive manufacturing process based on the concept of intensification of machining and application of multiaxis equipment is proposed. This approach made it possible to reduce the complexity of the manufacturing process in drilling, milling, and boring operations. Research has been conducted on the design, optimization, modeling, and production of fixtures for multiproduct manufacturing. The design of a flexible fixture for machining non-detachable connecting rods is provided, which allows adjustment of locating and clamping elements in a certain size range. Studies have shown an increase in machining productivity of the proposed manufacturing process from 1.7 to 3.9 times depends on batch size.

**Keywords:** Complex part · Manufacturing process · Fixture design · Locating · Multiaxis machining · Setup time

## 1 Introduction

The automotive industry is one of the priority domains in the world. The European Union holds one of the leading positions in terms of production and range of car models. Over the past five years, the development of electromobility has been actively underway. Therefore, by 2025, the leading European carmakers plan to abandon internal combustion engines completely. The complexity of automotive units is constantly increasing, along with the requirements for accuracy and quality of products [1].

Although the drive of the cars will be fundamentally new, the chassis and trans-gear elements will remain in most classic cars. Further development of manufacturing engineering in general and automotive engineering, in particular, is possible due to the implementation of innovative projects in the automotive industry. Innovations will increase product competitiveness by reducing the time of entering the market and by reducing unproductive time-consuming. Chassis and transmission components typically have a complex geometric shape consisting of a set of simple surfaces, such as (levers, connecting rods, clutch forks, and brackets). These parts require the highest tooling availability that can be achieved by new fixtures. Also, these fixtures must allow the setup of parts within a certain size range by adjusting the locating-and-clamping elements.

Therefore, it is important to implement flexible fixtures that can be adjusted to another type-size and, in some cases, to machining parts that are slightly different in design. The use of flexible fixtures in comparison to dedicated ones does not require storage for them, as flexible fixtures can replace several dedicated fixtures. Therefore, the design and manufacture of flexible fixtures that reduce the time and cost of machining is an urgent task for modern engineering.

The paper aims to develop an approach that improves the productivity of machining connecting rods in multiproduct manufacturing on CNC machining centers by introducing flexible fixtures.

## 2 Literature Review

In the paper [2], the authors noted the importance of maintaining the specified design tolerances and dimensions in order to avoid the possibility of the appearance of defects by optimizing the technological characteristics of fixtures and proposed a mathematical model for their determination. The paper [3] discusses the application of hybrid systems using industrial robots at the level of adjuster operators in detail. It is emphasized that the environmental aspects must be taken into account when designing manufacturing processes in advanced production. In paper [4], the authors applied the concept and implementation of Petri nets to measure and analyze the performance of flexible manufacturing systems by simulation in VisualSlam software. In paper [5], the authors consider different types of the flexibility of the manufacturing system, classification of manufacturing systems based on a combination of different forms of flexibility is given.

The authors [6] introduced a new method of optimal positioning of the locating and clamping elements of flexible fixtures with inspection and visualization on the example of thin-walled parts. An algorithm for determining the contact points of the workpiece with the functional elements of the fixture is developed [7], the implementation of which is carried out using augmented reality technology on the example of fork-type parts. In the study [8], an efficient algorithm for determining the optimal positioning of locating elements when machining complex parts is presented. In research [9], an optimization model was developed to minimize the time and costs of preparing modular fixtures with a grid of base holes. The use of this model is aimed at determining the optimal position for the placement of locating and clamping elements of fixtures, taking into account all possible movements and rotations of the workpiece in the machining process. In research [10], the authors proposed a general methodology for the design of flexible fixtures, based on which it is possible to compile 14 different fixture layouts in one reconfigurable fixture instead of six different fixtures that were previously used for the same technological tasks. When designing flexible fixtures, many factors must be considered, including production conditions [11, 12], equipment capabilities [13–17], cutting tools characteristics and coatings [18–20], design and technological features of machining parts [21–23], quality assurance [24, 25], power and dynamic characteristics of the machining process [26–29]. The design process of flexible fixtures is comprehensive and time-consuming, so it is advisable to automate the design and calculation procedures [30–32].

The paper [33] is aimed at determining the efficiency of work performance of workers in machine-building enterprises with the determination of the total and specific productivity of each worker, as well as the main factors that affect labor productivity. The paper [34] proposed a methodology for standardization of operations, reduction, and optimization of activities that do not affect the additional cost, and at the same time increase labor productivity in order to reduce the time spent on the example of standardization and optimization of the manufacture of automotive components. Publication [35] is devoted to the analysis of the efficiency of machine-building production based on four basic methodologies, presents the production situation, and its solution in the conditions of traditional and innovative enterprises. In [36], an estimation of production productivity as a function of a monitor to evaluate the quality of a manufacturing process and seven basic tools for finding variations of a manufacturing process is proposed.

### 3 Research Methodology

Connecting rods (Fig. 1) are the elements of crank mechanisms of reciprocating internal combustion pistons and compressors. They serve to transmit force from the piston and convert reciprocating motion into rotational motion of the crankshaft of the engine or, conversely, the rotating movement of the shaft into reciprocating motion. Connecting rods are also used in pumps, steam engines, and other types of drives. Most of the connecting rods have a complex geometric shape, which causes some difficulty in locating and clamping workpieces in machining operations. Complex design and technological improvement allow making the finished product more qualitative (increased resource of work, reduced mass, decreased time of manufacturing, etc.) with less cost, which is needed in the modern market.

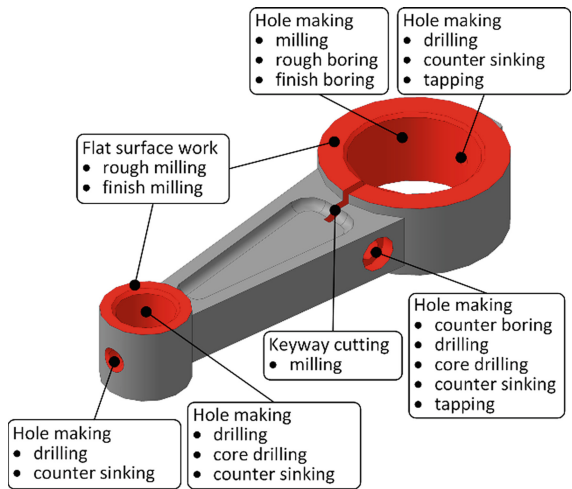
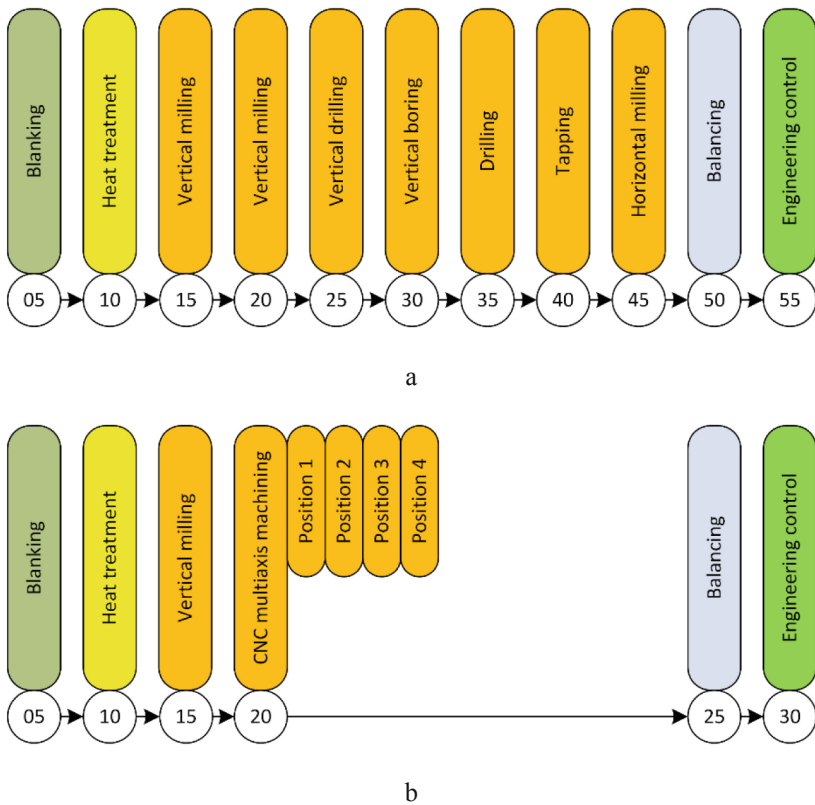


Fig. 1. Typical design and work surfaces of the connecting rod [1]



A typical manufacturing process of machining connecting rods is investigated. It consists of eleven operations; seven of them are drilling-milling-boring manufacturing operations, which require ten setups of the workpiece during machining (Fig. 2a). Extensive technological capabilities of modern CNC machining centers and the tendency to the intensification of the manufacturing processes allow carrying out the multiaxis machining of connecting rods at one setup by combining operations 20–45 of a typical manufacturing process into one – CNC multiaxis machining operation. This approach allows reducing the manufacturing process by five machining operations (Fig. 2b). Thus, the reduction of units of equipment from 5 machine tools to one CNC machining center and the number of fixtures from 5 dedicated fixtures to one flexible fixture are achieved.



**Fig. 2.** Comparison of the manufacturing routes for the machining connecting rods: a – typical manufacturing process; b – proposed manufacturing process [1]

Machining of all surfaces requiring drilling, milling, and boring operations can be carried out in four positions (Fig. 3), having pre-machined one of the planes of the connecting rod on the vertical milling operation (operation 15).

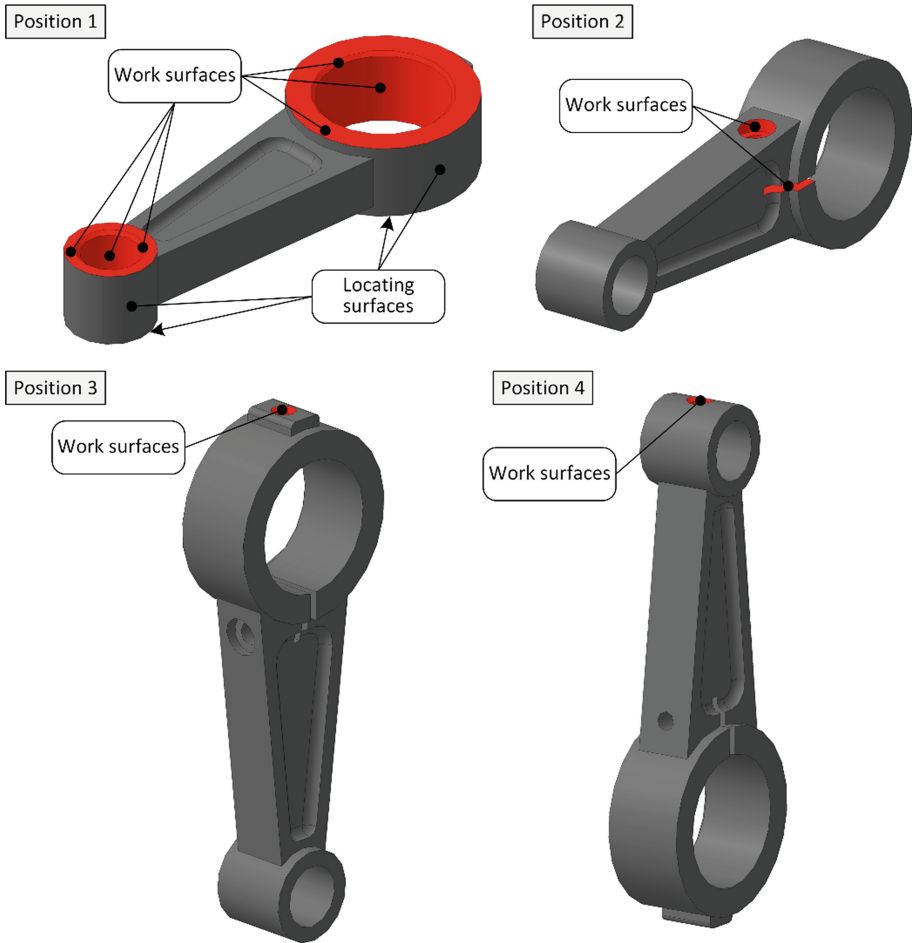


**Fig. 3.** Cut-map for machining connecting rods on the CNC multi-axis machining operation

The development of fixtures with a high degree of flexibility is an urgent task. Flexible fixtures require the implementation of fundamentally new schemes for the workpiece setup. Connecting rods have a quite different design and technological features that complicate the creation and implementation of a single manufacturing process for the group of parts.

Due to the constant improvement of machine and tool production, there is a need to improve the technology of manufacturing connecting rods. The high-performance CNC multi-axis equipment allows performing machining on one machine of a rather large group of various surfaces. The flexible fixture is designed for locating-and-clamping connecting rods of different sizes in the range of 100–120 mm long, 40–60 mm wide, and 15–25 mm high, which is controlled by adjusting the screw mechanisms that provide a change in the distance between the locating-and-clamping elements (Fig. 4).

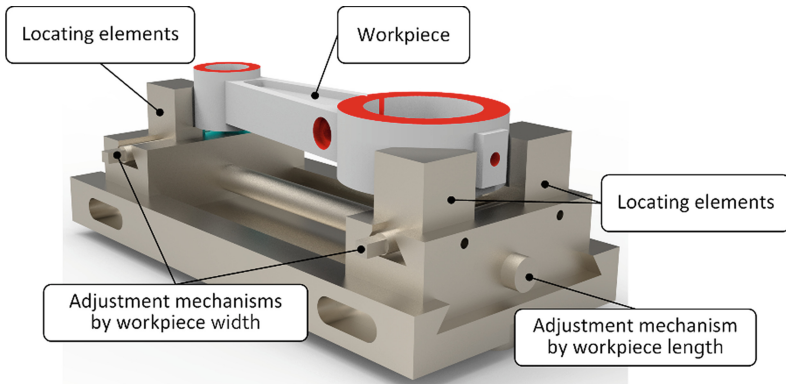


**Fig. 4.** Flexible fixture for the machining connecting rod on the CNC multiaxis machining operation

Flexible fixtures can be used on the machine table as well as on baseplates from different sets of modular fixtures. This technical solution, in combination with the rotating table of the machine, allows performing all drilling, milling, and boring operations with the constant fixing of the workpiece on one manufacturing operation at the CNC machining center.

Productivity is a fairly broad concept and, depending on the needs of the evaluation, is divided into absolute artificial productivity, the productivity of cutting, and the productivity of shaping. However, from the practical point of view, the most important indicator is the artificial productivity ( $Q_a$ ) of the machine tool, that can be determined by the time spent per unit of production or the amount of output machined per unit of time and is determined by the formula:

$$Q_a = 1/T_{mc}, \quad (1)$$

where  $T_{mc}$  – machining-calculation time, min.

The artificial productivity of the operation is divided into technological, theoretical, real, and actual. Technological productivity ( $Q_t$ ) is determined by the number of workpieces that can be machined per machine tool per unit of time in a continuous workflow, that is, the absence of idle time and auxiliary steps of the operation, or with complete overlapping of auxiliary time by the cutting time. It is determined by the time spent on machining ( $T_c$ ):

$$Q_t = 1/T_c. \quad (2)$$

The theoretical productivity ( $Q_{th}$ ) is the number of parts machined on the machine tool during continuous operation, i.e. without consideration or in the absence of off-cycle costs (idle time, the cost of servicing the workplace, and rest of the worker).

This productivity is defined for the structural diagrams of operations with automatic setup of parts by the formula:

$$Q_{th} = 1/T_{cycle}, \quad (3)$$

where  $T_{cycle}$  – the time of the working cycle in the transition of the machine tool to the automatic mode, min.

The real productivity operation ( $Q_r$ ) is determined by taking into account other elements of machining or machining-calculating time. For batch production the formula looks like:

$$Q_r = 1/T_{mc}. \quad (4)$$

The real productivity of the machine tool can be defined as follows:

$$Q_r = Q_{th} \cdot K, \quad (5)$$

where  $K$  is the coefficient that takes into account the off-cycle time costs. The value of the coefficient for batch production does not exceed 0.15.

The actual productivity ( $Q_{ac}$ ) takes into account the cases of different time losses in production conditions and is determined by:

$$Q_{ac} = \left(1 - \frac{\alpha}{100}\right) \left(1 - \frac{\beta}{100}\right) / T_{mc}, \quad (6)$$

where  $\alpha$  is the loss of idle time, %;  $\beta$  is the defective parts on this technological operation, %.

As the volumes of single-part manufacturing and medium-batch manufacturing are relatively small, the defective parts should not be allowed on any of the operations, and this requires that during the first workpiece control after the machining of each of the surfaces and the appropriate adjustment. Then, every subsequent part is fully controlled after machining of all surfaces on this operation without removing from the machine. Thus the defects are excluded.

Time losses on downtime are determined by the load factor of the equipment, which is 0.8–0.9 for single-part manufacturing and medium-batch manufacturing; therefore, 15% for downtime is taking into account.

## 4 Results

A comparison of machining productivity in two manufacturing processes is determined by the calculated time for machining in the previous studies [1] by plotting the percentages of time between the standard values for typical and the proposed manufacturing processes (Fig. 5).

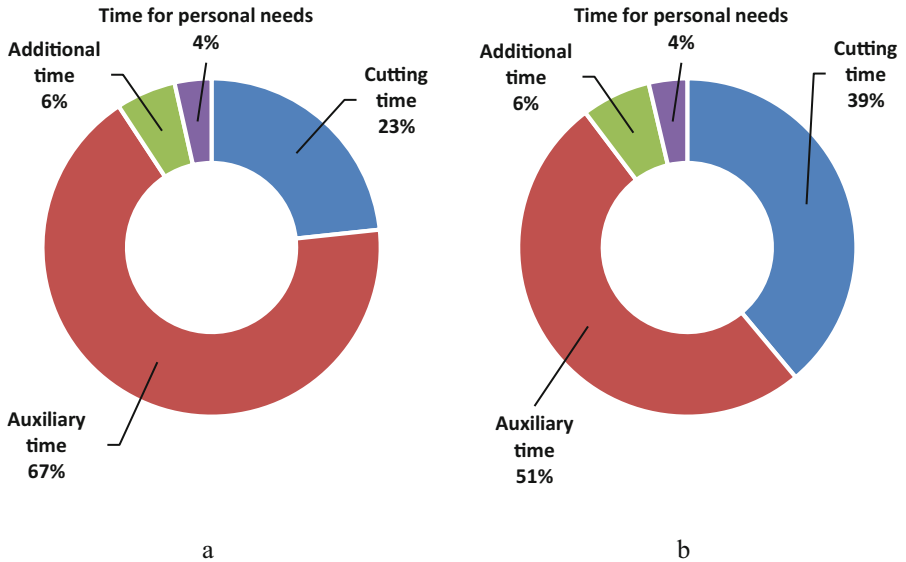


**Fig. 5.** Comparative analysis of typical (a) and proposed (b) manufacturing processes according to the structure of the machining time

In the proposed manufacturing process, the proportion of the cutting time (Fig. 5b) in the total volume of machining time is significantly higher than in the typical manufacturing process due to the reduction of auxiliary time.

The values of machining-calculation time for the typical and proposed manufacturing processes are calculated when changing the batch of parts from 1 to 200 pieces (Fig. 6). The curves corresponding to the values of different types of productivity typical (round marker) and proposed (triangle marker) manufacturing processes can be seen: technological (orange color); real (red); actual (blue) (Fig. 7).

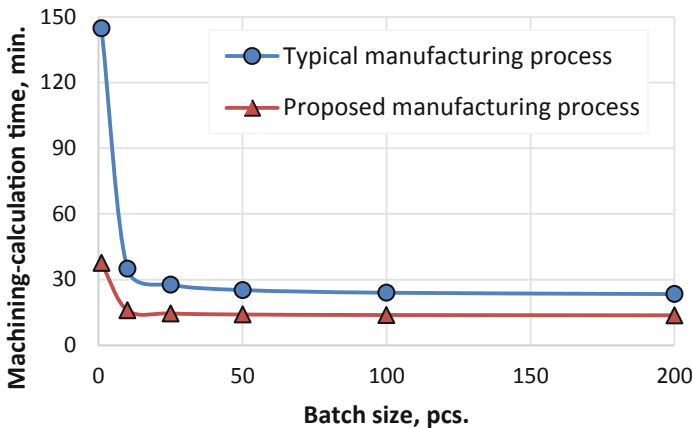


**Fig. 6.** Comparative analysis of manufacturing processes by the machining-calculation time

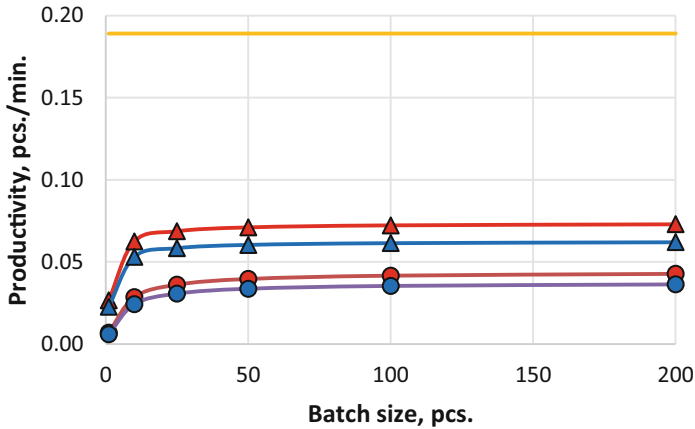


Fig. 7. Comparative analysis of manufacturing processes by productivity

The technological productivity for both manufacturing processes is equal, and the increase of other considered types of productivity in the proposed manufacturing process compared with the typical comprised from 1.7 to 3.9 times, which testifies to the improvement of the efficiency of the proposed manufacturing process overall under all similar conditions. At the same time, the greatest increase in productivity is observed for the batch size from 1 to 25 pcs.

## 5 Conclusions

The design of flexible fixtures for machining connecting rods on multiaxis CNC machining centers has been proposed, which allowed to offer a manufacturing process based on the principle of machining intensification and to reduce the number of drilling-milling-boring manufacturing operations from 7 to 2.

The comparative analysis of the time of the typical and the proposed manufacturing processes illustrated that in the proposed manufacturing process, the proportion of cutting time in the structure of machining time is higher than in the typical manufacturing process by 16%. The increase in productivity in the proposed manufacturing process was from 1.7 to 3.9 times for specific types of productivity and batch sizes.

Future studies will be directed to numerical modeling and experimental verification of the developed flexible fixture, as well as to the development of mechanisms for automated adjustment of the locating elements.

**Acknowledgment.** The research was realized within the project “Optimization of the Production Cycle of Complex Parts Manufacturing Using Modular Tooling” (State Reg. Number 0119U103186) funded by the Grant of the President of Ukraine for Young Scientists and the project “Development and Implementation of Energy Efficient Modular Separation Devices for Oil and Gas Purification Equipment” (State Reg. Number 0117U003931) funded by the Ministry of Education and Science of Ukraine.

## References

1. Ivanov, V., Dehtiarov, I., Pavlenko, I., Kosov, I., Kosov, M.: Technology for complex parts machining in multiproduct manufacturing. *Manag. Prod. Eng. Rev.* **10**(2), 25–36 (2019). <https://doi.org/10.24425/mper.2019.129566>
2. Ben, W.: The future of manufacturing: a new perspective. *Engineering* **4**, 722–728 (2018). <https://doi.org/10.1016/j.eng.2018.07.020>
3. Ambrogio, G., Gagliardi, F., Muzzupappa, M., Filice, L.: Additive-incremental forming hybrid manufacturing technique to improve customised part performance. *J. Manuf. Process.* **37**, 386–391 (2019). <https://doi.org/10.1016/j.jmapro.2018.12.008>
4. El-Tamimi, A.M., Abidi, M.H., Hammad, S.M., Aalam, J.: Analysis of performance measures of flexible manufacturing system. *J. King Saud Univ.* **24**(2), 115–129 (2012). <https://doi.org/10.1016/j.jksues.2011.06.005>
5. Lafou, M., Mathieu, L., Pois, S., Alochet, M.: Manufacturing system flexibility: product flexibility assessment. *Procedia CIRP* **41**, 99–104 (2016). <https://doi.org/10.1016/j.procir.2015.12.046>
6. Do, M.D., Son, Y., Choi, H.J.: Optimal workpiece positioning in flexible fixtures for thin-walled components. *Comput. Aided Des.* **95**, 14–23 (2018). <https://doi.org/10.1016/j.cad.2017.09.002>
7. Ivanov, V., Pavlenko, I., Liaposhchenko, O., Gusak, O., Pavlenko, V.: Determination of contact points between workpiece and fixture elements as a tool for augmented reality in fixture design. *Wirel. Netw.* (2019). <https://doi.org/10.1007/s11276-019-02026-2>
8. Zheng, Y., Qian, W.H.: A 3-D modular fixture with enhanced localization accuracy and immobilization capability. *Int. J. Mach. Tools Manuf* **48**(6), 677–687 (2008). <https://doi.org/10.1016/j.ijmactools.2007.10.022>
9. Tohidi, H., AlGeddawy, T.: Planning of modular fixtures in a robotic assembly system. *Procedia CIRP* **41**, 252–257 (2016). <https://doi.org/10.1016/j.procir.2015.12.090>
10. Yamaguchi, T., Higuchi, M., Nagai, K.: Assembly system by using prototype of active flexible fixture. In: Arai, E., Arai, T. (eds.) *Mechatronics for Safety, Security and Dependability in a New Era*, pp. 125–188. Elsevier (2007). <https://doi.org/10.1016/b978-008044963-0/50026-6>
11. Yarovy, Y., Yarova, I.: Energy criterion for metal machining methods. In: Ivanov, V., et al. (eds.) *Advances in Design, Simulation and Manufacturing II. DSMIE-2019. Lecture Notes in Mechanical Engineering*, pp. 378–387. Springer, Cham (2020). [https://doi.org/10.1007/978-3-030-22365-6\\_38](https://doi.org/10.1007/978-3-030-22365-6_38)
12. Kotliar, A., Basova, Y., Ivanov, V., Murzabulatova, O., Vasylytova, S., Litvynenko, M., Zinchenko, O.: Ensuring the economic efficiency of enterprises by multi-criteria selection of the optimal manufacturing process. *Manag. Prod. Eng. Rev.* **11**(1), 52–61 (2020). <https://doi.org/10.24425/mper.2020.132943>
13. Fesenko, A., Basova, Y., Ivanov, V., Ivanova, M., Yevsukova, F., Gasanov, M.: Increasing of equipment efficiency by intensification of technological processes. *Period. Polytech. Mech. Eng.* **63**(1), 67–73 (2019). <https://doi.org/10.3311/PPme.13198>
14. Kotliar, A., Basova, Y., Ivanova, M., Gasanov, M., Sazhniev, I.: Technological assurance of machining accuracy of crankshaft. In: Diering, M., Wiczorowski, M., Brown, C. (eds.) *Advances in Manufacturing II. Volume 5 - Metrology and Measurement Systems. MANUFACTURING 2019. Lecture Notes in Mechanical Engineering*, pp. 37–51. Springer, Cham (2019). [https://doi.org/10.1007/978-3-030-18682-1\\_4](https://doi.org/10.1007/978-3-030-18682-1_4)



15. Sokolov, V., Krol, O., Baturin, Y.: Dynamics research and automatic control of technological equipment with electrohydraulic drive. In: 2019 International Russian Automation Conference, RusAutoCon 2019. IEEE (2019). <https://doi.org/10.1109/rusautocon.2019.8867652>
16. Krol, O., Sokolov, V.: Development of models and research into tooling for machining centers. *East-Eur. J. Enterp. Technol.* **3**(1–93), 12–22 (2018). <https://doi.org/10.15587/1729-4061.2018.131778>
17. Józwick, J., Kuric, I., Łukaszewicz, A.: Analysis of the table motion of a 3-axis CNC milling machine tool at start-up and braking. In: Tonkonogyi V., et al. (eds.) *Advanced Manufacturing Processes. InterPartner 2019. Lecture Notes in Mechanical Engineering*, pp. 108–117. Springer, Cham (2020). [https://doi.org/10.1007/978-3-030-40724-7\\_11](https://doi.org/10.1007/978-3-030-40724-7_11)
18. Kostyuk, G.: Prediction of the microhardness characteristics, the removable material volume for the durability period, cutting tools durability and processing productivity depending on the grain size of the coating or cutting tool base material. In: Gapiński, B., Szostak, M., Ivanov, V. (eds.) *Advances in Manufacturing II. MANUFACTURING 2019. Lecture Notes in Mechanical Engineering*, pp. 300–316. Springer, Cham (2019). [https://doi.org/10.1007/978-3-030-16943-5\\_27](https://doi.org/10.1007/978-3-030-16943-5_27)
19. Kostyuk, G., Nechyporuk, M., Kostyk, K.: Determination of technological parameters for obtaining nanostructures under pulse laser radiation on steel of drone engine parts. In: 10th International Conference on Dependable Systems, Services and Technologies, DESSERT 2019, pp. 208–212. IEEE (2019). <https://doi.org/10.1109/dessert.2019.8770053>
20. Tarelnyk, V., Konoplianchenko, I., Tarelnyk, N., Kozachenko, A.: Modeling technological parameters for producing combined electrospark deposition coatings. *Mater. Sci. Forum* **968**, 131–142 (2019). <https://doi.org/10.4028/www.scientific.net/MSF.968.131>
21. Dodok, T., Čuboňová, N., Císar, M., Ivanov, V., Wiecek, D.: Influence of CNC milling strategies on complex surface machining. *IOP Conf. Ser. Mater. Sci. Eng.* **776**, 012002 (2020). <https://doi.org/10.1088/1757-899X/776/1/012002>
22. Cioată, V.G., Kiss, I., Alexa, V., Rațiu, S.A., Racov, M.: Study of the influence of the cutting temperature on the magnitude of the contact forces in the machining fixtures. *IOP Conf. Ser. Mater. Sci. Eng.* **294** (2018). <https://doi.org/10.1088/1757-899x/294/1/012072>
23. Dobrotvorskiy, S., Basova, Y., Ivanova, M., Kotliar, A., Dobrovolska, L.: Forecasting of the productivity of parts machining by high-speed milling with the method of half-overlap. *Diagnostyka* **19**(3), 37–42 (2018). <https://doi.org/10.29354/diag/93136>
24. Zaloga, V., Dyadyura, K., Rybalka, I., Pandova, I.: Implementation of integrated management system in order to enhance equipment efficiency. *Manag. Syst. Prod. Eng.* **27**(4), 221–226 (2019). <https://doi.org/10.1515/mspe-2019-0035>
25. Dymnyk, O., Denysenko, Y., Zaloga, V., Ivchenko, O., Yashyna, T.: Information support for the quality management system assessment of engineering enterprises. In: Ivanov, V., et al. (eds.) *Advances in Design, Simulation and Manufacturing II. DSMIE-2019. Lecture Notes in Mechanical Engineering*, pp. 65–74. Springer, Cham (2020). [https://doi.org/10.1007/978-3-030-22365-6\\_7](https://doi.org/10.1007/978-3-030-22365-6_7)
26. Cioată, V.G., Kiss, I., Alexa, V., Rațiu, S.A.: Study of the contact forces between workpiece and fixture using dynamic analysis. *J. Phys: Conf. Ser.* **1426**, 012040 (2020). <https://doi.org/10.1088/1742-6596/1426/1/012040>
27. Pavlenko, I., Trojanowska, J., Ivanov, V., Liaposhchenko, O.: Parameter identification of hydro-mechanical processes using artificial intelligence systems. *Int. J. Mechatron. Appl. Mech.* **2019**(5), 19–26 (2019)



28. Oborskyi, G., Orgiyan, A., Tonkonogyi, V., Aymen, A., Balaniuk, A.: Study of dynamic impacts at combined operations of the thin turning and boring. In: Tonkonogyi, V., et al. (eds.) *Advanced Manufacturing Processes. InterPartner-2019. Lecture Notes in Mechanical Engineering*, pp. 226–235. Springer, Cham (2020). [https://doi.org/10.1007/978-3-030-40724-7\\_23](https://doi.org/10.1007/978-3-030-40724-7_23)
29. Orgiyan, A., Tkachenko, B., Oborskyi, G., Balaniuk, A., Iorgachov, V.: Determining rational cutting modes for horizontal boring operation adjusted for the variable rigidity of the process system. In: Tonkonogyi, V., et al. (eds.) *Advanced Manufacturing Processes. InterPartner-2019. Lecture Notes in Mechanical Engineering*, pp. 246–253. Springer, Cham (2020). [https://doi.org/10.1007/978-3-030-40724-7\\_25](https://doi.org/10.1007/978-3-030-40724-7_25)
30. Wan, N., Wang, Z., Mo, R.: An intelligent fixture design method based on smart modular fixture unit. *Int. J. Adv. Manuf. Technol.* **69**, 2629–2649 (2013). <https://doi.org/10.1007/s00170-013-5134-3>
31. Ivanov, V., Vashchenko, S., Rong, Y.K.: Information Support of the computer-aided fixture design system. In: Ermolayev, V., et al. (eds.) *Proceedings of the 12th International Conference on ICT in Education, Research and Industrial Applications. Integration, Harmonization and Knowledge Transfer. ICTERI 2016*, vol. 1614, pp. 73–86. CEUR-WS.org (2016)
32. Haidabrus, B., Druzhinin, E., Elg, M., Jason, M., Grabis, J.: Programs to boost IT-readiness of the machine building enterprises. In: Ivanov, V., et al. (eds.) *Advances in Design, Simulation and Manufacturing II. DSMIE-2019. Lecture Notes in Mechanical Engineering*, pp. 75–84. Springer, Cham (2020). [https://doi.org/10.1007/978-3-030-22365-6\\_8](https://doi.org/10.1007/978-3-030-22365-6_8)
33. Sreekumar, M.D., Chhabra, M., Yadav, R.: Productivity in manufacturing industries. *Int. J. Innov. Sci. Res. Technol.* **3**(10), 634–639 (2018)
34. Antonioli, I., Guariente, P., Pereira, T., Pinto Ferreira, L., Silva, F.J.G.: Standartization and optimization of the automotive components production line. *Procedia Manuf.* **13**, 1120–1127 (2017). <https://doi.org/10.1016/j.promfg.2017.09.173>
35. Gamberini, R., Galloni, L., Lolli, F., Rimini, B.: On the analysis of effectiveness in a manufacturing cell: a critical implementation of existing approaches. *Procedia Manuf.* **11**, 1882–1891 (2017). <https://doi.org/10.1016/j.promfg.2017.07.328>
36. Azizi, A.: Evaluation improvement of production productivity performance using statistical process control, overall equipment efficiency, and autonomous maintenance. *Procedia Manuf.* **2**, 186–190 (2015). <https://doi.org/10.1016/j.promfg.2015.07.032>



# Optimization of the Technological Process Based on Analysis of Technological Damageability of Castings

Yaroslav Kusyi<sup>(✉)</sup>  and Vadym Stupnytskyi 

Lviv Polytechnic National University, 12, Bandera St., Lviv 79013, Ukraine  
jarkym@ukr.net

**Abstract.** Reasons for machine failures are analyzed in the article. The primary role of the machining and assembly process structure for the formation of the product's damages is noted. Improvement of the operating properties and reliability indicators are considered as a result of the pre-production technological system optimization as a part of the product's Life Cycle Support. The relationship between the technological damageability and the workpiece's material structure is presented in a formalized form. Methods for assessing the degree of the material's damage based on the results of direct and indirect measurements of the material's mechanical properties without destroying are analyzed. The method of experimental studies is described. The advantages of the method of LM-hardness analysis and evaluation of the heterogeneity of the workpiece's physical structure are submitted. The impact of the technological route structure on forming the process of product damage was studied based on experimental researches. Technological damageability is proposed to be used as a criterion for the analysis of the technological process of workpiece machining. This method is an energy approach to the research of the product's damage accumulation.

**Keywords:** Casting · Technological damageability · LM-hardness analyses method · Weibull homogeneity coefficient

## 1 Introduction

The most important criterion for the efficiency of mechanical engineering manufacturing is the harmonization of the technical requirements of the design documentation with the ensuring of the exploitation characteristics of parts and machines according to the modes and conditions of their work. Improving the efficiency of technological preparation as an important substage of the product/machine creation stage in their Life Cycle depends on the effective work in the following directions [1–5]:

1. automation of design and technological documents by means of CAD/CAM/CAE systems;
2. computerization of manufacturing using CIM-conception (CIM - Computer Integrated Manufacturing)

- implementation of PLM concepts (PLM - Product Lifecycle Management) with the design of functional-oriented engineering technologies by means of parallel engineering - CAPE (Concurrent Art-to-Product Environment).

At the same time, forecasting the part's behavior and ensuring the parameters of its reliability at all substages and stages of its Life Cycle is an important problem of the mechanical engineering industry.

Destruction of parts, according to the classical approach, as a rule, is connected with the formation of cracks in the places of local change in the physical and mechanical properties of parts. Grain borders are such places. Accumulation and alteration of defects in them under the action of operational and technological loads lead to the appearance of damage and the development of cracks. Nearly 50% of equipment failure, operating at low temperatures, is caused by the formation of damages developed between the crystal grains of the material [6].

Chemical fluctuations, changes in the initial structure, formation and interaction of pores and microcracks, etc. cause changes in the product materials on the nano-, micro- and macro-level in the conditions of operation.

Changes in the initial properties and condition of the part's material during operation lead to irreversible changes in the structure, occurring at all stages of deformation, and cause damage in materials and the risk of failure (see Fig. 1) [6–8].



**Fig. 1.** A simplified scheme for the formation of product failure.

The structure of the machining and assembly technological process has a decisive role in solving that problem. However, the influence of blanking operations on quality parameters in the design of modern technological processes is not studied enough. In addition, there is a lack of methodology of quantifying technological damages both on the blanking operation and during the technological process. Therefore, these questions require further fundamental theoretical and experimental research.

## 2 Literature Review

Parts and machines are characterized by the corresponding quality indicators, which are determined by their service position [9].

The quality of mechanical engineering products is characterized by the accuracy of sizes, parameters of the surface layer quality, operational characteristics and reliability parameters. The degree of conformity of a certain quality indicator is regulated by machining and assembly errors limited to the values of the corresponding tolerances [9, 10].

Error values are closely related to the structure of machining and assembly.

The transfer of object properties from previous to the following technological operations is called technological inheritance. Preservation of these properties in objects is called technological heredity [9, 11].

It has been investigated [9, 11] that the process of technological inheritance can be managed. At the same time, the properties positively affect the quality parameters, are preserved throughout the process, and negative factors are eliminated at the beginning of it.

However, in modern literature, the role of blanking operations in the analysis of the influence of technological inheritance on the quality parameters of part/machine is not sufficiently taken into account [11]. The structure and properties of blanks must be analyzed in close conjunction with the metal heredity from the liquid state. However, 75% of the properties are formed during the pouring and curing of the alloy during cooling. Only 25% of the properties of the mix are transferred to the blank during its manufacturing [11].

The need to take into consideration and analyse the behavior of materials at all stages of the product life cycle is integrated into the CAD/CAE/CAM environment [2, 8, 11, 12]. The task for the comprehensive analysis of materials for engineering products is considered in the work [13–15].

Modern methods of modeling foundry technologies permit to accurately calculate the temperature fields and forecast shrinkage defects in castings. But modern software cannot reliably identify the fracture zones in casting alloys, incorporating the factors that affect the initiation and propagation of cracks. Therefore, the theoretical and experimental studies to refine the mathematical models and software are needed [11, 12, 16].

The process of metal failure includes the next stages [1, 6]:

1. damage accumulation and breaking of the material continuity in the sphere of stresses and deformations;
2. development of microcracks in the field with defects;
3. growth of cracks and separation of the material under loads and displacements set at the boundaries of the blank.

In a majority of investigations on the causes of material fracture during exploitation, the technological damageability  $W$  is not associated with a workpiece structure. Only with the use of energy approaches to describe the processes of damage accumulation [11, 12], it is considered that, as a result of viscoplastic deformation, two types of micro-damages develop - along the body and along the grain boundaries.

Internal variables that determine the processes of damage accumulation are scalar parameters, such as the energy of damageability along the grain body  $W_p$  and the energy of damageability along the grain boundaries  $W_n$  [11, 12]:

$$W_k = \int_0^t w_k, \quad k = p, n. \quad (1)$$

where  $k$  is the current index;  $p$  is the index that characterizes the energy of damageability along the grain body;  $n$  is the index that characterizes the energy of damageability along the grain boundaries.

The damageability  $W_k$  depends on the history of the viscoplastic deformation of the material. Damageability along the body and the grain boundaries is characterized by the relative damage parameters  $W_p$  and  $W_n$ , respectively:

$$0 \leq W_p \leq 1, 0 \leq W_n \leq 1. \quad (2)$$

Total damageability of the material  $W$ :

$$0 \leq W \leq 1. \quad (3)$$

Increase in damageability [11]:

$$\Delta W = dW_n + dW_p, \quad (4)$$

where  $dW_n = dW_n(T, W_n, W_p)$ ,  $dW_p = dW_p(T, W_n, W_p)$ .

The total increase in damageability:

$$\begin{aligned} \Delta W &= dW_n + dW_p, \\ \Delta W_n &= dW_{nR} + dW_{n\delta}, \\ \Delta W_p &= dW_{pR} + dW_{p\delta} \end{aligned} \quad (5)$$

where  $dW_{nR}$ ,  $dW_{n\delta}$  are the increments of the grain-boundary damageability due to viscoplastic strain and as a result of changes in the conditions of deformation, respectively;  $dW_{pR}$ ,  $dW_{p\delta}$  are the increments of intragranular damageability, respectively, due to viscoplastic strain and as a result of a change in the type of the stress state and temperature.

The formation of technological damages during blanking operations, in particular foundry operations, their development during machining and exploitation and the change in the reliability of machine parts and machines under these conditions have not been adequately investigated.

In addition, there is no technique for calculating technological damageability after the operations of the technological process.

### 3 Research Methodology

#### 3.1 Methods of Research

The methods of assessing the degree of material damageability during the operating time based on the results of direct (weighting, methods of metallography, etc.) and secondary (ohmic resistance, acoustic emission, etc.) measurements of the metal mechanical properties without fractures are known [11, 12]. The use of these methods to assess material degradation due to accumulated damage during operating time leads to significant errors. The relationship between the measured parameters and the characteristics of the structural state for a wide class of materials is ambiguous. In addition, in some cases, for the implementation of such methods, samples with a current design need to be cut, which is not always possible.

The method of measuring the absolute values of the material hardness of the design at individual stages of operating time is the closest, in its technical essence, to the known methods. It is assumed that the hardness characteristics are correlated with the structure parameters. The degree of the material's damageability is analyzed based on this assumption. This method is not informative and accurate since the correlation between the material hardness and its damageability is very weak and not always unambiguous.

We used the LM-hardness method to analyze and evaluate the physical heterogeneity of the blank material structure. According to this method, the degree of dispersion of the characteristics of the material's mechanical properties after operating time at various stress levels is taken as a parameter of damageability. The scattering of the measurement results performed by identical devices and identical conditions is more representative regarding the correlation of the mechanical properties of the material and the structure state than the absolute values of the characteristics. This method is easier to implement using hardness as a mechanical characteristic. The hardness value is used for the indirect evaluation of properties [12].

Homogeneity is the parameter that integrally characterizes the state of the material when processing the results of hardness measurements. Homogeneity is estimated by the Weibull coefficient ( $m$ ). The higher value of the coefficient  $m$  corresponds to the low hardness dispersion and a low damageability degree; the lower value, on the contrary, corresponds to a higher degree of damageability [11, 12].

The Weibull homogeneity coefficient ( $m$ ) is calculated by [11]:

$$m = \frac{d(n)}{2,30259 S(\log(H))}, \quad (6)$$

where  $d(n)$  is a parameter that depends on the number of measurements,  $n$ ,

$$S(\log(H)) = \sqrt{\frac{1}{n-1} \sum_{i=1}^n (\log(H_i) - \log(\bar{H}))^2}, \quad (7)$$

$$\log(\bar{H}) = \frac{1}{n} \sum_{i=1}^n \log(H_i), \quad (8)$$

where  $H_i$  is the hardness value of  $i$  measurement;  $\bar{H}$  is the medium value of hardness for measurement results.

The technological damageability  $W$  is calculated by [11]:

$$W = \frac{m_{max} - m_i}{m_{max}}, \quad (9)$$

where  $m_i$  is the value of the Weibull coefficient on the  $i$ -th measurement line (plane);  $m_{max}$  is the maximum value of the Weibull coefficient for a series of measurements.

### 3.2 Planning of Experimental Researches

**Experimental Samples.** For experimental research, the blanks were casted in a metal mold. The blank dimensions were  $145 \times 60 \times 15$  mm. The blank was made of material AK21M2.5H2.5 State standard-GOST 1853-93.

**Machine-Cutting Tools and Equipment.** The casting was machined by the end milling. We used some tools: tools of the  $\varnothing 12$  mm ( $z = 2$ ) diameter for rough milling, tools of the  $\varnothing 16$  mm ( $z = 4$ ) diameter for semi-rough milling and finishing. The experimental sample was machined on the universal milling machine series 676.

**Technological Route and Cutting Parameters.** Two series of experimental researches for each machining were planned. We made two experimental series for result reproducibility. Different metal castings ensure each series of experimental researches. Technological route of blank manufacturing and next machining includes two variants – 1st variant: a) casting in a cold and warmed-over metal mold; b) rough milling; c) finishing; 2nd variant: a) casting in a cold and warmed-over metal mold; b) semi-rough milling; c) finishing. After that, the surface of the experiment sample was controlled by the measurement device. The cutting parameters are shown in Table 1.

**Table 1.** Cutting parameters for the type of machining

Type of machining	Cutting parameters			
	Rotary speed (n), $\text{min}^{-1}$	Cutting speed (V), m/min	Feed rate ( $S_{\text{min}}$ ), mm/min	Cutting depth (t), mm
Rough machining	700	26.39	100–120	1.0
Semi-rough machining	1050	52.78	13	0.3
Finishing	1050	52.78	13	0.3

**The Measurement Device.** Hardness was measured on the device TP-5006 by means of a  $\varnothing 3.175$  mm ball under loading with 588.4 N. In each experiment 30–35 measurements were performed.

## 4 Results

The Weibull homogeneity coefficient ( $m$ ), the technological damageability  $W$  is calculated by Eq. (6), (9) in Mathcad 15 medium using the research results. The diagrams  $m = f(n)$  and  $W = f(n)$  are presented in Fig. 2, 3, where  $n$  is the number of the machining method in the technological route.

The research results show a general tendency in the formation of the material surface layer after pouring metal into a cold and heated metal mold (Fig. 2, 3). It is found that, in general, the value of the Weibull coefficient ( $n$ ) on the blank surface is less, and the tendency to technological damageability ( $W$ ) is higher when pouring the

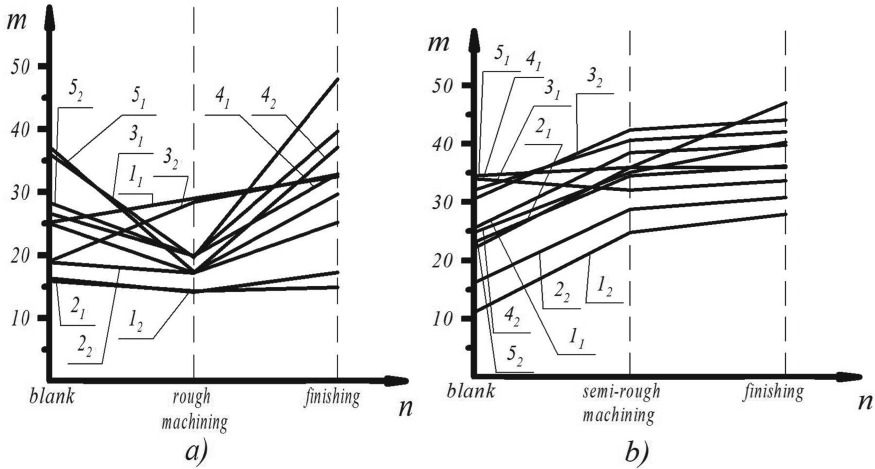


**Fig. 2.** Change of the Weibull homogeneity coefficient ( $m$ ) in the surface layer of the casting for the first (a) and second (b) variants of the technological route (1, 2 are the castings spilled in a cold metal mold, 3, 4, 5 are the castings spilled into a heated metal mold; indexes 1, 2 indicate the number of the melting blank).

liquid melt into cold molds than in the hot ones. This is explained by the lower level of heterogeneity development during crystallization under the conditions of a decrease in the temperature field between the crystallized metal and the form.

The analysis of the results obtained for the first variant of the technological route (blank - rough machining - finishing) after rough milling on a depth of 1 mm indicates a decrease in the value of the Weibull homogeneity coefficient ( $m$ ) and an increase in the values of technological damageability ( $W$ ) compared to similar measurements on the surface. This is due to the increase in the tendency toward material damageability in the deformation zone of the processed layer and the presence of significant residual tension after preprocessing by milling. Finish milling after preprocessing on a depth of 0.3 mm contributed to an increase in the Weibull  $m$  homogeneity coefficient and a decrease in the values of technological damageability ( $W$ ), which is due to the removal of a metal layer with a developed damageability during this machining (Fig. 2a, Fig. 3a). The increase of the Weibull homogeneity coefficient ( $m$ ) is 5.13 (that is 49.4%) after finish milling compared to the initial blank.

The analysis of the results obtained for the second variant of the technological route (blank – semi-rough machining - finishing) after semi-rough machining and finish milling on a depth  $h_1 = 0.3$  mm;  $h_2 = 0.6$  mm indicates a general trend toward an increase in the value of the Weibull homogeneity coefficient ( $m$ ) and a decrease in the value of the technological damageability ( $W$ ) compared to similar measurements on the surface. In this case, the dynamics of the change in the values of the Weibull homogeneity coefficient ( $m$ ) and technological damageability ( $W$ ) is more intensive for semi-rough milling. This is due to the removal of the defective surface layer of the blank with adjacent layers of oxides and dirt (see Fig. 2b; Fig. 3b). The Weibull homogeneity coefficient ( $m$ ) has increased to 1.14 (that is 60.2%) after finish milling compared to the initial blank, which is due to a reduction in material damage after machining.



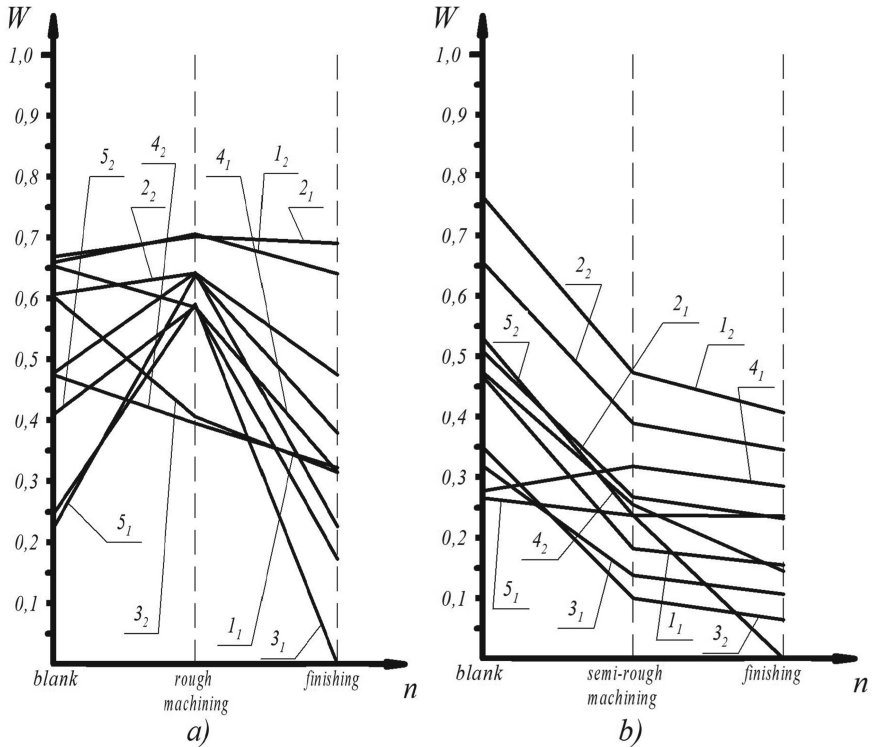


**Fig. 3.** Change of technological damageability ( $W$ ) in the surface layer of the casting for the first (a) and second (b) variants of the technological route (1, 2 - castings spilled in a cold metal mold, 3, 4, 5 - castings spilled into a heated metal mold; indexes 1, 2 indicate the number of the blank melting).

## 5 Conclusions

The main conclusions have been drawn based on the research results.

1. The technological damages on the surface layers of the parts during blanking operations and after machining should be analyzed by the level of hardness dispersion.
2. We propose to use the technological damageability ( $W$ ) described by means of energy approaches to the processes of damage accumulation as a criterion for the process analysis during blank machining.
3. Increasing force loads during rough machining, in particular milling, contribute to the production of a gradient structure in the blanks and the increase in the damageability of the surface layers. The reduction of the power characteristics of the cutting process at the finishing modes reduces the number of structural stress concentrators. It has a positive effect on the formation of the surface layer parameters and the behavior of the parts during their running.





4. Further research should be carried out for a wider nomenclature of machine parts and materials to introduce the proposed technique into the practice of modern mechanical engineering production.

## References

1. Stotsko, Z., Kuzin, O., Kuzin, M.: Use of modern tribology approaches for correcting the behaviour of adaptive biomechanical friction units. *Arch. Mater. Sci. Eng.* **2**(92), 49–52 (2018)
2. Lyashenko, B., Stotsko, Z., Kuzin, O., Kuzin, M., Mikosianchyk, O.: Determination of the optimal parameters of the structure of functional gradient materials using mathematical modelling approaches. *J. Achiev. Mater. Manuf. Eng.* **1–2**(92), 13–18 (2019)
3. Stotsko, Z., Kuzin, M.: Life cycle assessment of technical systems taking into consideration degradation processes in materials of constructions improving reliability of drill pipe by strengthening of thread connections of its elements. *Arch. Mater. Sci. Eng.* **1**(89), 5–8 (2019)
4. Gontarz, A., Hampl, D., Weiss, L., Wegener, K.: Resource consumption monitoring in manufacturing environments. *Int. Acad. Prod. Eng. (CIRP) Ann.* **26**(1), 264–269 (2015)
5. Kusyi, Y., Kuzin, O., Kuzin, M.: The dependence of intergrain damageability of casting on the technological treatment route. *East.-Eur. J. Enterp. Technol.* **1**(5/79), 39–47 (2016)
6. Lachmayera, R., Mozgova, I., Reimcheb, W., Colditzc, F., Mrozb, G., Gottwalda, P.: Technical inheritance: a concept to adapt the evolution of nature to product engineering. *Procedia Technol.* **15**, 178–187 (2014)
7. Kusyj, J., Kuzin, O., Kuzin, N.: Analysis of technological damageability of castings manufactured in sand molds. *Technol. Audit. Prod. Reserv.* **3**(1), 17–23 (2017)
8. Lebedev, A., Golubovskii, A., Lokoshchenko, E., Muzyka, A., Lamashevskii, N., Shvets, V., Efimenkova, E.: Assessment of the limiting levels of dispersed damage in materials under steady-state conditions of static and cyclic loading. *Strength Mater.* **44**, 579–584 (2012)
9. Wang, L.: *Dynamic Thermal Analysis of Machines in Running State*. Springer, London (2014)
10. Aftanaziv, I., Shevchuk, L., Strohan, O., Kuk, A., Samsin, I.: Improving reliability of drill pipe by strengthening of thread connections of its elements. *Sci. Bull. Natl. Min. Univ.* **4**, 22–29 (2019)
11. Blumenstein, V., Rakhimyanov, K., Heifetz, M., Kleptzov, A.: Problem of technological inheritance in machine engineering. In: *AIP Conference Proceedings*, vol. 1698, no. 1, pp. 2–7 (2016)
12. Blumenstein, V., Mahalov, V., Shirokolobova, F.: Finite element modeling of strengthening process by means of surface plastic deformation using a multiradius tool. *Mater. Sci. Eng.* **253**, 1–12 (2017)
13. Denkena, B., Mörke, T., Krüger, M., Schmidt, J., Boujnah, H., Meyer, J., Gottwald, P., Spitschan, B., Winkens, M.: Development and first applications of gentelligent components over their life-cycle. *J. Manuf. Sci. Technol.* **7**(2), 139–150 (2014)
14. Kundu, T.: *Epigenetics: Development and Disease*. Springer, Heidelberg (2013)
15. Cabej, N.: *Epigenetic Principles of Evolution*. Elsevier, Oxford (2012)
16. Bauerdick, C., Helfert, M., Petruschke, L., Sossenheimer, J., Abele, E.: An automated procedure for workpiece quality monitoring based on machine drive-based signals in machine tools. *Int. Acad. Prod. Eng. (CIRP) Ann.* **72**(1), 357–362 (2018)



# A Probabilistic-Statistical Model of Durability of Parts Under Cyclic Loading

Nataliia Lamnauer , Oleksandr Kupriyanov <sup>(✉)</sup> ,  
Anton Skorkin , and Oleg Kondratyuk 

Ukrainian Engineering Pedagogic Academy, 16, Universytets'ka St.,  
Kharkiv 61003, Ukraine  
a\_kupriyanov@uipa.edu.ua

**Abstract.** The article suggests the use of a probabilistic-statistical model for calculating the strength of parts under cyclic fatigue loads. Statistical analysis of the samples was carried out according to the results of a mass experiment on the strength of samples during fatigue tests. The numerical characteristics of the statistical sample are found: the average value, the corrected variance, the squared asymmetry coefficient, and the excess coefficient. As a result of the research, two models of the distribution of random variables were used: a three-parameter logarithmic-normal and a four-parameter model with upper and lower thresholds - the number of loading cycles. Estimates of the parameters of these two models were found using the moment method. The graphs of the distribution density functions of the two models were built based on the experimental results. To verify the adequacy of the models, sensitive functional characteristics were used, such as the average residual life and failure rate. The theoretical and empirical values of the functions are compared for the two models. It is shown statistically that the proposed four-parameter model is more adequate than the previously proposed three-parameter model (log-normal distribution). It is also shown that the four-parameter model proposed for assessing the strength of parts under cyclic loads is more physically adequate.

**Keywords:** Probabilistic-statistical model · Strength · Reliability · Cyclic load

## 1 Introduction

Elements of equipment and structures may experience variable loads. It is necessary to determine the strength and durability, including the residual life of elements having the fatigue nature of the failure. The problem of calculating the strength of parts under fatigue cyclic loads remains relevant. Modern research methods in this area actively use probabilistic-statistical analysis. It has now been proven to be more efficient than deterministic models.

High statistical technology is an integral part of any modern decision support system. High statistical technologies are statistical analysis procedures based on the latest achievements of applied mathematical statistics. The application of applied statistics gives a significant economic effect. For example, in the United States, it reaches at least \$20 billion annually in the field of statistical quality control.

More than 60 years have passed since the article “On the law of distribution of strength in fatigue tests” [1] was published in the scientific journal “Factory Laboratory”, No. 3, 1958. The paper presents a variant of one of the most massive tests (number of samples:  $n = 463$ , alloy grade B-95, stress:  $= 30 \text{ kg/mm}^2$ , cantilever bend). The authors conclude that even with heavy loads, you can see the sensitivity threshold in cycles  $N_{0,5} > 0$ . This is not visible with a small number of experiments. In addition, the feasibility of using a log-normal distribution through a statistical analysis of the results of tests is shown.

Currently, there have been major changes in connection with the development of programming. It became possible to better study the laws of distribution and carry out statistical analysis of time to failure of samples.

## 2 Literature Review

Scientists all over the world have been dealing with the issue of calculating the strength and reliability of parts under fatigue cyclic loads. Weibull distribution is especially often used to solve these problems. If you spend any amount of time in reliability engineering, you will undoubtedly encounter the Weibull distribution. Swedish engineer Waloddi Weibull introduced this probability distribution to the world in 1951 and it is still in wide use today [2]. This distribution is used to calculate the reliability of products in all areas of production. So, in [3] it was proposed rolling contact fatigue life evaluation using Weibull distribution. This text deals with solid mechanic aspects of contact fatigue including the description of an experimental study on contact fatigue. In the article measured data were analyzed using the Weibull distribution that is a continuous probability distribution, the gradients of which directly inform us about the shape and scale parameters corresponding to the characteristic life and failure rate of the specimen.

Recently, studies have appeared that use the exponentially transmuted Weibull distribution. A new generalization of the two-parameter Weibull distribution is presented. For this, a quadratic rank transmutation map was used. This new distribution is called the exponentially transmuted Weibull distribution (ETW). An advantage of the ETW distribution is its ability to model various forms of aging and destruction criteria. In addition, eleven life time distributions, such as the Weibull, Exponential Weibull, Rayleigh, and exponential distributions, follow as special cases [4–6].

However, any model is approximate, and work in this area should continue. There is a need to try using other models [7]. To verify the accuracy of the models, it is necessary to verify their compliance with the results of mass experiments. Another important aspect is checking the model for adequacy using sensitive functional characteristics.

A Lomax-Weibull distribution is proposed and developed by many scientists in order to assess the reliability of the systems and mechanisms. In the article [8], the new Lomax-Weibull distribution was introduced using the method of composition. Expressions for the moment generating function, hazard and survival functions were derived. The maximum likelihood method of estimation to derive the score functions for estimating the parameters of the distribution was suggested. A four-parameter

lifetime model named the Weibull inverse Lomax, is presented and studied in [9]. Maximum likelihood estimators along with asymptotic confidence intervals of population parameters and reliability function are constructed. The property of the consistency of maximum likelihood estimators has been verified based on simulated samples. The results are applied to real data.

In paper [10], a generalization of Additive Weibull distribution which is called exponentiated additive Weibull distribution was proposed. It includes a set of exponentiated distributions and represents a flexible model for reliability analysis such as reliability engineering, firmware reliability, decision-making reliability, and cost analysis. Some statistical properties of the new distribution are presented. The results showed that the new distribution provides a better fit than the existing one. A new four-parameter probability model, referred to the exponentiated Weibull Rayleigh distribution, is introduced in [11]. The essential statistical properties of the distribution are considered. The maximum likelihood estimators of population parameters are given in case of the complete sample.

The paper [12] introduces the transmuted exponentiated Weibull distribution by using the quadratic rank transmutation map technique studied by Shaw et al. This Weibull distribution contains eleven lifetime distributions as special cases. Maximum likelihood estimation is used for estimating the model parameters. The flexibility of the transmuted exponentiated Weibull distribution is assessed by applying mechanical data. Various modifications of the Weibull distribution are also proposed and fruitfully investigated in articles [13–16].

Other authors calculate reliability and risks using the Farmer’s diagram, which is complemented by the analytic hierarchy process and safety index [17], as well as analysis of various types of occurrence of cracks [18, 19].

### 3 Research Methodology

The research methodology is based on a comparison of two models of the distribution of random variables. A comparison of laws will consist of the following steps. First, we carry out a statistical analysis of the sample of the number of cycles  $H$  at a given load until the failure of the sample. Then, based on the results of mass tests, we compare the log-normal law of a random variable  $H$  with the law from [7]. In addition, for the two models studied, we apply sensitive functional characteristics to the type of distribution, such as the average residual life and failure rate. A comparison of the theoretical and empirical values of the functional characteristics for the two models will show which one is more suitable for applying the calculation of strength under cyclic loads.

The statistical analysis was performed for the log-normal law of mass experiments of samples from [1]. Statistical characteristics of a sample of measurement results were found. The average value of the number of cycles to failure is calculated. The average value of the number of cycles to failure is calculated by the formula:

$$\bar{H} = \sum_{j=1}^m x_j r_j / n = 168838,09, \text{ where } r_j - \text{the frequency of occurrence in the } j - \text{interval}$$

$$(n = \sum_{j=1}^m r_j m = 25 - \text{number of intervals}), x_j - \text{the average value in the indicated intervals}$$

[1], taken in physical values, since at large values the logarithm leads to a smoothing of the obtained values. The adjusted sample variance of the random variable was calculated –  $\mu_2 = 881264,14$ . The asymmetry coefficient was calculated –  $A_s = 1,6567$ . And excess coefficient was also calculated –  $E_s = 6,4757$ .

In [1], it is proposed to use the log-normal law of durability with a random variable –  $H$ , which distribution density has the formula [20]:

$$f(n; N_{0,5}; a; \sigma) = \frac{1}{(\eta - N_{0,5})\sqrt{2\pi\sigma}} e^{-\frac{[\ln(\frac{\eta - N_{0,5}}{2\sigma^2}) - a]^2}{2\sigma^2}}, \eta > N_{0,5}, \sigma > 0 \tag{1}$$

For this distribution law the expected values –  $M(N) = N_{0,5} + e^{a + \frac{\sigma^2}{2}}$ , variance –  $\mu_2 = e^{2a + \sigma^2} (e^{\sigma^2} - 1)$ , asymmetry coefficient –  $a_s = \sqrt{e^{\sigma^2} - 1} (e^{\sigma^2} + 2)$ .

Since for large samples, the numerical characteristics are stable and close to the theoretical numerical characteristics, we use the method of moments to estimate the parameters of the model (1).

We have a system:

$$\begin{cases} a_s = 1.6567, \\ \mu_2 = 881364.14, \\ M(H) = 168838.09. \end{cases} \tag{2}$$

It follows from the solution of system (2) that the parameters of the model (1):

$$\sigma^2 = 0.2299, \sigma = 0.4795, a = 12.0169 \text{ and } N_{0,5} = -16859.27$$

The negative value obtained  $N_{0,5}$  indicates that for the model (1) the left “tail” is very thin (the area of the curved triangle on the segment  $[N_{0,5}; 0]$  is equal  $0,9493 \cdot 10^{-6}$ ). Therefore, the statement about what  $N_{0,5} > 0$  is wrong if we assume that the distribution law is log-normal. For the law (1), there is a probability of obtaining  $N_{0,5} < 0$  for smaller ones  $S$ . This statement, what  $N_{0,5} > 0$  can be true only from physical considerations at certain loads on the sample, and not from the limitations of the experiment [21]. The model may be inadequate to the “true” and its estimates of the parameters may be unbiased or have a large variance.

The next step is to consider the proposed model in [7]. The distribution density of this model has the formula:

$$f(\eta; N_{0,5}; a; k; c) = \begin{cases} 0, \eta \notin (N_{0,5}, c) \\ \frac{1+k}{c - N_{0,5}} \left[ 1 - \left( \frac{\eta - a}{N_{0,5} - a} \right)^{\frac{1}{k}} \right], \eta \in [N_{0,5}, a] \\ \frac{1+k}{c - N_{0,5}} \left[ 1 - \left( \frac{\eta - a}{c - a} \right)^{\frac{1}{k}} \right], \eta \in (a, c] \end{cases} \tag{3}$$

where is  $a$  - the modal value,  $N_{0.5}$  - lower bound and  $c$  - upper bound,  $\eta, k$ - parameter of form.

To simplify the formula, we denote  $N_{0.5} = b$ . Then model (3) is defined, if  $k > 0$ ;  $k < -1$  where  $b < a < c$ . Moreover, when  $k < -1$  the value  $f(a)$  is unlimited, and when  $k > 0$  bounded, and when  $0 < k < 1$  the function  $f(\eta)$  is a smooth function, and when  $k \geq 1$  not smooth.

The mathematical expected value for the model (3):

$$M(H) = \frac{(b + c + 2ka + kb + kc)}{(4k + 2)},$$

Sample variance:

$$\mu_2 = \left( \frac{7b^2k^3 + 7k^3c^2 - 2bk^3c - 12bk^3a + 12k^3a^2 - 12ck^3a + 11b^2k^2 - 10bk^2c +}{+ 11k^2c^2 + 12k^2a^2 - 12bk^2a - 12ck^2a - 10bkc + 5kc^2 + 5b^2k + c^2 + b^2 - 2bc} \right) / \left( (12(3k + 1)(2k + 1))^2 \right) \tag{4}$$

Asymmetry and excess coefficients are rational functions of bulky parameters [10]. Therefore, they are not given.

Using the method of moments to estimate the parameters of model (3) according to the results of a sample from [1], we obtain:

$$k = -1.6520, N_{0.5} = -83406.41, a = 126943.42, c = 633374.52.$$

For model (3), the lower bound  $N_{0.5}$  is also negative, and the probability of obtaining a negative value of the lower bound is 0.0117.

So  $k < -1$ , then the straight line  $\eta = a$  is the equation of the vertical asymptote of the function  $f(\eta)$ . Cropping the value provided by the computer is enough to build a graph so that we can assume that the sum of the areas of the two cropped shapes is zero.

Plots of models (1) (Fig. 1) and (3) (Fig. 2) are constructed.

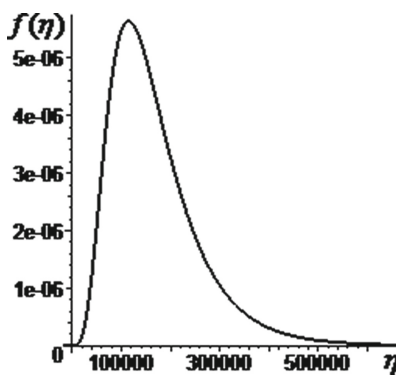


Fig. 1. The distribution density function of the model (1).

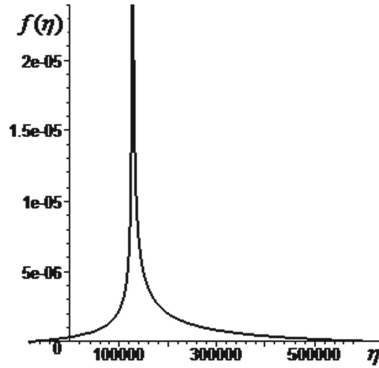


Fig. 2. The distribution density function of the model (3).

### 4 Results

Let's denote by  $F(\eta)$  and  $\tilde{F}(\eta)$ , respectively, the theoretical and empirical distribution functions of the random variable  $N$ . For model (1), this is determined using a special error function. The distribution function of the model (3) is not an elementary power function [22], like  $f(\eta)$ . Combining the three intervals at the beginning and four tables at the end [1] and adding empirical frequencies, we obtain for both models  $d\sqrt{n} < 1$ , where  $d = \max|F(\eta) - \tilde{F}(\eta)|$  for any  $\eta$ . It follows that the hypotheses about the laws (1) and (3) do not contradict the experimental data. It should be noted that consent does not always prove adequacy.

We used sensitive functional characteristics to model. Their form, established by experimental data, is one of the significant reasons for the proximity of the adequacy of the proposed model. One of these characteristics is the failure rate, which is « $\lambda$ -characteristic».

The theoretical « $\lambda$ -characteristic» is determined by the formula:  $\lambda(\eta) = f(\eta)/(1 - F(\eta))$ . The empirical « $\lambda$ -characteristic» was calculated by the formula [23]:  $(x_j) = r(x_j) / \left( \left[ n - \sum_{j=1}^{i-1} r(x_j) \right] (x_i - x_{i-1}) \right)$ , where  $r(x_j)$  is the number of failures in  $j$  interval. Graphs of theoretical and empirical « $\lambda$ -characteristic» were constructed for the model (1) (Fig. 3), and model (3) (Fig. 4).

The theoretical « $\lambda$ -characteristic» of the model (1) reaches its maximum value and monotonously decreases to zero, which is true from theoretical studies of the model (1) and which is physically impossible. The empirical « $\lambda$ -characteristic» of the model (1) shows that at first there is an increase in values, then these values decrease and increase again. Theoretical and empirical « $\lambda$ -characteristic» for the model (3) have the same tendency. At first, the values increase, then decrease and increase again. Note that at the end of the change in this characteristic the theoretical « $\lambda$ -characteristic» of the model (3) increases asymptotically to the value of the upper threshold of the number of cycles



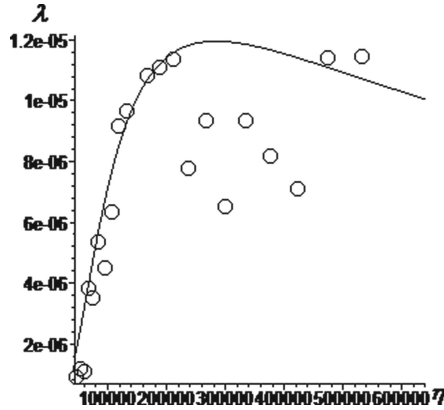


Fig. 3. Empirical and theoretical «λ-characteristic» for the model (1).

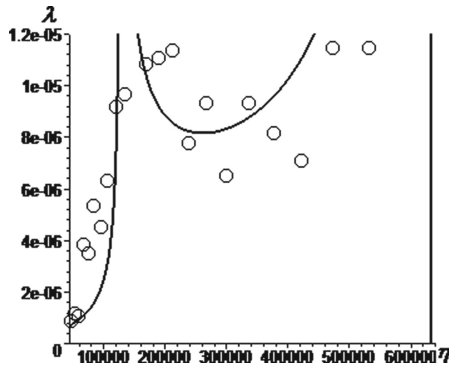


Fig. 4. Empirical and theoretical «λ-characteristic» for the model (3).

to failure. The «λ-characteristic» is the differential characteristic of the reliability function, and therefore less sensitive than the integral characteristic of the reliability function. An empirical sensitive characteristic is an empirical estimate of the average residual resource, especially in regards to the right «tail» of the distribution, where there is a sufficiently large spread, due to a decrease in the number of observations to obtain an estimate. For simplicity, we will call it «μ-characteristic» that is determined by the formula:  $\mu(\eta) = \int_{\eta}^{\infty} (1 - F(t)dt / (1 - F(\eta)))$ . Theoretical characteristics and empirical values were found at the points where the integral value was determined by the trapezoidal formula [24] for models (1) and (3).

Graphs of theoretical and empirical «μ-characteristic» were constructed for the model (1) (Fig. 5) and model (3) (Fig. 6).

From theoretical studies, it follows that «μ-characteristic» for small values is close to a linear dependence, what is observed for models (1) and (3).

For the theoretical model (1), the «μ-characteristic» monotonously decreases, and then monotonically increases to infinity, which is physically unfair. Empirical estimates

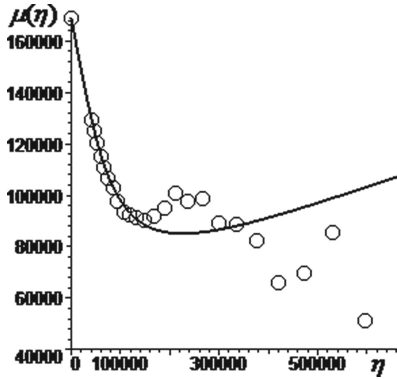


Fig. 5. Empirical and theoretical «μ-characteristic» for the model (1).

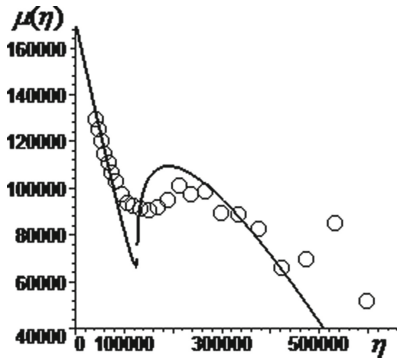


Fig. 6. Empirical and theoretical «μ-characteristic» for the model (3).

of the «μ-characteristic» indicate that at the beginning of the life of the sample the «extinction» of the weakest products takes place, then for the remaining ones, there is a slight «hardening» after which the «extinction» process begins again (Fig. 6). It can be seen that model (3) preserves the form of behavior - characteristics and shows a tendency to zero, which is physically natural. Note that in Fig. 4, 5, and 6, the intervals were not combined, which is used for the consent criteria. The last three empirical values obtained of the «μ-characteristic» have low accuracy since they have the largest intervals and the frequency of occurrence of each of the three is equal to one.

## 5 Conclusions

The undertaken researches bring to the following conclusions:

- It is not recommended to use the logarithmic law of the distribution of time to failure in the statistical processing of the results of fatigue tests. This has been proven using distribution-sensitive characteristics.

- The distribution model (3) is more suitable for calculation of operating time to failure during fatigue tests than the log-normal distribution.
- The statement from [1] that the lower bound of the operating time to failure is greater than zero can be false since the number of tests is limited. According to the proposed model, an estimate of the lower boundary gives a negative value.
- It is desirable to have not an interval of values of time to failure, but all the obtained values. This can provide more accurate estimates of model parameters and distribution-sensitive functional characteristics.






## References

1. Serensen, S., Kogaev, V., Stepnov, M., Hyacintov, V.: On the law of the distribution of durability during fatigue tests. *Factory Lab.* **3**, 324–329 (1958)
2. Mark, H.: How the Weibull Distribution Is Used in Reliability Engineering electronic resourcel. <https://www.allaboutcircuits.com/technical-articles/how-the-Weibull-distribution-is-used-in-reliability-engineering/>. Accessed 20 Dec 2019
3. Semrad, K., Cernan, J., Draganova, K.: Rolling contact fatigue life evaluation using Weibull distribution. *Mech. Mater. Sci. Eng.* **2**, 28–33 (2016)
4. Khan, M., King, R.: Transmuted modified Weibull distribution: a generalization of the modified Weibull probability distribution. *Eur. J. Pure Appl. Math.* **6**, 66–88 (2013)
5. Aryal, G.: Transmuted log-logistic distribution. *J. Stat. Appl. Probab.* **2**, 11–20 (2013)
6. Hady, A., Ebraheim, N.: Exponentiated transmuted Weibull distribution. A generalization of the Weibull distribution. *World Acad. Sci. Eng. Technol. Int. J. Math. Comput. Sci.* **8**, 903–911 (2014)
7. Lamnauer, N.: The model of the distribution of product sizes and its application for evaluating the accuracy of processing. *Bulletin of the National Technical University «Kharkiv Polytechnic Institute»*. Collection of scientific works. Series: Mathematical Modeling Engineering Technology **27**(98), 107 (2012)
8. Apam, B., Suleman, N., Adjei, E.: Lomax Weibull distribution. *Asian J. Probab. Stat.* **5**(3), 1–18 (2019)
9. Amal, H., Rokaya, M.: Weibull inverse lomax distribution. *Pakistan J. Stat. Oper. Res.* **15**(3), 587–603 (2019)
10. Ahmad, A., Ghazal, M.: Exponentiated additive Weibull distribution. *Reliab. Eng. Syst. Saf.* **193**, 1–12 (2020)
11. Elgarhy, M., Elbatal, I., Hamedani, G., Hassan, A.: On the exponentiated Weibull rayleigh distribution. *Gazi Univ. J. Sci.* **32**(3), 1060–1081 (2019)
12. Khan, M., King, R., Hudson, I.: Transmuted exponentiated Weibull distribution. *J. Appl. Probab. Stat.* **14**(2), 37–51 (2019)
13. Cordeiro, G., Ortega, E., Silva, G.: The Kumaraswamy modified Weibull distribution: Theory and applications. *J. Stat. Comput. Simul.* **84**(7), 1387–1411 (2014)
14. Provost, S., Saboor, A., Ahmad, M.: The Gamma-Weibull distribution. *Pak. J. Stat. Oper. Res.* **27**(2), 111–131 (2011)
15. Almalki, S., Yuan, J.: A new modified Weibull distribution. *Reliab. Eng. Syst. Saf.* **11**, 164–170 (2013)
16. Tahir, H., Cordeiro, M., Mansoor, M., Zubair, M.: The Weibull-Lomax distribution: properties and applications. *Hacetatepe J. Math. Stat.* **44**(2), 461–480 (2015)

17. Belodedenko, S.: Quantitative risk-analysis methods and mechanical systems safety. *Metall. Mining Ind.* **12**, 272–279 (2015)
18. Richard, H., Sander, M.: Crack initiation under cyclic loading. In: *Fatigue Crack Growth. Solid Mechanics and Its Applications*, vol. 227. pp. 239–250. Springer, Cham (2016)
19. Khamaza, L.: Generalized diagram of the ultimate nominal stresses (endurance limit) and the corresponding dimensions of the non-propagating fatigue cracks for sharp and blunt notches. *Strength Mater.* **51**, 350–360 (2019)
20. Levin, B.: *Handbook of reliability*, vol. 1. Mir, Moscow (1969)
21. Sozonov, Y., Shukailo, V.: Lower resource threshold for machine parts: scientific thought, pp. 131–132 (1982)
22. Lamnauer, N.: A general model for the distribution of linear part sizes and their application to improve product quality. *Bulletin of the National Technical University «Kharkiv Polytechnic Institute»*. Collection of scientific works. Series: *Mathematical Modeling in Engineering and Technology* **54**(1027), 134–143 (2013)
23. Kozlov, B., Ushakov, I.: Reference for the calculation of the reliability of electronics and automation equipment. *Soviet Radio*, p. 472 (1975)
24. Piskunov, N.: *Differential and integral calculus*, p. 456 (1985)



# Combined Thermo-Mechanical Techniques for Post-processing of the SLM-Printed Ni-Cr-Fe Alloy Parts

Dmytro Lesyk<sup>1</sup> , Silvia Martinez<sup>2</sup> , Oleksii Pedash<sup>3</sup> ,  
Vitaliy Dzhemelinskyi<sup>1</sup> , and Bohdan Mordyuk<sup>4</sup> 

<sup>1</sup> Laser Systems and Physical Technologies Department,  
National Technical University of Ukraine “Igor Sikorsky Kyiv Polytechnic  
Institute”, 37 Peremohy Ave., Kyiv 03056, Ukraine  
lesyk\_d@ukr.net

<sup>2</sup> Aeronautics Advanced Manufacturing Center, University of the Basque  
Country, 202 Bizkaia Science and Technology Park, 48170 Zamudio, Spain

<sup>3</sup> Metallurgical Engineers Department, MOTOR SICH JSC,  
15 Motorobudivnykiv Ave., Zaporizhzhia 69068, Ukraine

<sup>4</sup> Physical Principles for Surface Engineering Department,  
G.V. Kurdyumov Institute for Metal Physics of the NAS of Ukraine,  
36 Academician Vernadsky Blvd., Kyiv 03142, Ukraine

**Abstract.** The selective laser melting (SLM) is an additive manufacturing process applied to fabricate the metal parts owing to the melting of the metal powder in a layer by layer approach. The combined thermo-mechanical techniques for the post-processing of Ni-Cr-Fe alloy parts fabricated by the SLM process are proposed. In this study, the flat parts were fabricated using a nickel-based pre-alloyed Inconel 718 powder. The hot isostatic pressing (HIP) followed by homogenization (H) and/or aging (A) was carried out to modify the structure of the material and reduce the porosity. The shot peening (SP) and ultrasonic impact treatment (UIT) using a seven-pin impact head were applied to improve the surface texture parameters and stress state. The surface texture and hardness of the SLM-built and thermo-mechanical post-processed Inconel 718 specimens are studied and compared. Results indicated that the used mechanical surface treatments after heat treatments led to a further increase in the surface hardness and formation of a new surface microrelief. As compared to the SP process, the UIT process forms regular microrelief with smoother surface roughness and lower height profile parameters while the SP-induced surface hardness is higher than that of the UIT-processed specimen.

**Keywords:** Inconel 718 · Selective laser melting · Post-processing · Hot isostatic pressing · Homogenization · Aging · Shot peening · Ultrasonic impact treatment

## 1 Introduction

Manufacturing industries are always looking for improving techniques to lower cost, energy and expand their capability. Contrary to conventional manufacturing that often requires machining to remove superfluous material, additive manufacturing (AM) or

three-dimensional (3D) printing allows expanding manufacturing facility. By means of computer-aided design (CAD) or 3D object scanners, the metal components with precise geometric shapes can be created by AM techniques instead of conventional metal forming methods.

There are several advantages of AM processes. For example, metal 3D printing is a good approach for the manufacturing of complexly shaped parts that need to be strong and lightweight. Another significant benefit of 3D printing components is that metal AM wastes are less than 5% on average. Nevertheless, metal AM techniques still have some drawbacks. In particular, most 3D built-parts require post-processing to get the desired surface quality and properties of the material.

As a result, the development of new post-processing technologies is required to reduce or eliminate the superficial and volume defects in the metal AM parts.

## 2 Literature Review

Recently, the powder bed fusion, direct energy deposition, material extrusion, and binder or material jetting techniques have been developed to manufacture the 3D metal parts. In particular, the powder bed fusion process is implemented using a movable laser or electron beam, which selectively melts metal powder successively adding material layer by layer [1]. During the direct energy deposition, the metal wire or overblown metal powder is melted using a movable high-energy electron or a laser beam and selectively applied locally [2, 3]. The material extrusion process comprises a material drawing through a nozzle under constant pressure, its heating and further deposition layer by layer [4]. The binder jetting process involves one or more movable nozzles that are used to inject a liquid binder on the top of a powder bed, gluing the powder together [5].

The laser-based powder bed fusion technology, including selective laser melting (SLM) or electron beam melting (EBM) methods, is the most promising AM processes [1, 6]. The selective laser melting (SLM) process is one of the advanced manufacturing methods, which allows the production of the complexly shaped parts (material density is  $\sim 98\text{...}99\%$ ) by successive selective melting of the layers of metal powder on the top of the previous one using a scanning laser beam [7]. However, it should be also noted that the SLM-built components suffer from a relatively rough surface, residual sub-surface porosity, and tensile residual stress in the near-surface layers [8].

Currently, the thermal, mechanical, and chemical treatments may be used to improve the components fabricated by the SLM technique. The implementation of heat post-processing techniques in the AM routes, such as stress relieving (SR), hot isostatic pressing (HIP), solution (S) or homogenization (H), and aging (A) could minimize or eliminate only volume defects. In particular, the stress-relieving (SR) treatment is used before removing a part from the build plate. The HIP treatment is usually applied to eliminate porosity and increase the density of the material for critical applications where high fatigue/wear and corrosion resistance is required [9]. The solution (S), homogenization (H) and aging (A) treatments are applied for the improvement of material properties. The schematic representation of thermal cycles of the above-mentioned heat treatments is shown in Fig. 1.

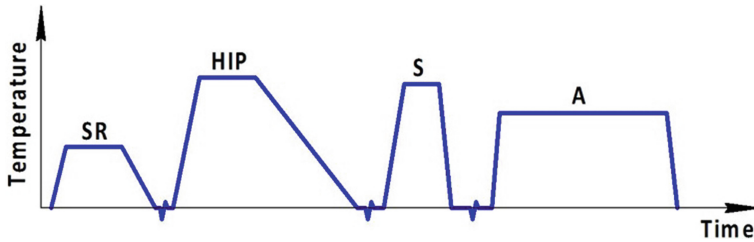


**Fig. 1.** Thermal cycle of stress relieving (SR), hot isostatic pressing (HIP), solution (S), and aging (A) processes.

Recently, various studies were carried out to explain the effects of heat post-processing techniques on the microstructure, porosity, hardness and residual stress in the SLM-built IN 718 alloy [7–9]. In particular, work by Kuo [9] shown that the HIP treatment followed by the direct aging process was the most effective technique among the heat treatments to improve the creep behaviour.

However, to improve the superficial properties in the metal parts fabricated by the SLM technique, the mechanical surface treatments combined with heat treatments should be applied. A barrel finishing [10], vibratory finishing [11], sandblasting [12], shot peening or water jet shot peening [12, 13], laser shock peening [14], cavitation peening [13], ultrasonic shot peening [15], ultrasonic nanocrystal surface modification [16], ultrasonic impact treatment [17, 18] are the most common mechanical post-processing techniques, which can be used in combination with heat treatments. The mechanical post-processing can be selected based on the operational requirements, geometry complexity, size of parts and required surface quality.

In the aviation and aerospace industries, it is known that the nickel and titanium alloys are widely used in high temperature. In particular, the nickel-based superalloys are an unusual class of metallic materials with an exceptional combination of high-temperature strength, toughness, and resistance to degradation in corrosive or oxidizing environments.

Work by Kim [15] shows that the USP process applied after the HIP treatment reduced the friction coefficient and wear resistance of USP-processed Ni-Cr-Fe alloy specimen as compared to polished specimen fabricated by direct metal laser sintering. It should also be noted that the HIP-treated Ti6Al4V alloy specimens after the ultrasonic surface mechanical attrition process provide significantly higher fatigue strength improvement as compared to that non-treated specimen manufactured by the SLM process [19]. At the same time, the attempts to use the shot peening and ultrasonic impact treatment combined with heat treatments to improve the surface layer properties of the SLM-printed Inconel (IN) alloy parts are virtually absent.

The purpose of this work is to develop the thermo-mechanical technique for the post-processing of Ni-Cr-Fe alloy parts fabricated by the SLM process. A study of the effects of the heat treatments followed by mechanical surface treatments on the surface texture and hardness of the SLM-built IN 718 parts is also addressed.

### 3 Research Methodology

The flat parts ( $40 \times 30 \times 3$  mm) were fabricated using a nickel-based pre-alloyed IN 718 powder with a particle size of  $10 \dots 55 \mu\text{m}$  (Fig. 1a). The chemical composition of the used powder is summarized in Table 1.

**Table 1.** Chemical composition of IN 718 powder.

Chemical composition (wt%)									
Ni	Cr	Nb	Mo	Ti	Al	C	Mn	Si	Fe
50–55	17–21	4.7–5.5	2.8–3.3	0.6–1.2	0.2–0.8	$\leq 0.08$	$\leq 0.35$	$\leq 0.35$	Balance

The selective laser melting (SLM) process was performed using an industrial Renishaw AM400 machine with a maximum build volume of  $248 \text{ mm} \times 248 \text{ mm} \times 285 \text{ mm}$  (Fig. 2a). The machine was equipped with a scanning optics (with a maximum scanning speed of  $7000 \text{ mm/s}$ ) and continuous wave ytterbium fiber laser with a maximum spot diameter of  $70 \mu\text{m}$  and laser power of  $400 \text{ W}$ . In particular, in this work, the turbine blade specimens were manufactured using a laser power of  $200 \text{ W}$  and a laser scanning speed of  $700 \text{ mm/s}$ . A multidirectional scanning strategy was used when the biaxial laser scanning patterns were rotated by  $67^\circ$  for each consecutive layer. The laser spot ( $70 \mu\text{m}$ ) was scanned in a single direction within  $5 \text{ mm}$  wide stripes. The SLM parameters were kept the same for all fabricated parts.

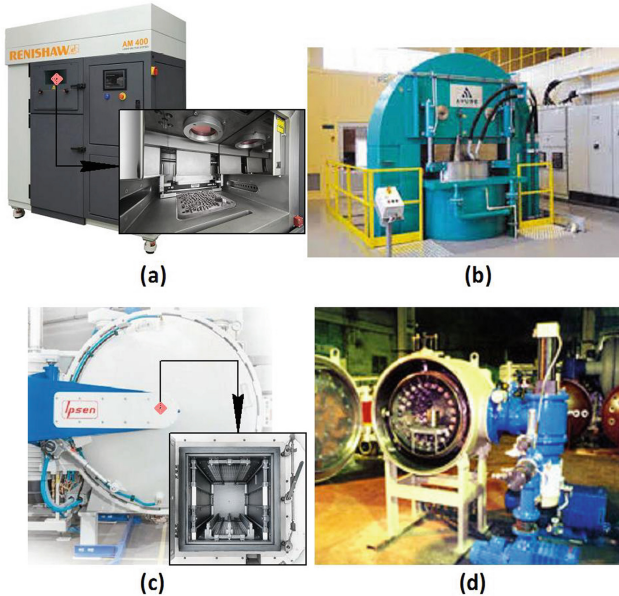


**Fig. 2.** General views of equipment for the SLM process (a), HIP treatment (b), the homogenization heat treatment (c), and aging heat treatment (d).



After the SLM process, to eliminate the internal porosity and increase the density of the material, all test SLM-built specimens were subjected to the HIP process per ASTM F3055 using a hot isostatic press QIH 0.9 x 1.5-2070-1400 MURC (Fig. 2b). The HIP treatment consisted of a heating temperature of 1160 °C and a pressure of 160 MPa for 3 h. To increase the cooling rate, the function of high-speed cooling was applied during the cooling of the specimens. After the HIP process, the HIP-processed specimens were subjected to both a double aging (A) process and homogenization (H) heat treatment followed by double aging heat treatment according to AMS 5662. In particular, the homogenization heat treatment of HIP-processed specimens was performed at the heating temperature of 1180 °C for 1 h using an IPSEN T2T vacuum furnace (Fig. 2c). The specimens were cooled in the furnace. The aging was carried out using an SNV 80 vacuum furnace at 720 °C for 8 h followed by furnace cooling to 620 °C and holding for 9 h (Fig. 2d). The cooling was performed in the furnace to 80 °C.

Two mechanical post-processing techniques, viz. the shot peening and ultrasonic impact treatment, were applied in the optimized parameters for surface treatment of heat-treated specimens (HIP+A, HIP+SA).

The shot peening (SP) treatment, which was implemented in this study at ambient temperature using industrial equipment, is known to produce severe plastic deformation of the treated surface due to the bombardment by metallic spherical shots (Fig. 3a). The SP process was implemented at a pressure of 0.55 MPa with a stand-off distance of ~20 mm for 1 min using steel balls of 0.5 mm diameter [20].

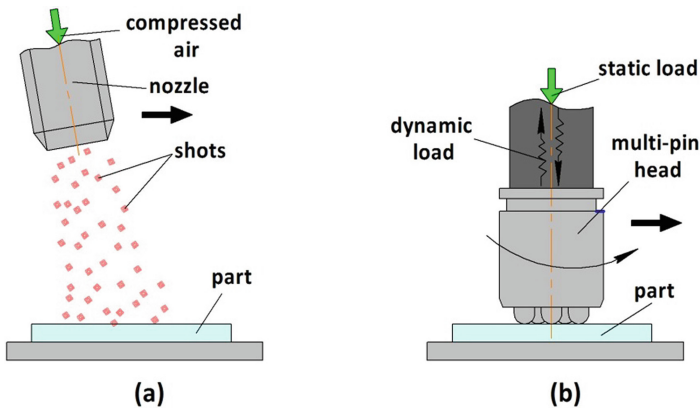


**Fig. 3.** Schemes of the SP (a) and UIT (b) processes.

The UIT of the SLM-built specimens also results in severe plastic deformation of the near-surface layers. A scheme of the UIT process using a multi-pin impact head is shown in Fig. 3b. The UIT equipment contained an ultrasonic generator with a frequency of 21.6 kHz, an acoustic vibration system with a piezoceramic transducer, a step-like horn, and a multi-pin impact head [21]. The high-frequency impacts ( $1 \pm 0.5$  kHz) were produced by seven cylindrical pins of 5 mm in diameter

positioned in the head that was forcedly rotated during the treatment (rotation speed of 76 rpm) to provide the lateral component of the load. The UIT duration was 2 min, the amplitude of the ultrasonic horn was  $\sim 18 \mu\text{m}$ , a static load on the acoustic system was 50 N, and a specimen feed rate was 600 mm/min.

The surface texture was studied using a 3D Taylor Hobson Form Talysurf 120 profilometer. The surface hardness of each specimen was registered using a hardness tester DIA TESTOR 2Rc at a load of 10 kgf ( $\text{HV}_{10}$ ). In all cases, a total of five measurements were carried out at different treated zones and the averaged magnitude was reported. The scatter of the experimental data was not exceeded by 2...5%.

## 4 Results

### 4.1 Surface Texture

The surface texture was characterized by the maximum height ( $S_z$ ) of the roughness profile curve according to ISO 25178 (Figs. 4 and 5).

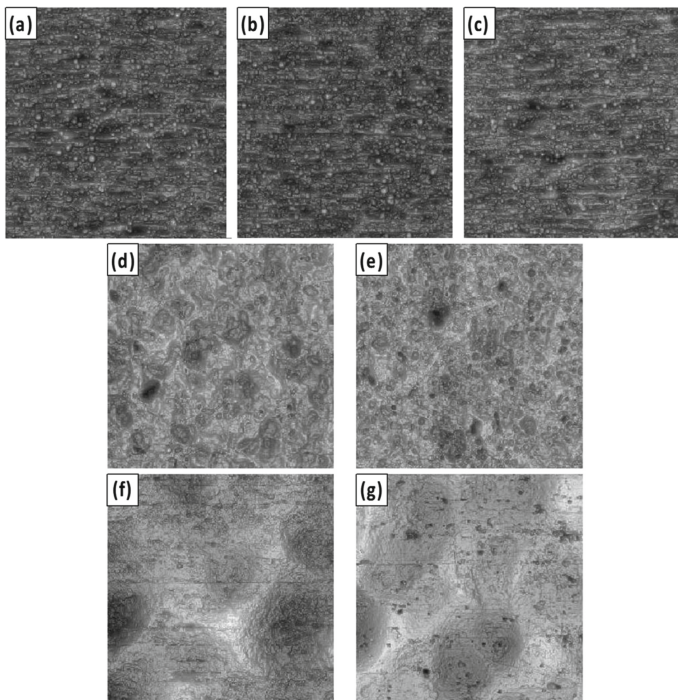


**Fig. 4.** Surface texture of the SLM-built (a) and HIP+HA (b), HIP+A (c), HIP+HA+SP (d), HIP+A+SP (e), HIP+HA+UIT (f), HIP+A+UIT (g) processed IN 718 specimens.

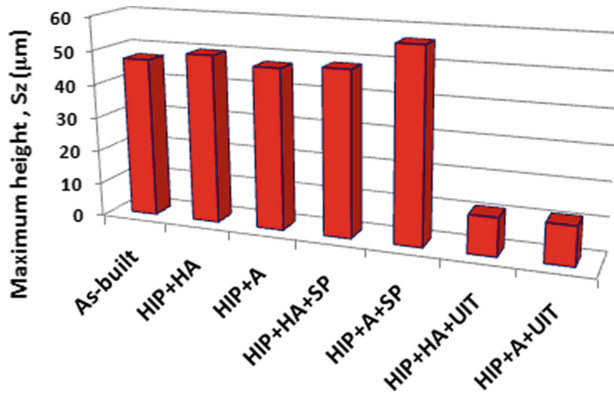


**Fig. 5.** Surface roughness profile maximum height magnitudes of the SLM-built and HIP+HA, HIP+A, HIP+HA+SP, HIP+A+SP, HIP+HA+UIT, HIP+A+UIT processed IN 718 specimens.

The maximum height parameter of SLM-built specimen is relatively high due to a large number of manufacturing surface defects, such as ellipsoidal and spherical balls, partially melted powder particles or spatters, open pores, as well as signs of the laser tracks (Fig. 4a). In particular, the  $S_z$  parameter is  $\sim 47 \mu\text{m}$  (Fig. 5). As compared to the  $S_z$  parameter of the SLM-built specimen, the heat treatments (HIP+HA, HIP+A) did not change the geometry of the treated surface (Fig. 4b, c).

Both shot peening and ultrasonic impact treatment after heat treatments led to a significant change in the shape of the profile/topography of the surfaces and formed a new wavy microrelief (Fig. 4d–g). As compared to the SP process ( $S_z = \sim 50 \mu\text{m}$ ), the UIT process forms regular microrelief with smoother surface roughness (the  $S_z$  parameter is  $\sim 11 \mu\text{m}$ ) and lower surface waviness owing to the application of the multi-pin ultrasonic tool, which produces the sliding impacts of pins by the specimen surface due to forced rotation of the impact head [21, 22].

As seen in Fig. 5, a remarkable reduction in the  $S_z$  parameter was observed after the UIT process as compared to those registered after the HIP+HA and HIP+A processes. In our experimental conditions, in comparison with the HIP+HA and HIP+A treated specimens the  $S_z$  parameter of the UIT-processed specimens were respectively decreased by 77.4% and 75.9%.

## 4.2 Surface Hardness

The surface hardness after the application of different post-processing techniques is shown in Fig. 6. The surface hardness of the SLM-built specimen ( $32.2 \text{ HRC}_{10}$ ) is increased after the application of all post-processing techniques. It is seen that as compared to the hardness of the SLM-built specimen, the HIP+HA, and HIP+A heat treatments led to the hardening via the formation of an equiaxed-grains structure with strengthening precipitates instead of a fine columnar-dendrite microstructure [7–9, 23]. The hardness of the surface layers of the HIP+HA and HIP+A processed specimens are higher than that of the SLM-built specimen by  $\sim 35\%$ .

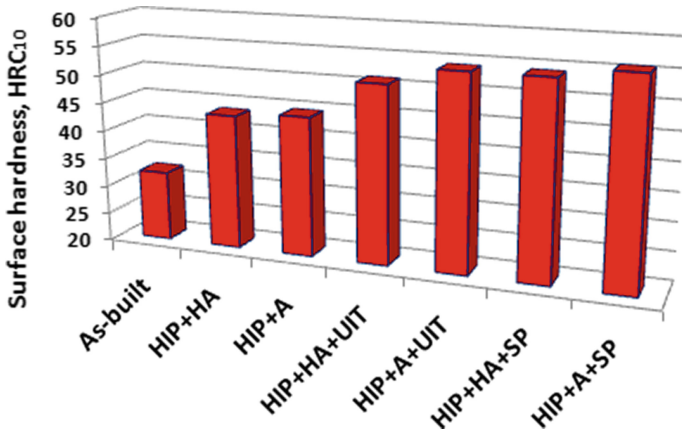


**Fig. 6.** The surface hardness of the SLM-built and HIP+HA, HIP+A, HIP+HA+SP, HIP+A+SP, HIP+HA+UIT, HIP+A+UIT processed IN 718 specimens.

It should be also noted that mechanical surface treatments after heat treatments led to a further increase in surface hardness. In comparison with the HIP+HA and HIP+A processed specimens, the surface hardness in the near-surface was increased by ~20% after the UIT process, while the SP-induced surface hardness (by ~25%) is slightly higher than that of the UIT-processed specimen.

Thus, the surface hardness increased by thermo-mechanical post-processing techniques in combination with the formed surface microrelief accompanied by the lower roughness profile parameters (Table 2) is expected to provide the enhancement in the fatigue life and corrosion/wear resistance of the Ni-Cr-Fe alloy parts fabricated by the SLM process.

**Table 2.** Surface texture parameters and hardness.

	Treatment						
	SLM-built	HIP+HA	HIP+A	HIP+HA+UIT	HIP+A+UIT	HIP+HA+SP	HIP+A+SP
Surface texture parameters ( $\mu\text{m}$ )							
<i>S<sub>a</sub></i>	3.79	4.20	3.73	1.19	0.72	3.26	3.41
<i>S<sub>p</sub></i>	29.1	31.3	26.6	5.46	6.74	21.6	23.2
<i>S<sub>v</sub></i>	18.0	18.4	20.8	5.71	4.69	26.9	33.3
<i>S<sub>z</sub></i>	47.1	49.7	47.4	11.2	11.4	48.5	56.5
Surface hardness (HRC <sub>10</sub> )							
	32.2	43.6	44.5	51.1	54.1	54.1	55.7

The type of an appropriate mechanical post-processing technique can be chosen based on the analysis of the shape and dimensions of the part to be treated [24]. The SP

(or sandblasting, laser shock peening, cavitation peening, barrel finishing) processes are rather controllable and flexible for surface treatment both small-sized and large-scale SLM-built parts.

## 5 Conclusions

The combined thermo-mechanical techniques applied in this study to improve the IN 718 alloy parts fabricated by the SLM process. The following conclusions can be drawn:

1. The combined thermo-mechanical techniques for post-processing both complexly shaped (SP) and large-scale (SP, UIT) or small-sized (SP) Ni-Cr-Fe alloy parts fabricated by the SLM process are proposed.
2. As compared to the surface roughness maximum height magnitudes ( $S_z \approx 47 \mu\text{m}$ ) of the SLM-built specimen, the HIP+HA and HIP+A processes did not change the geometry of the treated surface.
3. The SP and UIT processes after heat treatments (HIP+HA and HIP+A) led to a significant change in the shape of the surface profile and formed a new wavy microrelief. The UIT process forms regular microrelief with the smoother surface (the  $S_z$  parameter is about  $11 \mu\text{m}$ ) and lower surface waviness as compared to that produced by the SP process ( $S_z \approx 50 \mu\text{m}$ ).
4. The surface hardness of the SLM-specimen (32.2 HRC<sub>10</sub>) was increased after the HIP+HA and HIP+A treatments by about 35%. The heat treatments followed by mechanical surface treatments increased surface hardness by about 20–25%. As compared to the SLM-specimen, the combined treatment increased the surface hardness by 60...70%.

**Acknowledgments.** The authors would like to acknowledge S. Faust (Otto von Guericke University Magdeburg, Germany) for the surface topography measurements.

## References

1. Fousova, M., et al.: Influence of inherent surface and internal defects on mechanical properties of additively manufactured Ti6Al4V alloy: comparison between selective laser melting and electron beam melting. *Materials* **11**, 537 (2018)
2. Herzog, D., et al.: Additive manufacturing of metals. *Acta Mater.* **177**, 371–392 (2016)
3. Renderos, M., et al.: Microstructure characterization of recycled IN718 powder and resulting laser clad material. *Mater. Character.* **134**, 103–113 (2017)
4. Gonzalez-Gutierrez, J., et al.: Additive manufacturing of metallic and ceramic components by the material extrusion of highly-filled polymers: a review and future perspectives. *Mater.* **11**, 840 (2018)
5. Zhang, Y., et al.: Additive manufacturing of metallic materials: a review. *J. Mater. Eng. Perform.* **27**, 1–13 (2018)
6. Pereira, T., et al.: A comparison of traditional manufacturing vs additive manufacturing, the best method for the job. *Proc. Manuf.* **30**, 11–18 (2019)

7. Tucho, W.M., et al.: Microstructure and hardness studies of Inconel 718 manufactured by selective laser melting before and after solution heat treatment. *Mater. Sci. Eng. A* **689**, 220–232 (2017)
8. Raghavan, R., et al.: Effect of different heat treatments on the microstructure and mechanical properties in selective laser melting INCONEL 718 alloy. *Mater. Manuf. Process.* **32**, 1588–1595 (2017)
9. Kuo, Y.-L., et al.: The effect of post-processes on the microstructure and creep properties of alloy 718 built up by selective laser melting: a review. *Materials* **11**, 996 (2018)
10. Boschetto, A., et al.: Surface roughness and radiusing of Ti6Al4V selective laser melting-manufactured parts conditioned by barrel finishing. *Int. J. Adv. Manuf. Technol.* **94**, 2773–2790 (2018)
11. Bankowski, D., et al.: Vibratory machining effect on the properties of the aluminum alloys surface. *Arch. Foundry Eng.* **17**, 19–24 (2017)
12. Bagherifard, C.S., et al.: On the fatigue strength enhancement of additive manufactured AlSi10Mg parts by mechanical and thermal post-processing. *Mater. Des.* **145**, 28–41 (2018)
13. Soyama, H., et al.: The use of various peening methods to improve the fatigue strength of titanium alloy Ti6Al4V manufactured by electron beam melting. *AIMS Mater. Sci.* **5**, 1000–1015 (2018)
14. Sealy, M.P., et al.: Fatigue performance of biodegradable magnesium–calcium alloy processed by laser shock peening for orthopedic implants. *Int. J. Fatigue* **82**, 428–436 (2016)
15. Kim, J.D., et al.: Mechanical and tribological characteristics of sintered Fe-Ni-Cr alloy subjected to high-frequency ultrasonic peening. *Int. J. Surf. Sci. Eng.* **8**, 239–254 (2014)
16. Xing, X., et al.: Ultrasonic peening treatment used to improve stress corrosion resistance of AlSi10Mg components fabricated using selective laser melting. *Metals* **9**, 103–111 (2019)
17. Lesyk, D.A., et al.: Post-processing of the Inconel 718 alloy parts fabricated by selective laser melting: effects of mechanical surface treatments on surface topography, porosity, hardness and residual stress. *Surf. Coat. Technol.* **381**, 125136 (2020)
18. Zhang, M., et al.: Residual stress, defects and grain morphology of Ti-6Al-4V alloy produced by ultrasonic impact treatment assisted selective laser melting. *Appl. Sci.* **6**, 304–311 (2016)
19. Yan, X., et al.: Fatigue strength improvement of selective laser melted Ti6Al4V using ultrasonic surface mechanical attrition. *Mater. Res. Lett.* **7**, 327–333 (2019)
20. Lesyk, D.A., et al.: Surface finishing of complexly shaped parts fabricated by selective laser melting. In: Grabchenko's International Conference on Advanced Manufacturing Processes. InterPartner-2019. Lecture Notes Mechanical Engineering, pp. 186–195. Springer, Cham (2018)
21. Lesyk, D.A., et al.: Surface micror relief and hardness of laser hardened and ultrasonically peened AISI D2 tool steel. *Surf. Coat. Technol.* **278**, 108–120 (2015)
22. Lesyk, D.A., et al.: Effects of laser heat treatment combined with ultrasonic impact treatment on the surface topography and hardness of carbon steel AISI 1045. *Opt. Laser Technol.* **111**, 424–438 (2019)
23. Seede, R., et al.: Microstructural and microhardness evolution from homogenization and hot isostatic pressing on selective laser melted Inconel 718: structure, texture, and phases. *Manuf. Mater. Process.* **2**, 30 (2018)
24. Lesyk, D.A., et al.: Surface finishing of complexly shaped parts fabricated by selective laser melting. In: Grabchenko's International Conference on Advanced Manufacturing Processes. InterPartner-2019, pp. 186–195. LNME, Cham (2020)



# Theoretical Analysis of Conditions for Improving Gear Grinding Accuracy and Productivity

Fedir Novikov<sup>1</sup> , Vladimir Polyansky<sup>2</sup> , Igor Riabenkov<sup>3</sup> ,  
Andrii Hutorov<sup>4</sup> , and Oksana Yermolenko<sup>1</sup> 

<sup>1</sup> Simon Kuznets Kharkiv National University of Economics,  
9A Nauky Ave., Kharkiv 61166, Ukraine  
fokusnicl@rambler.ru

<sup>2</sup> LLC “Empire Metals”, 88 Grygorivske Rd., Kharkiv 61020, Ukraine

<sup>3</sup> Kharkiv Petro Vasylenko National Technical University of Agriculture,  
44 Alchevskyyh St., Kharkiv 61002, Ukraine

<sup>4</sup> NSC “Institute of Agrarian Economics”,  
10 Heroiv Oborony St., Kyiv 03127, Ukraine

**Abstract.** The aim of this study is a theoretical substantiation of the possibilities for increasing accuracy and productivity in gear grinding and determining the optimal machining conditions based on the reduction of elastic displacements arising in the technological system. The expediency of gear grinding using the profile copy method is shown based on a theoretical analysis of the conditions for increasing the accuracy and productivity of gear grinding operations. Compared to the traditional milling, this method has more significant technological capabilities in terms of improving the accuracy and productivity of machining. This machining effect appears while implementing the dead-stop grinding, which provides a significant reduction in elastic displacements that occur in the technological system due to the uneven removed stock. In this case, the main part of stock removal is carried out in terms of high-performance deep grinding. For the implementation of gear grinding using the profile copy method, an analytical ratio has been obtained to determine the lateral feed elastic displacement that occurs after each wheel pass. Using this ratio allows achieving high machining productivity with the required accuracy. It has also been found out that it is possible to increase the machining accuracy and productivity during milling by increasing the refinement of the wheel pass by reducing the conditional cutting stress. This can be achieved by using high porosity grinding wheels, providing a decrease in the friction intensity in the cutting zone due to their high cutting ability.

**Keywords:** Abrasive wheel · Dead-stop grinding scheme · Elastic displacement

## 1 Introduction

Gear grinding is the final operation of the gear teeth machining, providing high accuracy and quality of the finished surfaces. Traditionally, gear grinding operations are carried out by the milling method in milling cutters. Using high porosity abrasive wheels can significantly reduce the power and thermal tension of gear grinding; eliminate the formation of thermal damage, microcracks and other temperature defects on the finished surfaces. However, the machining productivity is relatively low, and in practice that leads to forcing cutting conditions, and as a result, decreasing the accuracy and quality of the machined surfaces. Therefore, instead of milling, gear grinding technology using the profile copy method is being increasingly used, implementing a scheme of high-performance deep grinding. In this case, the stock removal is carried out in one or several passes of the grinding wheel, which reduces the additional machining time for a rotary table in comparison with gear grinding in milling cutters. The main disadvantage of this gear grinding technology is the relatively low machining accuracy, which is mainly due to the uneven removed stock on both sides of the grinding wheel. The reason for this is the occurrence of thermoelastic deformations of the teeth during its thermal or/and chemical treatment and improper wheel installation in the machined gear wheel space. As a result, elastic displacements occur in the technological system, causing machining errors. In addition, uneven removed stock leads to increased thermal tension during grinding, as well as to the occurrence of temperature defects on the machined surfaces which requires a reduction in machining productivity. Regarding this, it is necessary to theoretically substantiate the conditions for increasing the efficiency of the gear grinding technology using the profile copy method.

## 2 Literature Review

The studies of gear grinding rules by the profile copy method have been paid less attention than the milling method in the scientific and technical literature [1, 2]. Meanwhile, the published works [3–5] revealed significant technological capabilities of this progressive gear grinding technology, which is implemented most fully on modern CNC gear grinding machines. In the work [6] we can see that specific example show the feasibility of measuring the accuracy parameters of machined gears using a coordinate measuring machine, which provides more accurate adjustment of the gear grinding machine and thereby reduces processing errors. However, there is no theoretical analysis of the conditions for increasing the accuracy and machining parameters in these works, which does not allow to provide a scientifically substantiated selection of rational gear grinding parameters. There are no theoretical solutions defining ways to increase the accuracy and processing parameters to a level that exceeds the level achieved by gear grinding using the rolling method.

Particularly valuable is the work [7] devoted to gear hobbling at finishing operations; however, it does not provide a comparison of this technology with modern gear grinding technologies.



The work [8] is devoted to the analytical determination of the cutting force during grinding and turbine blade machining. Nevertheless, it gives no calculation and analysis of elastic displacements that occur in the technological system under the influence of cutting forces, which, as a rule, predetermine the parameters of machining accuracy during gear grinding. The same conclusion can be made regarding the works [9, 10] devoted to the experimental determination of the cutting force during grinding and turbine blade machining.

It should be outlined that much less attention is paid to the studies of the power tension parameters during gear grinding than to the studies of the heat tension parameters and the search for ways to reduce the cutting temperature [11–13]. This is since gear grinding needs increased contact area of the wheel with the workpiece and it features increased cutting temperature. As a result, thermal damage and microcracks formation tend to increase in number on the machined surfaces, reducing the quality of machining.

### 3 Research Methodology

The analysis of literature showed no analytical ratio for determining the accuracy parameters of gear grinding connected to the occurrence of elastic displacements in the technological system. Thus, the distinctive features of the formation of machining errors are not substantiated theoretically during gear grinding using the profile copy and milling methods. This does not allow to reveal the potential technological capabilities of these gear grinding methods and theoretically determine the optimal machining conditions that provide a significant increase in accuracy and productivity. Therefore, our task is to mathematically describe the patterns of elastic displacements formation that occurs in the technological system during gear grinding using the profile copy and milling methods. It is necessary to establish the analytical relationship between the magnitude of the elastic displacement and the main processing time, and determine the most productive gear grinding method, taking into account the limitations on processing accuracy further. Also, there is a need to justify the optimal processing conditions on this basis, including the parameters of the grinding mode and the number of passes of the wheel. In this case, the processing accuracy is determined by the amount of elastic displacement: when it is smaller, then the processing accuracy is higher.

In work [14], a theoretical approach to optimizing gear grinding parameters by the profile copy method was proposed. Based on it, the optimal machining route is determined, consisting of 4 wheel passes when removing stock  $P = 0.4$  mm per side. The first pass is supposed to remove the main part of the stock (0.37 mm), and subsequent passes remove 0.01 mm per each pass. It was found out experimentally that such a route provides high machining productivity, but reduces machining accuracy. This takes place because with each subsequent wheel pass, due to a decrease in elastic displacements, the width of the space between the machined teeth increases, exceeding the permissible value. The gear space is broken down, which reduces machining accuracy. Under these conditions, the resulting machining errors can be eliminated by feeding the grinding wheel after each pass to the appropriate value.

To determine this feed value, it is advisable to study initially the changing nature in the elastic displacement  $y$  that occurs in the technological system in multi-pass grinding (for  $n$  passes of the grinding wheel) according to the dead-stop grinding scheme based on analytical dependencies [15]:  $y = P_y/c = P_z/(c \cdot K)$ , where  $c$  is a given rigidity of the technological system, N/m;  $K = P_z/P_y$  is a grinding coefficient;  $P_z, P_y$  is tangential and radial components of the cutting force, N.

Reporting in terms of  $P_z = \sigma \cdot F$ , the relationship between the elastic displacements  $y_n$  and  $y_{n-1}$  arising on the  $n$ -th and  $(n - 1)$ -th passes of the grinding wheel is established by the formula (1):

$$y_n = \frac{y_{n-1}}{\varepsilon} = \frac{t}{\varepsilon^n}, \tag{1}$$

where  $\sigma$  is the conditional cutting stress, N/m<sup>2</sup>;  $F = Q/V_c$  is the total instantaneous cross-sectional area of a slice of ganged grains of a grinding wheel, m<sup>2</sup>;  $Q = B_1 \cdot t \cdot V_{det}$  is the processing performance, m<sup>3</sup>/s;  $B_1$  is the grinding width, m;  $t$  is the grinding depth, m;  $V_c, V_{det}$  is the speed of a wheel and a workpiece, m/s;  $\varepsilon = \frac{c \cdot K \cdot V_c}{\sigma \cdot B_1 \cdot V_{det}}$  is the refinement of a wheel pass.

The total refinement of  $\varepsilon_0$  is equal to:

$$\varepsilon_0 = \frac{t}{y_n} = \varepsilon^n. \tag{2}$$

The larger the values of  $t$  and  $\varepsilon$ , the smaller the number of passes of the wheel  $n$ , the given value  $y_n$  can be achieved, which determines the machining error. Nevertheless, the main condition for increasing the refinement in the wheel pass  $\varepsilon$  is a decrease in the workpiece speed  $V_{det}$ . However, this leads to an increase in the main machining time  $\tau$ . Therefore, it is necessary to determine the optimal values of  $n$  and  $V_{det}$  at which the main machining time  $\tau$  takes the smallest value. Representing  $\tau = n \cdot L/V_{det}$  and

resolving the ratio  $\varepsilon = \frac{c \cdot K \cdot V_c}{\sigma \cdot B_1 \cdot V_{det}}$  to the workpiece speed  $V_{det}$ , we obtain:

$$\tau = \frac{n \cdot L \cdot \sigma \cdot B_1}{c \cdot K \cdot V_c} \cdot \sqrt[n]{\varepsilon_0}, \tag{3}$$

where  $L$  is the stroke length of the machine table, m.

It follows according to the ratio (3) that there is an extremum of the function  $\tau$  on  $n$ . Subordinating the ratio (3) to the necessary condition for the extremum ( $\tau'_n = 0$ ), we obtained  $\varepsilon_0 = e^n, n = \ln \varepsilon_0$ , respectively. The second derivative  $\tau''_n$  at the extremum of the function  $\tau$  is positive. Therefore, the minimum of the function  $\tau$  is realized, at which the refinement of the wheel pass  $\varepsilon$  is equal to the number  $e \approx 2.72$ .

The optimal workpiece speed  $V_{det}$  is determined by the ratio as follows:

$$V_{det} = \frac{c \cdot K \cdot V_c}{\sigma \cdot B_1 \cdot e} \tag{4}$$

It is possible to increase the workpiece speed  $V_{det}$  and, accordingly, reduce the main machining time  $\tau$  by decreasing the parameters  $\sigma$ ,  $B_1$  and increasing  $c$ ,  $K$ ,  $V_c$ . This is achieved mainly when using high porosity, impregnated and intermittent grinding wheels [15–19], featuring high cutting ability and providing a decrease in the friction intensity in the cutting zone.

It should be outlined that the patterns of change in the elastic displacement that occur under the conditions of an optimal dead-stop grinding scheme ( $\varepsilon = e$ ) are described by an analytical ratio:  $y_n = t \cdot e^{-n} = t \cdot e^{-\frac{V_{det}}{t} \tau}$ .

Therefore, over the machining time  $\tau$ , the value of  $y_n$  decreases exponentially, which corresponds to the known experimental data [15]. Thus, the dead-stop grinding scheme, due to the presence of an elastic system of the grinding machine, automatically implements the optimal grinding cycle with a refinement of  $\varepsilon = e \approx 2.72$ . This explains the high efficiency of applying the dead-stop grinding scheme in grinding to solve practical problems of ensuring high accuracy and machining productivity.

The drawn theoretical solutions were used to justify the technological possibilities of increasing accuracy and productivity during gear grinding, as well as when choosing the most productive gear grinding method and determining optimal processing conditions.

## 4 Results

When gear grinding using the profile copy method, the ratio for determining the amount of elastic displacement for various grinding wheel passes is as follows:

$$y_n = \frac{\Delta_0}{e^n}, \tag{5}$$

where  $\Delta_0$  is the displacement of the cone wheel axis relative to the gear space axis, m;

$\varepsilon = \frac{c \cdot K \cdot V_c}{2 \cdot \sigma \cdot B \cdot \cos \frac{\alpha}{2} \cdot S_0}$  is the refinement of a wheel pass;  $B_1$  is grinding width, m;  $\alpha$  is

the angle at the apex of the cone wheel;  $S_0$  is the longitudinal feed rate made by the grinding wheel along the tooth being machined, m/s.

The optimal longitudinal feed rate  $S_0$  is determined by:

$$S_0 = \frac{c \cdot K \cdot V_c}{2 \cdot \sigma \cdot B \cdot \cos \frac{\alpha}{2} \cdot e} \tag{6}$$

In this case, as with grinding according to the dead-stop grinding scheme, the optimal refinement value is  $\varepsilon = e \approx 2.72$ . Therefore, the technology of gear grinding using the profile copy method allows implementing the dead-stop grinding scheme, which is most effective from the viewpoint of ensuring high accuracy machining. In this instance, increasing the longitudinal feed rate  $S_0$ , according to the ratio (6), and reducing the main machining time  $\tau$  is possible due to decreasing  $\sigma$ ,  $B$ ,  $\alpha$  and increasing  $c$ ,  $K$ ,  $V_c$ .

To achieve the specified machining accuracy by eliminating the breakdown of the gear wheel space, it is necessary to feed the grinding wheel  $S_l$  after each double pass by a certain value  $S_{l,n}$  (Fig. 1).

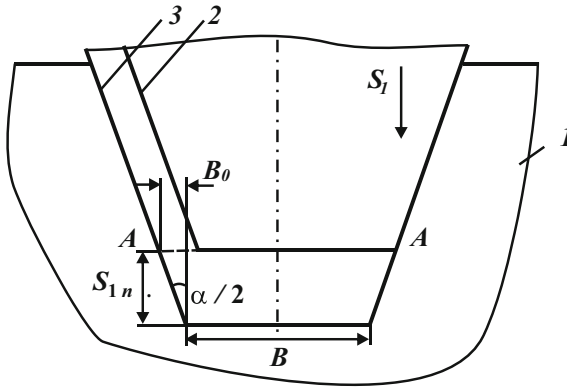


**Fig. 1.** The calculation scheme of gear grinding parameters using the profile copy method: 1 – gear; 2, 3 – grinding wheel positions at  $(n - 1)$  and  $n$  passes.

When calculating it, it is necessary to take into account the elastic displacement  $y_{n-1}$  that occurs in the technological system at the previous pass of the grinding wheel (in section A–A, see Fig. 1):

$$B + y_{n-1} = B + 2 \cdot B_0, \tag{7}$$

where  $B_0 = S_{1,n}/\text{tg}(\alpha/2)$  is the width of the grinding wheel cone portion at section level A–A, m;  $B$  is the width of the wheel’s peripheral part, m.

We get as follows:

$$y_{n-1} = \frac{2 \cdot S_{1,n}}{\text{tg} \frac{\alpha}{2}}. \tag{8}$$

According to the ratio (8), it follows that the transverse feed  $S_{l,n}$  is less than the elastic displacement  $y_{n-1}$ , since  $B_0 = S_{1,n}/\text{tg}(\alpha/2)$ . Therefore, in grinding, it is necessary to finely adjust the transverse feed  $S_{l,n}$  at each double pass of the grinding wheel, since it will vary within a few microns at the given machining error, for

example, 10  $\mu\text{m}$ . Failing to follow this condition will not ensure the required machining accuracy. As a result, there will be a breakdown of the gear wheel machined space, which is observed when using the gear grinding technology using the profile copy method.

When using gear grinding technology by the milling method, the stock on each side of the tooth being machined is removed separately by the end of the cup wheel according to the rigid multi-pass grinding scheme. So, the patterns of the elastic displacements formation that occur in the technological system by wheel passes are described as follows:

$$y_n = \frac{t}{\varepsilon} + \frac{t}{\varepsilon^2} + \dots + \frac{t}{\varepsilon^n} = \frac{SR}{n} \cdot \frac{(1 - \varepsilon^{-n})}{(\varepsilon - 1)}, \quad (9)$$

where  $t = SR/n$  – is the grinding depth, m;  $SR$  – is the stock removed, m;  $\varepsilon = \frac{c \cdot K \cdot V_c}{\sigma \cdot B_1 \cdot S_0}$  is the refinement of a wheel pass.

With an increase in the number of wheels passes  $n$ , the value of the elastic displacement  $y_n$  increases according to the law of geometric progression. Therefore, to ensure the given machining accuracy, it is necessary to make additional dead-stop wheel passes, which reduces productivity. From this viewpoint, the use of gear grinding using the profile copy method is more effective, because after several wheels pass, a dead-stop grinding scheme is implemented that allows maximum productivity with the given machining accuracy.

Based on the ratio (9), the elastic displacement change nature follows a more complex pattern than when grinding using the dead-stop grinding scheme, which is realized under gear grinding using the profile copy method, where  $\varepsilon_0 = \varepsilon^n = e^n$ . The elastic displacement  $y_n$  can be reduced by increasing  $n$  and  $\varepsilon$  values. However, the increase in  $n$  decreases machining productivity. The increase in the refinement of a wheel pass  $\varepsilon$  by reducing the longitudinal feed rate  $S_0$  also reduces machining productivity. Therefore, the main way to reduce  $y_n$  is to increase the refinement of a wheel pass  $\varepsilon$  by reducing the  $\sigma/K$  ratio and increasing the parameters  $c$  and  $V_c$ , which do not affect the machining productivity directly. For the practical implementation of these conditions, it is advisable to use grinding wheels with high cutting ability, as well as effective grinding methods.

It should be emphasized that when gear grinding using the milling method, i.e. when using multi-pass grinding, the grinding depth  $t$  has to be reduced and the longitudinal feed rate  $S_0$  has to be increased. This leads to a decrease in the refinement  $\varepsilon$ , however, it is not so efficient for reducing the elastic displacement  $y_n$  and machining errors.

When gear grinding according to the profile copy method which implements the deep grinding conditions, it is, on the contrary, necessary to increase the grinding depth  $t$  and reduce the longitudinal feed rate  $S_0$ . This automatically leads to an increase in the refinement of a wheel pass  $\varepsilon$ , to a decrease in the elastic displacement  $y_n$  and machining errors. Therefore, it is more efficient to use gear grinding by the profile copy method, which provides increased accuracy and machining productivity.

The calculated values of the ratio  $y_n/SR$  are represented in Tables 1, 2, based on the ratio (9) and the ratio  $\varepsilon_0 = \varepsilon^n$  (for gear grinding by the profile copy method). It is shown that the values  $y_n/SR$  (Table 2) are much less than the similar values given in Table 1.

**Table 1.** The calculated values of the ratio  $y_n/SR$ .

$\varepsilon$	n			
	2	3	4	5
1.5	0.555	0.490	0.400	0.347
2	0.375	0.292	0.234	0.193
3	0.222	0.160	0.123	0.100
4	0.156	0.109	0.083	0.066
5	0.120	0.083	0.062	0.050
6	0.097	0.066	0.050	0.040
7	0.081	0.055	0.041	0.033
8	0.070	0.047	0.036	0.029
9	0.062	0.042	0.031	0.025

**Table 2.** The calculated values of the ratio  $y_n/SR$ .

$\varepsilon$	n			
	2	3	4	5
1.5	0.44400	0.29600	0.19800	0.13200
2	0.25000	0.12500	0.06250	0.03100
3	0.11100	0.03700	0.01230	0.00410
4	0.06250	0.01560	0.03900	0.00098
5	0.04000	0.00800	0.00160	0.00032

So, when gear grinding according to the method of profile copying with  $n = 5$  and  $\varepsilon = e \approx 3$  (see Table 2), the ratio  $y_n/SR = 0.0041$ , and when gear grinding is done using the rolling method for the same values of  $n$  and  $\varepsilon$ , the ratio  $y_n/SR = 0.1$ , i.e. it is 24.4 times less. Therefore, the required machining accuracy in gear grinding using the profile copy method can be ensured at lower  $n$  and  $\varepsilon$  values, which allows increasing machining productivity.

The experimental studies of gear grinding, carried out at PJSC “Svet Shakhtyora” using the profile copy and milling methods confirmed the theoretical solutions obtained. It has been found out that gear grinding using the profile copy method is more productive; it allows increasing the productivity up to 5 times while ensuring a given machining accuracy. There is no thermal damage or microcracks on the finished surfaces, and it improves the machining quality. Gear grinding was performed using a high porosity abrasive wheel TIESP 400 × 32 × 127 93A60F15VPMF 601 W – 50 m/s from Winterthur (Austria) in a modern CNC gear grinding machine

HOFLER RAPID 1250 (Germany). The initial rotation speed was  $S_0 = 0,5$  m/min, and the further one was  $S_0 = 3$  m/min. Wheel fixing was carried out after machining four teeth. The roughness of the finished surface is  $R_a = 0,63 - 1,25$   $\mu\text{m}$ .

## 5 Conclusions

The theoretical analysis of the conditions for increasing the accuracy and productivity of gear machining in gear grinding operations is carried out. The expediency of gear grinding using the profile copy method is shown. Compared to milling, this method has more technological capabilities. It provides increased accuracy and machining productivity due to the implementation of the dead-stop grinding scheme, which reduces the elastic displacements that occur in the technological system due to uneven removed stock. In this case, the main part of stock removal is carried out in terms of high-performance deep grinding. For the implementation of gear grinding using the profile copy method, an analytical ratio has been obtained to determine the lateral feed elastic displacement that occurs after each pass. Using this ratio allows achieving high machining productivity with the required accuracy. It has also been found out that it is possible to increase machining accuracy and productivity while milling by increasing the refinement of the wheel pass by reducing the conditional cutting stress. This can be achieved by using high porosity grinding wheels, providing a decrease in the friction intensity in the cutting zone due to their high cutting ability.

## References




1. Lischenko, N.V., Larshyn, V.P., Nezhebovskiy, V.V.: Studying of the quality of the surface layer of gears with profile grinding. *Cutt. Tools Technol. Syst.* **89**(101), 88–99 (2018)
2. Riabchenko, S.V.: Grinding gears with disc wheels made of superhard materials. *Bull. Kharkiv Petro Vasylenko Natl. Tech. Univ. Agric.* **115**, 243–246 (2011)
3. Undewiss, S., Miller, B.: Grinding large module gears. *Gear solut.* 35–45 (2010)
4. Lishchenko, N.V., Larshin, V.P.: Profile gear grinding temperature determination. In: *Proceedings of the 4th International Conference on Industrial Engineering. Lecture Notes in Mechanical Engineering*, pp. 1723–1730 (2018)
5. Al Quran, F.M.F.: Theoretical corroboration of the selection criteria of the breaking-in and shape-copy gear teeth grinding methods. *Int. J. Mech. Prod. Eng. Res. Dev.* **8**(1), 389–392 (2018)
6. Kovalchuk, A.N., Nezhebovskiy, V.V.: Efficiency of using the GLOBAL PERFORMANCE 122210 coordinate measuring machine for measuring gear parts. *Bull. Kharkiv Petro Vasylenko Natl. Tech. Univ. Agric.* **101**, 214–225 (2010)
7. Kito, Y., Katsuma, T., Yanase, Y., Nose, Y.: Latest technologies for high-precision, high-efficiency gear grinding processing. *Mitsub. Heavy Ind. Tech. Rev.* **52**(3), 5–8 (2015)
8. Matarneh, M.E.: Improvement of abrasive and edge cutting machining efficiency through theoretical analysis of physical conditions. *Int. J. Mech. Prod. Eng. Res. Dev.* **8**(2), 249–262 (2018)
9. Stachurski, W., Midera, S., Kruszynski, B.: Determination of mathematical formulae for the cutting force  $F_C$  during the turning of C45 steel. *Mech. Mech. Eng.* **16**(2), 73–79 (2012)

10. Patil, R.A., Gombi, S.L.: Experimental study of cutting force on a cutting tool during machining using inverse problem analysis. *J. Braz. Soc. Mech. Sci. Eng.* **40**, 494 (2018)
11. Atlantic Gear Tooth Profile Grinding. [http://www.atlantic-schlifkrugi.ru/fileadmin/redaktion/bilder/downloads/kurzinformativen/EN\\_Zahnflankenprofilschleifen\\_01.pdf](http://www.atlantic-schlifkrugi.ru/fileadmin/redaktion/bilder/downloads/kurzinformativen/EN_Zahnflankenprofilschleifen_01.pdf). Accessed 15 May 2019
12. Nishimura, Y., Toshifumi, K., Yuji, A., Yoshikoto, Y., Koichi, M.: Gear grinding processing developed for high-precision gear manufacturing. *Mitsub. Heavy Ind. Tech. Rev.* **45**(3), 33–38 (2008)
13. Zaborowski, T., Ochendusko, R.: Grinding burns in the technological surface of the gear teeth of the cylindrical gears. *Mechanik* **10**, 135–139 (2017)
14. Novikov, F.V., Riabenkov, I.A.: Improved gear grinding gears. *Bull. Natl. Tech. Univ. «KhPI» Technol. Mech. Eng.* **33**(1205), 138–144 (2016)
15. Novikov, F.V.: *Mathematical Modeling and Optimization of Metalworking Processes*. Simon Kuznets Kharkiv National University of Economics, Kharkiv (2014)
16. Iakimov, O.O.: Influence of intermittent grinding wheel design on geometrical parameters of quality of the processed surface. *Cutt. Tool. Technol. Syst.* **85**, 323–330 (2015)
17. Tonkonogiy, V.M., Dmitrieva, C.Yu., Yakimov, A.A.: Prevention of the occurrence of parametric instability in the grinding of high-precision gears with intermittent elbor circles. *Mod. Technol. Eng.* **9**, 206–215 (2014)
18. Lavrinenko, V.I., Novikov, M.V.: *Extra materials in mechanical engineering: encyclopaedic handbook*. V. Bakul Institute for Superhard Materials of the NAS of Ukraine, Kyiv (2013)
19. Siziyy, YuA, Stalinskyi, D.V.: *Grinding Dynamics and Thermophysics*. Energostal, Kharkiv (2016)





# Ensuring the Bending Stiffness of Pre-compressed Cantilever Boring Bars During Fine Boring

Alexandr Orgiyan<sup>1</sup> , Vladimir Kobelev<sup>1</sup>, Vitalii Ivanov<sup>2</sup> ,  
Anna Balaniuk<sup>1</sup> , and Albakush Aymen<sup>1</sup>

<sup>1</sup> Odessa National Polytechnic University, 1, Shevchenko Ave., Odessa 65044,  
Ukraine

annabalanyuk24@gmail.com

<sup>2</sup> Sumy State University, 2, Rymaskogo-Korsakova St., Sumy 40007, Ukraine

**Abstract.** The research discovers ensuring technological and dynamic capabilities of fine boring due to the use of cantilever boring bars with increased bending stiffness. Experimental design of the cantilever boring bar and a method for increasing its bending stiffness for fine boring of long holes of small diameter ( $d = 10\text{--}20$  mm) with a ratio of  $l/d > 4$  is proposed. Bending stiffness increases due to preliminary compression of the outer layers of the boring bar hollow housing with a unique lock pin-drawbar. The experiments were carried out first on pipes of different lengths, in which the effect of the drawbar increased bending stiffness significantly, and then the experiments were carried out on small diameter boring bars. The results of all experiments show a significant increase in bending stiffness and vibration resistance of unique small diameter boring bars for boring long holes. To study the bending vibrations, a testing bench was assembled based on a finishing boring machine. The measurements were carried out using strain-gauge transducers power on via the differential circuit. It has been established that the effect of boring bar drawbar leads to an increase in bending stiffness by about 1.3–1.4 times, and the vibration amplitudes during cutting decrease by about 2–3 times.

**Keywords:** Lock pin-drawbar · Cutting tool holder nut · Bending oscillations

## 1 Introduction

The precision of a hole finishing for fine boring is characterized by indices very close to fine grinding, honing, and lapping-in. It should be noted that at present, fine boring successfully competes with honing and lapping-in operations, or is used in combination with these methods. Numerous studies contain recommendations on cutting conditions, the geometry of fine-cutting bits and tooling materials, as well as the influence of temperature in the cutting zone on the stability of the cutting process and tool wear [1–3].

In fine boring, small cutting forces do not cause significant elastic deformations and releases of the technological system elements. At the same time, when boring, the cutting process proceeds more intensively due to the peculiarities of chips formation

than during turning. With a decrease in the boring diameter, shrinkage of the chips decreases while the cutting force increases [4, 5].

Therefore, for fine boring, the geometry of the cutting bits and cutting conditions (primarily the cutting speed) depend not only on the material being machined but also on the diameter of the hole being machined and the design of the boring unit mandrel.

## 2 Literature Review

In the practice of edge cutting machining, cantilever boring bars are widely used, ensuring high boring accuracy and productivity, while the straightness of the axis of the boring hole is maintained, and there is no drill run-off. A boring unit (boring bar) for finishing boring is a no less responsible tool than the fine boring tool itself. The most commonly used mandrel design is a cylindrical rod 1, at one end of which there is a round flange 2 with a centering shank end 3 (Fig. 1).

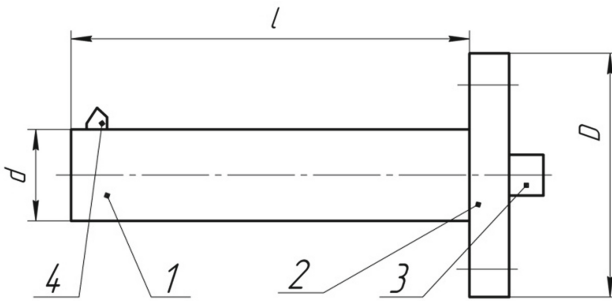


Fig. 1. Boring bar

The flange has holes for attaching the mandrel to the spindle of the boring head. A fine boring tool is attached at the other end of the mandrel rod 4. The other boring bar designs provide for the replacement of the cylindrical rod. Sometimes, there is either a Morse taper or quick-change cone with a drawbar and unique lock instead of a flange with a centering shank end.

The rigidity and vibration resistance of cantilever boring bars depends on the diameter of the cylindrical rod and are often characterized by the  $l/d$  ratio, where  $l$  – the length of the rod,  $d$  – its diameter. When the  $l/d$  ratio is more than 3, the use of cantilever boring bars is limited by reducing the bending stiffness values (reducing engineering rigidity), which results in a reduction in the vibration resistance of the spindle-boring bar subsystem.

Similar approaches devoted to static and dynamic analyses, vibration reliability, and developing the scientific approach of using artificial neural networks were investigated in [6, 7].

The experimental study of the bending vibrations of the developed threaded head design was carried out in paper [8]. The research [9] provides recommendations for

increasing the accuracy of horizontal boring operation adjusted for the variable rigidity of the processing system.

Studies of the vibrational features of cantilever boring bars lead to the dynamics of machine tools, at least, by the number of works published [10–13]. When cutting for machining specific workpieces, both adjustments with a rotating boring bar mounted on the spindle of the finishing-boring machine and adjustments with a non-rotating boring bar are used (while the workpiece undercut rotates, and the boring bar with the cutting bit has an axial feed).

The experimental results confirm the primary influence of the spindle and the boring bar on the formation of the deformative characteristics of the processing system. In experiments, the parameters of the boring bar subsystem – with a fixture (spindle – boring bar) were studied for the case of changing the boring bar's diameter and length ( $l/d = 3–6$ ,  $d = 10–20$  mm). The experimental results of vibrations of the cantilever boring bars mounted on the spindle heads of finishing and boring machines show that the connection between bending and torsional vibrations is weak, the frequencies of bending and torsional vibrations, virtually, do not coincide, while the forms of static bending when applying the radial force to the cutting bit, coincide with the spatial shape of the bending fluctuations. The length of the boring bar and the cutting depth chiefly affect the amplitudes of forced vibrations than the changes in the recommended limits of cutting and feed speeds. In specific boring conditions at the selected cutting conditions and the material being processed, the ultimate yield of the cutting bit is determined, which provides vibration-resistant machining. The ultimate yield, in this case, somewhat decreases with the increase in the bored hole diameter.

When conducting dynamic studies, they often use “long” boring bars that are convenient for model experiments, for which  $l/d > 3$ . The use of such boring bars allows considering the elastic-dissipative-inertial system as one-dimensional, whereas the closed dynamic system has a small margin of stability [14]. The importance of such experiments is determined by the fact that it is possible to establish the limiting boring conditions without the use of vibration dampers.

It was experimentally established that with an increase in the length of the boring bars for  $l/d > 3$ , the vibration intensity increases significantly, and the vibration frequency slightly differs from its natural frequency. According to the results of measuring the amplitudes of the oscillations, the limiting values of the boring bar length are set for the given values of its diameter, cutting depth, and the machined material. It has been established that the ultimate yield is a convenient critical indicator of vibration resistance.

To expand the technological capabilities of fine-boring cantilever boring bars, their rigidity and damping ability should be increased. Thus, the manufacture of boring bars entirely from hard alloy allows one to bore holes with  $l/d > 6$ , since the elastic modulus of a hard alloy is much higher than that of steel. To increase the boring bars damping, variable vibration dampers are often used: shock action or dynamic action [15]. However, the manufacture of carbide boring bars leads to a significant increase in their cost, and the use of vibration dampers requires unique shank ends for their accommodation [16].

Bending stiffness is the most crucial factor affecting the quality of the machined surface and limiting the use of cantilever tools for long holes. A review of the research

and technical literature did not reveal ways to increase the bending stiffness of the cantilever boring bar constructively.

### 3 Research Methodology

The research objective is ensuring the technological and dynamic capabilities of dedicated boring bars with increased bending stiffness. The idea of developing the boring bar design with increased bending stiffness is associated with the full use of prestressed reinforcement beams in the construction, as well as with the use of tensioned cables to increase the stability of high-rise buildings.

The first experiments confirming the effect of an increase in stiffness were carried out on tube samples.

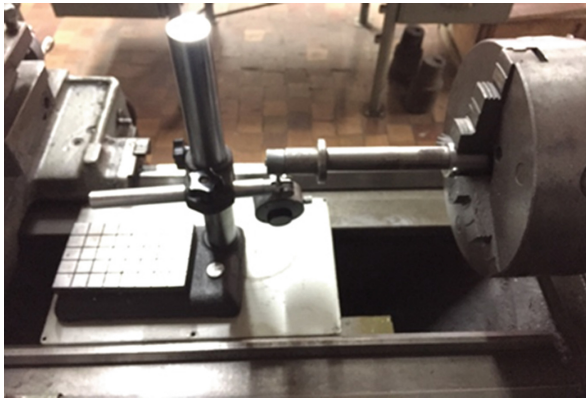


**Fig. 2.** Experimental test bench for measuring the bending stiffness of a pre-compressed pipe.

A tube with a lock pin one end of which is screwed into the sleeve refuse is inserted into the sleeve fixed in the lathe chuck. The second end of lock pin protrudes from the pipe and nut is screwed onto it, the end of which abuts against the other end of the pipe. One end of the pipe is pinned into the sleeve and cannot rotate relative to the sleeve. Using a torque screw, the nut creates a compressive force through the end of the pipe, while the lock pin is elongated due to this force.

In the experiments, the torque  $M$  was applied to the nut. The end of the pipe, after tightening up with specific torque, was loaded with radial forces. The displacement in the cross-section of the force application was measured to calculate the stiffness ratio. It should be noted that at values of the radial force close to 15 N, a slight decrease in the stiffness ratios is noted, which is possibly associated with contact deformations at the lock pin – nut and nut – pipe end joints. However, in all cases, an increase in the compression force leads to an increase in the bending stiffness ratios.

When performing a series of experiments with pipes of different sizes, it was found that with the increase in axial force, the bending stiffness increases. Table 1 shows

typical results of measurements of stiffness when loading the lock pin with different moment  $M$  (N•m) and the action of radial force.

**Table 1.** The experimental values of bending stiffness (N/μm) for the pipe (dout = 24 mm, l = 140 mm, dinn = 18 mm)

Radial force, N	M = 0 N•m	M = 10 N•m	M = 20 N•m	M = 40 N•m
5	0.5	0.71	1.0	1.25
10	0.52	1.0	1.25	1.5
15	0.47	0.75	0.85	1.0
20	0.51	0.8	0.9	1.2

The results of the experiments with pipes led to the development of a fairly simple design of an experimental cantilever boring bar with increased bending stiffness. The design of the experimental boring bar is provided in Fig. 2

The cantilever boring bar contains an elongated body 1, in which a cylindrical cavity with a diameter of  $d_0$  is made with an internal thread with a diameter  $M$  in its blind end, and a lock pin 2 with an external thread  $M$  at both ends.

The external thread  $M$  at one, conditionally right, end of the lock pin 2 corresponds to the internal thread  $M$  at the blind end of the cylindrical cavity  $d_0$  of the cantilever boring bar body 1. The lock pin 2 is screwed with one, conditionally right, end to refuse into the internal thread  $M$  of the cylindrical cavity of the of cantilever boring bar body 1. The cantilever boring bar also contains a cutting tool holder nut 3 screwed onto the other, conditionally left, end of the lock pin 2 t refuse, in the left butt end of the body 1 ( $T_1$  in Fig. 3) of the cantilever boring bar, a boring tool 4 mounted in the hole of the diameter  $d_p$  of the cutting tool holder nut 3.

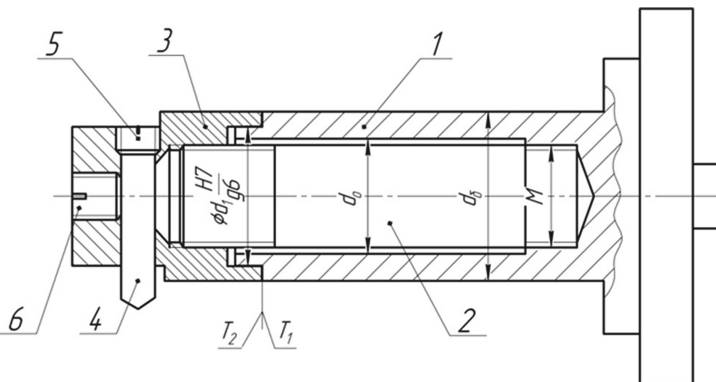


**Fig. 3.** Cantilever boring bar design.

The hole in the cutting tool holder nut 3 is made perpendicular to the axis of its rotation, and the boring tool 4 is set to the required distance using the adjusting screw 5

and secured using the locking screw 6. The ratio of the lock pin 2 length and the depth of the thread of the cutting tool holder nut 3 is chosen to provide a margin of the thread lead  $L$  (Figs. 3 and 4), which is greater by three thread steps.

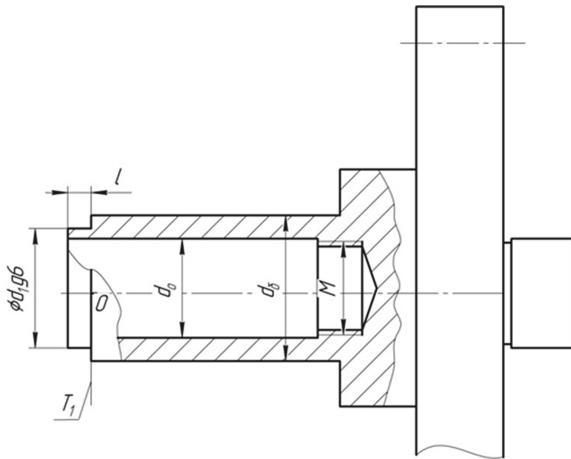


**Fig. 4.** The boring bar body.

The outer surface of the final, conditionally left, part of the cutting tool holder nut 3 is made hexagonal in its cross-section, for S wrench, and the length  $h$  of this part of the cutting tool holder nut 3 is selected so that it is sufficient to arrange the head of the torque wrench on it.

The butt end contact surfaces of the casing 1 of the cantilever boring bar and the tool holder nut 3 have a stepped shape with a fit and a gap of diameter  $d_1$  of type H7/g6, where the diameter  $d_1$  is assumed to be larger or equal to the diameters half-sum: the outer diameter of the boring bar body  $d_6$  and the diameter of the cylindrical cavity  $d_0$  of the boring bar body 1, and the ratio of the lengths of the steps of  $l$  – the boring bar body and  $l_1$  – the cutting tool holder nut is chosen so that the equality  $l_1 = l + (0.5 \dots 0.8)$  mm should be fulfilled.

On the lateral surfaces of the body 1 of the cantilever boring bar and the cutting tool holder nut 3, in the place of their ends  $T_1$  and  $T_2$  contact, a calibration scale is applied in the form of dashes, for establishing the compression force (Fig. 5, position 7). A method of increasing bending stiffness is implemented in the process of manufacturing a cantilever boring bar and its preparation for use.

In the elongated cylindrical body 1 of the boring rod, a cylindrical cavity is made with a diameter  $d_0$ , which is equal to 0.7...0.8 of the boring bar  $d_6$  outer diameter, in the blind end of which an internal thread  $M$  is cut. A lock pin 2 is arranged in the made cylindrical cavity so that one part of it should protrude from the cylindrical cavity of diameter  $d_0$ . The lock pin nominal diameter is equal to the nominal diameter of the cylindrical cavity, thus providing a placement with a wide gap.

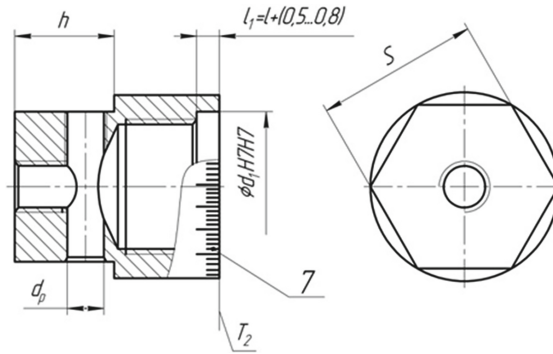


**Fig. 5.** Cutting tool holder nut.

After that, one, conditionally right, end of the lock pin 2 is fixed in the blind end of the cylindrical cavity having a diameter  $d_0$  in the housing 1 of the boring bar by screwing the lock pin 2 into the thread  $M$  to refuse.

Then, the cutting tool holder nut 3 is screwed manually onto the protruding, conditionally left, part of the lock pin 2 until resistance is felt, which is controlled by the absence of a gap between the butt ends of the boring bar body 1 and the cutting tool holder nut 3.

This initial state of the unloaded lock pin 2 is fixed by the coincidence of the bars of the scale 7 on the boring bar body 1 and the cutting tool holder nut 3, which is indicated as zero. Then, the cutting tool holder nut 3 is screwed onto the lock pin 2 using a torque wrench by the required number of scale divisions in the scale 7, and thereby an axial tension of the lock pin 2 and compression of the boring bar body 1 are achieved, which leads to an increase in the bending stiffness of the cantilever boring bar. An increase in the axial load  $P$  leads to an increase in the bending stiffness of the boring bar and is mainly limited by the thread strength.

## 4 Results

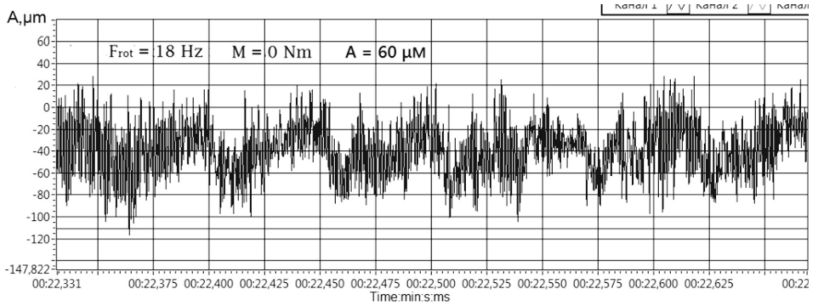
In experiments on pipes, to determine their bending stiffness, forces of 5 to 20 N and moments varying from 0 to 60 Nm were applied perpendicularly to the outer surface of the pipe. The same values of force  $P$  simulating the radial component of the cutting force and moments were applied to the tested boring bars of small diameter.

The axial forces of the screed acting on the boring bar were determined by calculating the transmission of torque on a torque wrench through the stud thread. The effect of the axial force  $P$  compressing the body of the boring bar is reflected in the experimental results of bending stiffness measuring (Table 2).

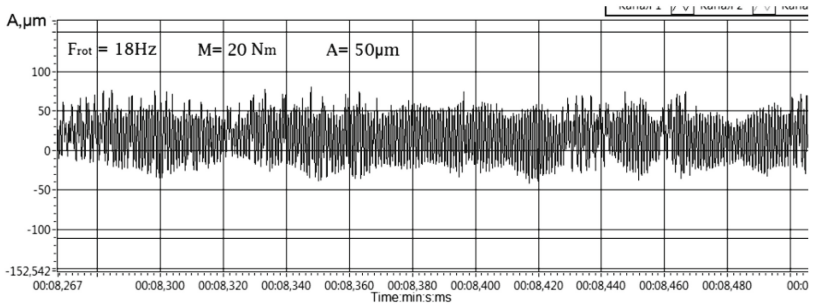
Table 2 shows, below the values of the applied moments  $M$ , the design values of the axial force  $P$  acting on the boring bar. To study the amplitudes of the bending vibrations of the compressed boring bars, an experimental test bench was assembled based on a finishing and boring machine. The measurements were carried out using

**Table 2.** Experimental values of bending stiffness for the boring bar  $l = 96$  mm,  $d = 16$  mm.

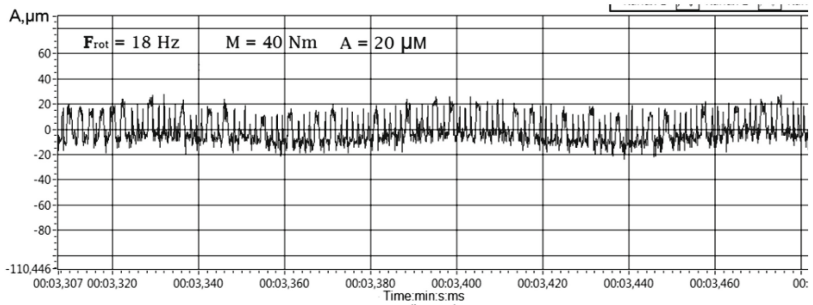
Radial force, N	Without compression ( $P = 0$ N)	$M = 10$ N·m ( $P = 3,500$ N)	$M = 20$ N·m $P = 7,500$ N	$M = 40$ N·m $P = 13,000$ N
5	3.3	4.1	4.3	4.5
10	3.3	4.2	4.4	4.5
15	2.5	2.5	3.2	4.0
20	2.7	2.3	3.4	4.1



a



b



c

**Fig. 6.** Oscillograms of the boring bar bending vibrations  $d = 16$  mm,  $l/d = 6$ : a – without compression; b –  $M = 20$   $\mu$ m; c –  $M = 40$   $\mu$ m



strain-gauge transducers power on via the differential circuit. Figure 6 provides the oscillograms of the studied boring bar's bending vibrations.

From the oscillograms, it follows that the oscillation amplitudes of the pre-compressed boring bar are 2–3 times lower compared to the amplitudes of an unstressed boring bar. The values of the oscillation amplitudes and loading conditions are given in Table 2.

## 5 Conclusion

The extension of technological and dynamic capabilities of fine edge boring with cantilever boring bars having increased bending stiffness was experimentally established. A simple boring bar design has been developed that implements a method of increasing bending stiffness. The effect of preliminary compression of the boring bar body results is an increase in bending stiffness by about 1.3–1.4 times compared to a boring bar without compression, and the amplitude of the forced vibrations during cutting decreases by about 2–3 times. This effect allows us to bore precise holes with a ratio  $l/d > 4$ . Theoretical studies of special boring bars vibrations, as well as boring errors, will be discussed in further publications.



## References

1. Suslov, A.G., Dalsky, A.G.: Scientific Foundations of Engineering Technology. Machine Building, Moscow (2002)
2. Jablonski, W.: Simulation of cutting process – modeling and applications, engineering the future. INTech (2010)
3. Usov, A., Oborskij, G.: The effect of thermomechanical phenomena on the stability of cutting process and wear of cutting tools. *SverkhtverdyeMaterialy* **6**, 66–71 (2003)
4. Mazur, N.P., Vnukov, Yu.N., Grabchenko, A.I., et al.: Fundamentals of the materials cutting theory, 2nd edn. NTU “KhPI”, Kharkiv (2013)
5. Altintas, V.: Manufacturing Automation: Metal Cutting Mechanics, Machine Tools Vibrations and CNC Design. Cambridge University Press, Cambridge (2012)
6. Pavlenko, I.: Static and dynamic analysis of the closing rotor balancing device of the multistage centrifugal pump. *Appl. Mech. Mater.* **630**, 248–254 (2014). <https://doi.org/10.4028/www.scientific.net/AMM.630.248>
7. Pavlenko, I.V., Simonovskiy, V.I., Demianenko, M.M.: Dynamic analysis of centrifugal machines rotors supported on ball bearings by combined application of 3D and beam finite element models. In: IOP Conference Series: Materials Science and Engineering, vol. 233, no. 1, p. 01253 (2017). <https://doi.org/10.1088/1757-899x/233/1/012053>
8. Oborskiy, G., Orgiyan, A., Tonkonogyi, V., Aymen, A., Balaniuk, A.: Study of dynamic impacts at combined operations of the thin turning and boring. In: Tonkonogyi, V., et al. (eds.) *Advanced Manufacturing Processes. InterPartner-2019. Lecture Notes in Mechanical Engineering*, pp. 226–235. Springer, Cham (2020). [https://doi.org/10.1007/978-3-030-40724-7\\_23](https://doi.org/10.1007/978-3-030-40724-7_23)

9. Orgiyan, A., Tkachenko, B., Oborskyi, G., Balaniuk, A., Iorgachov, V.: Determining rational cutting modes for horizontal boring operation adjusted for the variable rigidity of the process system. In: Tonkonogyi, V., et al. (eds.) *Advanced Manufacturing Processes. InterPartner-2019. Lecture Notes in Mechanical Engineering*, pp. 246–253. Springer, Cham (2020). [https://doi.org/10.1007/978-3-030-40724-7\\_25](https://doi.org/10.1007/978-3-030-40724-7_25)
10. Ostling, D., Tormod, I., Tjomsland, M., Standal, O., Mugaas, N.: Cutting process monitoring with an instrumented boring bar measuring cutting force and vibration. *Proc. CIRP* **77**, 235–238 (2018). <https://doi.org/10.1016/j.procir.2018.09.004>
11. Sørby, K., Østling, D.: Precision turning with instrumented vibration-damped boring bars. *Proc. CIRP* **77**, 666–669 (2018). <https://doi.org/10.1016/j.procir.2018.08.181>
12. Sørby, K., Sundseth, E.: High-accuracy turning with slender boring bars. *Adv. Manuf.* **3**(2), 105–110 (2015). <https://doi.org/10.1007/s40436-015-0112-7>
13. Siddhpura, M., Paurobally, R.: Experimental investigation of chatter vibrations in facing and turning processes. *Int. J. Mech. Aerosp. Ind. Mech. Manuf. Eng.* **7**(6), 968–973 (2013)
14. Schmitz, T.L., Scott Smith, K.: *Machining Dynamics: Frequency Response to Improved Productivity*, 2nd edn. Springer, Heidelberg (2008). <https://doi.org/10.1007/978-3-319-93707-6>
15. Kopelev, Yu.F., Orgiyan, A.A., Kobelev, V.M.: Parametric of oscillations of machine tools. In: Kopelev, Yu.F. (ed.). Publishing House ONPU, Odessa (2007)
16. Linchevsky, P.A. Dzhuguryan, T.G., Orgiyan, O.A.: Machining of parts on turning and boring machines. In: Linchevsky, P.A. (ed.). Tekhnika, Kyiv (2000)



# Improvement of the Accuracy of Grinding by Means of Coolant Supply

Mykhaylo Stepanov<sup>1</sup> , Maryna Ivanova<sup>1</sup> ,  
Petro Litovchenko<sup>2</sup> , Larysa Ivanova<sup>2</sup> , and Alexey Kotliar<sup>1</sup> 

<sup>1</sup> National Technical University “Kharkiv Polytechnic Institute”,  
2, Kyrpychova St., Kharkiv 61002, Ukraine  
ivanovamarynal@gmail.com

<sup>2</sup> National Academy of the National Guard of Ukraine,  
3, Zakhysnykiv Ukrainy Sq., Kharkiv 61000, Ukraine

**Abstract.** This article considers the issues related to various methods of supplying cutting fluid to the cutting zone during grinding. It is established that the improvement of the technique for supplying cutting fluids to the cutting zone is one of the promising directions for increasing the processing efficiency. In this regard, a method for supplying cutting fluid was proposed. To increase the accuracy of processing parts, grinding is performed without the contact of the heated liquid coolant with the surfaces of the grinding wheel head, headstock, and tailstock, bed, and table of the machine tool, as well as grinding waste. For the practical implementation of this method, a device was developed for supplying a liquid coolant during machining by external round grinding. This device contains a nozzle for grinding waste, a distributing nozzle, which covers the workpiece, and the receiver with air channels and radial nozzles made with different diameters. The research to determine the rational parameters (diameters and numbers of air nozzles) of this device is carried out.

**Keywords:** External round grinding · Coolant supply device · Cutting force · Nozzle · Air curtain

## 1 Introduction

The machining accuracy of parts on metal cutting machine tools depends on many different factors. There are various geometrical errors of the technological system elements (the machine tools, fixtures, cutting tools), their wear, temperature deformations, technological heredity, etc. In this regard, researchers are studying the possibility of controlling and reducing the influence of these factors on the accuracy of processing. Therefore, the research of possibilities of directed formation of indicators of quality by selecting technological operations and appointment of corresponding processing regimes is presented in the paper [1]. It has been noted that the structure and accuracy of the dimensions of the used technological equipment plays an important role in ensuring the accuracy of machining [2, 3].

A grinding process is accompanied by the transformation of mechanical cutting energy to heat, where the heat sources are primarily plastic strains occurring in the chip formation process, as well as friction [4].

The temperature rise in the workpiece is the main cause of changes in micro-hardness and internal stresses of the machined material, which can reduce the fatigue strength of machine parts, as well as decrease micro-hardness inside the surface layer [5]. The high temperature can cause structural changes in the surface layer, which noticeably decrease properties of the machined surface, its quality, and accuracy [6, 7].

Cutting fluids (coolants) are used to improve lubrication, flush away chips, reduce workpiece thermal damage, and improve the surface finish [8–11].

On the one hand, there are some negative aspects of the coolant application due to substances that are hazardous to the environment and machine operators [12]. As a result, the grinding fluid usage reduction is obtained by means of minimum quantity lubrication methods [8, 12, 13].

Moreover, liquid spraying, as it is known, has a negative effect, since the contact of the heated coolant with the elements of the machine tool causes additional heating, and therefore their deformation, which greatly influences the accuracy of the grinding workpieces. On the other hand, during grinding (especially of non-rigid details), elastic deformations occur under the action of the cutting force, which also worsens the accuracy parameters of machining. Therefore, much attention is paid to the development of various methods and devices for supplying fluid to the cutting zone.

The **purpose** of this paper is to increase the accuracy of grinding details by reducing temperature and elastic deformations by using air jets to eliminate the contact liquid coolant with the elements of the grinding machine and to increase its rigidity.

## 2 Literature Review

The specificity of the use of coolant during grinding is associated with the reproduction of conditions for improving the lubricating, dispersing, cooling, and other actions. Most efforts are directed to create a technique for supplying coolant to the grinding zone. Improving the technique for supplying coolant to the cutting zone is one of the promising areas for increasing grinding efficiency.

First, a classification of methods for supplying coolant to the grinding zone was developed [14, 15]. Later on, the systematization of coolant supply methods was carried out taking into account the latest data [16]. According to the new classification, the number of methods has been expanded to 29.

The authors [17] analyze methods of coolant supplying for flat grinding with the grinding wheel including the development of combined methods of coolant supplying. Besides, the method and theoretical justification for forming the coolant bath in the working area of the flat grinding machine are presented.

The authors [18] pointed out that a grinding wheel rotating at high circumferential speed induces a boundary-layer airflow, which possibly can detain the coolant from submerging into the grinding zone to prevent thermal damage. They investigated the interaction of the coolant with the grinding wheel under the influence of the airflow with different coolant nozzle types and parameters.

Moreover, a lot of work is devoted to determining the parameters of nozzles [19].

The authors of the paper [20] developed a method for supplying coolant, which is the creating of a continuous curtain around the working area. According to the authors, with such a coolant supply scheme, liquid spraying is absent or minimized.

### 3 Research Methodology

#### 3.1 Development of a Coolant Supply Device Design

To improve the accuracy of grinding, a coolant supply device has been developed [21]. When designing the device, we considered the fact that it should fulfill two functions:

1. the air flows that exit from the radial nozzles should create an air screen (curtain), which prevents the coolant from leaving the nozzle and hinders the coolant from contacting the machine tool elements;
2. air jets outgoing from the radial nozzles should create a lifting aerodynamic force that prevents the workpiece from moving under the action of the cutting force.

The device (Fig. 1) consists of a nozzle 2 and a receiver 5, which covers the workpiece 11 on the outer cylindrical surfaces and contains a pipe for grinding waste 9, a coolant exhaust pipe 8, air supply nozzles 4 and 6 connected to cavities 16, and 21 respectively; with air nozzles 17 in the side walls 12 and 13, which prevent coolant leakage in the gaps 15 between the cylindrical surface of the workpiece and the enveloping surfaces 23 of the nozzle 2, and 20 of the receiver 5.

Radial air nozzles 13, 22 and other parts are made with different diameters. The axis of the nozzle 22 with a maximum diameter coincides with the direction of action of the cutting force.

The device operates as follows. The coolant flow enters the nozzle 2, then, washing the workpiece 11 moves to the coolant outlet pipe 8 and is output to the coolant supply and cleaning subsystem.

Grinding waste enters the pipe 9, where the wall 10 prevents contact with the coolant flow, this is facilitated by a slot 18 located in the wall 10 connected to channel 19. Compressed air is supplied to the nozzle 18 through channel 19, which forms a separation screen between the grinding waste and the coolant. Jets of air flowing from the radial nozzles 17, 22 and others from the air screen, which prevents leakage and spraying of the coolant at the ends of the nozzle 2 and the receiver 5.

The manufacture of radial nozzles with different diameters contributes to the formation of aerodynamic airlifting forces, the resultant of which move in the direction opposite to the directions of the cutting force that occurs during grinding. This reduces the elastic deformation of the grinding machine parts.

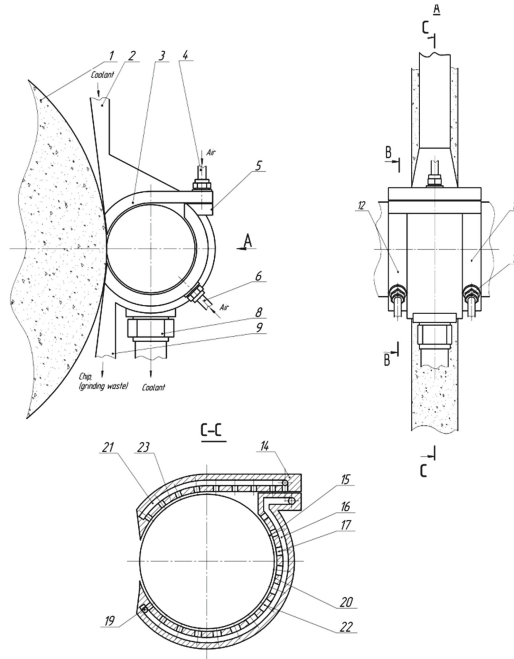


Fig. 1. The coolant supply device.

### 3.2 Determination of Rational Parameters of the Lubricant Coolant Supply Device

The task of creating an air curtain in the clearance between the workpiece and the nozzle elements is quite complex [22–26]. As a rule, the determination of the jet path and the main parameters of the curtain is based on solving differential equations of energy and impulse conservation.

However, given the small clearance between the workpiece and the nozzle elements, the insignificant distance between the axes of the nozzle holes, as well as the difference between the coolant pressure near the contact zone and the air pressure supplied, the task could be simplified.

To determine the rational parameters of the lubricant coolant supply device, the design diagram of the forces acting on the workpiece during grinding using a coolant and air jets was done (Fig. 2, 3).

To prevent the workpiece from moving, the following condition must be fulfilled

$$F_{cut} = F_{\Sigma} \tag{1}$$

where  $F_{cut}$  is cutting force, N;  $F_{\Sigma}$  is the total force resulting from leakage of jets from radial nozzles, N.

The cutting force is determined as

$$F_{cut} = \sqrt{F_y^2 + F_z^2}, \tag{2}$$

where  $F_y, F_z$  is radial and tangential components of the cutting force, N.

The total force is determined as

$$F_{\Sigma} = \sum_{i=1}^n \vec{F}_i = \vec{F}_1 + \vec{F}_2 + \vec{F}_3 + \dots + \vec{F}_n, \tag{3}$$

where  $F_i$  is the force vector arising from the flow of the air jet of the corresponding nozzle, N.

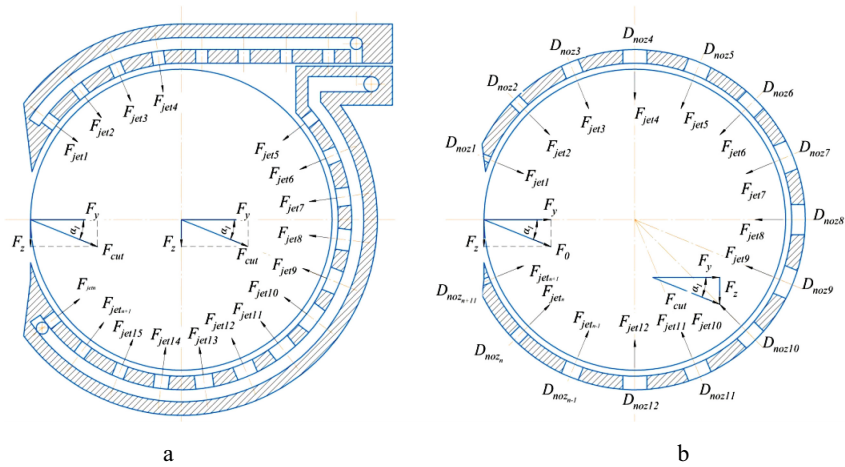


**Fig. 2.** The design diagram of the forces acting on the workpiece during the grinding using a coolant and air jets: a - initial; b - converted.

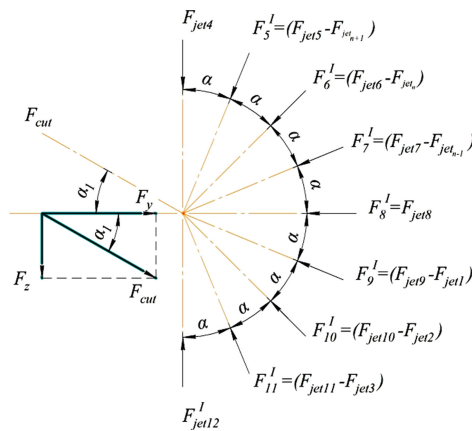


**Fig. 3.** The converted design diagram of the balance of forces acting on the workpiece during the grinding using a coolant and air jets.

The aerodynamic force for submerged jet acting on the surface of the workpiece with a clearance  $h < D_{noz}/4$ , taking into account the gas-dynamic force, can be determined by the formula

$$F_{jet} = \frac{\pi \cdot D_{noz}^2}{4} \cdot \rho_1 + k_c \cdot \mu \cdot A_n \cdot (P_1 - P_2), \quad (4)$$

where  $D_{noz}$  is nozzle diameter, mm;  $A_n$  is the minimum cross-sectional area, mm<sup>2</sup>;  $P_1, P_2$  is pressure before and after nozzle, Pa;  $\mu$  is flow rate coefficient,  $\mu \approx 0.61 \dots 0.7$ ;  $k_c = 0.5 \dots 0.6$ .

The minimum cross-sectional area is determined by the formula

$$A_n = \pi \cdot D_{noz} \cdot h, \quad (5)$$

where  $h$  is the clearance between the surface of the workpiece and the end face of the nozzle, mm.

Taking into account the formula (4), an aerodynamic force of jet acting for each nozzle can be founded

– for the first nozzle

$$F_{jet1} = \frac{\pi \cdot D_{noz1}^2}{4} \cdot \rho_1 + k_c \cdot \mu \cdot A_n \cdot (P_1 - P_2), \quad (6)$$

– for the second nozzle

$$F_{jet2} = \frac{\pi \cdot D_{noz2}^2}{4} \cdot \rho_1 + k_c \cdot \mu \cdot A_n \cdot (P_1 - P_2), \quad (7)$$

– for the  $n$ -th nozzle

$$F_{jetn} = \frac{\pi \cdot D_{nozn}^2}{4} \cdot \rho_1 + k_c \cdot \mu \cdot A_n \cdot (P_1 - P_2), \quad (8)$$

Balance Eqs. (1) are valid for a one-sided air barrier (curtain). Since the air barrier (curtain) in the designed device is organized on two sides, this equation will have the form

$$F_{cut} = 2 F_{\Sigma}. \quad (9)$$

The equation of the balance of forces acting on the workpiece taking into account the components of the cutting forces (Fig. 3):



– for the radial component

$$F_y = F'_8 + F'_7 \cdot \cos \alpha + F'_6 \cdot \cos 2\alpha + F'_5 \cdot \cos 3\alpha + \dots + F'_k \cdot \cos n\alpha + F'_9 \cdot \cos \alpha + F'_{10} \cdot \cos 2\alpha + F'_{11} \cdot \cos 3\alpha + \dots + F'_j \cdot \cos n\alpha. \quad (10)$$

– for the tangential component

$$F_z = -F'_7 \cdot \sin \alpha - F'_6 \cdot \sin 2\alpha - F'_5 \cdot \sin 3\alpha + \dots + F'_k \cdot \sin n\alpha + F'_9 \cdot \sin \alpha + F'_{10} \cdot \sin 2\alpha + F'_{11} \cdot \sin 3\alpha + \dots + F'_j \cdot \sin n\alpha. \quad (11)$$

The value of clearance between the surface of the workpiece and the nozzle exit section can be taken based on the condition

$$h < D_{noz}/4. \quad (12)$$

When determining the distance between the axes of the holes (and therefore the number of holes), a number of factors should be taken into account, among which the jet expansion angle is most important. According to the ASHRAE guide 1996, the air jet has a constant angle of 20–24° (an average of 22°), although some elements can give a wider jet expansion angle.

The efficiency of the device was evaluated by the value of the deformation of the joint “wheel-workpiece”  $\Delta_{F_y}$ . The experimental dependence obtained in the Experimental Design Bureau of Grinding Machines (the OKBSHs) is

$$\Delta_{F_y} = k_0 + k_1 \cdot F_y = 1.4 + 0.1 \cdot F_y \quad (13)$$

where  $F_y$  is the radial component of cutting force, H,  $F_y = 50 \dots 500$  N.

In our case, the formula (13) has the form

$$\Delta_{F_y} = k_0 + k_1 \cdot (F_y - F_{jet}). \quad (14)$$

## 4 Results

The diagrams of the action of the air jet forces on a workpiece show that all nozzles can be divided into two categories: with negative and positive effects (Fig. 4).

This is because the directions of the air jet force action at one part of the nozzles coincide and at the other part, it is opposite to the direction of the cutting force action. Therefore, when designing, this effect should be taken into account either by varying the diameters of the nozzles (minimizing the diameter of nozzles with a negative effect) or by varying the air pressure (decreasing the air pressure in front of nozzles with a negative effect).

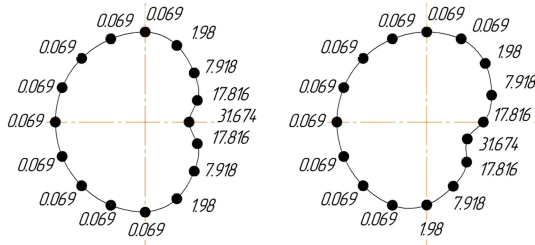


**Fig. 4.** Variants of diagram of the forces of the air jet action on the workpiece: air supply pressure  $P = 0.588$  MPa ( $6 \text{ kg/cm}^2$ ); clearance between the nozzles and the workpiece surface  $h = 0.5$  mm; infeed  $v = 1.4$  mm/min.

The following parameters have been varying during the experiment:

- the diameter of air nozzles is  $0.1 \dots 0.8$  mm (depending on the angular position of the nozzle);
- air supply pressure is  $0.098 \dots 0.588$  MPa ( $1 \dots 6 \text{ kg/cm}^2$ );
- the radial clearance between the nozzle end and the workpiece surface is  $0.5 \dots 0.8$  mm ( $0.05 \text{--} 0.08$  cm).

The graphs (Fig. 5) shows that within the investigated pressures, the total force of the action of the air jets on the workpiece surface can vary significantly (in 6 times). In addition, the changes in the radial clearance associated with the removal of the allowance during the final grinding hardly affect the value of the total force of action of the air jets.

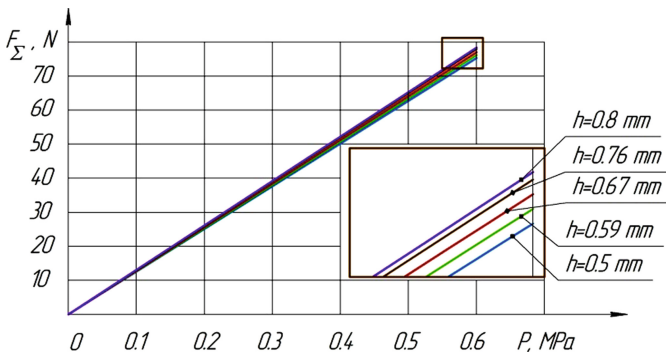


**Fig. 5.** The effect of air pressure and the clearance between the nozzles and the workpiece surface on the total force of the air jets.

The graph in Fig. 6 shows that in the pre-grinding mode, the effect of air jets action on the workpiece becomes smaller. This is because the force of the jet action formed by the pressure up to  $0.588$  MPa ( $6 \text{ kg/cm}^2$ ) is not large enough to counteract the cutting force. To solve this problem, it is necessary to increase the nozzle supply pressure.

This requires equipping the grinding machine tools with compressors and other equipment. In addition, this can lead to significant air expenses, reducing efficiency and increasing economic costs. Therefore, if it is possible, the diameters of nozzles with opposite directions of the air jet force action to the direction of the cutting force action should be increased, and the diameters of nozzles with coinciding directions of the air jet force action should be decreased. However, it is worth remembering that these nozzles must also provide an airlock (curtain).

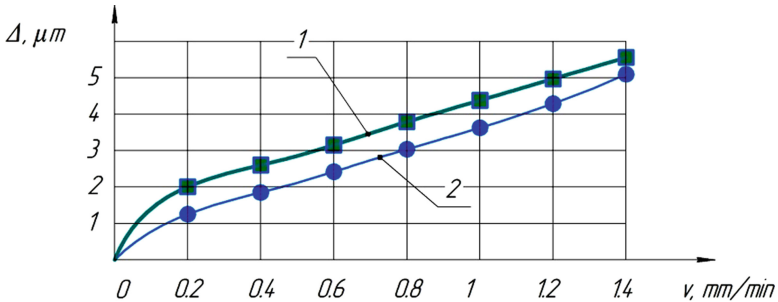


**Fig. 6.** The effect of air jets acting on the workpiece and infeed on the value of the joint deformation: 1 - without the using of air jets; 2 - using air jets (air supply pressure  $P = 0.588$  MPa ( $6 \text{ kg/cm}^2$ ); clearance between the nozzles and the workpiece surface  $h = 0.5$  mm).

It positively affects the joint deformation and reduces it from  $5.6 \mu\text{m}$  to  $5.4 \mu\text{m}$  for pre-grinding and from  $2 \mu\text{m}$  to  $1.2 \mu\text{m}$  for final grinding even within air jets pressure of  $0.588$  MPa ( $6 \text{ kg/cm}^2$ ).

## 5 Conclusions

1. The proposed method and device, involving isolating the coolant contact with the surfaces of the machine elements and increase the rigidity of the technological system of the machine, which occurs under the action of air jets formed in a certain way, can be used to increase the accuracy of grinding details by reducing the temperature and elastic deformations.
2. The clearance between the surface of the workpiece and the ends of the nozzles on the total force of the air jets is hardly affected.
3. The deformation due to the action of air jets can be reduced by 21%. This effect is achieved during final grinding, in particular, and the nature of the location of the nozzles is important.

The study of the action effect of the air jet (barrier) on the temperature state of the coolant liquid is planned for further research.

## References

1. Tkachuk, A., Zablotzkyi, V., Kononenko, A., Moroz, S., Prystupa, S.: Directed formation of quality, as a way of improving the durability of conjugated parts of friction pairs. In: Ivanov, V., et al. (eds.) *Advances in Design, Simulation and Manufacturing II, DSMIE 2019. Lecture Notes in Mechanical Engineering*, pp. 370–377. Springer, Cham (2020). [https://doi.org/10.1007/978-3-030-22365-6\\_37](https://doi.org/10.1007/978-3-030-22365-6_37)
2. Ivanov, V., Dehtiarov, I., Denysenko, Y., et al.: Experimental diagnostic research of fixture. *Diagnostyka* **19**(3), 3–9 (2018). <https://doi.org/10.29354/diag/92293>
3. Karpus, V.E., Ivanov, V.A.: Locating accuracy of shafts in V-blocks. *Russ. Eng. Res.* **32**(2), 144–150 (2012). <https://doi.org/10.3103/S1068798X1202013X>
4. Stachurski, W., Sawicki, J., Krupanek, K., et al.: Numerical analysis of coolant flow in the grinding zone. *Int. J. Adv. Manuf. Technol.* **104**(5–8), 1999–2012 (2019). <https://doi.org/10.1007/s00170-019-03966-x>
5. Grzesik, W., Kruszynski, B., Ruszaj, A.: Surface integrity of machined surfaces. In: Davim, J.P. (eds.) *Surface Integrity in Machining*, pp. 143–179. Springer, London (2010). [https://doi.org/10.1007/978-1-84882-874-2\\_5](https://doi.org/10.1007/978-1-84882-874-2_5)
6. Malkin, S., Guo, C.: *Grinding Technology: Theory and Application of Machining with Abrasives*, 2nd edn. Industrial Press Inc., New York (2008)
7. Jamshidia, H., Budak, E.: Grinding temperature modeling based on a time dependent heat source. In: Monostori, L. (eds.) *8th CIRP Conference on High Performance Cutting (HPC 2018)*. Elsevier Ltd. (2018), <https://doi.org/10.1016/j.procir.2018.09.020>. *Procedia CIRP*, vol. 77, pp. 299–302
8. Patil, P.J., Patil, C.R.: Analysis of process parameters in surface grinding using single objective Taguchi and multi-objective grey relational grade. In: Thomas, B.S. (eds.) *Perspectives in Science*, vol. 8, pp. 367–369. Elsevier GmbH (2016). <https://doi.org/10.1016/j.pisc.2016.04.077>
9. Tschätsch, H.: *Applied Machining Technology*. Springer, Heidelberg (2009). <https://doi.org/10.1007/978-3-642-01007-1>
10. Grzesik, W.: *Advanced Machining Processes of Metallic Materials*, 2nd edn. Elsevier, Amsterdam (2017)
11. Stepanov, M., Ivanova, L., Litovchenko, P., Ivanova, M., Basova, Y.: Model of thermal state of the system of application of coolant in grinding machine. In: Ivanov, V., et al. (eds.) *Advances in Design, Simulation and Manuf. DSMIE 2018. Lecture Notes in Mechanical Engineering*, pp. 156–165. Springer, Cham (2019). [https://doi.org/10.1007/978-3-319-93587-4\\_17](https://doi.org/10.1007/978-3-319-93587-4_17)
12. Czapiewski, W.: Methods of minimalization of coolant flow rate in the grinding processes – the review. *J. Mech. Energy Eng.* **1**(41), 2, 117–122 (2017)
13. Sadeghi, M.H., Hadad, M.J., Tawakoli, T., Vesali, A., Emami, M.: An investigation on surface grinding of AISI 4140 hardened steel using minimum quantity lubrication MQL technique. *Int. J. Mater. Form.* **3**, 241–251 (2010). <https://doi.org/10.1007/s12289-009-0678-3>
14. *Cutting fluids for metal cutting. Recommendations for use*. NIIMASH, Moscow (1979). (in Russian)
15. *Improving the efficiency of grinding operations by improving the technique of applying coolant. Guidelines*. NIIMASH, Moscow (1984). (in Russian)
16. Vasilenko, Yu.G.: Current state of coolant supply technology during grinding. *Eng. J.* **4**, 29–34 (2005). (in Russian)

17. Tyuhta, A.V., et al.: Ways to enhance environmental flat grinding by improving the technology of the coolant supply. In: Radionov, A.A. (eds.) 2nd International Conference on Industrial Engineering, ICIE 2016, vol. 150, pp. 1073–1080 (2016). <https://doi.org/10.1016/j.proeng.2016.07.217>
18. Baumgarta, C., Radziwill, J. J., Kustera, Fr., Wegener, K.: A study of the interaction between coolant jet nozzle flow and the airflow around a grinding wheel in cylindrical grinding. In: Outeiro, J., Poulachon, G. (eds.) 16th CIRP Conference on Modelling of Machining Operations, vol. 58, pp. 517–522 (2017). <https://doi.org/10.1016/j.procir.2017.03.261>
19. Irani, R.A., Bauer, R.J., Warkentin, A.: A review of cutting fluid application in the grinding process. *Int. J. Mach. Tools Manuf.* **45**, 1696–1705 (2005). <https://doi.org/10.1016/j.ijmachtools.2005.03.006>
20. Vasilenko, Yu.V., Tyukhta, K.S., Tyukhta, A.V.: The combined method of coolant supply during flat grinding by the periphery of the wheel. *Bull. Samara Center Russ. Acad. Sci.* **13**(4), 942–945 (2011). (in Russian)
21. Stepanov, M., Litovchenko, P., et al.: Coolant supply device. Patent of Ukraine № 136095 (2019). (in Ukrainian)
22. Diskin, M.E.: On the issue of calculating air curtains. *ABOK* **7**, 58–65 (2003). (in Russian)
23. Stroptin, A.S., Nikulin, M.V.: On the issue of calculating air-thermal curtains. *ABOK* **1**, 60–63 (2004). (In Russian)
24. Nikulin, M.V.: Heat exchange of an air curtain jet. *Hydromechanics of heating and ventilation devices*, pp. 27–33 (1989). (in Russian)
25. Elterman, V.M.: *Air curtains*. Engineering, Moscow (1966). (in Russian)
26. Titov, V.P.: Features of a jet of air curtains. *Thermal regime of heating, ventilation, air conditioning and heat and gas supply systems* 177, 3–15 (1980). (in Russian)



# Optimization of Modular Fixture Setup Time in an Automated Assembly Line

Hossein Tohidi<sup>1</sup>  and Tarek AlGeddawy<sup>2</sup>

<sup>1</sup> North Carolina State University, 111 Lampe Dr, Raleigh, NC 27607, USA  
atohidi@ncsu.edu

<sup>2</sup> Western Washington University, 516, High St., Bellingham, WA 98225, USA

**Abstract.** Designing and fabricating different fixtures are among the main barriers for manufacturing systems to produce a variety of products with different geometries. To overcome the time and costs associated with the frequent changes in fixture design, modular fixtures have been developed. The changeability plan of these fixtures is vital for changeable manufacturing systems, especially in automated systems in which robots are in charge of placing and securing parts in their respective places. In this paper, we are extending the model presented in the literature in two directions to further reduce the fixture setup time in a mid-volume mid-variety automated production system. First, we consider both vertical and horizontal movement of the robot to find the optimal changeability plan. Then, a new fixture design is introduced that improves the fixture modularity to hold more products with different geometries. The results prove that the newly proposed models can significantly reduce fixture setup time.

**Keywords:** Changeability · Robot travel path · TSP · Fixture design · MILP

## 1 Introduction

The models presented in [1] can optimally determine the location of each part on the modular fixture as well as the best dowel locations to fix a variety of products with different geometries using modular fixtures with minimal dowel replacements. This can be translated as vertical robot movement, taking a dowel out and inserting it in a new location, in the proposed assembly setting. However, the robot's horizontal movement, traveling between the new locations and current locations, have not been considered in that paper. Therefore, this paper presents a new mathematical formulation that can optimally reduce the total time associated with fixing parts on fixtures, considering the robot's horizontal and vertical movements. Also, the mathematical formulation presented in [1] is extended to another fixture design in order to improve the system performance by enabling it to adapt to more parts' geometries.

## 2 Literature Review

Changeability in manufacturing systems has been implemented in various industries over the last forty years to meet the challenge of changes in product demands [2–4]. For instance, BMW claims the uniqueness of each and every 7 Series vehicle that goes out of the manufacturing line as they can have  $10^{17}$  variations [5]. Although manufacturing a variety of products creates many challenges for manufacturing firms, it provides unique opportunities for firms that can adapt to this rapid change [6]. Changeability is an umbrella paradigm and consists of different manufacturing system characteristics, such as reconfigurability, flexibility, transformability, and agility [7]. Reconfigurability should be applied at all different levels of manufacturing systems, such as planning and control, system design, and machine design [8, 9]. On the system level, reconfigurability is enabled particularly by implementing modular equipment designs such as modular fixtures that can hold a variety of product geometries to reduce production expenses and improve the production rates [2, 3].

Fixtures are fundamental components of a manufacturing system and are used to hold a part securely during the manufacturing or assembly process. Fixture design is a complicated and precise process [4, 5] that can significantly impact the production time, the final cost and quality of the product [10, 11]. To overcome those issues, many researchers focus on designing flexible fixtures that can adapt to a variety of products with different geometries [12–14]. On the operational level, optimizing the changeability plan of those modular fixtures improves the performance of the manufacturing system [1].

This paper reconsiders a hole-pattern modular fixture presented in [1] to increase the changeability of an automated assembly system. In this assembly setting, a robot that is located on top of a conveyor belt loop places different parts on the modular fixture and secures them by inserting four pegs around each part. The more peg replacements occur, the longer fixture setup time is required. To read more about the problem context, readers are referred to [1] where three mathematical formulations, Basic model, LRTE and SLRTE, are presented to optimally determine parts as well as dowel locations to minimize the number of peg replacements. The Basic model only chooses the best locations among the set of potential peg locations, but the LRTE enables the rotation and translation of parts on the cradle to improve the fixture setup time. Finally, SLRTE enables the model to decide the sequence of jobs to be done. However, all models have only considered the robot's vertical movement. In other words, they have only minimized the time associated with lowering and raising the robot's arm to take out dowels and place them in other locations. However, the robot's horizontal movement, from a dowel current location to its new location, is also a significant portion of the fixture setup time that can be optimized. Also, with some modifications in the mathematical formulations presented in [1], they can be extended to be used for a new hole-pattern fixture design, which adds more flexibility to the fixture to provide sufficient forces to hold more parts' geometries. The new design is described in Sect. 3.

The rest of the paper is organized as follows: in Sect. 3, first, the Robot Travel Path Optimization Model (RTPOM) is presented. Then we discuss the need for the new

fixture design and present extensions in proposed models to be used for the new fixture design. The results are presented in Sect. 4, and finally, the conclusion is presented in Sect. 5.

### 3 Research Methodology

#### 3.1 Robot Travel Path Optimization Model (RTPOM)

The models presented in [1], Basic, LRTE, and SLRTE, enable the system to minimize the number of dowel replacement by considering different assumptions. In this section, a mathematical model is developed to not only determine the best peg locations between two successive parts but to figure out the optimized route that the robot should go through to replace the pegs as well. In other words, the problem lies in minimizing the number of pegs that need to be replaced and minimizing the robot’s travel path between current and future peg locations. These two objectives can translate into the robot’s vertical and horizontal movement. The less movement the robot needs to make, the less energy it consumes, and the less fixture setup time it requires.

As it has been proved in [1], finding the optimized parts and dowel locations is NP-Hard, and there is no polynomially solvable algorithm for this problem. Therefore, complicating the LRTE model by adding new decision variables and constraints to determine the robot’s horizontal movement is not justifiable. Therefore, to keep the model efficient for real industrial instances, the two aforementioned objectives are solved separately. In the first step, one of the presented models in [1], Basic, LRTE or SLRTE, is used to determine the parts’ position on the fixture as well as the best peg locations to minimize the number of pegs that need to be replaced. Then, the results are used in the second model (RTPOM) to figure out the minimum travel distance between different peg locations. The dynamic of the proposed method is mapped in Fig. 1.

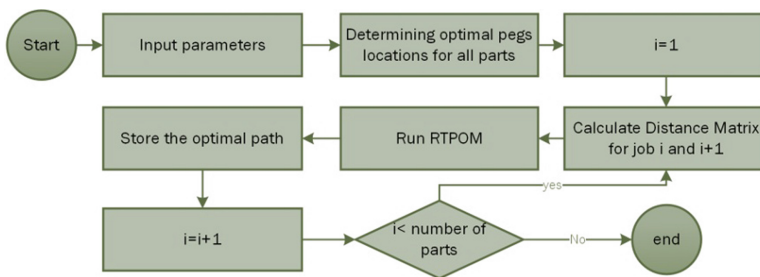


Fig. 1. Solution flowchart.

To discuss the RTPO model, assume that a set of x-y coordinates is given by running the LRTE model. Now, the problem is about finding the best path between the pegs to minimize the total travel distance. To illustrate the problem, let us take a look at the following Fig. 2.



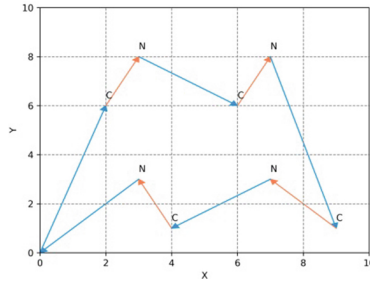


Fig. 2. A feasible travel path between current and future peg locations.

In this figure, 8 different coordinates are given in two different sets, the current (C) and the next (N) locations. A feasible route is a closed path that starts from the origin point (0, 0), visits one of the current locations in order to pick up a peg, then visits one of the new peg locations in order to insert the peg and so on so forth to the last pegs to be replaced. Finally, the robot goes back to the origin points to complete its closed tour for the first two parts. As implied, the problem statement is a type of well-known problem, the Travel Salesman Problem (TSP), which has been discussed in the literature for many years. However, there is a difference between this problem and a standard TSP model. In this problem, the robot needs to visit different sets of locations every other one. Because, as described, the robot must take a peg out from a current location and insert it in its new location. Therefore, the robot is not free to choose all locations among not-visited locations.

TSP models are usually defined by two sets of information: the number of cities to visit, and the distance between each pair of cities. In this paper, the number of cities and their locations is pre-defined by the LRTE model. Then, the results are used in another program to calculate the distance matrix for any two successive parts. The  $D_{ij}$  in that matrix is computed as Euclidean distance between every two pegs in new and current sets. To ensure the problem's logical constraint, i.e., avoiding visiting two points from one set in a row, the distance between them is defined as a big number, M.

The matrix given in Fig. 3 is symmetrical, meaning that the distance from point  $i$  to  $j$  is the same as the distance from  $j$  to  $i$ ,  $D_{ij} = D_{ji}$ . As mentioned before, half of the matrix is filled out with a big number, M, to enforce the logical constraints of the problem. For instance, after leaving the origin point (0, 0), the robot must visit one point from the set of current peg locations to take the peg out. That is to say, visiting any point from the set of next peg locations is logically wrong. Therefore, the distance between the origin point and the set of next locations is set to a big number. Also, after picking up a peg from the current set of peg locations, the robot must visit a location among new locations to insert the peg.

Note that the matrix size is not fixed, and is a function of the number of pegs that should be replaced between parts  $p_1$  and  $p_2$ ,  $n_{p_1,p_2}$ , and it is calculated as below:

	O	C1	C2	C3	C4	N1	N2	N3	N4
O	M	$D_{12}$	$D_{13}$	$D_{14}$	$D_{15}$				M
C1						$D_{26}$	$D_{27}$	$D_{28}$	$D_{29}$
C2						$D_{36}$	$D_{37}$	$D_{38}$	$D_{49}$
C3	M		M			$D_{46}$	$D_{47}$	$D_{48}$	$D_{59}$
C4						$D_{56}$	$D_{57}$	$D_{58}$	$D_{69}$
N1	$D_{61}$	$D_{62}$	$D_{63}$	$D_{64}$	$D_{65}$				
N2	$D_{71}$	$D_{72}$	$D_{73}$	$D_{74}$	$D_{75}$			M	
N3	$D_{81}$	$D_{82}$	$D_{83}$	$D_{84}$	$D_{85}$				
N4	$D_{91}$	$D_{92}$	$D_{93}$	$D_{94}$	$D_{95}$				

Fig. 3. Distance matrix.

Distance matrix size between  $p_1$  and  $p_2 = 2 * n_{p_1,p_2} + 1$   
 The problem formulation is given below:

$$\min \sum_i \sum_{i'} (D_{ii'} * X_{ii'})$$

$$\sum_{i'} X_{ii'} = 1 \quad \forall i$$

$$\sum_i X_{ii'} = 1 \quad \forall i'$$

$$U_i \leq n \quad \forall i | i \neq 1$$

$$U_i \geq 2 \quad \forall i | i \neq 1$$

$$U_1 = 1$$

$$U_i - U_{i'} \leq (n - 1) * (1 - X_{ii'}) \quad \forall i, i' | i \neq 1, i' \neq 1$$

where the objective function is to minimize the robot’s total travel distance, and  $D_{ii'}$  is the distance between two points  $i$  and  $i'$ . In this formulation,  $X_{ii'}$  is a binary variable that is equal to one, if the corresponding route between points  $i$  and  $i'$  is selected. Based on the formulation by Miller et al. [15], an extra variable  $U_i$  is defined to prevent a subtour from being created. Figure 4 presents an infeasible solution with subtours.

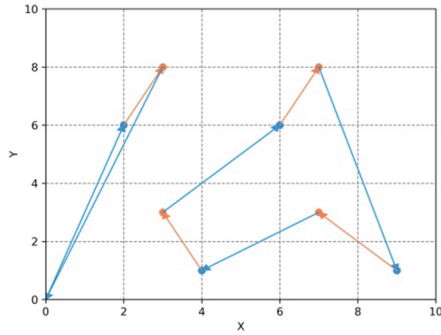


**Fig. 4.** Sub-tours to be prevented.

### 3.2 New Fixture Design

In this section, a new fixture design is introduced that can improve the system performance by enabling it to adapt to more parts' geometries. In the previous design, the fixture was sometimes unable to hold the part securely as inserting pegs in any of the holes cannot grab the part hard enough. This problem is shown in the following Fig. 5.

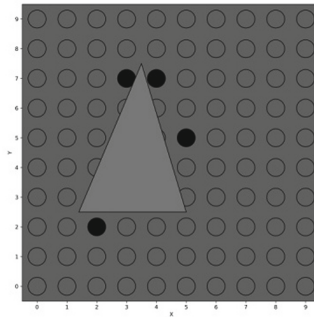


**Fig. 5.** Fixture unable to secure the part securely.

Due to the given part's geometries, the fixture is unable to keep the part securely. As depicted, two of four pegs could not touch the part, which means the part can move freely by importing any forces in those directions. To overcome this problem and increase the changeability of the proposed assembly system, a new fixture is designed by adding holes between every two rows and every two columns in the previous design. In this fixture, the number of holes is increased in the given  $10 \times 10$  surface area with the same size of the pegs' diameter. The isometric and top view of the designed fixture is given in Fig. 6a.

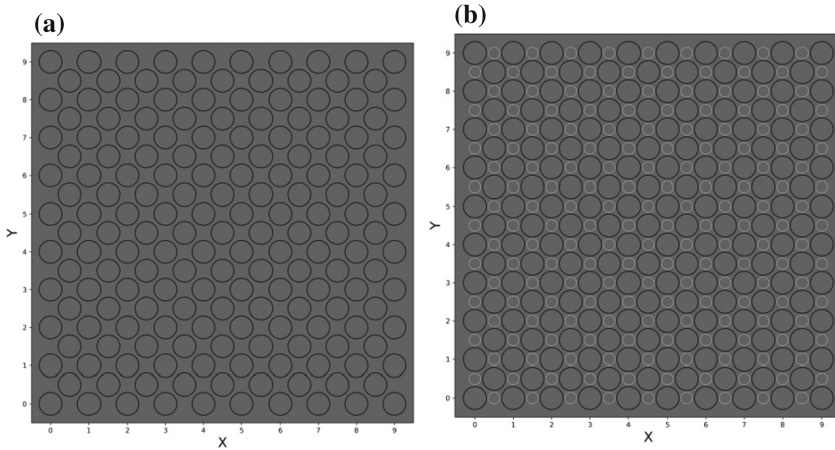


**Fig. 6.** a. New fixture design (left), b. New fixture design with adding imaginary holes (right).

To extend the mathematical models presented in [1] and apply them for the new fixture design, some constraints need to be modified, and one constraint should be added.

Let us take a look at Fig. 6.b. As depicted, imaginary holes (circles with dash lines) are added to the previous design in order to make it similar to the previous fixture. The number of rows and columns in this figure can be calculated using the following formula:

$$n_2 = 2 * n_1 - 1$$

where  $n_1$  and  $n_2$  are the number of rows in the previous and new fixture designs, respectively. Note that the same simple transformation is needed for the first and second coordinate parameters,  $px_{iwl\theta}$  and  $py_{iwl\theta}$ .

As shown, there are 19 holes in each row and each column in a  $10 \times 10$  fixture that was used in the previous section. In LRTE, two constraints determine the size of the fixture. These two constraints need to be redefined. In addition, to ensure that the imaginary holes are not selected, another constraint needs to be added. Note that the row number plus column number for imaginary holes are always odd numbers.

$$0 \leq x'_{iw} \leq 19$$

$$0 \leq y'_{iw} \leq 19$$

$$x'_{iw} + y'_{iw} = 2 * n_{iw}$$

where  $n_{iw}$  is an integer variable that can get any positive value.

## 4 Results

### 4.1 RTPOM Results

To illustrate the application of proposed methods in different instances, the same numerical examples presented in [1] have been reconsidered. As mentioned, the proposed dynamic framework in this paper can use any of the models to determine peg locations. Among them, LRTE and Basic models are used in the first step of the algorithm to find the optimal peg locations; then, RTPOM is used to find the optimized robot travel paths for three different instances.

For the first case with 5 different parts, the optimized routes that the robot should travel to replace the pegs are given in Fig. 7. By using the Basic Model, 14 pegs need to be replaced in total. The LRTE model significantly drops this number to 4 pegs, which is about a 72% reduction in vertical movements. Also, after finding the optimal path for both cases, a 42% improvement in horizontal movements has been observed. The optimal routes are drawn in Fig. 7 between each pair of successive jobs. Therefore, for planning 5 parts on the system, 4 graphs are drawn. In this figure, the red stars and green circles represent current and next peg locations, respectively.

The following table summarizes the results for three numerical examples (Table 1).

### 4.2 New Fixture Design Results

As explained in Sect. 3, the proposed methods can be applied in the new fixture design by making a few modifications. In this section, the similar cases of Sect. 4.1 are solved on the new fixture using the Basic and the LRTE models, and the results are compared with [1] (Table 2).

As shown, the new fixture design gave more flexibility to the proposed models to further improve the fixture setup time by reducing the number of pegs that need to be replaced. Note that in the table, the number of fixed pegs is reported. The number of replacements needed can be computed by  $(4 * \text{No. of parts}) - \text{No. of fixed pegs}$ .

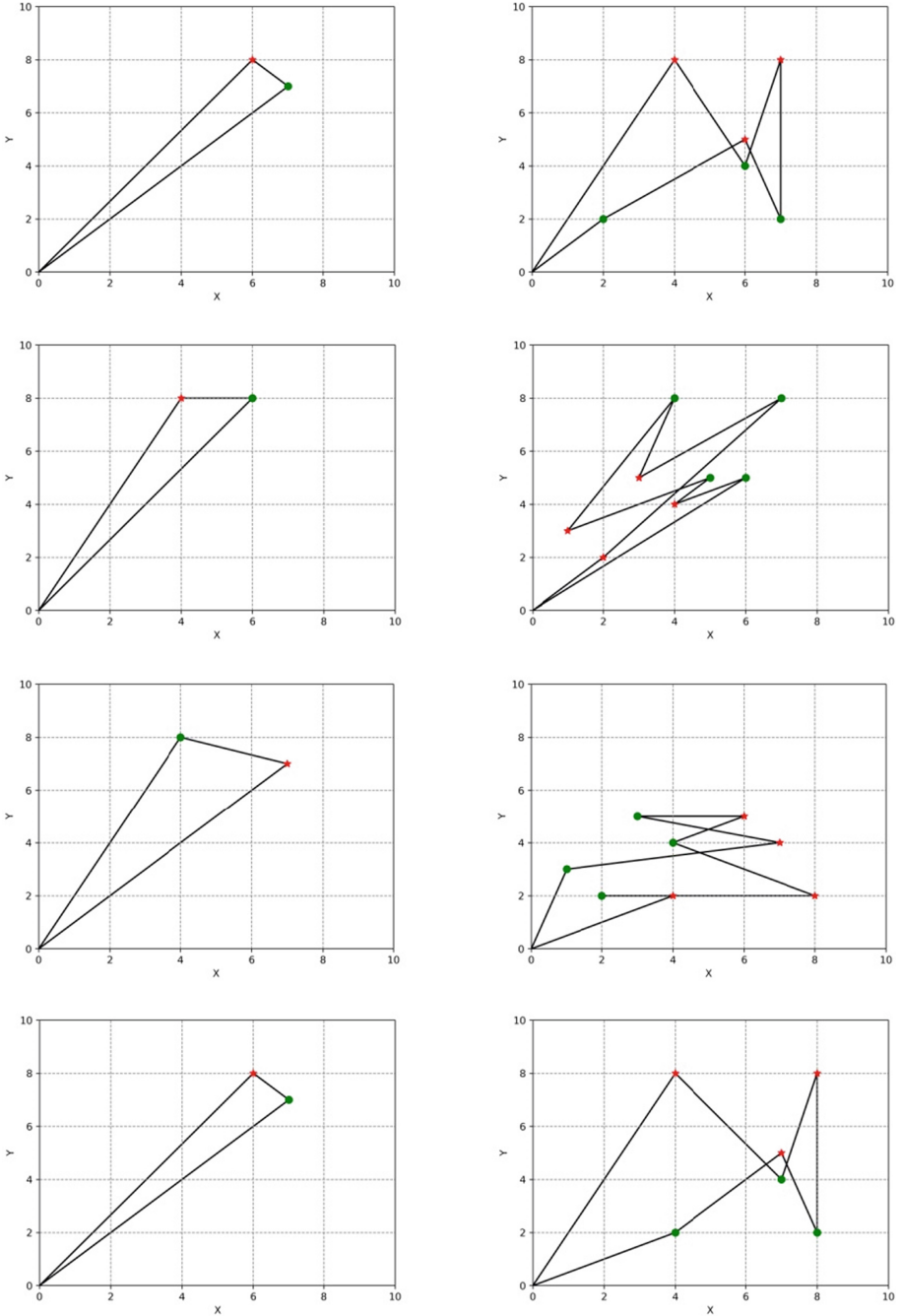


**Fig. 7.** Optimized robot travel path for fixing successive parts on the cradle for Case study 1 using: **a.** left column: LRTE and RTPO model; **b.** right column: Basic and RTPO Model.

**Table 1.** Summary of results.

Instance	Number of parts	Reduction in horizontal movement	Reduction in vertical movement
Example 1	5	42%	72%
Example 2	10	39%	59%
Example 3	50	56%	45%

**Table 2.** Summary of results for the new fixture design using LRTE and Basic Model.

Instance	Number of parts	Number of fixed pegs using basic model		Number of fixed pegs using LRTE	
		Former fixture	New fixture	Former fixture	New fixture
Example 1	5	2	2	12	16
Example 2	10	7	12	23	24
Example 3	50	29	29	110	121

## 5 Conclusions

The models presented in [1] minimize the robot's vertical movements in an automated mid-volume mid-variety assembly line by optimally determining the part as well as dowel locations. These models reduce the number of dowels that need to be replaced and, as a result, significantly reduce the fixture setup time. This paper extended the same idea in two directions. First, we proposed a new framework that uses the same models of [1] in its first step; then uses the results to optimally determine the robot's horizontal path to further reduce the fixture setup time. Second, a new fixture design is introduced in order to improve the system performance by enabling it to adapt to more parts' geometries. By making a few modifications, the models have been extended to be used for this new fixture design.

## References

1. Tohidi, H., AlGeddawy, T.: Change management in modular assembly systems to correspond to product geometry change. *Int. J. Prod. Res.* **57**(19), 6048–6060 (2018)
2. Yu, K., Wang, S., Wang, Y., Yang, Z.: A flexible fixture design method research for similar automotive body parts of different automobiles. *Adv. Mech. Eng.* **2**(10), 1–8 (2018)
3. Tohidi, H., Algeddawy, T.: Planning of modular fixtures in a robotic assembly system. *Proc. CIRP* **41**, 252–257 (2016)
4. Ansaloni, M., Bonazzi, E., Leali, F., Pellicciari, M., Berselli, G.: Design of fixture systems in automotive manufacturing and assembly. *Adv. Manuf. Sci. Eng.* **712**, 2913–2916 (2013)
5. Patil, T.D., Kavdikar, A.V., Nadar, A.T., Shirsat, G.M., Sanyashiv, A.V.: Design of fixture for cross hole drilling of Flange-Yoke. *Int. J. Mod. Eng. Res.* **6**, 19–24 (2016)







6. Bi, Z.M., Zhang, W.J.: Flexible fixture design and automation: review, issues and future directions. *Int. J. Prod. Res.* **39**(13), 2867–2894 (2001)
7. Maler-Sperdelozzi, V., Koren, Y.H.S.J., Hu, S.J.: Convertibility measures for manufacturing systems. *CIRP Ann.* **52**(1), 367–370 (2003)
8. Koren, Y.: General RMS characteristics, Comparison with dedicated and flexible systems. In: *Reconfigurable Manufacturing Systems and Transformable Factories*. Springer, Heidelberg (2006)
9. Chaube, A., Benyoucef, L., Tiwari, M.K.: An adapted NSGA-2 algorithm based dynamic process plan generation for a reconfigurable manufacturing system. *J. Intell. Manuf.* **23**(4), 1141–1155 (2012)
10. Jonsson, M., Ossbahr, G.: Aspects of reconfigurable and flexible fixtures. *Prod. Eng.* **4**(4), 333–339 (2010)
11. Wang, H., Rong, Y., Li, H., Shaun, P.: Computer aided fixture design: recent research and trends. *Comput. Des.* **42**(12), 1085–1094 (2010)
12. Arzanpour, S., Fung, J., Mills, J.K., Cleghorn, W.L.: Flexible fixture design with applications to assembly of sheet metal automotive body parts. *Assem. Autom.* **26**(2), 143–153 (2006)
13. Ivanov, V., Pavlenko, I., Kuric, I., Kosov, M.: Mathematical modeling and numerical simulation of fixtures for fork-type parts manufacturing. In: Knapcikova, L., Balog, M. (eds.) *Industry 4.0: Trends in Management of Intelligent Manufacturing Systems*. EAI/Springer Innovations in Communication and Computing, pp. 133–142. Springer, Cham (2019). [https://doi.org/10.1007/978-3-030-14011-3\\_12](https://doi.org/10.1007/978-3-030-14011-3_12)
14. Loharkar, P.K., Modeling, M.P.: Design and Fabrication of fixture for machining control lever of Tractor’s governor design and Fabrication of fixture for machining control lever of Tractor’s governor, pp. 1–6 (2018)
15. Miller, C.E., Tucker, A.W., Zemlin, R.A.: Integer programming formulation of traveling salesman problems. *J. ACM* **7**(4), 326–329 (1960)



# **Numerical Simulation and Experimental Studies**



# Investigation of Waveforms of Roller Bearing's Working Surfaces on Centerless Grinding Operations

Vasyl Chalyj<sup>1</sup> , Sergiy Moroz<sup>2</sup> , Vitaliy Ptachenchuk<sup>2</sup> ,  
Valentyn Zablotskyj<sup>2</sup>  , and Stanislav Prystupa<sup>2</sup> 

<sup>1</sup> PSC "SKF UKRAINE", 34, Bozhenka St., Lutsk 43017, Ukraine

<sup>2</sup> Lutsk National Technical University, 75, Lvivska St., Lutsk 43018, Ukraine  
{s.moroz, v.zablotskyj}@lntu.edu.ua

**Abstract.** The article investigated the formation of waviness on working surfaces rings of roller bearings, which causes the appearance of noise and vibration in the bearing units of machines and mechanisms. To establish patterns of appearance of waviness some principles of systems theory and mathematic simulation were used; in particular, the establishments of transfer functions, finding the equation of dynamics, usage of Laplace transformations to solve differential equations, building locus diagrams and others. For analysis, a centerless grinding system with some simplifications was considered as a linear, continuous, closed dynamic system. Based on this a flow-chart of plunge centerless grinding model on rigid shoes was compiled and the transfer function was found. The solution of the system's characteristic equation revealed the influence of waviness on the ground surface and the regeneration process of this waviness on the locus diagram of the displacement vector of the workpiece's center.

**Keywords:** Undulation · Dynamic stability · Centerless grinding · Rigid support

## 1 Introduction

When grinding the roller bearings of the roller bearings, it is necessary to ensure rapid removal of the allowance and processing performance [1–3], the final macro- and micro geometric accuracy of the machined surface [4]. It is known that the magnitude of the cut layer during grinding is proportional to the normal grinding force [5, 6], and the formation of the undulation of the workpiece is caused by deviations in the size of the cut layer or changes in the grinding force [7, 8]. The surface waviness depends on the materials of the workpiece and the grinding wheel, the removal performance of the allowance and the relative speed between the workpiece and the circle [9, 10]. The main variable for grinding analysis in most cases is the grinding force that is generated during the cutting process. In order to determine the optimal characteristics of the cutting force, many studies have been carried out [11]. Previous studies have found that the cutting force contains components that, by their parameters, influence the formation

of the operational characteristics of the surface being treated, and also form the microgeometry of the working surface.

Therefore, it is extremely important to use high-performance operations in the final stages of machining that can neutralize adverse hereditary traits and help stabilize and improve the quality of manufacturing of bearing parts. One such progressive and highly productive way of grinding the roller bearing raceways is centrifugal grinding with the support of parts on rigid supports.

## 2 Literature Review

Many years of research by domestic and foreign authors have revealed almost the whole range of factors that affect the quality of the sanded surface. The works [3, 12] set the basic regularities of the formation of a surface layer taking into account thermal processes in the cutting zone.

Also regularities of formation of macro- and microgeometric parameters of the precision of the polished surface and the influence on them of the speed of rotation of the circle, uneven wear, salinization and dulling, composition and methods of feeding ZOR are considered important.

The influence of the dynamic state of the machine, oscillatory processes, including due to the imbalance of the abrasive tool, and the role of the dynamic system of the machine in grinding is considered in [6, 13]. Some factors affecting the quality of grinding processing on automated machines, including those with active control, are considered in [2, 8]. The problems of formation and control of surface waviness are addressed work [10, 14]. However, in these works, there are no recommendations and studies of the processes of rolling waveforms of the roller bearings on the centerless grinding operations. Also, it was found that the vibroacoustic characteristics and performance of the rolling bearings depend on the ratio of the number of waves on the roller track of the ring  $k$  and the number of rollers in the bearing  $Z$ .

Among the scientific works concerning the problem of technological quality assurance of molding and performance characteristics of the parts of rolling bearings, there are four directions: geometric, based mainly on the dimensional analysis of technological processes and operations to achieve the desired level of accuracy of parts, components and products; technological, in which the quality of the surface is considered from the standpoint of interrelations with technological factors; rigid, which mainly investigates the elastic-mass characteristics of the nodes of the technological system, as well as their deformation of parts and their influence on the quality parameters of the forming surfaces; complex, which takes into account a set of factors that affect the quality of formation [15].

As a result of the analysis of literary sources and the conducted statistical analysis of production, the experience is established that the main reasons for the decline in performance (незавершение речення). Roller bearings such as durability, reliability, vibration, noise, rotation accuracy are the state of the geometric structure of the working surfaces of the rings and the physical and mechanical properties of the surface layer.

To characterize the forces acting on grinding, it is necessary to analyze two cases. First, static gravity, constant feed force, and constant torque for a steady-state process should be considered. Second, it is necessary to investigate the dynamic model because grinding is a dynamic process and involves instantaneous forces [8, 9]. In this paper, we analyze a dynamic model that is used to predict the dynamic stability of a centerless grinding process on rigid supports.

### 3 Research Methodology

#### 3.1 Analysis of Static State Forces of Centerless Grinding

Although most of the centerless grinding forces are short-lived, it is appropriate to investigate static or steady-state forces. Figure 1 shows a diagram of the process of centrifugal grinding on rigid supports with active forces. The action of the tangential forces of the supports  $F_A \cdot \mu_1$  and  $F_B \cdot \mu_1$  is neglected since they are not significant in comparison with other forces. The normal  $F_n$  and tangential  $F_t$  components of the grinding force together with the weight of the  $F_G$  part and the magnetic force  $F_M$  cause the reaction forces of the supports  $F_A$  and  $F_B$  to maintain a static equilibrium of the system. It is known that the tangential grinding force is about half of the normal grinding force [6] and depends on the type of grinding wheels.

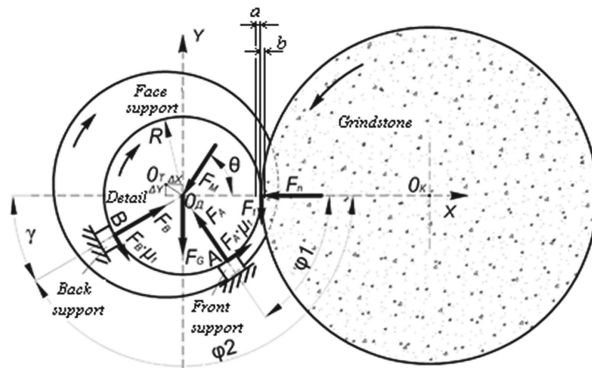


Fig. 1. Calculation scheme of operating forces at centerless cut-in grinding on rigid supports.

With centerless grinding on rigid supports, the back end of the workpiece is driven by a rotating electromagnet. This magnetic end support is mainly used to prevent the workpiece from rotating at the same speed as the grinding wheel. The speed of the workpiece is determined by the speed of rotation of the magnetic cartridge, which creates a relative speed between the workpiece surfaces and the grinding wheel. Quite often, the center of the workpiece is slightly shifted from the center of the end support ( $\Delta X$ ;  $\Delta Y$ ), to ensure constant contact of the workpiece with the supports.

Centrifugal grinding on rigid supports is characterized by two angles,  $\phi_1$  and  $\phi_2$  (see Fig. 1).  $\phi_1 \approx 60^\circ$  - the angle between the contact point grinding wheel - workpiece and

contact point front support - workpiece.  $\varphi_2 \approx 155^\circ \div 180^\circ$  - the angle between contact point grinding wheel - workpiece and contact point rear support - workpiece. The angle  $\gamma$  is defined as  $180^\circ - \varphi_2$  and is called the center height angle in circular centrifugal grinding to the pass. For this horizontal grinding feed configuration,  $\varphi_1$  should be less than  $90^\circ$  and  $\varphi_2 - \varphi_1$  should be less than  $180^\circ$ .

If the forces in Fig. 1 are balanced in the horizontal and vertical directions, then:

$$\sum F_x = -F_n - F_A \cdot \cos(\varphi_1) + F_B \cdot \cos(\gamma) + F_M \cdot \mu \cdot \cos(\theta) = 0 \quad (1)$$

$$\sum F_y = -F_t - F_G + F_A \cdot \sin(\varphi_1) + F_B \cdot \sin(\gamma) + F_M \cdot \mu \cdot \sin(\theta) = 0 \quad (2)$$

where  $\mu$  is the coefficient of friction between the end support and the rear end of the workpiece;  $\theta$  is the angle of application of magnetic force.

The force,  $F_G$ , in Eq. (2) can be neglected in comparison with other forces in the system. Because the angle  $\gamma$  is usually small compared to  $\varphi_1$ , most of the normal grinding force is offset by the back support (reaction of the  $F_B$  support) and the magnetic force of the end support. The tangential grinding force and the vertical component of the magnetic force of the end support are generally offset by the front support (reaction of the  $F_A$  support). If  $F_G$  is neglected and  $F_t/F_n$  is about 1/2, then Eqs. (1) and (2) combine, then we get:

$$F_A = \left( \frac{tg\gamma}{tg\gamma + tg\varphi_1} \right) \cdot \left( \frac{1 - 2 \cdot tg\gamma}{2 \cdot tg\gamma \cdot \cos\varphi_1} \right) \cdot F_n + \left( \frac{tg\gamma}{tg\gamma + tg\varphi_1} \right) \cdot \left( \frac{\cos\theta \cdot tg\gamma + \sin\theta}{tg\gamma \cdot \cos\varphi_1} \right) \cdot F_M \cdot \mu \quad (3)$$

Summing torques around the center of the part we get:

$$\sum M_{O_A} = F_t \cdot R - F_A \cdot \mu_1 \cdot R - F_B \cdot \mu_1 \cdot R - F_M \cdot \mu \cdot r = 0 \quad (4)$$

If a magnetic force is applied to a circular part, then  $r = R$  and the radius disappears from the equation. The supports are often made of hardened steel, so the friction-slip coefficient  $\mu_1$  between the workpiece and the supports is usually quite low. Assuming  $\mu_1 \rightarrow 0$ , then to maintain the relative rotation speed between the workpiece and the abrasive wheel while grinding  $F_M \cdot \mu \geq F_t$ . Therefore,  $F_M \geq F_t$ . The angle  $\gamma$  can be sufficiently increased with the constant magnetic force of the end support, where the normal grinding force will not be offset, which will push the workpiece out of the working area. To prevent this, the torque of the rear support must be balanced. Summarizing the torques of the rear support at the point of contact we obtain:

$$\sum M_B = -F_n \cdot R \cdot \sin\gamma + F_t \cdot R \cdot (1 + \cos\gamma) - F_A \cdot R \cdot \sin(\varphi_1 + \gamma) - F_M \cdot \mu \cdot R \cdot \sin(\theta - \gamma) \geq 0. \quad (5)$$

From Eqs. (3) to (5) determine the angle of application of  $F_M$ :

$$\theta \geq \arcsin(1/(2 \cos \gamma)) \quad (6)$$

Thus, using Eq. (5), the required magnetic force will be calculated with sufficient accuracy for practical application based on the force  $F_i$  for actual processing, depending on the grinding conditions, and according to (6) the angle of application of the magnetic force  $\theta$  depending on the selected angle adjusting the rear support  $\gamma$ .

### 3.2 Centrifugal Grinding Instant Analysis

If the rigidity of the machine in the initial position is acceptable, then only the geometry of the process is important. Instantaneous force can be obtained through the current cutting depth by summing the initial waviness of the workpiece and the current arc coordinate of the workpiece (given both rigid supports). An analysis of the impact of one projection on the workpiece shows that the instantaneous grinding force will change when the projection passes through the front support, then the rear support, and again when it directly meets the grinding wheel after one full rotation. These three geometric effects can be considered as three-time delays in the mathematical model. Thus, at any moment, the theoretical depth of cut can be found, knowing only the initial waviness of the workpiece and the time elapsed during grinding (at a constant rotational speed). The theoretical cutting depth can be converted to grinding power, knowing the cutting rigidity [9]. Cutting depth combined with cutting rigidity gives instant normal grinding force. The newly formed undulations are the result of a change in the actual cutting depth.

The temporal effects of the waviness components in the model are quite simple in origin. If there is one depression or protrusion on the workpiece, a temporary delay (angular velocity of the workpiece to the adjacent angle  $\varphi_1$ ) causes the projection to move from the grinding wheel to the front support. When the projection meets the front support, the workpiece moves up (parallel to the rear end support) and moves away from the grinding wheel by a value (Fig. 1). Assume the projection on the surface of the part is equal to a unit. Thus, the horizontal displacement of the center of the workpiece, and through the conditional unit of the projection is equal:

$$a = \frac{\sin(\varphi_2)}{\sin(\varphi_2 - \varphi_1)} \quad (7)$$

Similarly, there is a further delay when the projection passes through another support. If the protrusion falls on the second support forces the workpiece to press against the grinding wheel parallel to the front support, this increases the grinding force. This displacement  $b$  is horizontal in shape similar to the front bearing factor and for the unit of the magnitude of the projection is:

$$b = \frac{\sin(\varphi_1)}{\sin(\varphi_2 - \varphi_1)} \quad (8)$$

The part also has a third delay effect called regeneration. When the projection rotates 360° and returns to the grinding wheel, the instantaneous depth of cutting depends on the projection resulting from the previous rotation. Thus, the grinding force depends on the depth of cutting, the convexity or protrusion will increase the grinding force, while the concavity or depression will cause a proportional decrease in force.

Also, the grinding wheel has its regeneration effect based on the accidental formation of the waviness of the circle due to wear. The effect of regeneration of the grinding wheel affects the long grinding process, where the processing time exceeds the regeneration time, as well as in the case of a long period between edits of the grinding wheel. The regeneration of the part takes only a few seconds. Therefore, the regeneration effect of the grinding wheel is neglected as negligible compared to the effects of the workpiece. The grinding wheel will be considered perfectly circular with characteristics of constant and even wear. We accept constant cutting rigidity at grinding for constant values of removal of an allowance.

### 3.3 Theory and Equation of Geometry Adjustment of Centrifugal Mortise Grinding on Rigid Supports

For the study, we break down the model into sections and analyze each section separately with their subsequent association, to form conclusions. The proposed model uses Laplace operators to analyze the centerless grinding system (Fig. 2).

To solve the characteristic equation of the system  $1 + D(s) \cdot H(s) = 0$  and to find stable and unstable solutions, to separate the influence of geometry and the machine, we transform it to the form  $H(s) = -1/D(s)$ . Consider that

$$D(s) = \frac{1 - e^{-2\pi s}}{1 - ae^{-\varphi_1 s} + be^{-\varphi_2 s}}; H(s) = K \sum_{n=1}^m \frac{\omega_n^2}{S^2 + 2\xi\omega_n S + \omega_n^2} \tag{9}$$

For geometric analysis, we consider the machine to be infinitely rigid, so the previous equation will turn into

$$-1/D(s) = 0 \tag{10}$$

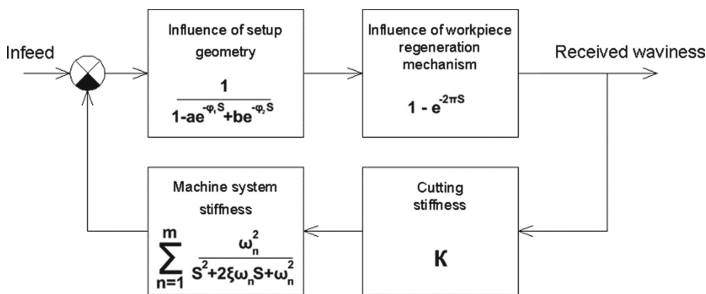


Fig. 2. Flowcharts for simplifying die-cut grinding on rigid supports.

Investigation of the transfer function and the solution of the characteristic equation will be solved by graphical methods.

In the Laplace region, the delay time is represented by an exponential function,  $e^{-\Omega s}$ , where  $\Omega$  is the phase angle, and  $s$  is the Laplace operator ( $s = \sigma + jn$ ). Investigating part of the Eq. (10) by presenting the waveform of the center of the displacement vector of the center of the workpiece (hereinafter the monograph) in the form of  $1/D(s)$ , the exponential phase shift of the angles of supports  $\varphi_1$  and  $\varphi_2$ :

$$1 - a \cdot e^{-\varphi_1 s} + b \cdot e^{-\varphi_2 s} = 0 \quad (11)$$

Since the Laplace operator,  $s = \sigma + jn$ , has both: real and imaginary parts, the exponentials in Eq. (6) are complex functions, that is:

$$e^{\sigma + jn} = e^{\sigma} \cdot (\cos(n) + j \sin(n)) \quad (12)$$

Let us distinguish between real and imaginary components:

$$\text{Re} = 1 - a \cdot e^{-\sigma\varphi_1} \cos(n\varphi_1) + b \cdot e^{-\sigma\varphi_2} \cos(n\varphi_2) \quad (13)$$

$$\text{Im} = a \cdot e^{-\sigma\varphi_1} \sin(n\varphi_1) + b \cdot e^{-\sigma\varphi_2} \sin(n\varphi_2) \quad (14)$$

These equations can be analyzed for different  $\sigma$ ,  $n$ ,  $\varphi_1$  and  $\varphi_2$  with the factors  $a$  and  $b$ , which are deduced in Eqs. (7) and (8).

The stability analysis is simpler when the stability limit  $\sigma = 0$  is observed in  $s = \sigma + jn$ . Thus after transformation of Eqs. (13) and (14) we have:

$$\text{Re} = 1 - a \cdot \cos(n\varphi_1) + b \cdot \cos(n\varphi_2) \quad (15)$$

$$\text{Im} = a \cdot \sin(n\varphi_1) + b \cdot \sin(n\varphi_2) \quad (16)$$

For any given debugging condition, the angles  $\varphi_1$  and  $\varphi_2$  will not be variable, so Eqs. (15) and (16) are plotted as complex functions of frequency,  $n$ . The moving hodograph vector of the center of a part in a complex plane is similar to circles around a point (1; 0). For different angles of adjustment of rigid supports the angular orientation of the hodograph changes.

Further studies have shown that slight changes in  $\sigma$  from the stability boundary  $\sigma = 0$  cause a change in the diameter of the center of motion of the moving center. This feature is used to evaluate the stability of the geometry of the rigid support.

Also, the importance and trends of factors  $a$  and  $b$  were established. In particular,  $a$  and  $b$  in Eq. (11) represent the effect of the projection on the cutting depth as it passes through the front and rear supports, respectively. Therefore, it is determined that  $\varphi_1$  or  $\varphi_2$  affects the normal component of the grinding force, the depth of cutting, the stability in the cutting zone and, as a consequence, the harmonics of the newly formed waviness.



360° rotation of the workpiece back to the grinding wheel represents the third delay time in the proposed model. The regeneration mechanism is very important since the instantaneous depth of cutting will depend heavily on the amount of allowance for the grinding wheel part, which will be caused by premature rotary cutting. The real and imaginary components in this case are:

$$\text{Re} = \frac{-1 + e^{-2\pi\sigma} \cos(2\pi n)}{1 + e^{-4\pi\sigma} - 2e^{-2\pi\sigma} \cos(2\pi n)} \quad (17)$$

$$\text{Im} = \frac{e^{-2\pi\sigma} \sin(2\pi n)}{1 + e^{-4\pi\sigma} - 2e^{-2\pi\sigma} \cos(2\pi n)} \quad (18)$$

For geometric analysis at the boundary of stability  $\sigma = 0$ , Eqs. (17) and (18) are reduced to simpler:

$$\text{Re} = \frac{-1}{2} \quad (19)$$

$$\text{Im} = \frac{\sin(2\pi n)}{2 - 2 \cos(2\pi n)} \quad (20)$$

Equation (20) ranges from plus infinity for integers (5,000, 6,000, etc.) and minus infinity for only slightly smaller than the target (5,999, 6,999, etc.). As  $\sigma$  changes from the stability limit  $\sigma = 0$ , the regeneration mechanism folds into itself and forms circles. The small deviations in  $\sigma$  significantly affect the size of these circles, which will become important when the rigidity of the machine is specified.

In the Laplace region, a multiplication action is required to combine the ripple mechanism and the regeneration mechanism. For graphical analysis, the mechanism of combined influence is found by multiplying the vector by the corresponding  $s = \sigma + jn$ . For this method, the vector from the origin for both the undulation and regeneration mechanisms is at the same frequency and  $\sigma$  (here,  $\sigma = 0$ ). In vector multiplication, the values of each vector are multiplied and the angles from the positive real axis are added.

Figure 3 shows the sampling elements of the combined operation of the hodograph with 2 to 10 harmonics under a particular tuning condition. These forms of hodographs are centered around a point  $(-0.5; 0)$  in a complex plane and have infinite asymptotes spanning from 0° to 360°. Asymptotes have imaginary components, starting with plus infinity for integer numbered harmonics (5,000, 6,000, etc.) and ending with minus infinity for numbers slightly smaller than integers (5,999, 6,999, etc.). It is characteristic that the asymptote is the most variable for these hodographs. This will confirm that asymptotes about 0° indicate geometric instability.

## 4 Results

The hyperbolas of the displacement and regeneration of the displacement hodograph are predicted to change in their asymptotic angles. It is found that the asymptotes follow the main tendency to increase by about  $2.5^\circ$  in harmony with even and odd, whole and near integer components grouping together about  $180^\circ$  from each other. We find the tendencies of the asymptote of angles with change  $\varphi_2$  for several harmonics at a constant angle of the front support,  $\varphi_1 = 55^\circ$ , namely a decrease in the asymptote of the angle with increasing  $\varphi_2$ .

Because asymptotes of angles follow clear arrays, interpretation of angles will be useful in understanding the geometry of centrifugal grinding processes. Two possible interpretations are proposed. First, it requires a deep analysis of the multiplication of the waveguide displacement and regeneration hodographs. The second, possible interpretation of the asymptote of angles comes from the observation of the graphical coincidence of the combined hodograph of the movement of regeneration mechanisms and the waviness with the hodograph of the motion of an infinitely rigid machine.

In the article, the mechanism of the influence of waviness was defined as unstable when the moving hodograph had a negative real part. The angle of the unstable hodograph of the movement of the undulation mechanism will be greater than  $90^\circ$  or less than  $-90^\circ$  from the positive real axis. Since the moving movement's hodograph is also in a certain region, its angle will also be similar at a certain frequency. When the mechanisms of waviness and regeneration coincide at a certain frequency, that is, their geometrical angles are canceled, then the combined moving hodograph will lead to hyperbole with asymptote  $0^\circ$  ( $-360^\circ$ ). This mechanism of coincidence implies geometric instability asymptote of a particular harmonic.

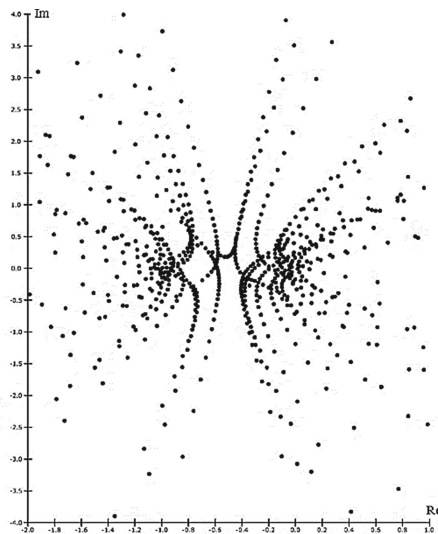


**Fig. 3.** Points from merged vectors of vectors for several harmonics under given debugging conditions. Asymptote angles differ from each other.

The moving hodograph of an infinitely rigid machine is the point of origin at the origin in a complex plane. Thus, the wave displacement and regeneration hodograph are centered around the point  $(-0.5; 0)$ , any particular displacement hodographs having an asymptote of about  $0^\circ$  are likely to intersect with the machine displacement hodograph. The graphical coincidence of the results in the mechanism of the corresponding influence for this particular frequency of waviness allows the growth of this harmonic due to instability in the cutting zone. This interpretation uses an infinitely rigid machine and therefore implies geometric instability of the waviness frequency based on the vector coincidence in the complex plane.

Since the asymptote angles depend on the number of projections (harmonics) and the geometry of the debugging, it is possible to predict, given the analysis above, which harmonics are unstable in the range of debugging conditions. If the asymptote angle of one harmonic is investigated throughout the complex geometry of debugging, then the theoretical geometric instability of this harmonic number will be observed when the asymptote angle is multiple of  $2\pi$  radians.

Figure 4 shows a general picture of the geometric instability of the undulations from 2 to 22 harmonics under the usual conditions of the geometry of centrifugal deburring based on asymptote angles. It also shows that most combinations of rigid support angles have some geometric instability and that harmonic instability is consistent with the array. For example, 12 harmonics are geometrically unstable in the region of  $\varphi_1 = 60^\circ$  and  $\varphi_2 = 165^\circ$ , 14 harmonics are unstable above and to the left about  $52^\circ$  and  $168^\circ$ , 16 harmonics up and to the left of 14, and so on. This chart allows you to choose a geometry for adjusting grinding on rigid supports that increases or decreases the parameters of a particular harmonic.

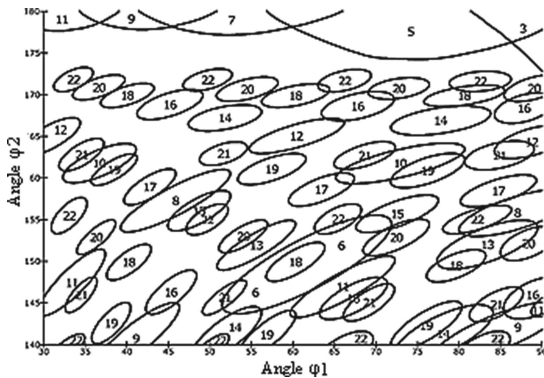


**Fig. 4.** The geometric instability waviness diagram is based on the angular analysis of the unified hodograph of moving on the boundary of stability within the ordinary geometry of centrifugal sanding.

## 5 Conclusions

Using the results of the above studies allows us to provide the necessary parameters of waviness on the working surfaces of the roller bearings. Taking into account the presented algorithm of research, it is possible to find the general picture of geometric instability of undulation under usual conditions of the geometry of debugging of center-free grinding.

The data presented in the paper provide a high probability of geometrical instability in the cutting zone when grinding, the diagram in Fig. 4 allows you to choose the geometry of adjustment of grinding on rigid supports, which predictably increases or decreases the parameters of a certain harmonics of waviness.

The control of the undulations of the surfaces of the bodies of rotation on the centerless grinding operations is an important condition for ensuring the optimum parameters of the quality of the working surfaces of the roller bearings and as a consequence of the operational characteristics of the bearing, such as noise, durability, reliability.




## References

1. Kudinov, A.: Qualitative identification of vibrations and forms of loss of vibration resistance in machine tools. *STIN* **7**, 15–21 (1999)
2. Kalchenko, V., Yeroshenko, A., Oyko, S.: Mathematical modeling of abrasive grinding working process. *Sci. Bull. Natl. Min. Univ.* **6**, 76–82 (2017)
3. Larshin, V., Lishchenko, N.: Adaptive profile gear grinding boosts productivity of this operation on the CNC machine tools. *Lecture Notes in Mechanical Engineering F2*, pp. 79–88 (2019)
4. Albizuri, J., Fernandes, M., Garitaonandia, I., Sabalza, X., Uribe-Etxeberria, R., Hernbndez, J.: An active system of reduction of vibrations in a centerless grinding machine using piezoelectric actuators. *Int. J. Mach. Tools Manuf.* **47**(10), 1607–1614 (2007)
5. Fedotkin, I.: *Mathematical Modeling of Technological Processes*. Librocom, Moscow (2016)
6. Tkachuk, A., Zablotskiy, V., Kononenko, A., Moroz, S., Prystupa, S.: Directed formation of quality, as a way of improving the durability of conjugated parts of friction pairs. In: Ivanov, V., et al. (eds.) *Advances in Design, Simulation and Manufacturing II. DSMIE 2019. Lecture Notes in Mechanical Engineering*. Springer, Cham (2019)
7. Yakimov, A., Novikov, F., Novikov, G., Serov, B., Yakimov, A.: *Theoretical foundations of cutting and grinding materials*. OGPU, Odessa (1999)
8. Fesenko, A., Basova, Y., Ivanov, V., et al.: Increasing of equipment efficiency by intensification of technological processes. *Period. Polytech. Mech. Eng.* **63**(1), 67–73 (2019). <https://doi.org/10.3311/PPme.13198>
9. Chalvi, V., Moroz, S., Ptsashenchuk, V.: Simulation of the formation of wavelength of working surfaces of roller bearings on centrifugal polishing operations. *Technol. Audit. Prod. Reserv.* **5**/7(25), 57–66 (2015)
10. Chetverzhuk, T., Zabolotnyi, O., Sychuk, V., Polinkevych, R., Tkachuk, A.: A method of body parts force displacements calculation of metal-cutting machine tools using CAD and CAE technologies. *Ann. Emerg. Technol. Comput. (AETiC)* **3**(4), 37–47 (2019)

11. Chaly, V.: Maintenance of the quality of working surfaces of rings of roller bearings with centrifugal mortise grinding by means of synthesis of optimum dynamic properties of the machine. *Scientific Notes. Interuniversity Collection* 29, 235–239 (2010)
12. Larshin, V., Lishchenko, N.: Gear grinding system adapting to higher CNC grinder throughput. *MATEC Web Conf.* **226**(04033), 1–6 (2018)
13. Stepanov, M., Ivanova, L., Litovchenko, P., Ivanova, M., Basova, Y.: Determination of parameters of cylindrical grinding with additional intermediate dressing. In: Ivanov, V., et al. (eds.) *Advances in Design, Simulation and Manufacturing II. DSMIE-2019. Lecture Notes in Mechanical Engineering*, pp. 330–340. Springer, Cham (2020). [https://doi.org/10.1007/978-3-030-22365-6\\_33](https://doi.org/10.1007/978-3-030-22365-6_33)
14. Stepanov, M., Ivanova, L., Litovchenko, P., Ivanova, M., Basova, Y.: Model of thermal state of the system of application of coolant in grinding machine. In: Ivanov V., et al. (eds.) *Advances in Design, Simulation and Manufacturing. DSMIE-2018. Lecture Notes in Mechanical Engineering*, pp. 156–165. Springer, Cham (2019). [https://doi.org/10.1007/978-3-319-93587-4\\_17](https://doi.org/10.1007/978-3-319-93587-4_17)
15. Lebedev, V.G., Klimenko, N.N., Uryadnikova, I.V., Chumachenko, T.V., Ovcharenko, A. V.: The definition of amount of heat released during metal cutting by abrasive grain and the contact temperature of the ground surface. *East. Eur. J. Enterp. Technol.* **5/7**(83), 43–50 (2016)



# Theoretical and Experimental Studies of Changes in the Workpiece Shape During Narrow Die Indentation

Vitalii Chukhlib<sup>1</sup> , Evhen Klemeshov<sup>2</sup>, Serhii Gubskiy<sup>1</sup> ,  
Anton Okun<sup>1</sup> , and Nikolay Biba<sup>3</sup>

<sup>1</sup> National Technical University “Kharkiv Polytechnic Institute”,  
2, Kyrpychova St., Kharkiv 61002, Ukraine  
profdnepro@gmail.com, gubskiyso@gmail.com,  
okunanton@gmail.com

<sup>2</sup> Z. I. Nekrasov Iron and Steel Institute of NAS of Ukraine,  
1, Starodubova Sq., Dnipro 49050, Ukraine  
gleb.gorban@gmail.com

<sup>3</sup> MICAS Simulations Ltd., 107, Oxford Road, Oxford OX4ER, UK  
micas@qform3d.co.uk

**Abstract.** The study performs the analysis of existing technological schemes of manufacturing crankshaft forgings. Advanced technology of the manufacturing is proposed based on this analysis. The influence of sizes of a tool and its indentation depth on the forming process of a workpiece is examined. As a result of the carried-out theoretical and experimental studies, dependency diagrams of the influence of the upper die thickness and its indentation depth on the change in sizes of the workpiece, namely the maximal widening, the lengths of the contact areas of the workpiece with the upper and lower dies and the value of the maximal workpiece diameter reduction is received. These diagrams can be used to determine optimal parameters of the process of the narrow die indentation into a workpiece to receive the optimal form of the workpiece, used for the subsequent forging. The comparison of the results of the experimental studies and computer simulation in the QForm V8 program showed appropriate convergence of the results.

**Keywords:** Narrow die · Indentation · Forging

## 1 Introduction

Nowadays, companies and enterprises, which produce forgings, tend to develop and implement resource-saving technologies due to strong demand for forgings made of alloyed or special steels. Such forgings, require a special mode of deformation to obtain high mechanical properties, which increases the cost of the forging production in comparison with the production of forgings made of plain carbon steels. Also, the forging process is characterized by the high consumption of metal that affects the cost of final products and associated with their further mechanical processing.

By focusing on the development of resource-saving technologies for forging, it is possible to pick out one product, which has high labour intensity. One of such products

is a crankshaft. The volume of metal, used for its manufacturing, is measured in tons. In most cases, alloyed steels are used. The improvement of the technology is of particular interest, because, when forging, a large part of the product is not only covered by an allowance but also by an overlap in a part of a shaft knee. In this case, tens or even hundreds of kilograms of metal are wasted during machining. Such removal of metal often facilitates the deterioration of mechanical properties of a product while in operation, because fibres of metal during machining are cut in the most responsible and heavily loaded places of the final product. Taking into account all the production features mentioned above, the development of resource-saving technologies of manufacturing crankshaft forgings is an important issue.

## 2 Literature Review

A technological process of manufacturing crankshaft forgings is a time-consuming process that consists of many forging operations and technological transitions [1–5]. Considering this, it is difficult to track from the beginning an impact of each forging operation on mechanical properties and the quality of a final forging as a whole. Each stage, whether it is a billet forging from an ingot or forging process of a crankshaft itself, requires separate consideration and study, since each step has a specific influence on the quality of forgings [6–15].

In [16], a labor intensity classification for the execution of forging forms is provided. According to this classification, crankshafts are the most complex forgings. C35, C40, C50, GS20Mn5, 40Mn4, 46Mn7 steels, and others are frequently used for producing most crankshafts of stationary, marine and diesel engines. Shafts of high-speed engines are manufactured from the same steels and of chrome, chrome-Nickel, chrome-molybdenum (41Cr4, 40NiCr6, 34CrMo4, 30CrNiMo8, 14NiCrMo134, etc.). Steels, alloyed with vanadium, chromium, molybdenum, and nickel have the increased hardness, ductility, wear resistance (26CrMo4, 41CrAlMo7, 40NiCrMo6, etc.) and are used to produce crankshafts of diesel engines with increased power. The use of carbon steel for crankshafts of engines with low and medium power is explained by low cost and excellent mechanical properties of these steels [17, 18].

An essential stage in the process of forging crankshafts that affect mechanical properties of forgings is a workpiece preparation stage. This stage includes roughing an ingot, setting and drawing to the size of a workpiece for the subsequent forging. Main parameters of the setting process, affecting the stress-strain state of the metal, are: 1) the shape factor of the workpiece ( $h/D$ ); 2) the degree of the deformation ( $\varepsilon$ ); 3) the strain rate ( $\dot{\varepsilon}$ ); 4) the temperature ( $T$ ). And main parameters of the forging drawing are: 1) the feed rate; 2) the degree of the unit compression; 3) the degree of the forging reduction during the deformation; 4) the shape factor of the workpiece; 5) the method of applying the deforming force (the canting scheme) [19].

The authors of the paper [20] conducted experiments using a computer simulation. Their results allowed them to define the influence of workpiece parameters - the shape factor ( $h/D$ ), and deformation parameters - the degree of the deformation ( $\varepsilon$ ), on the uneven deformation distribution in metal during the setting operation of an ingot with the subsequent forging drawing to a round cross-section. A canting scheme during the drawing of the ingot was grounded in [21].

In another paper [22], the authors considered various schemes of crankshaft forging that are used at the place of production. According to this source, the forging process of a crankshaft may vary depending on the design features of a shaft. However, forging a one-knee shaft has only one version. In this case, a round workpiece is marked along its length based on the calculated volume of metal, needed to forge bearing journals. Then it is performed the forging operation of fullering and forging the bearing journals.

The fullering operation can be performed using a special tool (fuller) with both round and triangular cross-sections and at a fullering depth of 100...300 mm. To fuller to a greater depth, the operation only with a triangular fuller is carried out. Since a tightening of metal edges occurs at the point of contact with the tool while forging. Therefore, a stock of metal to the knee height in 10 to 25% is provided [23]. At the same time, the central part of metal (shaft knee) remains with the same level of processing after setting and forging drawing of an ingot. This has a negative impact on the quality of forgings, because of the heterogeneity of mechanical properties in different parts of the shaft. In addition to this, when machining, a part of metal (overlap) is removed as a waste that negatively impacts the quality of forgings due to the cutting of metal fibres in the area of a crankpin [24].

Considering all the features mentioned above of the technology of manufacturing crankshaft forgings, improved technological forging scheme, which allows to channelling metal fibres in the area of a crankpin and shaft cheeks and reducing metal consumption during mechanical processing.

### 3 Research Methodology

Since the technology of manufacturing large crankshaft forgings involves the use of multiton metal ingots, that's why in some cases full-scale production experiments are difficult to conduct and not feasible from an economic point of view. For the investigation of developed technologies of manufacturing large crankshaft forgings, experiments with scaled models of real workpieces are used.

Therefore, in the paper, based on the analysis of technological schemes of manufacturing crankshaft forgings, as well as drawings of final details, a workpiece for the subsequent forging was chosen. This workpiece is a smooth shaft with a circular cross-section. Its cylinder length was selected based on the volume of metal for manufacturing one forging, as well as taking into account the scale factor. Therefore, a cylinder with a diameter of 40 mm and a length of 50 mm was a workpiece for a full-scale experiment. C1 grade lead was used as stock material. Figure 1 shows the workpieces used in experiments.

According to the technological scheme, developed by the authors and presented in Fig. 2, steel plates (thin die) with different thicknesses were used for the deformation of the workpieces.





**Fig. 1.** Lead workpieces used in experiments.

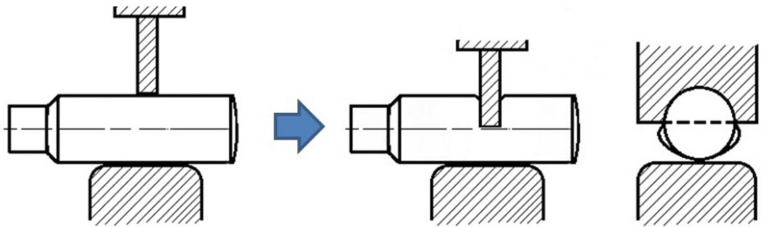


**Fig. 2.** A schematic representation of the indentation process of a narrow die into the workpiece.

Based on the analysis of final product drawings, we chose three fundamental values of the die thickness, corresponding to the distance between the knee cheeks taking into account allowances. These values of the die thickness for the full-scale experiment were 4 mm, 8 mm and 12 mm (Fig. 3). A lower deforming tool, in this case, was a setting plate. Also, based on the analysis of product drawings, the optimal indentation depth of a thin die was determined. This depth reached 50% of the workpiece diameter.



**Fig. 3.** Narrow dies with a thickness of 4 mm, 8 mm and 12 mm.

Application programs based on the finite element method are increasingly used in free forging process studies. One such program is the QForm V8 program, which allows calculating changes in the form of a workpiece and values of the stress-strain state of the metal.

The finite element method (FEM) has become a common practice for engineering analysis in different branches of human activities. Many users “idealize” results obtained with this method. However, it is important to keep in mind that FEM is a numerical method based on certain assumptions. In the process of formulating a problem, setting initial data, deriving equations and their numerical solving with visualization of results, some errors may occur. Therefore, to use QForm V8 properly and minimize possible errors, it is necessary to understand how the program works, how it uses the input data, how the initial data influence simulation results and how to interpret these results correctly. In this regard, it was decided to compare the final data of experimental studies and computer modelling to determine the accuracy of the chosen parameters of the developed technological scheme.

To simulate the indentation process of the thin die, 3D models of the dies and workpiece were created. It is known that the QForm V8 program allows simulating a flat deformation task as well, but in the processes of free forging it is necessary to consider changes in the form of the workpiece in volume. Figure 4 shows the workpiece and a deforming tool as an assembly.

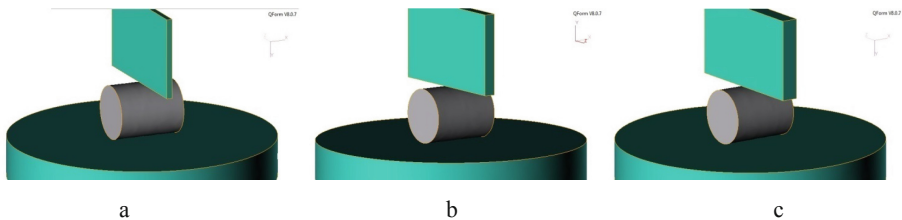


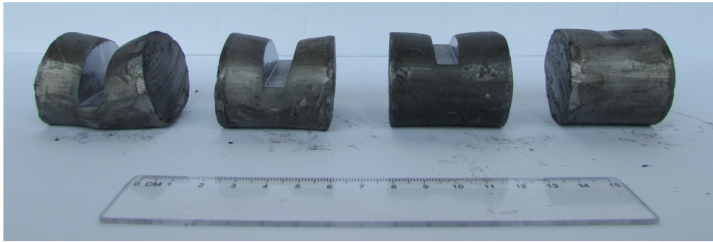
**Fig. 4.** The 3D model of the workpiece and the deforming tool created in the QForm V8 simulation program (the thickness of the narrow die is following: a – 4 mm; b – 8 mm; c – 12 mm).

## 4 Results

As a result of the computer simulation in the QForm V8 program and conducted a full-scale experiment, it was obtained the following workpieces, shown in Fig. 5.



a



b



c

d

e

**Fig. 5.** The changes in form of the workpieces after the indentation of the narrow die with a thickness of 4 mm (a) and 8 mm (b) received by the full-scale experiment and after the indentation of the narrow die with a thickness of 4 mm thick (c), 8 mm (d) and 12 mm (e) received using the computer simulation in the QForm V8 program.

As we can see from Fig. 5, the changes in the form of the workpiece after the narrow die indentation is complicated. Therefore, to describe the form of the workpiece after completing the deformation, the following parameters, shown in Fig. 6, were examined.

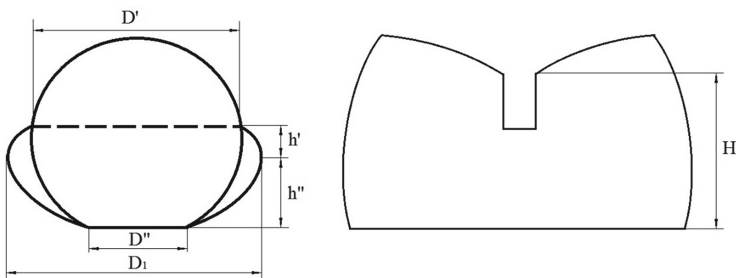


Fig. 6. A schematic representation of the workpiece after the deformation.

The basic geometrical size for comparison of all the measured values was the initial workpiece diameter  $D_0$ . It was equal to 40 mm. Measured values were as follows  $D_1$  (the maximal widening of the workpiece after the deformation),  $D'$  (the contact length of the workpiece and narrow die, that is indented),  $D''$  (the contact length of the workpiece and lower die),  $h'$  and  $h''$  (the height of the resulting metal flow from the contact zone of the workpiece with the die to the point with the maximum diameter  $h'$  and from this point to the contact zone of the workpiece with the lower die  $h''$ ),  $H$  (the minimal height of the workpiece). The value  $\Delta D$ , which was the difference between the initial diameter and maximum widening value of the workpiece, was used as well.

After analyzing the values mentioned above and comparing some of them with the initial diameter, the following dependency diagrams, depicted in Fig. 7, 8 and 9, were obtained.

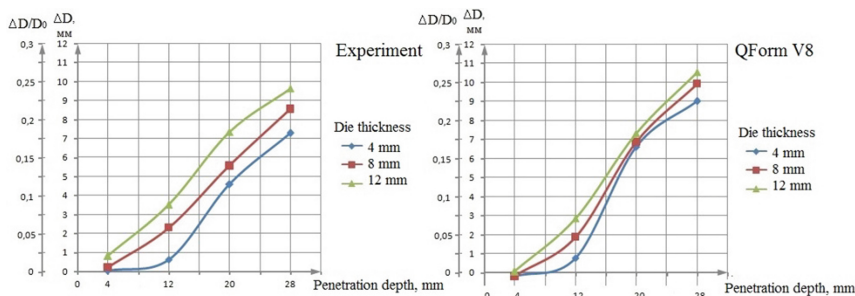
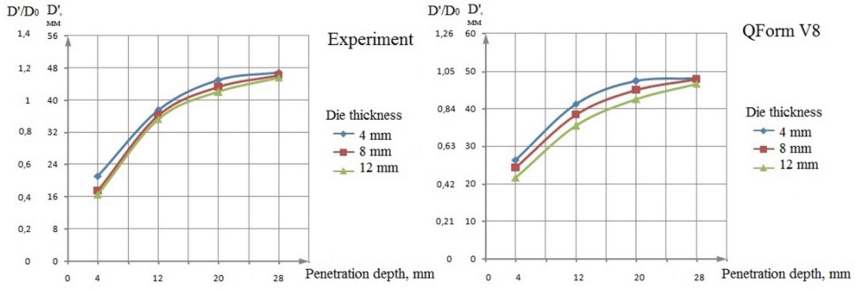
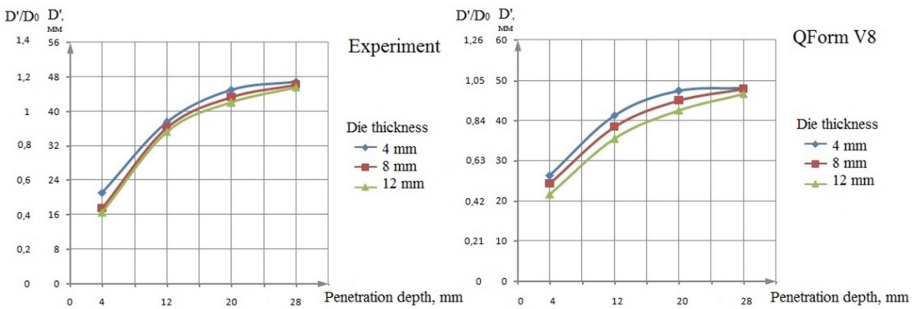


Fig. 7. Dependency diagrams of increasing the maximal widening of the workpiece ( $\Delta D$ ) on the indentation depth of the die.



**Fig. 8.** Dependency diagrams of increasing the contact zone length of the workpiece with the upper die ( $D'$ ) on the indentation depth of the die.



**Fig. 9.** Dependency diagrams of increasing the contact zone length of the workpiece with the lower die ( $D''$ ) on the indentation depth of the die.

As can be seen from Fig. 7, 8 and 9, with an increase of the indentation depth of the die, the value of the contact zone length of the workpiece with the upper and lower dies and the value of the maximal widening increase. It can also be noticed that the obtained dependencies are not linear. Therefore, it is possible to identify a particular area of the narrow die indentation depths with the corresponding optimal metal widening values and contact zone lengths. The optimal interval of the indentation depth for studied forging technological schemes is a depth within 12–20 mm. The use of the given dependencies is also possible to obtain forgings of crankshafts of other sizes with different spacings between the shaft cheeks and the crankpin thicknesses. Based on the received dependencies, it is possible to choose the optimal die thickness and indentation depth to make this in order to obtain the optimal workpiece form.

In addition, one of the tasks of the study was to confirm the adequacy of the selected process parameters with the help of the full-scale experiment and computer simulation in the QForm V8 program. As we can see from Figs. 5, 7, 8 and 9, dependency diagrams are quite similar. In some cases, the experimental data completely coincide with the results of the computer simulation in the QForm V8 program.

Further comparing the experimental data with the computer modelling results, it was found that in almost all studied cases errors do not exceed 10%. Therefore, it is acceptable. The results of the comparison also confirm that the tasks for the simulation were set correctly.

## 5 Conclusions

1. As a result of the analysis of the recent studies, publications and technological schemes of manufacturing crankshaft forgings, the general scheme to obtain a forged crankshaft from an ingot are created. Based on the analysis of the disadvantages of this scheme, the improved technology of manufacturing crankshaft forgings with obtaining a crankpin is developed. This technology is covered by an overlap in the standard scheme.
2. As a result of the carried-out theoretical and experimental studies of the indentation process of a narrow die into a workpiece, it is received the dependency diagrams of the influence of the upper die thickness and its indentation depth on the change in sizes of the workpiece, namely the maximal widening, the lengths of the contact areas of the workpiece with the upper and lower dies and the value of the maximal workpiece diameter reduction. According to these dependencies, it is possible to determine the optimal die thicknesses and indentation depth to get the highest manufacturability of the given operation.
3. The comparison of the results of the experimental studies and computer simulation in the QForm V8 program showed appropriate convergence of the results. The error did not exceed 10%, which could be interpreted as a good indicator. Therefore, the QForm V8 program allowed us to receive the excellent convergence of the results of the experimental and theoretical studies of the free forging processes.
4. Studying the dependencies of metal changes in form using the thin deforming tool, as well as determining the deformation conditions for closely approximating the shape and dimensions of the forgings to the finished product and creating an improved technology for manufacturing crankshaft type forgings have practical application.
5. Further investigation, based on the results of research, will consist in developing technological recommendations for the application of the improved method of manufacturing crankshaft forgings with obtaining a crankpin.






## References

1. Bogoyavlensky, A., Bogoyavlensky, M.: Calculation technological parameters of forging on hammers and presses (corrected proof). In: *Materials Today: Proceedings* (2019)
2. Alves, L.M., Martins, P.A.F.: Flexible forming tool concept for producing crankshafts. *J. Mater. Process. Technol.* **211**(3), 467–474 (2011)
3. Wu-jiao, X., Kai-qing, W., Jie, Z., et al.: Experimental and computational failure analysis of TR upset-bending equipment for heavy crankshaft with continuous grain flow. *Eng. Fail. Anal.* **17**(2), 546–554 (2010)

4. Zhang, Y., Hui, W., Dong, H.: Hot forging simulation analysis and application of microalloyed steel crankshaft. *J. Iron. Steel Res. Int.* **14**(5), 189–194 (2007)
5. Zhao, F., Wu, M., Jiang, B., et al.: Effect of nitrogen contents on the microstructure and mechanical properties of V-Ti microalloyed steels for the forging of crankshafts. *Mater. Sci. Eng. A* **731**, 360–368 (2018)
6. Park, H., Dang, X.: A study on the heating process for forging of an automotive crankshaft in terms of energy efficiency. *Proc. CIRP* **7**, 646–651 (2013)
7. Milenin, A., Rec, T., Walczyk, W., et al.: Model of curvature of crankshaft blank during the heat treatment after forging. *Proc. Eng.* **81**, 498–503 (2014)
8. Song, M.C., Moon, Y.H.: Coupled electromagnetic and thermal analysis of induction heating for the forging of marine crankshafts. *Appl. Therm. Eng.* **98**, 98–109 (2016)
9. Chval, Z., Cechura, M.: Optimization of power transmission on mechanical forging presses. *Proc. Eng.* **69**, 890–896 (2014)
10. Castro, G., Fernández-Vicente, A., Cid, J.: Influence of the nitriding time in the wear behaviour of an AISI H13 steel during a crankshaft forging process. *Wear* **263**(7–12), 1375–1385 (2007)
11. Raz, K., Kubec, V., Cechura, M.: Dynamic behavior of the hydraulic press for free forging. *Proc. Eng.* **100**, 885–890 (2015)
12. Zahalka, M.: Modal analysis of hydraulic press frames for open die forging. *Proc. Eng.* **69**, 1070–1075 (2014)
13. Gronostajski, Z., Hawryluk, M., Widomski, P., et al.: Selected effective methods of increasing the durability of forging tools in hot forging processes. *Proc. Manuf.* **27**, 124–129 (2019)
14. Alshammari, Y., Jia, M., Yang, F., et al.: The effect of  $\alpha + \beta$  forging on the mechanical properties and microstructure of binary titanium alloys produced via a cost-effective powder metallurgy route. *Mater. Sci. Eng. A* **769**, 138496 (2020)
15. Yakura, R., Matsuda, M., Sakai, T., et al.: Effect of inclusion size on fatigue properties in very high cycle region of low alloy steel used for solid type crankshaft. *Kobelco Technol. Rev.* **35**, 7–13 (2017)
16. Greger, M.: Forging. VŠB – Technical University of Ostrava, Ostrava (2014)
17. Sharma, P.C.: A Textbook of Production Technology (Manufacturing Processes). S. Chand & Company Pvt. Ltd, New Dehli (2012)
18. Citti, P., Giorgetti, A., Millefanti, U.: Mechanical characterization of a new low carbon bainitic steel for high performance crankshaft. *Proc. Struct. Integr.* **12**, 438–447 (2018)
19. Grinkevich, V., Chuhleb, V., Banashek, G., et al.: Theoretical studies of blacksmith broaching operations using the “passes” deformation scheme. *Visnyk NTU «KhPI»* **44**, 28–34 (2014). [in Russian]
20. Chuhlib, V., Klemeshov, Y., Grynkevych, V., et al.: The influence analysis of the parameters of the upsetting and its absence on the inequality of deformation during the forging of titanium alloys. *Visnyk NTU «KhPI»* **47**, 82–85 (2015). [in Ukrainian]
21. Chuhlib, V., Klemeshov, Y., Grynkevych, V., et al.: An investigation of the stress-strain state during the titanium alloy broaching for optimization of forging parameters. *Visnyk NTU «KhPI»* **24**, 159–166 (2015). [in Ukrainian]
22. Altan, T., Ngaile, G., Shen, G.: Cold and Hot Forging: Fundamentals and Applications. ASM International, West Conshohocken (2004)
23. Nisbett, E.: Steel Forgings: Design, Production, Selection, Testing, and Application. ASTM International, West Conshohocken (2005)
24. Chen, S., Qin, Y., Chen, J.G., et al.: A forging method for reducing process steps in the forming of automotive fasteners. *Int. J. Mech. Sci.* **137**, 1–14 (2018)



# A Numerical-Analytical Model of the Temperature Field Distribution During Orthogonal Cutting of Composites

Gennadii Khavin<sup>1</sup>  , Magomedemin Gasanov<sup>1</sup> ,  
Alexander Permyakov<sup>1</sup> , and Viktoria Nevludova<sup>2</sup> 

<sup>1</sup> National Technical University “KhPI”, 2, Kyrpychova St., Kharkiv 61002,  
Ukraine

[gennadii.khavin@gmail.com](mailto:gennadii.khavin@gmail.com)

<sup>2</sup> National University of Radioelectronics, 14, Nauky Ave., Kharkiv 61000,  
Ukraine

**Abstract.** The process of machining composite materials, as the phenomenon of targeted destruction of the surface layer, is accompanied by the release of a large amount of heat. That heat largely determines defines the picture of the stress-strain state in the tool-composite contact. The intensity and distribution of the temperature field mainly define the choice of the tool type and processing parameters which provide a given surface quality and productivity. A numerical-analytical model for determining the temperature field for orthogonal cutting of fiberglass with bundles reinforced is presented. The two-dimensional stationary problem of heat conduction of piecewise homogeneous bodies is solved by the boundary element method. An empirical relationship for average temperature and the heat source arising at the contact of the tool flank surface with the material being processed is used for as the boundary conditions in the model. The dependences of the maximum temperature on the feed, speed, and depth of cut are given. It is shown that to prevent the possible occurrence of thermal destruction and burns in each case, there is a limit combination of technological parameters – feed, speed and depth of cut.

**Keywords:** Reinforced polymers · Machining · Modeling · Thermal effects

## 1 Introduction

Physically, the process of cutting inhomogeneous composites has many times less loaded than when cutting metals. The phenomenon of material destruction is accompanied by the formation of fine-dispersed chips as a result of brittle fracture of the matrix and filler. The resulting fine-dispersed chips practically don't affect on the front surface of the tool and don't cause its heating and wearing. On the flank surface of the tool, there is an abrasive effect from the cut fibers (bundles), which is caused by the elastic recovery of the cut fibers (bundles) due to the high elastic properties of the glass or graphite filler. Thus, the intense friction occurs on the flank surface with the release of a large amount of heat, partial cleaning of the treated surface and, as a result, wears of the tool on the flank surface.

© The Editor(s) (if applicable) and The Author(s), under exclusive license  
to Springer Nature Switzerland AG 2020

V. Ivanov et al. (Eds.): DSMIE 2020, LNME, pp. 371–379, 2020.

[https://doi.org/10.1007/978-3-030-50794-7\\_36](https://doi.org/10.1007/978-3-030-50794-7_36)



The specificity of reinforced plastics properties determines the peculiarity of thermal phenomena that occur during the cutting. The low heat resistance of these materials limits the temperature in contact with the tool to approximately 300–350 °C, after which intensive thermal destruction and decomposition of the polymer binder begin. As a result, the quality of the treated surface is sharply deteriorated, up to the burns, and tool wear is intensified.

It is believed that the total amount of heat during cutting consists of the heat generated from deformations in the conditional shear plane, the heat from the friction of the chips on the face of the tool; heat from the friction of the flank surface and the workpiece processed; heat from the polymer mechanoluminescence transformations; and heat from the dispersion of the reinforcing fibers. Among these components, the main role is played by the heat generated by the friction the tool flank surface and the workpiece, which can be from 70 to 90% of the total amount of heat released.

Experimental observations have shown that heat from friction on the flank surface of up to 90% is removed by the tool, 5% is carried away by chips and only 5% is transferred to the treated surface of the composite. However, the heat released is capable of intense surface heating, which can lead to thermal decomposition of the binder and deterioration in the quality of processing. Therefore, in the general task of designing the process of cutting reinforced plastics, the limitation on the temperature in contact plays a crucial role, which in many cases determines the choice of technological parameters of cutting for a given type of reinforced plastic and material of the tool.

## 2 Literature Review

The machining of reinforced materials is accompanied by significant damage. Also, the contact zone is heated. Despite the importance of thermal effects in the processing of glass-reinforced plastics and other reinforced materials, this problem is not given enough attention in the scientific literature. The great difficulties associated with conducting experimental studies initiated the development of numerical and semi-analytical methods for studying thermal phenomena at the instrument-composite contact.

In [1], a three-dimensional (3D) finite-element model of orthogonal cutting of CFRP which includes thermal effects is presented. The strong influence of fiber orientation on the predicted thermal and mechanical interlayer damage was shown. The thermal damage zone was larger than the mechanical damage area. This fact confirms the importance of taking thermal effects into account when modeling the processing of reinforced plastics. Also, a three-dimensional numerical model was proposed for predicting the temperature distribution in [2]. Drilling experiments were carried out to verify the proposed numerical model and investigate the thermal damages with low-mild spindle velocities. Cutting heat easily accumulated in composites was drilled with low-mild spindle velocities for their poor thermal conductivity. Temperature distributions presented has diagonal direction was consistent with the fiber direction. With the high heat accumulation, although the drilled hole surface was damaged by the high temperature, the carbonation phenomenon was not serious for the low spindle velocity

drilling. For the mild spindle velocity drilling case, a serious carbonation phenomenon had been observed, and the heat-affected layer in the hole surface was about 0.3 mm.

An experimental investigation aimed at studying the thermal effects arising from the mechanical processing of composite materials is presented in [2]. For information about the temperature field of the cutting tool, a built-in wireless thermocouple is used. An infrared thermal imaging camera is used to collect data on the thermal state of the specimen. The results showed that vertical spindle processing and depth of cut have the most significant effect on the steady-state temperature distribution in contact. While the greatest influence on the magnitude of the cutting forces has a feed rate and depth of cut. The surface quality is especially sensitive when the cutoff value is reduced, which is explained by a decrease in the area of the heat source at the tool point.

In [3], it was experimentally shown that a high temperature in the cutting zone not only leads to a deterioration in the quality of the treated surface but also degrades the mechanical properties of the composite (tensile strength) with small cross-sections of the cut. The effect of tool wear is especially pronounced. The temperature increases, which leads to the destruction of the surface and the charring of the matrix.

In the study [4], the relationship between the value of the temperature in contact, the cutting force, and the technological processing parameters was experimentally studied. The thermocouple tool-blank method is used. The results were processed using the surface response method (RSM). The results of the analysis showed that the spindle speed is the main parameter that affects the cutting temperature, while the feed rate is a key parameter that affects the cutting force when milling FRP. It was shown that if the temperature in the cutting zone exceeds the glass transition temperature of the binder, then the matrix can no longer provide sufficient retention of the fibers, which leads to a sharp deterioration in the processing quality of the composite material.

In the study [5], orthogonal machining experiments were conducted to investigate the effects of cutting parameters, cutting tool geometric parameters, and material parameters on cutting temperature, and the prediction model of cutting temperature about fiber orientation angle was built. The experimental results revealed that the influence of cutting parameters on cutting temperature was not affected by the fiber orientation angle of carbon fiber reinforced polymer. Cutting tool geometric parameters have little effect on cutting temperature. Unlike metal materials, cutting temperature was greatly influenced by the fiber orientation angle. Cutting temperature for angles of less  $90^\circ$  was significantly higher than that for angles of more than  $90^\circ$ . The maximum temperature occurred at  $90^\circ$ . The influence of fiber orientation angle was shown in two aspects: changing the spring back of unidirectional-carbon fiber-reinforced polymer laminates in the cutting process, changing the material removal mechanism, which affected cutting temperature eventually.

The temperature field distribution during the drilling of composites is investigated using a combined approach of experimental, analytical, and numerical analysis of heat propagation modeling is considered in [6]. The experimental study aims to establish the change in thrust force and torque over time. Analytical modeling is used to estimate the heat flux at the tool-blank contact, and numerical simulation to analyze the heat distribution and estimate the maximum temperature level in the workpiece. This approach was used for a new and worn tool. The main advantage of the work is the development of a combined approach to predicting thermal damage. The numerical model showed

that the maximum temperature that occurs on the wall of the hole near the exit of the drill is an area where mechanical delamination is usually observed. The occurrence of thermal damage in the event of excessive wear increases the risk of a defect at the outlet of the hole.

In the study [7], the cutting temperature during milling of the composite was measured by three different methods: a thermocouple tool-blank method, an integrated thermocouple and a scanning electron microscope (SEM). The main goal was to determine the glass transition temperature of the binder (resin), as the main criterion for damage to reinforced plastic. In the experiments, the measured temperature exceeded the glass transition temperature. It was shown that the temperature of the treated surface layer drops sharply with distance from the surface. The depth of damage depends on the thermal conductivity of the composite. The binder was not damaged even at a cutting speed of 300 m/min, which serves as the basis for the application of high-speed milling. Also, the problem of heat generation and distribution in edge trimming of carbon-fiber-reinforced polymers was investigated in [8]. Measurements of boundary temperatures allowed the determination of the proper magnitude of heat flux applied to the workpiece and the cutting tool. It was found that less than 16% of the total heat is conducted into the workpiece and that higher feed speeds allowed less heat to conduct into the workpiece. The depth of heat penetration into the workpiece caused the temperature to reach the glass transition temperature of the epoxy only for the slower feed speed.

The effect of cutting temperature when drilling holes with a cemented carbide spherical end-milling cutter in CFRP is investigated in [9]. Despite the high quality of the holes, it is noted that the cutting temperature adversely affects the quality and strength of CFRP when it exceeds the temperature of the thermal stability of epoxy resin. The authors believe that the speed of rotation during the spiral cutting of carbon fiber plates improves the cutting process. It is shown that the cutting temperature decreases with increasing rotational speed and, due to the reduction in contact time, the time of heat propagation to the workpiece is reduced.

### 3 Research Methodology

The known theoretical relationships for the temperature field in processed fiberglass (GFRP), based on the processing of experimental results, have several significant drawbacks that limit their practical use. In particular, these include:

- determined by some average temperature of the surface layer, which may differ significantly from the maximum instantaneous temperature;
- a limited range of changes in the technological parameters of the processing and the discrepancy with the experimental data, if high cutting speeds, increased depths of removal and feed are used;
- the structure of laying, interlacing, and thickness of fibers (bundles) of reinforcing filler are practically not taken into account.

To further develop theoretical research methods and an analytical description of the temperature field, create new models that more reliably describe phenomena in contact

fiberglass-tool, and also to solve the temperature distribution problem when cutting fiberglass across fibers (bundles), the following calculation model was used.

The steady-state heat conduction two-dimensional problem for the bundle-binder (matrix)-bundle model was solved by the boundary element method, Fig. 1, where  $t$  is the depth of cut;  $\lambda_f, \lambda_b$  – thermal conductivity of the filler (bundle) and binder (matrix). An epoxy binder and a bundle of alumina-borosilicate glass fibers were considered. Geometrical dimensions of the selected fragment:  $A_1B_1 = 1000 \mu\text{m}$ ,  $AB = 1500 \mu\text{m}$ ,  $A_1A = A_2A_3 = 270 \mu\text{m}$ ,  $AA_2 = 180 \mu\text{m}$ . These geometrical data are taken from the solution of the stress-strain state task for a tool-fiberglass contact problem which was considered in [10]. In formulating this task, the following assumptions were made:

- within the framework of the theory of elasticity, the design scheme does not distinguish between cases when a load is first applied, then a temperature field in the contact, or vice versa, there is a temperature field first, and then a load is applied;
- the steady-state heat conduction two-dimensional problem for contacting isotropic bodies is solved;
- physical-mechanical properties of processed fiberglass are considered to be independent of temperature.

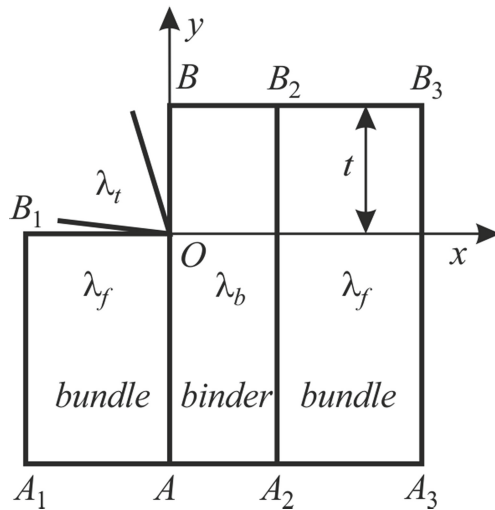


**Fig. 1.** General calculate scheme for the problem of temperature field determining.

The assumption of the stationary the process of thermal conductivity is explained as follows. Due to the very low thermal conductivity coefficient, the heat flux is perceived by the surface layers of fiberglass and there is practically no heating to the bottom. Also, it is assumed that the discrete contact of the tool when cutting bundles is a source of heat, and heat from the contact directly binder with the rear surface is missing or slightly. The physical-mechanical properties of the processed fiberglass are considered

to be independent of temperature since there are no specific data on quantitative dependence.

For the accepted calculation model (Fig. 1), the following thermal boundary conditions were assumed. Along the lines,  $A_1B_1$ ,  $AA_1$ ,  $AA_2$ ,  $A_2A_3$ ,  $A_3B_3$ , the mean temperature was set  $\theta = 196.99 \cdot V^{0.38} S^{0.08} t^{0.34}$ . This ratio is a modification of the experimental dependence for the average temperature [11], obtained from the determination of the temperature during fiberglass turning with carbide cutters. The cutting conditions and the geometric parameters of the tool were taken:  $V = 1\text{--}4$  m/s;  $S = 0.2\text{--}0.6$  mm/rev;  $t = 0.5\text{--}2.0$  mm;  $\alpha = 20^\circ$ ,  $\gamma = 10^\circ$ ,  $\varphi = 45^\circ$ ,  $\varphi_1 = 15\text{--}45^\circ$ , where  $V$  is the cutting speed;  $S$  is feed;  $t$  is the depth of cut;  $\alpha$ ,  $\gamma$  are clearance and face angles;  $\varphi$ ,  $\varphi_1$  are main and auxiliary angles.

The mean temperature value is obtained by processing (averaging) the experimental data measured at some distance from direct contact of the instrument with the glass bundle. Therefore, it can be taken as a condition of the first kind for the presented fragment in Fig. 1. At the boundaries of  $BB_2$ ,  $B_2B_3$ ,  $OB$ , and  $OB_1$ , the condition of the absence of heat exchange is established  $\partial\theta/\partial n = 0$ , where  $n$  is the external normal to the surface. On the coupling surfaces of the bundle and the binder  $OA$  и  $A_2B_2$ , a fourth kind condition was adopted, namely, the equality of temperatures and the absence of heat flows through the coupling surfaces.

The heat source is the friction of the tool and the processed fiberglass on the flank surface of the tool of width  $b$  over the contact area of length  $a$ . Based on this, in the neighborhood of point  $O$  along the length  $a$ , a uniformly distributed heat flux was applied by the intensity  $q = Q_{fg}/(a \cdot b)$ , where  $Q_{fg}$  is the total amount of heat entering the material. This value is part of the total heat during the cutting process  $Q$ . It is known that only a small amount of heat enters directly into the material being processed, due to the low thermal conductivity of the GFRP components. To determine this quantity, the simplest known ratio is used [12].

$$Q = Q_t + Q_{gf} = Q \frac{\lambda_t}{\lambda_{gf} + \lambda_t} + Q \frac{\lambda_{gf}}{\lambda_{gf} + \lambda_t}, \quad (1)$$

where  $\lambda_t$ ,  $\lambda_{gf}$  are thermal conductivity of the tool material and glass-reinforced plastic.

From experimental studies on the processing of glass-reinforced plastics, it is known that almost all the heat is produced as a result of the frictional interaction of the tool and the workpiece on the back surface. Heat generation due to friction on the flank surface of the tool is determined, first of all, by the acting normal force and interaction conditions at the contact area. Using the Coulomb-Amonton friction law traditionally used in engineering practice, the ratio for determining the total amount of heat can be represented as  $Q = P_y \cdot f \cdot V/I$ , where  $P_y$  is normal cutting force;  $f$  is the friction coefficient and  $I$  is the mechanical equivalent of heat.

The value  $P_y$  can be calculated using the dependence on the normal component of the cutting force [13]. The friction coefficient or coefficient external friction of the system tool material-fiberglass, in general, depends on a large number of factors [11, 14], in particular, the speed of interaction, contact stress, temperature, etc. Data on the value of the friction coefficient is very small. Therefore, based on the results given in

[11], for the speed range  $V = 1\text{--}4$  m/s, the value of the friction coefficient was taken  $f_0 = 0.3$ .

Then, as a boundary condition over the surface of the interaction between the tool and fiberglass, the condition of the heat flux impact with a specific uniformly distributed intensity is taken

$$q = P_y \cdot f_0 \cdot V \cdot \lambda_{gf} / (\lambda_t + \lambda_{gf}) / (a \cdot b) \quad (2)$$

The given calculation scheme is not complete and perfect. However, it models with sufficient reliability the most significant factors influencing the temperature field distribution in the filler-binder system. Also, the presented model makes it possible by calculation to predict an increase in temperature in contact compared to the calculated average value.

## 4 Results

Using the proposed model for describing the temperature field in a tool-fiberglass contact, a numerical study was performed using the boundary element method [15]. During the calculations, the following values of thermal physic quantities, geometrical parameters and coefficients were taken:  $\lambda_t = 54.4$  W/(m · °C);  $\lambda_{gf} = 0.8$  W/(m · °C);  $f_0 = 0.3$ ;  $a = 10$  μm;  $b = 1000$  μm;  $I = 4.184$  s/W. The value of  $P_y$  was calculated from the relations  $P_y = 158.1 \cdot V^{-0.08} S^{0.33} l^{0.49}$ .

Figure 2 presents the calculated dependencies of the average and maximum temperature in the contact on the feed, speed, and depth of cut. The analysis of the dependencies presented in Fig. 2a (for a constant cutting depth of 0.5 mm) allows us to draw the following conclusions. Average and maximum temperatures increase with increasing cutting and feed rates. If we assume that the epoxy binder (matrix) degradation temperature is 300–350 °C, then for a feed range of more than 0.3 mm/rev and a cutting speed of more than 3 m/s, intense thermal destruction will be observed. For the entire range of feeds, the increase in cutting speed 4 times leads to an increase in the maximum temperature of about 2 times. On the other hand, an increase in feed by 12 times from 0.05 to 0.6 mm/rev leads to an increase in the maximum temperature by about 1.5 times, while the average temperature only increases by 1.2 times. An increase in cutting speed has a greater effect on the temperature rise in the contact than an increase in feed. For a cutting depth of 0.5 mm at a speed of up to 3 m/s for feeds up to 0.3 mm/rev, the maximum temperature values are safe from thermal decomposition. However, for feeds above 0.3 mm/rev, the likelihood of burns and deterioration in the quality of the treated surface appears. For cutting speeds above 4 m/s, for almost all feeds, one can expect the thermal decomposition of the binder (matrix) and the appearance of burns.

Figure 2b for a cutting speed of 2 m/s shows the dependence of the average and maximum temperature on the feed for different cutting depths. It can be concluded that a possible temperature rises above 300 °C should be expected from a cutting depth of 1 mm for all feeds above 0.15 mm/rev. A further increase in the depth of cut can lead to an increase in temperature at the contact and the appearance of thermal

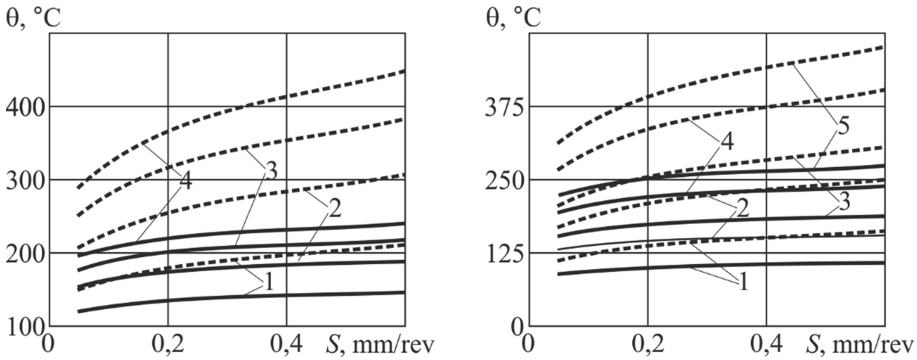


**Fig. 2.** The dependence of the maximum (.....) and average temperature (—) in the cutting zone: a) at a constant value of the cutting depth  $t = 0.5$  mm and cutting speed: 1 – 1 m/s; 2 – 2 m/s; 3 – 3 m/s; 4 – 4 m/s; b) with a constant value of cutting speed 2 m/s and value of the cutting depth: 1 – 0,1 mm; 2 – 0,3 mm; 3 – 0,5 mm; 4 – 1,0 mm; 5 – 1,5 mm.

decomposition of the binder (matrix). Increasing the thickness of the cut to 1.5 mm requires a maximum reduction in feed at the minimum cutting speed.

## 5 Conclusions

A numerical-analytical model for describing the distribution of a stationary temperature field in a tool-composite contact, in the process of orthogonal cutting is proposed. The ratio for the average temperature obtained by processing the experimental data was used as the boundary conditions. The boundary element method was used to solve the problem of heat conduction of piecewise homogeneous bodies. The numerical-analytical approach to determine the maximum temperature within the framework of the stated constraints allows one to approximately predict the value of the maximum temperature, possessing versatility concerning the type and structure of the composite material.

The task of determining the maximum temperature values when cutting epoxy fiberglass reinforced with bundles of alumina-borosilicate glass fibers was considered. The obtained dependences of the maximum temperature on the feed, speed, and depth of cut allowed drawing the following conclusions:

- the average and maximum temperatures increase with increasing cutting speed and feed, and for cutting speeds above 4 m/s for almost all feeds, one can expect the appearance of thermal destruction of the binder and the appearance of burns;
- as the limiting depth of cut, we can recommend a value of no more than 1 mm, a cutting speed of no more than 3 m/s and a feed of no more than 0.3 mm/rev, at a given temperature of thermal destruction 300–350 °C;
- the implementation of these restrictions in the fiberglass processing at low cutting speed with a bar blade can guarantee the absence of thermal destruction of the binder (matrix) and, as a result, the absence of sticking it onto the flank surface of

the tool. The adoption of such measures ensures high tool life with given requirements to the quality of the surface to be treated.






## References

1. Santiuste, C., Diaz-Alvarez, J., Soldani, X., Miguelez, H.: Modeling thermal effects in machining of carbon fiber reinforced polymer composites. *J. Reinf. Plast. Compos.* **33**(8), 758–766 (2014)
2. Bao, Y.-J., Hao, W., Gao, H., Jiu, X.-S., Wang, Y.-Q.: Numerical and experimental investigations on temperature distribution of plain-woven aramid fiber-reinforced plastics composites with low-mild spindle velocities. *Int. J. Adv. Manuf. Technol.* **99**, 613–622 (2018)
3. Kerrigan, K., O'Donnell, G.E.: On the relationship between cutting temperature and workpiece polymer degradation during CFRP edge trimming. *Procedia CIRP* **55**, 170–175 (2016)
4. Delahaigie, J., Chatelain, J.-F., Lebrun, G.: Influence of cutting temperature on the tensile strength of a carbon fiber-reinforced polymer. *Fibers* **5**(4), 46, 1–16 (2017)
5. Quinglong, An., Chen, J., Cai, X., Peng, T., Chen, M.: Thermal characteristic of unidirectional carbon fiber reinforced polymer laminates during orthogonal cutting. *J. Reinf. Plast. Compos.* **37**(13), 905–916 (2018)
6. Díaz-Álvarez, J., Olmedo, A., Santiuste, C., Henar Miguélez, M.: Theoretical estimation of thermal effects in drilling of woven carbon fiber composite. *Materials* **7**, 4442–4454 (2014)
7. Yashiro, T., Ogawa, T., Sasahara, H.: Temperature measurement of cutting tool and machined surface layer in milling of CFRP. *Int. J. Mach. Tools Manuf.* **70**, 63–69 (2013)
8. Sheikh-Ahmad, J.Y., Almaskar, F., Hafeez, F.: Thermal aspects in machining CFRPs: effect of cutter type and cutting parameters. *Int. J. Adv. Manuf. Technol.* **100**, 2569–2582 (2019)
9. Sakamoto, S., Iwasa, H.: Effect of cutting revolution speed on cutting temperature in helical milling of CFRP composite laminates. *Key Eng. Mater.* **523–524**, 58–63 (2012)
10. Verezub, N.V., Tarasyuk, A.P., Khavin, G.L., Getmanov, A.A.: *Mechanical Processing of Fibrous Polymer Composites*. KharkovHNADU (HADI), (2001). (in Russian)
11. Stepanov, A.A.: *Cutting of high-strength composite polymeric materials*. Mashinostroenie, L. (1987). (in Russian)
12. Rudnev, A.V., Korolev, A.A.: *Processing cutting fiberglass*. Mashinostroenie, M. (1969). (in Russian)
13. Verezub, N.V.: *The scientific basis of highly efficient processes for the mechanical processing of polymer composites*. Thesis Doctor of Technical Sciences, Kharkov (1995). (in Russian)
14. Kobayashi, A.: *Machining of Plastics*. McGraw-Hill, New York (1967)
15. Khavin, G.L.: Calculation of the contact interaction of the piecewise homogeneous bodies by the direct boundary element method. *Eng. Probl.* **28**, 28–33 (1987). (in Russian)





# Simulation of Thin-Walled Parts End Milling with Fluid Jet Support

Serhii Kononenko , Sergey Dobrotvorskii ,  
Yevheniia Basova , Ludmila Dobrovol'ska ,  
and Vitalii Yepifanov 

National Technical University “Kharkiv Polytechnic Institute”,  
2, Kyrpychova St., Kharkiv 61002, Ukraine  
e.v.basova.khpi@gmail.com

**Abstract.** One of the biggest barriers in the formation of surfaces of the thin-walled parts is the difficulties of prediction and prevention of deflections. The research is focused on the use of fluid jet support in processing as the technique to increase material cutting stability. The analysis of existing methods of deviations prevention is made. A preliminary number of simulations are proposed to define dynamic cutting parameters, apply it to the fluid jet simulation, and investigate the influence on the frequency part structure characteristics. The simulation results are allowed to trace the change in the natural frequency of the part and part with jet support. The potential fluid flow speed is established. The degree of the stress caused by directional fluid jet force is calculated. The technique is novel and useful in the sense that it is supported by fluid flow jet that can theoretically be organized on the existing equipment basis. The solution does not significantly affect the characteristics of the equipment structure while saving dimensional parameters. Matching between nozzle diameters and efficiency of fluid jet support is presented. Considerable oscillation amplitude reduction of the thin-walled part was observed using the proposed solution.

**Keywords:** Thin-walled parts · Fluid jet support · High-speed milling · SPH-particles · Undesirable deflections · Oscillation amplitude

## 1 Introduction

Deflections and vibrations of the thin-walled parts are one of the biggest barriers in enhancing the accuracy of the metal cutting operation. Parts with thin-walled elements are used in certain branches of industry as aircraft manufacturing, drive production, due to its lightweight with high efficiency. There are a lot of impellers, turbine blades, and other essential parts, united by difficulties in the processing - low ability to resist static and dynamic loads, geometrical deviations, vibrations, large deflections, and poor surface quality.

The most common aspects which should be considered during the processing of thin-walled parts are heat, force, and vibration. Heat transfer and deformation in thin-walled parts are significant which leads to difficulties in compliance with technological requirements. Rational use of coolant fluid has an influence on the temperature in the

cutting zone, cutting force and tool wear. From this point of view proposed fluid jet support particularly attractive to study as the existing equipment in most cases has units providing fluid high-pressure supply.

When the tooth cuts into the material the number of force components directed toward the surface and produces a large amount of the geometrical deviations. But as much thin-walled parts are malleable to pressure on the surface from the processing side as the part structure is malleable to deflect from the reverse side. Therefore, it is necessary to investigate the compensation contribution of the fluid jet support technique to the deflection degree of the part.

Another important aspect is vibration. In the processing, the rotating tool generates a cyclic load. In case the frequency of load matches the natural frequency of the thin-walled part, the amplitude of the oscillation increases [1–3]. Therefore, any external impact, such as fluid jet support on the structure influences the oscillation frequency characteristics.

## 2 Literature Review

From the studies' analysis, it has been found that a lot of attention is paid to the problems caused by the low stiffness of the thin-walled parts.

A lot of authors in their researches suggest a dedicated fixture as a way to compensate for the small rigidity of the part. The solution [4] represents spring fixture support for circular thin-wall components. The device minimizes vibrations, reconfigurable, and increases damping. The results of the numerical simulation research [5] and experimental studies [6] of the flexible fixtures have a significant impact on the technological assurance of the manufacturing processes.

Research [7] reveals the details of the generation mechanism of process damping and proves that the velocity-dependent mechanism more than the plowing one dominates the process damping effect in thin-wall part milling.

The research on the titanium alloy parts milling with air-jet assistance [8] provides conclusions of the effectiveness of this technique – the machine surface roughness errors decreased by 21%, the acceleration of the vibration by 46%, the cutting force by 10%. The finish quality of the surface of the part is better than by experiments without assistance. Additional processing assistance can improve the stability of the process.

The aim of the study on fundamentals of the optimization of machining process planning [9] is related to the improvement of preliminary technological preparation of manufacturing of aluminum alloy thin-walled parts.

Thing-walled parts are easily distorted under the processing of each material layer. Modeling of distortion due to processing of thin-walled components depicts, that the distortion of the structure is extremely related to the residual stress induced by manufacturing processes like heat treatment, forming or machining [10].

The analysis of moving fixtures and influence on deformation suppression during the milling process of thin-walled structures [11] represents the new tool-part-fixture system. The system assumes that the support of the cutting process with a special cylindrical roller is performing along the cutting line, thus affecting the static and dynamic deviations and changing the frequency characteristics of the structure as a

whole. The experimental results provide that the method suppresses the milling deflection effectively.

One of the studies is related to online error compensation [12]. It is based on the electrical component, which is called a piezoelectric actuator. The system is correcting the position of the tool-part during processing. The system is separate and is no influence on the machine tool control system or programming trajectories.

The number of studies proves that the milling path optimization is an efficient way to improve thin-walled cutting stability [13, 14].

Many solutions are proposed for the layout of the clamping, study on the optimization of the clamping force [15–19], improvement of dynamic machinability [20–22].

### 3 Research Methodology

The research methodology is based on the numerical deflections’ analysis [1] Fig. 1. The researched object is a sample of aluminum alloy thin-walled elements of the blade. The directional cutting force and stress obtained during fluid jet simulation are applied in the harmonic response analysis. At each stage calculations compared with the finite element analysis. Finally, the prediction of the oscillation amplitude for high-speed end milling with fluid jet support is presented.

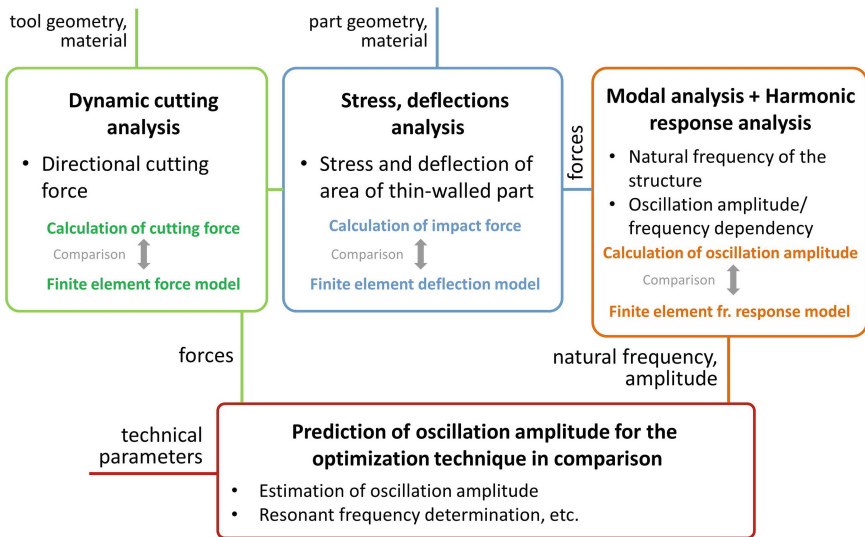
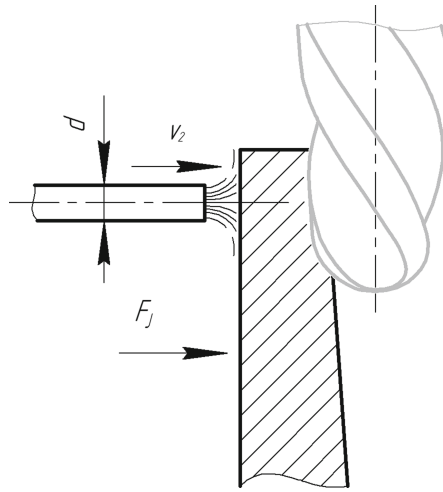


Fig. 1. The research methodology scheme.

### 3.1 Formulation of the Fluid Jet Support



**Fig. 2.** The scheme of fluid jet support.

To perform the simulation of fluid flow it is necessary to define the force value that acting towards the surface and speed of the fluid flow. For this purpose, Bernoulli's principle (1) and the continuity equation are used (2).

$$p_1 + \frac{1}{2}\rho v_1^2 + \rho gh_1 = p_2 + \frac{1}{2}\rho v_2^2 + \rho gh_2, \quad (1)$$

where  $p$  is static pressure,  $\rho$  – density,  $g$  – gravitational acceleration,  $v$  – velocity, it is assumed that elevation  $h = 0$ . The friction energy loss of flow through the nozzle will come out mainly in the reduction of pressure. But for preliminary analysis purposes, the friction impact on the system is neglected. The material of the nozzle and length of the line are considered neither in calculation nor in simulation.

The geometry of the nozzle is a thin tube with a circular cross-section Fig. 2. Simulation is performed for nozzles with diameters 2 and 4 mm.

Continuity Eq. (2) states that in a steady flow (flow rate is stable) the inflow is equal to outflow. The equation is based on the law conservation of mass.

$$\rho A_1 v_1 = \rho A_2 v_2 = const, \quad (2)$$

The flow rate  $Q = A \cdot v_2$ , where  $A$  is an area of cross-section,  $A = \pi d^2 / 4$ ,  $v$  – the flow speed [8]. Based on the momentum statement, the jet force:

$$F_J = \rho Q v_2 = \rho \frac{1}{4} \pi d^2 v_2^2 = \frac{1}{2} \pi d^2 p_1. \quad (3)$$

## 4 Results

### 4.1 Cutting Force Finite Element Analysis

The input parameters are: a thin-walled blade with variable distribution of stiffness (the thinnest area of the blade is 3.7 mm and the thickest is 8.7 mm), the material is aluminum alloy, spindle speed is 5000 rpm, feed is  $0.015 \text{ m}\cdot\text{s}^{-1}$ . The mathematical model of cutting a thin-walled element is defined in a previous study [1].

To reduce the computational cost, the dynamic cutting analysis is made only for the quarter of the part. The tool is a conical 3-blade end mill.

In the previous study, the error of the method was established near 15%. The instability of force values probes was observed. The mesh density was 0.5 mm. In this study the density of the mesh in the region of cutting is improved up to 0.15 mm, the geometric parameters of the 3D model of the tool were optimized (edge angle, edge thickness, smoothness of the lines, etc.), enhanced the quality of the mesh elements in the cutting area - hex elements are selected. The probes are taken in the  $Y$  direction. The probes values of the directional cutting force are close to each other along the milling line and equal  $P_{v\ fea} = 200 \text{ N}$ . The graph of the stress-step time dependency is obtained in Fig. 3.

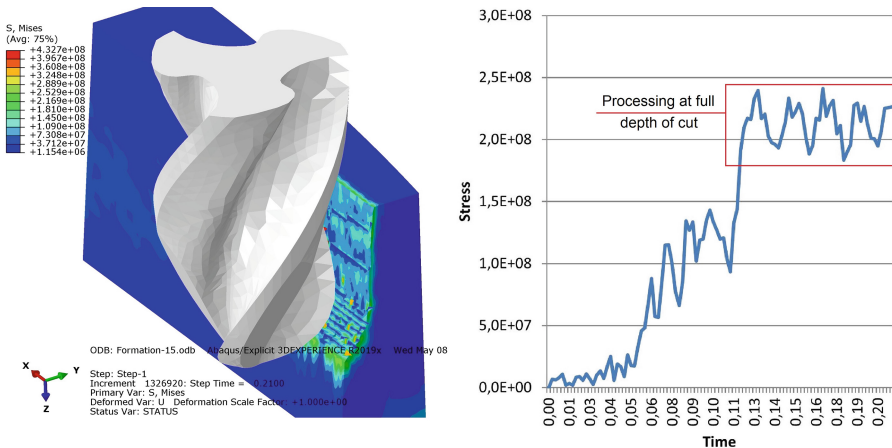


Fig. 3. Model of analysis and graph of the stress.

### 4.2 Fluid Jet Support Finite Element Analysis

The SPH-particles (Smoothed-particle hydrodynamics) are used to model the fluid flow. SHP method is suited to simulate the cases dominated by complex boundary

dynamics when the surface flows are free and the boundary displacement is large. The computational cost of the SPH method per amount of particles is significantly less than the cost of the grid-based method per amount of cells when the metric of interest is related to fluid density.

The input parameters are: water density is  $997 \text{ kg}\cdot\text{m}^{-3}$ , speed of sound in water is  $1400 \text{ m}\cdot\text{s}^{-1}$ , impact jet force is obtained from Eq. (3)  $F_J = 18 \text{ N}$ , initial distance between jet and part is  $2 \text{ mm}$ , fluid pressure  $p_1 = 2.8 \text{ MPa}$ , flow speed  $v_2 = 75 \text{ m}\cdot\text{s}^{-1}$ , nozzle diameter is  $2 \text{ mm}$ .

To perform the simulation the jet is imported as a solid element, but after the initial setting the solid elements of the jet in the input file should be deleted (except nodes), mass elements type should be changed to PC3D particle elements. The simulation Fig. 4 and the graph of the displacement dependency Fig. 5 are obtained.

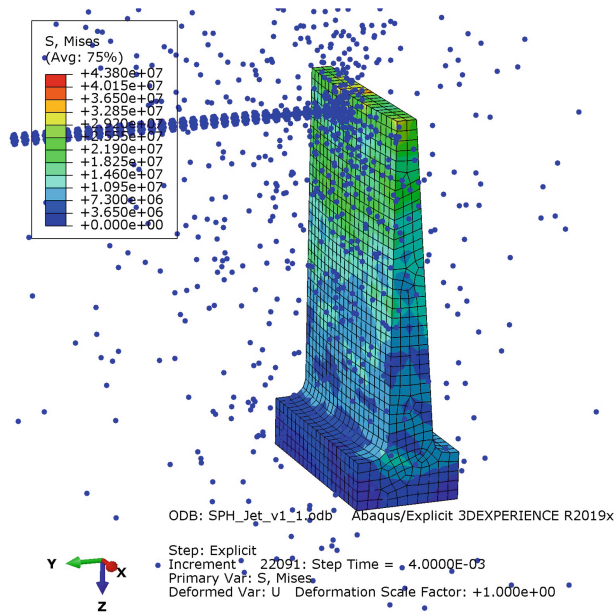


Fig. 4. Model of the stress under the fluid jet impact.

The graph Fig. 5 shows that the less nozzle diameter the more speed of flow, therefore more impact force. The maximum deflection for the  $2 \text{ mm}$  and  $4 \text{ mm}$  nozzle diameters:  $-100 \text{ }\mu\text{m}$  and  $-17 \text{ }\mu\text{m}$  respectively.

### 4.3 Modal and Harmonic Response Analyses

The natural frequency of the part is a necessary aspect in determining the resonant frequency. If the external cyclic load frequency coincides with the natural frequency of the thin-walled element, resonance occurs and the amplitude of the oscillations

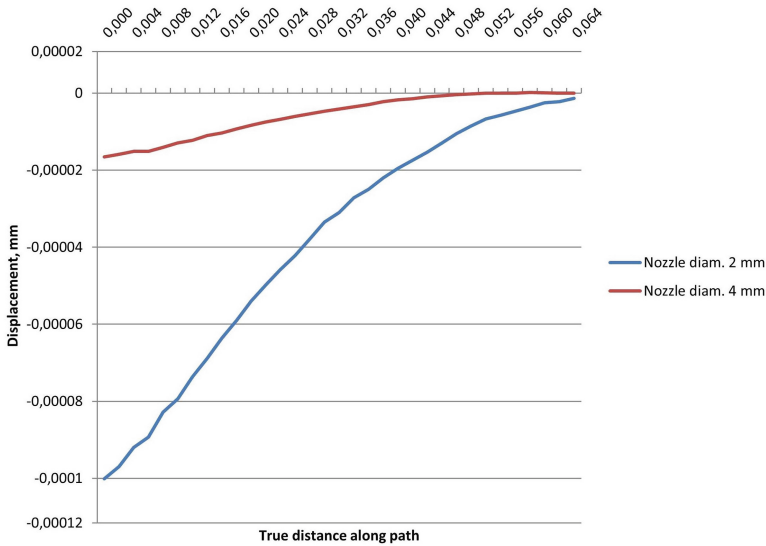


Fig. 5. Graph of displacement for 2 mm and 4 mm nozzle diameter.

increases. In milling mechanical system the main oscillation generator is a turning cutting tool. Every time the tooth cuts into the material the part loses its stable state.

Any external impact on the system alters its natural frequency – the more support the system gets the higher frequency needs to achieve the oscillation. In order to shift the resonant frequency and reduce the oscillation amplitude the fluid jet support (FJS) is used.

For the modal analysis to imitate the fluid jet support the Elastic Support in the CAE program is selected. The “Elastic Foundation Stiffness” (EFS) or “Elastic Support” is a way of specifying a spring stiffness per unit area that only acts in the direction normal to the face of the element. In Workbench Mechanical, the Elastic Support can be scoped on any 3D face. The area of the face where the fluid jet is directed is selected, and the applied force is 18 N for a 2 mm nozzle jet, the average deflection of this area is 0.05 mm thus the  $EFS = 1.4 \text{ N}\cdot\text{mm}^{-2}$ .

Max Modes to find in the modal analysis is 6, Fixed Support is the base surface of the model, Elastic Support for the FJS is the face of jet impact. The modal results are listed, Hz: 1728, 5137, 5839, 7603, 13097, 17771. The modal results with FJS, Hz: 2313, 5355, 5839, 7734, 13174, 17823.

As expected the frequency values of the modal analysis are higher for processing with FJS.

Harmonic response analysis predicts the dynamic action of the structures, giving the knowledge of whether or not the structure will safely overcome resonance.

The graph on Fig. 6 and Table 1 depict the frequencies of oscillation amplitudes – resonance values of oscillations of the part under the load  $Pv\ fea = 200 \text{ N}$ . For the conventional machining without FJS resonance amplitude is 2.793 mm. The natural

frequency is 1650 Hz. For the FJS machining, the maximum amplitude is 1.4109 mm. The natural frequency is 2320 Hz.

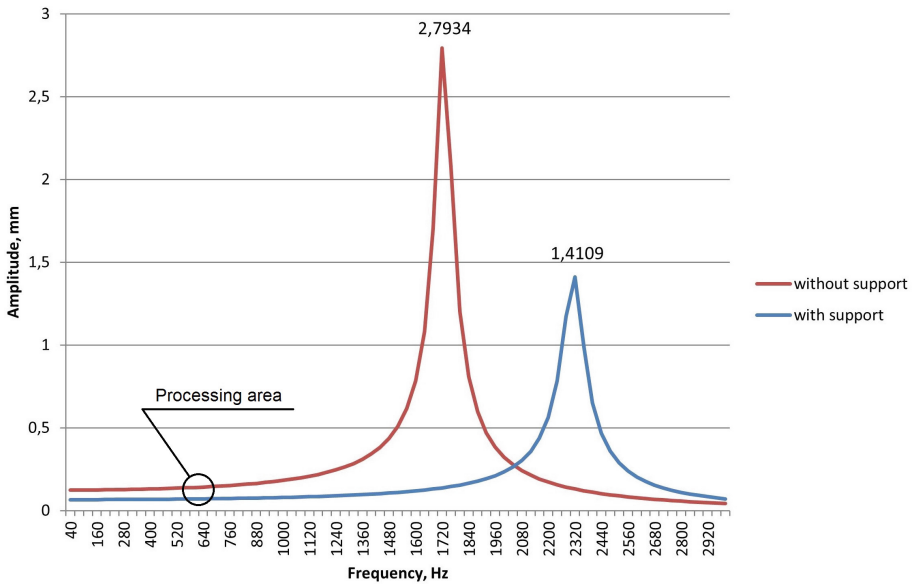


**Fig. 6.** Oscillation Amplitudes without and with fluid jet support.

The rotation  $n$  of the milling tool for machining is near 12000 rpm. The milling tool has 3 cutters, so the frequency of contact of the cutters with the surface is multiplied by 3. Thus generated frequency is near 600 Hz, which matches to 0.139 mm amplitude without FJS and 0.07 mm with FJS.

Both machining methods are far from the resonance frequency, so milling can be performed with safety. The oscillations with the FJS technique are decreased by 50%.

**Table 1.** A shortened list of frequencies and corresponding amplitudes.

Frequency, Hz	Amplitude without FJS, mm	Amplitude with FJS, mm
40	0,124	0,066
360	0,129	0,067
680	0,145	0,072
1000	0,181	0,079
1640	1,082	0,124
1960	0,383	0,211
2280	0,142	1,173
2600	0,077	0,203
2920	0,048	0,084



## 5 Conclusion

Based on the literature analysis, it can be concluded that there are many solutions to reduce the negative effects in the processing of thin-walled parts. The approach in this research proves the effectiveness of the designed solution and the ability to perform simulation of processing with fluid jet support. The fluid jet analysis is executed using the SPH-particles method. Cutting force  $P_{v\,fea} = 200$  N. Flow jet force  $F_J = 18$  N for the nozzle 2 mm. Maximum of displacement for the 2 mm nozzle is greater by 80% then for 4 mm, which is caused by a highly increased speed of flow impact.

As a result of harmonic analysis, the amplitude of the oscillations with the FJS technique is decreased by 50%.

## References

1. Dobrotvorskiy, S., Basova, Y., Kononenko, S., Dobrovolska, L., Ivanova, M.: Numerical deflections analysis of variable low stiffness of thin-walled parts during milling. In: Ivanov, V., et al. (eds.) *Advances in Design, Simulation and Manufacturing II, DSMIE-2019*. LNME, pp. 43–53. Springer, Cham (2020)
2. Kononenko, S., Dobrotvorskiy, S., Basova, Y., Gasanov, M., Dobrovolska, L.: Deflections and frequency analysis in the milling of thin-walled parts with variable low stiffness. *Acta Polytech.* **59**, 283–291 (2019)
3. Bashistakumar, M., Pushkal, B.: Finite element analysis of orthogonal cutting forces in machining AISI 1020 steel using a carbide tip tool. *J. Eng. Sci.* **4**(1), A11–A15 (2017)
4. Kolluru, K., Axinte, D.: Novel ancillary device for minimising machining vibrations in thin wall assemblies. *Int. J. Mach. Tools Manuf.* **85**, 79–86 (2014)
5. Ivanov, V., Mital, D., Karpus, V., Dehtiarov, I., Zajac, J., Pavlenko, I., Hatala, M.: Numerical simulation of the system “fixture–workpiece” for lever machining. *Int. J. Adv. Manuf. Technol.* **91**(1–4), 79–90 (2017). <https://doi.org/10.1007/s00170-016-9701-2>
6. Ivanov, V., Dehtiarov, I., Denysenko, Y., Malovana, N., Martynova, N.: Experimental diagnostic research of fixture. *Diagnostyka* **19**(3), 3–9 (2018). <https://doi.org/10.29354/diag/92293>
7. Feng, J., Wan, M., Gao, T.-Q., Zhang, W.-H.: Mechanism of process damping in milling of thin-walled workpiece. *Int. J. Mach. Tools Manuf.* **134**, 1–19 (2018)
8. Liu, C., Sun, J., Li, Y., Li, J.: Investigation on the milling performance of titanium alloy thin-walled part with air jet assistance. *Int. J. Adv. Manuf. Technol.* **95**, 2865–2874 (2017)
9. Vukman, J., Lukić, D., Milošević, M., Borojević, S., Antić, A., Đurđev, M.: Fundamentals of the optimization of machining process planning for the thin-walled aluminium parts. *J. Prod. Eng.* **19**(2), 53–56 (2016)
10. Schulze, V., Arrazola, P., Zanger, F., Osterried, J.: Simulation of distortion due to machining of thin-walled components. *Proc. CIRP* **8**, 45–50 (2013)
11. Fei, J., Lin, B., Xiao, J., Ding, M., Yan, S., Zhang, X., Zhang, J.: Investigation of moving fixture on deformation suppression during milling process of thin-walled structures. *J. Manuf. Process.* **32**, 403–411 (2018)
12. Diez, E., Perez, H., Marquez, J., Vizan, A.: Feasibility study of in-process compensation of deformations in flexible milling. *Int. J. Mach. Tools Manuf.* **94**, 1–14 (2015)
13. Wang, M.-H., Sun, Y.: Error prediction and compensation based on interference-free tool paths in blade milling. *Int. J. Adv. Manuf. Technol.* **71**, 1309–1318 (2014)

14. Ratchev, S., Govender, E., Nikov, S., Phuah, K., Tsiklos, G.: Force and deflection modelling in milling of low-rigidity complex parts. *J. Mater. Process. Technol.* **143–144**, 796–801 (2003)
15. Wan, X.-J., Hua, L., Wang, X.-F., Peng, Q.-Z., Qin, X.: An error control approach to tool path adjustment conforming to the deformation of thin-walled workpiece. *Int. J. Mach. Tools Manuf.* **51**, 221–229 (2011)
16. Ramanaiah, B.V., Manikanta, B., Ravi Sankar, M., Malhotra, M., Gajrani, K.: Experimental study of deflection and surface roughness in thin wall machining of aluminum alloy. *Mater. Today Proc.* **5**, 3745–3754 (2018)
17. Padmanaban, K.P., Prabhakaran, G.: Dynamic analysis on optimal placement of fixturing elements using evolutionary techniques. *Int. J. Prod. Res.* **46**, 4177–4214 (2008)
18. Vasundara, M., Padmanaban, K.P.: Recent developments on machining fixture layout design, analysis, and optimization using finite element method and evolutionary techniques. *Int. J. Adv. Manuf. Technol.* **70**, 79–96 (2013)
19. Ivanov, V.: Process-oriented approach to fixture design. In: Ivanov, V., et al. (eds.) *Advances in Design, Simulation and Manufacturing, DSMIE 2018*. LNME, pp. 42–50. Springer, Cham (2019)
20. Wan, X.-J., Zhang, Y.: A novel approach to fixture layout optimization on maximizing dynamic machinability. *Int. J. Mach. Tools Manuf.* **70**, 32–44 (2013)
21. Ivanov, V., Dehtiarov, I., Pavlenko, I., Kosov, I., Kosov, M.: Technology for complex parts machining in multiproduct manufacturing. *Manage. Prod. Eng. Rev.* **10**(2), 25–36 (2019)
22. Usatyi, O., Avdieieva, O., Maksiuta, D., Tuan, P.: Experience in applying DOE methods to create formal macromodels of characteristics of elements of the flowing part of steam turbines. In: *17th Conference of Power System Engineering, Thermodynamics and Fluid Mechanics, AIP Conference Proceedings, Pilsen, Czech Republic*, vol. 2047, no. 1, p. 020025 (2018)



# Research of Thermomechanical Processes When Processing Cylindrical Surfaces with Wear-Resistant Coatings

Maksym Kunitsyn<sup>(✉)</sup>  and Anatoly Usov 

Odessa National Polytechnic University,  
1, Shevchenko Ave., Odessa 65044, Ukraine  
kunitsyn.maksim@gmail.com

**Abstract.** The possibilities of technical support of the quality of finishing processing of the cylinder working surfaces using coatings of wear-resistant materials are considered. For this, a design scheme is proposed for determining the stress-strain state of the cylinder-coating system. The influence of the processing regimes of a cylindrical group with a wear-resistant coating on its physical and mechanical characteristics is determined. The dependence of SIF on the delamination angle  $\alpha$  and the roughness of the working area of the cylindrical surface  $R_a$  is presented. A design scheme is proposed for studying the mutual influence of exfoliation sections on stress intensity in a wear-resistant coating. The effect of particles on the wear resistance of the coating deposited by the electrochemical method is determined. A study of composite materials based on Ni/Ni-TiO<sub>2</sub> in a scanning electron microscope. The calculated and experimental values of the ultimate dimensions of crack-like defects during grinding of wear-resistant coatings are considered. The dependence of crack formation on the surface of the surface processed by grinding under the cutting depth and tool characteristics is determined.

**Keywords:** Durability · Reliability · Wear resistance · Delamination · Thermomechanical processes · Diamond abrasive processing · Tribocorrosion

## 1 Introduction

Analyzing the literature on tribology revealed that the operating costs of all technological cycles of machines exceed the costs of producing new equipment. In developed countries, the losses caused by friction and wear, account for 4...5% of national income [1–3].

The wear resistance of parts that work in conditions of sliding friction and have cylindrical surfaces, determines the durability of many machines [4]. Solving the problem of wear resistance of machine parts will lead to an increase in machine durability [5, 6]. Thus, the current area of research today is to increase the wear resistance of machine parts [7].

## 2 Literature Review

Often, qualitative modification of the structural composition in all the main elements of the material is not taken into account when protecting related parts from production and improving the quality of products, therefore this problem is solved taking into account the modification of the surface layer of the composite material because in this case only the surface layer is strengthened [1, 2]. The hardening of the surface layer is understood as increasing the mechanical characteristics such as hardness [8, 9].

Various methods of hardening have been proposed in a large number of works, which were devoted to improving the mechanical characteristics of rubbing surfaces [1, 2]. The use of modern methods for producing wear-resistant coatings using composite materials based on compounds such as oxides, nitrides, and carbides is today a promising direction for the development of surface-strengthening technologies [6, 7]. The creation of hardening coatings from dissimilar materials leads to the formation of a fundamentally new composite material of the surface layer, which has not only high strength, but also sufficient ductility, as well as increased wear resistance, and not only to the modification of the surface layer [10, 11].

## 3 Research Methodology

The paper describes the study of thermomechanical processes in products with reinforcing composite coatings during processing and operation to determine the conditions for the formation of various defects such as cracks, chips, and delaminations of coatings from the base material, as well as their elimination taking into account the technological parameters of finishing, hereditary defects arising during coating operations taking into account the physico-mechanical state of the surface layer.

The research helped to define the parameters of delamination at which the destruction of the composite coating occurs, taking into account the roughness of the working surface of the cylinder, its geometrical error, as well as the physico-mechanical properties of the material of the cylinder and reinforcing wear-resistant composite coating.

The stress-strain state of the cylinder-coating system is depicted in the analytical model (Fig. 1).

Let's consider the heat equation for a two-layer cylinder with symmetric heating, with free heat transfer from the inner and outer surfaces of the cylinder. The temperature and heat flux of the vicinity of the interface varies continuously. The obtained problem is to find a continuous temperature function  $t_i(r, \tau)$  in the domain  $D[R_1 \leq r \leq R_3, 0 \leq \tau < \infty]$ , satisfying the equation [12–15]:

$$\frac{\partial t_i}{\partial \tau} = a_i \left( \frac{\partial^2 t_i}{\partial r^2} + \frac{1}{r} \frac{\partial t_i}{\partial r} \right), \quad (1)$$

where  $i = 1$  for the first area  $D[R_1 \leq r \leq R_3, 0 \leq \tau < \infty]$

$i = 2$  for the second area  $D[R_1 \leq r \leq R_3, 0 \leq \tau < \infty]$

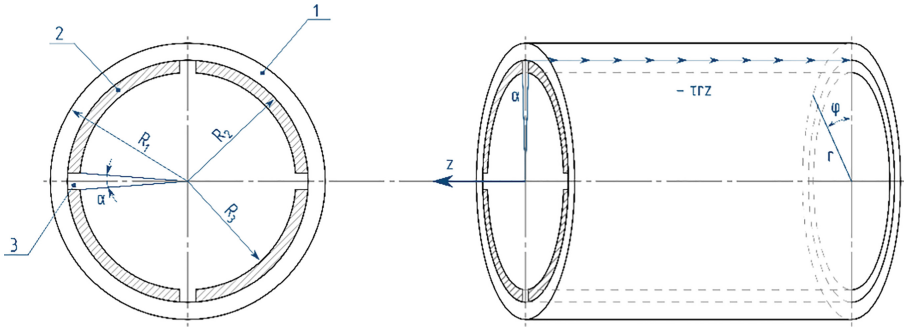


**Fig. 1.** The calculation scheme for determining the stress-strain state: 1 – the cylinder body; 2 – the body of the coating; 3 – areas of absence (exfoliation) of the coating.

Boundary conditions:

$$\begin{aligned} \frac{\partial t_1}{\partial r} - h_1[t_1 - T_1(\tau)] &= 0, \text{ at } r = R_1, \\ \frac{\partial t_2}{\partial r} - h_2[t_2 - T_2(\tau)] &= 0, \text{ at } r = R_3, \end{aligned} \tag{2}$$

pairing conditions:

$$t_1 = t_2, \lambda_1 \frac{\partial t_1}{\partial r} = \lambda_2 \frac{\partial t_2}{\partial r}, \text{ at } r = R_2; \tag{3}$$

initial condition:

$$t_i(r, 0) = \Phi_i. \tag{4}$$

Here  $a_i, h_i, \lambda_i$  are the coefficients of thermal diffusivity, relative heat transfer, and thermal conductivity, respectively, of the coating ( $i = 2$ ) and the base material ( $i = 1$ ).

The final solution to the problem is written as:

$$t_i(r, \tau) = \psi_i(r, \tau) + \sum_{n=1}^{\infty} \exp(-\gamma_n^2 \tau) \left[ \bar{\Theta}_n(0) + \int_0^{\tau} \frac{d\bar{\psi}_n(\bar{\tau})}{d\bar{\tau}} \exp(-\gamma_n^2 \bar{\tau}) d\bar{\tau} \right] u_{in}(r).$$

Here  $\psi_i(r, \tau) = [T_2(\tau) - T_1(\tau)](A_i \ln r + B_i) + T_i(\tau)$ .

To determine the stress-strain state of a coated cylinder exposed to a temperature field, the following problem is considered. A two-layer unlimited hollow cylinder is subject to the action of the temperature field  $t_i = t_i(r, \tau)$ . The material of the cylinder and the coating are in contact over the entire interface and, therefore, movements on the interface will be continuous. Another condition at the interface is obtained from the condition of continuity of normal stresses  $\sigma_r$ . On the outer surfaces,  $\sigma_r$  is assumed to be

zero. Thus, the following problem is to find the continuous deformation function  $u_i(r, \tau)$  in the domain  $D[R_1 \leq r \leq R_3, 0 \leq \tau \leq \tau_0]$  satisfying the equation:

$$\frac{1}{c_i^2} \frac{\partial^2 u_i}{\partial \tau^2} = \frac{\partial^2 u_i}{\partial r^2} + \frac{1}{r} \frac{\partial u_i}{\partial r} - \frac{u_i}{r^2} - m_i \frac{\partial t_i}{\partial r}, \tag{5}$$

where  $i = 1$  for the first area when  $r$  changes from  $R_1$  to  $R_2$  and  $i = 2$  for the second area, when  $r$  changes from  $R_2$  to  $R_3$ ;  $u_i(r, \tau)$  – the displacement;  $c_i$  – the propagation velocity of expansion waves in an elastic medium.

Boundary conditions:

$$\begin{aligned} \frac{\partial u_1}{\partial r} + p_1 u_1 &= m_1 t_1, \text{ at } r = R_1, \\ \frac{\partial u_2}{\partial r} + p_2 u_2 &= m_2 t_2, \text{ at } r = R_3; \end{aligned} \tag{6}$$

pairing conditions:

$$u_1 = u_2, p_{12} \frac{\partial u_1}{\partial r} + q_{12} u_1 = \frac{\partial u_2}{\partial r} + p_{12} m_1 t_1 - m_2 t_2 \text{ at } r = R_2; \tag{7}$$

initial condition:

$$u_i(r, 0) = \Phi_i(r), \frac{\partial u_i(r, 0)}{\partial \tau} = \Psi_i(r). \tag{8}$$

Having analyzed the calculated dependencies, the area of the peeling of the coating from the base material increases with increasing roughness of the inner surface of the cylinder because of the friction process in this area.

This means that the destruction of the coating will occur when the process stresses exceed the adhesion strength  $\sigma_{adh}$  in magnitude.

Figure 2(a) shows the processing mode of the working surfaces of the cylinder which provides the roughness to maintain the functional properties of the coated piston-cylinder group [1, 2, 6, 7, 14–16].

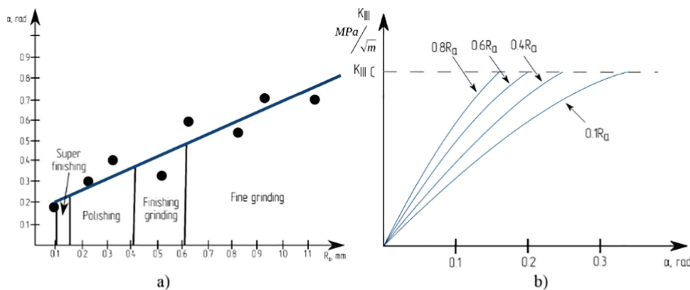


**Fig. 2** a) The influence of the processing regimes of the coated cylindrical group on its characteristics; b) SIF dependency onto detachment angle  $\alpha$  and cylinder surface's working area roughness  $R_a$ .

The quality of the machined surfaces of the cylindrical group will be ensured if, using the control technological parameters, we select such processing modes, cutting fluids and tool characteristics that the current grinding temperature  $T_i(r, \tau)$  and heat flux  $q(r, \tau)$ , stresses  $\sigma(r, \tau)$  will not exceed their limiting values [14, 15].

The processing of materials and alloys without grinding cracks can be achieved if the stresses formed in the intensive cooling zone are limited by the limiting values:

$$\sigma_{max}(r, \tau)|_{r=R_1} = 2G \frac{1 + \nu}{1 - \nu} \alpha_t T_k \operatorname{erf}\left(\frac{r}{2\sqrt{\alpha\tau}}\right) \leq [\sigma_{adh}] \tag{9}$$

Let  $U_z^{(i)}, U_r^{(i)}, U_\phi^{(i)}$  denote the displacement of the points of the cylinder-coating system in the direction of the corresponding coordinates of the cylindrical system  $(z, r, \phi)$ . Since under the influence of technological coupling stresses  $\tau_{rz}$  in system 1-2 (Fig. 1), the displacements  $U_z(r, \phi)$  will be nonzero, the Lamé equations can be written in the form:

$$\mu^{(i)} \Delta^2 U_z^{(i)} = \mu^{(i)} \left( \frac{\partial^2 U_z^{(i)}}{\partial r^2} + \frac{1}{r} \cdot \frac{\partial U_z^{(i)}}{\partial r} + \frac{1}{r^2} \cdot \frac{\partial^2 U_z^{(i)}}{\partial \phi^2} \right) = 0. \tag{10}$$

Or  $U_z(r, \phi) = W(r, \phi), 0 \leq r \leq R_z, -\pi \leq \phi \leq \pi$  the equation (26) takes the form:

$$\Delta W(r, \phi) = \frac{\partial^2 W}{\partial r^2} + \frac{1}{r} \cdot \frac{\partial W}{\partial r} + \frac{1}{r^2} \cdot \frac{\partial^2 W}{\partial \phi^2} = 0. \tag{11}$$

Boundary conditions:

$$\tau_{rz}|_{z=R_2} = 0, \tag{12}$$

$$\tau_{rz}(R_1 - 0, \phi, T) = \tau_{rz}(R_1 + 0, \phi, T) = -\tau_{adh}, |\phi| \leq \alpha. \tag{13}$$

Defect conditions:

$$W(R_1 - 0, \phi, T) - W(R_1 + 0, \phi, T) = \begin{cases} \chi(\phi), & -\alpha \leq \phi \leq \alpha \\ 0, & |\phi| > \alpha \end{cases}. \tag{14}$$

The conditions of continuity of tangential stresses at the cylinder-coating interface:

$$\tau_{rz}(R_1 - 0, \phi, T) = G_1 \frac{\partial W}{\partial r} \Big|_{r=R_1-0},$$

$$\tau_{rz}(R_1 + 0, \phi, T) = G_2 \frac{\partial W}{\partial r} \Big|_{r=R_1+0},$$

$$\begin{aligned} \tau_{rz}(R_1 - 0, \phi, T) - \tau_{rz}(R_1 + 0, \phi, T) &= G_1 \frac{\partial W}{\partial r} \Big|_{r=R_1-0} - G_2 \frac{\partial W}{\partial r} \Big|_{r=R_1+0} \\ &= G_1 \langle W'(R_1, \phi) \rangle - (G_2 - G_1) \frac{\partial W}{\partial r} \Big|_{R_1} = 0. \end{aligned}$$

Equations (11)–(14) constitute an anti-plane problem for the cylinder-coating system taking into account a defect of the delamination, which arises because of the roughness of the working surface of the cylinder or its non-circularity.

The solution to the discontinuous problem can be obtained in the form [12–15]:

$$W_n(r) = \int_0^{R_2} G(r, \rho) f(\rho) d\rho + \sum_{j=0}^1 r_j W_{n,j}(r) + grad T \tag{15}$$

In this problem, of practical interest is the stress intensity factor (SIF) at the delamination edges at  $\phi = -\alpha - 0$  and at  $\phi = \alpha + 0$ , i.e.:

$$K_{III}^- = \lim_{\phi \rightarrow -\alpha-0} \sqrt{2\pi(-\alpha - \phi)} \tau_{rz}(R_1, \phi, T), \tag{16}$$

$$K_{III}^+ = \lim_{\phi \rightarrow \alpha+0} \sqrt{2\pi(\phi - \alpha)} \tau_{rz}(R_1, \phi, T) \tag{17}$$

Taking into account the substitution  $\phi = \alpha\phi'$  and symmetry, these relations will take the form [12, 13]:

$$K_{III}^\mp = \lim_{\phi' \rightarrow \mp 1 \mp 0} \sqrt{2\pi\alpha(\mp 1 \mp \phi')} \tau_{rz}(R_1, \alpha\phi', T)$$

and at the same time [12–15]:

$$\begin{aligned} \tau_{rz}(R_1, \alpha\phi', T) &= \frac{-(h+1)G_1}{2\pi^2(2+h)\alpha} \\ &\times \frac{d^2}{d\phi'^2} \int_{-1}^1 X(\alpha\phi') \left[ \ln \frac{1}{|\phi' - \psi'|} + R^*(\alpha\phi', \alpha\psi') \right] d\psi'. \end{aligned} \tag{18}$$

Using the correlation between the roughness of the working zone of the cylinder and the value  $(-\alpha, \alpha)$  of the coating peeling section during various finishing operations: fine grinding, finishing grinding and polishing, we find the SIF dependence  $K_{III} = f(\alpha)$  (Fig. 2 (b)).

We find the calculated values of  $K_{III}$  depending on the magnitude of the defect  $(-\alpha, \alpha)$  delamination by the given values of  $\tau_{adh}$  of the adhesion of the coating to the cylindrical surface, at different values of the tool surface roughness (Fig. 2 (b)) (Fig. 3).



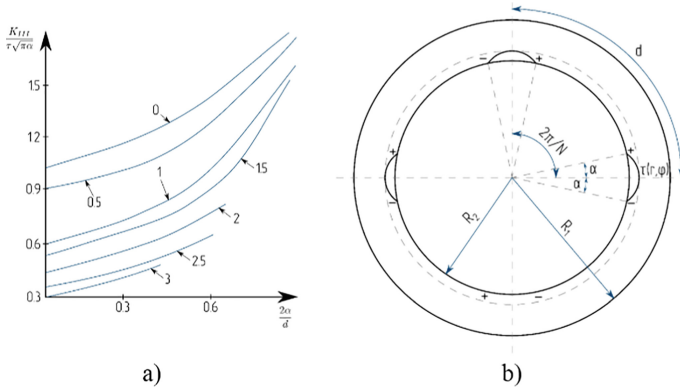


**Fig. 3** a) Dependency of SIF  $\frac{K_{III}}{\tau\sqrt{\pi a}}$  at longitudinal displacement; b) Calculation scheme for researching the reciprocal influence between detachment areas and stress intensity  $K_{III}$ .

### 4 Results

To ensure the required reliability and durability of the coated cylindrical group, it is necessary to provide a roughness of  $0.8 \leq Ra \leq 1,2$  when applying coatings on their working surfaces. Such roughness can be achieved through finishing grinding and subsequent finishing polishing.

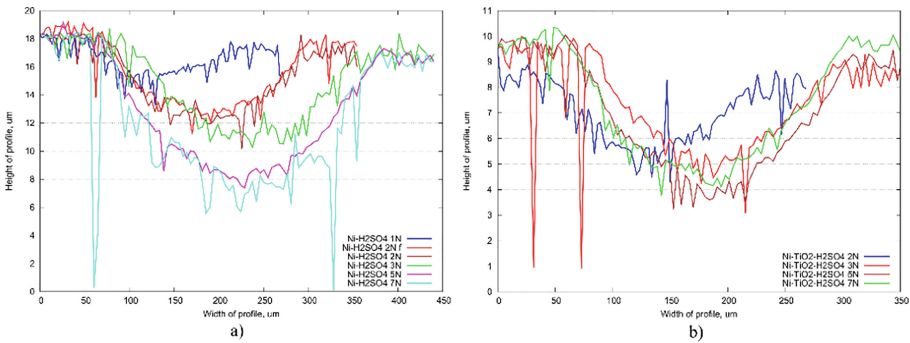


**Fig. 4.** The effect of particles on the wear resistance of an electrochemical deposited coating: a) nickel coating, b) Ni-TiO<sub>2</sub> coating.

To confirm the above analytical model, tribocorrosion studies of Ni/Ni-TiO<sub>2</sub>-based composite materials obtained by electrochemical deposition were carried out [18].

Electrochemical deposition of coatings was carried out using Autolab and the Nova program with the following parameters [18]:

- Mode – Galvanostatic;
- Current range – 100 mA;
- Bandwidth – High stability;

- Apply current – 0.035 A/dm<sup>2</sup>;
- Duration – 1800 s;
- Interval time – 0.1;

After tribocorrosion studies of Ni/Ni-TiO<sub>2</sub> materials, it was determined that for Ni coating, an increase in the depth and width of cracks is noticeable, depending on the increase in load with constant exposure time. Here, the crack profile for the Ni-TiO<sub>2</sub> coating does not change with increasing load and constant time. One can single out the positive effect of TiO<sub>2</sub> particles in the coating, which increases the protective functions of the coating against mechanical abrasion, and the load for Ni-TiO<sub>2</sub> ceases to play such a significant role (Fig. 4) [18].

The adequacy of the constructed model was tested experimentally on duplex steel samples (Table 1), on the surface of which a wear-resistant Ni-TiO<sub>2</sub>-based coating with a thickness of 0.4–0.6 mm was deposited by electrochemical deposition. To calculate the parameters of defect-free processing, the following physical and mechanical characteristics were used:  $KS = 2 \text{ MPa m}^{1/2}$ ;  $\alpha = 8.58 \text{ K}^{-1}$ ;  $G = 168 \text{ GPa}$ .

To check the criterion for the absence of grinding cracks on the surface to be treated, the contact temperature in the grinding zone was determined. Taking into account the fact that the dominant factor of the grinding modes affecting the thermal stress of the grinding process is  $h$  – the depth of grinding, the dependence  $T = f(h)$  was found. The remaining modes were selected from the conditions of maximum performance while maintaining the required quality. So, when grinding the coating with circles made of polycrystalline-crushed diamonds (Fig. 5: curve 1), circles made of synthetic diamonds (Fig. 5: curve 2), circles made of white electrocorundum (Fig. 5: curve 3), the remaining grinding modes were selected as follows:  $V_g = 0.17 \text{ m/s}$ ;  $V_{cr} = 30 \text{ m/s}$ ;  $S_{non} = 5 \text{ mm}$ .

**Table 1.** The chemical composition of duplex steels

Type / %	Cr	Ni	Mo	N	Sec. phases
Depleted	20–24	1–5	0.1–0.3	0.1–0.22	24–25
Standard	21–23	4.5–6	2.5–3.5	0.1–0.22	33–35
Saturated	24–29	4.5–8	2.7–4.5	0.1–0.35	>40
Enriched	27	6.5	5	0.4	49

Experimental studies have shown that circles from natural and synthetic diamonds have a stable cutting ability, high dimensional stability, have relatively low temperature in the grinding zone, which also affects the absence of cracks at large grinding depths (compared to circles made of white electrocorundum) [11].

It was found that grinding the coating with circles made of polycrystalline-crushed diamonds (Fig. 5: curve 1) was the most productive while maintaining the required quality.

The results of the study of the microhardness of the treated surface and the microstructure of the surface layer indicate that in the range of the studied modes there are no structural changes after grinding the wear-resistant Ni-TiO<sub>2</sub> coating. The diagram (Fig. 6) shows that while maintaining the quality characteristics of wear-resistant coatings the most productive tool for processing wear-resistant coatings are No. 6 and No. 7, which allow processing this surface at great depths of cut.

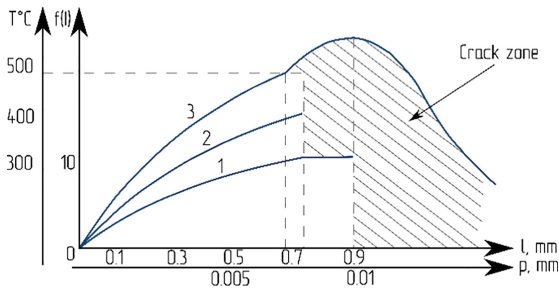


**Fig. 5.** Calculated and experimental values of the limiting sizes of crack-like defects when grinding wear-resistant coatings based on Ni-TiO<sub>2</sub> coatings in circles: 1 - circles made of polycrystalline-crushed diamonds; 2 - circles made of synthetic diamonds; 3 - circles made of white electrocorundum).

The nature of the crack formation of coatings depending on the characteristics of the wheels, cutting conditions can be followed using the criterion of the limiting heat flux  $q^*$ . The heat flux entering the part during grinding is not only a function of cutting modes —  $V_g, V_{cr}, t_{shl}, P_Z$ , but also the characteristics of wheels — the hardness of the bond, the graininess of the properties of cutting grains, their hardness, etc. its value of the limiting heat flux at which coatings containing defects of  $2l$  in size will not be subject to cracking [8, 10, 11].

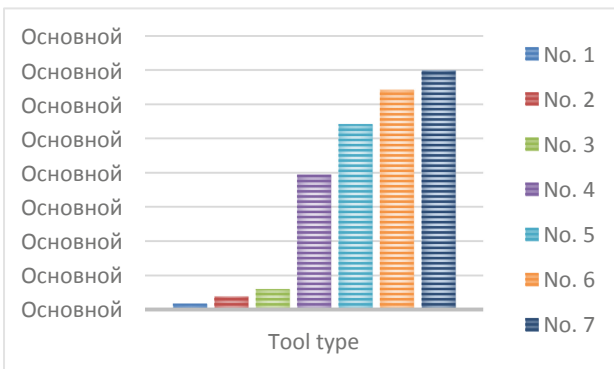


**Fig. 6.** Cracking on the surface of a wear-resistant coating processed by grinding, depending on the depth of cut and the characteristics of the tool.

## 5 Conclusions

An analytical model has been developed to determine the thermomechanical state of the working surface of a cylinder with a wear-resistant coating having partial detachment areas during application. The possibilities of technological support for the quality of finishing processing of the cylinder working surfaces using coatings of wear-resistant materials are considered. For this, a design scheme is proposed for determining the stress-strain state of the cylinder-coating system. The influence of the processing regimes of a cylindrical group with a wear-resistant coating on its physical and mechanical characteristics is determined. The dependence of SIF on the delamination angle  $\alpha$  and the roughness of the working area of the cylindrical surface  $R_a$  is presented. A design scheme is proposed for studying the mutual influence of exfoliation sections on stress intensity in a wear-resistant coating. The effect of particles on the wear resistance of the coating deposited by the electrochemical method is determined. Tribocorrosion studies of composite materials based on Ni/Ni-TiO<sub>2</sub> obtained by electrochemical deposition were carried out. A study of composite materials based on Ni/Ni-TiO<sub>2</sub> in a scanning electron microscope. The calculated and experimental values of the ultimate dimensions of crack-like defects during grinding of wear-resistant coatings are considered. The dependence of crack formation on the surface of the surface processed by grinding under the cutting depth and tool characteristics is determined. The technological quality assurance of the finish treatment of cylindrical surfaces with wear-resistant coatings based on Ni-TiO<sub>2</sub> by a rational choice of processing modes, and the characteristics of the tool taking into account hereditary defects during coating, is presented.




## References

1. Storozhev, V.P.: Causes and Patterns of Gradual Failures of the Main Tribological Objects of the Ship's Energy System and Increase of Their Resource. TOC, Odessa (2002). (in Russian)
2. Levchenko, A.A., Evdokimov, V.D.: The influence of technological heredity in the production of spare parts on hydrogenation of parts and their wear resistance. *Problems of Technology* **2**, 23–28 (2006). (in Russian)
3. Garkunov, D.N., Kornik, P.I.: Types of Friction and Wear Operational Damage to Machine Parts. MSHA, Moscow (2003). (in Russian)
4. Batako, A.D., Rowe, W.B., Morgan, M.N.: Temperature measurement in high efficiency deep grinding. *Int. J. Mach. Tools Manuf* **45**(11), 1231–1245 (2005)
5. Balohonov, R.R.: Surface layers and internal interfaces in heterogeneous materials. SO RAN, Novosibirsk (2006). (in Russian)
6. Sun, Y., Flis-Kabulska, I., Flis, J.: Corrosion behaviour of sediment electro-codeposited Ni–Al<sub>2</sub>O<sub>3</sub> composite coatings. *Mater. Chem. Phys.* **145**(3), 476–483 (2014)
7. Aruna, S., William Grips, V., Rajam, K.: Ni-based electrodeposited composite coating exhibiting improved microhardness, corrosion and wear resistance properties. *J. Alloys and Compounds* **468**(1–2), 546–552 (2009)
8. Usov, A.V.: Mathematical modeling of control processes for the coating of structural elements based on SIE. *Mechanical Engineering Issues* **13**(1), 98–109 (2010)

9. ASTM B254-92(2014): Standard Practice for Preparation of and Electroplating on Stainless Steel. ASTM International, West Conshohocken (2014)
10. Oborskiy, G.A., Daschenko, A.F., Usov, A.V., Dmitrishin, D.V.: System modeling. Astroprint, Odessa (2013). (in Russian)
11. Davim, J.P.: Machining. Fundamentals and Recent Advances. Springer, London (2008)
12. Carslaw, H.S.: Introduction to the Mathematical Theory of the Conduction of Heat in Solids (Classic Reprint). Fb&c Limited, London (2017)
13. Carslaw, H.S., Jaeger, J.C.: Conduction of Heat in Solids. Clarendon Press, Oxford (1986)
14. Chen, L., Wang, L., Zeng, Z., Xu, T.: Influence of pulse frequency on the microstructure and wear resistance of electrodeposited Ni–Al<sub>2</sub>O<sub>3</sub> composite coatings. *Surf. Coat. Technol.* **201** (3–4), 599–605 (2006)
15. Kim, K.T., Kim, D.W., Kim, S.H., Kim, C.K., Choi, Y.J.: Synthesis and improved explosion behaviors of aluminum powders coated with nano-sized nickel film. *Appl. Surf. Sci.* **415**, 104–108 (2017)
16. Kalpakjian, S., Schmid, S.R.: Manufacturing Engineering and Technology. Pearson, Upper Saddle River (2014)
17. Surjya, K.M.: Fracture Mechanics. Cambridge University Press, Cambridge (2015)
18. Kunitsyn, M.V., Usov, A.V.: Tribocorrosion research of NI-Al<sub>2</sub>O<sub>3</sub>/TiO<sub>2</sub> composite materials obtained by the method of electrochemical deposition. *Modern Technologies in Mechanical Engineering* **12**, 61–70 (2017)



# Investigation of the Grinding Process Considering the Increase of the Active Surface of Abrasive Grains

Maksym Kurin<sup>(✉)</sup> , Serhii Nyshnyk , and Anatolii Dolmatov 

National Aerospace University “Kharkiv Aviation Institute”,  
17, Chkalova St., Kharkiv 61070, Ukraine  
m.kurin@khai.edu

**Abstract.** The problems of the grinding process of difficult-to-process materials are analyzed. The main factors influencing the efficiency of preserving the parameters of the quality of the surface and the surface layer are the cutting modes, characteristics of the abrasive wheel and lubricating and cooling technological environments are defined. At the same time, all these factors indirectly affect the efficiency of processing due to wear, blunting and salinization of the grinding wheel. The study of the kinematics of the microcutting process with round external and internal grinding of surfaces was conducted. It has been determined that the work of plastic deformation is the main source of heat formation during grinding. The method of calculation of processes of plastic deformation, based on the closed system of equations of mechanics of continuous media is considered. In the experimental part of the work, the research of the influence of technological regimes and the characteristics of the abrasive tool on the energy indices of the process of round external grinding of hard-working materials has been carried out.

**Keywords:** Microcutting · Kinematics of the process · Heat stress · Energy-Intensive processes · Plastic deformation · Dissipation energy · Deformation power

## 1 Introduction

In the modern aircraft engine industry, the development of technology for the production of GTE parts occurs by increasing their processing with an abrasive tool. Due to the increasing number of grinding operations and requirements for quality production surfaces, the goal is efficiency abrasive processing methods [1, 2].

The need to predict the force and other characteristics of the grinding process around the periphery of the grinding wheel requires their analytical description. In this connection, the question arises of the study of the kinematics of shaping during grinding and the establishment of the most important grinding equations describing the geometric parameters of the tool’s contact with the workpiece. The latter include the equation of the trajectory of the micro-cutting by the grinding grain, the length of contact of the tool with the workpiece, the layer thickness removed by one grain of a wheel, and others.

Thus, studies aimed at improving the efficiency of grinding due to the improvement of existing forming processes of products of intractable metals and alloys are relevant.

## 2 Literature Review

Making of details of the aviation engine is related to the treatment of workpieces with special physical and mechanical properties - corrosion resistance, heat resistance, high-temperature strength, and high strength. These materials belong to the group of intractable materials. Literature sources, which studies the issues of increasing the efficiency of the grinding process of intractable materials are considered. It is established that the main factors that influence the efficiency of processing while maintaining the quality parameters of the top surface and surface layer are the cutting modes, the characteristics of the abrasive wheel, and the lubricant-cooling agent. At the same time, all these factors indirectly affect the efficiency of processing due to wear, blunting and salinization of the grinding wheel [3–10].

The analysis shows that one of the most rational ways to increase the efficiency of the grinding process is the choice of rational processing modes. In this case, there is a comprehensive solution to the problem: first, the need to use expensive lubricant-cooling agents reduced, and second, the need for special grinding wheels and their frequent trueing is reduced [1–9, 11–13].

A large number of analytical and empirical dependencies for determining such parameters of the grinding process, as the number of cutting grains and the shape of their cutting part, the geometric parameters of the chip and the contact zone, the cutting force and the contact temperature, testifies both to the complexity of its adequate description, and to the fact that grinding theory is imperfect and needs further development.

## 3 Research Methodology

### 3.1 Investigation of Kinematics and Micro-cutting Process During Grinding

The principle of standard grinding methods has been used to establish the basic kinematic parameters, which is that when specifying some arbitrary motions of the grinding wheel and details, any grinding method may be obtained as a separate case [14].

To determine the orientation angle of the cutting grain it is necessary to find the angle between the vector of absolute cutting speed and the vector of the speed of movement of the grain relative to the axis of the circle rotation (in a moving coordinate system associated with the circle) (Fig. 1).

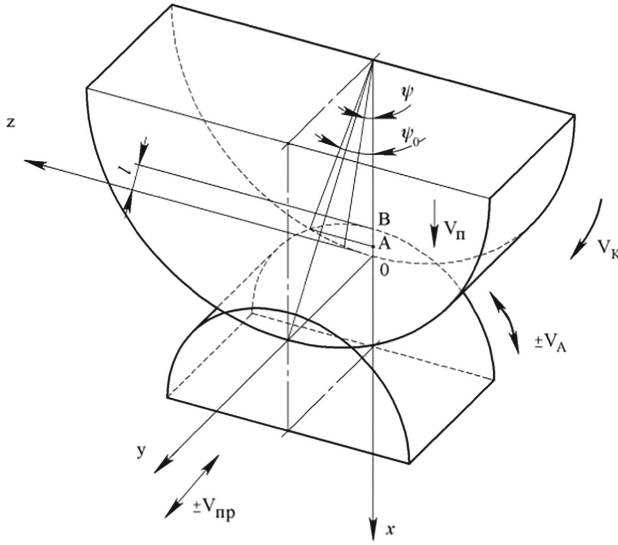


**Fig. 1.** Scheme for calculating the basic kinematic parameters of the grinding process [14].

It is described as follows.

$$\phi = \arccos \left[ \frac{V_k - (V_n \cdot \sin \psi \pm V_\delta \cdot \cos \psi)}{\sqrt{V_k^2 - 2 \cdot V_n \cdot V_k \cdot \sin \psi \pm 2 \cdot V_\delta \cdot V_k \cdot \cos \psi + V_n^2 + V_{np}^2 + V_\delta^2}} \right], \quad (1)$$

$$0 \leq \phi \leq \pi.$$

Determine the orientation angle within the contact angle:

$$\Delta\phi = \left| \phi|_{\psi=\psi_0} - \phi|_{\psi=0} \right|, \quad (2)$$

where

$$\psi_0 \approx 2 \cdot \sqrt{\frac{d \cdot l}{D \cdot (d + D)}}.$$

Based on the obtained equations, the orientation angle change within the contact angle was calculated, depending on the speed of rotation of the workpiece and the speed of longitudinal feed of the workpiece for external and internal grinding for different cutting depth, and graphs have been plotted (Figs. 2, 3 and 4).

Changing the orientation of the grain relative to the cutting velocity vector contributes to the increase in the total area of discrete contact sites (contact) of the grain with the treated surface and chips, which descends while reducing the contact time of the sites.



These graphs show that increasing rotation speed of the circle and the speed of longitudinal feed of the workpiece leads to a decrease in the total area of discrete contact pads (touch) of the grain, and an increase in the speed of workpiece rotation - to the rise in the entire area of discrete pads of contact (touch) of the grain.

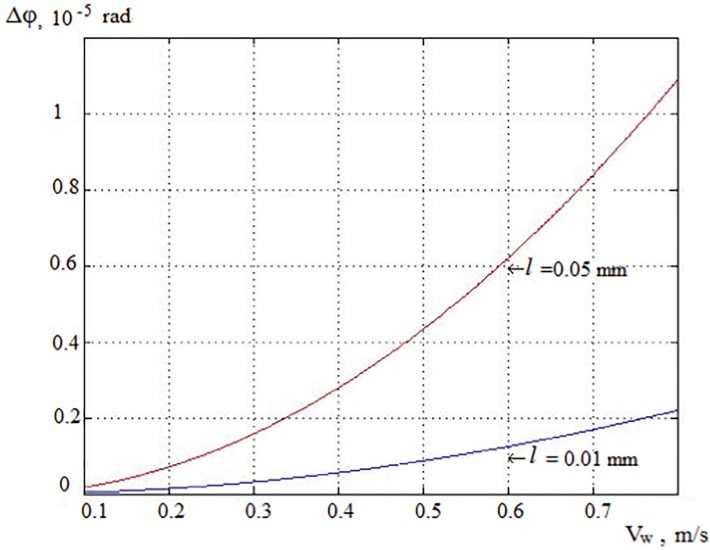


Fig. 2. Changing the orientation angle within the contact angle depending on the speed of rotation of the part for external grinding.

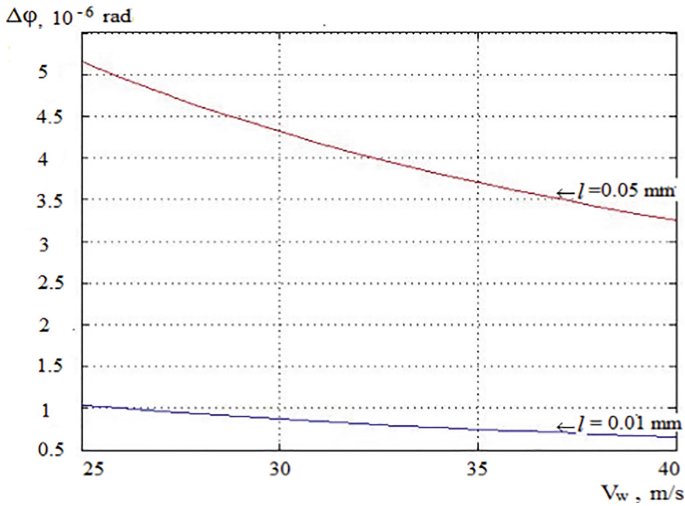
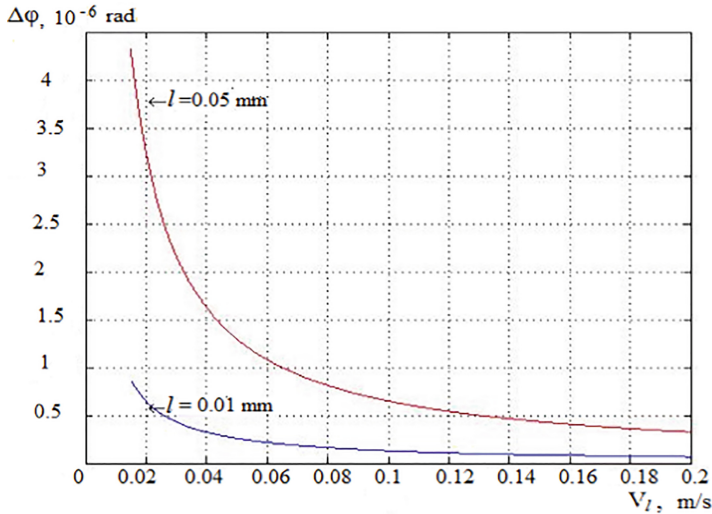


Fig. 3. Changing the orientation angle within the contact angle depending on the speed of rotation of the part for external grinding.



**Fig. 4.** Changing the orientation angle within the contact angle depending on the speed of longitudinal feeding of the part for external grinding.

## 4 Results

### 4.1 Investigation of Power-Strength Parameters of Grinding Process

The study of the energy-power characteristics of the grinding process was carried out based on the hypothesis of a generalized cutter with a continuous cutting edge. Part of the abrasive grains acting over the bond identified with rotational ellipsoids. The essence of the proposed methodology is based on the conceptual model of abrasive grain that it is the equivalent that reflects all the cutting properties of the abrasive wheel.

Establishing a direct correlation makes it possible to find the value of the forward angle of the equivalent grain  $\gamma$ , which is quantitatively related to the coefficient of the reference curve:

$$\operatorname{tg}|\gamma| \approx \frac{1}{v} \quad (3)$$

The cutting properties of the abrasive tool do not depend on the values of the grinding mode parameters, and  $\gamma$  is meant to be a constant that quantitatively expresses the cutting properties of a particular brand of the abrasive tool.

Theoretical research has resulted in analytical dependencies, not only describing the metal flow in the deformation zone but also being suitable for calculating the energy-power characteristics of the process, without the use of a vast array of empirical dependencies that do not fully reflect the physics of the process and are limited by the narrow scope of experimental research.

Based on the velocity field, which is given by parametric equations [15] (4)

$$\begin{cases} V_x(x, y) = V_0[\omega(x, y)]^{-\frac{1}{2}} \left[ \frac{(x \cdot \cos \alpha - y \cdot \sin \alpha) \cdot e^2 \cdot \sin \alpha + y}{\sqrt{e^2 - 1}} \right]; \\ V_y(x, y) = V_0[\omega(x, y)]^{-\frac{1}{2}} \left[ \frac{(x \cdot \cos \alpha - y \cdot \sin \alpha) \cdot e^2 \cdot \cos \alpha - x}{\sqrt{e^2 - 1}} \right]; \\ \omega(x, y) = \frac{e^2 \cdot [x_0 \cdot \cos \alpha \pm \sqrt{\sin^2 \alpha \cdot (1 - e^2) \cdot ([a(x, y)]^2 \cdot (e^2 \cdot \sin^2 \alpha - 1) - x_0^2}]}{(1 - e^2 \cdot \sin^2 \alpha)^2} \\ \quad + [a(x, y)]^2; \\ a(x, y) = \sqrt{\frac{(x \cdot \cos \alpha - y \cdot \sin \alpha)^2 \cdot e^2 - (x^2 + y^2)}{(1 - e^2)}}. \end{cases} \quad (4)$$

dependencies are obtained for the calculation of deformation constituents, strain rates, and their intensities:

$$e_{xx} = \int \varepsilon_{xx} dt; \quad e_{yy} = \int \varepsilon_{yy} dt; \quad e_{xy} = \int \varepsilon_{xy} dt \quad (5)$$

$$\varepsilon_i = \frac{\sqrt{2}}{3} \cdot \sqrt{(\varepsilon_{xx} - \varepsilon_{yy})^2 + e_{yy}^2 + e_{xx}^2 + \frac{3}{2} \cdot e_{xy}^2}; \quad (6)$$

$$e_i = \frac{\sqrt{2}}{3} \cdot \sqrt{(e_{xx} - e_{yy})^2 + e_{yy}^2 + e_{xx}^2 + \frac{3}{2} \cdot e_{xy}^2}. \quad (7)$$

These dependencies make it possible to calculate the energy dissipation function, which can be expressed by the intensity of stresses and strain rates by the formula:

$$E = \sigma_i \cdot \varepsilon_i. \quad (8)$$

To determine the deformation power, the energy dissipation function must be integrated by volume:

$$N = \iiint_v E dv, \quad (9)$$

where  $\sigma_i$  is the intensity of stresses;  $\varepsilon_i$  is the intensity of strain rates.

The stress intensity for different deformed media is a complex function of the strain intensity, strain rate, temperature, time, and other parameters.

Metals and alloys are a group of materials that are strengthened during plastic deformation. The stress intensity is a function of the strain intensity only:

$$\sigma_i = \sigma_m \cdot e_i^n, \quad (10)$$

where  $n$  is the index of strain hardening;  $e_i$  is the intensity of deformation;  $\sigma_m$  is the yield strength.

An example is considered: the operation of grinding a part of an alloy BT3-1, the speed of rotation of the abrasive wheel  $V_{wh} = 30$  m/c, the speed of rotation of the workpiece  $V_w = 30$  m/min, cutting depth  $t = 0.02 \cdot 10^{-3}$  m. Parts were machined with an abrasive wheel 63C40CM2K with geometry  $\gamma = \alpha = 101.6^\circ$  (Fig. 5).

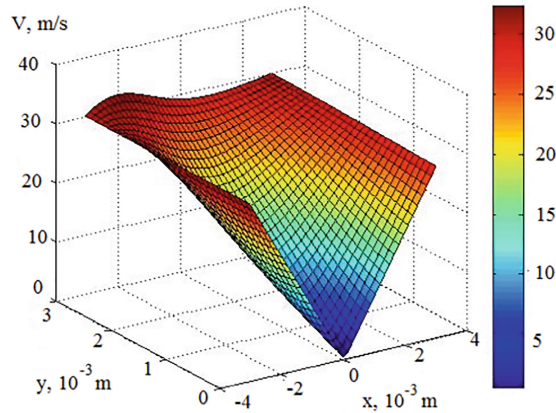


Fig. 5. Particle velocity field.

The calculation of the deformation power according to the above algorithm gives the following result –  $N \approx 9.93$  W. Below there is the experimental investigation of the total cutting forces, which is converted to the single grain power and agrees to the theoretical calculations.

#### 4.2 Effect of Grinding Modes on Cutting Forces

The influence of technological regimes and the characteristics of the abrasive tool on the energy indices of the process of round external grinding of hard-working materials as 12X17H2, 30XГСА, ЖС6-K, BT-3, OT-4 has been carried out. The change in the physical and mechanical properties of the treated materials at a depth of the molded surface layer was evaluated by changing the micro-hardness and microstructure. The grinding process for the BT3-1 alloy has been shown in Fig. 6. The nature of the change in the performance of other processed materials is similar.

As can be seen from the graphs in Fig. 6, the dependence is observed: with increasing the speed of rotation of the workpiece with constant cutting depth, the cutting force decreases intensively (curve t4, which corresponds to a depth of 0.05 mm).

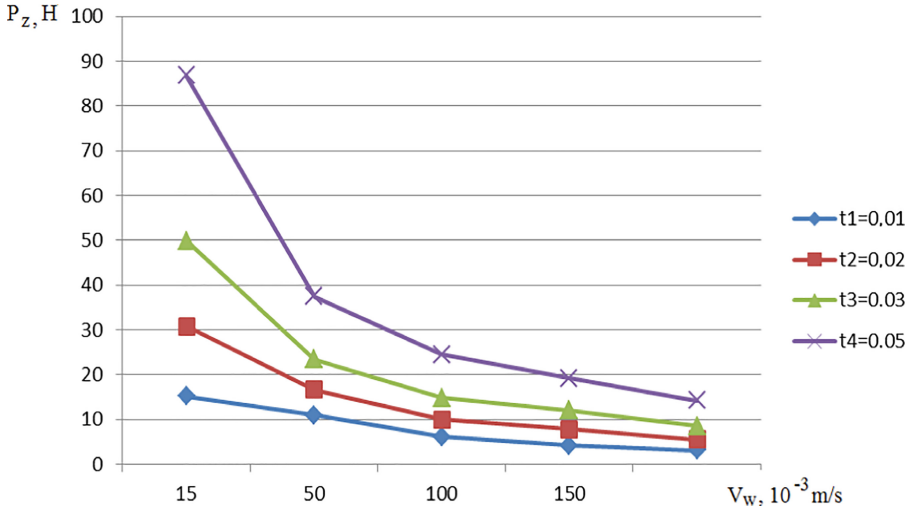


**Fig. 6.** The dependence of the cutting force on the speed of rotation of the workpiece  $V_w$  at different grinding depth 63C40CM2K for material BT3-1.

The reason is that the higher the speed of rotation of the workpiece, the greater the contact area of the abrasive grain with the grinding surface, the higher the number of non-blunt discrete contact areas (touching) of the grain involved in cutting, which consequently reduces the cutting force that falls on each grain at the same cutting depth.

Similarly, the specific grinding intensity influence the cutting force can be explained. The higher the speed of the longitudinal feed of the workpiece, the smaller the contact area of the abrasive grain with the grinding surface.

This is confirmed by the results of theoretical studies presented in Figs. 2, 3 and 4.

It can be stated that when increasing the grain size of the wheel, the value of the cutting force is almost unchanged. However, when machining the surface with an abrasive wheel 63C16CM2K, there is an increase in cutting forces for the BT3-1 material and a decrease for the OT4. This can be explained by the fact that in the first case, a stronger bond of grains, which affects their dullness, and in the second, less durable, where the mode of self-exacerbation occurs.

The physical and mechanical properties of the treated materials in the depth of the formed surface layer were evaluated by the change in microhardness, as well as by the results of microstructure analysis. The microhardness of the materials was determined according to the conventional method using the PMT-3 instrument by the method of oblique grinding.

When grinding the sample using basic technology, a layer with a minimum microhardness at a depth of 0.1 mm is formed in the near-surface zone. The reason for the formation of such a layer is the phase transformations that occur at elevated contact temperatures. When grinding according to the proposed technology, on the contrary, there is an additional hardening of the surface layer of metal to a depth of 0.25... 0.3 mm, as evidenced by the increase in microhardness.

During metallographic studies, no changes were observed in the surface microstructure of all the treated samples (Fig. 7).

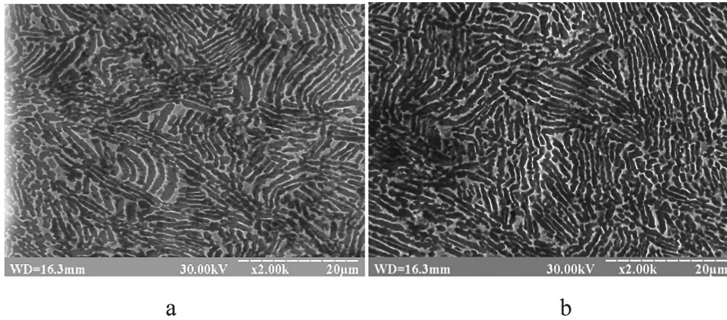


**Fig. 7.** The structure of the BT3-1 material at different depths.

The surface temperature of treated areas was measured in the zone located directly in front of the grinding wheel using an IR-1000L pyrometer solely for comparing its value in different modes. It was found that with an increase of speed rotation part, a decrease in contact temperature is observed.

## 5 Conclusions

The importance and relevance of the research topic have been confirmed. The kinematics of the formation of circular grinding was investigated, and the parametric equations of the trajectories of the abrasive grain motion, the absolute speed of the abrasive grain movement, the angle of orientation of the cutting grain relative to the velocity vector and the area of the active surface of the cutting grain were obtained.

The calculation of the change of the orientation angle within the contact angle, depending on the speed of the circle rotation, the speed of rotation of the workpiece and the speed of longitudinal feeding of the workpiece for external and internal grinding for different cutting depth done.

For the theoretical study of the energy-power parameters of the circular grinding process, a method of calculating the processes of plastic deformation of metals, based on a closed system continuum mechanics equations is proposed.

As a result of complex experimental studies it is established that the provision of technological modes of processing based on the criteria conditions during grinding leads to a qualitative and quantitative change in the parameters of the chip formation process:

- cutting forces are reduced by 1.1... 1.3 times;
- contact temperature decreases from 5 to 15%;

- the physical and mechanical properties of the formed surface layers change both qualitatively and quantitatively in the direction of increasing the operational properties;
- the need for lubricant-cooling agent consumption is reduced by up to 15%, with the requirements for their properties becoming less critical;
- increases the resistance of the abrasive tool.

The recommendations on the improvement and expansion of the technological modes of grinding are given.

## References

1. Poklad, V.A., Abysov, I.A., Starkov, V.K., Ryabtsev, S.A.: Surface-layer properties of turbine-blade tailpiece in deep grinding by highly porous wheels. *Russ. Eng. Res.* **11**(30), 1132–1136 (2010)
2. Krymov, V.V.: Production of gas turbine engine blades. Mashinostroenie, Moscow (2002)
3. Hessel, D., Karyazin, A., Starkov, V.K., Ryabtsev, S.A., Gorin, N.A.: High-efficiency rotary dressing method for cubic boron nitride wheels. *J. Superhard Mater.* **3**(37), 194–201 (2015)
4. Grigoriev, S.N., Starkov, V.K., Gorin, N.A., Krajnik, P., Kopač, J.: Creep-feed grinding: an overview of kinematics, parameters and effects on process efficiency. *J. Mech. Eng.* **4**(60), 213–220 (2014)
5. Kopač, J., Krajnik, P.: High-performance grinding - a review. *J. Mater. Process. Technol.* **175**(1), 278–284 (2006)
6. Rowe, W.B.: Towards high productivity in precision grinding. *Inventions* **3**(2), 1–16 (2018)
7. Rowe, W.B.: Temperatures in grinding-a review. *J. Manuf. Sci. Eng.* **139**(12), 1–6 (2017)
8. Kurin, M.O., Surdu, M.V.: The concept of the mechanism and kinetics of influence of mechanochemical processes on edge cutting machining. *Metallofizika i Noveishie Tekhnologii* **3**(39), 401–424 (2017)
9. Surdu, N.V.: Improving the grinding efficiency of hard-to-machine materials by improving the kinematics of processes. IPMash NAS of Ukraine, Kharkiv (2005)
10. Dolmatov, A.I., Kabatov, A.A., Kurin, M.A.: Investigation and optimization of diamond smoothing technology as applied to stainless steel details for aircraft engines and aggregates. *Metallofizika i Noveishie Tekhnologii* **10**(35), 1407–1423 (2013)
11. Badger, J., Murphy, S., O'Donnell, G.E.: Acoustic emission in dressing of grinding wheels: AE intensity, dressing energy, and quantification of dressing sharpness and increase in diamond wear-flat size. *Int. J. Mach. Tools Manuf.* **125**, 11–19 (2018)
12. Zhang, L., Rowe, W.B., Morgan, M.N.: An improved fluid convection solution in conventional grinding. *J. Eng. Manuf.* **227**(6), 332–338 (2013)
13. Sipailov, V.A.: Grinding thermal processes and surface quality control. Mashinostroenie, Moscow (1978)
14. Evseev, D.G., Salmikov, A.N.: The physical basis of the grinding process. Izdatelstvo Saratovskogo universiteta, Saratov (1978)
15. Kurin, M.O.: Hyperbolae method analysis of a wedge flow at free cutting. *Metallofizika i Noveishie Tekhnologii* **7**(40), 859–876 (2018)



# Processing of Parts Under Pulse Loading of a Vibrating Hopper

Volodymyr Symoniuk , Viktor Denysiuk ,  
and Yurii Lapchenko  

Lutsk National Technical University, 75, Lvivska St., Lutsk 43018, Ukraine  
yuralap@gmail.com

**Abstract.** In the article, the critical analysis of the current state of processing of vibrating methods of grinding, the advantages of their existing methods of processing machine parts and devices with traditional grinding are indicated. The inspection of the developed vibration installation, the influence of the regime of vibrating on the movement of the working environment in a vibration bunker are analyzed, the process of conducting a scientific experiment is planned. The results of experimental researches on the process of vibroabrasive processing of details, the reproducibility of the experiment, and the reliability of the obtained results were considered. It has been determined that the results of mathematical modelling coincide with the results of the experiment. To determine the patterns vortex circulation movement of the working environment, a specially introduced coordinate system was used and a single shooting was performed, which made it possible to determine the movements of parts and abrasive granules. In addition, from the analysis of demonstration shooting, the trajectory of parts movement in the volume of the working environment was predicted. The analysis of technological possibilities of vibroprocessing in a wide range of frequency and oscillation scope is carried out. The reasons for the problem selection of optimum modes of vibration processing and possible directions for overcoming them are presented. different modes of vibration machine operation are modeled. The results of the analysis made it possible to determine the principles of optimal selection of vibration treatment modes. The method of operation of a vibrating machine with the most effective use of mechanical energy of vibrations is established.

**Keywords:** Vibroprocessing · Vibrosetting · Circulation movement · Electromagnetic · Abrasive material · Vibrohopper

## 1 Introduction

The relevance of vibration abrasive methods for machining parts is explained by the advantages of this method over traditional finishing operations such as ripping, grinding, polishing [1–6]. Vibroabrasive treatment allows providing mechanization of the machining process, to improve the processing of geometrically complex external and internal hard-to-reach surfaces of details, as well as the processing of fragile and non-rigid parts without disturbing their geometric shape and damage to the surfaces [2, 4, 7, 8]. The use of vibration treatment as a finishing operation can significantly reduce



the cost of manufacturing parts with a surface roughness  $R_a > 0$ . Vibration processing, which provides micro-roughness of the order of  $0.15\text{--}0.25\ \mu\text{m}$ , in some cases, can replace fine tuning, the cost of which is 4–5 times higher. The accuracy of the geometric shape of the workpiece obtained by grinding is not compromised, as a result of vibration removes a layer of the metal, not more than  $1\text{--}2\ \mu\text{m}$  [4, 5, 9–11].

## 2 Literature Review

Information technical sources indicate the high performance of vibration processing [1, 4, 5, 12–14]. However, the lack of complete information on the processes that occur during the machining of details in the work environment and the technological capabilities of vibration treatment, as well as recommendations for the technological support of mechanical vibration abrasion impedes the widespread industrial implementation and further development of this progressive method [2, 4, 7, 8, 15]. The interest in vibrating abrasive methods of machining parts is explained by the advantages of this method over such traditional finishing operations as ripping, grinding, and polishing as it provides the mechanization of the machining process, machining of geometrically complex external, and internal hard-to-reach surfaces of details and not the machining of the curves of the details, as well as machining and damage to surfaces and parts that tend to clutch when machined in rotating drums. An important advantage of vibration treatment is the high stability of the machining results of all parts in one batch, which is especially important when machining high precision parts.

## 3 Research Methodology

The vibration unit (Fig. 1) contains a working chamber mounted on the supports connected to the base, the ends of each are equipped with springs, and the bottom of the working chamber is equipped with vibrators made in the form of electromagnets. The number of supports and electromagnets is four. Depending on the sequence of activation of the electromagnets, the necessary circulating motion of the working medium is formed [4]. The working environment is a quasi-homogeneous liquid-fluid substance with nonlinear characteristics. At a shock impulse load, the vibrating hopper of the working environment changes its properties. Shock loads can be carried out symmetrically when all four electromagnets are switched on and in asymmetric schemes [4, 8–10]. Moving elements of the working environment cause circulatory motion, which is formed in radial planes (Fig. 2). Equivalent flow lines (element trajectories) are closed and are annular lines having lower branches L1, L2, L3, L4 and upper branches L5, L6, L7, L8. The circulation is slow. It covers the entire volume of the work environment. The circulating motion looks like a vortex ring centered at points O1 and O2. Thus, at the impulse load of the vibrating hopper in the working environment, there is a vortex circulation motion, which covers the spherical region. In the center of the spherical region (points O1 and O2), there is a focus of the current, where its translational velocity is close to zero. The basic provisions of the theory of hydraulic shock

are used to calculate the dynamic parameters of the environment during the shock impulse loading. The propagation time of the shock wavefront from the bottom of the vibrating hopper to the free surface is the phase of the hydraulic shock  $\tau$ :

$$\tau = \frac{H}{v_a} \tag{1}$$

where  $H$  – the height of the working environment;  $v_a$  – shock wave speed.



**Fig. 1.** The vibration installation.

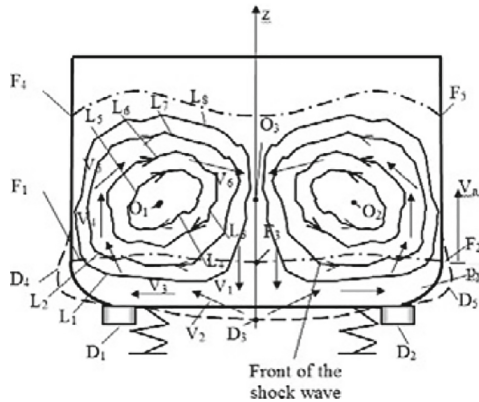


**Fig. 2.** The scheme of axisymmetric vertical movement of the vibrating hopper and circulation of the working environment.

The pressure increase is determined by the energy balance equation. In a hydraulic impact, the kinetic energy of the working environment  $E_k$  is converted into the potential energy of compression of the environment  $E_{np}$  and the potential energy of the

deformed bottom of the walls of the vibrating hopper  $E_{nm}$ . Thus, the energy balance equation is as follows:

$$E_k = E_{nm} + E_{np} + E_d \quad (2)$$

where  $E_d$  – energy lost to environmental resistance and non-linear deformation processes in the work environment.

The kinetic energy of the medium moving with the average velocity  $v_0$  in the vibro-bunker height  $H$  and radius  $r_0$  is determined by the equation:

$$E_k = 0,5\rho\pi r_0^2 H v_0 \quad (3)$$

where  $\rho$  – the average equivalent density of the working environment, which includes the parts and pellets of the abrasive.

The potential energy of the compressed work environment is equal to the work of compression under the action of shock change of pressure  $\Delta p_y$  and is defined as:

$$E_{np} = 0,5\rho\pi r^2 \Delta p_y \Delta W \quad (4)$$

Where  $\Delta H$  – changing the height of the working environment;  $\Delta W$  – changing the volume of the work environment.

Assume in the first approximation that the change in the volume of the working environment depends linearly on the change in pressure:

$$\Delta W = \frac{W \Delta p_y}{E_a} \quad (5)$$

where  $W$  – a volume of the work environment;  $E_a$  – the average value of the equivalent modulus of elasticity of the working environment.

Defining the volume of the environment as  $W = \rho\pi r^2 H$ , we obtain an expression for the potential energy compression of the working environment:

$$E_{np} = \frac{0,5\rho\pi r_0^2 H (\Delta p_y)^2}{E_a} \quad (6)$$

The potential energy of deformation of the vibrohopper walls is:

$$E_{nm} = 0,5\Delta p_y \rho\pi r_0 H \Delta r$$

where  $\Delta r$  – vibrating hopper wall deformation in the radial direction.

According to Guka Law:

$$\Delta r = \frac{\sigma r}{E}$$

where  $\sigma$  – normal stress in the material of the vibrohopper;  $E$  – elasticity module of the vibrohopper wall.

Define the tension as:

$$\sigma = \frac{\Delta p_y r}{\delta}$$

where  $\delta$  – hopper wall thickness.

The potential energy deformation:

$$E_{nm} = \frac{\pi r^3 H}{\delta E} (\Delta p_y)^2 + E_{bm}$$

$$E_{bm} = \frac{\pi r^3}{\delta E} K_d (\Delta p_y)^2$$

where  $E_{bm}$  – the potential energy hopper bottom,  $K_d$  – factor.

Set the value of energies in the energy balance equation and get:

$$0,5\pi r^2 H \rho V_0^2 = \frac{\pi r^2 (H + K_d)}{\delta E} (\Delta p_y)^2 + \frac{\pi r^2 H}{2E_a} (\Delta p_y)^2 \quad (7)$$

Shock pressure values:

$$\Delta p_y = \rho V_0 V_a \quad (8)$$

where,  $V_a = \sqrt{\frac{E_p}{\rho}}$  – the shock wave propagation speed;  $E_p$  – the attached bunker elasticity module.

## 4 Results

Experimental researches were carried out for the clarification dependence of indicators of intensity and quality of vibroprocessing from the amplitude of oscillation of the vibrohopper. The duration of each experiment was 3 h. Mark is abrasive 38A (normal electrocorundum). The details of the type of bodies of rotation, which have external and internal cylindrical, flat and torsion surfaces, which are obtained in different ways (milling, precision) and have different initial roughness are used as test samples. This allows determining the degree of processing of each type of surface, estimate the degree of rounding of sharp edges. Samples from two different materials are used in experiments to clarify the dependence of indicators of the intensity and quality of vibration processing from the amplitude and frequency of oscillations: from non-magnetic steel 1.4878 and brass CW607N. In the study of the influence of the electromagnetic field on the process of vibroabrasive processing, it was used as the experimental samples of the ring of Cardan bearings after punching of steel (100Cr6). Experiments were conducted in the following sequence: flushing specimens with a warm soapy solution of dirt; drying of samples; determination of the primary mass of  $m_1$ , gram and roughness  $Ra_1$ , mkm samples for processing; tagging on swatches

conducting research; cleaning and flushing of samples from abrasive residues; drying; measuring of the mass of  $m_2$ , gram, and roughness of  $Ra_2$ , mkm samples after processing; calculation of metal chip removal by the weighing of marked samples by the formula:

$$Q = m_1 - m_2 \tag{9}$$

Based on obtained values, the graphs of the dependence of metal chip removal  $Q$ , gram and roughness  $Ra$ , mkm from amplitude  $A$ , frequency  $f$  for each material (steel 1.4878 and brass CW607N) were constructed. As a result of the experiment, the following values of a span of a container oscillation were obtained depending on a load of its working mixture (Table 1).

**Table 1.** Results of experimental measurement of a range of container oscillations, mm.

Download level	0 kg			1,5 kg			3 kg			
№ repeattiness	1	2	3	1	2	3	1	2	3	
Number of the electromagnet	1	2,0	1,5	2,0	1,5	1,5	1,5	1,0	1,0	1,0
	2	2,5	1,5	2,0	1,5	1,5	2,0	1,0	1,5	1,0
	3	2,5	2,5	2,0	1,5	1,0	1,0	1,0	1,0	1,0
	4	2,5	2,5	2,5	2,0	1,5	2,0	2	1,5	1,5
Arithmetic mean	2,4	2,0	2,1	1,6	1,4	1,6	1,2	1,2	1,1	
Quadratic mean	2,4	2,0	2,1	1,6	1,4	1,7	1,3	1,3	1,1	

In the table you can see that the average of the arithmetic and the average quadratic value of a span of vibrations are not significantly different, that is, it is possible to conclude about small random error measurements. Based on Table 1, a table is compiled for mathematical processing of experiment results (Table 2). This data evaluates the criterion of Kohrena:  $G = 0,722$ . The table value of the Kohrena  $G_T = 0,977$ . Since the value of the criterion of Kohrena, suggested by the experiment results, is less than the table, the experimental data can be considered authentic, and the experiment itself is reproducible. According to experimental data, the projection of the three points of the dependence of the range of vibrations of the container from its load working mixture is:

$$R = b_0 + b_1m + b_2m^2 \tag{10}$$

where  $R$  – container oscillations;  $m$  – the weight of container loading;  $b_0, b_1, b_2$  – extrapolating factors.

**Table 2.** Experimental results.

Download level, kg	Oscillation frequency by repetition, mm			The arithmetic mean, mm	Dispersion, mm <sup>2</sup> I
	I	II	III		
0	2,4	2,0	2,1	0	2,4
1,5	1,6	1,4	1,6	1,5	1,6
3	1,2	1,2	1,1	3	1,2

The method of sequential lookup in Eq. (6) of experiment data in each of three points is found extrapolating coefficient (with precision to two significant digits). After that, the Eq. (6) took the form:

$$R = 2,17 - 0,52 m + 0,06 m^2 \quad (11)$$

Adequacy of this equation is tested according to the Fisher criterion. For Eq. (11) variance of adequacy is  $S_{ad}^2 = 1,417 \times 10^{-4}$ . In accordance with the criterion of Fisher,  $F = 7,077 \cdot 10^{-3}$ . A table value for the Fisher criterion for this case is  $F = 5,987$ . Since the value of the Fisher criterion for Eq. (11) is less than the table value for this case, the description of the dependence of the range of vibration of the container from its loading by the Eq. (11) can be considered adequate.

The measurement of circulating vortex movement of the working environment was carried out under different laws of management of electromagnetic drives [4]. An optical method is applied when measuring the position of the elements of the working environment. The wood surveying of the surface of the working environment in the vibrobunker is carried out. The frame rate was 1 s. The coordinates of the working environment element and their change by individual frames are defined in cartesian rectangular and polar in curved or special coordinate systems.

We will accept a cartesian rectangular coordinate system XOY with a center in the central part of the vibrobunker (Fig. 3). For several adjacent frames, we define the coordinates of separate abrasive granules or the marker. We will establish successive provisions of individual granules on the surface of the working environment. The array of vectors of the position of separate individual elements in the form of a set of vectors:

$$\begin{bmatrix} X_{A1} \\ Y_{A1} \end{bmatrix}, \begin{bmatrix} X_{A2} \\ Y_{A1} \end{bmatrix}, \dots, \begin{bmatrix} X_{An} \\ Y_{An} \end{bmatrix}; \begin{bmatrix} X_{B1} \\ Y_{B1} \end{bmatrix}, \begin{bmatrix} X_{B2} \\ Y_{B1} \end{bmatrix}, \dots, \begin{bmatrix} X_{Br} \\ Y_{Br} \end{bmatrix}; \begin{bmatrix} X_{C1} \\ Y_{C1} \end{bmatrix}, \begin{bmatrix} X_{C2} \\ Y_{C1} \end{bmatrix}, \dots, \begin{bmatrix} X_{Cq} \\ Y_{Cq} \end{bmatrix}.$$

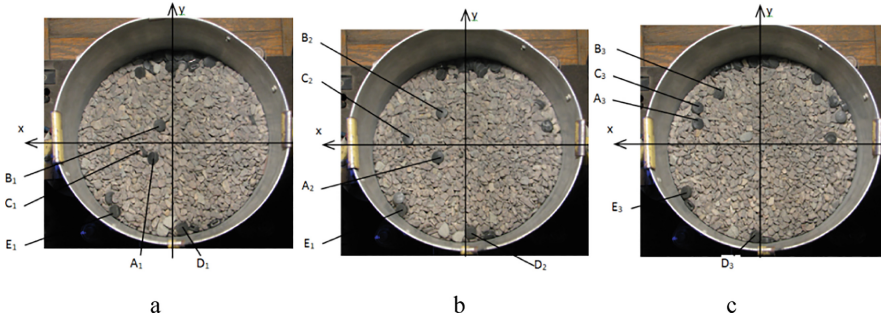


**Fig. 3.** The scheme of determining the position of details on separate shooting frames when using a cartesian rectangular coordinate system.

Vectors determine the position of an element of the working environment on the surface in the form of points  $A_1, A_2, A_n; B_1, B_2, B_r; C_1, C_2, C_q$ . To determine the speed of the slow circulating movement of the working environment are determined by increments of coordinates of elements in the neighboring positions, which are formed in the form of vectors:

$$\left[ \begin{matrix} \Delta_x A_1 \\ \Delta_y A_1 \end{matrix} \right], \left[ \begin{matrix} \Delta_x A_2 \\ \Delta_y A_2 \end{matrix} \right], \dots, \left[ \begin{matrix} \Delta_x A_n \\ \Delta_y A_n \end{matrix} \right]; \left[ \begin{matrix} \Delta_x B_1 \\ \Delta_y B_1 \end{matrix} \right], \left[ \begin{matrix} \Delta_x B_2 \\ \Delta_y B_2 \end{matrix} \right], \dots, \left[ \begin{matrix} \Delta_x B_n \\ \Delta_y B_n \end{matrix} \right]; \left[ \begin{matrix} \Delta_x C_1 \\ \Delta_y C_1 \end{matrix} \right], \left[ \begin{matrix} \Delta_x C_2 \\ \Delta_y C_2 \end{matrix} \right], \dots, \left[ \begin{matrix} \Delta_x C_n \\ \Delta_y C_n \end{matrix} \right].$$

Resulting increments can be submitted in the form of the distances between the individual provisions of points. For example, point A.

$$\Delta_{A1} = \sqrt{\Delta_{xA1}^2 + \Delta_{yA1}^2}, \dots, \Delta_{Ai} = \sqrt{\Delta_{xAi}^2 + \Delta_{yAi}^2}$$

The average speed of the circulating movement was defined from the dependencies:

$$v_{xA1} \approx \frac{\Delta_{xA1}}{\Delta t}, \dots, v_{yA1} \approx \frac{\Delta_{yA1}}{\Delta t}$$

Thus, the field of velocity on the surface of the working environment was defined. To improve the quality of the field, velocities are introduced in a special coordinate system. They allow defining the features of a local Vortex motion desktop (coordinate system in the form of an arc  $K_1M_1$  (Fig. 4), provide an opportunity to identify local moving items in the diametric intersection of the working environment. The coordinate system in the form of an arc or line allows installing features and limits of the current. This system allows determining the degree of the passing of the elements into the work environment. Similarly, the coordinate system in the form of a closed polygon (polyhedron) is used. In Figure ABCD, the elements combined in a quadrilateral are shown. Its move from the frame to frame describes the average speed of the elements of the working environment within the quadrangle. The deformation of the quadrangle characterizes the differences between the elements of the working environment.

Change the position of the quadrangle, in particular, its surface characterizing the local vortex movement of elements of the work environment.

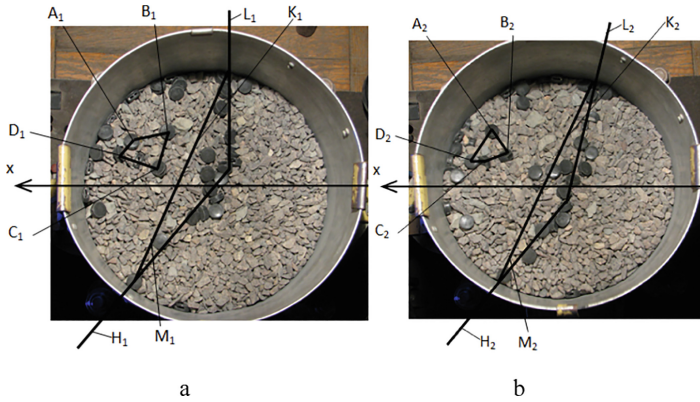


**Fig. 4.** The determination of regularities of the vortex circulation movement working environment with the use of especially typed coordinate systems.

A frame-by-frame survey provides an opportunity to determine the rotational movements of the parts and abrasive granules. For this purpose, bullets of cylindrical shape with a small value (in the form of the disc) are applied. On individual frames, registered angular position details and use the normal to its control surface (Fig. 5). Vectors of normal for neighboring leaders  $\vec{n}_2, \vec{n}_3, \vec{n}_4, \vec{n}_5$  are determined by the position of the disc. An angular position of the parts is determined by the angle  $\theta$ , which is associated with the ratio of axes of an ellipse, respectively:

$$\theta = \arccos\left(\frac{b}{a}\right).$$

The angular position of the disc in the plane of the coordinate axes XOY is determined by an angle  $\varphi$  between the small axis of an ellipse and the X-axis. The analysis of time-lapse shooting can predict the trajectory of the parts in the volume of the work environment. The definition of the forecast trajectory of movement simulates the scheme (Fig. 5). For details (markers) frame-by-frame shooting is made. On frames fixed position details, starting from the point of the  $A_1$  and ending point of the AK.

Further reorganization of the frame-by-frame shooting took as long as the piece again appeared on the surface (about point  $A_1$ ). Trajectories of the details are shown with the dotted line. The time of finding parts in the volume of the work environment is exactly determined.



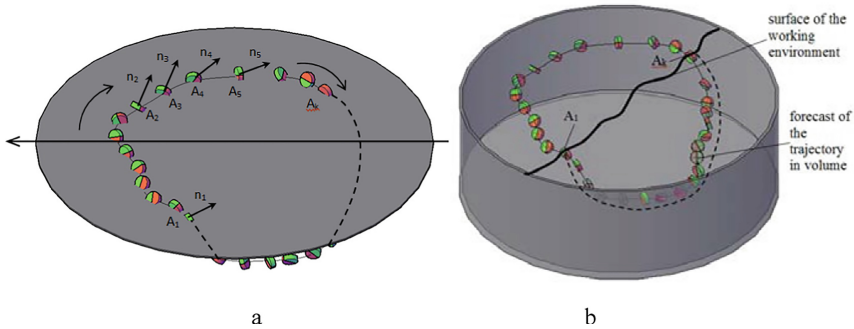


**Fig. 5.** The determination of the predictive values of the trajectory of motion of the parts in the volume of work environment: a – fixed movement parts on the surface; b – the spatial movement of parts (the trajectory shown in the dotted line).

## 5 Conclusions

The result of studies showed that the shock impulse load on the vibrobunker lead to a slow circulation of the movement work environment. This movement intensification in the non-symmetrical shock load. The circulation motion is circular or arcuate vortex ring that covers the entire volume of the desktop environment. To determine the nature of the Vortex motion, the application of the law changes the amount of movement in the integral form for the selected control the volume of the working environment is accepted. The average speed of the circulating movement depends on the intensity of impact, speed vibrobunker to the punch, and the mass of the working environment. The angular speed of the vortex movement is proportional to the average velocity of the circulating traffic. In the working environment, a movement of individual items (blasting media granules) is chaotic, which is caused by shock loads of the granules from the neighboring granules. The chaotic movement manifests itself in the form of deviations of the trajectory of a single pellet from the high trajectory of a circulating movement. The deviation of the trajectory is close to harmonic (sinusoidal).




## References

1. Blekhman, I.I., Blekhman, L.I., Yaroshevich, N.P.: Upon drive dynamics of vibratory machines with inertia excitation. *Obogashchenie Rud* 49–53 (2017)
2. Blekhman, I.I., Kremer, E.B.: The dynamics of a complex machine assembly: vibration-induced drag on the rotation. *J. Mach. Manuf. Reliabil.* **46**(4), 330–335 (2017)
3. Filimonihin, G.B., Yacun, V.V.: Investigation of the process of excitation of dual-frequency vibrations by ball auto-balancer of GIL 42 screen. *East.-Eur. J. Enterp. Technol.* **1**(7(79)), 17–23 (2016)
4. Strutinski, V.B., Symonyuk, V.P., Denysiuk, V.Y.: Improvement of equipment and process of shock-pulse processing of parts in vibrobunker: monograph. SPD Gadjak Zhanna Volodymurivna, Lutsk (2016)

5. Filimonikhin, G., Yatsun, V., Dumenko, K.: Research into excitation of dual frequency vibrational-rotational vibrations of screen duct by ball-type auto-balancer. *East-Eur. J. Enterp. Technol.* **3**(7(81)), 47–52 (2016)
6. Symonyuk, V., Denysiuk, V., Lapchenko, Y.: Experimental study of circulating vortex movement working environment in vibrobunker. *Mech. Mater. Sci. Eng. J.* **12** (2017)
7. Symonyuk, V.P., Fedorchuk, O.V., Denysiuk, V.Y., Kaidyk, O.L., Lapchenko, Y.S.: Lutsk national technical university. Ukraine patent 126090 (2018)
8. Pavlenko, I.V., Yukhymenko, M.P., Lytvynenko, A.V., Bocko, J.: Solving the nonstationary problem of the disperse phase concentration during the pneumoclassification process of mechanical mixtures. *J. Eng. Sci.* **6**(1), F1–F5 (2019)
9. Blekhman, I.I., Indeitsev, D.A., Fradkov, A.L.: Slow motions in systems with inertial excitation of vibrations. *J. Mach. Manuf. Reliabil.* **37**(1), 21–27 (2008)
10. Balthazar, J.M., Mook, D.T., Weber, H.I., Brasil, M.L.R.F., Fenili, A., Belato, D., Felix, J.L. P.: An overview on non-ideal vibrations. *Meccanica* **38**(6), 613–621 (2003)
11. Blekhman, I.I., Vasil'kov, V.B., Yaroshevich, N.P.: On some opportunities for improving vibration machines with self-synchronizing inert vibration exciters. *J. Mach. Manuf. Reliabil.* **42**(3), 192–195 (2013)
12. Filimonihin, G.B., Yacun, V.V.: Method of excitation of dual frequency vibrations by passive autobalancers. *East-Eur. J. Enterp. Technol.* **4**(776), 9–14 (2015)
13. Artyunin, A.I., Eliseyev, S.V.: Effect of “crawling” and peculiarities of motion of a rotor with pendular self-balancers. *Appl. Mech. Mater.* **373–375**, 38–42 (2013)
14. Yatsun, V., Filimonikhin, G., Dumenko, K., Nevdakha, A.: Equations of motion of vibration machines with a translational motion of platforms and a vibration exciter in the form of a passive auto-balancer. *East-Eur. J. Enterp. Technol.* **5**(1(89)), 19–25 (2017)
15. Yatsun, V., Filimonikhin, G., Dumenko, K., Nevdakha, A.: Search for two-frequency motion modes of single-mass vibratory machine with vibration exciter in the form of passive auto-balancer. *East-Eur. J. Enterp. Technol.* **6**(7(90)), 58–66 (2017)



# Finite Element Analysis of Profile Grinding Temperature

Natalia Lishchenko<sup>1</sup> , Vasily Larshin<sup>2</sup> ,  
and Sergey Uminsky<sup>3</sup> 

<sup>1</sup> Odessa National Academy of Food Technologies,  
112, Kanatna St., Odessa 65039, Ukraine

<sup>2</sup> Odessa National Polytechnic University, 1, Shevchenko Ave.,  
Odessa 65044, Ukraine

vasilylarshin@gmail.com

<sup>3</sup> Odessa State Agrarian University, 13, Panteleimonivs'ka St.,  
Odessa 65012, Ukraine

**Abstract.** The analysis of equations for determining the grinding temperature taking into account the curvature of the grinding profile, is performed. Mathematical models of the temperature field were proposed, which makes it possible to identify the influence of the curvature radius of the surface to be ground on the grinding temperature in the range from a semicircular profile to a linear one as the radius of the semicircular profile tends to infinity. The variation range of the curvature radius is established, in which the curvature of the profile being ground can be neglected when calculating the grinding temperature. The influence of the profile curvature radius on the maximum grinding temperature was established using both direct calculating and computer simulating of the temperature field by the analytical model and the finite element method (FEM), respectively. Grinding temperature FEM simulation results differ by no more than 0.5% compared to the analytical model under otherwise similar conditions. It is established that the FEM simulation is more suitable due to its greater sophistication, which makes it possible considering the individual geometric features of the surface to be ground as well as any instantaneous distribution of the heat flux in the grinding zone. At the same time, an analytical model for direct calculating of the grinding temperature takes much less time to get a result and can be used in computer monitoring and grinding diagnosing of subsystems on CNC machines.

**Keywords:** Curvature radius · Temperature field · Heat flux · Analytical model · Finite element method · FEM simulation

## 1 Introduction

Taking into account the surface curvature influence on the grinding temperature is essential in grinding the bearing's raceways, semicircular profile thread grinding, profile grinding the gear teeth, etc. In real profile grinding, the curvature of the surface being ground is different and can be variable for different points of the surface, e.g. in profile gear grinding. Promising methods that take into account a large number of

factors inaccessible to the analytical model, including the profile curvature factor, are simulation methods for which the following special computer programs have been developed viz. ELCUT, COSMOS/M, ADINAT, ANSYS, NASTRAN, LS-DYNA, STAR-CD, and COMSOL Multiphysics. They are mostly based on the FEM simulation; however, it takes a lot of time to determine the grinding temperature and not acceptable for rapid control of the profile grinding operation on CNC machines. The temperature determination by the analytical equation does not have this drawback. However, the problem is in obtaining an analytical model (an equation), which can be obtained theoretically and then experimentally tested. Therefore, the comparative study of the temperature field in profile grinding using an analytical mathematical model and FEM simulation was performed in the paper.

## 2 Literature Review

The temperature in the grinding zone is one of the factors limiting the performance of the grinding operation [1, 2]. To optimize grinding parameters, it is necessary to have accurate information about the grinding temperature, which can be obtained by pure theoretical methods [3, 4], theoretical methods with experimental verification through heat itself and thermal burns which are a result of this temperature appearance [5–20], as well as by the temperature field FEM simulation [21–25]. The practical application of the temperature studies listed above for the monitoring and diagnosing of computer subsystems on CNC grinding machines is considered in works [26, 27].

The review showed that theoretical methods are based on the analysis of a temperature field mathematical (analytical) model, which acts within the framework of the so-called phenomenological approach. Existing analytical models are obtained under certain assumptions; they are as follows: the heat flux constancy, the profile simple geometric shape of the contact zone surface to be ground. Besides, even with these assumptions, the analytical models taking into account surface curvature are quite complicated. At the same time, based on the literature review, the following scientific hypothesis has arisen. If the dimensions of the elementary surface being ground are sufficiently long and when the Peclet number is greater than 5, the grinding temperature field can be described quite well by a correctly selected analytical model for the corresponding elementary geometric surface.

## 3 Research Methodology

It is convenient to take the threaded surface of the lead screw with a semicircular thread profile as a profile-grinding example with different profile curvatures when the curvature radius  $R$  is changed. By changing the radius  $R$  of the semicircular profile of the thread, it is possible to establish the influence of the grinding profile curvature on the grinding temperature. The following equation was found for the case in question [28].

$$T(r, \tau) = -\frac{2qR}{\pi\lambda} \int_0^\infty (1 - \exp(-F_0\zeta^2)) \frac{J_0(\zeta \frac{r}{R})Y_1(\zeta) - Y_0(\zeta \frac{r}{R})J_1(\zeta)}{\zeta^2(J_1^2(\zeta) + Y_1^2(\zeta))} d\zeta, \quad (1)$$

where  $r$  is the current radius vector of the surface point;  $F_0 = a\tau/R^2$  is the Fourier number;  $\tau$  is the heat source time, s;  $q$  is the heat flux, W/m<sup>2</sup>;  $R$  is the cylindrical surface radius (or radius of the cylindrical heat source);  $\lambda$  is the thermal conductivity of the workpiece material, W/(m · °C);  $J_0, J_1$  are the Bessel functions of first kind of zero and first order;  $Y_0, Y_1$  are the Bessel functions of second kind of zero and first order;  $\zeta$  is integration variable.

Equation (1) is the solution of the following one-dimensional differential equation of the heat conduction

$$\frac{\partial T}{\partial \tau} = a \left( \frac{\partial^2 T}{\partial r^2} + \frac{1}{r} \frac{\partial T}{\partial r} \right).$$

For example, Eq. (1) one can be used for the grinding temperature determination in the semicircular thread profile grinding under the second kind boundary condition and zero initial condition, i.e.

$$-\lambda \frac{\partial T}{\partial r} = q = \text{const, if } r = R;$$

$$T(r, \tau) = 0, \text{ if } r \geq R \text{ and } \tau = 0.$$

In turn, Eq. (1) is the closest analog of the following solution of the one-dimensional differential equation of heat conduction when  $R \rightarrow \infty$  [28]:

$$T(x, \tau) = \frac{2q\sqrt{a\tau}}{\lambda} \left( \frac{1}{\sqrt{\pi}} \exp\left(\frac{-x^2}{4a\tau}\right) - \frac{x}{2\sqrt{a\tau}} \operatorname{erfc} \frac{x}{2\sqrt{a\tau}} \right), \quad (2)$$

where  $x$  is the current coordinate, which is perpendicular to the heat source surface;  $a$  is the thermal diffusivity of the workpiece material being ground, m<sup>2</sup>/c.

To determine the depth  $x$  of the temperature penetration into the thread surface layer it is necessary to take into account the formula

$$\frac{r}{R} = \frac{R+x}{R}.$$

We can write Eq. (1) in the form

$$T(x, \tau) = -\frac{2qR}{\pi\lambda} \int_0^\infty \left( 1 - \exp\left(\frac{-a \cdot \tau}{R^2} \zeta^2\right) \right) \frac{J_0\left(\zeta \frac{R+x}{R}\right)Y_1(\zeta) - Y_0\left(\zeta \frac{R+x}{R}\right)J_1(\zeta)}{\zeta^2(J_1^2(\zeta) + Y_1^2(\zeta))} d\zeta. \quad (3)$$

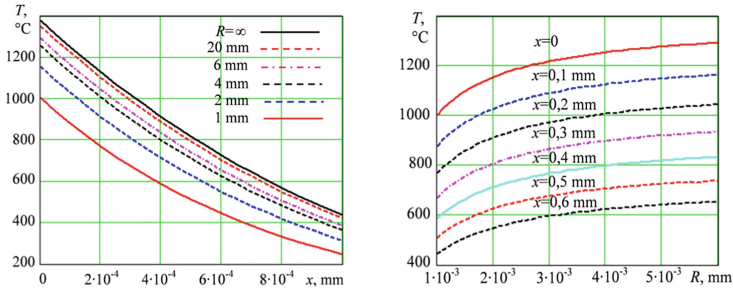


**Fig. 1.** Grinding temperature distributions over the surface layer depth  $x$  (left) and profile curvature radius  $R$  (right).

The temperature calculation is performed using the formula (3) for different radius  $R$  of the profile being ground in the range of  $1 \leq R \leq 6$  mm and for different values  $0 \leq x \leq 0.6$  mm (Fig. 1). To solve this problem in the MathCAD 2000 Professional environment, it is necessary to specify three groups of input parameters viz. the thermal group ( $a$ ,  $\lambda$ ), geometric group ( $R$ ,  $x$ ) and energetic group ( $q$ ,  $\tau$ ). The calculations were performed for  $\lambda = 30$  W/(m  $\cdot$   $^{\circ}$ C),  $q = 40 \cdot 10^6$  W/m $^2$ , and for the heat source time duration  $\tau = 0.1$  s.

It can be seen that a change in radius  $R$  from 1 to 3 mm significantly affects the surface temperature both at  $x = 0$  (i.e., on the surface being ground) and its distribution over the surface layer depth (Fig. 1). At the same time, a change in radius  $R$  from 4 to 6 mm slightly affects the temperature (Fig. 1). For example, a change in radius  $R$  from 4 to 6 mm on the surface ( $x = 0$ ) leads to an increase in the grinding temperature from 1120  $^{\circ}$ C to 1136  $^{\circ}$ C (by 3.1%), while with an increase  $R$  from 1 to 3 mm the temperature increases from 1003  $^{\circ}$ C to 1219  $^{\circ}$ C (by 21.5%).

Figure 1 also shows the temperature distributions over the depth of the surface layer, which is obtained by the Eq. (2) for a flat heat source when the curvature radius tends to infinity ( $R \rightarrow \infty$ ). The condition  $R = \infty$  is the limiting case of the calculation by Eq. (3) with  $R \rightarrow \infty$ . Thus, the curves in Fig. 1 shows the close agreement of Eqs. (2) and (3) in the specified range of variables  $R$  and  $x$ . You can see at what values of the radius  $R$  the thermo-physical calculations for the semicircular thread profile can be carried out using Eq. (2), obtained for a flat heat source. So, for example, at  $R = 6$  mm, the difference in calculations according to Eqs. (2) and (3) at a depth of a double temperature drop ( $x = 0.6$  mm) is 724.06  $^{\circ}$ C and 653.9  $^{\circ}$ C (Fig. 1), respectively, i.e., no more than 11%, which is acceptable for engineering calculations at the grinding operation design stage.

Equation (3) describes the temperature on an ideal cylinder at a constant heat flux and can be used to describe the temperature field in the area of the contact zone, which is remote from this zone. To illustrate the temperature field at all points of the contact zone, you can use the FEM based simulation method, for example, implemented in the COMSOL Multiphysics program.

To solve the problem using the “COMSOL Multiphysics”, the following sequence of actions may be used.

1. Selection of the dimension of the model. In the Model Wizard window, the following is selected: 3D, 2D Axisymmetric; 2D, 1D Axisymmetric; and 1D, 0D.
2. Selecting the physical section: Heat Transfer in Solids (should be chosen), Heat Transfer in Fluids, Diffusion, Fluid Dynamics, Structural Mechanics, Acoustics, etc.
3. Selection of a stationary (Stationary) or non-stationary (Time Dependent) process to be studied.
4. Creating the geometric object, for which FEM simulation will be performed. This object can be created using constructors embedded in COMSOL Multiphysics or special programs (for example, AutoCAD) and imported into COMSOL Multiphysics.
5. Set the thermo-physical properties of the material (thermal conductivity, material density, heat capacity at constant pressure).
6. Set the initial conditions (Initial Values).
7. Set the boundary conditions (Boundary conditions).
8. Divide the region into finite elements. By default, the COMSOL Multiphysics program builds a triangular grid in two-dimensional mode and a tetrahedral (triangular pyramid) grid in three-dimensional mode.
9. Chose a solver.
10. Visualize the results.

The equation of thermal conductivity in COMSOL Multiphysics window is as follows

$$\rho C_p \frac{\partial T}{\partial t} + \rho C_p \mathbf{u} \cdot \overline{\nabla T} + \overline{\nabla} \cdot \mathbf{q} = Q, \quad (4)$$

where  $\rho$  is the material density,  $\text{kg/m}^3$ ,  $C_p$  is the specific heat capacity,  $\text{J}/(\text{kg} \cdot ^\circ\text{C})$ ,  $\mathbf{u}$  is the velocity vector,  $\text{m/s}$ ,  $\overline{\nabla T}$  is the temperature gradient,  $^\circ\text{C}/\text{m}$ ,  $\mathbf{q}$  is the heat flux vector,  $\text{W}/\text{m}^2$ ,  $Q$  is the heat source power per unit volume,  $\text{W}/\text{m}^3$ .

The velocity vector can be written as

$$\mathbf{u} = u_x \mathbf{i} + u_y \mathbf{j} + u_z \mathbf{k}.$$

where  $u_x$ ,  $u_y$ ,  $u_z$  are components of the velocity vector in the thermal conductivity medium,  $\text{m/s}$ ;  $\mathbf{i}$ ,  $\mathbf{j}$ ,  $\mathbf{k}$  are single vectors or orts in the Cartesian coordinate system.

The temperature gradient  $\overline{\nabla T}$  or  $\overline{\text{grad} T}$  is a vector that is directed normal to an isothermal surface in the direction of temperature increase and is numerically equal to a temperature change per unit length, i.e.

$$\overline{\text{grad} T} = \mathbf{n} \frac{\partial T}{\partial n} \quad \text{or} \quad \overline{\nabla T} = \mathbf{n} \frac{\partial T}{\partial n},$$

where  $\mathbf{n}$  is the normal unit vector;  $\overline{\nabla}$  is the vector differential operator, i.e. a symbolic vector that replaces the gradient symbol  $T$ .

In the Cartesian coordinate system, the  $\overline{\nabla}T$  gradient vector of the function  $T$  denoted by as the following vector

$$\overline{\nabla}T = \frac{\partial T}{\partial x} \cdot \mathbf{i} + \frac{\partial T}{\partial y} \cdot \mathbf{j} + \frac{\partial T}{\partial z} \cdot \mathbf{k}.$$

Since  $\mathbf{n} = \mathbf{i} + \mathbf{j} + \mathbf{k}$  then

$$\frac{\partial T}{\partial n} = \frac{\partial T}{\partial x} \cdot \mathbf{i} + \frac{\partial T}{\partial y} \cdot \mathbf{j} + \frac{\partial T}{\partial z} \cdot \mathbf{k} \quad (5)$$

The scalar product of two vectors  $\mathbf{u}$  and  $\overline{\nabla}T$  can be written as

$$\mathbf{u} \cdot \overline{\nabla}T = u_x \frac{\partial T}{\partial x} + u_y \frac{\partial T}{\partial y} + u_z \frac{\partial T}{\partial z}, \quad (6)$$

where  $u_x, u_y, u_z$  are the  $\mathbf{u}$  vector projections on the corresponding coordinate axes  $x, y, z$ .

The vector of the heat flux

$$\mathbf{q} = -\lambda \overline{\nabla}T.$$

The scalar product of two vectors  $\overline{\nabla}$  and  $\mathbf{q}$

$$\overline{\nabla} \cdot \mathbf{q} = -\lambda \left( \frac{\partial^2 T}{\partial x^2} + \frac{\partial^2 T}{\partial y^2} + \frac{\partial^2 T}{\partial z^2} \right). \quad (7)$$

The vector-scalar transformations carried out above explain the close agreement between the analytical model and FEM simulation. The more simple the geometric shape of the profile being ground is, the closer the results of determining the temperature during analytical modeling and FEM simulation will be. In other words, during the FEM simulation at each point of the profile, the usual analytical model operates, and the FEM simulation takes into account the “interaction” (mutual influence) of these “instantaneous” analytical models, i.e., takes into account the vector nature of heat fluxes and temperature gradient. During FEM simulation, any value of the heat flux can be set (and this will be taken into account) at each point on the grinding zone surface. In contrast, in the analytical model, the heat flux is either constant or equal to some average value.

In the case under consideration, all derivatives with respect to the coordinate  $z$  are equal to zero. Thus, the use of the vector form for describing the temperature field in “COMSOL Multiphysics” allows us to solve the problem of determining the temperature considering the influence of the geometric shape of the surface being ground.



### 4 Results

The influence of the curvature of the grinding surface on the grinding temperature is revealed in Fig. 1 mentioned above. For example, it was found that when the radius of curvature of the abrasive surface is more than 6 mm when grinding steels, the influence of the curvature on the grinding temperature could be neglected.

To establish an agreement of the analytic model and FEM simulation in the COMSOL Multiphysics program, we will formulate the following problem. It is necessary to determine the maximum grinding temperature  $T_{MAX}$  on the surface ( $x = 0$ ) with the following initial data:  $\lambda = 30 \text{ W/(m} \cdot \text{ }^\circ\text{C)}$ ;  $a = 8.4 \cdot 10^{-6} \text{ m}^2/\text{c}$ ;  $c = 455 \text{ J/(kg} \cdot \text{ }^\circ\text{C)}$ ;  $\rho = 7850 \text{ kg/m}^3$ ;  $q = 40 \cdot 10^6 \text{ W/m}^2$ ,  $\tau = 0.1 \text{ s}$ ;  $1 \leq R \leq 6 \text{ mm}$ .

In the COMSOL Multiphysics program, a geometric model (Fig. 2, left) with different circumference radii is created, and temperature distribution is obtained (Fig. 2, right).

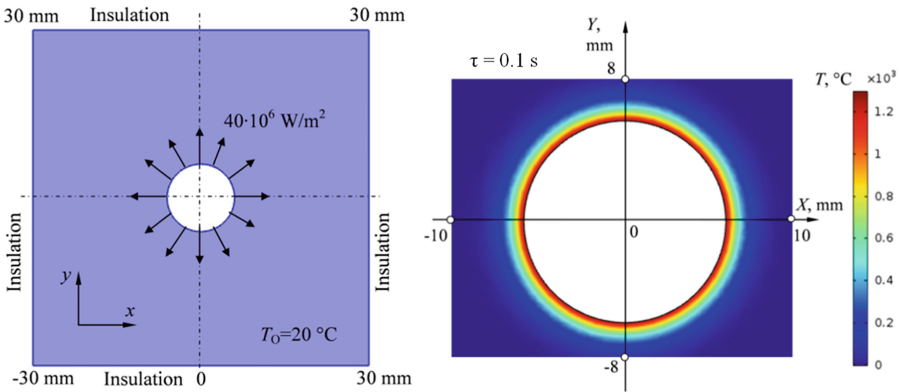


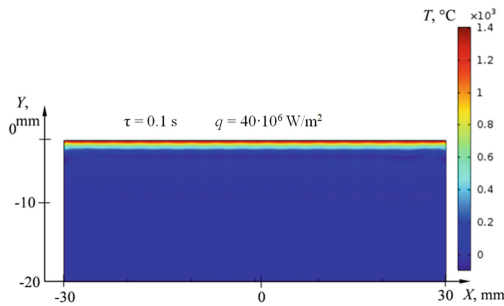
**Fig. 2.** 2D Model geometry with boundary conditions (left) and temperature distribution (right) for internal cylinder surface.

The maximum temperatures found by the two methods (Table 1) are close. The difference between them (i.e., analytical approach and FEM simulation) is no more than 0.4%. The maximum temperature found by Eq. (2) for a semi-limiting thermal source is 1379 °C, and that using FEM simulation is 1404 °C (Fig. 3). The difference here will be 2%.

Thus, in “COMSOL Multiphysics”, the temperature field is obtained based on the solution of the differential heat equation in the partial derivatives. The number of these equations is determined by the number of sections, of which the contact zone is composed. Within each section, the required initial and boundary conditions operate, and these conditions change discretely when moving from one section to another. Thus, it is possible to take into account the variable heat flux within the contact zone under boundary conditions of the second kind, the instantaneous curvature of the profile to be ground, etc.

**Table 1.** Comparison of the analytically and FEM calculated maximal surface temperatures.

$R$ , mm	$T_1$ , °C by analytical model	$T_2$ , °C by FEM solution	Difference $\delta$ , %
1	1003	1004	0.1
2	1155	1157	0.17
3	1219	1221	0.16
4	1254	1257	0.24
5	1277	1281	0.31
6	1293	1298	0.39

**Fig. 3.** Temperature distribution on depth obtained for the flat surface.

## 5 Conclusions

1. The grinding temperature is one of the factors limiting the performance of the profile grinding operation; therefore, the temperature information can use to optimize the grinding parameters during the production, as well as production preparation stages.
2. The grinding temperature is conventionally determined either theoretically or experimentally, based on the mathematical models of the temperature field and using the sensors for direct and indirect measurements, respectively. In the paper, another method is considered and investigated, which consists in geometric modeling (creating a model) and FEM simulation (observing and studying the temperature field using the established geometric model and vector form of the Fourier law of thermal conductivity). The physical essence of temperature modeling and simulation has been revealed; it consists in using a vector model of the temperature field and naturally (as it is) takes into account the geometric shape of the surface to be ground.
3. The difference between the estimates of the temperature field by the analytical scalar and simulation vector models of the temperature field is established. On the example of semicircular profile grinding, this difference (for maximum surface temperatures) does not exceed 0.5% for the conditions under consideration.
4. The influence of the grinding surface curvature on the grinding temperature is revealed. For example, it was found that when the grinding surface curvature radius

is more than 6 mm, and when grinding workpiece of steel, the influence of the curvature on the grinding temperature could be neglected.

5. The study made it possible to justify the conditions under which there is the opportunity of using an analytical model to determine the profile grinding temperature using the computer subsystems for grinding operation monitoring and diagnosing on modern CNC grinding machines. Namely, the proposed analytical model with a linear profile (as opposed to a semicircular profile) can be used to determine the maximum temperature of profile grinding, if two conditions are met. The first is the Peclet number, which is more than 5. The second is the profile curvature radius, which is more than 6 mm in profile grinding the steel workpiece. Other conditions and recommendations, not listed here, can be similarly established based on the data presented in the paper.






## References

1. Larshin, V., Lishchenko, N.: Gear grinding system adapting to higher CNC grinder throughput. *MATEC Web Conf.* **226**, 04033 (2018)
2. Larshin, V., Lishchenko, N.: Adaptive profile gear grinding boosts productivity of this operation on the CNC machine tools. In: Ivanov, V., et al. (eds.) *CONFERENCE 2019, LNME*, pp. 79–88. Springer, Cham (2019)
3. Deivanathan, R., Vijayaraghavan, L.: Theoretical analysis of thermal profile and heat transfer in grinding. *Int. J. Mech. Mater. Eng. (IJMME)* **8**(1), 21–31 (2013)
4. Tan, J., Jun, Y., Siwei, P.: Determination of burn thresholds of precision gears in form grinding based on complex thermal modelling and Barkhausen noise measurements. *Int. J. Adv. Manuf. Technol.* **88**(1–4), 789–800 (2017)
5. Jun, Y., Ping, L.: Temperature distributions in form grinding of involute gears. *Int. J. Adv. Manuf. Technol.* **88**(9–12), 2609–2620 (2017)
6. González-Santander, J.L.: Maximum temperature in dry surface grinding for high Peclet number and arbitrary heat flux profile. *Hindawi Publishing Corporation Mathematical Problems in Engineering*, pp. 1–9 (2016)
7. Foeckerer, T., Zaeh, M., Zhang, O.: A three-dimensional analytical model to predict the thermo-metallurgical effects within the surface layer during grinding and grind-hardening. *Int. J. Heat Mass Transf.* **56**, 223–237 (2013)
8. Lishchenko, N., Larshin, V.: Comparison of measured surface layer quality parameters with simulated results. *Appl. Aspects Inf. Technol.* **2**(4), 304–316 (2019)
9. Zhang, L.: Numerical analysis and experimental investigation of energy partition and heat transfer in grinding. In: Salim Newaz Kazi, M. (eds.) *Heat Transfer Phenomena and Applications*, Sense Publishers, Rotterdam, The Netherlands (2012)
10. Tahvilian, A.M., Champlaud, H., Liu, Z., Hazel, B.: Study of workpiece temperature distribution in the contact zone during robotic grinding process using finite element analysis. In: *8th CIRP Conference on Intelligent Computation in Manufacturing Engineering*, Ischia, Italy, pp. 205–210 (2013)
11. Li Hao, N., Axinte, D.: On a stochastically grain-discretised model for 2D/3D temperature mapping prediction in grinding. *Int. J. Mach. Tools Manuf* **116**, 1–27 (2017)
12. Jermolajev, S., Epp, J., Heinzl, C., Brinksmeier, E.: Material modifications caused by thermal and mechanical load during grinding. In: *3rd CIRP Conference on Surface Integrity (CIRP CSI)* (2016). *Procedia CIRP* **45**, 43–46

13. Jermolajev, S., Brinksmeier, E., Heinzl, C.: Surface layer modification charts for gear grinding. *CIRP Ann. Manuf. Technol.* **67**(1), 333–336 (2018)
14. Heinzl, C., Sölter, J., Jermolajev, S., Kolkwitz, B., Brinksmeier, E.: A versatile method to determine thermal limits in grinding. In: 2nd CIRP Conference on Surface Integrity (CSI) (2014). *Procedia CIRP*, vol. 13, pp. 131–136
15. Vrkoslavová, L., Louda, P., Malec, J.: Analysis of surface integrity of grinded gears using Barkhausen noise analysis and X-ray diffraction. In: 40th Annual Review of Progress in Quantitative Nondestructive Evaluation APP Conference Proceedings, vol. 1581, pp. 1280–1281 (2014)
16. Crow, J.R., Michael, A.: Pershing standard samples for grinder burn etch testing. *Gear Technology*, pp. 54–56 (2018)
17. Zaborowski, T., Ochendusko, R.: Grinding burns in the technological surface of the gear teeth of the cylindrical gears. *MECHANIK NR 90*, 880–884 (2017)
18. de Lima, A., Gâmbaro, L.S., Junior, M.V., Baptista, E.B.: The use of cylindrical grinding to produce a martensitic structure on the surface of 4340 steel. *J. Braz. Soc. Mech. Sci. Eng.* **33**, 34–40 (2011)
19. Rena, X., Hu, H.: Analysis on the temperature field of gear form grinding. *Appl. Mech. Mater.* **633–634**, 809–812 (2014)
20. Beizhi, L., Dahu, Z., Zhenxin, Z., Qiang, Z., Yichu, Y.: Research on workpiece surface temperature and surface quality in high-speed cylindrical grinding and its inspiration. *Adv. Mater. Res.* **325**, 19–27 (2011)
21. Lishchenko, N., Larshin, V.: Gear-grinding temperature modeling and simulation. In: Radionov, A., et al. (eds.) *Proceedings of the 5th International Conference on Industrial Engineering (ICIE 2019)*, vol. 2, pp. 289–297. Springer (2019)
22. Yadav, R.K.: Analysis of grinding process by the use of finite element methods. *ELK Asia Pacific J. Manuf. Sci. Eng.* **1**(1), 35–42 (2014)
23. Linke, B., Duscha, M., Vu, A.T., Klocke, F.: FEM-based simulation of temperature in speed stroke grinding with 3D transient moving heat sources. *Adv. Mater. Res.* **223**, 733–742 (2011)
24. Sharma, C., Ghosh, S., Talukdar, P.: Finite element analysis of workpiece temperature during surface grinding of inconel 718 alloy. In: 5th International & 26th All India Manufacturing Technology, Design and Research Conference, IIT Guwahati, Assam, India, pp. 420-1–420-6 (2014)
25. Patil, P., Patil, C.: FEM simulation and analysis of temperature field of environmental friendly MQL grinding. In: *Proceedings of the International Conference on Communication and Signal Processing 2016 (ICCASP 2016)*, pp. 182–186 (2017)
26. Lishchenko, N., Larshin, V.: Temperature models for grinding system state monitoring. *Appl. Aspects Inf. Technol.* **2**(3), 216–229 (2019)
27. Chen, X., Öpöz, T.: Effect of different parameters on grinding efficiency and its monitoring by acoustic emission. *Prod. Manuf. Res. Open Access J.* **4**(1), 190–208 (2016)
28. Carslaw, H.S., Jaeger, J.C.: *Conduction of Heat in Solids*, 2nd edn. Oxford University Press, Oxford (1959)



# Influence of the Thread Profile Accuracy on Contact Pressure in Oil and Gas Pipes Connectors

Oleh Onysko<sup>(✉)</sup> , Volodymyr Kopei , Iuliia Medvid ,  
Lolita Pituley , and Tetiana Lukan 

Ivano-Frankivsk National Technical University of Oil and Gas,  
15, Karpats'ka St., Ivano-Frankivsk 76019, Ukraine  
o.onysko@nung.edu.ua

**Abstract.** Pipeline connectors of the oil and gas assortment must ensure good screwing and durability during it. These operating requirements depend to a large extent on the contact pressure between the thread surfaces of the pin and the box at the start of screwing and in the fully screwed state. The paper presents the study of the dependence of the contact pressure between the threads of the box and the pin, depending on the accuracy of the profile of the threads. The contact pressures at the time of insertion of the pin into the box are investigated based on theoretical assumptions about the effect of the weight of the drill pipe stand on the example of the tool joint 2 7/8 Reg. Based on the finite element method for the 114 mm diameter tubing connector, the contact pressure inside the connector, depending on the accuracy of the thread profile is investigated. Studies show that at the time of insertion of the pin into the drill pipe box, the pressure changes by almost 10% depending on the upper and lower limit of the thread profile deviations. In a finally screwed state, the contact pressure increases twice if the pin thread profile is made on upper limit deviation, and at the box, the thread profile is made as nominal.

**Keywords:** Threading tool-joint · Tapered thread · Finite element model · Process of screwing · Pin and box

## 1 Introduction

Tapered thread is used for connecting pipes of the oil and gas assortment as a whole, and in particular for connecting of drill pipes as well as oil well tubing. The quality of these joints is determined by the following characteristics: tightness and mechanical durability. The mechanical durability depends mainly on the contact pressures that occur between the thread surfaces of the two connection pieces - the pin and the box. The pressure increase leads to the improvement of the friction force between the thread surfaces. This leads to the loss of the initial shape of the thread profile and as a consequence, on the reduced functionality of the connection, i.e. the decrease of mechanical durability and tightness of the tool joint. So, reducing contact pressures in the process of screwing in oil and gas pipes is a very actual issue. Therefore, in the opinion of the authors, the influence of the precision of the profile manufacturing on the

size of the contact pressures at the moment of start and final screwing of the pin in the box should be investigated.

## 2 Literature Review

The contact pressure between the drill string tool joint thread surfaces of the box and the pin is investigated at the theoretical level in work [1]. In this paper, the value of contact pressure is determined for two fundamentally different periods of the joint screw process. The first period is just when the pin is installed into the box, and the second period when there is a process of finally screwing the pin into the box.

In [2] thorough analytical studies of the contact pressure between the groove surfaces at the time of clamp are carried out. However, the authors do not consider contact pressures during the screwing process. The work [4] also contains an in-depth analytical exploration of the contact pressures, but it applies only to cylindrical thread. Paper [5] is concerned with studies of contact pressures in the tapered thread, but their change in the screwing process is not considered. The article [6] contains a study in general of contact pressures in thread joints without relation to the tapered thread connections of the pipe oil and gas assortment. The work [7] is related to relationships of the oil and gas profile, but the dependence of the thread parameters on the geometrical parameters of the cutter is investigated without studying the effect of received profile accuracy on the contact pressure. In [8], a study of the influence of contact pressures on the operational efficiency of a pipe connection is shown. In [9], the accuracy of contact pressures in premium joints is investigated using ultrasound, but not concerning their dependence on the profile of the thread. In [10], on the basis of the analytical solution of the contact problem for a three-component body, the conditions for the compatibility of deformations from the fatigue and the conical connection of the “nipple and coupling” is studied. Design [11, 12], technological [13], and operating methods [14, 15] are used to improve the operability of drilling equipment and tools. Features of contact interaction of shells with aggregate taking into account Poisson effect are considered in articles [16, 17]. The analysis of friction contact of individual elements of oil and gas equipment under conditions of the cyclic heat load is carried out in the article [18]. In [19, 20], the authors investigate the contact pressures but only depending on the geometrical parameters of the cutter.

## 3 Research Methodology

Figure 1 shows the scheme of the moment of setting the pin into the box (the pin is highlighted in dark gray), but the contact is not on their crests but on their longer flanks. For a better illustration of this moment, the diagram shows the points  $A$  and  $F$  located on a line parallel to the axis of the thread 1. This line is the direction in which the pin is set down into the box along. Unlike the variant of contact, I (see Fig. 1), in this case, point  $B$  on the crest of the pin corresponds to the point  $F$ , that is, the crest of the pin moved down past the crest of the box and touch to the flank of the box 5. This corresponds to the initial distance  $X_0$  between the crests of the pin and the box.

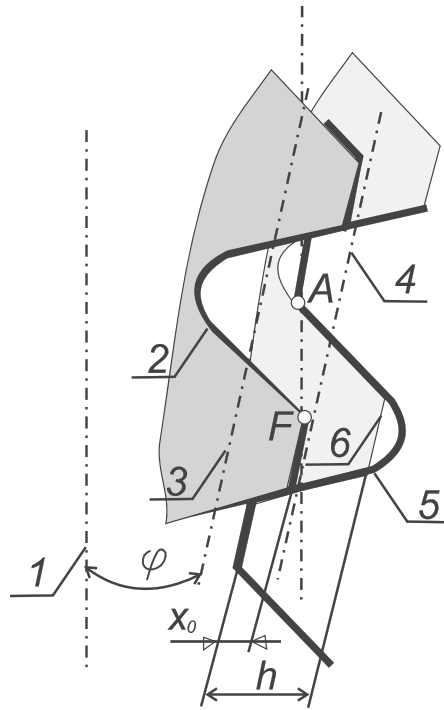


**Fig. 1.** Scheme of the moment of installing pin into the box by use the surface of the thread flanks. Numbers mean: 1– axis of the tapered thread joint, 2 – profile of the pin thread, 3 – pitch diameter of the pin thread, 4 – pitch diameter of the box thread, 5 – profile of the box thread, 6 – profile of the box thread at the moment of the full screwing.

Formula 1 in accordance to [1] describes the area of contact between the flank of the pin and the box at the moment of the installation of the pin into the box (see Fig. 3):

$$F_c = \frac{\pi(P - 2a)}{4P \cos \alpha} \left[ \left( d_1 - 2h + K \left( 1 - \frac{K}{2} \operatorname{tg} \alpha \right) (P - 2a) \right)^2 - (d_1 - KL)^2 \right], \text{ (mm}^2\text{)}, \quad (1)$$

The screw-in process begins immediately after the moment the pin is installed into the box and ends when the pitch diameter of the pin coincides with the pitch diameter of the box, and the crest of the pin moves to the value of  $(h - X_0)$ . This position of the pin is shown in light gray and is indicated in Fig. 3.

Formula 2, according to the data [1] shows the functional dependence of the area of the mutual contact of the thread's surface of the pin and the box in the process of screwing them. This screwing has a certain number of revolutions  $m$ . So distance  $X$  depends on the number of revolution  $m$ .

$$F_k = \frac{\pi m}{4 \cos \alpha} \left[ (d_1 - 2h + KP_1 \cdot m)^2 - (d_1 - KL)^2 \right], \text{ (mm}^2\text{)} \quad (2)$$

where  $Fk$  – the area of mutual contact between the pin and the box in the process of screwing them on the value of  $X$ , corresponding to a certain number of revolutions of the pin  $m$ ;

$h$  – thread height truncated (mm);

$d_l$  – the largest outer diameter of the pin thread on the large base of the taper;

$P_l$  – the pitch is defined between the larger flanks

$K = 2tg\varphi$  – taper of thread.

$L$  – the length of the tapered thread.

According to standard API 7 the length of the tapered thread of the pin is determined by the equation:

$$L = l_n - 12,7, (\text{mm}^2)$$

where  $l_n$  – the length of the tapered part of the pin.

## 4 Results

According to the same scheme, the pressure  $p_c$  from the weight of the drill string stand is transmitted to the side of the flank and corresponds to the moment of installation of the pin into the box, according to Fig. 1. This pressure can be calculated by the formula:

$$p_c = \frac{M \cdot 10^4 \cos\alpha}{F_c}, (\text{MPa})$$

where  $F_c$  – area  $\text{mm}^2$ , which is calculated by the formula 4;

$\alpha$  –profile angle.

For analytical research, one of the tool joint tapered thread, namely 2 7/8 Reg. The weight of the drill string stand is 256 kg.

The magnitudes of the contact pressures with full screwing ( $m = 3.86$ ) are shown in column 4, and when fitted by the sides - in column 5 (a reference to Table 1).

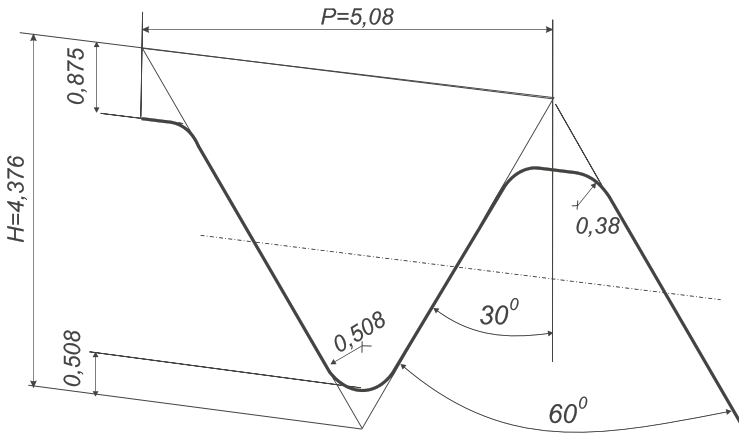
Judging from the value of column 4, there is no significant effect of the profile angle on the value of the contact pressure between the threads of the pin and the box if fully screwed. However, column 5 indicates a certain effect of the deviation of the profile angle (according to the standard  $\pm 0.5^\circ$ ), the contact pressure is varied from 2.28 to 2.31, which in the absolute measure is 0.03 mm, and relative measure is defined as 1.3%, which also indicates a slight influence of the accuracy of profile angle execution on the change in the value of contact pressure at the time of mounting the pin in the box. But this study was conducted without taking into attention the difference in accuracy of the profile of the pin and box.

Figure 2 presents a schematic diagram of a tapered thread in accordance with Form I, which is named by 2 7/8 Reg.



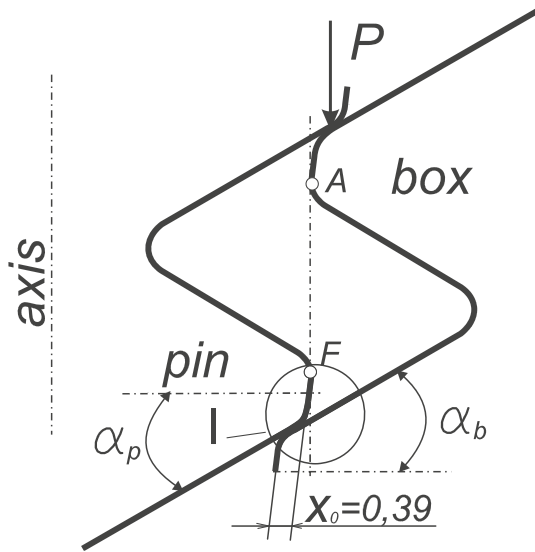
**Table 1.** Results of theoretical studies of contact pressure between the tapered thread surfaces of the tool joint 2 3/8 Reg at the time of the installation of the pin into the box and in the finally screwing. Load 256 kg.

№	Contact area, mm <sup>2</sup>		Contact pressure, MPa		Thread profile $\alpha$ , °
	$F_k$	$F_c$	Finally screwing $p_k$	Between flanks $p_c$	
1	2	3	4	5	6
1	8209	968,49	0,27	2,29	30
2	8216	969,45	0,27	2,28	30,1
3	8224	970,42	0,27	2,28	30,2
4	8232	971,39	0,27	2,28	30,3
5	8179	972,36	0,27	2,29	30,4
6	8187	973,34	0,27	2,29	30,5
7	8172	963,76	0,27	2,31	29,5
8	8179	964,69	0,27	2,31	29,6
9	8187	965,63	0,27	2,30	29,7
10	8194	966,58	0,27	2,30	29,8
11	8203	967,53	0,27	2,29	29,9



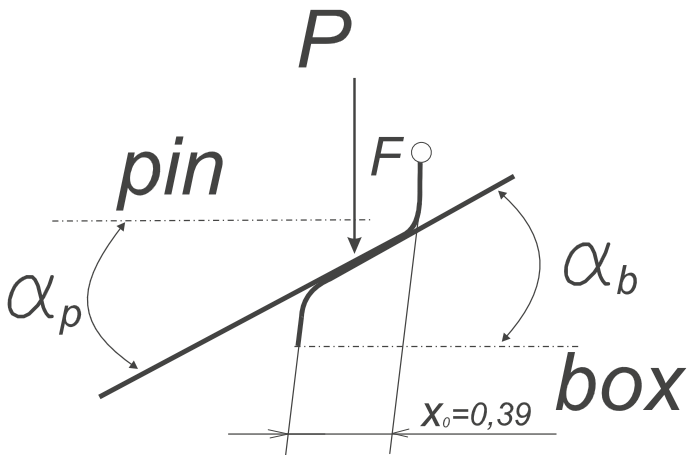
**Fig. 2.** The scheme of the tapered thread in form I according to the API standard: P - pitch, H - the height of the output triangle cut. I screwing.

Based on the sizes shown in Fig. 2, as well as using the diagram of mounting the nipple in the sleeve of Fig. 1, the size of X0 is determined graphically. Figure 3 shows the mounting of the nipple in the coupling along the AF line, which is parallel to the cut axis. The value of X0 is equal to 0,39 mm. This study was conducted without taking into account the difference in the accuracy of the profile of the pin and box.



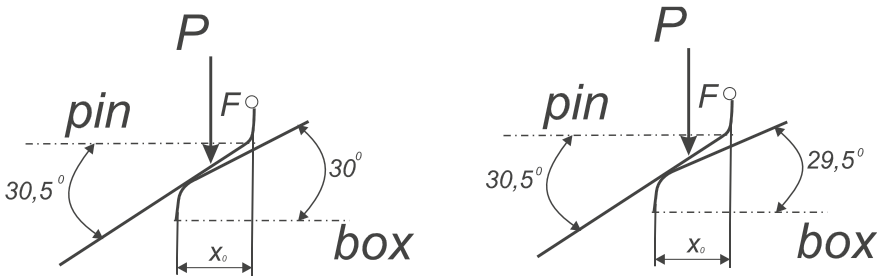
**Fig. 3.** Schematic diagram of the determination of the contract value  $X_0$  of the box and the pin at the time of its installation.

Figure 4 is a view of Fig. 3 for more detailed consideration (see sign I on Fig. 3).



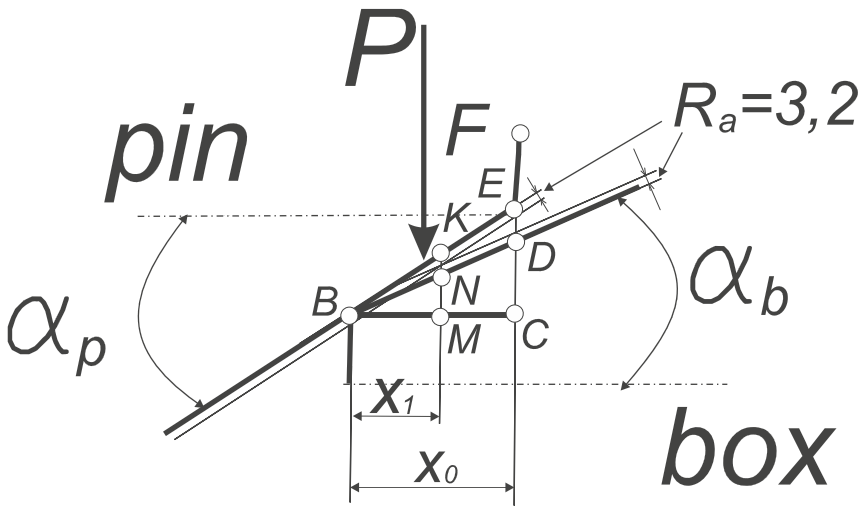
**Fig. 4.** Schematic diagram of the determination of the contract value  $X_0$  of the box and the pin at the time of its installation.

Figure 5 shows a diagram of the installation of the pin in the box considering deviations from the nominal value of the profile angle of their thread.



**Fig. 5.** Scheme of installation of the pin in the box, taking into account the deviations from the nominal value of the profile angle: Left: The profile of the pin thread is made according to the upper limit. Right: The profile of the pin thread is made according to the upper limit, and the box thread profile is made according to the lower limit.

In Fig. 6, the scheme in Fig. 5 is complemented by the effect of roughness. According to ARI 7, it is  $R_a$  3.2.  $X_1$  - corresponds to the length of contact of the cut surfaces, taking into account the roughness.



**Fig. 6.** Scheme of installation of the pin into the box considering deviations from the nominal value of the profile angle and roughness of thread.

From Scheme 6, provided that  $KN = 2 * Ra = 6,4$  after certain trigonometric transformations we get  $x_1 = 0.91x_0$ .

Therefore, the contact area of the nipple and coupling  $Fc' = 0.91Fc$ . Accordingly, the contact pressure  $Pc' = pc/0.91$ , which means increasing by 9%. So the full increase is more than 10%.

Consider axisymmetric finite element models of drilling tool joints ZN-80 GOST 5286 with Z-66 GOST 28487 threads (2 3/8 REG API Spec. 7 equivalents). The joint

make-up was simulated by axial deformation 0.2 mm of the box shoulder. The external axial tensile load is 1.0 MN. Also, consider models of the threaded connection of non-upset tubing with outside diameter 114 mm according to GOST 633-80 (4-1/2 non-upset tubing coupling API Spec. 5CT equivalents). A connection with hand-tight make-up (with a standoff value 6.5 mm) is considered as the most serious case for connection leak tightness. At the upper end of the pin acts a constant pressure - 155 MPa, which simulates the external tensile load. These threads have a nominal profile of the thread in the coupling ( $\alpha = 30^\circ$ ) and modified profile of the thread in the pin ( $\alpha = 30.5^\circ$ ). Material plasticity and friction are simulated. It is noticeable that the differences in the profile angles cause increasing of the contact pressure  $P_c$  on the root of the pin profile and on the crest of the coupling profile (Fig. 7). The contact pressure values  $P_c$  on the loaded side of the thread profile in the area of the minor diameter increased by 2–5 times. This is especially true for the middle part of the thread - turns from 4 to 8. However, in the area of the major diameter, their values are zero. This creates the conditions for the penetration of liquid.

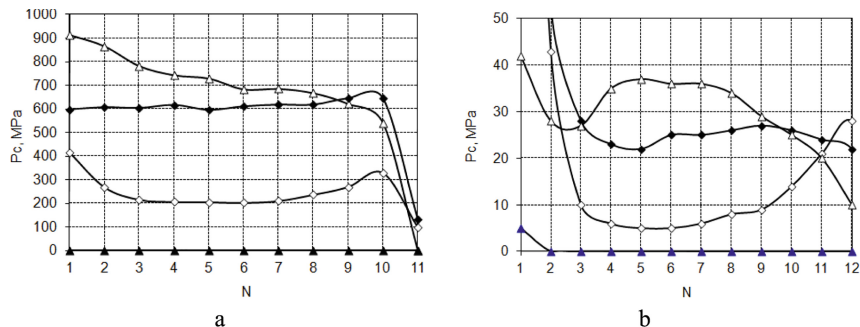


**Fig. 7.** The contact pressure  $P_c$  on the loaded profile side of the  $N$  thread of the pin in the area of the minor ( $\diamond, \blacklozenge$ ) and major ( $\square, \blacktriangle$ ) diameters:  $\square, \triangle, \circ$  -  $\alpha = 30.0^\circ$ ;  $\blacksquare, \blacktriangle, \blacklozenge$  -  $\alpha = 30.5^\circ$ ; a - drilling tool joints ZN-80; b - connection of non-upset tubing 114 mm.

### 5 Conclusions

1. The contact pressure between the drill string tapered thread surfaces at the time of insertion of the pin into the box is dependent on the profile angle of the thread within its standard tolerance of  $\pm 0.5^\circ$ , which means that the difference in contact pressure depending on the accuracy of the profile may be up to 10%.
2. The difference in the profile angles of the box and the pin of  $0.5^\circ$  or more is the cause of a significant increase in contact pressures in the zone of the minor diameter of the pin thread and the appearance of gaps in the zone of the major diameter. The significant increase in contact pressure in local areas can cause plastic deformation and thread failure. Gaps create conditions for the penetration of liquid.

In the future, it is planned to do the same research of small diameter tapered thread.






## References

1. Onysko, O., Havryliv, Y., Kopey, V., Medvid, I., Vryukalo, V.: Theoretical studies of the contact pressure value between the surfaces of the pin and the box in the small diameter drill pipes connectors. In: Ziobro, J. (ed.) CONFERENCE 2019, Napędy pojazdów. Modelowanie komputerowe konstrukcji i układów technologicznych, pp. 202–210. Wydawnictwo Uniwersytetu Rzeszowskiego, Rzeszów (2019)
2. Xu, H., Shi, T., Zhang, Z., Shi, B.: Loading and contact stress analysis on the thread teeth in tubing and casing premium threaded connection. *Math. Probl. Eng.* <http://www.hindawi.com/journals/mpe/2014/287076/>. Accessed 03 Jan 2020
3. Wang, W., Marshek, K.: Determination of the load distribution in a threaded connector having dissimilar materials and varying thread stiffness. *J. Eng. Ind.* **1**(117), 1–8 (1995)
4. Chen, S., An, Q., Zhang, Y., Gao, L., Li, Q.: Loading analysis on the thread teeth in cylindrical pipe thread connection. *J. Pressure Vessel Technol.* **3**(132), 0312021–0312028 (2010)
5. Baragetti, S.: Effects of taper variation on conical threaded connections load distribution. *J. Mech. Des.* **2**(124), 320–329 (2002)
6. Sugino, M., Nakamura, M., Yamaguchi, S., Daly, D., Briquet, G., Verger, E.: Development of an innovative high-performance premium threaded connection for OCTG. In: Proceedings of the 10th Offshore Technology Conference (OTC 2010), Houston, USA, pp. 1883–1891 (2010)
7. Wang, J., Mathew, P., Li, X., Huang, C., Zhu, H.: Experimental study on cutting characteristics for buttress thread turning of 13%Cr stainless steel. In: *Key Engineering Materials. Advances in Materials Processing IX*, vol. 443, pp. 262–267 (2010)
8. Luo, S., Wu, S.: Effect of stress distribution on the tool joint failure of internal and external upset drill pipes. *Mater. Des.* **52**, 308–314 (2013)
9. Hamilton, K., Wagg, B., Roth, T.: Using ultrasonic techniques to accurately examine seal surface contact stress in premium connections. In: Proceedings of the SPE Annual Technical Conference and Exhibition, ATCE 2007, Anaheim, CA, USA, vol. 5, pp. 3461–3471 (2007)
10. Shats'kyi, I., Lyskanych, O., Kornuta, V.: Combined deformation conditions for fatigue damage indicator and well–drilling tool joint. *Strength Mater.* **48**, 469–472 (2016)
11. Levchuk, K., Moisyshyn, V., Tsydylo, I.: Influence of mechanical properties of a material on dynamics of the stuck drilling pipes. *Metallophys. Adv. Technol.* **38**(12), 1655–1668 (2016). [in Ukrainian]
12. Vlasiy, O., Mazurenko, V., Ropyak, L., Rogal, O.: Improving the aluminum drill pipes stability by optimizing the shape of protector thickening. *East-Eur. J. Enterp. Technol.* **1**(7(85)), 25–31 (2017)
13. Ropyak, L., Shuliar, I., Bohachenko, O.: Influence of technological parameters of centrifugal reinforcement upon quality indicators of parts. *East-Eur. J. Enterp. Technol.* **1**(5(79)), 53–62 (2016)
14. Moisyshyn, V., Levchuk, K.: The impact of vibration mechanism' zone installation on the process of retrieving stuck drill pipes. *Min. Min. Deposits* **10**(3), 65–76 (2016)
15. Skitsa, L., Yatsyshyn, T., Liakh, M., Sydorenko, O.: Ways to improve safety of pumping-circulatory system of a drilling rig. *Min. Min. Deposits* **12**(3), 71–79 (2018)
16. Bulbuk, O., Velychkovych, A., Mazurenko, V., Ropyak, L., Pryhorovska, T.: Analytical estimation of tooth strength, restored by direct or indirect restorations. *Eng. Solid Mech.* **7**(3), 193–204

17. Shatskyi, I., Popadyuk, I., Velychkovych, A.: Hysteretic properties of shell dampers. In: Awrejcewicz, J. (ed.) *Dynamical Systems in Applications. DSTA 2017. Springer Proceedings in Mathematics & Statistics*, vol. 249, pp. 343–350. Springer, Cham (2018)
18. Volchenko, N., Volchenko, A., Volchenko, D., Poliakov, P., Malyk, V., Zhuravliov, D., Vytvytskyi, V., Krasin, P.: Features of the estimation of the intensity of heat exchange in selfventilated disk–shoe brakes of vehicles. *East.-Eur. J. Enterp. Technol.* 1(5(97)), 47–53 (2019)
19. Kopei, V., Onysko, O., Panchuk, V.: The application of the uncorrected tool with a negative rake angle for tapered thread turning. In: Ivanov, V., et al. (eds.) *Advances in Design, Simulation and Manufacturing II. DSIME 2019. LNME*, pp. 149–158. Springer, Cham (2019)
20. Kopei, V., Onysko, O., Panchuk, V.: Computerized system based on FreeCAD for geometric simulation of the oil and gas equipment thread turning. In: *IOP Conference Series: Materials Science and Engineering*, vol. 477, p. 012032 (2019)



# Numerical Simulation of Local Plastic Deformations of a Cylindrical Workpiece of a Steel Wheel Rim

Yuliia Salenko<sup>1</sup> , Ruslan Puzyr<sup>2</sup> , Oleksandr Shevchenko<sup>1</sup> ,  
Viktoriia Kulynych<sup>1</sup> , and Oleksandr Pedun<sup>1</sup> 

<sup>1</sup> Kremenchuk Mykhailo Ostrohradskyy National University,  
20, Pershotravneva St., Kremenchuk 39600, Ukraine

<sup>2</sup> Kremenchuk Mykhailo Ostrohradskyy National University College,  
7, Chumatskyi Shliakh St., Kremenchuk 39621, Ukraine  
puzyruslan@gmail.com

**Abstract.** The presented studies of the process of radial-rotational profiling of the rims of the wheels of vehicles are aimed at studying the field of stress-strain. An attempt is made to simulate this dynamic process by a static finite element model. This statement of the problem justifies itself from the viewpoint of the physical nature of the method in a finite minimum time. The von Mises stress intensity during plastic deformation of a cylindrical workpiece by a pair of solid-state profile rollers is determined, and the distribution pattern of meridional stresses and displacements of the workpiece sections is shown. The results are compared with existing analytical models for profiling the wheel rim. Numerical modeling of the process of deformation of a cylindrical workpiece by a pair of rollers showed that opposite stresses act both in the tangential and in the meridional direction in the deformation zone. The magnitude and direction of the tangential stresses coincide with both modeling techniques. The distribution pattern of the meridional stresses acting in the deformation zone is contradictory. It is shown that the workpiece changes shape during loading. If some zones are stretched, then other zones are necessarily compressed, i.e. the shell is deformed along the entire peripheral surface. This circumstance allows us to assume the possibility of a directed influence on the deformation zone by applying additional forces to the free sections of the workpiece.

**Keywords:** Finite-element model · Shell · Meridional stresses

## 1 Introduction

The manufacture of wheel rims of vehicles from steel cylindrical workpieces is based on the methods of sheet stamping (drawing, crimping, distribution), rotary drawing and radial-rotational profiling [1–3]. The last method for the production of steel rims was most widely used since it has many advantages such as high productivity, the accuracy of the geometric dimensions of the products and minimal energy costs due to the local action of the tool on the workpiece. However, the competitiveness of wheel production depends on the degree of knowledge of this issue, which will predetermine the

possibilities of a directed influence on the quality and cost of products. It also makes possible to scientifically substantiate and identify individual technological parameters or their combination, which have the most significant impact on the course of the profiling process and semi-finished [4, 5].

## 2 Literature Review

World trends to improve radial-rotational profiling technologies focus on obtaining rims of the minimum thickness difference to reduce metal consumption and increase the operational characteristics of the wheels [6, 7]. Therefore, the data found in scientific journals indicate an increasing interest in determining the laws of the process of radial-rotational profiling from a theoretical point of view. An explanation of the established opinions about this process from the standpoint of the shells of rotation theory and, as a result, the identification of new patterns of the method will give a powerful impetus to the application of theoretical results in practice in the form of creating new schemes and methods of profiling.

Therefore, the greatest attention is for determining the stress-strain state in the deformation zone. Moreover, many authors consider the equilibrium of the workpiece element with axial symmetry and the joint solution of simplified equations with plasticity conditions by the engineering method [8–11]. However, this approach is not approved in the technical theory of shells and does not allow revealing all the features of their plastic deformation. Great emphasis is placed on modeling the profiling process by numerical methods, where not only deformation of a complex spatial body can be taken into account, but also metal hardening, a local type of loading, the anisotropy of the workpiece material, etc. [12–17]. Sometimes modeling a sheet blank instead of a cylindrical one leads to incorrect results from the physical side of the phenomena occurring in the center of plastic deformation and beyond [17]. Much attention is also paid to experimental methods for studying the stress field with the local application of forces to the shell or plate [18–22]. However, in this case, the obtained results relate to certain, specific conditions of shaping and it is not possible to extend them to the entire range of produced rims.

Therefore, the goal of this study was the finite element modeling the local deformation of a cylindrical workpiece by a pair of profiling rollers in static mode and comparing the results with existing analytical solutions. As well as determining the deformation of peripheral zones, which is not described in the considered studies.

## 3 Research Methodology

It was studied the distribution of the stress-strain field during the static introduction of profiling rollers into a cylindrical workpiece. This statement of the problem is close to the first transition of radial-rotational profiling. Firstly, the tool and the workpiece do not rotate, secondly, the cylinder is modeled as a workpiece, and thirdly, the initial and acquired metal anisotropy is not taken into account. However, if we imagine the mutual rotational movement of the tool and the workpiece in the instantaneous period, i.e.



when time tends to zero, we get a picture of the introduction of stopped rollers in the shell. This makes it possible to study the distribution of the stress-strain tensor on every small segment of the semi-finished product generatrix and to extend the results to the workpiece as a whole during rotation of the tool. An important advantage of such coverage of the issue is that many analytical models of the radial-rotational profiling process do not take into account the rotation of the tool, the complex semi-finished product profile and anisotropy, which means that there is a possibility to compare the results of both methods.

The finite element modeling of the process was carried out in a special complex of solid modeling Simulia Abaqus – student edition, which is provided by an engineering company «TESIS». The workpiece was set using the finite elements system with a hexahedral shape. The method of its construction was extrusion, element type C3D8R with linear order from the standard library from the category 3D Stress. The dimensions of the workpiece and tool were assigned based on the data of the PJSC “Kremenchuk Wheel Plant” for the size of the wheel rim W12–24 (Fig. 1a). The workpiece had such dimensions: the diameter of the cylinder – 568 mm; height – 380 mm; wall thickness – 4.5 mm. The upper and lower rollers had the following geometric characteristics: upper - shelf zone diameter – 500 mm; stream zone diameter – 564 mm; shelf zone length – 95 mm; stream zone lengths – 95 mm; lower - shelf zone diameter – 564 mm; stream zone diameter – 450 mm; shelf zone length – 90 mm; stream zone length – 95 mm. The radii of the mating zones of the shelves with the zones of the walls and walls with the mounting stream for the upper and lower roller were the same and amounted to 5 mm. The rollers were modeled by standard elements from the discharge of solid-state quadrangular, and their grid was generated in a freeway. The element type was R3D4. Figure 1b shows the model assembly with a generated finite element mesh.

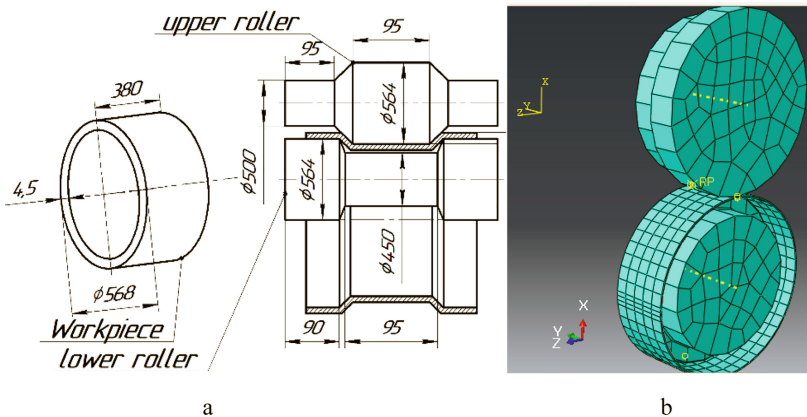


**Fig. 1.** Workpiece and tool dimensions (a) and the mesh of finite elements on the assembly in the model of deformation of a cylindrical workpiece with two rollers (b).

The material of the cylindrical workpiece is isotropic with the following mechanical characteristics: density – 7800 kg/m<sup>3</sup>; elastic modulus – 210 GPa; Poisson’s ratio – 0,28; tensile strength – 320 MPa; yield strength – 230 MPa [23, 24]. The true stress diagram was approximated by the dependence  $\sigma_{0.2} = 230 + 3.46\epsilon^{0.6}$  [25, 26]. The model was assembled with the assignment of reference points on the tool since it was a nondeformable solid with axial symmetry in the form of a shell. The workpiece was a deformable solid in a three-dimensional setting. The type of interaction between the inner and outer cylindrical surfaces of the workpiece and the rollers was specified as contact with the final formulation of the slip and mechanical constraints in the form of a slip with a friction coefficient 0.15 [3–33] and normal components [27, 28]. The workpiece was secured against rotation around its axis; no restrictions were imposed on the remaining degrees of freedom. The lower roller at the initial step was set to be completely limited from displacements and rotations, and the upper roller at the reference point had a displacement of 4.5 mm, which corresponded to one loading step. The value of the specified movement was selected according to the technological process of manufacturing the wheel rim W12–24 [29, 30].

### 4 Results

As it was mentioned above, taking into account the deformation of the workpiece (which is a shell of rotation) leads to the appearance of deformation effects unnoticed by early studies [11–13, 19–21]. Figure 2 shows the distribution of the intensity of stresses according to Mises and tensile stresses.

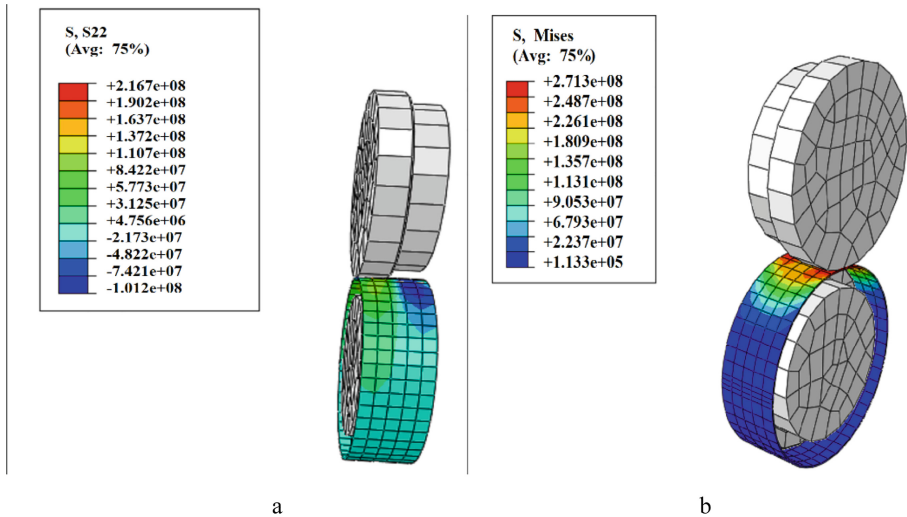


**Fig. 2.** Distribution of meridional stresses (a) and stress intensity according to Mises (b) upon the deformation of a cylindrical workpiece by fixed rollers.

The highest stress intensity was observed in the deformation zone along the bisector of the coverage angle of the workpiece by rollers. Here it reached values up to 271 MPa. As decreasing from the center of the deformation zone, the values of stress intensity decreased. On the way to the deformation zone, their value did not exceed the values of 203 MPa. The peripheral part of the workpiece, free from the action of the load, was also subjected to the action of internal stresses. However, their intensity was several orders of magnitude lower and ranges from 0.133 MPa to 23 MPa. The shell was deformed as a structure, the local action of the load spread throughout the workpiece, but to varying degrees. In confirmation of all the above, Fig. 3 shows the resulting displacements of various zones of the loaded cylinder along the coordinate axes.

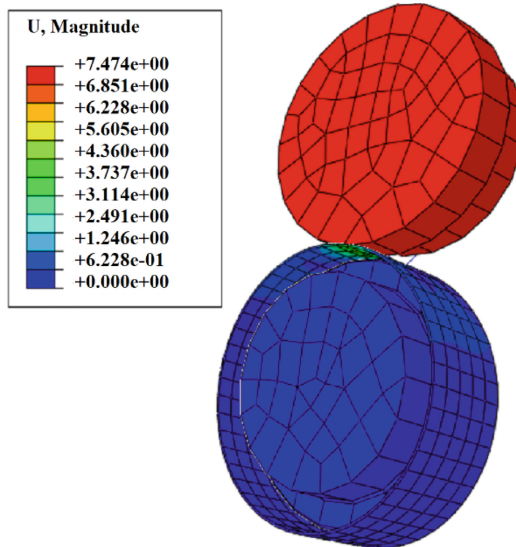


**Fig. 3.** The total movement of the workpiece elements.

In the zone of direct plastic deformation, the workpiece is shifted by an amount almost equal to the feed (4.36 mm) in the direction of the force. However, this zone is not the only one that moves in space. As we can see, two areas are formed behind the focus of plastic deformation, in which the total displacements approach 1.2 mm. This revealed pattern is of practical interest in creating new methods of profiling, for example, with a modified scheme of the external influence of the tool [1, 34, 35]. Here, the upper roller is colored with red, since all its points receive an offset in the direction of the vertical axis of 7.47 mm.

It is also of interest to compare the data obtained with existing calculation methods applicable to radial-rotational profiling. In [2, 5, 12, 20, 22, 36–38] formal dependencies obtained for calculating the components of the stress tensor with the local application of forces by rollers to a cylindrical workpiece. Here, Kirchhoff-Love's hypotheses are used as assumptions, as well as assumptions of the technical theory of

shells [39–41]. The equilibrium equations of the momentless theory of shells were solved by substituting single or double trigonometric series together with the conditions for the transition to the plastic state without taking into the account hardening and anisotropy of the workpiece metal [42–45]. For the crimp section, the dependence for calculating the meridional internal forces has the form

$$N_{xob} = \frac{4}{90} \frac{\sigma_s n l h}{R_0^2 m^3 \pi^3} \cos n\phi \cdot \left[ \phi_{0n} R_n \left( 1 - \sin \frac{m\pi x}{l} \right) + \phi_{0v} R_v \left( 1 + \sin \frac{m\pi x}{l} \right) \right]. \quad (1)$$

For the distribution area

$$N_{xraz} = \frac{\phi_{0v}}{90} \frac{4R_v \sigma_s n l h}{R_0^2 m^3 \pi^3} \cos n\phi \sin \frac{m\pi x}{l}, \quad (2)$$

- $\phi_{0v}, \phi_{0n}$  – the angle of the capture of the workpiece by the inner and outer rollers, respectively (degrees);
- $R_v$  – inner roller radius (m);
- $h$  – workpiece thickness (m);
- $R_n$  – outer roller radius (m);
- $\sigma_s$  – yield strength of the metal of the workpiece (Pa);
- $x$  – coordinate along the axis of the cylinder (m);
- $l$  – cylinder length (m);
- $\phi$  – coordinate in the tangential direction (degrees);
- $n, m$  – the number of deformation waves in the tangential and meridional directions.

Substituting the initial data for the wheel rim W12–24 in the Eqs. (1), (2), we will have a picture of the distribution of the stress field. To display the calculation results, graphs are constructed in the environment Mathcad (Fig. 4).

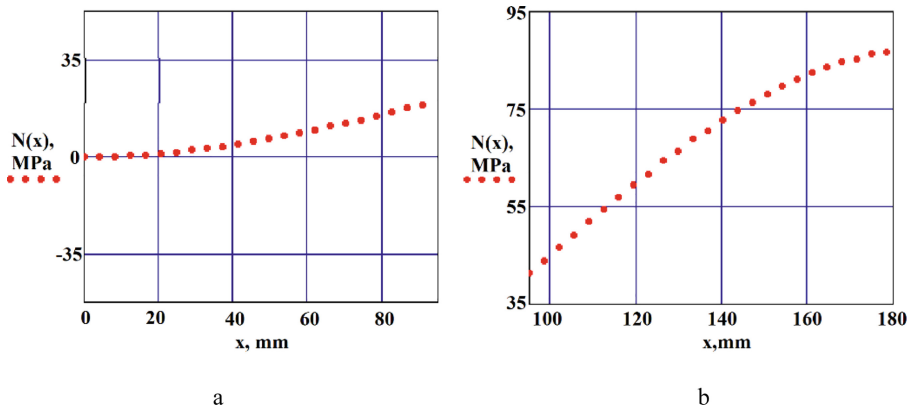


**Fig. 4.** Distribution of normal meridional stresses along the bisector of the contact angle: a) - distribution zone; b) - crimp zone.

The analysis of numerical and analytical results shows that the lowest meridional stresses act on the end face of the workpiece and are equal to zero for the analytical model and 0.47 MPa for the numerical in the distribution zone. The highest tensile stresses are observed for the theoretical model in the crimp zone - 82 MPa, for the numerical model - 110 MPa. However, as can be seen from Fig. 2 (b), compressive axial stresses appear in the deformation zone of the numerical model. Analytical solutions do not consider it. In the zone of the strain jump, where the tangential strain changes the sign from plus to minus, a jump in tensile stresses appears in the theoretical model. They increase more than twice. The numerical picture of the distribution of meridional stresses looks different. In the zone of change of the sign of tangential deformation, the meridional stresses become compressive and reach up to half of the yield strength of the material. This phenomenon is most likely due to the effect on the deformation zone outside the contact zones of the workpiece, which is not taken into account by the theoretical formulation of the problem. Figure 2 (b) shows that the zone of compressive meridional stresses originates just outside the contact zone and extends to the deformation zone. Therefore, this question remains open but proves the effect on the focus of plastic deformation of the peripheral zones of the workpiece. The distribution and comparison of tangential stresses are not given due to the sufficient coincidence of the results of both methods.

## 5 Conclusions

Thus, the following conclusions can be made. Numerical modeling of the process of deformation of a cylindrical workpiece by a pair of rollers shows that opposite stresses act both in the tangential and meridional directions in the deformation zone. The magnitude and direction of the tangential stresses coincide with both modeling techniques. The distribution pattern of the meridional stresses acting in the deformation zone is contradictory. Finite-element modeling shows the presence of compressive meridional stresses in the deformation zone, which form behind the plastic deformation zone and extend to it. This phenomenon contradicts analytical solutions, wherein the place of the sign of tangential deformation a jump in the magnitude of tensile meridional stresses are observed. Over the entire length of the workpiece zone covered by plastic deformation, meridional stresses are tensile. This position is consistent with the prevailing opinion about the pattern of stress distribution during radial-rotational profiling. Moreover, in this zone, the greatest thinning of the metal is observed in the profile of the finished wheel rim. This just indicates the tensile nature of the meridional stresses. Therefore, this issue requires further research. However, the fact of the influence of non-contact zones on the deformation zone is indisputable.

The workpiece changes its shape during loading. If some zones are stretched, then other zones are necessarily compressed, i.e. the shell is deformed along the entire peripheral surface. This circumstance allows assuming the possibility of a directed influence on the deformation zone by applying additional efforts to the free sections of the workpiece. This, in turn, should lead to the management of the stress-strain state of the profiling process as a whole and the regulation of the thickness difference of the final product.

## References

1. Wang, X., Jin, J., Deng, L.: Review: state-of-the-art of stamping-forging process with sheet metal blank. *J. Harbin Inst. Technol.* **24**, 1–16 (2017). <https://doi.org/10.11916/j.issn.1005-9113.17005>
2. Puzyr, R., Kukhar, V., Maslov, A., Shchipkovskiy, Y.: The development of the method for the calculation of the shaping force in the production of vehicle wheel rims. *Int. J. Eng. Technol.* **7**(4.3), 30–34 (2018)
3. Markov, O., Perig, A., Zlygoriev, V., Markova, M., Kosilov, M.: Development of forging processes using intermediate workpiece profiling before drawing: research into strained state. *J. Braz. Soc. Mech. Sci. Eng.* **39**(4), 4649–4665 (2017). <https://doi.org/10.1007/S40430-017-0812-Y>
4. Puzyr, R., Savelov, D., Argat, R., Chernish, A.: Distribution analysis of stresses across the stretching edge of die body and bending radius of deforming roll during profiling and drawing of cylindrical workpiece. *Metall. Min. Ind.* **1**, 27–32 (2015)
5. Wang, X., Li, L., Deng, L., et al.: Effect of forming parameters on sheet metal stability during a rotary forming process for rim thickening. *J. Mater. Process. Technol.* **223**, 262–273 (2015). <https://doi.org/10.1016/j.jmatprotec.2015.04.009>
6. Rout, M., Pal, K., Singh, S.: Prediction of edge profile of plate during hot cross rolling. *J. Manuf. Process.* **31**, 301–309 (2018). <https://doi.org/10.1016/j.jmapro.2017.11.024>
7. Markov, O., Zlygoriev, V., Gerasimenko, O., Hrudkina, N., Shevtsov, S.: Improving the quality of forgings based on upsetting the workpieces with concave facets. *East. Eur. J. Enterpr. Technol.* **5**/1(95), 16–24 (2018). <https://doi.org/10.15587/1729-4061.2018.142674>
8. Liu, Y., Qiu, X.: A theoretical study of the expansion metal tubes. *Int. J. Mech. Sci.* **114**, 157–165 (2016). <https://doi.org/10.1016/j.ijmecsci.2016.05.014>
9. Wang, Z., Zhang, Q., Liu, Y., Zhang, Z.: Robust and accurate geometric model for automated design of drawbeads in sheet metal forming. *Comput. Aided Des.* **92**, 42–57 (2017). <https://doi.org/10.1016/j.cad.2017.07.004>
10. Faraj, M., Li, X.: Determination of springback in sheet metal forming. *The annals of “dunarea de jos” university of galati V*, pp. 129–134 (2009)
11. Chigirinsky, V., Legotkin, G., Slepynin, A., Kozlov, V., Dragobetsky, V.: Mechanisms of plastic deformation in case of production of thin-walled rolled stock of the special purpose. *Metall. Min. Ind.* **11**, 222–230 (2015)
12. Bi, D., Yang, G., Chu, L.: Numerical simulation on spinning forming process of automotive wheel rim. *Mater. Sci. Forum* **704–705**, 1458–1464 (2012)
13. Bhattacharyya, S., Adhikary, M., Das, M., Sarkar, S.: Failure analysis of cracking in wheel rims – material and manufacturing aspects. *Eng. Fail. Anal.* **15**(5), 547–554 (2008). <https://doi.org/10.1016/j.engfailanal.2007.04.007>
14. Kil, T., Lee, J., Moon, Y.: Quantitative formability estimation of ring rolling process by using deformation processing map. *J. Mater. Process. Technol.* **220**, 224–230 (2015). <https://doi.org/10.1016/j.jmatprotec.2015.01.006>
15. Takayuki, H., Takashi, N., Cristian, T., Akitake, M., Hirohiko, J.: Finite element simulation of springback in sheet metal forming using local interpolation for tool surfaces method. *Int. J. Mech. Sci.* **50**, 175–192 (2008)
16. Chou, N., Hung, C.: Finite element analysis and optimization on springback reduction. *Int. J. Mach. Tools Manuf.* **39**(3), 517–536 (1999)
17. Mohan, R., Udayakumar, A., Selvarajan, S.: Innovative concept of correlating roll forming process with pressing simulation by using Altair HyperWorks. *Simul. Innov.* **1**, 1–9 (2013)

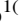




18. Jurkovic, M., Jurkovic, Z., Obad, M.: An investigation of the force and torque at profile sheet metal rolling – input data for the production system reengineering. *Tehnički Vjesnik* **22** (4), 1029–1034 (2015). <https://doi.org/10.17559/TV-20150310092726>
19. Jurković, M., Mustafić, E.: Mathematical modeling of the torque driving electric motor production line to the profiling forming thin sheets. In: *Proceedings International Scientific Conference on Production Engineering*, Budva, pp. 47–52 (2013)
20. Puzyr, R., Haikova, T., Majernik, J., Karkova, M., Kmec, J.: Experimental study of the process of radial rotation profiling of wheel rims resulting in formation and technological flattening of the corrugations. *Manuf. Technol.* **18**(1), 106–111 (2018). <https://doi.org/10.21062/ujep/61.2018/a/1213-2489/mt/18/1/106>
21. Puzyr, R., Haikova, T., Trotsko, O., Argat, R.: Determining experimentally the stress-strained state in the radial rotary method of obtaining wheels rims. *East. Eur. J. Enterpr. Technol.* **4**(1(82)), 52–60 (2016). <https://doi.org/10.15587/1729-4061.2016.76225>
22. Puzyr, R., Savelov, D., Shchetynin, V., Levchenko, R., Haikova, T., Kravchenko, S., Yasko, S., Argat, R., Sira, Y., Shchipkovakyi, Y.: Development of a method to determine deformations in the manufacture of a vehicle wheel rim. *East. Eur. J. Enterpr. Technol.* **4**(1 (94)), 55–60 (2018)
23. Markov, O., Zlygoriev, V., Gerasimenko, O., Hrudkina, N., Shevtsov, S.: Improving the quality of forgings based on upsetting the workpieces with concave facets. *East. Eur. J. Enterpr. Technol.* **5**(1(95)), 16–24 (2018). <http://doi.org/10.15587/1729-4061.2018.142674>
24. Geselbracht, M.J., Ellis, A.B., Penn, R.L., Lisensky, G.C., Stone, D.S.: Mechanical properties of metals: experiments with steel, copper, tin, zinc, and soap bubbles. *J. Chem. Educ.* **71**(3), 254 (1994)
25. Aliiev, I., Aliieva, L., Grudkina, N., Zhibankov, I.: Prediction of the variation of the form in the processes of extrusion. *Metall. Min. Ind.* **3**(7), 17–22 (2011)
26. Sosenushkin, E., Yanovskaya, A., Sosenushkin, A., Emel'yanov, V.: Mechanics of nonmonotonic plastic deformation. *Russ. Eng. Res.* **35**(12), 902–906 (2015). <https://doi.org/10.3103/s1068798x15120199>
27. Ogorodnikov, V., Dereven'ko, I., Sivak, R.: On the influence of curvature of the trajectories of deformation of a volume of the material by pressing on its plasticity under the conditions of complex loading. *Mater. Sci.* **54**(3), 326–332 (2018)
28. Titov, V., Zlochevskaya, N., Kachan, A.: Features of integrated manufacture of blade workpieces from eutectically strengthened titanium alloys. *Metallurgist* **58**(1–2), 141–148 (2014)
29. Haikova, T., Puzyr, R., Dragobetsky, V., Symonova, A., Vakylenko, R.: Finite-element model of bimetal billet strain obtaining box-shaped parts by means of drawing. In: Ivanov, V., et al. (eds.) *Conference 2019, DSMIE*, pp. 85–94. Springer, Lutsk (2019). [https://doi.org/10.1007/978-3-030-22365-6\\_9](https://doi.org/10.1007/978-3-030-22365-6_9)
30. Zagirnyak, M., Drahobetskyi, V.: New methods of obtaining materials and structures for light armor protection. In: Krivanek, V. (eds.) *Conference 2015, ICMT*, pp. 1–6. OPROX, Inc., Brno (2015)
31. Matsuda, K., Hashimoto, D., Nakamura, K.: Real contact area and friction property of rubber with two-dimensional regular wavy surface. *Tribol. Int.* **93**(part B), 523–529 (2016)
32. Jin, J.-S., Deng, L., Wang, X.-Y., Xia, J.-C.: A new rotary forming process for rim thickening of a disc-like sheet metal part. *J. Mater. Process. Technol.* **212**(11), 2247–2254 (2012). <https://doi.org/10.1016/j.jmatprotec.2012.06.013>
33. Savelov, D., Dragobetsky, V., Puzyr, R., Markevych, A.: Peculiarities of vibrational press dynamics with hard-elastic restraints in the working regime of metal powders molding. *Metall. Min. Ind.* **2**, 67–74 (2015)

34. Maslov, A., Batsaikhan, J., Puzyr, R., Salenko, Y.: The determination of the parameters of a vibration machine for the internal compaction of concrete mixtures. *Int. J. Eng. Technol.* **7**(4.3), 12–19 (2018)
35. Logesh, K., Bupesh Raja, V., Gokula Krishnan, D., Azeemudeen, M., Andrew, N., Hariprasath, K.: Experimental investigation and analysis of tensile and forming behaviour of cold rolled sheet. *Int. J. Mech. Eng. Technol.* **8**(11), 252–264 (2017)
36. Susheel, S.: Reducing number of spots using fem technique. *Int. J. Res. Dev.* **4**(9) (2018)
37. Thomas, T., Nair, S., Garg, K.: Elasto-plastic stress analysis and fatigue life prediction of a freight car wheel under mechanical and cyclic thermal loads. *Comput. Struct.* **17**(3), 313–320 (1983)
38. Attwood, D., Nicolich, M., Doney, K., Smolar, T., Swensen, E.: Valve wheel rim force capabilities of process operators. *J. Loss Prev. Process Ind.* **15**, 233–239 (2002)
39. Woldstad, J., McKulkin, M., Bussi, C.: Forces applied to large hand wheels. *Appl. Ergon.* **26** (5), 55–60 (1995)
40. Miehe, C., Schotte, J., Lambrecht, M.: Homogenization of inelastic solid materials at finite strains based on incremental minimization principle - application to the texture analysis of polycrystals. *J. Mech. Phys. Solids* **50**, 2123–2167 (2002)
41. Akbulut, H.: On optimization of a car rim using finite element method. *Finite Elem. Anal. Des.* **39**, 433–443 (2003)
42. Li, J., Zhang, X.: A criterion study for non-singular stress concentrations in brittle or quasi-brittle materials. *Eng. Fract. Mech.* **73**(4), 505 (2006)
43. Markov, O., Gerasimenko, O., Khvashchynskyi, A., Zhytnikov, R., Puzyr, R.: Modeling the technological process of pipe forging without a mandrel. *East. Eur. J. Enterpr. Technol.* **3**(1 (99)), 42–48 (2019). <http://doi.org/10.15587/1729-4061.2019.167077>
44. Shiozawa, K., Morii, Y., Nishino, S.: Subsurface crack initiation and propagation mechanism in high-strength steel in a very high cycle fatigue regime. *Int. J. Fatigue* **28** (11), 15–21 (2006)
45. Akiniwa, Y., Stanzl-Tschegg, S., Mayer, H.: Fatigue strength of spring steel under axial and torsional loading in the very high cycle regime. *Int. J. Fatigue* **30**(2), 20–57 (2008)





# Peculiarities of Interaction of Micro-roughnesses of Contacting Surfaces at FANT

Ihor Shepelenko<sup>1</sup> , Yakiv Nemyrovskiy<sup>1</sup> , Yuri Tsekhanov<sup>2</sup> ,  
Sergii Mahopets<sup>1</sup> , and Oleh Bevz<sup>1</sup> 

<sup>1</sup> Central Ukrainian National Technical University, 7, Universytetskyi Ave.,  
Kropyvnytskyi 25006, Ukraine  
kntucpfzk@gmail.com

<sup>2</sup> Voronezh State Technical University, 84, 20 let Oktyabrya St.,  
Voronezh 394026, Russia

**Abstract.** Based on the theory of cutting mechanics, using a model experiment, the basic laws of the interaction of surface microroughness with a tool have been established, which allow developing a theoretical model for the first stage of finish anti-friction non-abrasive processing (FANT), which will ensure the efficient course of the micro-cutting process and the filling of microcavities with anti-friction material. It is noted that during the interaction of cast-iron micro-roughness with a brass tool, the top of the microroughness dulls with the formation of a rounding radius. The mechanism of forming the radius of rounding of micro-roughness is shown, a significant interdependence between it and the front cutting angle is established. The phenomena occurring on the back surface of micro-roughness are revealed. The ways to improve the efficiency of the micro-cutting process by ensuring the established values of the rake cutting angle are proven. It is proposed to consider the application of FANT anti-friction coatings from the perspective of a systematic approach and the principles of self-organization, which will make it possible to predict the achievement of optimal quality parameters of the surface layer: equilibrium roughness, favorable microrelief, required hardening, and residual stresses.

**Keywords:** Finish anti-friction non-abrasive treatment · Anti-friction coating · Micro-cutting · Contact interaction · Cutting angle · Rounding radius

## 1 Introduction

Current trends in the development of world engineering are aimed at a significant increase in the operational properties of machines and mechanisms, primarily by improving the quality of work surfaces of parts. The creation of new and improvement of existing technological methods should be aimed at improving the quality of work surfaces by achieving optimal operational properties of machine parts.

The main parameters of surface quality - physical and mechanical properties and geometric characteristics of the surface layer, which largely determine the operational properties, are formed throughout the entire technological process, however, the finishing operations have the greatest influence. An important role in the formation of

physical and mechanical properties is played by the intermediate environment through which the interaction of microroughness of the contacting surfaces occurs. Therefore, one of the ways to improve the quality of parts during their manufacture and repair, and hence their operational properties, is to create an intermediate environment by modifying the worksurface through creating and applying coatings in finishing operations. In these cases, when choosing a method for producing coatings, preference should be given to technologies that ensure the formation of contacting surfaces with a given set of operational properties.

Such coatings can be obtained using the technology of finish anti-friction non-abrasive treatment (FANT), realized due to the frictional interaction of the tool being machined with the surface of the treated workpiece. The friction of the contacting surfaces in the presence of a process fluid ensures the transfer of the tool material and the formation of an antifriction coating up to 5  $\mu\text{m}$  thick on the surface of the part, as a result of which it acquires high antifriction properties.

The formation of the FANT anti-friction coating largely depends on the conditions under which the tool contacts with the surface to be treated, and the shape and size of micro-roughness determine the quality of the resulting coating and its continuity [1]. The study of the features of contacting surfaces, as well as the establishment of the basic laws, will improve the quality of the antifriction coating, and hence the operational properties of the part. Thus, carrying out special studies of the interaction of contacting surfaces during the application of coatings FANT seems very relevant.

## 2 Literature Review

The existing hypotheses explaining the mechanism of the formation of an antifriction coating during FANT are described in a number of works [2–6]. According to the research [2], the process of frictional deposition of films of plastic materials is connected with the fulfillment of the conditions of complete weldability of the applied coating material with the base material and the presence of a surface-active medium (SAM) in the contact zone. It also indicates the need to create a set of theoretical prerequisites for obtaining high-quality anti-friction coating FANT, namely:

- micro cutting conditions;
- conditions of plastic contact;
- seizing criteria;
- optimal coating conditions.

Directly, according to [2, 3] the process of frictional material transfer can be divided into two stages:

- plastic displacement of the starting material carried out by micro-roughness of the surface on which the coating is applied, which proceeds to destruction by micro-cutting;
- seizure of the particles formed as a result of micro-cutting with the surface onto which the transfer occurs.

Microscopic analysis of the particles contained in glycerine after coating showed that when a high-quality film is formed in the contact zone “friction rod - surface to be treated”, a micro-cutting process must necessarily take place [2].

It should be noted that despite the difference in approaches and interpretation of the process of forming the FANT coating by the friction-mechanical method, the authors of the studies [2–6] agree on the importance and necessity of implementing the conditions of micro-cuts, the fulfillment of which is associated with certain requirements for micro-roughness of contact surfaces:

$$\frac{2h_i}{r} = 1 - \frac{2\tau_n}{\sigma_T} \leq 0,02, \quad (1)$$

where

- $h_i$  – the height of a single microroughness;
- $r$  – the radius of the apex of a single microroughness;
- $\tau_n$  – tangential component of adhesive bond strength;
- $\sigma_T$  – yield strength of the brass rod.

The FANT anti-friction coating application model is considered in detail in the works of German researchers [7], where it is also indicated that the process of micro-cuts of a copper alloy prevails at the initial moment of tribo-interaction. The presence of SAM formed as a result of glycerine tribodestruction allows loosening of oxide layers on friction surfaces and plastic deformation of particles of the transferred metal in the friction zone. Some particles are compressed in the hollows between the protrusions of the roughness, which causes a general decrease in the roughness parameter of the treated surface. Under the influence of high local compressive forces, the particles are pressed, and their adhesive bond is formed between themselves and with the substrate.

Based on experimental data and a theoretical discussion of the formation of coatings during FANT, the authors of the study [8] established that tool wear and material transfer occur due to micro-cuts by the surface roughness of the workpiece. This phase is characterized by high pressure and the associated introduction of protrusions of the surface roughness of the part into the surface of a softer material, forming coatings.

According to the studies [9], as a result of plastic deformation in the near-surface volumes, crushing and micro-cuts of micro protrusions occur, and an increase in temperature in the contact zone leads to a decrease in the yield strength of the material. As a result, the transfer of plastic metal particles to a solid substrate, their deformation, and the formation of new adhesive bonds are observed.

Of course, the formation of friction coatings has its characteristics, requiring a detailed and in-depth study. In our opinion, an important reserve for improving the quality of the FANT anti-friction coating is the study of the contact interaction of the micro-roughness of the treated surface with a tool to create favorable conditions for micro-cutting.

The work is aimed at studying the characteristics of the interaction of micro-roughness of the treated surface with a tool to create favorable conditions for micro-cutting.

### 3 Research Methodology

Experimental studies of contact interaction were carried out on special samples of gray cast iron GG20 (DIN, Germany) and brass CuZn37 (DIN, Germany), simulating the microroughness of the treated cast iron surface. The choice of these materials is due to the following. Gray cast iron is widely used for the manufacture of parts working in a pair of friction, for example, cylinder liners. However, when applying the FANT anti-friction coating on the surface of cast iron parts, difficulties arise due to the presence of free graphite in the structure of cast iron, which prevents the adhesion of the anti-friction coating with the base material. Considering the possibility and expediency of processing parts from gray cast iron GG20 FANT, the bulk of the experiments were performed on this material. Given the plastic properties, brass CuZn37 was used in studies as an anti-friction material.

To study the contact interaction of micro-roughness during micro-cuts during FANT, the method of the theory of similarity and dimensions was used, and the following model experiment was carried out. A brass sample in the form of a plate was mounted on the working table of the milling machine, and a replaceable cast iron cutter was installed in a tailored device with an indicator head, the microgeometry of the cutting part of which simulated a separate micro-roughness of the surface of the workpiece. The rake cutting angle varied within  $\gamma = +5\text{--}15^\circ$ . A diagram of the interaction of contacting surfaces during a model experiment is shown in Fig. 1.

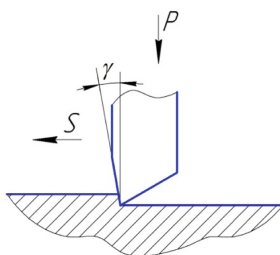


**Fig. 1.** The scheme of contacting surfaces when modeling micro-cuts with a rake cutting angle  $\gamma$ .

The load  $P$  on the brass plate was provided by the vertical feed mechanism of the machine table and was controlled by the indicator head. Its value was chosen so that the small depth of penetration of the cutter corresponded to the conditions for the interaction of micro-roughness of the workpiece with a brass bar. Supply  $S$  was carried out by moving the machine table manually. Thus, moving under a fixed load, a cast-iron cutter cuts off a layer of anti-friction metal (brass), thereby simulating the process of micro-cutting of contacting surfaces (Fig. 2). For more accurate reproduction of the FANT process, technical glycerine was supplied to the friction zone, which degreased the surface, destroyed the oxide film and created the necessary conditions for the setting of the base material with the coating.

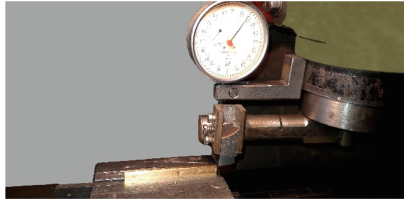


**Fig. 2.** The working area of the equipment when modeling micro-cuts with FANT.

When conducting a model experiment, the forces of contact interaction were measured using the designed device with an indicator head (Fig. 2), the roughness parameters of the studied surfaces were determined on a Talysurf-5 profilograph-profilometer with a microrelief profilogram recorded. The geometric parameters of the micro-cutter model, the processes occurring on the surfaces of the studied samples were studied using MIM-7 and «Altami» metallographic microscopes, as well as a ZEISS EVO 50XVP scanning electron microscope at the V. Bakul Institute for Superhard Materials of the National Academy of Sciences of Ukraine.

#### 4 Results

Let's consider the contact interaction of a single micro-roughness formed during the processing of a surface from brass CuZn37 with a cutter from cast iron GG20. In the beginning, the micro-cutting process is carried out with a sharpened cutter, the initial radius of the cutting edge of which is  $r = 0.008\text{--}0.015$  mm. It is significantly less than the thickness of the removal  $t_p$ . The interaction diagram of such a cutter with the surface of a brass sample is shown in Fig. 3.

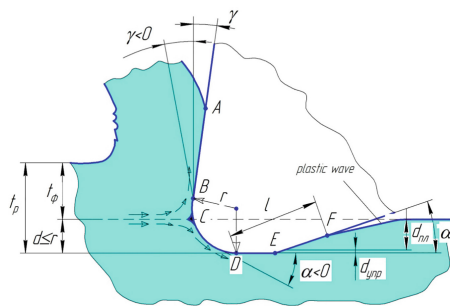


**Fig. 3.** The scheme of interaction of a single micro-roughness with the treated surface during FANT.

As it follows from Fig. 3, the contour of the cutting wedge consists of the following parts: **AB** is the rectilinear part of the contour of the front surface, sharpened with a rake angle  $\gamma > 0^\circ$ ; **BC** is a rounded portion of the front surface in which  $\gamma > 0^\circ$ ; the **CD** is

the rounded part of the contour of the rear surface, in which the rear angle  $\alpha > 0^\circ$ . The length of this section is practically determined by the process of plastic recovery since the amount of elastic recovery of the processed material  $d_{ynp} < d_{nr}$ .

Thus, the front surface of the cutting wedge consists of two parts  $L = AB + BC$ , and its rear surface of length  $L_I$  consists of three parts  $L_I = CD + DE + EF$ . Point  $C$  corresponds to the section of the front and back surfaces of the wedge.

Let's consider this scheme in more detail. According to the data [10], the workpiece material deposited onto the cutting wedge at point  $C$  is divided into two flows, one of which moves along the tool's front surface, and the second layer, of thickness  $d$ , is deformed by the back surface of the cutting wedge. In this case, the real cut surface passes through point  $C$  and the actual cut depth does not coincide with the nominal thickness  $t_p$  of the surface cut. The author [10] recommends determining the position of point  $C$  and the value of  $d$  by a sequential decrease in the thickness of the cut-off layer until the termination of micro-chip formation.

In our case, point  $C$  is the dividing point of the entire layer to be removed with a thickness of  $t_p$ , namely, to the layer of material that goes into micro-chips with the actual cutting depth  $t_\phi$  and to the layer that is processed by surface plastic deformation by the radius portion of the back surface. Its value  $d \leq r$ , meaning  $t_p \sim t_\phi + r$ , where  $r$  is the blunting radius of the tip of the cutter changing during operation.

Experimental studies have shown that with a decrease in the rake cutting angle  $\gamma$ , the radius of rounding of the micro-cuts increases (Fig. 4). This indicates that the cutting edge of the cast iron cutter wears out intensively in the process of interaction with the brass surface, and this happens already at the very beginning of the interaction, and the wear itself is like micro-cracking, which undergoes frictional wear soon after stabilization of the blunting form. After that, a layer of brass sticks to the contact surface, which plays the role of a solid lubricant, and the shape of the cutting wedge finally stabilizes. It's worth to be noted that this form of the cutting blade corresponds to the principle of self-organization of the process [11], and, consequently, to the minimum power of micro-cutting.

It should also be noted that the wear rate of the cutting blade directly depends on the angle  $\gamma$ , which is illustrated by the data shown in Fig. 5.

From Fig. 5 it follows that the actual thickness of the cut with a decrease of  $\gamma$  from  $+5^\circ$  to  $-5^\circ$  decreases in proportion to the angle, and then monotonically decreases to  $0^\circ$  at a value of  $\gamma = -15^\circ$ . This is explained by the intensive formation of the wear radius of the cutting edge (Fig. 4).

Therefore, to intensify the first stage of FANT chip formation, single micro-roughness of the treated surface should interact with the brass surface having an angle  $\gamma \geq 0^\circ$ .

The increase in the radius of rounding of the cutting edge intensifies the next stage of the FANT process - the interaction of the rear surface of the tool with a brass surface.

In the contact zone of the processed material on the back surface, high contact pressures are exceeding 3 times the yield strength of brass and approximately equal to its  $HV$  hardness. Therefore, a layer of plastically hardened material  $d_{nr}$  is formed on the back surface of the tool and a film of adhesive-adhering brass appears (Fig. 6).

This film starts playing the role of the third body, i.e. solid lubricant, preventing further blunting of the micro roughness peaks, and the further value of the rounding

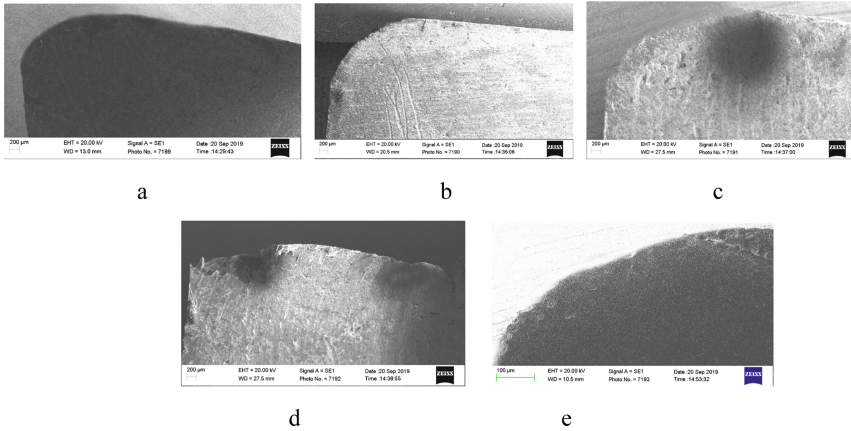


**Fig. 4.** Cast iron micro-cutter rounding radius at rake cutting angle  $\gamma$ : a)  $\gamma = +5^\circ$ ; b)  $\gamma = 0^\circ$ ; c)  $\gamma = -5^\circ$ ; d)  $\gamma = -10^\circ$ ; e)  $\gamma = -15^\circ$ , increase 50.

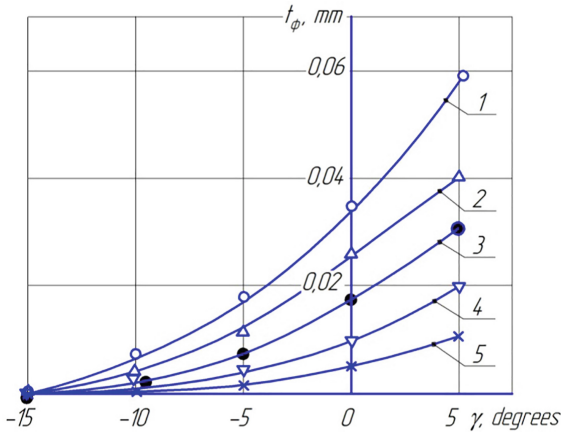


**Fig. 5.** The dependence of the actual thickness of the cut  $t_\phi$  on the rake cutting angle  $\gamma$  when simulating micro-cuts with casting iron of the brass surface at nominal thicknesses of the cut  $t_{nom}$ , mm: 1 – 0,6; 2 – 0,4; 3 – 0,3; 4 – 0,2; 5 – 0,1.

radius  $r$  is stabilized. It should be noted that the condition for the interaction of brass with the back surface of the micro-cutter model (micro roughness apex) depends on the angle  $\gamma$ , which mainly determines the wear of the cutting edge.

This is confirmed by the experimental data shown in Fig. 7. It follows that the length of the contact along the rear face  $l$  depends on the angle  $\gamma$ , and as the angle  $\gamma$  decreases, the value of  $l$  increases slightly (Fig. 7, curve 2), which is apparently due to the complete interaction of the  $CD$  section (Fig. 3) with brass and the absence of a micro-cutting process. The adhesive interactions of the rear surface of the cutter model with brass also increase with decreasing angle  $\gamma$  and reaches its maximum at  $\gamma = -15^\circ$ .



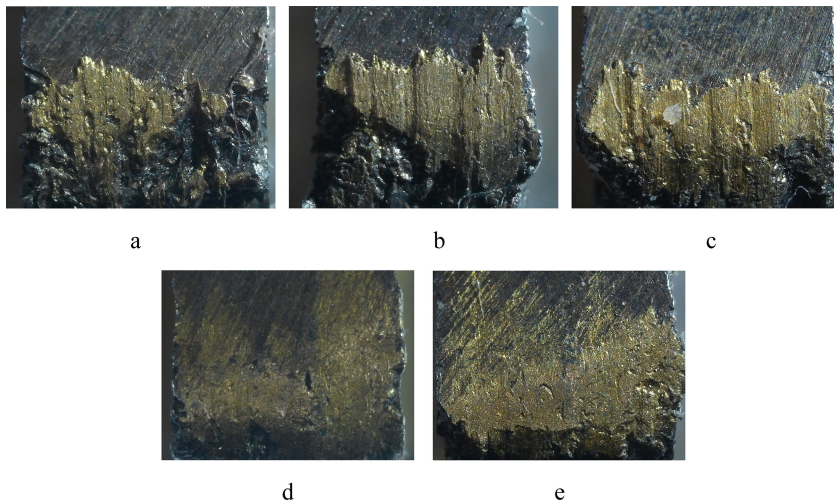


**Fig. 6.** Sticking of brass on the rear surface of the cutter made of cast iron when rubbing brass with a rake cutting angle  $\gamma$ : a)  $\gamma = +5^\circ$ ; b)  $\gamma = 0^\circ$ ; c)  $\gamma = -5^\circ$ ; d)  $\gamma = -10^\circ$ ; e)  $\gamma = -15^\circ$ , increase 30.

This is evidenced by curve 1 (Fig. 7), which shows the change in the percentage of the area covered with brass, referred to the total contact area.

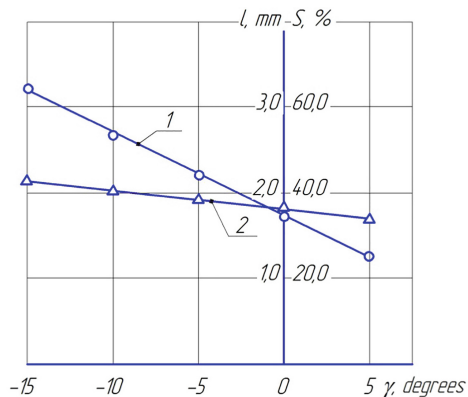


**Fig. 7.** The dependence of the brass coating area of the contact surface  $S$  (curve 1) and the contact length  $l$  (curve 2) on the angle  $\gamma$  when modeling micro-cuts made of cast iron GG20 of the surface of brass CuZn37 at  $t_{НОМ} = 0,6$  mm.

Thus, the FANT process can also be intensified due to the interaction of the brass surface with individual micro-roughness at negative values of the angle  $\gamma$ . One example of the implementation of this condition is the implementation of the reciprocating



working movement of the brass tool, and the angle in forwarding motion is  $\gamma \geq 0^\circ$  and in backward  $\gamma < 0^\circ$  only further brass sticking will occur.

The study of the conditions of contact interaction showed a significant mutual influence of the tool (a single microroughness) and the brass surface with which the microparticles were removed. This micro-chip, located in the cavities of micro-roughness, reduces roughness and forms a brass coating in the second stage. Therefore, the FANT process itself must be considered from the perspective of a systematic approach and the principles of self-organization [11]. In this case, the interaction of a single micro-roughness with a brass surface will be a non-equilibrium thermodynamic process where self-organizing reactions take place [12].

As the internal manifestation of such self-organization it is to expect the following:

- the development of equilibrium roughness (coinciding with the operational), regardless of the initial microgeometry of the friction surface;
- increasing the actual contact area, rounding the tops of micro-roughness due to running-in wear;
- obtaining hardening of the surface layer and the formation of favorable residual stresses.

## 5 Conclusions

Analysis of the above material allows formulating the following conclusions:

1. The regularities of the interaction of the micro-roughness of the treated surface with the tool at FANT, which are determined by the principle of adaptability of the tool-blank system, have been experimentally established.
2. It is proved that during the interaction of micro-roughness with a brass tool, a blunted peak of micro-roughness with a rounding radius is formed almost immediately, which subsequently remains practically unchanged.
3. The formation of the rounding radius at the initial stage occurs due to micro destructions, which finishes its formation due to wear from friction forces after reaching the optimum micro-cutting process from the viewpoint of minimum energy. Moreover, the radius of the rounding of the cutting edge depends on the values of the rake cutting angle  $\gamma$ .
4. On the back surface of the cutter model, micro-roughness is three times higher there than the yield strength of the brass sample due to the presence of high contact pressures there, antifriction material (brass) adheres. In the future, these plots will play the role of foci of the adhesion of the brass film on the surface processed by the friction-mechanical method.
5. From the viewpoint of the maximum efficiency of the micro-cutting process and filling the cavities between micro-roughness, their geometry should provide a rake cutting angle  $\gamma = 0^\circ - 5^\circ$ .
6. The revealed regularities of the interaction of the micro-roughness of the workpiece with a brass tool allow developing a theoretical model for the first phase of the

FANT, which ensures the efficient course of the process of micro-cutting and filling microcavities with rubbed material.

7. It is proposed to consider the FANT process from the standpoint of a systematic approach and the principles of self-organization, which will make it possible to predict the achievement of optimal quality parameters of the surface layer: equilibrium roughness, favorable microrelief, required hardening and residual stresses.

## References

1. Shepelenko, I., Nemyrovskiy, Y., Tsekhanov, Yu., Posviatenko, E.: Modeling of contact interaction of micro roughness at FANP. In: I-th International Scientific and Technical Conference «Prospects for the Development of Mechanical Engineering and Transport-2019», pp. 218–219 (2019)
2. Kharchenkov, V.S., Pogonyshev, V.A., Lemeshko, V.I.: Optimization of surface roughness when applying soft run-in films by finish antifriction nonabrasive treatment. *J. Frict. Wear* **20**, 82–85 (1999)
3. Bersudskij, A.L.: The mechanism of formation of antifriction coatings during hardening treatment. *VESTNIK of Samara University. Aersp. Mech. Eng.* **2**(10), 81–84 (2006). (in Russian)
4. Zinin, M.A., Gavrilov, S.A., Shchedrin, A.V., Garkunov, D.N.: Influence of metal-cladding additivite valena on combined machining. *Russ. Eng. Res.* **31**, 880 (2011). <https://doi.org/10.3103/S1068798X11090292>
5. Ragutkin, A.V., Sidorov, M.I., Stavrovskij, M.E.: Some aspects of antifriction coatings application efficiency by means of finishing nonabrasive antifriction treatment. *J. Min. Inst.* **236**, 239–244 (2019). <https://doi.org/10.31897/PMI.2019.2.239>
6. Rybakova, L.M., Kuksenova, L.I., Nazarov, Y.A.: Structure of steel 50G after antifriction nonabrasive finish treatment of the surface and evaluation of the quality of the modified layer. *Met. Sci. Heat Treat.* **34**, 622–629 (1992). <https://doi.org/10.1007/BF00776900>
7. Polzer, G.: Basics of Friction Coating under Conditions of Selective Transmission. *R.R.M. (Repairs. Recovery. Modernization)* **10**, 23–28 (2010). (in Russian)
8. Shepelenko, I.V., Posviatenko, E.K., Cherkun, V.V.: The mechanism of formation of anti-friction coatings by employing friction-mechanical method. *Prob. Tribol.* **1**, 35–39 (2019). <https://doi.org/10.31891/2079-1372-2019-91-1-35-39>
9. Karakozov, Je.S., Mustafaev, R.I., Mel'nikov, N.V.: Current state of friction welding (review). *Weld. Prod.* **8**, 2–5 (1989). (in Russian)
10. Rozenberg, Ju.A.: *The Mechanics of the Cutting Process*. Kurgan University Publishing House (2005). (in Russian)
11. Kosteckij, B.I.: Structural and energetic adaptability of materials during friction. *Frict. Wear* **2**, 201–212 (1985). (in Russian)
12. Jakubov, F.Ja., Kim, V.A.: *Structural and Energetic Aspects of Hardening and Increasing the Durability of the Cutting Tool*. Crimean Educational and Pedagogic State Publishing House (2005). (in Russian)



# The Influence of Milling Parameters on Cutting Forces in High-Speed Milling of Polymer Materials

Alper Uysal<sup>1</sup>(✉) , Eshreb Dzhemilov<sup>2</sup> ,  
and Ruslan Dzhemalyadinov<sup>2</sup> 

<sup>1</sup> Yildiz Technical University, Yildiz, Besiktas, 34349 İstanbul, Turkey  
auysal@yildiz.edu.tr

<sup>2</sup> Crimean Engineering and Pedagogical University, 8, Uchebniy Side St.,  
Simferopol 29501, Republic of Crimea

**Abstract.** This article presents the results of experimental studies during high-speed end milling of pure and carbon black reinforced polyamide materials depending on the cutting conditions used. The physicomaterial properties of such materials largely depend on the technological requirements of their manufacture. The high elastic properties of the polymer materials and their composites contribute to an increase in the contact area of the tool with the workpiece, especially on the back surface, thereby leading to an increase in the cutting forces. The result of this phenomenon causes a decrease in the critical wear threshold of the tool compared to metal processing. Based on this experimental study, it was found that milling of pure polyamide couldn't be performed at the cutting speeds beyond 500 m/min due to the occurring high temperature at the contact area. The cutting forces for both polymer materials increased as the feed and cutting speed increased. Furthermore, when comparing carbon black reinforced and pure polyamide materials, it was observed that more cutting force is needed for milling of pure polyamide material.

**Keywords:** High-speed milling · Carbon black reinforced polyamide · Cutting forces

## 1 Introduction

The development in the engineering industry promotes the use of new structural materials. Advanced properties of some polymer-based composites can significantly increase the operational characteristics of the finished product and reduce its cost in comparison with a metal alloy analogue. In such materials, one of the elements acts as the matrix, and the other has the role of reinforcement. The matrix serves for reinforcement material protection, stress distribution among reinforcement materials and form definition of the manufactured composite part. The presence of reinforcing fibres in the composition provides high mechanical properties. However, even though the blanks from composite materials on a polymer basis are made by casting, which allows getting the product close in configuration to the finished part, there is a need for

mechanical processing of several surfaces: processing of flat surfaces, grooves, and holes of the required quality [1, 2].

The study of the processes occurring in the contact zone of a cutting tool with a workpiece made of composite material is an urgent scientific and practical task. The solution of it will increase the tool life, improve the surface quality and reduce the proportion of rejection and the overall self-value of the final parts.

This work aims to study the effects of cutting speed and feed on the cutting force during high-speed milling of pure and carbon black reinforced polyamide materials.

## 2 Literature Review

Polymer-based carbon-containing composite materials are used in many fields, especially in the engineering, aviation, and shipbuilding industries. The mechanical processing of composite materials with a polymer matrix, in particular, reinforced with carbon fibres, glass fibres, carbon black, etc. is a complicated technical task, since these materials have low density, high elastic modulus, and strength, low thermal conductivity and friction coefficient.

This leads to the fact that the type and processing conditions must be selected at the same time taking into account several parameters: polymer base; curing options; the presence, appearance, orientation and structure of the reinforcements; the presence of the coating and the process itself [3, 4]. The effect of temperature on mechanical properties and tensile creep responses of Wood/PVC (WPVC) composite materials were investigated [3]. The experimental results indicate that the mechanical strength of WPVC composites decreased significantly at a temperature higher than 50 °C. At the same time, the modulus of elasticity was affected significantly at a temperature higher than 60 °C. The material properties at large deformation as mechanical strength are more sensitive to the temperature change than the mechanical modulus at small deformation. Chen et al. [4] constructed a theoretical model to predict the cutting and thrust forces in orthogonal cutting of UD-CFRP under the entire range of fibre orientation varying from 0° to 180° based on the theory of beams on elastic foundation and the principle of minimum potential energy. The researcher concluded that fibre orientation has the most significant influence on cutting and thrust forces, followed by the depth of cut, and finally, rake angle. Thus, it is unacceptable to apply similar process parameters with metal alloys in the cutting of polymer and polymer-based composite materials.

Features of the composite materials cutting, depending on their material specifications, are in the relative complexity of obtaining a surface of the required quality because of the delamination of the material upper layers and the appearance of microcracks on the surface [5, 6]. High hardness of reinforcements leads to an increase in abrasive tool wear. Low thermal conductivity leads to the destruction of the polymer matrix and the appearance of burns on the surface of the material. Caggiano [7] has studied the milling FRP composite and showed that material behaves non-homogeneous and depends on diverse reinforcement and matrix properties, reinforcement architecture and orientation, and the relative content of matrix and reinforcement. To reduce the typical damages, such as delamination and fibre protrusions at

different ranges of fibre orientation angle, some authors suggested performing an initial scoring along the contour via grinding or laser cutting. Others proposed oscillated milling to reduce delamination. Uhlmann et al. [8] have shown that significant improvement in the process of reliability and productivity can be made by implementing innovative CFRP-designed CVD diamond coated cutting tools. The deposition of the diamond at a lower temperature than currently industrially undertaken is possible, and the use of SiC interlayers for the machining of CFRPs with diamond-coated tools exhibits potential. For some composite materials, in particular polyamides, it is not allowed to use cutting lubricants during machining due to the high level of moisture absorption. The high elastic properties of composite materials contribute to an increase in the contact area between cutting and workpieces, and this leads to an increase in the cutting forces. The result of this phenomenon is a decrease in the critical wear threshold of the tool compared to metal processing [9–11]. Khairusshima et al. [9] addressed the issue of determining the effects of cutting parameters on the surface roughness and delamination in milling of CFRP by using a solid uncoated carbide cutting tool. The spindle speed, feed rate and depth of cut were the factors while surface roughness and delamination were recorded as a response. It was observed that the feed rate was the most significant factor affecting surface roughness (Ra) and delamination factor in the cutting of CFRP. Karatas and Gokkaya [10] reported that an increment in feed rate caused higher compressive forces and an increase in cutting speed and a reduction in feed rate caused higher hole surface quality in the machining of CFRP and GFRP composite materials. Despite there are some studies on the cutting of fibre-reinforced composite materials [12–17], there is a lack of research on the cutting of particle reinforced composite materials.

### 3 Research Methodology

Experimental studies were carried out by milling of pure polyamide (PA 6) and carbon black reinforced polyamide materials. The pure polyamide material is Eurotec® brand, and the carbon black reinforced polyamide material is the Premix brand. The technical specifications for these materials used in the experimental studies are given in Table 1 and Table 2.

Pure and carbon black reinforced polyamide materials were produced in a plastic injection molding machine with dimensions of  $150 \times 150 \times 10$  mm Fig. 1.

Before production, all granular polymer materials were dried at  $60^\circ\text{C}$  for 2 h. The dried granules were melted at  $260^\circ\text{C}$  in a plastic injection machine and injected into the mold cavity with a pressure of 70 MPa. In this process, the mold was heated to  $60^\circ\text{C}$  in advance. The samples for carbon black reinforced polyamide are given in Fig. 2.

Milling operations were performed in a CNC machining center, shown in Fig. 3, using an uncoated WC (Tungsten Carbide) end mill of 8 mm diameter with two cutting edges. Gisstec SC16 speeder head which can operate at a maximum of 24,000 rpm was used to reach the rotational and cutting speed values given in Table 3. The cutting forces were measured by the Kistler brand 9257BA model dynamometer.

The milling conditions during the experiments are shown in Table 3.

**Table 1.** Technical specifications for pure polyamide.

Specification	Pure Polyamide (PA 6)
Density [ $\text{g}\cdot\text{cm}^{-3}$ ]	1.14
Upper operating temperature limit (short time) [ $^{\circ}\text{C}$ ]	160
The upper limit of operating temperature (long time) [ $^{\circ}\text{C}$ ]	85
Lower operating temperature limit [ $^{\circ}\text{C}$ ]	-40
Melting temperature [ $^{\circ}\text{C}$ ]	220
Yield strength [MPa]	76
Shear strength [MPa]	45
Elastic modulus [MPa]	3250
Elongation at break [%]	$\geq 50$
Elongation at yield [%]	4.5–20
Impact toughness (Izod, thickness 4 mm, 23 $^{\circ}\text{C}$ ) [ $\text{KJ}\cdot\text{m}^{-2}$ ]	5.5
Bending temperature (0.45 MPa) [ $^{\circ}\text{C}$ ]	125–175
Coefficient of friction	0.4
Volume resistance [Ohm-cm]	$\geq 10^{14}$
Surface resistance [Ohm]	$>10^{13}$
Thermal conductivity [ $\text{W}\cdot\text{m}^{-1}\cdot\text{K}^{-1}$ ]	0.28
Coefficient of thermal expansion [ $^{\circ}\text{C}^{-1}$ ]	$0.9 \times 10^{-4}$
Shore hardness D	66

**Table 2.** Technical specifications for carbon black reinforced polyamide.

Specification	Carbon black reinforced polyamide
Density [ $\text{g}\cdot\text{cm}^{-3}$ ]	1.25
Tensile strength [MPa]	68
Yield strength [MPa]	70
Elongation at break [%]	12
Elongation at yield [%]	8
Elastic modulus [MPa]	3100
Impact toughness (Izod, thickness 4 mm, 23 $^{\circ}\text{C}$ ) [ $\text{KJ}\cdot\text{m}^{-2}$ ]	6
Impact strength of the notch (according to Charpy, thickness 4 mm, 23 $^{\circ}\text{C}$ ) [ $\text{KJ}\cdot\text{m}^{-2}$ ]	6
Softening point (Speed A) [ $^{\circ}\text{C}$ ]	218
Softening point (Speed B) [ $^{\circ}\text{C}$ ]	188
Bending temperature (0.45 MPa) [ $^{\circ}\text{C}$ ]	104
Bending temperature (1.8 MPa) [ $^{\circ}\text{C}$ ]	59
Volume resistance [Ohm-cm]	$<50$
Surface resistance [Ohm]	$<10^4$
Casting shrinkage [%]	1.2–2.2
Shore hardness D	72

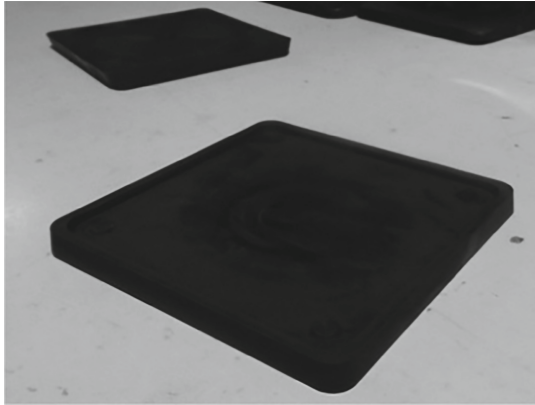


**Fig. 1.** Samples for carbon black reinforced polyamide.

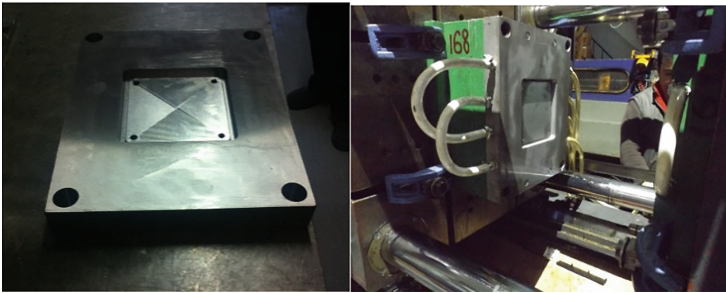


**Fig. 2.** Mold for samples.



**Fig. 3.** CNC machining centre.

**Table 3.** Milling parameters.

Rotational speed, n (rpm)	Cutting speed, V (m·min <sup>-1</sup> )	Feed, f (mm·rev <sup>-1</sup> )	Depth of cut, a (mm)
15000	377	0.05	2
17000	427	0.07	
21000	527	0.09	
23000	578	0.13	

## 4 Results

Based on the results of experiments conducted at the Yildiz Technical University Machining Laboratory, the influences of the selected milling parameters on cutting forces during high-speed milling of pure and carbon black reinforced polyamide materials are investigated. In Fig. 4, the machined slots are given. In Fig. 5 and Fig. 6, the cutting force results are given.

**Fig. 4.** Surface sample after milling.

As can be seen from Fig. 5 and Fig. 6, the cutting forces increased as the feed and cutting speed increased in milling of both polyamide materials [18]. Additionally, when comparing carbon black reinforced and pure polyamide materials, a more cutting force was needed to cut the pure polyamide material. This is because the black carbon reinforcement incorporated in the polyamide material facilitates the cutting process due to both the lubricant property of the carbon and the high thermal conductivity of the carbon black.

Also, it was observed that pure polyamide material could not be processed at the cutting speeds of 527 m/min and 578 m/min while performing experimental studies at high speeds. This is not the case with carbon black reinforced polyamide material. It was observed that the polymer was melted by the heat generated during the cutting process since the pure polyamide material is an insulator material. As the black carbon



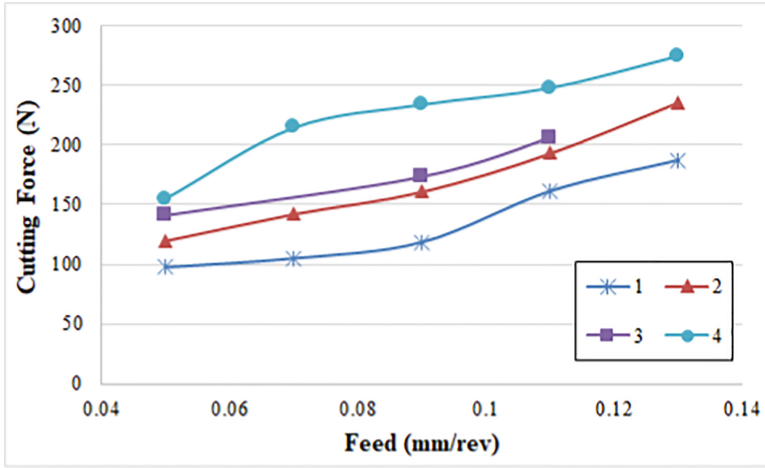


**Fig. 5.** Cutting force variation with feed-in milling of carbon black reinforced polyamide at the cutting speed of 1:  $377 \text{ m}\cdot\text{min}^{-1}$  (15000 rpm); 2:  $427 \text{ m}\cdot\text{min}^{-1}$  (17000 rpm); 3:  $527 \text{ m}\cdot\text{min}^{-1}$  (21000 rpm); 4:  $578 \text{ m}\cdot\text{min}^{-1}$  (23000 rpm).

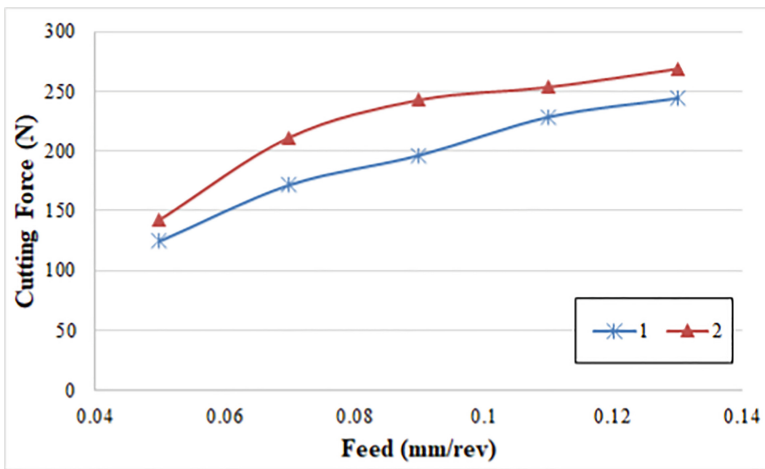


**Fig. 6.** Cutting force variation with feed-in milling of pure polyamide at the cutting speed of 1:  $377 \text{ m}\cdot\text{min}^{-1}$  (15000 rpm); 2:  $427 \text{ m}\cdot\text{min}^{-1}$  (17000 rpm).

reinforcement increased the thermal conductivity of the polymer material, we might conclude that this material was less affected by the heat generated in the cutting zone.

## 5 Conclusion

Carbon black reinforced polymer materials find many application areas, especially in the automotive and packaging industries. Although these materials can be mostly produced by plastic injection, the final process is machining operations. When the studies on both these materials and general-purpose polymer materials are examined, it is seen that the revolution speeds (cutting speeds) are selected low. However, in this experimental study, the cutting forces were investigated in high-speed milling of pure and carbon black reinforced polyamide materials at various cutting speeds and feeds. In this respect, the experimental study is the first. Based on the measurement results, the cutting forces increase as the cutting speed and feed increase in milling of both materials. Besides, it was seen that more cutting force was needed in milling of pure polyamide material as comparing black carbon reinforced and pure polyamide materials.

Further studies are expected to be carried out using cryogenic cooling in the machining of polymer materials to achieve a better and more efficient process.

## References




1. Tushar, U.J., Hemant, A.M.: Machining of plastics: a review. *Int. J. Eng. Res. General Sci.* **3** (2), 577–581 (2015)
2. Priyansh, P., Vijay, Ch., Kundan, P., Piyush, G.: Milling of polymer matrix composites: a review. *Int. J. Appl. Eng. Res.* **13**(10), 7455–7465 (2018)
3. Pulngern, T., Chitsamran, T., Chucheepsakul, S., Rosarpitak, V., Patcharaphun, S., Sombatsompop, N.: Effect of temperature on mechanical properties and creep responses for wood/PVC composites. *Constr. Build. Mater.* **111**, 191–198 (2016)
4. Chen, L., Zhang, K., Cheng, H., Qi, Z., Meng, Q.: A cutting force predicting model in orthogonal machining of unidirectional CFRP for entire range of fibre orientation. *Int. J. Adv. Manuf. Technol.* **89**, 833–846 (2017). <https://doi.org/10.1007/s00170-016-9059-5>
5. Kumaran, S.T., Kurniawan, R., Park, K.M., Byeon, J.H., Koilraj, J.K.M.: Review on the methodologies adopted to minimize the material damages in drilling of carbon fiber reinforced plastic composites. *J. Reinf. Plast. Compos.* **38**(8), 268–351 (2019)
6. Bhatnagar, N.: On the machining of fiber reinforced plastic (FRP) composite laminates. *Int. J. Mach. Tools Manuf.* **35**, 701–716 (1995)
7. Caggiano, A.: Machining of fibre reinforced plastic composite materials. *Materials* **11**(3), 442 (2018)
8. Uhlmann, E., Richarz, S., Sammler, F., Heitmüller, F., Bilz, M.: Machining of carbon fibre reinforced plastics. In: *New Production Technologies in Aerospace Industry - 5th Machining Innovations Conference*, pp. 19–24 (2014)
9. Khairurshima, M.K.N., Aqella, A.K.N., Sharifah, I.S.S.: Optimization of milling carbon fibre reinforced plastic using RSM. *Procedia Eng.* **184**, 518–528 (2017)
10. Karataş, M.A., Gökkaya, H.: A review on machinability of carbon fiber reinforced polymer (CFRP) and glass fiber reinforced polymer (GFRP) composite materials. *Def. Technol.* **14** (4), 318–326 (2018)
11. Sreenivasulu, R.: Optimization of surface roughness and delamination damage of GFRP composite material in end milling using Taguchi design method and artificial neural network. *Procedia Eng.* **64**, 785–794 (2013)

12. Guo, D.M., Wen, Q., Gao, H., Bao, Y.J.: Prediction of the cutting forces generated in the drilling of carbon-fibre-reinforced plastic composites using a twist drill. *Proc. Inst. Mech. Eng. Part B: J. Eng. Manuf.* **226**, 28–42 (2012)
13. Kishore, R.A., Tiwari, R., Rakesh, P.K., Singh, I., Bhatnagar, N.: Investigation of drilling in fibre-reinforced plastics using response surface methodology. *Proc. Inst. Mech. Eng. Part B: J. Eng. Manuf.* **225**, 453–457 (2012)
14. Rubio, J.C., Panzera, T.H., Abrao, A.M., Faria, P.E., Davim, J.P.: Effects of high speed in the drilling of glass whisker-reinforced polyamide composites (PA66 GF30): statistical analysis of the roughness parameters. *J. Compos. Mater.* **45**(13), 1395–1402 (2011)
15. Gaitonde, V.N., Karnik, S.R., Rubio, J.C., Abrao, A.M., Correia, A.E., Davim, J.P.: Surface roughness analysis in high-speed drilling of unreinforced and reinforced polyamides. *J. Compos. Mater.* **46**(21), 2659–2673 (2012)
16. Uysal, A., Altan, M., Altan, E.: Effects of cutting parameters on tool wear in drilling of polymer composite by Taguchi method. *Int. J. Adv. Manuf. Technol.* **58**(9–12), 915–921 (2012). <https://doi.org/10.1007/s00170-011-3464-6>
17. Ramesh, B., Elayaperumal, A., Satishkumar, S.: Drillability study of pultruded and sheet moulding compound thick polymeric composites. *Proc. Inst. Mech. Eng. Part B: J. Eng. Manuf.* **231**(2), 268–285 (2017)
18. Lazarevic, D., Madic, M., Jankovic, P., Lazarevic, A.: Surface roughness minimization of polyamide PA-6 turning by Taguchi method. *J. Prod. Eng.* **15**(1), 29–32 (2012)

# **Advanced Materials**



# Influence of Modifiers-Ligatures on the Properties of Cast Aluminum Alloy AK5M2 for the Automotive Industry

Kristina Berladir<sup>1</sup>(✉) , Tetiana Hovorun<sup>1</sup> , Oleksandr Gusak<sup>1</sup>,  
Yaroslav Reshetniak<sup>1</sup> , and Djanibek Khudaybergenov<sup>2</sup>

<sup>1</sup> Sumy State University, 2 Rymkogo-Korsakova St., Sumy 40007, Ukraine  
kr.berladir@pmtkm.sumdu.edu.ua

<sup>2</sup> MANGANROBOT S.r.L., Via Ala di Stura 67, 10148 Turin, Italy

**Abstract.** The paper analyzes the effectiveness of modifying aluminum alloys with active additives of microcrystalline alloys of different types. Production technologies have been developed, and the optimum amount of the most effective modifiers and active reinforcing additives for silumin made from recyclable materials has been determined; the connection of changes of structure with the parameters of mechanical properties of secondary silumin was established. It was found that the optimum amount of modifier-ligature Al-Ti5 was 0,1% by weight of liquid metal. Using more modifiers is not rational from the standpoint of materials science, economics, and ecology. The addition of such additive provided in the cast and heat-treated material an increase in the hardness by (20–30)% and tensile strength by (15–25)% due to the change in shape and dispersion of the formed intermetallic phases, reduction of porosity and increase in density. The use of non-deficient, cheap and environmentally friendly active additives in combination with traditional refining-modifying treatment can provide a significant increase in the properties of cast aluminum alloy products and are recommended for use in industry.

**Keywords:** Aluminium alloy · Silumin · AK5M2 · Modifiers · Ligature · Structure · Hardness · Tensile strength

## 1 Introduction

The continuous growth of aluminum alloy production is related to their widespread use due to their valuable mechanical, physical, and corrosion properties in different sectors of the world economy [1–4] (Fig. 1). This may lead to a shortage of aluminum in the global market, according to data [5] (Fig. 2).

The main driving force behind the increase in aluminum alloys production so far is the increase in their consumption in the transport sector, and especially in the automotive industry. Such parts of automotive as crankcase, cylinder blocks, cylinder heads, pulleys, etc. are produced from aluminum alloys (mainly silumin). That is why the need for light car body constructions, lightweight suspension components, and engines determines progress in the development of new casting technologies and alloys that adapted to processes such as low and high-pressure casting, thixo- and rheocasting.

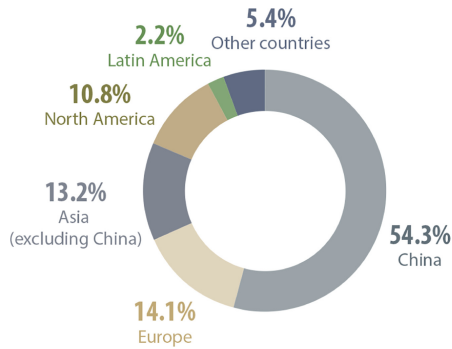


Fig. 1. The largest world consumers of aluminum [1].

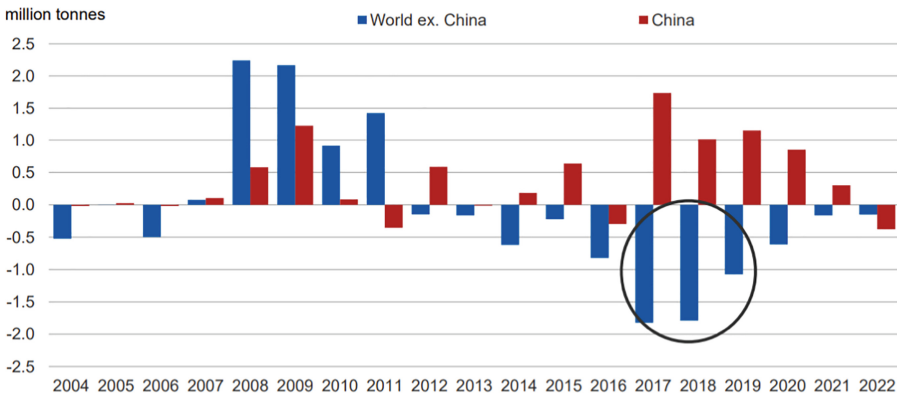
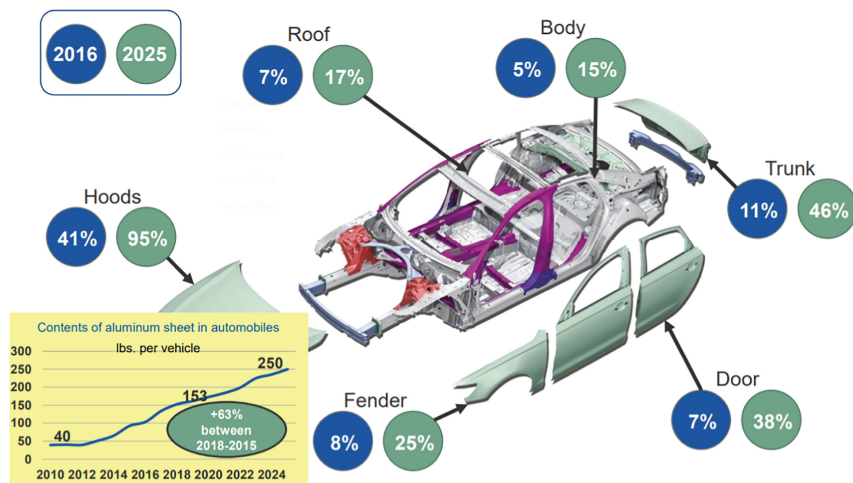


Fig. 2. Aluminum market balance [5].

The problem of increasing the mechanical and operational properties of cast aluminum alloy products – silumin remains relevant in the theory and practice of foundry production. It is particularly necessary to highlight the problem of obtaining aluminum alloys from waste and scrap of machine-building enterprises, the so-called secondary alloys.

## 2 Literature Review

The main consumer of secondary silumin is the automotive industry. Automobile companies are continually working to increase the use of aluminum alloys in the design of the car [5] (Fig. 3). This is due to several fundamental reasons: it reduces the weight of the vehicle, which reduces fuel consumption; aluminum alloy wastes are completely recycled without polluting the environment. The problem of improving the quality of aluminum alloys is relevant for all developed countries [6–9].



**Fig. 3.** The dynamics of the use of aluminum alloy products in automobiles [4].

One way to solve such problems is modification – the process of influencing the crystallization and structure of the material by introducing special additives-modifiers [10–14].

Despite the widespread use of ligatures for modification, there is no single set of quality requirements. Recent work in the field of structural heredity in the system «charge-melt-cast product» showed that the structure of the ligature has a significant impact on the crystallization process, structure, and properties of the modified alloy [15].

One of the strongest modifiers of dendrites of the  $\alpha$ -solid solution is titanium and boron. When hit by a melt, they form the ultrafine intermetallic compounds  $AlB_2$ ,  $TiB_2$ ,  $TiAl_3$ ,  $ZrAl_3$ , which are crystallization centers. Since these elements have a high melting point, in practice, they are introduced into the melt or in the form of aluminum ligatures or the form of complex salts of type  $K_2TiF_6$ ,  $KBF_4$ ,  $K_2ZrF_6$  [16].

Additives of Ti (up to 1,7%) or B (up to 0,07%) in the casting alloys of  $AlSiCu$  cause the grinding grain and reduction of interdendritic distances. An important point in improving the efficiency of modifying ligatures is not only the chemical composition but also the method of obtaining and further processing them. Thus, the production of Al-B-Ti ligatures in the self-propagating high-temperature synthesis (SHS) allows reducing the nucleation phase. Al-Sr-Ti-B and Ni-Cr-Al-Ti ligatures are offered as complex modifiers acting on the dendrites of  $\alpha$ -solid solution and eutectic. Moreover, the use of nanopowders for their production instead of fusing the usual way ligatures several times increases the mechanical properties [17].

The results of numerous studies [18–23] allow us to conclude that the effectiveness of modifying ligatures should be determined not only by their composition but also by the method of their production.

The influence of modifying and complex processing of the AK6M2 melt was investigated by the authors [24] with the use of fine-grained modifiers and refining fluxes. Applied modifiers were  $AlSr_{10}$ ,  $AlTi_5$ , and  $AlTi_5B_1$ . The content of Sr and Ti

varied in the range of 0,01–0,02%. In some cases, the melt was treated with fluxes. The greatest modification effects were achieved with the addition of 0,02% Sr (roll and deformed AlSr10 ligatures) and 0,02% Ti (AlTi5 roll ligatures). The best results are obtained on an alloy modified with AlTi10 industrial ligatures in combination with Arsal 2120 flux and AlSr10 without flux. The use of ligatures obtained by special processing methods can reduce their costs when modifying aluminum-silicon alloys by 2–3 times.

Therefore, the main aim of the research is to develop scientific and technological fundamentals for the formation of secondary silumin; to increase the performance of their mechanical and operational properties in the cast and heat-treated states to the level of primary alloys.

### 3 Research Methodology

AK5M2 is a popular aluminum alloy that has low cost, durability, and relative plasticity. The alloy belongs to the group of Al-Si-Cu system, with good plasticity and high enough hardness, and it is used for the manufacture of carburetor housings, fuel pumps, various types of covers, small nozzles, etc. The main characteristics of the material are given in Table 1 and Table 2 (according to DSTU 2839-94 (GOST 1583-93)).

**Table 1.** The chemical composition of the material AK5M2 (wt%)

Fe	Si	Mn	Ni	Ti	Al	Cu	Mg	Zn	Impurities
Up to 1,3	4–6	0,2–0,8	Up to 0,5	0,05–0,20	85,90–94,05	1,5–3,5	0,2–0,8	Up to 1,5	All 2,8

**Table 2.** The main properties of the material AK5M2

Indicator	Value
Short-term tensile strength, MPa	118–206
Elongation, %	0,5–2,0
Brinell hardness, MPa	65–75

The investigated alloys were obtained in industrial production by melting scrap and non-ferrous metal waste in accordance with DSTU 3211-95. When casting into the mold, the temperature of the alloy was  $750 \pm 10$  °C. The modification was performed by introducing Al-Ti5 ligatures (Table 3) over a wide concentration range.

**Table 3.** The chemical composition of the Al-Ti5 ligature (wt%)

Ti	Fe, max.	Si, max.	V, max.	Other, max.
4,5–5,5	0,40	0,30	0,30	0,05



Upon receipt of the ligature, the content of Al-Ti ligatures was 0; 0,05; 0,10 and 0,15%. In the Al-Ti ligature used in the form of a bar, titanium is contained in the form of the intermetallic compound  $Al_3Ti$ , which is in the form of block inclusions, evenly distributed in the matrix of pure aluminum. The specific density of the ligature is  $\rho = 2,5 \text{ g/cm}^3$ . The introduction of a small amount of titanium into aluminum and its alloys is a traditional method of reducing grain. Titanium is best introduced into ligature in aluminum-based alloys in the form of ingots or bars for continuous feeding into the pouring chute of the furnace.

Technology for the introduction of ligatures in silumin AK5M2:

1. Removal of scale from the surface of the melt.
2. Adding ligature to the silumin melt at normal operating temperature (720–740 °C).
3. Thorough mixing of the melt to ensure uniformity and complete absorption of the alloying element.

Control of the chemical composition was carried out continuously at all stages of the process of obtaining aluminum alloys.

After obtaining silumin to improve their properties for samples without additives and with active additives, the following heat treatment was carried out:

1. Annealing – at a temperature of 400 °C with cooling in a furnace to 200 °C, then – in the air to room temperature. The exposure time is 2 h.
2. Quenching – at  $(525 \pm 5)$  °C with cooling in water. Exposure time is an hour;
3. Tempering – at  $(175 \pm 5)$  °C. Exposure time is 4–5 h.

The obtained cylindrical blanks were honed, micro-grinders were prepared, and then mechanical tests and microstructure tests were performed.

Metallographic analysis of the structure was performed on MIM-7 and MIM-8 microscopes at 200-fold magnification, as well as by high-resolution metallography on a Tescan-VEGA 3 scanning electron microscope.

The microstructure of the alloys was studied on sanding molds and after heat treatment without etching, as well as after etching with Keller's reagent composition: HCl – 1,5 mL; HF – 1 mL;  $HNO_3$  – 2,5 mL;  $H_2O$  – 95 mL, which is used for nonferrous alloys.

The strength and plasticity of the alloys were determined on samples with a diameter of 10 mm and a working length of 50 mm, made according to DSTU 2839-94 (GOST 1583-93).

## 4 Results

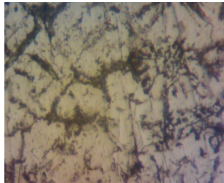
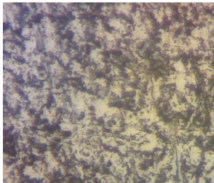
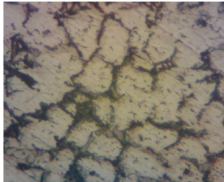
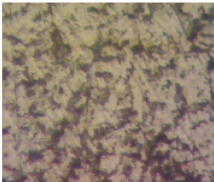
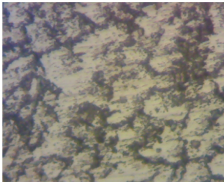
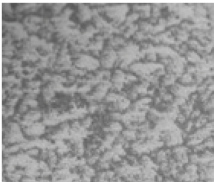
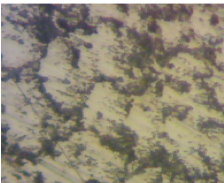
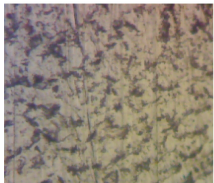
In this work, we investigated the structure and properties of the aluminum cast alloy AK5M2 (silumin) in its original and modified state; cast and heat-treated state.

**4.1 Study of Microstructure**

The study of the microstructure of the samples is shown in Table 4 and Fig. 4. The main structural components of the pre-eutectic silumin of the Al-Si-Cu system, which are melted from primary metals, are the primary crystals of a solid aluminum solution  $Al_\alpha$  and the double eutectic  $Al_\alpha + Si$ . In secondary silumin, which almost always contain significant amounts of iron and copper, double eutectic is rare.

The microstructure of the original pre-eutectic silumin AK5M2 (Table 4) consists of a solid solution of silicon in aluminum and eutectic, in which silicon is in the form of coarse needle and plate inclusions. There are also intermetallic phases that correspond to the literature data [25].

**Table 4.** The structure of the secondary alloy AK5M2 + Ti-Al, x200

The content of the modifier, wt. %	The state of the alloy	
	cast	heat treated
0		
0,05		
0,10		
0,15		

No less promising a way to further increase of the strength, heat and corrosion resistance and other operational and technological characteristics by alloying aluminum alloys with metals that are insoluble or practically insoluble in solid aluminum, but forming different intermetallic compounds ( $\text{Al}_6\text{Mn}$ ,  $\text{Al}_3\text{Ti}$ ,  $\text{Al}_3\text{Zr}$ ,  $\text{Al}_3\text{Ni}$ ,  $\text{Al}_3\text{Fe}$ , etc.) [26].

In this regard, modification of such alloys is aimed at grinding eutectic silicon. In the AK5M2 alloy, after the introduction of the modifying particles, there is redistribution of structural components and dispersion of eutectic silicon (Table 4). The needles of eutectic silicon ground and become a more compact rounded shape, reducing the size of the dendrites of the  $\alpha$ -solid aluminum solution, which agrees well with the data [27].

When alloy modification is 0,05; 0,1; 0,15% (wt.) The ti-al structure has become finely dispersed and finely differentiated (Table 4); this is explained by the grain score, which was determined according to GOST 5639-82. The main task of titanium in the alloy is the grinding of the grain in castings, which significantly improves the strength and uniformity of properties throughout the volume. Particles of eutectic silicon have diminished in size, becoming compact in planar and skeletal shape. The releases of iron-containing phases were evenly spaced along the section of the grinder. A further increase in the number of modifiers affected the coarseness of the structure and the increase in the size of eutectic grains. The iron-containing phases were encountered in the form of plates that reached considerable sizes and focused on specific sections of the grinder.

We have observed an active change of structure during the processing. It was accompanied by a decrease in the size of the selection fields of  $\alpha$ -solid silicon solution in aluminum and the grinding of complex intermetallic phases, a decrease in their average parameter of the form  $\lambda c$  (ratio of the maximum length of inclusions to their width) while increasing the dimension (Table 4). When the content of 0,05% Al-Ti grain score before heat treatment was 3–4, after heat treatment – 4–5; at 0,1% before heat treatment – 4–5, after heat treatment was 6–7; at 0,15% before heat treatment – 3–4, after heat treatment was 5–6, respectively.

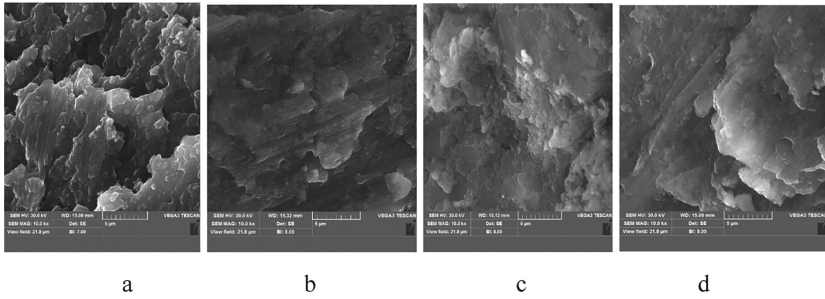
The duration of the treatment process was 5–10 min and it depends on the volume of liquid metal. During the processing, an active change of structure was noted. On the example of the secondary alloy AK5M2 dependencies of influence of the quantity of the modifier on the properties and the parameter of the form of inclusions in the cast state and after heat treatment (Fig. 4) according to the proposed model are established.

The obtained data allowed to optimize the amount of modifier at the level of 0,10% by weight of liquid metal.

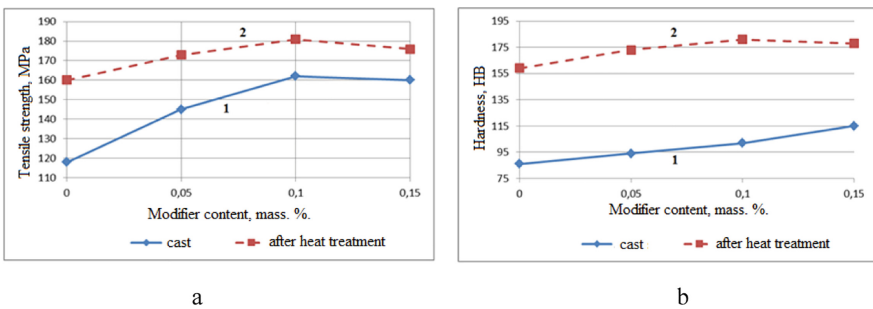
## 4.2 Determination of Properties

Figure 5 shows the dependences of the mechanical properties of secondary silumin AK5M2 on the concentration of the Ti-Al modifier.

The experiment found that the value of the optimal additive modifier-ligature Ti-Al for processing secondary silumin AK5M2, obtained by traditional technology with the level of mechanical properties corresponding to the primary according to DSTU 2839-94 (GOST 1583-93), was 0,1% by weight of liquid metal.



**Fig. 4.** Microstructures performed using Tescan-VEGA 3 REM: a, b – AK5M2; c, d – AK5M2 + Ti-Al (0,10%); a, c – cast; b, d – heat treated.



**Fig. 5.** Effect of Ti-Al modifier on mechanical properties of secondary alloy AK5M2: 1 - in the cast state; 2 - after heat treatment.

This active additive provided in the heat-treated material a hardness increase of 1,5–1,8 times compared to the cast and 1,2–1,3 times compared to the heat-treated without the addition of Ti-Al (Fig. 5, b), the tensile strength is increased by 1,15–1,25 times in comparison with the cast and in 1,1–1,2 times compared to heat-treated without adding Ti-Al (Fig. 5, a). Even without heat treatment, the addition of the ligature increases the hardness and tensile strength of secondary silumin AK5M2 by 1,2–1,4 times (Fig. 5). This is due to the change in the form and dispersion of the intermetallic phases, increasing the density and reducing the porosity.

Increasing the level of mechanical properties provided refining-modifying action of the components included in the modifier. Grinding the grain of a solid solution of silicon in aluminum was achieved due to the presence in the modifier of titanium, which in the melt formed refractory dispersed particles of intermetallic  $TiAl_3$ , thus providing a sufficiently large number of additional centers of crystallization.

The modified AK5M2 cast aluminum alloy with the optimum amount of 0,1% Ti-Al alloy modifier was introduced at the production of RELIT LLC, which proves the high efficiency of the proposed technological solutions.

## 5 Conclusions

1. It is shown that improving the quality of AK5M2 silumin obtained from 100% recyclable material to the level of primary, possibly due to the use of modifying ligatures.
2. It was found that the optimum amount of Ti-Al ligature modifier is 0,1% by weight of liquid metal. Using more modifiers is not rational from the standpoint of materials science, economics, and ecology.
3. The addition of the specified modifying ligature provided in the cast and heat-treated material increases hardness by (20–30)% and tensile strength - by (15–25)% due to the change in shape and dispersion of the formed intermetallic phases, porosity reduction, and density increase.

## References

1. Aluminum facts. <https://www.nrcan.gc.ca/our-natural-resources/minerals-mining/minerals-metals-facts/aluminum-facts/20510>. Accessed 13 Oct 2019
2. Vakulenko, I.A., Nadezhdin, Y.L., Sokirko, V.A., et al.: Electric pulse treatment of welded joint of aluminum alloy. *Sci. Prog. Transp. Bull. Dnipropetrovsk Natl. Univ. Railway Transp.* **4**(46), 73–82 (2013)
3. Hovorun, T.P., Berladir, K.V., Pererva, V.I., Rudenko, S.G., Martynov, A.I.: Modern materials for automotive industry. *J. Eng. Sci.* **4**(2), F8–F18 (2017). [https://doi.org/10.21272/jes.2017.4\(2\).f8](https://doi.org/10.21272/jes.2017.4(2).f8)
4. Telang, A.K., Rehman, A., Dixit, G., Das, S.: Alternate materials in automobile brake disc applications with emphasis on Al composites – a technical review. *J. Eng. Res. Stud.* **1**(1), 35–46 (2010)
5. Aluminium Market Outlook... trade rises to top of the agenda. [https://cdn.ymaws.com/www.aec.org/resource/resmgr/Annual\\_Meeting/Materials/3\\_FRI\\_Wittbecker\\_180316\\_AEC\\_pdf](https://cdn.ymaws.com/www.aec.org/resource/resmgr/Annual_Meeting/Materials/3_FRI_Wittbecker_180316_AEC_pdf). Accessed 12 Oct 2019
6. Pietrowski, S., Gumieny, G., Pisarek, B., Wladysiak, R.: Kontrola produkcji wysokojakosciowych stopow odlewniczych metoda ATD. *Archiwum technologii maszyn i automatyzacji* **24**(3), 131–144 (2004)
7. Lipinski, T.: Improvement of mechanical properties of AlSi7 Mg alloy with fast cooling homogeneous modifier. *Arch. Foundry Eng.* **8**(1), 85–88 (2008)
8. Lyutova, O.V.: Improving the casting properties of secondary aluminum alloys. *Sci. Prog. Transp. Bull. Dnipropetrovsk Natl Univ. Railway Transp.* **3**(45), 53–59 (2013)
9. Santhosh, M.S., Sasikumar, R.: Influences of aluminium/E-glass volume fraction on flexural and impact behaviour of GLARE hybrid composites. *J. Eng. Sci.* **6**(1), C6–C10 (2019). [https://doi.org/10.21272/jes.2019.6\(1\).c2](https://doi.org/10.21272/jes.2019.6(1).c2)
10. Klyszewski, A., Lech-Grega, M., Szymanski, W., Zelechowski, J.: The structure and properties of sheets made from aluminium and aluminium alloys for use in transport industry. In: *Proceedings of IX International Conference «Aluminium in Transport»*, pp. 203–217. Institute of Non-Ferrous Metals, Cracow, Tomaszowice (2013)
11. Hovorun, T.P., Pylypenko, O.V., Hovorun, M.V., Dyadyura, K.O.: Methods of obtaining and properties of wear-resistant coatings Ti and N and Ti, Al and N. *J. Nano Electron. Phys.* **9**(2), 02026-1–02026-7 (2017). [https://doi.org/10.21272/jnep.9\(2\).02026](https://doi.org/10.21272/jnep.9(2).02026)

12. Degula, A.I., Govorun, T.P., Kharchenko, N.A., Khyzhnyak, V.G., Karpets, M.V., Myslyvchenko, O.M., Smetanin, R.S.: Investigation of phase and chemical composition of complex carbide coatings. *Metallofiz. Noveishie Tekhnol.* **37**(11), 1461–1476 (2015)
13. Budnik, A.F., Rudenko, P.V., Berladir, K.V., Budnik, O.A.: Structured nanoobjects of polytetrafluoroethylene composites. *J. Nano Electron. Phys.* **7**(2), 02022-1–02022-9 (2015)
14. Berladir, K., Gusak, O., Demianenko, M., Zajac, J., Ruban, A.: Functional properties of PTFE-composites produced by mechanical activation. In: Ivanov, V., et al. (eds.) *Advances in Design, Simulation and Manufacturing II. DSMIE-2019. Lecture Notes in Mechanical Engineering*, pp. 391–401. Springer, Cham (2020). [https://doi.org/10.1007/978-3-030-22365-6\\_39](https://doi.org/10.1007/978-3-030-22365-6_39)
15. Boyko, V., Prach, O.L., Trudonoshyn, O.I., Mykhalekov, K.V.: Eutectic spheroidization in Al-7Mg-3Si casting alloys during solution treatment. In: 16th International Scientific and Technical Conference of Non-Ferrous Metal Casting «Science and Technology», Krakow, pp. 21–27 (2013)
16. Volochko, A.T., Korolev, S.P., Galushko, A.M., Shegidevich, A.A.: Analysis of the structure formation of silumins. In: *Proceedings of the National Academy of Sciences of Belarus. Physico-Technical Series*, vol. 3, pp. 18–25 (2013)
17. Volochko, A.T.: Modification of eutectic and primary silicon particles in silumins. *Dev. Prospects Cast. Metall.* **4**(81), 38–45 (2015)
18. Material Qualification in the Automotive Industry. <https://www.cargroup.org/publication/material-qualification-in-the-automotive-industry-2/>. Accessed 12 Oct 2019
19. Surappa, M.K.: Aluminium matrix composites: challenges and opportunities. *Sadhana* **28**(1–2), 319–334 (2003)
20. Mityayev, A.A., Volchok, I.P., Frolov, R.A., Loza, K.N., Gnatenko, O.V., Lukinov, V.V.: Complex modification of secondary silumins. *Sci. Prog. Transp. Bull. Dnipropetrovsk Natl Univ. Railway Transp.* **6**(54), 87–96 (2014)
21. Tian, X., Zhu, A., Wei, J., Han, R.: Preparation and forming technology of particle reinforced aluminum matrix composites. *Mater. Sci.: Adv. Compos. Mater.* **1**(1), 1–9 (2017)
22. Sudnik, L.V., Rudnitskiy, K.F., Rudnitskiy, F.I., Nikolaychik, Yu.A.: Management of the formation of the structure of cast alloys in the process of recycling metal waste. *Cast. Metall.* **1**, 32–36 (2015)
23. Demchenko, M.V., Gaponova, O.P., Myslyvchenko, O.M., Antoszewski, B., Bychenko, M. M.: Microstructure and properties of AlCrFeCoNiCux high-entropy alloys. *J. Eng. Sci.* **5**(1), C11–C15 (2018). [https://doi.org/10.21272/jes.2018.5\(1\).c3](https://doi.org/10.21272/jes.2018.5(1).c3)
24. Nikitin, K.V., Nikitin, V.I., Timoshkin, I.Y., Krivopalov, D.S., Chernikov, D.G.: Hereditary influence of the structure of charge materials on the density of aluminum alloys of the Al-Si system. *Russ. J. Non-Ferrous Metals* **56**(1), 20–25 (2015)
25. Shportko, A.Yu., Mazur, V.I., Slukhovskiy, O.I.: The effect of thermal treatment of the Al-10.6% Si melt on the short-range order parameters of the liquid phase. *Message 2. Theory Pract. Metall.* **3**, 48–52 (2005)
26. Yelagin, V.I.: Ways of development of high-strength and heat-resistant structural aluminum alloys in the XXI century. *Metall. Heat Treat. Metals* **9**, 3–11 (2007)
27. Mavhungu, S.T., Akinlabi, E.T., Onitiri, M.A., Varachia, F.M.: Aluminum matrix composites for industrial use: advances and trends. *Procedia Manuf.* **7**, 178–182 (2017)



# Influence of Surface Hardened Nanocrystalline Layers on the Resistance of Contact Fatigue Destruction

Volodymyr Gurey<sup>(✉)</sup>  and Ihor Hurey 

Lviv Polytechnic National University, 12, Bandera St., Lviv 79013, Ukraine  
vgurey@gmail.com

**Abstract.** The conducted research has shown that in the process of frictional treatment of test-pieces made of Steel 40NiCr6 and Steel CT80 after hardening and low-temperature tempering, a hardened nanocrystalline layer is formed on the surface layer. The grain size of the hardened surface layer was 20–60 nm near the treated surface. The value of a hardened layer's TEF that allows us to estimate the thermodynamic state of the metal was determined. After friction treatment, the residual compression stresses are formed in the hardened layer.

Experiments have shown that in the case of frictional treatment, the shape of the working surface of the tool significantly affects the nature of the redistribution of residual stresses of the first kind. Thus, when hardening the Steel 40NiCr6 test-pieces, residual compression macrostresses occur in the hardened and low-temperature tempered state. The conducted research has shown that frictional treatment increases the resistance to fatigue destruction during contact loading. Thus, the increase in the durability of Steel CT80 after frictional treatment reaches 1.6...1.8 times compared to unhardened test-pieces. The crack is formed in the area of tensile loads and passes through the base metal.

**Keywords:** Nanocrystalline layer · Friction hardening · Residual stress · Contact fatigue

## 1 Introduction

The performance of the machine parts depends on the physical and mechanical characteristics and the condition of the surface and surface layer of the metal. In the surface layers, under various load schemes (bending, contact, wear), the highest stresses occur. The thermodynamic state of the surface becomes more non-equilibrium under the influence of a corrosive medium. The surface of machine parts is weakened by various stress concentrators. These are marks, structural concentrators, cracks, corrosion centers, scores, etc. Under cyclic loading, these concentrators intensify the fatigue processes in the surface layer of the material. During the manufacture of machine parts, it is necessary to ensure optimal surface quality parameters, such as roughness, macro and microstructure of the material, hardness, magnitude and signs of residual macro stresses, and others. They are obtained by applying various methods of surface hardening of machine parts [1].

The durability of many products is determined by the resistance of the surface layers to destruction during the contact interaction of the work surfaces of the conjugated parts. Such parts, which operate in the conditions of contact interaction, include bearings, gear teeth, rollers, and others. Destruction during alternating, shock and contact load usually begins with the surface layer of metal. A distinctive feature of contact fatigue destruction is localization with high-stress gradients in relatively small volumes of parts' surface layers. They can exceed the elastic limit and lead to the building of cracks. The quality of the metal's surface layer significantly affects the performance of the products during operation [2].

## 2 Literature Review

Durability during contact loading is significantly influenced by surface stereometry (surface roughness, marks, scratches, etc.). They are stress concentrators in which fatigue stresses accumulate [3]. Stress concentrators become the source of the surface cracks grid formation, which then propagates into the depth of the metal surface layer and leads to the formation of pitting which damages the conjugated surface of the contacting parts from the contact load [4].

The grain size, structure, chemical composition, and hardness of the surface layer of the conjugated surfaces of the contacting parts are also significantly influenced by the fatigue load process [5].

It is known that residual stresses formed in the surface layer of the metal affect the durability of the product during operation [6]. Residual stresses in the surface layers of the products' work surfaces are formed during the finishing methods of treatment. Residual compression macrostresses increase durability, and tensile stresses - on the contrary - reduce it [7]. The formation of the magnitude, pattern, and depth of arrangement of residual stresses is influenced by many factors, and namely by plastic deformation of the surface layer (its intensity and magnitude), temperature in the processed area, phase and structural transformations that occur during surface treatment [8].

During contact fatigue loading, the surface layers obtain a complex load [9]. Therefore, not all surface treatments and hardening methods used to increase durability during friction are effective and suitable during fatigue, and especially contact fatigue loading [10].

Hardened nanocrystalline white layers are quite effective for increasing durability during friction [11]. The influence of hardened layers on fatigue during contact loading has not been studied sufficiently. Hardened nanocrystalline layers have a higher hardness than the main metal; the question is whether the surface layer will be exfoliated during contact loading [12].

Therefore, the purpose of this research is to study the effect of a hardened nanocrystalline layer on the fatigue strength during contact loading.



### 3 Research Methodology

During the contact of the hot needle with the metal, temperature-electromotive force (TEF) is formed, the value of which depends on the physical properties of the material of the investigated needles and metal. The determination of microTEF is carried out by the following method: the needle is made of tungsten because it has stable physical properties in the temperature range 20–150 °C, high hardness to obtain a sharply pointed needle, low thermal conductivity, is not oxidized at the temperature of experiments. The needle temperature was constant and equal to  $65 \pm 5$  °C. The contact temperature of the needle and test metal was monitored using a platinum sample. The temperature-electromotive force of tungsten relative to platinum is  $E_{W-Pt} = 11,2 \mu\text{V/K}$ . The tungsten needle with the heater was installed at the location of the indenter on the PMT-3 microhardness tester. MicroTEF was determined by the potentiometric method [13].

Residual stresses were determined on cylindrical test-pieces with a diameter of 20 mm and a length of 150 mm after frictional hardening. The strain gauges were bonded only on one side of test-pieces. Before the measurement, strain gauges were calibrated and a calibration curve was determined. In sequential removal of thin layers  $\delta_1, \delta_2, \delta_3, \dots, \delta_n$ , using electrochemical etching, on the opposite surface of the test-piece the magnitude of deformation was determined. One half of the workpiece was given a coat of waterproof lacquer to provide etching on one side only. Electrochemical etching was carried out at a current density of  $I = 5 \text{ A/dm}^2$  at a constant speed. During the etching, electrolyte stirring was observed and, after a delay, the deformation was measured. The residual stresses were determined from the deformations occurring in the cylindrical test-piece after frictional hardening.

Studies of resistance to fatigue destruction during contact loading were performed on circular test-pieces with a 35 mm diameter made of Steel 40NiCr6 and Steel CT80 after hardening and low-temperature tempering on three-roller equipment. External pressure rollers with a 50 mm diameter and 8 mm radius of the contact surface were located at an angle of 120° to each other and, using a special device, were pressed against the test-piece (Fig. 1). This design of the device provided an even clamping of each roller to the test-piece, and contact loads were not transmitted to the spindle bearings. The pressure rollers were made of 100Cr6 EN steel after hardening and low-temperature tempering (hardness 61–63HRC). The rotation was provided to the test-piece at a frequency of  $50 \text{ s}^{-1}$ , and the pressure rollers rotated freely in the bearings. The studies were performed using mineral oil.

The working parts of the test-pieces were hardened by friction treatment. The friction treatment of the test-pieces was carried out on a special device mounted on a lathe. Mineral oil containing active additives was used as the process medium [14]. Two different discs made of stainless steel were used as a tool for friction treatment. One disc had a smooth working surface; the other one had multi-directional grooves on the working surface [15]. The roughness of the test-pieces' working surfaces after friction treatment was  $R_a = 0.25\text{--}0.56 \mu\text{m}$ , after grinding it was  $R_a = 0.50\text{--}0.63 \mu\text{m}$ .

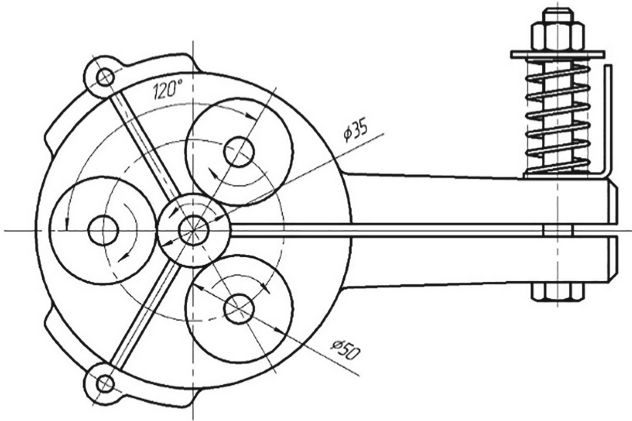


Fig. 1. Equipment for the study of fatigue resistance.

## 4 Results

Metallographic examinations have shown that, after frictional treatment, a hardened (white) layer with a nanocrystalline structure is formed in the surface layers of test-pieces made of Steel 40NiCr6 and Steel CT80. The thickness of the hardened layer and its microhardness depend on the treatment modes, the shape of the tool's working part, the carbon content in the steel, as well as the preceding thermal processing of the test-pieces.

After friction treatment of the test-pieces made of Steel 40NiCr6 with a tool with a smooth working part, the thickness of the hardened layer was 170–190  $\mu\text{m}$ , and its microhardness was 7.6 GPa. The microhardness of the original structure was 5.5 GPa. After friction treatment with a tool with multi-directional grooves on the working part, the thickness of the hardened layer was 200–220  $\mu\text{m}$ , and its microhardness increased to 8.6 GPa (Fig. 2).

With the increase of carbon content in the steel, the quality of the hardened layer improves greatly. The highest quality of the hardened layer was obtained on eutectoid Steel CT80. As metallographic examinations of test-pieces made of Steel CT80 showed, the thickness of the hardened layer reaches 250–280  $\mu\text{m}$  after friction treatment with a tool that had a smooth working surface. The formed white layer is homogeneous, and its microhardness is 9.1 GPa against 6.6 GPa in the original structure. Hardening with the tool which has grooves increases the thickness of the white layer up to 300  $\mu\text{m}$  and the microhardness up to 11 GPa.

X-ray analysis showed that the grain size of the hardened surface layer was 20–60 nm near the surface with a smooth transition to the base material structure in deeper layers. The structure of the obtained hardened surface layer after friction hardening is a nanocrystalline one.

During the contact load, in addition to the normal pressure force, tangential forces act, which try to move one of the surfaces relative to the other. The presence of a tangential force is reflected in the contact zone stress distribution. When the roller

touches the test-piece - it mimics the work of the rolling bearings - a complex system of tangent forces is created on the working surface, which creates the corresponding elastic micro-movements. Such phenomena severely change the distribution of stresses in the metal and contribute to the increase of tensile stresses. A thin layer of metal - which is plastically deformed by the previous load - has residual compression stresses, and tensile stress occurs in the layer below it. As a result of such actions, the surface layers are uplifted, the material density changes and a subsurface crack is formed, which mainly turns into pitting. Non-metallic inclusions, carbide liquation and heterogeneity of structure are sources of stress concentration that contribute to accelerating the formation of subsurface cracks and pitting.

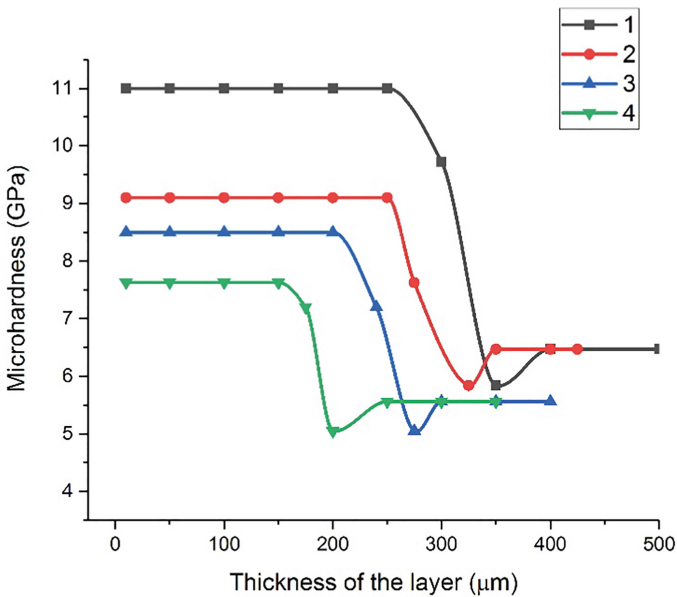


**Fig. 2.** Microhardness of the hardened layer obtained in Steel CT80 (1, 2) and Steel 40NiCr6 (3, 4) after friction hardening: 1, 3 – disk (tool) with multi-directional grooves on the working surface; 2, 4 – disk (tool) with a smooth working surface.

It is known that the value of Temperature-Electromotive Force (TEF), allows us to estimate the thermodynamic state of metal caused by a change in mainly chemical and phase composition [10]. So, for example, if concerning tungsten, the TEF of the ferrite phase is positive, then it is negative concerning austenite and graphite. It is shown that the stresses shift the TEF only to the positive side, and the stronger the greater their magnitude. The given data show the possibility of applying the TEF measurement method to control the degree of plastic deformation in various methods of metal hardening, and to evaluate changes in the structure and phase composition of the metal.

The studies have shown that the highest TEF value was registered in steel with low carbon content and in an equilibrium state. After frictional treatment, the TEF shifts to

the negative side; this indicates an increase in carbon in the surface layer of steel and a change in its phase composition (increase in the amount of residual austenite). Steel quenching shifts the TEF to the negative side.

Experiments have shown that the TEF value of the hardened nanocrystalline white layer is much smaller than that of the original metal. With the increase of carbon in the steel, as well as after quenching, the TEF value decreases. The TEF value of the white layer obtained on Steel CT80 goes down much more to the negative side than on the white layer on Steel 40NiCr6. The change of the TEF parameter both of the base steel and the white layer correlate completely with the change in the carbon content and residual austenite in the metal. The more residual austenite and carbon is in the metal, the lower the TEF parameter. This indicates a significant difference between the white layers obtained on different steels, which correlates well with the microhardness, the carbon content in the white layer, and the phase composition (Fig. 3).

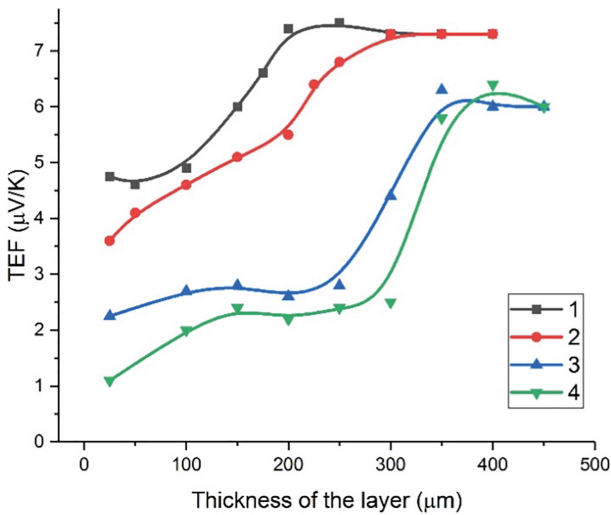


**Fig. 3.** Temperature-Electromotive Force (TEF) of the hardened layer obtained on Steel 40NiCr6 (1, 2) and Steel CT80 (3, 4) after friction hardening: 1, 3 – disk (tool) with a smooth working surface; 2, 4 – disk (tool) with multi-directional grooves on the working surface.

In the case of friction treatment, in the surface layers, a hardened white layer with a nanocrystalline structure is formed; the layer consists of highly dispersed martensite, residual austenite, and very dispersed carbides. Martensite has a higher specific volume than perlite, ferrite or austenite. In addition, the martensite in the white layer is very fragmented and has a higher volume than the martensite of hardening. Therefore, in the white layers, mainly compressive residual stresses of the first kind appear.

Experiments have shown that, in the case of frictional treatment, the shape of the working surface of the tool significantly affects the nature of the redistribution of residual stresses of the first kind. Thus, when hardening the Steel 40NiCr6 test-pieces,

residual compression macrostresses occur in the hardened and low-temperature tempered state. After hardening with a tool which has grooves on the working plate, the residual stresses extend to a greater depth and have a greater magnitude compared to the stresses obtained after hardening with a tool which has a smooth working surface. The largest amount of residual stress is formed near the surface. With the increase of the depth, the residual stresses decrease, then reverse the sign and become tension stresses. It should be noted that the change in the sign of stress occurs at a depth greater than the hardened layer, i.e. at the base metal. The same pattern is observed with the hardening of Steel CT80 (Fig. 4).

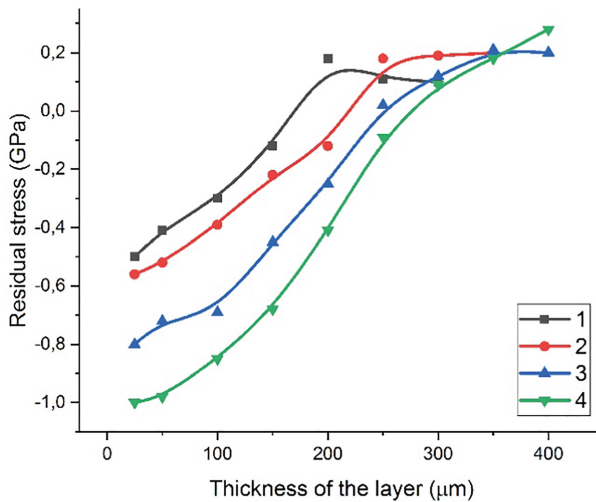


**Fig. 4.** Residual stress of the hardened layer obtained on Steel 40NiCr6 (1, 2) and Steel CT80 (3, 4) after friction hardening: 1, 3 – disk (tool) with a smooth working surface; 2, 4 – disk (tool) with multi-directional grooves on the working surface.

In cases of frictional hardening using the tool with grooves on the working part, an intensive shear sign-changing deformation of the surface layer of metal takes place, and it extends to a greater depth than when the tool with a smooth working part is used. Therefore, the residual stresses increase in magnitude and depth of occurrence.

Experiments have shown that friction hardening significantly increases the resistance to contact fatigue destruction of steels. Thus, after friction hardening with a smooth work surface tool, the contact durability of hardened and low-temperature tempered Steel 40NiCr6 test-pieces increased by 1.7 times and, after hardening with a tool which has grooves on the work surface, it increased by 1.9 times compared with the non-hardened ones.

Friction hardening of Steel CT80 in the hardened and low-temperature tempered state with a smooth work surface tool increases the resistance to contact fatigue destruction only by 1.4 times, and when hardened with a tool which has grooves on the

work surface, it increases by 1.6 times. It should be noted that the higher the hardness of the base metal, the less the effect of friction hardening on the durability of the steel under contact load (Fig. 5).

The increased resistance to fatigue destruction upon contact loading of steels after frictional hardening can be explained by the fact that the white layers have a higher hardness and, at the same time, a higher stickiness than the base metal structure. The stickiness of the white layers is increased by residual austenite (in Steel CT80 residual austenite equals 35%). During the formation of the white layers, the diffusion and redistribution of carbon and other elements in the surface layer of the metal take place. The structure of the white layer is more dispersed than the basic structure. The dislocation density is also increased in the hardened layer (in Steel CT80 dislocation density equal to  $2.4 \cdot 10^{11} \text{ cm}^{-2}$ ). Together, all these parameters lead to the deceleration of the processes of accumulation of micro damages, formation, and spreading of fatigue cracks and formation of pitting at contact loading.

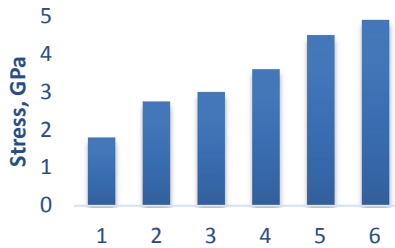


**Fig. 5.** Contact fatigue of the hardened layer obtained on Steel 40NiCr6 (1, 2, 3) and Steel CT80 (4, 5, 6): 1, 4 – unhardening test-pieces; 2, 5 – after friction hardening used disk (tool) with the smooth working surface; 3, 6 – after friction hardening used disk (tool) with multi-directional grooves on the working surface ( $N = 5 \cdot 10^7$  cycles).

Since the white layers have a high hardness, which is higher than that of the basic structure, the question arises as to whether they will during the contact load. The metallographic analysis showed that no exfoliation of the white layer takes place under contact loading; the crack arises under the surface layer in the area of the tensile residual stresses and passes through the base metal.

## 5 Conclusions

After frictional treatment of test-pieces made of Steel 40NiCr6 and Steel CT80, after hardening and low-temperature tempering, a hardened nanocrystalline layer is formed in the surface layer. The thickness and microhardness of the hardened layer are influenced by the shape of the tool's working surface. After treatment with multi-directional grooves on the working part, the thickness and microhardness of the hardened layer are greater than that of the one treated with a tool that has a smooth working surface.

The TEF parameter of the hardened nanocrystalline layer decreases to the negative side and completely correlates with the change of microhardness, as well as with phase composition.

After friction treatment, the residual compression stresses are formed in the hardened layer.

Friction treatment effectively increases the resistance of steel to fatigue destruction during contact loading. The durability of hardened test-pieces is influenced by the shape of the work surface of the tool used in treatment. The formation of pitting occurs on the base metal, in the area of residual tensile stress.






To increase the durability of parts during the action of contact fatigue loads, it is necessary to form surface nanocrystalline hardened layers, which will have high hardness, plastic deformation, and residual compression stresses.

## References

1. Terentyev, V.F., Korableva, S.A.: *Fatigue of Metals*. Science, Moscow (2015). (in Russian)
2. Pollock, T.M., Tin, S.: Nickel-based superalloys for advanced turbine engines: chemistry, microstructure and properties. *J. Propul. Power* **22**, 361–374 (2006)
3. Colas, R., Totten, G.E.: *Encyclopedia of Iron, Steel and Their Alloys*. CRC Press Taylor & Francis Group, Boca Raton, London, New York (2016)
4. Farahmand, B.: *Virtual Testing and Predictive Modeling. For Fatigue and Fracture Mechanics Allowables*. Springer, Dordrecht, Heidelberg, London, New York (2009)
5. Murakami, Yu.: *Metal Fatigue: Effects of Small Defects and Nonmetallic Inclusions*. Elsevier, Oxford (2002)
6. Abuzaid, W., Sehitoglu, H., Lambros, J.: Plastic strain localization and fatigue micro-crack formation in Hastelloy X. *Mater. Sci. Eng. A* **561**, 507–519 (2013)
7. Schijve, J.: *Fatigue of Structures and Materials*. Springer, Amsterdam (2009)
8. Suresh, S.: *Fatigue of Materials*, 2nd edn. University Press, Cambridge (2004)
9. Rudenko, S.P., Valko, A.L.: *Contact fatigue of gear wheels of power-driven machines*. Belaruskaya navuka, Minsk (2014)
10. Yushchenko, K.A., Borisov, Yu.S., Kuznetsov, V.D., Korzh, V.M.: *Surface Engineering*. Naukova dumka, Kyiv (2007)
11. Hurei, I., Kyryliv, V., Bassarab, A.: Erosion resistance of 40Kh steel after mechanical-pulse treatment. *Mater. Sci.* **40**, 296–301 (2004)
12. Knauth, P., Schoonman, J.: *Nanostructured materials. Selected synthesis methods, properties and applications*. Kluwer Academic Publishers, New York, Boston, Dordrecht, London, Moscow (2004)
13. Blatt, F.J., Schroeder, P.A., Foiles, D., Greig, C.L.: *Thermoelectric Power of Metals*. Plenum Press, New York, London (1976)
14. Hurey, I., Gurey, V., Dmyterko, P., Babiarz, R.: The research in to components of friction force tool part during friction hardening of plate steel faces. *Adv. Manuf. Sci. Technol.* **3**, 56–64 (2014)
15. Chyr, I., Jachymek, M., Hurey, I., Gurey, V., Shynkarenko, H.: Computer simulation of friction hardening of superficial layers of machine details. In: Gajek, M., Hachkewych, O., Stanik-Besler, A. (eds.) *Manufacturing Processes. Some Problems*. Basic Science Applications, vol. 1, pp. 49–62. Politechnika Opolska, Opole (2012)



# Numerical Simulation of Elasto-Plastic Behavior of Isotropic Composite Materials

Anton Karvatskii , Ihor Mikulionok , Serhii Leleka  ,  
and Vladyslav Solovei 

National Technical University of Ukraine “Igor Sikorsky Kyiv Polytechnic Institute”, 37, Peremohy Ave., Kiev 03056, Ukraine  
sleleka@rst.kpi.ua

**Abstract.** Tools in the form of methodology and software for the numerical study of the thermal-elastoplastic state of coke-pitch composites using the example of isostatic graphite production technology have been developed. A closed mathematical formulation and a method for numerically solving an elastoplastic problem with isotropic hardening based on an implicit inverse mapping algorithm are considered. Using the finite element method, the corresponding program code was developed and verified. A comparison of the results with the data of numerical analysis obtained using the ANSYS Mechanical APDL software product shows that, with isotropic hardening, the maximum discrepancy does not exceed 1.13%, and for ideal plasticity, it is no more than 3.58%. The calculations of the thermal-elastoplastic behavior of the coke-pitch composite in the technological stage of the production of isostatic graphite blanks are performed. It is shown that in the case of non-compliance with the temperature regimes at the initial stages of roasting, plastic deformations occur in the isostatic graphite blanks, which lead to cracking and deterioration of the uniformity of the physical properties of the finished products.

**Keywords:** Composite material · Elastoplasticity · Numerical analysis · Implicit algorithm · Isostatic graphite

## 1 Introduction

One of the composite materials with properties close to isotropic can include coke-pitch mixtures, which are the basis for the production of isostatic graphite (IG) [1, 2]. The composition of these mixtures includes pitch (matrix) and fine (30–150  $\mu\text{m}$ ) or fine-grained (10–30  $\mu\text{m}$ ) filler – coke [3, 4]. Owing to the uniqueness of the physicochemical properties, isostatic graphite has been extremely widely used in various fields of science and technology: from metallurgy and mechanical engineering to atomic and renewable energy [5, 6]. The technological cycle of industrial production of isostatic graphite is divided into the following stages: the first stage is the selection, preparation of raw materials, the preparation of a coke-pitch mixture (composite), as well as the isostatic pressing of “green” blanks, the second stage is the burning of blanks and the third is graphitization [4, 6]. The plastic properties of the composite material for the production of isostatic graphite are shown at the stages of pressing and burning [4, 7].



## 2 Literature Review

Available literature does not contain information on the results of modeling the elastic-plastic behavior of coke-pitch composites at the stages of the production of isostatic graphite blanks, and the mechanical properties are mainly given in the certificates of manufacturers and only for the finished product, which may be associated with the high commercial potential of this technology. In [7, 8], based on well-known analytical solutions for the normal components of the thermal stress tensor in a cylindrical body, the limiting radial temperature differences in composite graphite billets were estimated at the burning stage.

One of the first significant works devoted to implicit algorithms for solving elastoplastic problems is an article by Simo and Taylor [9], which introduced such important concepts as sequential tangential operators and the inverse mapping algorithm. It is shown that for the case independent of the speed of the elastoplastic behavior of the material, the so-called inverse mapping algorithms ensure that the quadratic velocity of the asymptotic convergence of the schemes of iterative solutions based on the Newton method is preserved. In this work, examples of numerical solutions of problems with isotropic and kinematic hardening for the associative flow law are given, as well as a problem with the non-associative Drucker-Prager flow law.

The theoretical foundations for solving a wide class of elastoplastic problems using various modifications of the inverse mapping algorithm are most fully described in [10, 11]. The paper [12] presents a mathematical formulation of the problem of the elastic-plastic state of bulk material based on the classical Drucker-Prager model. Using the inverse mapping algorithm, numerical experiments were carried out using an example of a material characterized by an associative flow law for various values of the angle of repose.

In the considered works [9–12], there are no closed formulations of the problems of thermo-elastic plasticity of composite materials and examples of their numerical implementation that could be directly applied to improve the technology for producing isostatic graphite.

In connection with the foregoing, this work is aimed at developing tools for the numerical study of the elastoplastic state of coke-pitch composites using isostatic graphite technology.

## 3 Research Methodology

### 3.1 Mathematical Statement of the Problem

According to the incremental theory of plasticity, the mathematical model of the isotropic material independent of the speed of the elastoplastic behavior of the isotropic material includes the equilibrium equation, the generalized Hooke law, and the geometric equation written through increments of physical quantities [10–12]:

$$\begin{cases} \nabla \cdot \hat{\boldsymbol{\sigma}} + \rho \hat{\mathbf{b}} = 0; \\ \hat{\boldsymbol{\sigma}} = \frac{E}{1+\nu} \left( \hat{\boldsymbol{\varepsilon}} + \frac{\nu}{1-2\nu} \text{tr}(\hat{\boldsymbol{\varepsilon}}) \hat{\mathbf{I}} \right) - \hat{\boldsymbol{\sigma}}^0; \\ \hat{\boldsymbol{\varepsilon}} = \frac{1}{2} (\nabla \hat{\mathbf{u}} + \hat{\mathbf{u}} \nabla) = \hat{\boldsymbol{\varepsilon}}^{el} + \hat{\boldsymbol{\varepsilon}}^{pl}, \end{cases} \quad (1)$$

where  $\dot{\hat{\boldsymbol{\sigma}}}$  is symmetric stress increment tensor of the second rank, Pa;  $\rho$  is density, kg/m<sup>3</sup>;  $\dot{\mathbf{b}}$  is vector increment of mass forces, N/kg;  $E$  is the modulus of elasticity under uniaxial tension (compression), Pa;  $\nu$  is Poisson's ratio;  $\dot{\hat{\boldsymbol{\epsilon}}}$  is symmetric increment tensor of the total deformations of the second rank;  $\hat{\mathbf{I}}$  is unit tensor of the second rank;  $\text{tr}()$  is tensor trace operator;  $\dot{\hat{\boldsymbol{\sigma}}}^0$  is increment tensor of initial stresses, Pa;  $\dot{\hat{\boldsymbol{\epsilon}}}^{el}$ ,  $\dot{\hat{\boldsymbol{\epsilon}}}^{pl}$  are the elastic and plastic components of the tensor of the increment of total deformations  $\dot{\hat{\boldsymbol{\epsilon}}}$ , respectively;  $\dot{\mathbf{u}}$  is the displacement increment vector, m.

In the case of isotropic hardening, the material yield condition takes the following form [10, 11]

$$F(\hat{\boldsymbol{\sigma}}, \boldsymbol{\varepsilon}_{eq}^{pl}) = \sigma_{eq} - \sigma_y(\sigma_{y0}, \boldsymbol{\varepsilon}_{eq}^{pl}), \tag{2}$$

where  $F$  is the function of the surface fluidity of the material;  $\sigma_{eq}$  is Mises equivalent stress, Pa;  $\sigma_y(\sigma_{y0}, \boldsymbol{\varepsilon}_{eq}^{pl})$  is yield point of the material, taking into account isotropic hardening according to the linear law, Pa;  $\boldsymbol{\varepsilon}_{eq}^{pl}$  is Mises equivalent plastic deformation;  $\sigma_{y0}$  is the initial value of the yield strength of the material, Pa.

The initial conditions for (1) and (2)

$$\dot{\hat{\boldsymbol{\sigma}}}^0 = 0. \tag{3}$$

The boundary conditions for (1) and (2):

- displacement vector

$$\mathbf{u}|_{S_u} = 0, \tag{4}$$

where  $S_u$  is the surface (or surface point) on which the components of displacement are specified, m<sup>2</sup>;

- symmetry

$$\mathbf{n} \cdot \mathbf{u}|_{S_{su}} = 0, \tag{5}$$

where  $\mathbf{n}$  is the vector of the external normal to the surface of the body;  $S_{su}$  is surface symmetry of the body, m<sup>2</sup>;

- external pressure

$$(\hat{\boldsymbol{\sigma}} \cdot \mathbf{n}) \cdot \mathbf{n}|_{S_p} = p, \tag{6}$$

where  $p$  is the external pressure set on the surface of the body  $S_p$ , Pa.

### 3.2 The Methodology of Numerical Research

Consider the theoretical foundations of the implicit Return-Mapping Algorithms [10, 11] using the example of solving the problem of the elastic-plastic behavior of isotropic

material. In the case of the occurrence of elastoplastic deformations in the material, taking into account the temperature load, elastic stresses are determined by the equation

$$\hat{\sigma} = \overset{4}{\hat{C}} : (\hat{\varepsilon}^{tr} - \hat{\varepsilon}^{pl} - \hat{\varepsilon}_T), \quad (7)$$

where  $\overset{4}{\hat{C}}$  is the fourth-rank tensor of the elastic constants of the material, Pa;  $\hat{\varepsilon}^{tr}$  is a tensor of test (full) deformations of the second rank, which is determined in the approximation of an elastic medium;  $\hat{\varepsilon}_T(\beta, T, T_{ref})$  is temperature strain tensor;  $\beta$  is coefficient of linear thermal expansion (CLThE), K<sup>-1</sup>;  $T, T_{ref}$  are the current absolute temperature and the absolute reference temperature, respectively, K.

Under the associative law of plastic flow, the increment of plastic deformations is determined by the relation

$$\Delta \hat{\varepsilon}^{pl} = \Delta \lambda \hat{\mathbf{m}}, \quad (8)$$

where  $\Delta \hat{\varepsilon}^{pl}$  is an increment of plastic deformation at the  $i$ -th step of loading;  $\Delta \lambda$  is the scalar associative factor (plasticity coefficient), which is determined by the formula

$$\Delta \lambda = \frac{\hat{\mathbf{m}} : \overset{4}{\hat{C}} : \hat{\varepsilon}^{tr}}{\hat{\mathbf{m}} : \overset{4}{\hat{C}} : \hat{\mathbf{m}}^{T+h}}, \quad (9)$$

where  $\hat{\mathbf{m}}$  is the derivative of the plasticity function (2) with respect to the stress tensor;  $h$  is hardening module, Pa.

Using the inverse Euler method, Eq. (7), taking into account (8) and (9) for  $k+1$  the loading step, can be easily transformed to

$$\hat{\sigma}^{k+1} = \hat{\sigma}^{tr} - \Delta \lambda^{k+1} \overset{4}{\hat{C}} : \hat{\mathbf{m}}(\hat{\sigma}^{k+1}), \quad (10)$$

where  $\hat{\sigma}^{k+1}$  is the elastic stress tensor at the loading step, Pa;  $\hat{\sigma}^{tr}$  is test stress tensor determined in the approximation of an elastic body, Pa.

Formula (10) describes the mapping of the test stress tensor in the direction of the yield surface  $F$ . Therefore, this method of solving the elastic-plasticity problem is called the inverse mapping algorithm [10].

System of Eqs. (10), taking into account the symmetry of the stress tensor, has seven unknowns, i.e. six independent components  $\hat{\sigma}^{tr}$  and plasticity coefficient  $\Delta \lambda$ . In this regard, to close the system of Eqs. (10), it is necessary to supplement it with a scalar Eq. (2) of the form

$$F(\widehat{\boldsymbol{\sigma}}^{k+1}, \Delta\lambda) = 0. \tag{11}$$

Equation (11) ensures the fulfillment of the yield condition at the end of each  $k$ -th stage of loading.

To apply the Newton method, the nonlinear system of Eqs. (10), (11) must be rewritten in the residual format (12). Moreover, to represent the tensors  $\widehat{\boldsymbol{\sigma}}^{k+1}$ ,  $\widehat{\boldsymbol{\sigma}}^{tr}$  and  $\widehat{\mathbf{m}}$  in the form of vectors, it is necessary to make the transition to six-dimensional space, taking into account their symmetry. This makes it possible to replace tensors of the second rank  $\widehat{\boldsymbol{\sigma}}^{k+1}$ ,  $\widehat{\boldsymbol{\sigma}}^{tr}$  and  $\widehat{\mathbf{m}}$  with the corresponding vectors  $\boldsymbol{\sigma}^{k+1}$ ,  $\boldsymbol{\sigma}^{tr}$  and  $\mathbf{m}$  with six components, and instead of using the tensor of the fourth rank  $\widehat{\mathbf{C}}$ , use the tensor of the second rank of elastic constants  $\widehat{\mathbf{D}}^{el}$  of dimension six:

$$\begin{cases} \mathbf{r}_\sigma = \boldsymbol{\sigma}^{k+1} - \boldsymbol{\sigma}^{tr} + \Delta\lambda^{k+1} \widehat{\mathbf{D}}^{el} \cdot \mathbf{m}(\boldsymbol{\sigma}^{k+1}); \\ r_F = F(\boldsymbol{\sigma}^{k+1}, \Delta\lambda^{k+1}). \end{cases} \tag{12}$$

To solve the system of nonlinear Eqs. (12), Newton’s method (13) or linearization by Newton’s method (14) are used, the iterative procedures of which are respectively written as follows:

$$\begin{pmatrix} \boldsymbol{\sigma}_{j+1}^{k+1} \\ \Delta\lambda_{j+1}^{k+1} \end{pmatrix} = \begin{pmatrix} \boldsymbol{\sigma}_j^{k+1} \\ \Delta\lambda_j^{k+1} \end{pmatrix} - \left[ \begin{array}{cc} \frac{\partial \mathbf{r}_\sigma}{\partial \boldsymbol{\sigma}} & \frac{\partial \mathbf{r}_\sigma}{\partial \Delta\lambda} \\ \frac{\partial r_F}{\partial \boldsymbol{\sigma}} & \frac{\partial r_F}{\partial \Delta\lambda} \end{array} \right]^{-1} \begin{pmatrix} \mathbf{r}_\sigma^j \\ \mathbf{r}_F^j \end{pmatrix}, \tag{13}$$

or

$$\left[ \begin{array}{cc} \frac{\partial \mathbf{r}_\sigma}{\partial \boldsymbol{\sigma}} & \frac{\partial \mathbf{r}_\sigma}{\partial \Delta\lambda} \\ \frac{\partial r_F}{\partial \boldsymbol{\sigma}} & \frac{\partial r_F}{\partial \Delta\lambda} \end{array} \right] \begin{pmatrix} \delta\boldsymbol{\sigma}_j^{k+1} \\ \delta\Delta\lambda_j^{k+1} \end{pmatrix} = \begin{pmatrix} \mathbf{r}_\sigma^j \\ \mathbf{r}_F^j \end{pmatrix}, \begin{pmatrix} \boldsymbol{\sigma}_{j+1}^{k+1} \\ \Delta\lambda_{j+1}^{k+1} \end{pmatrix} = \begin{pmatrix} \boldsymbol{\sigma}_j^{k+1} \\ \Delta\lambda_j^{k+1} \end{pmatrix} + \begin{pmatrix} \delta\boldsymbol{\sigma}_j^{k+1} \\ \delta\Delta\lambda_j^{k+1} \end{pmatrix}. \tag{14}$$

Here, the index  $k$  refers to the loading step, and the index  $j$  refers to the number of iterations according to Newton’s method.

The use of linearization of a system of equations of the form (14) and its solution by the Gaussian elimination method instead of inverting the matrix in (13) using a unit matrix allows significantly reducing the number of arithmetic operations at each iteration step by approximately  $2n(n - 1)^2$ , where  $n$  is the dimension of the system of equations.

For  $k = 1$ , the usual elastic problem with respect to complete displacements under the boundary conditions (4)–(6) is solved and the tensor of test stresses is determined. Further, in the part of the body in the elastoplastic state, tensors of the increment of plastic deformations and elastic stresses are determined from solution (14) and the initial stresses are found by the formula

$$\boldsymbol{\sigma}^{0(k)} = \Delta\lambda^{(k)} \widehat{\mathbf{D}}^{el} \cdot \mathbf{m}^{(k)}. \quad (15)$$

The following integration steps (1), (2) for  $k > 1$  are performed only with a load with initial stresses (15), (16) under boundary conditions (4), i.e. without taking into account external and internal load. In this case, the elastic problem is also solved and the vector of increment of displacements  $\Delta\mathbf{u}^k$  is determined and the components of the vector of full displacements are determined, according to which new values of the components of the test stress tensor are found. Then, from solution (14), new values of the components of the tensors of the increment of plastic strains and elastic stresses are determined for the part of the body in the elastoplastic state. Next, to perform the next loading step, we find the tensor of the increment of initial stresses according to the formula

$$\boldsymbol{\sigma}^{0(k)} = \Delta\lambda^{(k)} \widehat{\mathbf{D}}^{el} \cdot \mathbf{m}^{(k)} - \boldsymbol{\sigma}^{0(k-1)}. \quad (16)$$

The plastic strain tensor is determined by the formula

$$\boldsymbol{\varepsilon}^{pl(k)} = \boldsymbol{\varepsilon}^{pl(k-1)} + \Delta\lambda^{(k)} \mathbf{m}^{(k)}.$$

The criterion for the completion of calculations may be the fulfillment of one of the conditions

$$|\Delta\mathbf{u}^k| \leq \delta_u \text{ or } \left| \boldsymbol{\varepsilon}_{eq}^{pl(k)} \right| \leq \delta_\varepsilon.$$

To apply the described methodology to the problems of the elastoplastic state of isotropic composite materials, it is necessary to determine their effective physical and mechanical properties. For this, one can either use the additive relations [13] using the known properties of the constituents (matrix and filler) of the composite or experimentally determine the effective values of these properties [7].

Additive relations [13] have the general form

$$P_{\text{comp}} = P_f V_f + P_m V_m,$$

where  $V_f$ ,  $V_m$  are the volume fractions of the filler and matrix, respectively; indices comp, f, m relate to the composite, filler, and matrix, respectively;  $P$  is one of the physical properties of the composite, filler, and matrix, respectively.

When solving the unbound thermo-elastic-plastic problem (7), which takes place in IG technology, to determine the temperature field, it is necessary either to solve the non-stationary (stationary) heat conduction problem with the corresponding initial and boundary conditions [14] or to set the known temperature field in advance.

### 3.3 Software Implementation of the Calculation Method

For the numerical implementation of the above algorithm, the finite element method (FEM) was used [9–12] and the Mathcad programming environment [15]. To build the

geometry and tetrahedron mesh of the model, free open source code is used – a CAD system for grid generation Gmsh [16]. To visualize the results of calculations of physical fields, the free open software code ParaView was used [17]. Testing of the developed program code for solving the problem of elastic-plasticity with isotropic hardening was performed using an example of a material with the mechanical properties of carbon steel.

To fulfill the conditions on the yield surface (11) with an accuracy of 10–6 in each plastic finite element (FE), iterations must be performed 6 times, and to achieve an accuracy of 0.1% in determining the components of the displacement vector, 10–15 loading steps are required initial stresses when solving the global system of discrete FEM equations.

**Test.** The problem of elasticity is taking into account the isotropic hardening of a thick-walled cylinder with radii  $r_1/r_2 = 0.05/0.08$  m. Material is steel ( $E = 2 \cdot 10^5$  MPa,  $\nu = 0.3$ ,  $\sigma_{y0} = 320$  MPa,  $h = 1.5 \cdot 10^3$  MPa). The pressure on the inner wall of the cylinder is  $p = 150$  MPa.

The grid convergence of the solution to the problem was determined by the double recount method. As a result, it was found that the computational grid of the test problem, consisting of 2041 linear tetrahedral FEs and 743 nodes, leads to an error in the determination  $\sigma_{eq}$  of not more than 0.5%.

**Table 1.** Results of a comparison of solutions to the plasticity problem taking into account isotropic hardening.

Type of solution	$u_s$ , m	$\sigma_{eq}$ , MPa	$\varepsilon_{eq}^{el}$	$\varepsilon_{eq}^{pl}$
ANSYS, nodes 774, FEs – 2209	$8.61 \cdot 10^{-5}$ – 0.000112	213–322	0.001064– 0.001608	0– 0.001217
Mathcad, nodes 743, FEs – 2041	$8.675 \cdot 10^{-5}$ – 0.00011204	215.3– 321.83	0.001076– 0.001607	0– 0.001218
Error, %	0.75–0.038	1.08– 0.053	1.13–0.06	0–0.08

Note:  $u_s = |\mathbf{u}|$  is the displacement vector module;  $\sigma_{eq}$  is Mises equivalent stresses;  $\varepsilon_{eq}^{el}$  and  $\varepsilon_{eq}^{pl}$  are equivalent Mises elastic and plastic deformations, respectively.

**Table 2.** The results of a comparison of the solutions of the plasticity problem for ideal plasticity.

Type of solution	$u_s$ , m	$\sigma_{eq}$ , MPa	$\varepsilon_{eq}^{el}$	$\varepsilon_{eq}^{pl}$
ANSYS, nodes 774, FEs – 2209	$8.62 \cdot 10^{-5}$ – 0.000113	213–320	0.001066– 0.0016	0–0.001128
Mathcad, nodes 743, FEs – 2041	$8.615 \cdot 10^{-5}$ – 0.0001111	212.8–320	0.001068– 0.00162	0– 0.00115825
Error, %	0.058–1.68	0.094–0	0.84–1.25	0–3.58

The results of a numerical solution of the elastoplastic problem for cases of isotropic hardening and ideal plasticity and their comparison with data obtained using the ANSYS Mechanical APDL software product [18] are given in Table 1 and 2.

The results of numerical modeling of physical fields in solving the test problem of elasticity using the developed software code confirm the possibility of its practical application.

### 4 Results

The following are the results of a numerical analysis of the elastic-plasticity of coke-pitch composite blanks in the production of isostatic graphite.

To conduct studies of thermo-elastic plasticity at the early stages of the burning of IG blanks, the composition of the coke-pitch composite was used, including calcined pitch coke as a filler with an average grain size of 15 μm and a matrix of high-temperature pitch (HTP) in an amount of 40% (by weight) [7]. The softening temperature of the HTP is 140 °C. Pitch coke is characterized by physical properties close to isotropic [19], which positively affects the properties of the finished IG. The calcination temperature of coke exceeds the burning temperature of the IG blanks, which minimizes its shrinkage during the heat treatment. The physical properties of the coke-pitch composite used in the calculations are given in Table 3.

**Table 3.** Physico-mechanical properties of IG blanks at the burning stage [7] (composition: calcined coke (15 μm) + 40% HTP).

$t, \text{ }^\circ\text{C}$	$\rho, \text{ kg/m}^3$	$c_p, \text{ J/(kg K)}$	$\lambda, \text{ W/(m}\cdot\text{K)}$	$E, \text{ MPa}$	$\sigma_c, \text{ MPa}$	$\sigma_t, \text{ MPa}$
20	1420	670	0.60	3800	12.0	3.1
100	1380	950	0.77	5000	12.0	3.1
200	1450	1180	0.90	8400	20.6	5.3

Note:  $t$  is temperature;  $\rho$  is density;  $c_p$  is mass isobaric heat capacity;  $\lambda$  is a coefficient of thermal conductivity;  $\sigma_c, \sigma_t$  are the compressive and tensile strengths, respectively.

In the calculations, the Poisson’s ratio, CLThE, the yield strength and the hardening modulus of the IG blanks were taken equal to  $\nu = 0.235, \beta = 1.8 \cdot 10^{-4} K^{-1}, \sigma_{y0} = 3 \text{ MPa}$  and  $h = 0 \text{ MPa}$ , respectively. When heated, the composite material of the IG blanks behaves differently: to the softening temperature of the pitch (matrices) expand, and after the onset of destruction, accompanied by gas-fission, it shrinks with the formation of semicoke and coke in the temperature range of more than 250 °C, which leads to an increase in its density [7, 20].

The calculations were performed for vertically standing IG blanks with a diameter of 300 mm and a height of 500 mm, taking into account gravitational and temperature loads on a finite element mesh consisting of 4762 linear tetrahedral FEs and 1311 nodes. The temperature load in the form of radial temperature drops across the workpieces varied within the range  $\Delta T_r = 5\text{--}15$  K.

Analysis of the calculation results shows that:

- a significant part of the IG blank under the influence of temperature loading is in the plastic state;
- in the upper part along the axis of the workpiece, gravitational compressive forces and temperature expansion cancel each other out, which results in minimal equivalent elastic deformations and, accordingly, equivalent Mises stresses.

Irreversible plastic deformations worsen the uniformity of the composite and provoke cracks nucleation at the initial stage of burning, i.e. to reach the level of softening temperatures of the matrix material, the beginning of destruction and intense gas evolution.

## 5 Conclusions

Tools have been developed in the form of methodology and software for the numerical study of the thermal-elastoplastic state of coke-pitch composites in the production technology of isostatic graphite.

Verification of the program code developed in the Mathcad environment is carried out using the example of a numerical solution of the test problem of the elastic-plasticity of isotropic material. A comparison of the results with the data of numerical analysis obtained using the ANSYS Mechanical APDL software product shows that, with isotropic hardening, the maximum discrepancy does not exceed 1.13%, and for ideal plasticity, it is no more than 3.58%.

A numerical analysis of the thermo-elastic-plastic state of composite IG blanks during the burning process is carried out. It is shown that in the early stages of burning at radial temperature gradients of large 33 K/m in the coke-pitch composite, undesirable plastic deformations may occur, which can contribute to the initiation of cracks and reduce the uniformity of the composite material.

## References






1. Chung, D.D.L.: Composite Materials: Science and Applications. Springer, London (2010). <https://doi.org/10.1007/978-1-84882-831-5>
2. Askeland, D.R., Phule, P.P.: The Science and Engineering of Materials, 5th edn. Thomson, Toronto (2006)
3. Kostikov, V., Samoylov, V., Beylina, N., Ostronov, B.: New high-strength carbon materials for traditional technologies. Russ. Chem. Mag. **48**(5), 64–75 (2004). (in Russian)



4. Asao, O.: High density isotropic graphites and glassy carbons. Japanese situation: production, properties and applications. Universidad de Alicante. Secretariado de Publicaciones, Alicante (1997)
5. Global Isostatic Graphite Market 2015 Industry Trends, Analysis & Forecast to 2020. QY Research, Florida (2015)
6. Karvatskii, A., Leleka, S., Pedchenko, A., Lasariev, T.: Investigation of the current state of isostatic graphite production technology. *Technol. Audit Prod. Reserves* **2/1**(34), 16–21 (2017)
7. Samoylov, V.: Receiving fine carbon fillers and development of the production technology of fine-grained graphites on their basis. Doctoral thesis, Research Institute of Constructional Materials on the Basis of Graphite «NIIGrafit», Moscow (2006). (in Russian)
8. Shuvalov, E.: About distribution of temperatures and thermal tension in carbon and graphite bodies of a cylindrical form. *Collect Works Chelyabinsk Electrometallurgical Plant* **2**, 200–214 (1970). (in Russian)
9. Simo, J., Taylor, R.: Consistent tangent operators for rate-independent elastoplasticity. *Comp. Methods Appl. Mech. Eng.* **48**, 101–118 (1985)
10. de Borst, R., Crisfield, M.A., Remmers, J.J., Verhoosel, C.V.: *Nonlinear Finite Element Analysis of Solids and Structures*. Wiley, New York (2012)
11. Zienkiewicz, O., Taylor, R., Fox, D.: *The Finite Element Method for Solid and Structural Mechanics*, 7th edn. Elsevier Ltd., Oxford (2014)
12. Karvatskii, A., Panov, E., Pedchenko, A., Shkil, V.: Modification of implicit algorithm for solving a problem on the elastic plasticity of bulk materials. *Eastern-European Journal of Enterprise Technologies* **5**(7(89)), 17–23 (2017)
13. Jones, R.: *Mechanics of Composite Materials*, 2nd edn. Taylor & Francis, Philadelphia (1999)
14. Karvatskii, A., Leleka, S., Pedchenko, A., Lazariev, T.: Numerical analysis of physical fields of graphitization process of electrode production in Castner's furnace. *East.-Eur. J. Enterp. Technol.* **6**(5(84)), 19–25 (2016)
15. PTC Mathcad. <https://www.ptc.com/en/products/mathcad>. <http://www.ptc.com/engineering-math-software/mathcad/>. Accessed 29 May 2019
16. Gmsh: a three-dimensional finite element mesh generator with built-in pre- and post-processing facilities. <http://gmsh.info/>. Accessed 29 May 2019
17. ParaView. <https://www.paraview.org/>. Accessed 29 May 2019
18. Thompson, M., Thompson, J.: *ANSYS Mechanical APDL for Finite Element Analysis*. Butterworth-Heinemann, Oxford (2017)
19. Ostrovskiy, V., Beylina, N., Lipkina, N., Sinelnikov, L.: Peak coke as filler of constructional graphites. *Chem. Solid Fuel* **1**, 56–61 (1995)
20. Gromov, B., Panov, Ye., Bozhenko, M., Vasilchenko, G., Karvatskii, A., Shilovich, I.: *Burning and Start of Aluminum Electrolyzers*. Ore and Metals Publishing House, Moscow (2001)



# Simulation of the Process of Obtaining Nanostructures During Laser Radiation on Materials, Cutting Tools and Parts

Gennadiy Kostyuk<sup>1</sup>, Viktor Popov<sup>2</sup>,  
Mykola Nechyporuk<sup>1</sup>, Olecsandr Tymofyeyev<sup>3</sup>,  
and Hanna Yevsieienkova<sup>1</sup>

<sup>1</sup> National Aerospace University Named by N.Ye. Zhukovsky “KhAI”, 17, Chkalov St., Kharkiv 61070, Ukraine

[g.kostyuk@khai.edu](mailto:g.kostyuk@khai.edu)

<sup>2</sup> Joint Stock Company “FED”, 132, Sumska St., Kharkiv 61023, Ukraine

<sup>3</sup> Kharkiv Himprom Ltd., 22, Promyslova St., Vasyshchevo 62495, Ukraine

**Abstract.** The likelihood of obtaining nanostructures on solid alloys (K20 and VK 8 (MC 347)) was compared under the action of laser radiation with a heat flux density of  $10^{12}$ – $10^{16}$  (W/m<sup>2</sup>) with a duration of  $10^{-12}$ – $10^{-16}$  (s) and spot size contact  $5 \cdot 10^{-7}$  and  $10^{-6}$  m. The zone where the formation of nanostructures was considered the region where the temperature is in the range of 500–1500 K, its growth rate exceeds  $10^7$  (K/s). The technological parameters of laser radiation are obtained at which these conditions are met. The zones of formation of nanostructures depending on the heat flux density on the time of action of the ionizing radiation are determined. It is shown that it is necessary to take into account the rate of temperature rise and the probability of thermoelastic destruction due to the action of temperature stresses. In low-speed temperature rise formed micro and submicrostructure that has been confirmed experimentally. For the first time, the influence of grain formation energy on temperature development, its rate of change, temperature stresses and the possibility of nanostructures formation is taken into account. The comparison shows that the zone of technological parameters at which nanostructures are realized for the (MC347) hard alloy with the laser contact size  $R = 10^{-6}$  m differs little (MC347) is more likely, and for  $R = 5 \cdot 10^{-7}$  m it is significantly more for carbide HA (MC347).

**Keywords:** Nanostructure · Submicrostructure · Technological parameters · Steel · Hard alloy · Pulse laser radiation

## 1 Introduction

The use of a particular hard alloy for hardening leads to the fact that it is necessary to choose the tool depending on the final result of hardening. That is, how effectively will be formed nanostructures under the action of femtosecond lasers.

It is important to determine what amount of cobalt (in percentage terms) will be in the solid alloy, which will strengthen its positions more effectively. For this, the effect

of a femtosecond laser on a hard alloy was investigated K20 (Co 4%) and MC347 (Co 8%). So, we looked at two single carbides hard alloy with different contents of cobalt, differing in two times. This made it possible to determine how effectively it will be formed this or that alloy. That is the range of technological parameters in which a nanostructure will be formed in one way or another. At what, the most effective will be considered the alloy for which the range of technological much wider. So, the probability of obtaining nanostructures will be much higher. Application of femtosecond laser operating at high frequencies positives leads to the fact that energy consumption in the process of hardening much smaller than obtaining the same volumes of nanostructures using conventional lasers. All this determined the subject of the study.

## 2 Literature Review

Currently, the search for new methods for obtaining nanostructures is of great interest [1–5]. One of which is the laser treatment of the surface of the material [6–10].

Advances in the development of a wide range of lasers have opened up new opportunities in the field of material processing. Laser treatment of materials is a rapid and local energy exposure that results in electronic and thermodynamic nonequilibrium. The paper [11] deals with laser processing of films and nanostructures of metal oxides for various applications. The latest achievements in the field of laser treatment of metal oxides are summarized.

In [12] the influence of laser glazing on the behavior of nanostructured heat-protective coatings was investigated. The results showed that the service life of the plasma-sprayed was increased approximately twice due to laser glazing. Reducing the reactive specific surface area of the dense glazed layer with molten salts and improving stress accommodation through the mesh cracks formed during laser glazing were the main mechanisms of strengthening, providing an extension of the service life of nanostructured heat-protective coatings.

Knowing which kind of micro/nanostructure contributes significantly to the stability of the Cassie-state, especially at low temperatures and pressures is extremely relevant [13]. In this paper, using a femtosecond laser, several types of typical micro/nanostructures with different topography features on metal surfaces were manufactured. These surfaces have been modified with fluoroalkylsilane to produce superhydrophobicity. The stability of the Cassie-states of these surfaces was studied using condensation and evaporation experiments. Special attention is paid to the dependence of the stability of the Cassi-state on the produced micro/nanostructures and laser processing parameters. The results show that some superhydrophobic surfaces, even with high contact angles and low sliding angles under normal conditions, are unstable under low temperature or external pressure.

The work [14] deals with the preparation of micro/nanostructure on the surface of stainless steel using a nanosecond laser in various gas media. It was found that the dimensional characteristics of micro/nanostructures are particularly influenced by the speed of laser scanning, as well as the gas medium. The chemical composition of the structures can be regulated by the parameters of laser treatment. Studies have shown that the oxygen-rich environment promotes the growth of nanostructures.

The paper [15] was described as a new self-assembly phenomenon of the metal-phthalocyanine chloride nanostructures and its influence on the linear optical properties as well as the Second Harmonic Generation process. The self-assembly phenomenon was achieved through an annealing process carried out immediately after the deposition process.

### 3 Research Methodology

For technological purposes, a focused source of coherent radiation is used, the heat flux density of which is distributed in the focal plane  $q(r)$ ,  $q_0$ ,  $q_n$ ,  $q_{V0}$ . These values were obtained in the works [4, 5].

The heat balance is represented in the expression:

$$\begin{aligned}
 & C[T]\gamma[T] \frac{dT(x, y, z, t)}{dt} + C[T]\gamma[T] \frac{dT(x, y, z, t)}{dy} \cdot V_n + C[T]\gamma[T]\tau_p \frac{d^2 T(x, y, z, t)}{dt^2} \\
 & = \nabla \lambda [T] \nabla T(x, y, z, t) + C[T]\gamma[T]V_{TM} \frac{\partial T(x, y, z, t)}{\partial x} - AL_{III} \gamma[T] \frac{dV_{III}}{dt} + B \frac{q_n(r, t)}{0.1\delta} \quad (1) \\
 & \pm D \frac{dW(x, y, z, t)}{dt} \pm m_a C_a [T_a] \frac{dn_a}{dt} (T_a - T(x, y, z, t)) \pm P_{T.X.P} (n_A, n_B, T, t_e) \frac{dn_{A(B)}}{dt} L_{T.X.P} \\
 & + q_v(z) + \overline{E}_{cr} \cdot \overline{E}_{cr} = \frac{E_{cr}}{v_{nc} 2\tau_i}.
 \end{aligned}$$

where  $C[T]$  and  $\gamma[T]$  is the specific heat and density of the target material corresponding to a temperature  $T$ ;  $\tau_p$  is the relaxation time temperature by one Kelvin;  $V_n$  is the velocity of the plasma flow of laser radiation or the target relative to it;  $L_{III}$  and  $L_{T.X.P}$  are specific heat of fusion and thermochemical reaction;  $V_{qb}[T]$  – the displacement speed of the evaporation front;  $V_{III}$  – the volume of molten metal;  $W(x, y, z, t)$  – the energy of deformation of a unit volume target;  $m_a$  – a mass of the diffusing atom;  $C_a [T_a]$  is the heat capacity of the diffusing material at a temperature  $T_a$ ;  $P_{T.X.P} (n_A, n_B, T, t_{B3})$  – the probability of thermochemical reactions that depend on the concentration of the reagents;  $n_A$  and  $n_B$ , are the temperature  $T$  and the time of interaction;  $t_{B3}$ ;  $n_A$  and  $n_B$  are the concentration of the reactants that determine the possibility of a reaction;  $E_{cr}$  is the energy of crystallization of grain (equal to the energy of atomization of grain);  $V_{nc}$  is the volume of the nanocluster;  $\tau_i$  is laser pulse time.

The amount change of heat in a unit volume (the first term in the left part of the equation) is realized by moving the laser radiation flow along the treated surface or moving the target relative to the laser radiation flow at the rate of  $V_n$  (the second term); thermophysical processes: effects on the heat transfer of the final rate of heat propagation (the third term), thermal conductivity (the first term on the right), displacement of the evaporation front (the second term), melting (the third term); collision processes: volumetric heat source due to the action of laser radiation (the fourth term), thermoelastic, thermoplastic and thermo-fatigue processes that determine the energy of deformation of the material of elementary volume (the fifth term); diffusion processes

that determine the heat transfer of the diffusing material (the sixth term); thermochemical processes associated with the implementation of chemical reactions between the part material and the coating material or between the components of alloys and composite materials, the volumetric heat source due to the action of the light-beam flow [4].

Heat flow on the target surface is created by the following factors:

- collision processes: heat released on the surface due to the action of laser radiation (the first term on the right), the heat flux withdrawn from the thermoelectrons (the second term), and secondary photons (the third term);
- thermophysical processes: removal of heat flow with evaporated material (fourth term), the material in the liquid phase, if the conditions for its release (fifth term), thermal radiation of the heated surface (sixth term) and condensed atoms, previously evaporated (seventh term);
- plasma chemical processes, realized by the reactions of the laser radiation flux with the evaporated material of the part or adsorbed gases (eighth term); this energy is transmitted by radiation.

The energy transfer is also carried out by the radiation of the laser radiation quantum flux (the last term):

$$-\lambda [T] \frac{\partial T(x, y, z, t)}{\partial x} = F_{i,r} - F_{m_2} - F_{\phi} - F_{ucn} - F_m - \sigma \varepsilon T^4(0, y, z, t) \pm F_{\text{smo}} + F_{\text{flx}} + \sigma \varepsilon_c T_c^4, \quad (2)$$

where  $\sigma$  is the Stefan-Boltzmann constant;  $\varepsilon$  and  $\varepsilon_-$  are the degree of blackness of the target surface and the medium;  $T_c$  is the temperature of the medium.

Each term is considered in more detail in [3, 4].

## 4 Results

The results of calculations of temperature fields, temperature stresses, and temperature growth rates under the action of radiation sources with heat flux densities from  $10^{11}$  to  $10^{17}$  W/m<sup>2</sup> for operating times from  $10^{-16}$  to  $10^{-10}$  s on the VK VK4 are considered, the results of which are shown in Fig. 1. It can be seen that with an increase in the heat flux density, temperatures increase at almost all studied depths – from 0 to  $9,5 \cdot 10^{-7}$  m at an operating time of  $10^{-10}$  s. Actions with shorter times retain almost the same character of the dependence of temperature on the heat flux density, the character is preserved, but the temperature values are significantly reduced. The obtained temperature distributions of the heat flux density show that for shorter times of the heat flux action, more successful temperature distributions are realized at higher heat flux densities ( $10^{15} \dots 10^{16}$  W/m<sup>2</sup>), whereas at  $10^{-14}$  s this region of nanostructure production lies already at heat flux densities from  $10^{13}$  to  $10^{15}$  W/m<sup>2</sup>, at large times of  $10^{-12}$  s, this region moves towards lower heat flux densities and lies in the region from  $10^{12}$  to  $10^{14}$  W/m<sup>2</sup>. For a time of  $10^{-10}$  s, this region already lies in the range from  $10^{12}$  to  $10^{13}$  W/m<sup>2</sup>. From these graphs, it is possible to assess the possibility of obtaining nanostructures in short times, i. e., at the femtosecond and picosecond ranges, but these

graphs are insufficient to assess the possibility of obtaining nanostructures. It is also necessary to determine the rate of temperature rise from the heat flux density at the same time (from  $10^{-16}$  to  $10^{-10}$  s).

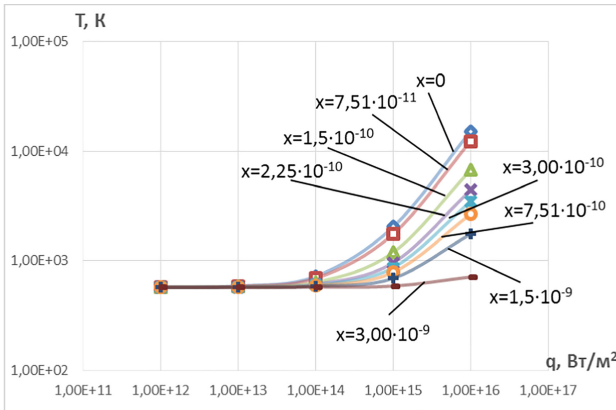


**Fig. 1.** The dependence of the maximum temperature in the area of the LI on VK4 from the heat flux density at different depths at the time of action:  $t = 10^{-15}$  s.

Analysis of the dependence of the rate of temperature change over time on the heat flux density at different depths and times of the heat flux from  $10^{-16}$  to  $10^{-10}$  s (Fig. 2). It can be seen that the rate of temperature change varies from  $10^{13}$  to  $10^{17}$  K/s, with a decrease in the action time, these speeds increase, and at a time of  $10^{-12}$  s they already approach  $10^{15} \dots 10^{18}$  K/s. A further decrease in time to  $10^{-14}$  s, speeds approach  $10^{17} - 10^{19}$  K/s, and at  $t = 10^{-16}$  s, the rate of temperature increase approaches  $10^{19} \dots 10^{20}$  K/s. It is seen that such high growth rates contribute to the formation of nanostructures and obviously can significantly accelerate this process. In Fig. 3 shows the dependences of temperatures at different depths in the area of the LI on the VK4 TS on the heat flux density at the same action times ( $10^{-16} - 10^{-10}$  s). It can be seen that with increasing heat flux density, the values of temperature stresses increase significantly from  $10^8$  to  $10^{13}$  Pa. These stresses in absolute value exceed the tensile strength, but since they act in a pulsed manner in a short time, the fracture does not occur (deformation energy is insufficient). For small heat fluxes, temperature stresses accelerate the formation of nanostructures, and for large ones, starting from  $10^{14} - 10^{16}$  W/m<sup>2</sup>, they can independently form nanostructures due to the deformation of the atomic lattice of the material.

Similar studies were conducted for the beam radius  $R = 10^{-6}$  m, the results of which are shown in Fig. 4. It can be seen that the nature of the curves in the dependencies of the volume of nanograins on the minimum (Fig. 4a) and maximum (Fig. 4b) depths is preserved, but the grain volume increased by almost an order of magnitude. The fraction of nanostructured grains decreases significantly, which can be seen by comparing the location of the dashed lines in Figs. 4a and 5b with the same in Fig. 4a and b. It is seen that an even larger proportion of grains in the case of a spot size with

$R = 10^{-6}$  m goes into the region of submicrostructures, which allows one to choose the size of the LI spot and its technological parameters.

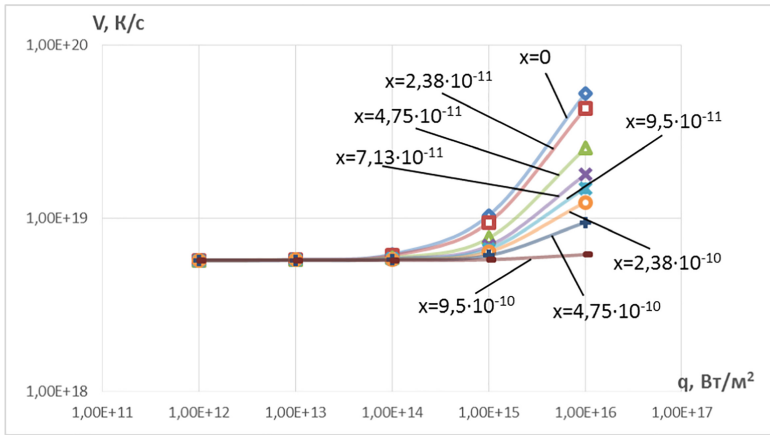


**Fig. 2.** Dependence of the rate of temperature change in the area of LI on VK4 on the heat flux density at different depths at the time of action:  $t = 10^{-16}$  s.

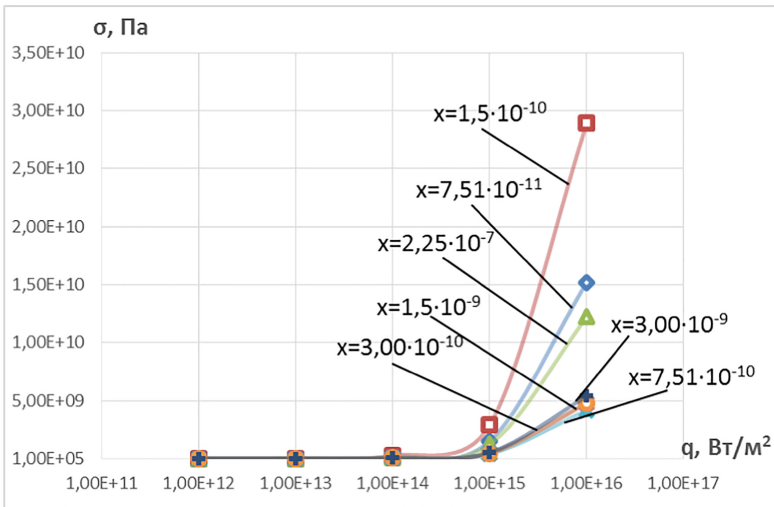
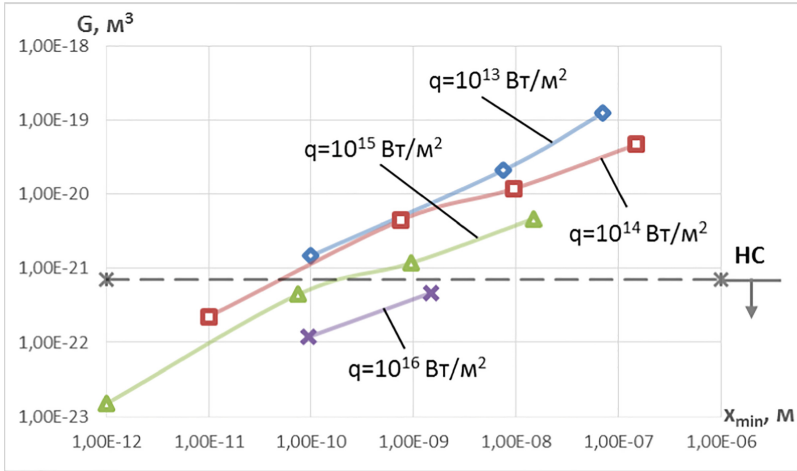
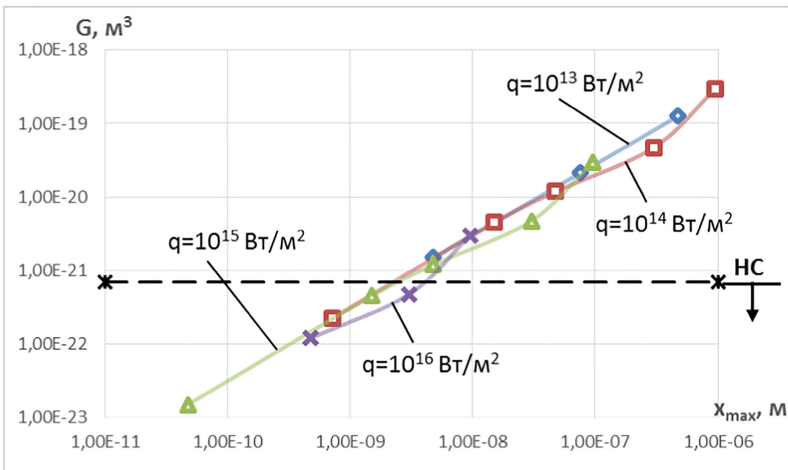


**Fig. 3.** The dependence of temperature stresses in the area of the LI on VK4 on the density of the heat flux at different depths at the time of action:  $t = 10^{-15}$  s.



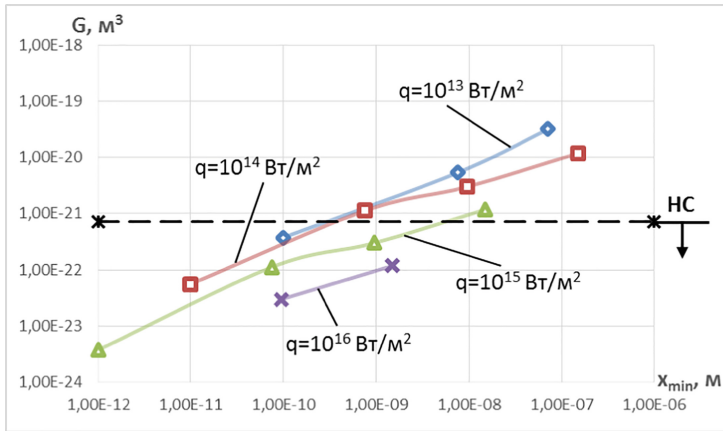
a



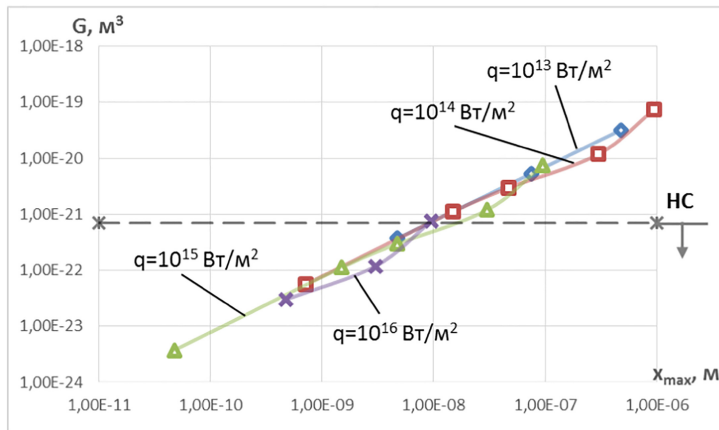
b

**Fig. 4.** Dependence of the nanocluster volume  $G$  on the minimum (a) and maximum depth (b) when exposed to laser radiation with different heat flux densities  $q$  laser radiation for TC VK8 with spot radius  $R = 10^{-6}$  m.





a



b

**Fig. 5.** Dependence of the nanocluster volume  $G$  on the minimum (a) and maximum depth (b) when exposed to laser radiation with different heat flux densities  $q$  laser radiation for TC VK8 with spot radius  $R = 5 \cdot 10^{-7}$  m.

## 5 Conclusions






For the first time, the influence of grain formation energy (nanostructure) on temperature development, its rate of change, temperature stresses and the possibility of nanostructures formation is taken into account. The influence of technological parameters (heat flux density  $10^{-15}$ – $10^{-16}$  W/m<sup>2</sup> and time of its action  $10^{-15}$ – $10^{-14}$  s), as well as the size of the spot on the possibility of nanostructures flight, was studied. It is shown that with a decrease in the size of the spot, the number of technological parameters for which it is possible to obtain nanostructures increases.

## References

1. Ono, T., Fujimoto, Y., Tsukamoto, S.: First-principles calculation methods for obtaining scattering waves to investigate transport properties of nanostructures. *Quantum Matter* **1**(1), 4–19 (2012)
2. Boles, M.A., Ling, D., Hyeon, T., Talapin, D.V.: The surface science of nanocrystals. *Nat. Mater.* **15**(2), 141 (2016)
3. Kostyuk, G., Popov, V., Kostyk, K.: Computer modeling of the obtaining nanostructures process under the action of laser radiation on steel. In: *CEUR Workshop Proceedings*, vol. 2353, pp. 729–743 (2019)
4. Kostyuk, G., Nechyporuk, M., Kostyk, K.: Determination of technological parameters for obtaining nanostructures under pulse laser radiation on steel of drone engine parts. In: *10th International Conference on Dependable Systems, Services and Technologies (DESSERT)*, Leeds, United Kingdom, pp. 208–212. IEEE (2019)
5. Alaa, F.I.I., Akimov, O., Golovko, L., Goncharuk, O., Kostyk, K.: The study of the influence of laser hardening conditions on the change in properties of steels. *East.-Eur. J. Enterp. Technol.* **2**(5), 69–73 (2016)
6. Jung, W.B., Cho, S.Y., Suh, B.L., Yoo, H.W., Jeon, H.J., Kim, J., Jung, H.T.: Polyelemental nanolithography via plasma ion bombardment: from fabrication to superior H<sub>2</sub> sensing application. *Adv. Mater.* **31**, 1805343 (2018)
7. Fortov, V.E., Ivlev, A.V., Khrapak, S.A., Khrapak, A.G., Morfill, G.E.: Complex (dusty) plasmas: current status, open issues, perspectives. *Phys. Rep.* **421**(1–2), 1–103 (2005)
8. Xiao, J., Liu, P., Wang, C.X., Yang, G.W.: External field-assisted laser ablation in liquid: an efficient strategy for nanocrystal synthesis and nanostructure assembly. *Prog. Mater. Sci.* **87**, 140–220 (2017)
9. Lu, K.: Stabilizing nanostructures in metals using grain and twin boundary architectures. *Nat. Rev. Mater.* **1**(5), 16019 (2016)
10. Alaa, F., Akimov, O., Kostyk, K.: Development of a combined technology for hardening the surface layer of steel 38Cr2MoAl. *East.-Eur. J. Enterp. Technol.* **2**(11), 56–62 (2017)
11. Palneedi, H., Park, J.H., Maurya, D., Peddigari, M., Hwang, G.T., Annapureddy, V., Lee, K. J.: Laser irradiation of metal oxide films and nanostructures: applications and advances. *Adv. Mater.* **30**(14), 1705148 (2018)
12. Ghasemi, R., Shoja-Razavi, R., Mozafarinia, R., Jamali, H., Hajizadeh-Oghaz, M., Ahmadi-Pidani, R.: The influence of laser treatment on hot corrosion behavior of plasma-sprayed nanostructured yttria stabilized zirconia thermal barrier coatings. *J. Eur. Ceram. Soc.* **34**(8), 2013–2021 (2014)
13. Long, J., Pan, L., Fan, P., Gong, D., Jiang, D., Zhang, H., Zhong, M.: Cassie-state stability of metallic superhydrophobic surfaces with various micro/nanostructures produced by a femtosecond laser. *Langmuir* **32**(4), 1065–1072 (2016)
14. Luo, F., Ong, W., Guan, Y., Li, F., Sun, S., Lim, G.C., Hong, M.: Study of micro/nanostructures formed by a nanosecond laser in gaseous environments for stainless steel surface coloring. *Appl. Surf. Sci.* **328**, 405–409 (2015)
15. Zawadzka, A., Waszkowska, K., Karakas, A., Plóciennik, P., Korcala, A., Wisniewski, K., Sahraoui, B.: Diagnostic and control of linear and nonlinear optical effects in selected self-assembled metallophthalocyanine chlorides nanostructures. *Dyes Pigm.* **157**, 151–162 (2018)



# Strength Properties Control of Mixtures Based on Soluble Glass with Ethers Solidifiers

Olga Ponomarenko<sup>1</sup> , Tatyana Berlizeva<sup>1</sup> , Igor Grimzin<sup>2</sup> ,  
Nataliia Yevtushenko<sup>1</sup> , and Tatiana Lysenko<sup>3</sup> 

<sup>1</sup> National Technical University “Kharkiv Polytechnic Institute”, 2, Kyrpychova St., Kharkiv 61002, Ukraine

berlizeva.tatyana@gmail.com

<sup>2</sup> Research and Production Center “European Engineering Technologies”, 101, Big Panasovskaya St., Kharkiv 61017, Ukraine

<sup>3</sup> Odessa National Polytechnic University (ONPU), 1, Shevchenko Ave., Odessa 65044, Ukraine

**Abstract.** The paper presents the mechanism of solidifying mixtures on a soluble glass base with complex ethers solidifiers, such as ethylene glycol acetates, triacetate with furfuryl alcohol and furfuryl oxypropyl cyclocarbonates. The castings comparative manufacturing technology based on cold-solidifying mixtures on soluble glass with these solidifiers is given. To experimentally determine and establish the regularities of increasing of the compressive strength of the mixture using ether hardeners and technological additives: ethylene glycol monoacetate (EGMA), ethylene glycol diacetate (EGDA), ethyl silicate (ES-40), ethylene glycol (EG), tetraethoxysilane (TEOS), triacetate with furfuryl alcohol (TAC with FA) and furfuryl oxypropyl cyclocarbonates are established. The basic physical and mechanical properties of mixtures with these additives, such as compressive strength, survivability, friability, gas permeability, and knocking-out ability were determined by standard methods according to the state standards (GOST). The most effective ethers solidifiers, which allow obtaining high-quality mixtures on soluble glass with the highest strength properties, were determined.

**Keywords:** Cold-solidifying mixture · Soluble glass · Ethylene glycol acetates · Furfuryl oxypropyl cyclocarbonates · Triacetate with furfuryl alcohol

## 1 Introduction

There is a large number of methods for the manufacture of casts and cores using numerous mixtures in modern foundry production. One of the most common is cold-solidifying mixtures (CSM). Depending on the nature of the binder, cold-solidifying mixtures can be divided into mixtures with organic (lignosulphonate, resins, etc.) and inorganic (soluble glass, phosphates, etc.) binders [1, 2].

One of the commonly used methods is the process of manufacturing cores and casts on soluble glass (SG), and the technology for their production is used at many enterprises. This is because soluble glass is an affordable, inexpensive and non-toxic

binder. The use of SG as a binder for the manufacture of casting and core mixtures allows us to obtain more durable casts, reduce the metal consumption of castings by producing thinner products and improve the quality of castings.

Depending on the nature of solidifying, these mixtures can be divided into mixtures with a solidifier introduced together with a binder during their preparation, and mixtures solidified by blowing with a gaseous solidifier during or after filling equipment by them and their solidification [1–3].

## 2 Literature Review

The main disadvantage when using soluble glass cold-solidifying mixtures solidified by CO<sub>2</sub>, SO<sub>2</sub> or by heat drying is the formation of fusible silicates at temperatures above 700 °C, which lead to sintering of the mixtures and an increase in their residual strength and deterioration of knocking-out ability [4].

The knocking-out ability of soluble glass mixtures depends on the content of soluble glass and its module. With an increase in the content of soluble glass and a decrease in its module (due to an increase in the liquid phase upon heating), knocking-out ability deteriorates. The knocking-out ability of liquid-glass mixtures is affected not only by the temperature of cast heating but also by the casting shrinkage. Since the steel shrinkage became greater than that of cast iron, the knocking-out ability of cores in steel castings is 1.5–1.6 times worse than that of cast iron [5].

Reducing the amount of soluble glass in the casting mixture is the simplest and most cost-effective way. However, in most cases, such a technological implementation leads to deterioration in the properties of the casting mixture itself.

One of the ways to improve the knocking-out ability of cast and core mixtures is the process of using compound ethers in conjunction with SG [6].

Therefore, the development and introduction into production of new complex additives for CSM on SG regulating the strength properties of mixtures is an urgent task of foundry production.

## 3 Research Methodology

The research is aimed at developing effective compositions of soluble glass cast and core mixtures with complex additives that allow you to control the strength of the casts and cores at the stage of their preparation, while maintaining the basic properties of the mixtures, such as survivability, gas production, gas permeability, friability and contribute to softening the mixture after pouring with metal and their cooling.

During the experiments, the mixture was prepared as follows: per 100 mass% of sand, we took 4 mass% of soluble glass with a module of 2,36 and a density of 1,47 g/cm<sup>3</sup>. As a filler of the casting mixtures, quartz sand of the grade 2K<sub>1</sub>O<sub>1</sub>O<sub>2</sub> GOST 2138-91 was used [7, 8].

The paper has researched such properties as compressive strength, survivability, friability, gas permeability, knocking-out ability.

Casting materials must have properties that meet certain cast or core mixtures; conditions for knocking-out casts and removing requirements: manufacturing techniques for casts and cores; conditions for the interaction of the cast with liquid metal during casting, solidification, and cooling of the casting; core preparation technologies [9–11].

The mechanical properties determine the strength characteristics of the mold during its manufacture, as well as when pouring it with alloy and solidifying the casting.

Testing the compressive strength of the mixtures was carried out in accordance with GOST 23409.7–78 (strength in the “wet” state) and GOST 23402.9–78 (strength in the “dry” state). For this purpose, a set was used to determine the tensile strength of cast and core mixtures of modules 04116Y with a device for compressing dry samples up to 15 MPa manufactured by UkrNIILitmash by special order of National Technical University “Kharkiv Polytechnic Institute”.

Technological properties characterize the conditions for obtaining high-quality casts and cores, as well as the conditions for the manufacture of castings with the lowest labor input and high surface quality (without cracks and blockages).

The starting materials should provide the technological properties of the mixtures on soluble glass binders, such as survivability, friability and knocking-out ability.

Survivability of self-hardening mixtures is the main parameter limiting the production cycle of cores and foundry casts. The survivability index of cold-solidifying mixtures usually was the length of time (in minutes), after which the value of its strength decreased by 30% of the maximum one.

Friability of cast and core mixtures in accordance with GOST 23409.9–78 was determined on standard cylinder specimens with a diameter and height of 50 mm. Samples were tested in the dry state. The evaluation of the friability of the mixture was made according to the amount of weight loss by a standard sample placed in a rotating wire roller, while the friability rate was expressed as a percentage.

The knocking-out ability of a mixture means the removing complexity degree of cores from castings and castings from molds. One of the simplest and most affordable methods for quantification of the knocking-out ability used in this paper was to determine the residual strength of heated and cooled reference materials. The essence of the method is as follows: the manufactured standard cylindrical samples are matured for 24 h, after which they are placed in a muffle furnace and kept at a temperature of 800 °C for 1 h. Then they are cooled and tested for strength. The difference in the readings of the strength characteristics of the samples, which were kept for 24 h and the samples subjected to heat treatment, indirectly characterizes the knocking-out ability parameter of castings.

The hydraulic properties of the mixtures mainly determine the gas formation conditions and the gaseous products removal from the mold cavity when casting with alloy, thermophysical properties – the conditions of thermal processes during solidification of the casting in the mold.

Gas permeability is a property of various porous materials, which is characterized by the ability to pass gases through itself and is one of the most important properties of casting and core mixtures. Insufficient gas permeability of the mixtures complicates the

removal of gaseous products from the mold cavity during the pouring period. The gas permeability of casting and core mixtures was determined by blowing air through a standard sample made from a tested casting or core mixture GOST 23409.12–78.

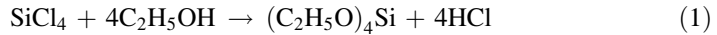
## 4 Results

Three series of experiments were carried out to study the effectiveness of mixtures on soluble glass with ether additives.

The first series of experiments were carried out to establish the physicommechanical properties of mixtures based on ethylene glycol acetates (EGA). Ethylene glycol monoacetate (EGMA) and ethylene glycol diacetates (EGDA) were used as the basis for ether solidifiers [6].

Ethylene glycol (EG), tetraethoxysilane (TEOS), ethyl silicate (ES-40) were added to EGMA and EGDA in an amount of up to 10%. TEOS and ES-40 are silicon-organic compounds. They can also play the role of SG solidifying agents when using minimal doses of amine type catalysts that accelerate the hydrolysis of siloxanes in an alkaline medium with the release of silicic acid.

Orthosilicic acid ethyl ester  $(C_2H_5O)_4Si$ , also called tetraethoxysilane, is the product of the reaction of ethyl alcohol with silicon tetrachloride. This reaction can be written as follows:



Ethylsilicate and tetraethoxysilane solutions are colloidal solutions – a sol that transforms into a silica gel that binds sand grains.

EG, TEOS and ES-40 additives were introduced in different quantities. The amount of EG ranged from 5 to 10 mass% of the amount of solidifier EGMA, and TEOS and ES-40 - from 1 to 3 mass% of the amount of hardener EGMA and EGDA.

The mixture was prepared as follows: 0.4–0.6 mass% of ether solidifiers with additives was added per 100 mass% of silica sand, then they were mixed for 3 min and then 4 mass% of sodium soluble glass was administrated and stirred for another 2 min.

The paper investigates 19 compositions of mixtures with soluble glass based on ether solidifiers with additives. The samples compressive strength data analysis showed that the highest compressive strengths are achieved in CSM on soluble glass with solidifiers of the following compositions: 1) EGDA – 91 mass% with EG – 9 mass% and 2) EGMA – 98 mass% with TEOS – 2 mass%.

The compressive strength of mixtures with solidifiers of the first composition is the following: after 1 h – 0,8 MPa, after 3 h 1,2 MPa; for the second composition – after 1 h – 1,0 MPa, after 3 h – 1,4 MPa [12, 13].

When using the studied ether solidifiers with additives, the residual strength decreases by 1,4 ... 1,6 times and amounts to 3 ... 5 MPa. For the test samples, friability after 24 h was  $\leq 0.15\%$ , gas permeability was more than 120 units. The research results showed that the survivability of mixtures using soluble solidifiers varied widely and ranged from 8 to 50 min.

The use of compound ethers can reduce the consumption of soluble glass, improve the quality of mixtures, as well as reduce the residual strength of the molds and cores and reduce the defect of castings.

The authors' papers [14, 15] studied the physical and mechanical properties of mixtures and established the effectiveness of introducing into a mixture of soluble glass with triacetin additives.

For the second series of experiments, an additive was proposed in which, besides triacetin (TAC), a certain amount of furfuryl alcohol (FA) was introduced.

The mixture was prepared as follows: 0,4 mass% of a liquid additive of triacetin with furfuryl alcohol (TAC with FA) was added per 100 mass% of silica sand in a ratio of 1:1, then was stirred for 3 min, and then 4 mass% of sodium soluble glass was introduced and was stirred for another 2 min.

The solidifying of a mixture containing TAC with FA occurs according to the reactions in Fig. 1.

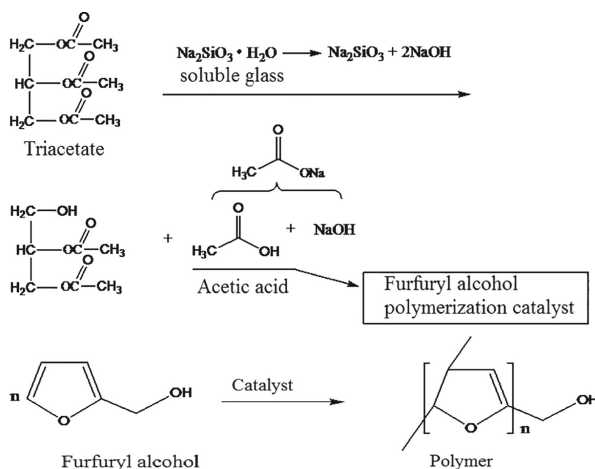


Fig. 1. The solidifying reaction of a mixture containing TAC with FA.

The solidifying of the composition begins with the hydrolysis of soluble glass with the subsequent acetic acid release and the formation of silicic acid and its condensation into a gel.

When furfuryl alcohol is added to the mixture, a three-dimensional polymer is formed. After pouring with metal, the polymer network formed by alcohol partially destructs, reducing the residual strength of the mixture.

The mixture was prepared in a similar way for experiments. First, a special TAC additive with FA was introduced and the mixture was stirred for 3 min, then soluble glass was added and mixed for another 2 min.

Indicators of compressive strength after 1 h – 1,08 ... 1,3 MPa; after 3 h – 1,40 ... 1,85 MPa; after 24 h – 2,57 ... 3,34 MPa. Survivability indices – 9 ... 30 min., friability – 0,1 ... 0,5%, residual strength – 1,04 ... 3,42 MPa [11].

As a result of studies of the strength characteristics of CSM, a special additive based on triacetate with furfuryl alcohol (TAC with FA), which allows increasing the compressive strength after 1 h compared to EGMA and EGDA. The residual strength of the mixture after pouring with metal and cooling was reduced by 4 ... 6 times compared with the CO<sub>2</sub> process.

The third series of experiments investigated the physical and mechanical properties of casting mixtures based on soluble glass with the addition of furfuryl oxypropyl cyclocarbonates (FOPCC). It aims to study the effect of additives on the knocking-out ability of mixtures.

A new universal additive obtained in NTU “KhPI” – furfuryl oxypropyl cyclocarbonates (FOPCC) based on raw materials of plant origin (Ukrainian Patent UA No. 95138) was proposed for the third series of experiments. The universal additive FOPCC is an environmentally friendly material since when pouring metal into the cast as a result of thermochemical destruction, FOPCC decomposes and releases CO<sub>2</sub> and water vapor into the environment in the volume of the formed composition.

The scheme of the process of solidifying mixtures on soluble glass with FOPCC can be represented by the scheme in Fig. 2.

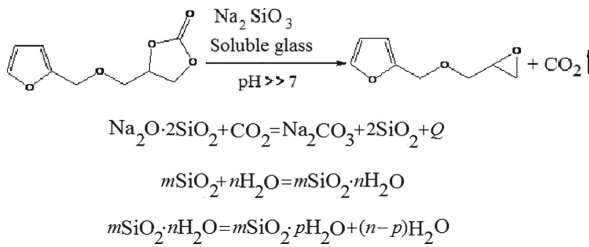


**Fig. 2.** The scheme of the process of solidifying mixtures on soluble glass with FOPCC.

The composition solidifies (quartz sand + FOPCC + soluble glass) during the interaction of the FOPCC universal additive with soluble glass. Any cyclocarbonates (propylene cyclocarbonate, FOPCC, etc.) in an alkaline medium (pH >> 7) are unstable and decompose with the release of CO<sub>2</sub>, which reacts with soluble glass to form polysilicates in the volume of the formed composition. Such systems can be attributed to nanostructured composite materials because the interaction processes between FOPCC and SG take place on the surface of quartz sand in monomolecular layers.

FOPCC organic additive has a dual function: it stabilizes the dispersion of filler particles (silica sand), since FOPCC molecules envelop the particles, creating additional solvation shells, on the one hand, and low surface tension weakens capillary forces in the pores and this determines the degree of compression during maturation (drying), on the other hand.

The most important characteristic of a silica system, when used as a binder, is the gellation time – the time for the sol-gel transition takes place. The main stage in the process of gel formation is the collision of two silica particles with a fairly low charge



on the surface. During the interaction of such particles between them, siloxane bonds are formed that irreversibly hold the particles together.

The highest gelation rate is approximately  $\text{pH} = 5$ . The moment of decomposition of FOPCC with the release of  $\text{CO}_2$ , is precisely connected with a sharp decrease in the  $\text{pH}$  of soluble glass and the system is converted from the sol structure to the gel structure, and the presence of an organic residue in the system in the form of furfuryl glycidyl ether accelerates the growth of the gelation rate.

The softening of the moldable mixture is associated with the thermal destruction process of furfuryl glycidyl ether according to the scheme in Fig. 3.

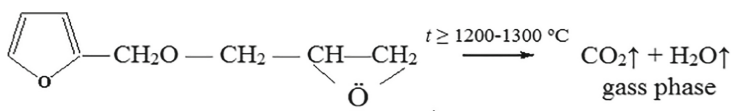
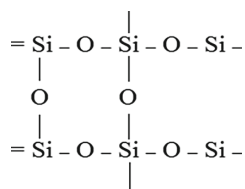


**Fig. 3.** Scheme of the process of softening the molding sand with FOPCC.

FOPCC is an environmentally friendly material since when metal is poured into a cast as a result of thermochemical destruction, it decomposes and releases  $\text{CO}_2$  and water vapor into the environment in the volume of the formed composition.

Thus, the role of  $\text{CO}_2$ , which is released from the FOPCC in the process of forming casts or cores, is to bind (neutralize) a “very alkaline” SG solution and upon reaching  $\text{pH} = 5$  a gel is formed with the structure of the polysilicate.

The introduction of FOPCC into the composition has a double function - it leads to the formation of  $\text{SiO}_2$  nanoparticles, which act as crystallization and nucleation centers, and the released  $\text{CO}_2$  (inside) brings the  $\text{pH}$  value to the optimal rates of soluble glass sol transition into a gel with a polysilicate structure and tetrahedral bonds.



As a result of the experiments, the main properties of the properties of CSM on soluble glass using FOPCC were determined: compressive strength, survivability, gas production, gas permeability, friability, and knocking-out ability, which affect the quality of castings in sand molds. The compressive strength indices for the technological sample, on average, are: after 1 h – 1.8–2.0 MPa; after 3 h – 2.5–3.0 MPa; after 24 h – 3.5–4.0 MPa. The survivability of the mixture is within 10–20 min. Friability of mixtures is in the range of 0.10–0.24%, gas permeability >400 units, residual strength – 0.74–2.06 MPa.

The compressive strength of mixtures on soluble glass with various ethereos solidifiers based on all experiments is presented in the form of dependencies in Fig. 4.

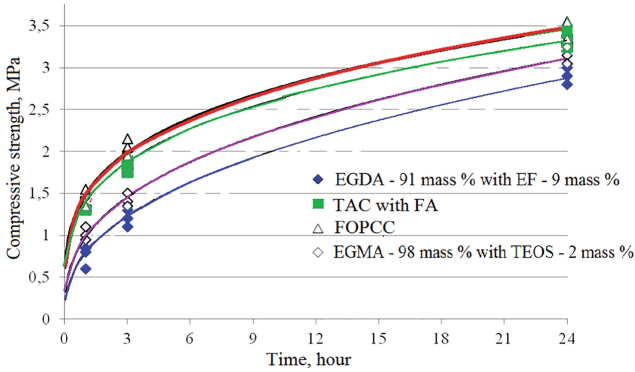


**Fig. 4.** The compressive strength of mixtures on soluble glass with various ethers solidifiers.

The presented dependencies in a general form can be described by an exponential function  $y = ax^n$  and presented in the form of mathematical dependences having the form of a parabola of the  $n^{\text{th}}$  order, for  $n < 1$ .

Table 1 shows the mathematical dependences of the increase in the strength of the mixture in time and the reliability of the approximation  $R^2$ ,  $y$  is the compressive strength of the mixture, MPa,  $x$  is time, hours.

**Table 1.** Mathematical dependences of increasing the strength of a mixture based on SG with EGA.

Composition of solidifiers based on ethers solidifiers	Mathematical dependences of the strength of the mixture	Approximation confidence value $R^2$
EGDA – 91 mass% with EG – 9 mass%	$y = 0,786 \times 0,407$	$R^2 = 0,998$
EGMA – 98 mass% with TEOS – 2 mass%	$y = 0,974 \times 0,364$	$R^2 = 0,996$
TAC with FA	$y = 1,387 \times 0,275$	$R^2 = 0,999$
FOPCC	$y = 1,408 \times 0,267$	$R^2 = 0,995$

The mathematical dependences of the compressive strength of the mixture correlate well with the approximation confidence value.

During the experiments, special attention was paid to the knocking-out ability of mixtures of residual strength, because the knocking-out process is the most difficult operation in terms of sanitary and hygienic conditions from the entire casting production cycle, which is accompanied by a large dust, gas, heat and high noise level.

The paper used the method of residual strength of heated and cooled standard samples to determine the quantitative assessment of knocking-out ability.

Figure 5 shows the residual strength of mixtures with various solidifiers.

Table 2 presents the characteristics of the mixtures based on additives studied in this work.

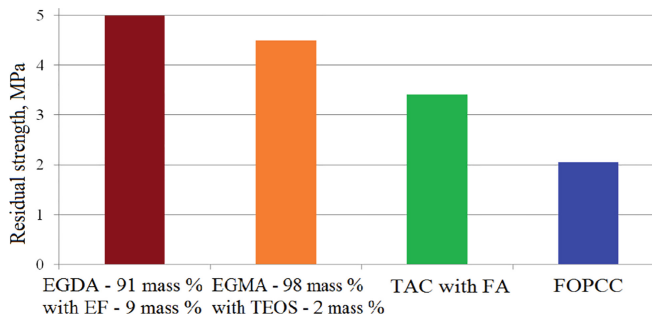


**Fig. 5.** The residual strength of mixtures on SG with various ethers solidifiers.

**Table 2.** Physical, mechanical and technological properties of soluble glass mixtures with additives.

Parameter	Units of measurements	Additive		
		EGA	TAC with FA	FOPCC
The mass ratio in the mixture	Soluble glass/additive	4,0/(0,4...0,6)	4,0/(0,5...3,0)	4,0/(0,3...0,4)
Survivability	min	8...50	10...20	12...25
Friability	%	≤ 0,15	0,1...0,5	0,066...0,13
Gas production	cm <sup>3</sup> /g	13...16	less than 10,5	4,9...7,4
Gas permeability	un.	more than 120	more than 120	450...500
Compressive strength	MPa			
1 h		0,45...1,1	1,08...1,3	1,27...1,45
3 h		0,95...1,4	1,40...1,85	1,73...2,05
24 h		1,90...2,5	2,57...3,34	2,14...3,43
Residual strength	MPa	3,0...5,0	1,05...3,42	0,74...2,06
Notional value		1,1	1,3...1,4	1,1

The analysis of comparative characteristics showed that at present the most promising is the use of TAC with FA special additive and FOPCC universal additive in mixtures with soluble glass.

## 5 Conclusions

1. The regularities of increasing the compressive strength of the mixture were experimentally determined and established using ether solidifiers and processing aids ethylene glycol monoacetate (EGMA), ethylene glycol diacetate (EGDA), ethyl silicate (ES-40), ethylene glycol (EG), tetraethoxysilane (TEOS).

2. A special additive for CSM on soluble glass based on triacetate with furfuryl alcohol (TAC with FA) has been proposed and tested, which allows increasing the compressive strength after 1 h compared to EGMA and EGDA. The residual strength of the mixture after pouring with metal and cooling was reduced by 4–6 times compared with the CO<sub>2</sub> process.
3. A new universal additive for CSM on SG based on furfuryl oxypropyl cyclocarbonates has been developed, which allows us to increase the strength of casts and cores at the stage of their preparation and helps to weaken the mixture after pouring with metal and cooling them. The universal additive FOPCC is an environmentally friendly material since when pouring metal into the mold as a result of thermal degradation, FOPCC decomposes and releases CO<sub>2</sub> and water vapor into the environment in the volume of the formed composition (Ukrainian Patent UA No. 95138).
4. The basic properties of CSM on SG using the universal additive FOPCC are determined: strength, survivability, gas production, gas permeability, friability, moisture, and residual strength, on which the quality of castings when casting in sand molds depends.
5. The use of soluble ethereal additives reduces the consumption of soluble glass to 2.5–4.0% and thereby by 1.5–2.0 times improves the knocking out ability of molds and core. Mixed additives of esters consisting of 2–3 items, a special additive TAC with FA and a universal additive FOPCC are effective.
6. The technological process of preparation of cold-hardening mixtures on liquid glass with the use of additives FOPCC was developed to obtain high-quality castings, which are introduced at the enterprises of Ukraine and in the educational process for the student's specialty "Equipment and technology of foundry production".






## References

1. Kukuy, D.M., Skvortso, V.A., Ektova, V.K.: Theory and technology of foundry. Design PRO, Minsk (2000)
2. Dobosz, S.M., Grabarczyk, A., Major-Gabryś, K., Jakubski, J.: Influence of quartz sand quality on bending strength and thermal deformation of moulding sands with synthetic binders. *Arch. Foundry Eng.* **15**(2), 9–12 (2015)
3. Dambatta, M.S., Izman, S., Yahaya, B., Lim, J.Y., Kurniawan, D.: Mg-based bulk metallic glasses for biodegradable implant materials: a review on glass forming ability, mechanical properties, and biocompatibility. *J. Non-Cryst. Solids* **426**, 110–115 (2015)
4. Kukuy, D.M., Melnikov, A.P., Rovin, S.L.: Technology of processes of mixture preparation and manufacturing of sand foundry molds. BNTU, Minsk (2009)
5. Boldin, A.N., Davydov, N.I., Zhukovsky, S.S.: Foundry Moulding Material Forming. Core Mixtures and Coatings. Mashinostroenie, Moscow (2006). Reference book
6. Huminski, YuYu., Rovin, S.L.: Environmentally friendly superfine modified ultrafine liquid glass binder. *Cast. Metall.* **3**, 41–45 (2019)
7. Saikaew, C., Wiengwiset, S.: Optimization of molding sand composition for quality improvement of iron castings. *Appl. Clay Sci.* **67**, 2–31 (2012)

8. Bakis, R., Koyuncu, H., Demirbas, A.: An investigation of waste foundry sand in asphalt concrete mixtures. *Waste Manage. Res.* **24**(3), 26–274 (2006)
9. Chaudhari, S., Thakkar, H.: Review on analysis of foundry defects for quality improvement of sand casting. *Int. J. Eng. Res. Appl.* **4**(3), 615–618 (2014)
10. Dariko, R.: Criteria for an advanced assessment of quality of moulding sands with organic binders and reclamation process products. *China Foundry* **10**(3), 181 (2013)
11. Dobosz, S.M., Jelínek, P., Major-Gabrys, K.: Development tendencies of moulding and core sands. *China Foundry* **8**(4), 438–446 (2011)
12. Zinchenko, P.S., Aksenenko, M.P., Yovbak, A.V., Orendarchuk, Y.V.: Application of liquid glass mixtures with a low content of liquid glass as a factor in improving the quality of castings for engineering purposes. *Journal «ScienceRise»* **5/2**(22), 6–9 (2016)
13. Huminski, YuYu., Rovin, S.L.: Application of a liquid glass binder modified by ultra-dispersed materials. *Foundry* **11**, 17–20 (2019)
14. Berlizeva, T.V., Ponomarenko, O.I.: Investigation of the effect of complex softening additives on the properties of cold-hardening mixtures on liquid glass. *Metall. Min. Ind.* **4**, 27–30 (2014)
15. Schetinin, A.A., Ammer, V.A., Turischev, Y.Y.: Advantages and prospects of using cold-hardening mixtures in the manufacture of critical and highly loaded castings for the aviation industry. *Bull. Voronezh State Tech. Univ.* **3**(13), 68–70 (2017)



# Design of New Nanocoatings Based on Hard Alloy

Viktor Popov<sup>1</sup> , Gennadiy Kostyuk<sup>2</sup> , Olecsandr Tymofyeyev<sup>3</sup> ,  
Kateryna Kostyk<sup>4</sup> , and Olena Naboka<sup>4</sup> 

<sup>1</sup> Joint Stock Company “FED”, 132, Sumska St., Kharkiv 61023, Ukraine

<sup>2</sup> National Aerospace University named by N.Ye. Zhukovsky “KhAI”,  
17, Chkalova St., Kharkiv 61070, Ukraine

<sup>3</sup> Kharkiv Himprom Ltd., 22 Promyslova St., Vasyshecho 62495, Ukraine

<sup>4</sup> National Technical University “Kharkiv Polytechnic Institute”,  
2, Kyrpychova St., Kharkiv 61002, Ukraine  
eklitus@gmail.com

**Abstract.** The paper investigates the possibility of creating high-entropy nitride, carbide, boride, sulfide, phosphide and oxide nanocoatings on hard alloy T12A based on hafnium, zirconium, molybdenum, tungsten, yttrium, and nickel. The study of obtaining coatings and nitrides, carbides, borides, sulfides, phosphides and oxides directly in the body of the material at ion energies in the range from 200 to  $2 \cdot 10^4$  eV with charge numbers from 1 to 3. Characteristics such as the grain volume for all these ions and nitrogen ions and the depth of their occurrence are obtained, which allows us to estimate the layers of nanostructures from compounds and elements or submicrostructures that can be formed by these high-entropy coatings. It is shown that it is possible to avoid the production of intermetallic compounds due to the high mobility of nitrogen, carbon, boron, sulfur, phosphorus and oxygen ions. It is shown that to obtain effective high-entropy coatings, it is necessary to provide an appropriate space-time distribution law of the ion supply to the CT material by controlling the installation.

**Keywords:** Highly entropic coatings · Submicrostructures · Nanostructures · Solid solutions · Intermetallide

## 1 Introduction

Currently, the study of high-entropy alloys is relevant. It is known that due to the formation of solid solutions they have high hardness and other high physical and mechanical characteristics [1–3]. There are attempts to create coatings from highly entropic alloys [4] and even experimentally get nitrides based on highly entropic alloys, but there are no theoretical works in the field of creating layers of nitride, carbide, boride, and oxide high-entropy coatings.

All this testifies to the urgency and timeliness of creation of the theory of obtaining nanostructural high-entropy coatings on the material of cutting tools.

The appearance of a new class of materials - high entropy alloys, their application can significantly improve the physical and mechanical characteristics of parts and cutting tools (CT), but they contain expensive components: hafnium, zirconium, tungsten, molybdenum and other rare-earth metals. Using these metals, it is possible to create nitride, carbide, boride and oxide coatings on the surface of CT, and their characteristics can be the same or even higher than those of high-entropy alloys. It is necessary that in the composition of high-entropy alloys were at least five different elements. As the number of elements increases, the entropy increases the same will be in the case with an increase in the number of carbides, nitrides, oxides, and borides. And one element should not be more than 30%. Obviously, for that coatings, new opportunities arise, which we still do not suspect, because they can create solid solutions with superhigh physical and mechanical characteristics, and form intermetallics, that possessing high plasticity, which, with their small amount, contribute to the realization of the properties of coatings that will effectively withstand to impact loads. All of this testifies to the timeliness and importance of ongoing research. Taking into account the adhesion interactions of the corresponding nitrides, carbides, borides and oxides with the treated material, it is possible to select surface layers with minimal adhesion interaction that will significantly reduce the adhesive wear of the coating on the CT and will reduce the cutting forces. This will increase the efficiency and effectiveness of cutting tools, taking into account the formation of nanostructures (NS).

The interaction of beryllium and magnesium with sulfur leads to the production of compounds BeS and MgS, which have a melting point exceeding 2000 °C, which allows increasing the operating temperature of the structure. Refractory sulfides will significantly increase the prospects for the use of magnesium alloys and beryllium for parts operating at elevated temperatures and requiring minimal weight.

Metal compounds with phosphorus may have a higher hardness than the base metal. Thus, magnesium forms  $Mg_3P_2$  and  $MgP_4$  compounds in the pulsed synthesis of elements at a temperature of 330–530 °C the passage of phosphorus vapor over the heated metal or at super-high pressure. With titanium, phosphorus forms a whole gamut of compounds  $Ti_3P$ ,  $Ti_2P$ ,  $Ti_2P_3$ ,  $Ti_4P_3$ ,  $Ti_5P_3$ ,  $TiP$  and  $TiP_2$ , the first 5 are obtained by melting in an arc furnace from the elements or tip ligatures are obtained by reaction between  $TiCl_4$  and  $PH_4$ , as well as by pulsed synthesis from the elements or by the interaction of titanium powder with PH, synthesis from the elements at 650 °C is obtained  $TiP_2$ .

Based on the above, it is possible to determine the use of a compound with sulfur and phosphorus: sulfur can be used as resistant temperature coatings (such as aluminum oxide), magnesium and beryllium sulfides, which can even work successfully on their own at high temperatures (up to 2000 °C), phosphides have a higher hardness and can increase wear resistance in abrasive wear can be used with magnesium sulfides, which provide high wear resistance of the surface at high temperatures, titanium phosphides together with nitrides, carbides, etc., borides can solve the problem of reducing the abrasive wear of parts and cutting tools.

## 2 Literature Review

At present the question of the creation of highly entropic alloys is regarded, which can be used in the machinery due to the high hardness, strength at significant temperatures, significantly less creep than traditional construction materials, which is also an important characteristic [1–5]. At the same time, the problem of obtaining NS in highly entropic alloys and coatings from the constituent of these alloys has not even been practically investigated experimentally (there are fragmentary data on the possibility of obtaining NS), and there are no another theoretical researches on obtaining the NS, except our [6–11].

Paper [12] reviews experimental research on nanocomposite protective coatings of various chemical compositions and structures. For adaptive multielement and multi-layer systems with specific phase composition, structure, substructure, stress state, and high functional properties, formation conditions are considered; the behavior of such systems under extreme operating conditions and in tribological applications is examined; the structural, phase and chemical composition are discussed as well as the hardness, friction and wear at elevated temperatures; and the adhesive strength of hierarchical protective coatings is analyzed.

The formation of the (TiZrNbHfTa)N/WN multicomponent coating is considered in the paper [13]. The structural investigations showed the formation of a simple disordered solid solution in (TiZrNbHfTa)N layer, b-W<sub>2</sub>N phase in WN layer with the fcc crystal structure and highly disordered bcc (1 1 0) and (2 2 0) -oriented high-entropy alloy phases, regardless of the applied bias potential. It was shown that with increasing of substrate bias from –90 to –280 V, there is a slight decrease of hardness from 34 to 31 GPa and increase of Young's modulus from 325 to 337 GPa, which can be explained by the annihilation of point defects and precipitation of relatively softer metallic phase.

The authors of work [14] believe that one of the most perspective directions of the development of surface engineering concerns hard multicomponent coatings prepared using PVD technologies. The authors present the results of the analysis of the transmission rate of the chemical composition of cathodes composed based on elements with different melting points (Al, Ti, Cr). It was presented the influence of the chemical composition of two and three-component cathodes on the chemical composition of the obtained coating in this work. The study was carried out with the EDS method using a scanning electron microscope with a chemical composition analyzer.

Multicomponent coatings with layers containing different functionality are of interest for a variety of applications, including electronic devices, energy storage, and biomaterials, according to the authors of the paper [15]. A comprehensive geometrical behavior against the multicomponent nano-activating flux, multi-walled carbon nanotubes-titanium oxide (MWCNTs-TiO<sub>2</sub>), was configured in the study [16].

The paper [17] presents some of the directions of developing the plasma electrolytic oxidation (PEO) technique to form the coatings with magnetic, catalytic, biocompatible or biocidal properties on the valve metals and alloys. It reflects the relationships between the structure, composition and functional properties of PEO coatings. The data presented suggest that PEO is an effective method of physicochemical synthesis on



metals and alloys of the surface layers with different chemical composition and certain characteristics.

Modern works do not consider the possibility of obtaining nanostructures and nanostructured coatings from sulfides and phosphides (sulfur and phosphorus ions), which can also be used to create nanostructured layers and nanocoatings with high wear resistance at high temperatures. The above shows that the use of magnesium sulfides and phosphides in coatings can significantly improve the performance of magnesium alloys, especially at high temperatures, which is an urgent and timely task for the aviation and automotive industry.

All this indicates that there is a significant need for the development of researches on the production of coatings of nitrides, carbides, borides, oxides and other solid compounds in the case of the formation of a highly entropic coating.

### 3 Research Methodology

The possibility of creating nitride, carbide, boride, sulfide, phosphide and oxide coatings on hard alloy T12A was investigated. The possibility of applying nitrides, carbides, borides, and oxides of hafnium, zirconium, molybdenum, tungsten, yttrium, and Nickel was considered. The results are obtained based on solving the joint problem of thermal conductivity and thermoelasticity determined the volume of grain and the depth of its occurrence for the considered elements, as well as nitrogen, carbon, boron, sulfur, phosphorus, and oxygen.

For three coordinates, we have an equation in finite differences. We carry out the calculation of these equations in the proposed equal to zero temperature stresses and obtain the temperature field by which we calculate the temperature stresses and the coefficient determining the influence of the final heat propagation velocity  $\tau R$ . We check the compatibility of the deformation, if not implemented, we introduce additional temperature stresses. With all this taken into account, we obtain the adjusted temperature at the first step, when the heat balance is satisfied. In the rest for the second and subsequent steps are repeated. It is considered how the time is calculated for which the temperature will change by one Kelvin at a distance of one meter. So, for example, the table gives the necessary values of the quantities to determine the corresponding value of the thermal conductivity coefficient.

### 4 Results

The possibility of creating high-entropic nitride, carbide, boride and oxide coatings on a solid T12A alloy was researched, and the possibility of applying nitrides, carbides, borides and oxides of hafnium, zirconium, molybdenum, tungsten, yttrium, and nickel was considered. For that, based on the joint problem of thermal conductivity and thermoelasticity, the volume of grain and the depth of occurrence for the elements considered, as well as nitrogen, carbon, boron, and oxygen were determined. For nitrogen, the dependence of the grain volume of the maximum and minimum depth of occurrence was found. It was determined that the volume for low energies of the order

of 200 eV corresponds to the nanograins, whereas at higher energies it exceeds them, the depth of occurrence of the volume in the first case lies in the range  $8.6 \cdot 10^{-10} \dots 3.9 \cdot 10^{-9}$  m – the minimum and  $2.7 \cdot 10^{-9} \dots 6.8 \cdot 10^{-9}$  m – the maximum.

The production of carbides requires the supply of carbon ions, which can be obtained directly from the carbon electrode by using a magnetron or from gases containing carbon. For carbon, dependences of the grain volume, the minimum depth, and the maximum depth of occurrence allow obtaining a space picture of the formation of grain in the zone of the carbon ion actis. It can be seen that nanograin can be obtained at ion energies from 200 to 2000 eV, while near 20 keV the probability of its formation is low, and for charge numbers 2 and 3 it is generally impossible. The range of minimum depths of occurrence is  $1.2 \cdot 10^{-9} \dots 9.29 \cdot 10^{-8}$  m, and the maximum depth of occurrence is  $2.94 \cdot 10^{-9} \dots 1.07 \cdot 10^{-7}$  m. It can be seen that in this case the maximum depth of the zone where the grain is formed is increased, practically up to ten micrometers, which in the last case forms submicrograin.

For the case of the action of boron ions, the grain size increases: it lies in the range of  $4.4 \cdot 10^{-9} \dots 1.364 \cdot 10^{-7}$  m. So, in the last case, we deal with submicrograin, the depth of its occurrence: the minimum lies in the range of  $1.2 \cdot 10^{-9} \dots 9.29 \cdot 10^{-8}$  m, and the maximum –  $2.9 \cdot 10^{-9} \dots 1.07 \cdot 10^{-7}$  m. In this case, the depths of occurrence exceed all the previous ones, so well as the grain size.

The transition to oxygen ions (for the formation of oxides) leads to a significant reduction in grain size to  $3.94 \cdot 10^{-9} \dots 1.04 \cdot 10^{-7}$  m, the latter value already corresponds to submicrograin. The range of depths of occurrence of the grain:  $7.49 \cdot 10^{-9} \dots 6.4 \cdot 10^{-8}$  m - the minimum and  $2.65 \cdot 10^{-9} \dots 7.7 \cdot 10^{-8}$  m - the maximum values.

In the future, depending on which sequence of layers we want to obtain based on the adhesive [2] and strength properties [3] of the coating, we select the surface layer of the coating and their alternation. To fulfill the high-entropy condition, we determine the fraction of hafnium involved in the process, taking into account the requirement which zirconium should not exceed 30%. Then we estimate the duty cycle of the voltage pulses on the evaporator with the ZrHf20 cathode and the fraction of the remaining components for which it is necessary to have one two-component cathode with a component ratio 50%/50% and two evaporators with one-component cathodes (moreover combining in the two-component cathode elements with close partial pressures at the same temperatures). Next, we consider (depending on the chosen sequence of layers), the first layer is external, for it we choose the range of depths: minimal and maximal, and also the grain size. The second in-depth will be a layer of compounds, elements (or intermetallic compounds) depending on the nature of the operation of the CT: if the CT works with a shock load, the second layer should be made of pure metal (intermetallic) or a compound that dampens the information of the first layer. The second in-depth will be a layer of compounds, elements (or intermetallic compounds) depending on the nature of the CT works: if the CT works with an impact load than the second layer should be made of pure metal (intermetallic) or from a compound that dampens the information of the first layer. Subsequent layers can be from chemical compounds.

It was found that the volume corresponding to the NS is realized up to ion energy of the order of 700–800 eV and depth: for a minimum of  $0 \dots 2.2 \cdot 10^{-8}$  m; for the maximum –  $1.8 \cdot 10^{-9} \dots 3.2 \cdot 10^{-8}$  m. It is seen that with increasing ion mass, the volumes

of NS and the depth of their occurrence are significantly reduced. This trend is tracked for practically all the ions considered. In order for nitrides to form, the charge and energy of the nitrogen ions are such like, and the depth of its occurrence must be close to that obtained for hafnium.

Turning to the zirconium ( $Zr^+$ ) dependencies, we find that NS is realized for practically all the energies studied. Moreover, at 200 eV the depths of occurrence are the minimum  $-0-6.3 \cdot 10^{-10}$  m; the maximum  $3.34 \cdot 10^{-9}-5.43 \cdot 10^{-9}$  m. At 2000 eV the minimum  $-6.37 \cdot 10^{-10}-5.37 \cdot 10^{-9}$  m; Maximum  $-5.4 \cdot 10^{-9} \dots 1.25 \cdot 10^{-8}$  m. For 20 keV, the minimum depth of occurrence is  $4.6 \cdot 10^{-9} \dots 2.48 \cdot 10^{-8}$  m; the maximum is  $1.54 \cdot 10^{-8}-3.52 \cdot 10^{-8}$  m.

From a comparison of the depths of NS for hafnium and zirconium ions with the penetration of nitrogen ions, we see that many nitrogen energies cannot be used, because the depth of their penetration is greater, and in many of the regimes nitrides, carbides, borides, and oxides will not be formed, but there will be a rather large amount of intermetallides that have small physical and mechanical characteristics, so consequently there will be zones in the material with reduced properties, that will not provide the appearance of highly entropic nitride coatings with good characteristics.

For molybdenum ( $Mo^+$ ), the depth of occurrence of NS at an energy of 200 eV is the minimum  $-0-1.18 \cdot 10^{-9}$  m, the maximum  $-1.89 \cdot 10^{-9}-4.49 \cdot 10^{-9}$  m. At an energy of 2000 eV: the minimum  $-6.12 \cdot 10^{-10}-5.65 \cdot 10^{-9}$  m; the maximum  $-5.59 \cdot 10^{-9}-1.23 \cdot 10^{-8}$  m. At 20 keV: the minimum  $-4.47 \cdot 10^{-9}-2.44 \cdot 10^{-8}$  m; the maximum  $-1.52 \cdot 10^{-8}-3.48 \cdot 10^{-8}$  m.

For tungsten ( $W^+$ ) ions, similar graphs are presented. The depths of occurrence of the NS at an energy of 200 eV are the minimum  $-0-9.89 \cdot 10^{-10}$  m, the maximum  $-1.77 \cdot 10^{-9}-4.33 \cdot 10^{-9}$  m. At an energy of 2000 eV: the  $-4.38 \cdot 10^{-10}-5.1 \cdot 10^{-9}$  m; the maximum  $-5.17 \cdot 10^{-9}-1.17 \cdot 10^{-8}$  m. At 20 keV: the minimum  $-3.79 \cdot 10^{-9}-2.19 \cdot 10^{-8}$  m; the maximum  $-1.42 \cdot 10^{-8}-3.20 \cdot 10^{-8}$  m.

It is seen that the depths of occurrence of HC are significantly different from those required for nitrogen ions, and it is necessary to select very carefully the energies and charges to obtain nitrides at a certain depth.

Depths of occurrence of NS for yttrium ions ( $Y^+$ ) at an energy of 200 eV are the minimum  $-0-1.23 \cdot 10^{-9}$  m, the maximum  $-1.92 \cdot 10^{-9}-4.54 \cdot 10^{-9}$  m. At an energy of 2000 eV: the minimum  $-6.53 \cdot 10^{-10}-5.79 \cdot 10^{-9}$  m. The maximum  $-5.45 \cdot 10^{-9}-1.25 \cdot 10^{-8}$  m. At 20 keV: the minimum  $-4.65 \cdot 10^{-9}-2.49 \cdot 10^{-8}$  m; the maximum is  $1.55 \cdot 10^{-8}-3.55 \cdot 10^{-8}$  m.

It is seen that in this case, for almost all energies, the depths are small, except that only the energy of 20 keV, that cannot always be realized in this installation, because the energy of nitrogen is much less, at which their depths are commensurable.

For nickel ( $Ni^+$ ), the dependencies of the NS volume and the minimum and a maximum depth of occurrence were found. Depths of occurrence of NS at an energy of 200 eV are the minimum  $-0-1.52 \cdot 10^{-9}$  m, the maximum  $-2.1 \cdot 10^{-9}-4.79 \cdot 10^{-9}$  m. At an energy of 2000 eV: the minimum  $-9.24 \cdot 10^{-10}-6.63 \cdot 10^{-9}$  m; the maximum  $-5.77 \cdot 10^{-9}-1.35 \cdot 10^{-8}$  m. At 20 keV: the minimum  $-5.7 \cdot 10^{-9}-2.87 \cdot 10^{-8}$  m; the maximum  $-1.7 \cdot 10^{-8}-3.95 \cdot 10^{-8}$  m.

For a nickel, the depth of occurrence is close to the depths of nitrogen deposition, which contributes to the efficient formation of HC from nitrides. The minimum and

maximum depths of grain occurrence decrease with ion mass increasing, and grain volumes are decreased significantly. The energy zone where it is possible to obtain nanostructures increases, which has a positive effect on the physic and mechanical characteristics of the coating, which for a nanostructured grain has a large microhardness, yield stress, ultimate strength. Corrosion resistance is also increased, while the ability to absorb impact loads due to a decrease in the modulus of elasticity is increased. It allows us to withstand high loads in the elastic zone, that is, for large deformations we have low stresses.

Dependences of nanocluster volume, minimum and maximum depth of NC on phosphorus ion energy are obtained. It can be seen that the volume of NC ranges from  $3.58 \cdot 10^{-28}$  to  $8.56 \cdot 10^{-24} \text{ m}^3$  (200 eV,  $z = 1$  and 20 keV,  $z = 3$ ), respectively, the minimum depth is from  $0-2.01 \cdot 10^{-8}$ , the maximum is from  $1.43 \cdot 10^{-9}$  to  $3.25 \cdot 10^{-8}$  m (respectively 200 eV,  $z = 1$  and 20 keV,  $z = 3$ ).

The transition to sulfur ions ( $S^+$ ) leads to a decrease in the volume of NC to  $3.58 \cdot 10^{-28}$ – $7.82 \cdot 10^{-24} \text{ m}^3$ , the minimum depth will be  $0-1.92 \cdot 10^{-8}$  and the maximum  $1.4 \cdot 10^{-9}$ – $3.14 \cdot 10^{-8}$  m, respectively, at  $E_i = 200 \text{ eV}$ ,  $z = 1$  and  $E_i = 20 \text{ keV}$ ,  $z = 3$ .

It is seen that the values for these ions are close, but for phosphorus, they are greater, since its atomic weight is less (30.97 AE) than that of sulfur (32.068), close values are reduced with a slight difference in the masses of ions. All this allows almost in the same layers to obtain phosphides and sulfides and this layer will increase both wear resistance and performance at sufficiently high temperatures (up to 2000 °C).

The actual size of the nanosilver for sulfides varies from 5.6 to 26 nm, for phosphorus ions and from 5 to 24 nm, that is, nanostructured layers can be realized for phosphides and sulfides.

The possibility of nitride formation taking into account the spatial nature of the action of nitrogen ions and basic metals was considered. A high-entropy coating with six metals can be realized in a VT2-MBC installation, where there are four evaporators, two of which will contain cathodes of pure metals, and the other two will have two-component cathodes. So, for example, if one of the cathodes will be from the ZrHf20 (20% Hf + 80% Zr), to ensure the production of a highly entropic coating, hafnium must be 7.5%, and zirconium is 30% - the maximum possible amount of one component in the highly entropic coating. Then the calculations show that the remaining elements should be contained 15.6% in both single-component cathodes and the two-component cathode. The calculations show that the operating time of the cathode with the material of the ZrHf20 should be four times less than the operating time of the remaining ones, which will ensure the required component ratio. The cathode must work periodically to ensure that the corresponding component ratios in the highly entropic nitride, carbide, boride and oxide coatings are obtained with the minimum amount of intermetallic compounds and amorphous phase.

Carrying out these calculations, we choose a sequence of layers: on the surface, there should be a layer from the compound having a minimum of adhesive interaction with the material being processed [7, 18]. Other layers are located taking into account the required operating mode of the CT (processing of high-strength and hardened steels, the nature of cutting - continuous, intermittent, etc.).

The algorithm for selecting the regimes for obtaining highly entropic nitride, carbide, boride and oxide coatings will be as follows:

- Having determined the sequence of the layers of compounds in-depth and by using the graphs, we select the energies of the ions of nitrogen, carbon, boron, and oxygen and the corresponding energies of the ions of hafnium, zirconium, molybdenum, tungsten, yttrium, and nickel at which the depths of their occurrence will be close to obtaining compounds at the required depth.
- Estimating the layer thicknesses for the corresponding energies and the charge number, for example, for the case of the spherical geometry of the grain, for which, by the simplest geometric transformations, we will get the time of layer formation.

$$t_i = \frac{e}{V_i} \cdot \frac{(h_i - h_{i-1})}{j_{eff}}. \quad (1)$$

Where  $e$  – the charge of an electron;  $V_i$  – the volume of grain;  $h_i$  and  $h_{i-1}$  – the coordinates of the end and beginning of the layer;  $j_{eff}$  – the effective current density, which is equal to the first critical density  $j_{eff} = j_{cr}^I$  [19] or possible for using the installation  $j_{eff} = j_{in}$ .

Assuming the cylindrical geometry of the grain, and by using simple geometric transformations, we obtain:

$$t_i = \frac{16 \cdot \pi \cdot e}{9 \cdot V_i^{2/3} \cdot j_{eff}}. \quad (2)$$

The notation is similar to the notation of expression 1.

- Having determined the time of obtaining each of the layers, we provide these regimes in the technology, then we close the chain that is necessary for the realization of the technology: the energy of ions of all sorts, their charge, the necessary current density for ions of each sort, and the operating time of the corresponding ion source. In the final analysis, we obtain a Spatio-temporal picture of the technological process with the calculated grain parameters.

It is necessary to provide a Spatio-temporal distributive law of ions in the material of a part to obtain effective high-entropy nitride, carbide, boride and oxide coatings.

## 5 Conclusions

Investigations of the action of ions B, O, N, Al, Ti, Cr with the energy of 200, 2000 and 20000 eV on carbide CT T12A were carried out. As a result of the combined action of the considered types of ions, we can obtain a high-entropy coating. Taking into account the action of nitrogen ions, that is, selecting the appropriate ion energy, it is possible to obtain a high-entropy nitride, carbide, boride, sulfide, phosphide or oxide nanostructured coating.

By creating layers of high-entropy nitride, carbide, boride, sulfide, phosphide, and oxide nanostructured coatings and selecting a sequence of layers (the first on the surface taking into account the adhesive interaction with the material being processed), we can design an effective cutting tool of high performance. The use of phosphorus and sulfur ions will allow obtaining almost the same volume of grains and the depth of their formation, so there is a real opportunity to create layers at the same time successfully working at sufficiently high temperatures (sulfides) with high resistance to abrasive wear (phosphides).

It is shown that to obtain effective high-entropy coatings, it is necessary to provide an appropriate space-time distribution law of the ion supply to the CT material by controlling the installation.

An algorithm for selecting technological modes for obtaining high-entropy nitride, carbide, boride and oxide nanocoating with alternating layers is proposed, taking into account the adhesive interaction of the surface layer with the processed material.

The study of the grain size in a hard alloy T12A showed the realization of the possibility of obtaining nanostructures.





## References

1. Yeh, J.W., Chen, Y.L., Lin, S.J., Chen, S.K.: High-entropy alloys. A new era of exploitation. In: *Materials Science Forum*, vol. 560, pp. 1–9 (2007)
2. Zhang, Y., Zuo, T.T., Tang, Z., Gao, M.C., Dahmen, K.A., Liaw, P.K., Lu, Z.P.: Microstructures and properties of high-entropy alloys. *Prog. Mater. Sci.* **61**, 1–93 (2014)
3. Ivchenko, M.V., Pushin, V.G., Wanderka, N.: High-entropy equiatomic alloys AlCrFeCoNiCu: hypotheses and experimental facts. *J. Tech. Phys.* **84**(2), 57–64 (2014)
4. Blinkov, I.V., Volkhonsky, A.O., Anikin, V.N.: Phase composition and properties of wear-resistant Ti-Al-Cr-Zr-Nb-N coatings, obtained by physical vapor deposition. *Phys. Chem. Mater. Process.* **37**, 37–44 (2010)
5. Pogrebnyak, A.D., Bagdasaryan, A.A., Yakushchenko, I.V., Beresnev, V.M.: Structure and properties of high-entropy alloys and nitride coatings on their basis. *Adv. Chem.* **83**(11), 1027–1061 (2014)
6. Kostyuk, G.: Prediction of the microhardness characteristics, the removable material volume for the durability period, cutting tools durability and processing productivity depending on the grain size of the coating or cutting tool base material. In: *Advances in Manufacturing II. Lecture Notes in Mechanical Engineering*, pp. 300–316 (2019)
7. Hartland, G.V.: Optical studies of dynamics in noble metal nanostructures. *Chem. Rev.* **111**(6), 3858–3887 (2011)
8. Manikandan, A., Antony, S.A., Sridhar, R., Ramakrishna, S., Bououdina, M.A.: Simple combustion synthesis and optical studies of magnetic  $Zn_{1-x}Ni_xFe_2O_4$  nanostructures for photoelectrochemical applications. *J. Nanosci. Nanotechnol.* **15**(7), 4948–4960 (2015)
9. Kostyuk, G., Popov, V., Kostyk, K.: Computer modeling of the obtaining nanostructures process under the action of laser radiation on steel. In: *CEUR Workshop Proceedings*, vol. 2353, pp. 729–743 (2019)
10. Alaa, F., Akimov, O., Kostyk, K.: Development of a combined technology for hardening the surface layer of steel 38Cr2MoAl. *East.-Eur. J. Enterp. Technol.* **2**(11), 56–62 (2017)
11. Norhasri, M.M., Hamidah, M.S., Fadzil, A.M.: Applications of using nano material in concrete: a review. *Constr. Build. Mater.* **133**, 91–97 (2017)

12. Pogrebnjak, A.D., Bagdasaryan, A.A., Pshyk, A., Dyadyura, K.: Adaptive multicomponent nanocomposite coatings in surface engineering. *Phys. Usp.* **60**(6), 586–607 (2017)
13. Bagdasaryan, A.A., Pshyk, A.V., Coy, L.E., Kempinski, M., Pogrebnjak, A.D., Beresnev, V. M., Jurga, S.: Structural and mechanical characterization of (TiZrNbHfTa) N/WN multilayered nitride coatings. *Mater. Lett.* **229**, 364–367 (2018)
14. Kacprzyńska-Gołacka, J., Słomka, Z., Osuch-Słomka, E., Rydzewski, M., Mazurkiewicz, A., Smolik, J.: The dependence of the chemical composition of Al-Ti-Cr multi-component coatings on parameters of the arc-evaporation process. *J. Mach. Constr. Mainten. Problemy Eksploatacji* **3**, 53–57 (2017)
15. Liu, X., Liu, W., Carr, A.J., Vazquez, D.S., Nykypanchuk, D., Majewski, P.W., Bhatia, S. R.: Stratification during evaporative assembly of multicomponent nanoparticle films. *J. Colloid Interface Sci.* **515**, 70–77 (2018)
16. Muzamil, M., Wu, J., Akhtar, M., Patel, V., Majeed, A., Yang, J.: Multicomponent enabled MWCNTs-TiO<sub>2</sub> nano-activating flux for controlling the geometrical behavior of modified TIG welding joint process. *Diam. Relat. Mater.* **97**, 107442 (2019)
17. Rudnev, V.S., Lukiyanchuk, I.V., Vasilyeva, M.S., Medkov, M.A., Adigamova, M.V., Sergienko, V.I.: Aluminum-and titanium-supported plasma electrolytic multicomponent coatings with magnetic, catalytic, biocide or biocompatible properties. *Surf. Coat. Technol.* **307**, 1219–1235 (2016)
18. Kostyuk, G., Nechyporuk, M., Kostyuk, K.: Determination of technological parameters for obtaining nanostructures under pulse laser radiation on steel of drone engine parts. In: 10th International Conference on Dependable Systems, Services and Technologies (DESSERT), Leeds, United Kingdom, pp. 208–212. IEEE (2019)
19. Boles, M.A., Ling, D., Hyeon, T., Talapin, D.V.: The surface science of nanocrystals. *Nat. Mater.* **15**(2), 141 (2016)



# Structure and Corrosion Resistance of Vacuum-Arc Multi-period CrN/Cu Coatings

Hanna Postelnyk<sup>1</sup> , Oleg Sobol<sup>1</sup> , Ondrej Chocholatý<sup>2</sup> ,  
and Sergey Knyazev<sup>1</sup> 

<sup>1</sup> National Technical University “Kharkiv Polytechnic Institute”,  
2, Kyrpychova St., Kharkiv 61002, Ukraine

annapostelnyk@ukr.net

<sup>2</sup> University of West Bohemia, 2732/8, Univerzitni St.,  
301 00 Pilsen, Czech Republic

**Abstract.** The influence of deposition conditions (pressure, bias potential, layer thickness) on the structure and corrosion resistance of vacuum-arc multi-period CrN/Cu coatings is studied. For research, we used the methods of precision XRD, scanning electron microscopy with energy dispersive microanalysis, impedance spectroscopy, and potentiodynamic polarization tests to detect corrosion resistance in a solution of 0.9% NaCl. According to structural studies, phases with an fcc crystal lattice are formed in the layers: Cu and CrN mononitride. In CrN layers obtained at the highest bias potential of  $-200$  V, a change in the lattice period associated with the action of compression stresses was revealed. Tests for corrosion resistance showed that for all the samples studied, the corrosion process has a predominantly anodic reaction. The most corrosion-resistant coatings are those obtained at a pressure of  $5 \cdot 10^{-4}$  Torr and the greatest bias potential of  $-200$  V in constant rotation mode. The feature of such coatings is the smallest thickness of copper and CrN layers (about 8 nm), the presence of compression stresses (which enhances adhesion between the layers), and the absence of a pronounced texture (the paths of easy diffusion are minimized).

**Keywords:** Composite coatings · Bias potential · Phase composition · Corrosion rate · Polarization curves · Electrochemical impedance spectroscopy

## 1 Introduction

The introduction of many modern progressive technologies requires the creation of new materials and the improvement of the properties of already known ones. The task of creating materials with desired properties can be solved through the use of structural engineering [1]. The structural engineering method has shown particularly high efficiency in predicting the properties of materials, the formation of which occurs under highly nonequilibrium conditions. Due to this, it became possible to achieve a wide range of phase, structural, and stress-strain states that cannot be achieved under equilibrium conditions. Such materials include coatings obtained by the vacuum-arc method [2, 3]. In the vacuum-arc method, nitrides are the most technologically



advanced, which provides good wear resistance and corrosion resistance [4, 5]. As a result of this, it was possible to create vacuum-arc multi-period coatings based on transition metal nitrides with very high physical and mechanical properties. In such nanocomposites, chromium nitride has a good prospect for use as a relatively inexpensive and effective material for protection against electrochemical corrosion. In addition, CrN exhibits high-temperature stability and has a relatively low coefficient of friction [5, 6].

## 2 Literature Review

Austenitic steels are widely used for the manufacture of technical and medical instruments, implants, screws for various purposes, etc. [7, 8]. However, this steel class has low wear resistance and does not have high corrosion resistance (e.g., low resistance to pitting corrosion). It is known that the main cause of corrosion and fatigue wear is the presence of chloride ions in the technological and biological environment [9]. One of the effective ways to extend the service life of such materials is to apply protective coatings that increase the corrosion resistance and wear resistance [10, 11]. The use of the vacuum-arc method allows one to obtain materials that can work under conditions of high temperatures, pressures, and also under the action of aggressive media [12, 13].

A feature of nitride coatings is that they are biocidal [14], i.e. leading to the death of bacteria on their surface. Therefore, nitride coatings can be used for medical instruments, accessories, etc. [15, 16]. In addition, nitrides have a relatively high wear resistance, which significantly exceeds the wear resistance of steels, and nitrides of transition metals are usually more stable in an aggressive environment than many marks of steel. Chromium nitride has good mechanical and corrosive properties and is used as a protective coating at elevated temperatures [17, 18]. A disadvantage of chromium nitride coatings is their relatively high fragility. To increase the plastic properties of chromium nitride coatings, multi-period composites with plastic layers of transition group metals can be used as a component.

Copper has high ductility and practically does not interact with nitrides, and therefore is a very promising material for increasing the ductility of multilayer composites.

Therefore, this work is aimed at studying the effect of technological conditions for the production of multi-period CrN/Cu coatings on their structural-phase state and electrochemical characteristics of corrosion in physiological saline using open-circuit potential, impedance spectroscopy, and potentiodynamic polarization.

## 3 Research Methodology

Coating substrates were made of AISI 321 austenitic steel. The coatings on the substrate were deposition by the vacuum-arc method at the “Bulat-6” installation with various technological parameters of deposition (Table 1). The working gas pressure ( $P_N$ ) during deposition of coatings varied within  $4 \cdot 10^{-3} \div 5 \cdot 10^{-4}$  Torr; the bias

potential supplied to the substrate was  $-65$  or  $-200$  V. The choice of such regimes was due to the need to verify the influence on the structure and properties of the ion bombardment factor during deposition. The greatest influence of ion bombardment was provided by the  $U_b = -200$  V mode at  $P_N = 5 \cdot 10^{-4}$  Torr. In this case, the continuous mode (with a constant rotation speed of the substrate during the deposition process) provided the largest specific volume of the mixed material at the interface between the layers. The  $U_b = -65$  V,  $P_N = 4 \cdot 10^{-3}$  Torr mode is standard for applying CrN coatings with less influence of the ion bombardment factor. In this mode, due to different deposition times, the thickness of the layers changed. This was necessary to change the specific volume of the mixed layer at the boundary (such a volume decreases with increasing layer thickness). Therefore, the deposition was carried out from two sources (Cr and Cu) in the regimes with constant rotation speed (rotation speed of 8 rpm) and in discrete mode (with a stop for 20 s near each of the plasma sources).

**Table 1.** Technological parameters of deposition.

Series	$P_N$ , Torr	$U_b$ , V	The condition for obtaining
1	$5 \cdot 10^{-4}$	$-200$	Constant rotation
2	$4 \cdot 10^{-3}$	$-65$	Constant rotation
3	$4 \cdot 10^{-3}$	$-65$	20 s interval, 180 layers

The deposition was carried out from two sources (Cr and Cu) in the regimes with constant rotation speed (rotation speed of 8 rpm) and in discrete mode (with a stop for 20 s near each of the plasma sources).

The phase-structural state of the samples was studied by X-ray diffractometry using a DRON-4 apparatus (Cu- $K_\alpha$  radiation). For monochromatization of the detected radiation, a graphite monochromator installed in the secondary beam (in front of the detector) was used [19]. The tables of the Powder Diffraction File international center were used to decode the diffraction patterns. The separation of profiles into components was carried out using the “NewProfile” software package. The surface morphology of the coated samples was investigated using scanning electron microscopy (SEM) (Philips XL30 ESEM).

Coatings were examined for their corrosion resistance during electrochemical processes. Electrochemical tests were carried out using a 3-electrode cell with a capacity of 200 ml and a Biologic SP-150 potentiostat. The cell consists of a coated sample (working electrode), a saturated calomel electrode (reference electrode), and a platinum electrode (counter electrode). Corrosion resistance was assessed by measuring the open-circuit potential for 1.5 h in a solution of 0.9% NaCl at room temperature.

Impedance spectroscopy was performed in the frequency range from  $10^{-2}$  to  $10^5$  Hz. The potentiodynamic polarization test was carried out in the range from  $-0.60$  to  $+1$  V at a scan speed of 1 mV/s. The contact area of the sample with the electrolyte was  $0.196$  cm<sup>2</sup>.

## 4 Results

The classical research scheme of modern materials science suggests the following sequence: composition (elemental and phase) - structure (substructure) - properties. Therefore, the first step was the study of elemental and phase compositions. Figure 1 shows the energy dispersive spectra (the top elemental composition calculated from them is shown on the right) of series 1 and 3 before the corrosion test.

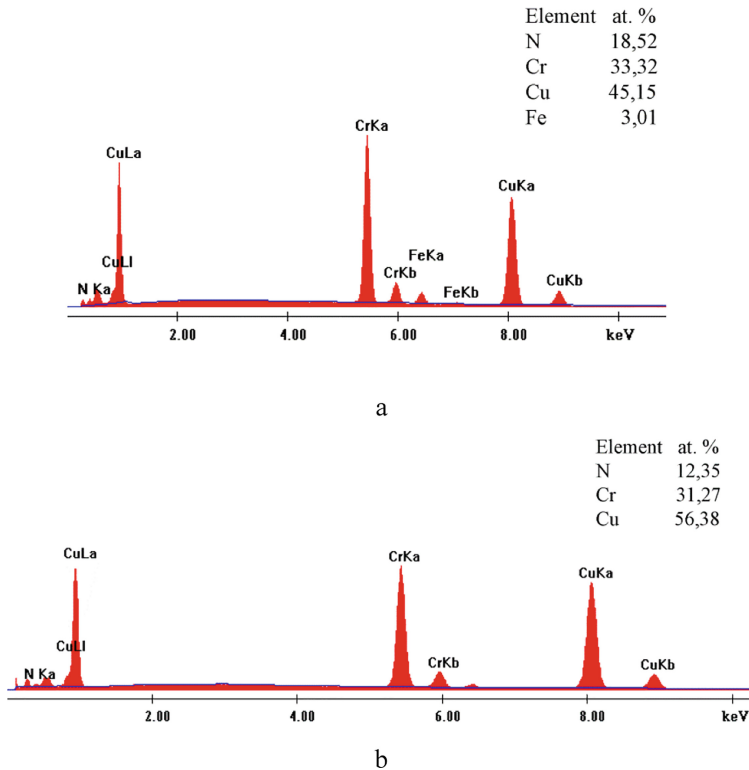


**Fig. 1.** Energy dispersive spectra with data on the elemental composition of series 1 (a) and 3 (b) before corrosion tests.

It can be seen that for series 3 obtained in the discrete mode, the relative copper content is much larger. Since, according to the experimental conditions, individual layers of copper were deposited, a large content indicates a greater thickness of the Cu layer.

To study the phase-structural state, the XRD method was used. The X-ray diffraction spectra of the coatings are shown in Fig. 2.

The spectra in Fig. 2 show that the positions of the diffraction peaks correspond well to the fcc lattices of the two phases CrN (JCPDS 76-2494) and Cu (JCPDS 89-2838). The relatively high intensity of the (111) CrN peak for samples of the 2nd series

(spectrum 2 in Fig. 2) indicates the presence in the CrN layers of a predominant orientation with the [111] axis perpendicular to the growth plane. For coatings of the 1st and 3rd series, large peaks are characteristic of the peaks from the (200) plane. The lattice periods calculated from the position of the peaks remain practically unchanged for the Cu layers and amount to  $a_{Cu} = 3,595 \text{ \AA}$ .

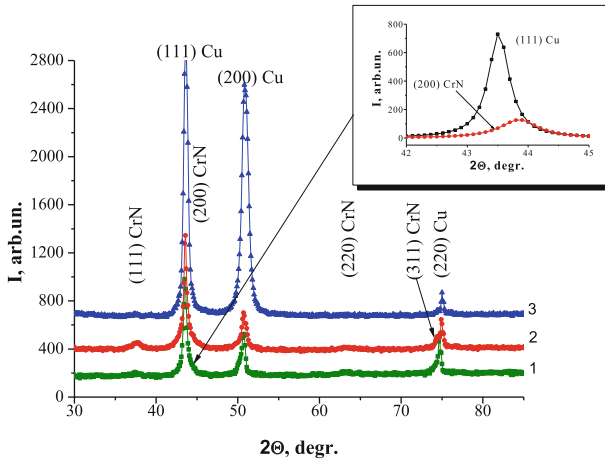


**Fig. 2.** Plots of diffraction spectra and decomposition of a complex diffraction profile of series 1 into components (insert in the upper right corner). (1 –  $P_N = 5 \cdot 10^{-4}$  Torr,  $U_b = -200$  V (continuous operation); 2 –  $P_N = 4 \cdot 10^{-3}$  Torr,  $U_b = -65$  V (continuous mode); 3 –  $P_N = 4 \cdot 10^{-3}$  Torr,  $U_b = -65$  V (discrete mode, 20 s)

For thinner CrN layers, period changes are observed. The smallest value is  $a_{Cu} = 4.1402 \text{ \AA}$  (for a sample from the 2nd series), and for samples of series 1 and 3, the period is somewhat longer and is  $a_{CrN} = 4.1568$  (1 series) and  $a_{CrN} = 4.1541 \text{ \AA}$  (3 series). The most likely reason for this change is the formation of compression stress in the CrN layers.

As a result of the corrosion tests, the potential ( $E_{corr}$ ) and current ( $I_{corr}$ ) of corrosion were established (which were calculated using the Tafel extrapolation method). Potentiodynamic polarization curves are shown in Fig. 3.

As can be seen from Fig. 3 - the process is controlled mainly by the anode part of the polarization curves [20]. From the above curves, the slope coefficients of the rectilinear portion of the anodic and cathodic parts  $\beta_a$  and  $\beta_c$  are obtained.

Since the anodic reaction takes precedence for the corrosion process on coatings (the substrate is more electronegative than coatings), the rate of continuous corrosion and not the porosity of the protective coating can be taken into account, for example in [21].

The corrosion rate is proportional to the current of corrosion and was calculated by the formula

$$CR = \frac{I_{corr} \cdot K \cdot EW}{d \cdot A}, \quad (1)$$

where CR is the corrosion rate, mm/year;  $I_{corr}$  - corrosion current, mA; K is the conversion factor determining the unit of measurement of the corrosion rate; EW - equivalent weight, gram-equivalent; d is the density, g/cm<sup>3</sup>; A is the sample area, cm<sup>2</sup>.

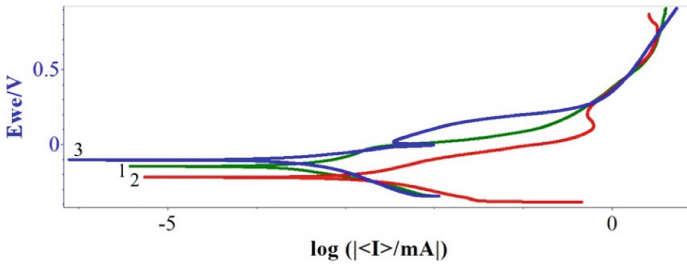


**Fig. 3.** Potentiodynamic polarization curves.

The calculation results are given in Table 2.

**Table 2.** Potentiodynamic polarization test results.

Series	$E_{corr}$ , mV	$I_{corr}$ , mA	$\beta_a$ , mV	$\beta_c$ , mV	CR mm/year
1	-99,241	$2,08 \cdot 10^{-4}$	68,3	149,8	$9,78 \cdot 10^{-3}$
2	-200,829	$8,72 \cdot 10^{-4}$	95,1	106,1	$41 \cdot 10^{-3}$
3	-229,129	$1,69 \cdot 10^{-3}$	550,4	218,3	$79,6 \cdot 10^{-3}$

Samples with a minimum corrosion current have the lowest corrosion rate. The best indicators of corrosion resistance are provided by coating samples obtained at a relatively low nitrogen pressure. Such coatings are practically not textured (Fig. 2) and therefore have few easy diffusion paths (due to a large number of misoriented intergranular boundaries). Moreover, the use of the constant rotation mode of the substrate has a clear advantage over the discrete deposition mode (due to the formation of thinner (nanometer) layers). Therefore, high corrosion resistance is most likely ensured by low diffusion mobility and rapid formation of an oxide film under conditions of oxygen deficiency during testing.

For a better understanding of the kinetics of the process, a graph of the potential change versus time is constructed and analyzed (Fig. 4).

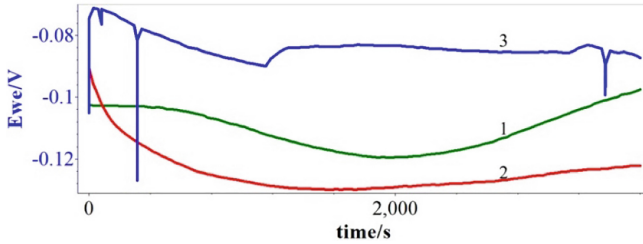


**Fig. 4.** Curves of the corrosion potential over time.

As can be seen from the curves in Fig. 4 for series 3, a sharp dissolution of the coating (first minute of testing) followed by passivation is characteristic. The presence of peaks and a change like a curve may indicate damage to the passivating layer and the protective coating as a whole. To verify this assumption, the surface morphology of the samples was studied after corrosion tests (Fig. 5).

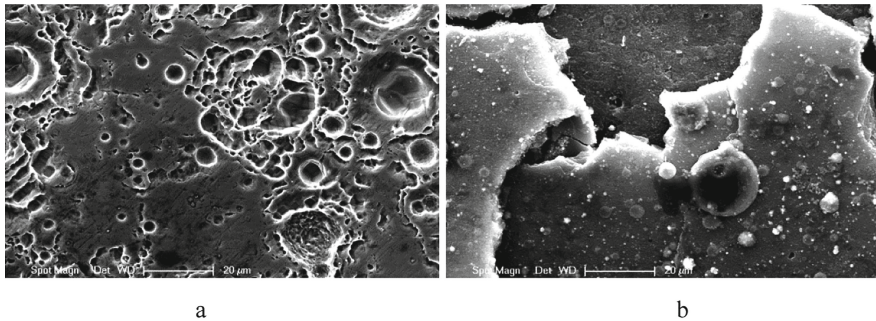
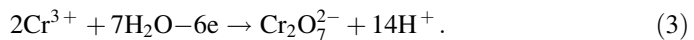
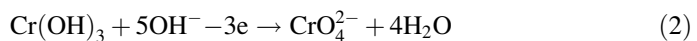


**Fig. 5.** Surface morphology of series 1 (a) and 3 (b) after corrosion tests in 0.9% NaCl.

From Fig. 5b (series 3), total surface destruction is seen, which is consistent with the course of curve 3 in Fig. 4. Energy dispersive analysis (Fig. 1b), performed before corrosion tests, showed an increased copper content, which indicates a different thickness of the layers in the coating under a discrete deposition mode. As a result, during the corrosion process, copper was dissolved in the electrolyte (after corrosion tests, the amount of copper decreased to 6.66 at.%, While the number of other elements increased: N – 39.96 at.%, Cr – 52.14 at.%) causing damage to the coating.

Samples obtained in other modes (Fig. 4, curves 1, 2) tend to passivation and superpassivation, which is associated with an increase in the valence of chromium ( $\text{Cr}^{3+}$ ) with the implementation of reactions:



A study of the surface of such coatings, such as series 1, after corrosion tests (Fig. 5a), confirms the absence of destruction, only the formation of “pits” with a developed surface relief is observed (the elemental composition of the coating remains almost unchanged).

As can be seen from a comparison of the curves of changes in potential, coating morphology, phase-structural state, and elemental composition, the resistance of coatings is ensured by the technological conditions for their production, mainly, by the continuous rotation of the substrate, which determines a small layer thickness of about 8 nm.

To obtain additional data on the corrosion resistance of the coatings, the polarization resistance was calculated using the formula

$$R_p = \frac{\beta_a \cdot \beta_c}{2,303 \cdot I_{corr} \cdot (\beta_a \cdot \beta_c)}. \quad (4)$$

The charge transfer resistance was also evaluated through protective coatings using Nyquist curves. The curves themselves for the systems under consideration are shown in Fig. 6. Comparing the diameters of the loops on the Nyquist graph, we can evaluate the corrosion properties of the samples: loops of larger diameter correspond to greater corrosion resistance.

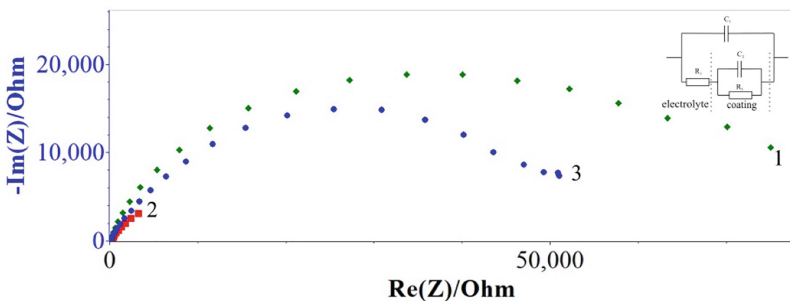


**Fig. 6.** Nyquist curves and equivalent circuit model “electrolyte-coating”. ( $C_1$ ,  $C_2$  – the capacity of the double layer and coating, respectively;  $R_1$ ,  $R_2$  – resistance of the electrolyte and phases in the coating, respectively)

This simulated equivalent circuit (Fig. 6) is in good agreement with the experimental values.

Corrosion processes associated with stray currents, charge accumulation and charge transfer through the electrolyte-coating interface can provide clarifying data necessary for understanding the corrosion resistance under real conditions. The data from calculations by formula (2)  $R_p$  (polarization resistance) and graphical calculations of the Nyquist curves (Fig. 6)  $R_{ct}$  (charge transfer resistance) are presented in Table 3.

**Table 3.** Corrosion resistance indicators according to the results of calculations of the Tafel curves and graphical analysis of Nyquist curves.

Series	$I_{\text{corr}}$ , mA	$R_p$ , Ohm·cm <sup>2</sup>	$R_{\text{ct}}$ , Ohm·cm <sup>2</sup>
1	$2,08 \cdot 10^{-4}$	19208	14677
2	$8,72 \cdot 10^{-4}$	4900	3274
3	$1,69 \cdot 10^{-3}$	7840	10515

## 5 Conclusions

Studies have shown that the composite multi-period CrN/Cu coatings obtained under different application conditions in the environment of the formation of chloride ions, for the protective mechanism, are anode. Technological formations of coatings with high corrosion resistance were determined: reduced nitrogen pressure ( $5 \cdot 10^{-4}$  Torr), high bias potential ( $-200$  V) and deposition mode, which leads to the smallest layer thickness (about 8 nm). With these parameters, a structure is formed without a pronounced predominant orientation, and a large bias potential of  $-200$  V allows the mixing process to go through at the interlayer boundary and leads to the formation of compressive stresses. When using the lower bias potential of  $U_b$  during the deposition process, the corrosion resistance of the coatings decreases significantly, and the corrosion rate increases by more than 4 times. The reason for this may be significantly less mixing at the interface between the layers (and, accordingly, a decrease in adhesive bond). With an increase in the thickness of the layers, at which the specific contribution of the mixed layer to the total thickness decreases, the corrosion rate increases even 2 times.

The assessment showed that with a coating thickness of about  $10 \mu$ , its work resource in the environment of the formation of chloride ions is about a year.

With a greater thickness of the copper layers (added as a stress relaxer in the microvolumes of the coating), destruction of the coating occurs due to the intense dissolution of the copper layers.

## References

1. Sobol', O.V., Andreev, A.A., Gorban', V.F., Stolbovoy, V.A., Meylekhov, A.A., Postelnyk, A.A.: Possibilities of structural engineering in multilayer vacuum-arc ZrN/CrN coatings by varying the nanolayer thickness and application of a bias potential. *Tech. Phys.* **61**(7), 1060–1063 (2016)
2. Öztürk, A., Ezirmik, K.V., Kazmanlı, K., Ürgen, M., Eryılmazb, O.L., Erdemirb, A.: Comparative tribological behaviors of TiN, CrN and MoNCu nanocomposite coatings. *Tribol. Int.* **41**(1), 49–59 (2008)
3. Polychronopoulou, K., Rebholz, C., Demas, N.G., Polycarpou, A.A., Gibson, P.N.: Effect of Cu content on the tribological performance of Cr-N coatings at high temperatures ( $840^\circ\text{C}$ ). In: *ASME/STLE 2009 International Joint Tribology Conference*, pp. 115–117 (2009)



4. Conde, A., Navas, C., Cristóbal, A.B., Housden, J., de Damborenea, J.: Characterisation of corrosion and wear behaviour of nanoscaled e-beam PVD CrN coatings. *Surf. Coat. Technol.* **201**(6), 2690–2695 (2006)
5. Dinu, M., Mouele, S.M., Parau, A.C., Vladescu, A., Petrik, L.F., Braic, M.: Enhancement of the corrosion resistance of 304 stainless steel by Cr–N and Cr(N, O) coatings. *Coatings* **8** (132), 1–20 (2018)
6. Martínez, E., Romero, J., Lousa, A., Esteve, J.: Wear behavior of nanometric CrN/Cr multilayers. *Surf. Coat. Technol.* **163–164**, 571–577 (2003)
7. Wang, Q., Zhou, F., Wang, C., Yuen, M.F., Wang, M., Qian, T., Matsumoto, M., Yan, J.: Comparison of tribological and electrochemical properties of TiN, CrN, TiAlN and a-C: H coatings in simulated body fluid. *Mater. Chem. Phys.* **158**, 74–81 (2015)
8. Hsu, C.H., Huang, C.K., Ou, K.L.: Improvement on hardness and corrosion resistance of ferritic stainless steel via PVD-(Ti, Cr)N coating. *Surf. Coat. Technol.* **231**, 380–384 (2013)
9. Sun, Y., Rana, V.: Tribocorrosion behaviour of AISI 304 stainless steel in 0.5 M NaCl solution. *Mater. Chem. Phys.* **129**, 138–147 (2011)
10. Kim, Y.J., Byun, T.J., Lee, H.Y., Han, J.G.: Effect of bilayer period on CrN/Cu nanoscale multilayer thin films. *Surf. Coat. Technol.* **202**, 5508–5511 (2008)
11. Niu, Y., Wei, J., Yu, Z.: Microstructure and tribological behavior of multilayered CrN coating by arc ion plating. *Surf. Coat. Technol.* **275**, 332–340 (2015)
12. Sobol, O.V., Andreev, A.A., Gorban, V.F., Meylekhov, A.A., Postelnyk, A.A., Stolbovoy, V.A.: Structural engineering of the vacuum arc ZrN/CrN multilayer coatings. *J. Nano Electron. Phys.* **10**, 06030-1–06030-5 (2018)
13. Sobol', O.V., Postelnyk, A.A., Meylekhov, A.A., Andreev, A.A., Stolbovoy, V.A., Gorban, V.F.: Structural engineering of the multilayer vacuum arc nitride coatings based on Ti, Cr, Mo and Zr. *J. Nano Electron. Phys.* **9**(3), 03003-1–03003-6 (2017)
14. Osés, J., García Fuentes, G., Fernández Palacio, J., Esparza, J., Antonio García, J., Rodríguez, R.: Antibacterial functionalization of PVD coatings on ceramics. *Coatings* **8**(5), 197–208 (2018)
15. Schmitz, T.: Functional coatings by physical vapor deposition (PVD) for biomedical applications. Würzburg (2016)
16. Kuppusami, P., Elangovan, T., Murugesan, S., Thirumurugesan, R., Khan, S., George, R.P., Ramaseshan, R., Divakar, R., Mohandas, E., Mangalaraj, D.: Microstructural, nanomechanical and antibacterial properties of magnetron sputtered nanocomposite thin films of CrN/Cu. *Surf. Eng.* **28**, 134–140 (2012)
17. Martínez, E., Sanjines, R., Karimi, A., Esteve, J., Levy, F.: Mechanical properties of nanocomposite and multilayered Cr–Si–N sputtered thin films. *Surf. Coat. Technol.* **180–181**, 570–574 (2004)
18. Benkahoul, M., Robin, P., Martinu, L., Klemberg-Sapieha, J.E.: Tribological properties of duplex Cr–Si–N coatings on SS410 steel. *Surf. Coat. Technol.* **203**, 934–940 (2009)
19. Sobol', O.V., Shovkoplyas, O.A.: On advantages of X-ray schemes with orthogonal diffraction vectors for studying the structural state of ion-plasma coatings. *Tech. Phys. Lett.* **39**(6), 536–539 (2013)
20. Ramoul, C., Beliardouh, N.E., Bahi, R., Nouveau, C., Abdelghani, D., Walock, A.: Surface performances of PVD ZrN coatings in biological environments. *Tribol. Mater. Surf. Interfaces* **13**, 12–19 (2018)
21. Montesano, L., Gelfi, M., Pola, A., Colombi, P., La Vecchia, G.M.: Corrosion resistance of CrN PVD coatings: comparison among different deposition techniques. *La Metallurgia Italiana* **2**, 3–11 (2013)



# Effect of Morphological Features on Dielectric Properties of Plasma Electrolytic Oxidation Coatings on D16T Aluminum Alloy

Elena Sevidova<sup>1</sup> , Larisa Pupan<sup>1</sup> , Yuriy Gutsalenko<sup>1</sup> ,  
Aleksandr Rudnev<sup>1</sup> , and Oksana Titarenko<sup>2</sup>

<sup>1</sup> National Technical University “Kharkiv Polytechnic Institute”,  
2, Kyrpychova St., Kharkiv 61002, Ukraine

<sup>2</sup> National Academy of the National Guard of Ukraine,  
3, Zakhysnykiv Ukrainy Sq., Kharkiv 61001, Ukraine  
oksanatitarenko4179@gmail.com

**Abstract.** The article focuses on the results of the surface morphology and dielectric properties research of the plasma electrolytic oxidation (PEO) coatings produced in the alkaline-silicate electrolytes in galvanostatic (GS) mode using rectified anode current. PEO coatings were formed on the samples of wrought aluminum alloy D16T used normally for the manufacturing of the diamond grinding wheels bodies. The influence of PEO factors on the porosity (quantity, shape, size, structure and its distribution on the surface) and dielectric properties (volume resistivity, electrolytic strength) was studied. It was established that through porosity increases in the series of solutions: 12 g/L LG (“liquid glass” (LG), a technical-grade sodium silicate solution) < 1 g/L KOH + 6 g/L LG (alkaline-silicate solution) < 2 g/L KOH + 12 g/L LG. The accordingly sizes of pores are 10...15  $\mu\text{m}$ , up to 1  $\mu\text{m}$  and 2...10  $\mu\text{m}$ . The through porosity increases in each electrolyte with increasing of anode current density from 5 to 15  $\text{A}/\text{dm}^2$ . The smallest relative increase in porosity is observed in the samples oxidated in sodium liquid glass solution 12 g/L LG. It was demonstrated that the dielectric properties research results qualitatively correlate with the micro geometric and morphology characteristics. The electrolyte composition is a major factor affecting the volume resistivity and electrolytic strength. The coatings produced in 12 g/L LG technical-grade sodium solution have the best dielectric properties, corresponding to the smallest through the porosity of these samples.

**Keywords:** Morphology · Through porosity · Surface · Galvanostatic mode · Alkaline-silicate electrolyte · Liquid glass · Electricity mode · Current density · Volume resistivity · Electrolytic strength

## 1 Introduction

Plasma electrolytic oxidation coatings (PEO coatings) on light alloys, including aluminum, have a wide range of functional properties and are used in various industries, in particular, mechanical engineering, for restoring worn surfaces of parts, providing wear resistance or resistance to aggressive environments. PEO coatings are commonly

applied to friction pairs, plain bearings, gears, pistons, cylinders, face seals for internal combustion engines and machine tools.

A rather new and promising trend in this field is increasing the efficiency of using a diamond-abrasive tool in a combined diamond-spark grinding (DSG) by creating the selective dielectric protection on mounting surfaces. The most important requirements for the coatings of this application are high dielectric properties – electric strength, electrical resistance, etc.

These properties largely depend on the morphological characteristics of PEO coatings.

## 2 Literature Review

Morphological surface features of PEO coatings on light alloys (Al, Ti, Mg) are characterized by extremely developed relief, high roughness, and porosity indices. In general, these features can both improve and degrade the characteristics of products, depending on the exploitation conditions of their applications.

Sufficient attention is devoted to the study of surface morphology of PEO coatings on aluminum alloys, due to their unique properties, such as high specific strength, corrosion resistance, weldability, and deformability. In addition to the effect of increasing the corrosion resistance, the application of PEO coatings also increases the hardness of the surface layer, its wear resistance, and dielectric properties. It allows extending the application areas of the appropriate products significantly and makes them multifunctional [1–6].

Among the characteristics of surface morphology of PEO coatings, the most attention is devoted to the study of porosity, primarily through, caused by the nature of the oxidation process. Porosity is an integral structural component of PEO coatings and undoubtedly affects the efficiency of their use.

Most of the works deal with the effect of porosity on corrosion and wear resistance, which determines the most common application areas of coatings [1, 7–11]. The studies indicate a negative effect of through porosity on the corrosion properties of coatings. Since porosity formation cannot be prevented when the PEO process, it is important to search the ways of reducing the size and relative amount of pores to obtain the quality layers uniform in a structure. It is determined that nature, qualitative and quantitative indicators of through porosity are affected by many parameters – the electrolyte composition and concentration, the base material structure, as well as current density, voltage, temperature and oxidation time. The results of studies on through porosity reduction by controlling the oxidation parameters are presented in [4–6, 12–15].

In particular, according to the statement about the key role of the electrolyte composition in the formation of the coatings morphological features, PEO processes in electrolyte suspensions containing powders of varying dispersion degrees (from nanometers to tens of micrometers) and nature (carbides, nitrides, diamond, graphite, etc.) are quite promising [13, 14, 16–19]. The decrease in porosity is explained by the incorporation of the filler solid particles into the structure of the coatings. For example, the addition of  $AL_2O_3$  sol in the electrolyte solution reduces through the porosity of the coatings almost 90 times [19].

The problem of porosity can also be solved by the use of a two-stage process, which involves the formation of a pre-porous layer and its further filling with sol-gel oxide by chemical technology [20].

The study of coatings operation in the wear mode has shown that porosity is an ambiguous factor in this case. In general, the porosity reduces the wear resistance of coatings [1, 8, 9, 21]. But in some applications, for example in friction pairs, medical products (bioactive coatings), a porous structure may be useful. In particular, during friction in the lubricating medium, the oil used enters the pores of coatings, which are a kind of reservoir for its accumulation. Further, the lubricant sequentially enters the friction zone, which significantly reduces the wear process [1, 12]. Thus, porosity plays a positive role in improving process efficiency. The paper [12] also notes that a similar pore designation can be used to incorporate the corrosion inhibitors.

The relationship between porosity as a structural component of the surface of the coating and their dielectric properties is much less. These properties are decisive for PEO coatings in diamond-abrasive tools in the DSG process [22–24].

When using PEO coatings for electrical insulation, it is to be expected that porosity, particularly through, can impair dielectric properties. First of all, this applies to electric strength, since it is much lower for air than for the main substance.

**The purpose of this work** is a qualitative assessment of through porosity effect on the dielectric characteristics of PEO coatings on D16T alloy, depending on the formation mode (the electrolyte composition, coatings thickness, current density).

### 3 Research Methodology

D16T wrought aluminum alloy was the experimental sample material due to its usual use for the manufacture of diamond grinding wheels in the DSG process.

To obtain insulating coatings, the samples were oxidated at a laboratory installation in the galvanostatic (GS) mode using rectified anode current. The main advantage of the GS mode is a high efficiency, i.e. high build-up rate of functional protective coatings controlled by current density.

Plasma electrolytic oxidation was carried out in different solutions of alkaline-silicate electrolytes – technical-grade sodium liquid glass (silicate) – LG solution, technical-grade sodium liquid glass and alkali solution (KOH + LG) with the corresponding concentrations: 12 g/l LG; 2 g/l KOH + 12 g/l LG; 1 g/l KOH + 6 g/l LG.

The selection of electric modes for the study was carried out based on the literature review and taking into account the results of previous studies [9, 10].

The thickness of the coatings on D16T alloy was measured by a non-destructive method using the NOVOTEST TP-1 eddy current thickness gauge. The measurement error was  $\pm 1.5 \mu\text{m}$ . The GS mode in all the tested electrolytes provided the formation of coatings with a thickness of 30...45  $\mu\text{m}$  meeting the requirements for insulating properties.

To study the through porosity, after oxidation, the samples were washed with running water, degreased ( $\tau \sim 1 \text{ min}$ ) in soda ash solution (40 g/l) heated to 45...50 °C. After washing, the samples were immersed ( $\tau \sim 15 \text{ s}$ ) in the pickling solution – a mixture of nitric and hydrofluoric acids (1:1) and then in the contact copper isolation

solution ( $\tau \sim 5$  min) containing 20 g/l copper sulfate and 10 g/l sulfate and hydrochloric acids.

The washed and dried samples were examined using the *USB Supereyes B008* microscope to obtain general information on the relative number and distribution of pores over the surface; magnification – 30...80. Additionally, to identify the shape, structure, and size of pores, the studies were performed using the *JEOLJSM-840* electron scanning microscope at a magnification of 200...2000.

Volume resistivity and electric strength were used as indicators of the dielectric properties of PEO coatings.

Electrical resistance  $\rho$  was measured according to the standard procedure (Fig. 1). The method involves determining the volume leakage current, depending on the applied voltage. The E6-13 teraohmmeter was used for measurements, the operating voltage was 100 V.

Volume resistivity  $\rho_v$ ,  $\Omega \cdot \text{m}$ , was calculated by the results of the electrical resistance  $\rho$  measurement:

$$\rho_v = R_v \cdot \frac{S}{h} \quad (1)$$

where  $R_v$  is the total electrical resistance of the insulating coating limited by two metal electrodes,  $\Omega$ ;  $S$  is the cross-sectional area of the contact electrode,  $\text{m}^2$ ;  $h$  is the coating thickness, m.

The anode current (50 Hz) measurement of the electric strength of the coatings (breakdown voltage) was performed. The equipment included a high-voltage transformer, protective resistor of 5 k $\Omega$  and device for smooth voltage control. The measurements were carried out at the high-voltage side. The number of breakdowns was at least 5. The circuit of needle electrodes when measuring the breakdown voltage was similar to the electrical resistance circuit (Fig. 1).

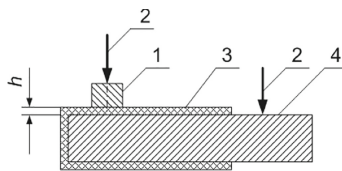


**Fig. 1.** Circuit of measuring electrodes on the sample for electrical resistance registration: 1 – copper support-current collector; 2 – pair of probe electrodes; 3 – PEO coating with thickness  $h$ ; 4 – base aluminum alloy material.

The electric strength of the coatings  $E$ ,  $\text{V}/\mu\text{m}$ , was calculated by the formula:

$$E = \frac{1}{n} \sum_{i=1}^n \frac{U_i}{h} \quad (2)$$

where  $n$  is the number of measurements;  $U_i$  is the breakdown voltage, V;  $h$  is the average coating thickness,  $\mu\text{m}$ .

## 4 Results

The electrolyte composition and current density were selected of many oxidation parameters as the most influential in the formation of the surface structure of PEO coatings, as shown by previous studies [10].

Analysis of the results of microscopic examination of the surface of insulating coatings on D16T alloy produced in the GS mode in different electrolytes at the same density (Fig. 2) allows making appropriate generalizations.

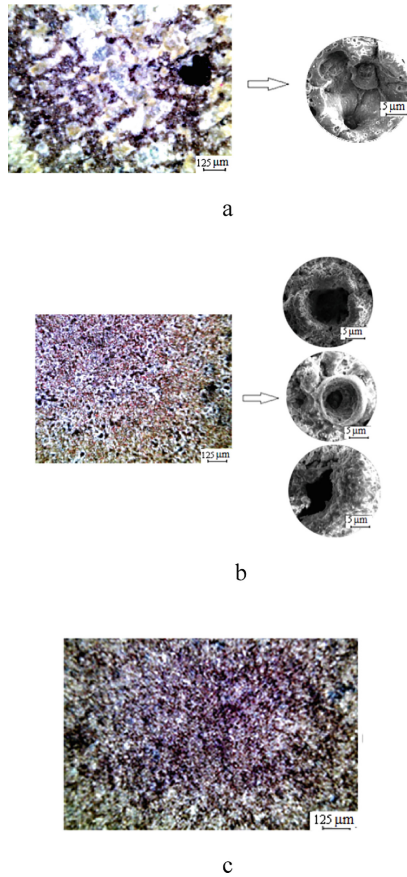


**Fig. 2.** The surface of the D16T samples with PEO coatings produced in the GS mode at current density  $j = 10 \text{ A/dm}^2$  in different electrolytes: a – 0:12; b – 2:12; c – 1:6.

In particular, the lowest regular through porosity is characteristic for PEO coatings produced in 12 g/l LG (0:12) technical-grade sodium liquid glass solution (Fig. 2a). The deposits of contact copper, the egress of which is a direct sign of the through character of pores, are observed only in separate crater structural elements of rather large size of 10...15  $\mu\text{m}$  (Fig. 2a), which are probably produced during the microarc-to-arc transition.

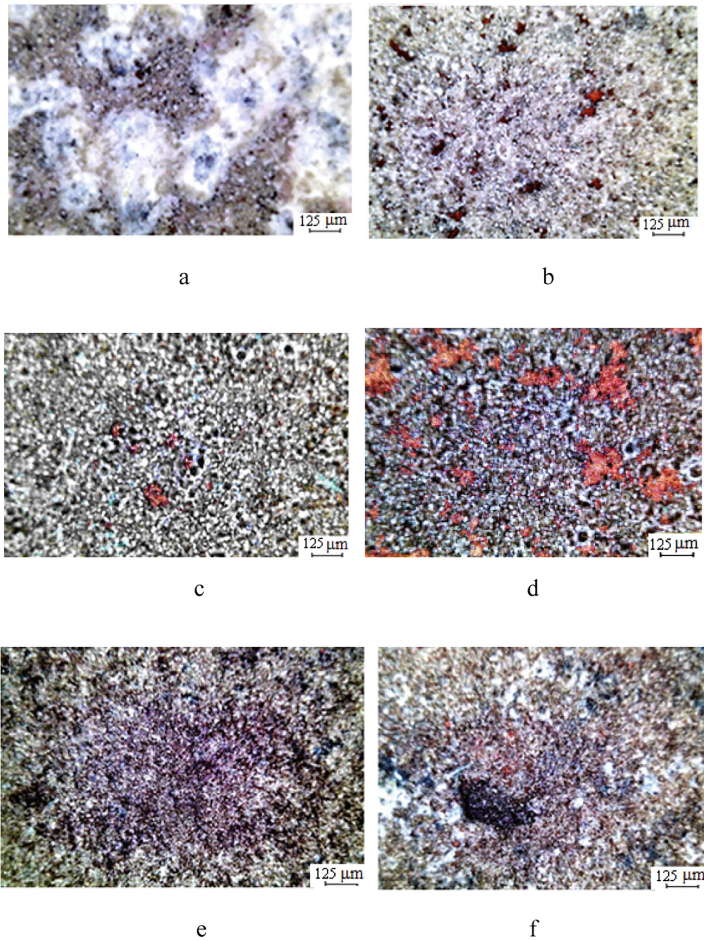


**Fig. 3.** Effect of current density of PEO coatings formation in different electrolytes on the D16T surface: a, b – 0:12; c, d – 2:12; e, f – 1:6; a, c, e –  $j = 5 \text{ A/dm}^2$ ; b, d, f –  $j = 15 \text{ A/dm}^2$ .



On the coatings produced in sodium liquid glass and alkali solution with the concentration of 2 g/l KOH + 12 g/l LG (2:12), a large number of systemic open pores of size 2...10  $\mu\text{m}$  and copper inclusions of 3...6  $\mu\text{m}$  are recorded over the entire surface, indicating the presence of through porosity (Fig. 2b). Along with porosity, open porosity is also a possible negative factor affecting the dielectric properties. Different shapes of open pores (round, oval, irregular) (Fig. 2b) may indicate the nonlinear pore propagation in the coatings, as well as the different degrees of their closing. Comparing to the surface of 0:12 solution coatings, the copper deposits on the samples oxidized in 2:12 solutions are more evenly distributed.

Relatively lower (by number and linear size) open porosity is characteristic for the oxide layers produced in 1 g/l KOH + 6 g/l LG (1:6) solution (Fig. 2c). Copper inclusions are also smaller in size, up to 1  $\mu\text{m}$ .

It should be noted that the thickness of the coating in this electrolyte is the smallest – 37  $\mu\text{m}$  (43 and 44  $\mu\text{m}$  in 0:12 and 2:12 solutions, respectively). This factor also affects the through porosity index, in particular, impairs it.

In general, if we evaluate the surface quality of the coatings by the relative number and size of pores, we can conclude that through porosity increases in the series of solutions: 0:12 < 1:6 < 2:12.

Analysis of micrographs in Fig. 3, reflecting the surface of the coatings produced in the GS mode at different current densities  $j$ , shows that through porosity increases in each electrolyte with increasing  $j$  from 5 to 15  $\text{A}/\text{dm}^2$ .

According to the obtained results, there is a significant dependence of volume resistivity on the electrolyte composition: the highest  $\rho_v$  values are characteristic for the coatings produced in 0:12 solution, the smallest – for the electrolyte oxidation coatings produced in 2:12 solution.

These data correlate qualitatively with the results of microscopic studies of PEO coatings, Figs. 2 and 3.

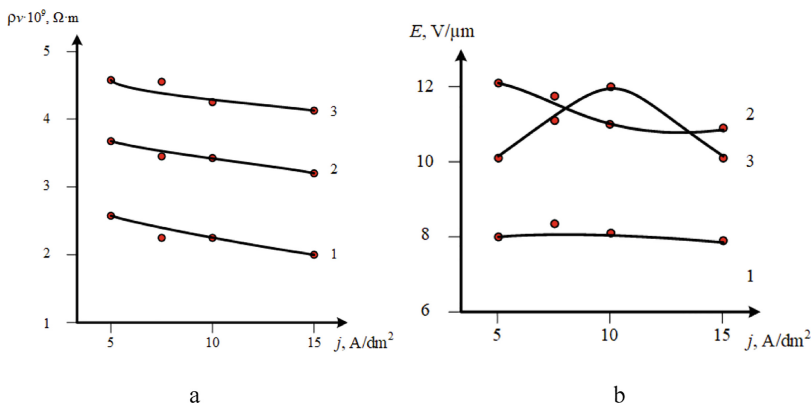


**Fig. 4.** Volume resistivity  $\rho_v$  (a) and electric strength  $E$  (b) of PEO coatings produced in the GS mode in different electrolyte solutions, depending on anode current density: 1 – 2 g/l KOH + 12 g/l LG; 2 – 1 g/l KOH + 6 g/l LG; 3 – 12 g/l LG.



An analysis of  $\rho_v$  values of the coatings on D16T alloy produced in the GS mode at different current densities  $j$  shows that volume resistivity is almost independent of this indicator. Reduction of  $\rho_v$  for the coatings obtained in 0:12 solution is within the margin of error. A slight trend of  $\rho_v$  decrease with increasing  $j$  for the samples oxidated in 1:6 and 2:12 solutions is most likely due to the increase in the number of pores.

The nature of changes in electric strength  $E$ , depending on the studied factors (electrolyte composition, current density) has a certain analogy with the corresponding dependencies of volume resistivity (Fig. 4a, b) and also correlates qualitatively with the results of microscopic analysis.

In particular, the  $E$  indicator is more sensitive to the qualitative and quantitative electrolyte composition. The lowest values of the maximum breakdown voltage and, accordingly, electric strength is determined on the PEO coatings obtained in a more concentrated 2:12 electrolyte (Fig. 4b), where the largest number of through pores is recorded. Rather higher  $E$  and  $\rho_v$  values are characteristic for the coatings produced in silicate (0:12) and dilute alkaline silicate (1:6) solutions, where the number of through pores is smaller compared to the samples oxidated in 2:12 solution.

## 5 Conclusions

Based on the research performed, it was established that there is a qualitative correlation between the nature of through porosity in the plasma electrolytic oxidation coatings on D16T alloy and their dielectric properties.

The through porosity increases in the series of solutions: 12 g/L LG < 1 g/L KOH + 6 g/L LG < 2 g/L KOH + 12 g/L LG with increasing of anode current density from 5 to 15 A/dm<sup>2</sup>. The accordingly sizes of pores are 10...15  $\mu\text{m}$ , up to 1  $\mu\text{m}$  and 2...10  $\mu\text{m}$ .

Increased through porosity of the coatings obtained in the galvanostatic mode in the 2 g/l KOH + 12 g/l LG electrolyte is one of the major reasons for the deterioration of their dielectric properties – the lowest values of resistivity and electric strength.

The coatings produced in 12 g/l LG technical-grade sodium liquid glass solution have the best dielectric properties, corresponding to the smallest through the porosity of these samples.

Further studies are related to the realization of the PEO process in suspension electrolytes to reduce the porosity and, accordingly, to improve the dielectric characteristics of the coatings on aluminum alloys.

It is also planned to continue research on the surface morphology and dielectric properties of PEO coatings on cast aluminum alloys to expand the range of structural materials for the manufacture of grinding wheels used in combined diamond-spark grinding.

## References

1. Hussein, R.O., Northwood, D.O.: Production of anti-corrosion coatings on light alloys (Al, Mg, Ti) by plasma-electrolytic oxidation (PEO). In: *Developments in Corrosion Protection*, 201–239. InTech, Rijeka (2014)
2. Suminov, I.V., Belkin, P.N., Apelfeld, A.V., Ludin, V.B., Krit, B.L., Borisov, A.M.: *Plasma-Electrolytic Modification of the Surface of Metals and Alloys: Book 2*, vol. 2. Technosfera, Moscow (2011). (in Russian)
3. Curran, J.A., Clyne, T.W.: Porosity in plasma electrolytic oxide coatings. *Acta Mater.* **54** (7), 1985–1993 (2006)
4. Orlova, D.V., Trushkina, T.V., Vakhteev, E.V., Alyakretsky, R.V.: The study of porosity of oxide coatings on aluminum alloys. In: *MAI Proceedings: Network Scientific Magazine* vol. 68, p. 14327084 (2013). (in Russian)
5. Famiyeh, L., Xiaohu, H.: Plasma electrolytic oxidation coatings on aluminum alloys: microstructures, properties, and applications. *Mod. Concepts Mater. Sci.* **2**(1), 000526 (2019)
6. Sotomonte, S.F., Pinzon, C.B., Vegrara S.G.: Growth of PEO ceramic coatings on AA 2024-T3 aluminium alloy. *J. Phys.: Conf. Ser.* **687**, 012037 (2016)
7. Zhang, P., Nie, X., Hu, H.: Wear and galvanic corrosion protection of Mg alloy via plasma. SAE Technical Paper 2009-01-0790 (2009)
8. Montoya, R.D.Z., Vera, E.L., Pineda, Y.T., Cedeno, M.L.: Effect of the layer of anodized 7050-T6 aluminum corrosion properties. *J. Phys.: Conf. Ser.* **786**, 012032 (2017)
9. Xie, H., Cheng, Y., Li, S., Cao, J., Cao, L.: Wear and corrosion resistant coatings on surface of cast A356 aluminum alloy by plasma electrolytic oxidation in moderately concentrated aluminate electrolytes. *Trans. Nonferrous Met. Soc. China* **27**(2), 336–351 (2017)
10. Ji, S., Weng, Y., Wu, Z., Ma, Z., Tian, X., et al.: Excellent corrosion resistance of P and Fe modified micro-arc oxidation coating on Al alloy. *J. Alloys Compd.* **710**, 452–459 (2017)
11. Shao, L., Li, H., Jiang, B., Liu, C., Gu, X., Chen, D.: A comparative study of corrosion behavior of hard anodized and micro-arc oxidation coatings on 7050 aluminum alloy. *Metals* **8**(3), 165 (2018)
12. Walsh, F.C., Low, C.T.J., Wood, R.J.K., Stevens, K.T., Archer, J., Poeton, A.R., Ryder, A.: Plasmaelectrolytic oxidation (PEO) for production of anodized coatings on light weight metal (Al, Mg, Ti) alloy. *Trans. Inst. Metal Finish.* **87**(3), 122–135 (2009)
13. Wang, X., Wu, X., Wang, R., Qiu, Z.: Effect of  $\text{Na}_3\text{AlF}_6$  on the Structure and Mechanical Properties of Plasma Electrolytic Oxidation Coatings on 6061 Al alloy. *Int. J. Electrochem. Sci.* **8**, 4986–4995 (2013)
14. Aliramezani, R., Raeissi, K., Santamaria, M., Hakimizad, A.: Characterization and properties of PEO coatings on 7075 Al alloy grown in alkaline silicate electrolyte containing  $\text{KMnO}_4$  additive. *Surf. Coat. Technol.* **329**, 250–261 (2017)
15. Hussein, R.O., Zhang, P., Xia, Y., Nie, X., Northwood, D.O.: The effect of current mode and discharge type on the corrosion resistance of plasma electrolytic oxidation (PEO) coated magnesium alloy AJ62. *Surf. Coat. Technol.* **206**(7), 1990–1997 (2011)
16. Wang, P., Pu, J., Xiao, Y.-T., Hu, W.-J., Wu, T., Cao, W.-J., Gong, Z.-Y., Huang, M.: Effect of graphite additives in electrolytes on characteristics of micro-arc oxidation coatings on 7E04 aluminum alloy. *Surf. Rev. Lett.* **26**(4), 18501780 (2019)
17. Wu, X., Qin, W., Guo, Y., Xie, Z.: Self-fabricative coating grown by micro-plasma oxidation on aluminum alloys in the solution of aluminate-graphite. *Appl. Surf. Sci.* **254**(20), 6395–6599 (2008)

18. Liu, Y., Xu, J., Gao, J., Yuan, Y., Gao, C.: Influences of additive on the formation and corrosion resistance of micro-arc oxidation ceramic coatings on aluminum alloy. *Phys. Procedia* **32**, 107–112 (2012)
19. Laleh, M., Sabour Rouhaghdam, A., Shahrabi, T., Shanghi, A.: Effect of alumina sol addition to micro-arc oxidation electrolyte on the properties of MAO coatings formed on magnesium alloy AZ91D. *J. Alloys Compd.* **496**(1–2), 548–552 (2010)
20. Xu, X., Lu, P., Guo, M., Fang, M.: Cross-linked gelatin/nanoparticles composite coating on microarc oxidation film for corrosion and drug release. *Appl. Surf. Sci.* **256**(8), 2367–2371 (2010)
21. Arrabal, R., Mohedano, M., Matykina, E., Pardo, A.: Characterization and wear behaviour of PEO coatings on 6082-T6 aluminium alloy with incorporated  $\alpha$ -Al<sub>2</sub>O<sub>3</sub> particles. *Surf. Coat. Technol.* **269**, 64–73 (2015)
22. Gutsalenko, Yu.G., Sevidova, E.K., Stepanova, I.I., Strel'nitskij, V.E.: Evaluation of dielectric properties of micro-arc coatings on deformable aluminum alloys. *Probl. At. Sci. Technol.* **114**, 125–127 (2018)
23. Gutsalenko, Yu.G., Sevidova, E.K., Stepanova, I.I.: Evaluation of technological capability to form dielectric coatings on AK6 alloy, using a method of microarc oxidation. *Surf. Eng. Appl. Electrochem.* **55**(5), 602–606 (2019)
24. Sevidova, E., Gutsalenko, Yu., Rudnev, A., Pupan, L., Titarenko, O.: The study of surface microgeometry and morphology of plasma electrolytic oxidation dielectric coatings on aluminum alloys. In: Ivanov, V., et al. (eds.) *Advances in Design, Simulation and Manufacturing II. DSMIE-2019, LNME*, pp. 302–310. Springer, Cham (2020)



# Structural Engineering of Nanocomposite Coatings Based on Tungsten and Titanium Carbides

Oleg Sobol<sup>1</sup> and Osman Dur<sup>2</sup>

<sup>1</sup> National Technical University “Kharkiv Polytechnic Institute”,  
2, Kyrpychova St., Kharkiv 61002, Ukraine  
sool@kpi.kharkov.ua

<sup>2</sup> Hacettepe University Technopolis, Üniversiteler Mahallesi 1596. Cadde 6.  
F-Blok Kat: 3 Bey-tepe, 06800 Ankara, Turkey

**Abstract.** The elemental and phase compositions, structure, substructure, and mechanical properties of nanocomposite coatings based on a quasibinary system of tungsten and titanium carbides are studied. It was found that as a result of selective sputtering during coating formation, it is enriched with heavy tungsten atoms in comparison with the sputtered target. The content of carbon atoms varies in proportion to the change in the content of titanium atoms in the coating, which is determined by the higher binding energy in the Ti-C system compared to W-C. With a low content of titanium atoms in the coating (up to 7 at.%), a two-phase state is formed in the coating from (Ti, W)C (with an fcc crystal lattice (structural type NaCl) and W<sub>2</sub>C (with a hexagonal close-packed lattice) phases. Characteristic concentration regions with a certain growth rate of crystallites and the formation of a microstrain state. It has been established that in areas with low concentrations of impurity elements, hardness maxima are detected which are associated with the formation of a two-phase state and the appearance of a predominant orientation of crystallites with the [111] axis perpendicular to the growth plane. The hardness of nanocomposite coatings is significantly higher than the hardness of basic WC and TiC coatings and corresponds to a superhard state with the maximum value (39.1 GPa).

**Keywords:** Quasibinary system · Nanocomposite · Phase composition · Crystallites · Texture · Microstrain · Hardness

## 1 Introduction

Currently, structural engineering is the most effective method of achieving the necessary (high) functional properties [1, 2]. This is determined by a significant expansion of the capabilities of controlling the structural state under nonequilibrium conditions (which is characteristic of modern methods of obtaining materials) [3, 4]. And the highest functional properties were achieved by using materials from the interstitial phases [5, 6]. The possibilities of surface structural engineering in recent years have been significantly expanded by using highly nonequilibrium processes in the formation of materials [7, 8]. As a result of this, it was possible to create artificial composite

materials (nanocomposites) with ultra-high hardness and strength [9, 10]. Nanocomposites (i.e., composites based on nanosized elements) are created based on two structural approaches: by stratification of supersaturated solid solutions into several phases (mainly by spinodal-like mechanisms) [11, 12] and by creating multilayer composite materials [13, 14].

## 2 Literature Review

In multi-element nanocomposites, the highest functional characteristics were achieved in Ti-Si-N materials as a result of decomposition (in the spinodal type) with the formation of nanosized crystallites in an amorphous matrix [15, 16]. The use of silicon is determined by the fact that silicon is slightly soluble in nitride systems of transition metals and such systems (supersaturated with Si atoms) tend to decompose and form composites with high hardness [17, 18].

Another type of system in which an increase in properties can be achieved by spinodal decomposition is quasibinary systems [19, 20]. The greatest effect can be achieved with the formation of quasibinary systems under highly nonequilibrium conditions [21]. Under such high nonequilibrium conditions, the process of material formation takes place under ion-plasma deposition methods [22, 23].

The functional properties of quasibinary systems of interstitial phases are largely determined by the binding forces in their binary components [24, 25]. To estimate the bond strength, the enthalpy of formation  $\Delta H_{298}^0$  can be used. A necessary condition for spinodal decomposition in quasibinary systems of interstitial phases is a significant difference  $\Delta H_{298}^0$  of their constituent components.

Among transition metal carbides, the highest heat of formation, and therefore the highest resistance to thermal effects, are carbides of metals of the 4th group of elements, and the lowest heat of formation is inherent in carbides of metals of the 6th group [26].

In the temperature range of 20 ... 900 °C in the equilibrium state, carbides of metals of the 4th group have a simple cubic crystal lattice of the structural type NaCl. In contrast, carbides of metals of the 6th group have more complex types of crystal lattices (orthorhombic or hexagonal).

Under nonequilibrium conditions for the formation of materials by cathodic sputtering due to the high rate of thermalization of the energy of the deposited particles, a simpler cubic crystalline structure such as NaCl [27]. Under conditions close to equilibrium in the W-C system, such a structure is formed only at temperatures above 2000 °C. In a crystal lattice of a structural type NaCl, atoms of one sort are located in the octahedral environment of atoms of another sort. A feature of the NaCl type cubic lattice is the high resistance of the structure to non-stoichiometry. This explains the stabilization of phases with a structural type of NaCl when deviating from stoichiometry under the influence of radiation-stimulated processes during the deposition of coatings of interstitial phases [28, 29].

The combination of metal carbides of the 4th (TiC) and 6th groups (WC) into the quasibinary WC-TiC system allows one to obtain a unique combination of two-phase

states in a single composite (thermodynamically equilibrium (TiC) and nonequilibrium (WC)). Such a combination can be the basis for obtaining materials with unique structural state and high functional (primarily mechanical) properties.

Therefore, in this work, the aim was to determine the structural engineering capabilities for the TiC-WC quasibinary carbide system with a change in the composition and deposition temperature of vacuum condensates (obtained by magnetron sputtering method) based on them.

### 3 Research Methodology

Coatings were obtained by ion sputtering of a target—a cathode. For sputtering, a planar magnetron circuit was used.

Sputtering targets were manufactured by hot pressing at a temperature of  $T_{hp} \approx 1700$  °C. The targets for quasibinary systems were two-phase and contained TiC phases with a cubic lattice of the NaCl structural type and a WC phase with a simple hexagonal lattice. The used targets of different compositions are shown in Table 1.

**Table 1.** Composition of sputtered targets and coatings formed at  $T_S = 700$  °C.

Series number	Composition of the sputtered target	Coating composition, at. %		
		Ti	W	C
1	5 mol% TiC – 95 mol% WC	2.6	63.3	34.1
2	10 mol% TiC – 90 mol% WC	6.1	56.1	37.8
3	60 mol% TiC – 40 mol% WC	30.9	27.8	41.3
4	90 mol% TiC – 10 mol% WC	48.1	10.3	41.6
5	100 mol% TiC	51.2	–	48.8

Sputtering was carried out in an inert gas Ar at a pressure of 0.2 ... 0.3 Pa. The applied spray voltage of 320...400 V ensured the flux density of the deposited metal atoms  $j_{Me} \approx (2...9)10^{15} \text{ cm}^{-2}\text{c}^{-1}$ . Two substrate temperatures were used in the deposition of ( $T_s$ ) 300 °C and 700 °C. The coating thickness was 1.2 ... 1.7  $\mu\text{m}$ . As substrates, polished single crystal silicon and stainless steel plates were used.

The phase composition of coatings was investigated by X-ray diffraction analysis using the DRON-4 system with Cu-K $\alpha$  radiation (0.154 nm) according to the Bragg-Brentano scheme. To monochromatize the detected radiation, we used a graphite monochromator, which was installed in the secondary beam (in front of the detector) [30]. 2Theta range varied from 20 to 80° with a step duration of 0.01°.

To decode the diffraction spectra, tables of the Powder Diffraction File international center for diffraction data were used [31].

Electron microscopy studies were carried out using a JEOL - 2100 transmission electron microscope and an FEI Nova NanoSEM 450 scanning electron microscope. The elemental composition of the coatings was studied by analyzing the characteristic X-ray spectra generated by the electron beam in a scanning electron microscope.

The microhardness was measured by the Vickers method at a load of 0.5 N.

## 4 Results

The primary study of coatings was to study the surface and side morphology. Figure 1 shows the corresponding images of coatings obtained at different substrate temperatures during deposition ( $T_s$ ).

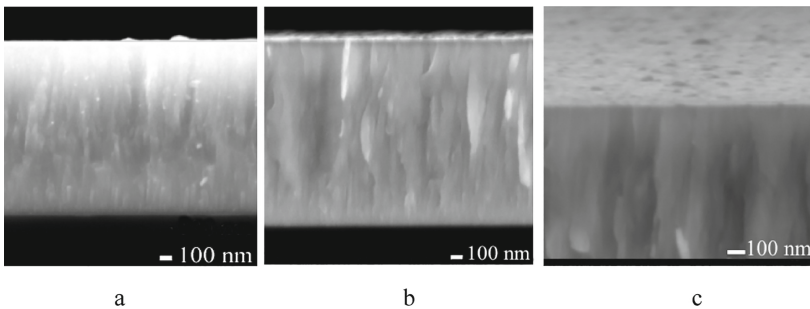


**Fig. 1.** Side cross-sectional photos of coatings obtained by sputtering a target with a composition of 10 mol% TiC - 90 mol% WC at  $T_s = 300$  °C (a), 700 °C (b), and the surface of the coating obtained at 700 °C (c).

It can be seen that the coatings obtained at a relatively low  $T_s = 300$  °C have a practically unoriented structure with the multidirectional growth of nanometer-sized crystallites (Fig. 1a). With an increase in  $T_s$ , condensates form with an oriented growth of crystallites in the direction of particle incidence. It is seen that in the coatings formed at  $T_s = 700$  °C, the formation of a fibrous type structure occurs (Fig. 1b). As can be seen from the lateral section of this coating, oblong columns are formed with a base size of 15–25 nm and a height of 300–400 nm. This leads to an inhomogeneous morphology of the surface layer of such a coating (Fig. 1c).

The second important characteristic of coatings is their composition. Figure 2 shows a map of the element distribution in a coating obtained at  $T_s = 700$  °C on a silicon substrate. It can be seen that all elements (W, Ti, and C) are evenly distributed over the coating volume. There is no predominant distribution of elements at the boundary with the substrate and on the surface.

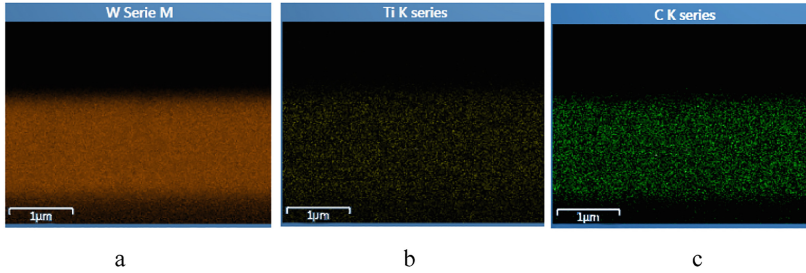


**Fig. 2.** Map of distribution of tungsten (a), titanium (b) and carbon (c) over the volume of the coating.

The data obtained based on such an elemental analysis are summarized in Table 1. It can be seen that, in comparison with the targets that were sprayed, the content of the heaviest tungsten atoms by mass increases in the coatings. The reason for the increase in the W content in the coating may be secondary selective sputtering from the deposition surface of lighter Ti and C atoms. Moreover, with an increase in the relative content of titanium atoms in the target, the intensity of the secondary sputtering increases. This is manifested in a change in the ratio of Ti/W atoms in the coatings compared with the target from 0.78 (when spraying a target with a composition of 5 mol% TiC - 95 mol% WC) to 0.52 (when spraying a target with a composition of 90 mol% TiC - 10 mol% WC). Along with a change in the Ti/W ratio, the carbon content also changes in the surface. However, in this case, a different type of dependence is observed: the relative content of C atoms in the coatings increases with increasing Ti content. The observed trend can be associated with a significantly higher heat of formation of titanium carbide compared with tungsten carbide ( $-183.8$  kJ/mol and  $-37.7$  kJ/mol, respectively). This determines the high resistance of TiC with increasing temperature.

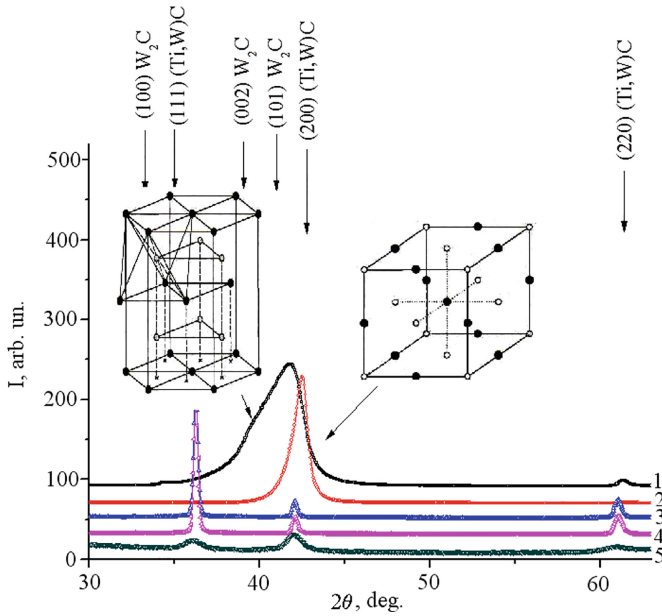
The effect of the composition of the sputtered target on the phase composition of the coatings was analyzed according to X-ray diffraction data. Figure 3 shows XRD patterns for coatings of different compositions obtained at  $T_S = 700$  °C.

It can be seen that for series 1 and 2 (in which the Ti content is 2.6 at.% and 6.1 at.%), a two-phase state forms. This is the (Ti, W)C phase with the fcc crystal lattice (a structural type of NaCl) and the  $W_2C$  phase with the hcp crystal lattice (lattice types are shown schematically in Fig. 3). With a higher Ti content, a single-phase state (Ti, W)C is formed in the coating phase with fcc crystal lattice.

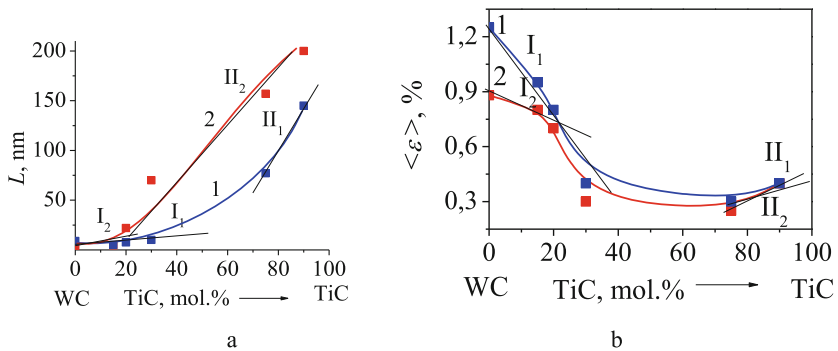
Analysis of their substructure (crystallite size  $L$  and microstrain  $\langle \epsilon \rangle$ ) was carried out by the approximation method for the (Ti, W)C phase with a cubic crystal lattice. The content of the TiC component in the sputtering target was chosen as the change parameter.

Figure 4 shows the corresponding dependencies of  $L$  and  $\langle \epsilon \rangle$  on the composition at temperatures  $T_S = 300$  °C and  $700$  °C. One can see a similar character of the dependencies with increasing TiC content (increasing  $L$  and decreasing  $\langle \epsilon \rangle$ ). The reason for such changes is the strengthening of the interatomic bond with an increase in





**Fig. 3.** XRD patterns of the coatings of the TiC-WC quasibinary system obtained at  $T_S = 700$  °C for different compositions of the sprayed target: 1–5% mol% TiC–95 mol% WC, 2–10% mol% TiC–90 mol% WC, 3–75% mol% TiC–25 mol% WC, 4–90% mol% TiC–10 mol% WC, 5–100% mol% TiC.



**Fig. 4.** The dependence of the crystallite size (a) and microstrain (b) of the coatings on the content of the TiC component in the sputtering target: 1 -  $T_S = 300$  °C, 2 -  $T_S = 700$  °C; I and II - concentration areas with a characteristic change in the parameter.

the Ti content in the nodes of the crystal lattice. In this case, two characteristic regions can be distinguished in the concentration dependences  $L(C_{TiC})$  and  $\langle \epsilon \rangle(C_{TiC})$  (Fig. 4, labeled I and II).

Processing the obtained dependencies and identifying characteristic regions of the dependence of the rate of change of crystallite size on the TiC content in the coating ( $I_1$ ,  $II_1$ , and  $I_2$ ,  $II_2$  for curves 1 and 2 in Fig. 4, respectively) showed that in the case of small  $T_S = 300$  °C, the region  $I_1$  with a low crystallite growth rate of 0.29 nm/mol% (in this case, the final crystallite size after coating formation remains virtually unchanged) occupies a concentration range from 0 to 40 mol%. Region  $II_1$  is characterized by a high crystallite growth rate (about 4.22 nm/mol%) and corresponds to a concentration region of 70 to 90 mol%.

For coatings deposited at large  $T_S = 700$  °C, the beginning of region  $II_2$  shifts toward a lower TiC content and, as a result, region  $II_2$  corresponds to a larger concentration gap. Thus, region  $I_2$  with a low crystallite growth rate of 0.42 nm/mol% corresponds to a range of TiC content from 0 to 20 mol%. And region  $II_2$  with a high crystallite growth rate (2.89 nm/mol%) is in the range TiC content from 20 to 90 mol%.

Figure 4 shows that in the concentration gap  $II_2$  there is a proportional dependence  $L(C_{TiC})$ . This may be due to the sufficiently high mobility of the deposited atoms. Such conditions lead to a more uniform (with a low content of structural defects) structure of the crystal lattice of the (Ti, W)C phase with an increase in the specific content of titanium atoms.

An analysis of the dependence of microstrain on the concentration of the TiC component in the coating indicates that the  $\langle \varepsilon \rangle$  value is mainly affected by the small content of the components (TiC in the case of a base from WC and vice versa).

At  $T_S = 300$  °C (curve 1 in Fig. 4b, in the range of up to 40 mol% TiC dissolved in WC and up to 30 mol% WC dissolved in TiC), a pronounced concentration dependence  $\langle \varepsilon \rangle (C_{TiC})$  is observed. In these concentration regions, upon dissolution of TiC (with a large  $\Delta H_{298}^0$ ) in WC (with a relatively small  $\Delta H_{298}^0$ ), the rate of change of the dependence  $\langle \varepsilon \rangle (C_{TiC})$  is greatest and amounts to 0.024%/mol% (region  $I_1$ ). When WC is dissolved in TiC (i.e., in this case, the base material has a large  $\Delta H_{298}^0$  value), the concentration dependence has a smaller slope, which corresponds to a rate of change of 0.005%/mol% (region  $II_1$ ).

For high temperature,  $T_S = 700$  °C (curve 2 in Fig. 4b), the microstrain for pure WC is much smaller and amounts to 0.88%. This can be attributed to significantly larger atoms that are deposited, which promotes the recombination of defective sites. In the region of TiC content up to 20 mol% in WC, the rate of change  $\langle \varepsilon \rangle (C_{TiC})$  is much lower and amounts to 0.0087%/mol% (region  $I_2$ ). Upon dissolution of WC in TiC (up to 30 mol%), the rate of change of  $\langle \varepsilon \rangle (C_{TiC})$  is 0.0086%/mol% (region  $II_2$ ). Note that for both  $T_S$  the lowest value  $\langle \varepsilon \rangle$  corresponds to content close to equiatomic (for Ti and W atoms).

The most universal method, microhardness measurement, was used to determine the mechanical characteristics of coatings. Figure 5 summarizes the microhardness of the coatings obtained by sputtering targets of different compositions. The deposition temperature of the coatings is 700 °C.

Figure 5 shows that the hardness of the nanocomposite significantly exceeds the hardness of pure WC and TiC coatings. Moreover, there are 2 maxima in the dependency. These maxima are located in the region of low concentrations of the second

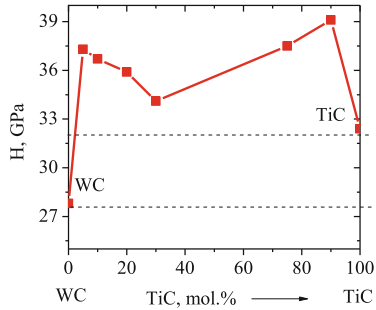


**Fig. 5.** Dependence of the microhardness of coatings deposited at  $T_S = 700\text{ }^\circ\text{C}$  on the TiC content in sputtered targets (dashed lines show hardness values for WC and TiC, respectively).

phase. Moreover, in the case of low TiC content, the peak of the maximum hardness corresponds to the formation of a two-phase state (Fig. 3). And for a small WC content in the base TiC material, the peak in hardness corresponds to a single-phase state of a solid solution with a predominant orientation of crystallites with an axis [111] perpendicular to the growth plane.

## 5 Conclusions

1. The dependence of the growth morphology of composite coatings based on a quasi-binary system of tungsten and titanium carbides on the deposition temperature has been revealed. With an increase in the deposition temperature from  $300\text{ }^\circ\text{C}$  to  $700\text{ }^\circ\text{C}$ , the coating structure changes from a practically non-oriented structural state with multidirectional crystallite growth to a fibrous structure with an explicit growth texture.
2. As a result of selective sputtering during coating formation, it is enriched with heavy W atoms in comparison with the sputtered target.
3. The content of carbon atoms increases in proportion to the increase in the content of titanium atoms in the coating, which is determined by the higher binding energy in the Ti-C system compared to W-C.
4. At a low content of titanium atoms in the coating (up to 7 at.%), a two-phase state is formed in the coating from (Ti, W)C (with an fcc crystal lattice (a structural type of NaCl) and  $W_2C$  (with a hexagonal close-packed lattice) of phases.
5. According to the data of substructural characteristics, characteristic concentration regions with a certain growth rate of crystallites and the formation of a microstrain state are revealed.
6. An increase in the deposition temperature leads to a shift in the high growth rate of crystallites to the region of low concentrations and a decrease in the magnitude of microstrain.
7. The presence of two maxima on the concentration dependence of the hardness of the coatings was established. These maxima are located in the region of low concentrations of impurity elements (Ti in basic tungsten carbide and W in basic

titanium carbide) and are associated with the formation of a two-phase state and the appearance of a predominant orientation of crystallites with the [111] axis perpendicular to the growth plane.






## References

1. Morton, B.D., Wang, H., Fleming, R.A., Zou, M.: Nanoscale surface engineering with deformation-resistant core-shell nanostructures. *Tribol. Lett.* **42**(1), 51–58 (2011)
2. Bourebia, M., Laouar, L., Hamadache, H., Dominiak, S.: Improvement of surface finish by ball burnishing: approach by fractal dimension. *Surf. Eng.* **33**(4), 255–262 (2017)
3. Sobol', O.V., Andreev, A.A., Gorban, V.F.: Structural engineering of vacuum-arc multiperiod coatings. *Met. Sci. Heat Treat.* **58**(1), 40–42 (2016)
4. Mayrhofer, P.H., Mitterer, Ch., Wen, J.G., Greene, J.E., Petrov, I.: Self-organized nanocolumnar structure in superhard TiB<sub>2</sub> thin films. *Appl. Phys. Lett.* **86**(13), 131909(3) (2005)
5. Musil, J.: Hard nanocomposite coatings: thermal stability, oxidation resistance and toughness. *Surf. Coat. Technol.* **207**, 50–65 (2012)
6. Sobol', O.V., Postelnyk, A.A., Meylekhov, A.A., Andreev, A.A., Stolbovoy, V.A., Gorban, V.F.: Structural engineering of the multilayer vacuum arc nitride coatings based on Ti, Cr, Mo and Zr. *J. Nano Electron. Phys.* **9**(3), 03003-1–03003-6 (2017)
7. Sobol', O.V., Meylekhov, A.A.: Conditions of attaining a superhard state at a critical thickness of nanolayers in multiperiodic vacuum-arc plasma deposited nitride coatings. *Tech. Phys. Lett.* **44**(1), 63–66 (2018)
8. Mayrhofer, P.H., Mitterer, Ch., Hultman, L., Clemens, H.: Microstructural design of hard coatings. *Prog. Mater. Sci.* **51**(8), 1032–1114 (2006)
9. Euchner, H., Mayrhofer, P.H.: Designing thin film materials-Ternary borides from first principles. *Thin Solid Films* **583**, 46–49 (2015)
10. Tsai, Y.-Z., Duh, J.-G.: Thermal stability and microstructure characterization of CrN/WN multilayer coatings fabricated by ion-beam assisted deposition. *Surf. Coat. Technol.* **200**(5–6), 1683–1689 (2005)
11. Zhang, R.F., Veprek, S.: On the spinodal nature of the phase segregation and formation of stable nanostructure in the Ti-Si-N system. *J. Mater. Sci. Eng. A* **424**(1–2), 128–137 (2006)
12. Veprek, S., Veprek-Heijman, M., Karvankova, P., Prochazka, J.: Different approaches to superhard coatings and nanocomposites. *Thin Solid Films* **476**(1), 1–29 (2005)
13. Sobol', O.V., Andreev, A.A., Gorban, V.F., Meylekhov, A.A., Postelnyk, H.O., Stolbovoy, V.A.: Structural engineering of the vacuum Arc ZrN/CrN multilayer coatings. *J. Nano Electron. Phys.* **8**(1), 01042-1–01042-4 (2016)
14. Yang, Q., He, C., Zhao, L.R., Immarrigeon, J.-P.: Preferred orientation and hardness enhancement of TiN/CrN superlattice coatings deposited by reactive magnetron sputtering. *Scripta Mater.* **46**(4), 293–297 (2002)
15. Li, S.Z., Shi, Y., Pen, H.: Ti-Si-N films prepared by plasma-enhanced chemical vapor deposition. *Plasma Chem. Plasma Process.* **12**(3), 287–297 (1992)
16. Veprek, S.: The search for novel, superhard materials. *J. Vac. Sci. Technol. A* **17**, 2401–2420 (1999)
17. Zhang, X.D., Meng, W.J., Wang, W., Renh, L.E., Baldo, P.M., Evans, R.E.: Temperature dependence of structure and mechanical properties of Ti-Si-N coatings. *Surf. Coat. Technol.* **177–178**, 325–333 (2001)

18. Endrino, J.L., Palacín, S., Aguirre, M.H., Gutiérrez, A., Schäfers, F.: Determination of the local environment of silicon and the microstructure of quaternary CrAl(Si)N films. *Acta Mater.* **55**(6), 2129–2135 (2007)
19. Schmalzried, C., Telle, R., Freitag, B., Mader, W.: Solid state reactions in transition metal diboride-based materials. *Z. Metallkd.* **92**(11), 1197–1202 (2001)
20. Shibuya, M., Yamamoto, Y., Ohyanagi, M.: Simultaneous densification and phase decomposition of TiB<sub>2</sub>-WB<sub>2</sub> solid solutions activated by cobalt boride addition. *J. Eur. Ceram. Soc.* **27**(1), 307–312 (2007)
21. Euchner, H., Mayrhofer, P.H., Riedl, H., Klimashin, F.F., Limbeck, A., Polcik, P., Kolozsvári, S.: Solid solution hardening of vacancy stabilized Ti<sub>x</sub>W<sub>1-x</sub>B<sub>2</sub>. *Acta Mater.* **101**, 55–61 (2015)
22. Musil, J., Kos, Š., Zenkin, S., Číperová, Z., Javdošňák, D., Čerstvý, R.: β-(Me<sub>1</sub>, Me<sub>2</sub>) and MeN<sub>x</sub> films deposited by magnetron sputtering: novel heterostructural alloy and compound films. *Surf. Coat. Technol.* **337**, 75–81 (2018)
23. Musil, J., Bell, A.J., Vlček, J., Hurkmans, T.: Formation of high temperature phases in sputter deposited Ti-based films below 100°C. *J. Vac. Sci. Technol. A* **14**, 2247 (1996)
24. Jansson, U., Lewin, E.: Sputter deposition of transition-metal carbide films - a critical review from a chemical perspective. *Thin Solid Films* **536**, 1–24 (2013)
25. Zhang, Y., Li, J., Zhou, L., Xiang, S.: A theoretical study on the chemical bonding of 3d-transition-metal carbides. *Solid State Commun.* **121**(8), 411–416 (2002)
26. Kuo, L.-Y., Shen, P.: On the condensation and preferred orientation of TiC nanocrystals – effects of electric field, substrate temperature and second phase. *Mater. Sci. Eng. A* **276**(1–2), 99–107 (2000)
27. Sobol, O.V.: Structural engineering vacuum-plasma coatings interstitial phases. *J. Nano Electron. Phys.* **8**(2), 02024-1–02024-7 (2016)
28. Krzanowski, J.E., Endrino, J.L.: The effects of substrate bias on phase stability and properties of sputter-deposited tungsten carbide. *Mater. Lett.* **58**, 3437–3440 (2004)
29. Romanus, H., Cimalla, V., Schaefer, J.A.: Preparation of single phase tungsten carbide by annealing of sputtered tungsten-carbon layers. *Thin Solid Films* **359**, 146–149 (2000)
30. Sobol', O.V., Shovkoplyas, O.A.: On advantages of X-ray schemes with orthogonal diffraction vectors for studying the structural state of ion-plasma coatings. *Tech. Phys. Lett.* **39**(6), 536–539 (2013)
31. Smith, D.K., Jenkins, R.: The powder diffraction file: past, present, and future. *J. Res. Natl. Inst. Stand. Technol.* **101**(3), 259–271 (1996)



# Numerical Simulation of the Microstructure of Structural-Inhomogeneous Materials

Oleg Zabolotnyi<sup>(✉)</sup> , Viktoriya Pasternak , Igor Andrushchak ,  
Nataliia Ilchuk , and Kostiantyn Svirzhevskiy 

Lutsk National Technical University, 75, Lvivska St., Lutsk 43018, Ukraine  
volynasi@gmail.com

**Abstract.** The algorithm of the process of filling the powders of structurally inhomogeneous materials (SIM). Based on the developed computer program for modeling the process of random packaging of various particles of the charge (powder), the structural characteristics of the source material were predicted (aluminum, copper, saponite). Classification of structurally inhomogeneous materials by size and particle shape is presented. The research of separate areas of the microstructure of particles of structurally inhomogeneous materials by the application program is substantiated Smart-eye. The microstructure of inhomogeneous materials obtained as a result of the entanglement of particles was investigated. The functional dependencies of porosity on the computer-simulation modeling of densities of various shapes and sizes of particles in the mold are investigated.

Thus, there are grounds for asserting that the developed software for the process of formation of structurally inhomogeneous materials with the help of mathematical and computer modeling can be used to predict existing or create new composites with specified properties for operation under certain conditions, as well as the dynamic calculation of composite media taking into account the size of structural elements, establishing a correlation between components, structure, and properties.

**Keywords:** Porosity · Microstructure · Algorithm · Modelling · Forecasting · Inhomogeneous materials · Particle formation · Structural characteristics

## 1 Introduction

The level of modern science allows us to process a large volume of information that promotes the emergence of new methods and approaches to the microstructure analysis. One of these areas is the computer-simulation modeling of the structurally inhomogeneous materials. It should be noted that this direction allows for revealing concrete observations and statements of facts to predict various properties of materials, products, and processes. In turn, computer-information technologies began to be used intensively from the 90s of the last century and in the field of materials science, creating a new discipline – “computer material science”.

Obtaining new materials with qualitative structural properties is possible with the help of the traditional technology of powder metallurgy. When manufacturing such

materials with the necessary complex of features, it is required to control the parameters of their structure in the process of technology implementation at all stages. This concerns, first of all, operations of filling the mold. Real powders have a diverse form and wide gamma along with granulometric composition. In the case of the use of particles of natural, spherical shape, we obtain materials with more or less homogeneous properties by volume. The use of irregularly shaped particles complicates the situation. Exploring the structures and physical-mechanical characteristics of the blanks obtained by such particles in field experiments are difficult due to the large variety of powders in shape and size. Therefore, research on the structure of such materials based on irregular and spherical particles using computer-simulation modeling is an urgent task.

## 2 Literature Review

Across the world, many scientists are involved in the issues of forecasting the properties of materials. A study of the physicomechanical properties of inhomogeneous materials of his time involved a relatively significant number of researchers, among which it is important to note [1, 2]. The results obtained in these studies are phenomenological, and therefore the mechanical properties in most cases are not correlated with the structure of materials. Also, considerable attention is paid to the stability of multifractal spectra relative to the change in brightness, rotation, and scale of the image of structurally inhomogeneous materials. The study of optimization of acoustic control of inhomogeneous materials using methods of planning and statistical modeling of a complete two-level factor experiment is covered in the study [3].

It should be noted that structurally inhomogeneous materials are the most widespread among natural and artificial ones. They are widely used in various industries, construction, water supply, and more [4]. In their structure, these materials are very diverse, and the properties of these materials are different [5]. In turn, structurally inhomogeneous materials are characterized by several physical-mechanical and technological properties. These include particle shape, size and particle size distribution (granulometric composition), specific surface (dispersion) [6, 7] and also, the hardness of the particles, the pixometric density of particles, the boundary conditions and the formation of powder particles, fluidity, etc. [8].

One of the main factors determining the quality of the sintered parts is the granulometric composition of the source material. For a well-compressed preform and after the next sintering of products with a given porosity, a powder is required fractions form with specific particle sizes and the ratio of these fractions to each other [9].

An essential condition for the further development and improvement of this industry is to provide it with modern computer and mathematical modeling, suitable for efficient classification of used materials in size to optimize their granulometric composition. Therefore, approaching the problem of computer modeling of the structure needs to be differentiated to each group of structurally inhomogeneous materials to take into account their properties. However, the division of materials and their properties into groups is conditional. Therefore, structurally inhomogeneous materials, at first glance, can be easily classified according to the number of components or the number

of phases forming the material. It implies that each component has at least one distinctive feature, either physical or statistical, concerning another. However, such a division of materials is entirely arbitrary, since in statistical mixtures for each component, it can be divided into groups by other features. Therefore, the classification of inhomogeneous materials depends on the tasks that need to be solved for these materials [10]. And also, the feature of these works is that the main factors of structurally inhomogeneous materials that influence the change of parameters of an elastic wave are investigated [11]. However, despite the efforts of scientists, several problems in the field of computational materials science are still open. Therefore, further research is crucial that requires more integrated approaches, including the use of new functional materials and structures. And also, new ideas, methods and principles of construction, implementation of higher accuracy of reliable measurement channels, and hence the implementation of fundamental and applied research using the latest methods and technologies of production.

### 3 Researches Methodology

The purpose of the research is to develop a computer program for modeling the process of random packing of various particles of a charge (powder), as well as to investigate the functional dependencies of porosity and structure based on computer simulation of densities of different shapes and sizes of particles in a mold.

To conduct a scientific study of structurally inhomogeneous materials (SIM), the developed software was used to simulate the filling of particles of different shapes and sizes in a rectangular container. Since the initial stage of powder metallurgy technology is the filling packing of powder to mold with a sufficiently low filling density, it is important to optimize the packing density of monodisperse and polydisperse particles to minimize porosity and achieve the best functional properties of the pressed material.

It should be noted that modeling the structure of structurally inhomogeneous materials makes it possible to obtain additional information about the processes that occur during their manufacture and operation and thus facilitate the control and optimization of their manufacturing processes. To predict the physical and mechanical properties of structurally inhomogeneous materials, a quantitative model of their microstructure takes an important place, which allows us to judge the degree of their inhomogeneity and, consequently, porosity. In this case, it is a spherical, sphero-quadrant and triangular shape of the particles, which allows us to establish the relationship between the porosity and the coordination number of particles. It should also be noted that the coordination number allows us to evaluate the quality of the structure of structurally inhomogeneous materials and serves as a reference point for the construction of approximations of the physical characteristics of the porosity.

Some physical and structural characteristics of composite materials to some extent depend on the shape of the particles, so when studying these characteristics on mathematical models, it is necessary to take into account the deviation of the particle shape from the spherical one. And when modeling packages of spherical and non-spherical elements, there are some general principles, which consist in a random drawing of the parameters of these elements and their location in space (in the



package), in the sequence of the packaging of these elements, in the methods of constructing algorithms and programs. The basis of the fill is to check the conditions of non-intersection (1) of elements of random filling as each other, both among themselves and with the boundaries of the hypothetical container. The interface of the developed computer program for modeling the process of random packing of different charge fractions in a rectangular container is shown in Fig. 1.

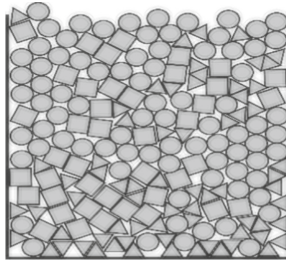


**Fig. 1.** Filling particles in different shapes and sizes.

In particular, for the modeling of packages, each element was described by ten generalized coordinates: three coordinates of the center ( $x_{ki}, y_{ki}, z_{ki}$ ) one of the hemisphere, the lengths of three pivots and the three Euler angles, as well as the radius of the cross-section of the cylinder ( $R_i$ ). The condition of not crossing (one-way contact with the possibility of lagging) of spheres in the bases of different cylinders is written in the form:

$$(X_{ki} - X_{pj})^2 + (Y_{ki} - Y_{pj})^2 + (Z_{ki} - Z_{pj})^2 \geq (R_{ki} - R_{pj})^2 \tag{1}$$

The proposed computer-simulation model describes the non-stationary processes associated with free filling-packed particles. To do this, unlike existing geometric-statistical models, it is recommended to simulate the dynamic interaction of systems from the particles, which is quite possible to be implemented using modern high-performance computer technology. The displacement of each lobe in the formulation of a two-dimensional problem was described by the differential equations of their plane-parallel motion:

$$m_i \frac{d^2 x_i}{dt^2} = T_{xi}, \quad m_i \frac{d^2 y_i}{dt^2} = -m_i g + T_{yi}, \quad J_i \frac{d^2 \varphi_i}{dt^2} = M_i \tag{2}$$

where  $m_i$  – is the mass of the  $i$ -th particle (proportional to its volume or area);  $J_i$  – is its central moment of inertia;  $T_{xi}, T_{yi}$  – are the components of the main vector of external forces acting on the particle from other particles and the walls of the hopper;  $M_i$  – is the sum of the moments of these forces relative to the centre of mass of the particle. The unknown components of the forces of interaction between the particles were determined from the conditions of one-way contact of the type (1). To simplify the simulation, it was considered that the interaction of the particles occurs by a completely

inelastic smooth impact since, during the filling of the charge, the reflection of the particles was not observed, with the change of their motion in the opposite direction. The integration of the received system of differential equations with restrictions imposed at each step was carried out by the fourth-order numerical Runge–Kutta method with a steady step.

It is known that vibration is used to seal the structurally inhomogeneous materials before sintering and thus reduce their porosity. The algorithm of filling the hopper with slices of polyhedra using vibration vibrations takes into account the influence of vertical and horizontal vibrations as separate factors, as well as the effect of interaction between particles and their movement relative to each other. The algorithm is designed in such a way that the seals under the influence of vibration may start at any time of the program.

The amplitude and frequency of the oscillations were the values characterizing the vibration in the algorithm. The structural characteristics of backfills were determined by the amplitude of oscillations  $A$ , the frequency of oscillations  $\omega$ , particle sizes and their percentage in the charge. The variable parameter was also the period of overlapping vibrations. The vibration parameters were changed using the vibration control panel. The algorithm of the model provides that the procedure of overlapping horizontal and vertical lines is similar. The difference between them was that the main for the implementation of horizontal oscillations was the  $X$ -coordinate, and for vertical-the  $Y$ -coordinate. The algorithm provides the possibility of simultaneous exposure to horizontal and vertical oscillations. The ratio of horizontal and vertical oscillations, which are applied simultaneously, makes it possible to study the stages of the filling process.

The Fig. 2 presents the results of the study of the effect for a fixed time (10 min after filling) of the combined action of horizontal and vertical vibrations with an amplitude of 1 mm and a variable frequency  $\omega$  in the case of particles of round, triangular and square shapes with a characteristic size of  $24 \mu$  are presented.

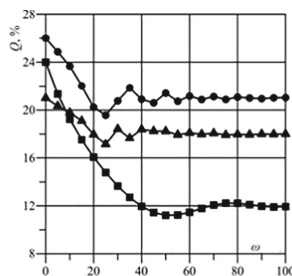


**Fig. 2.** Effect of vibration frequency  $\omega$  on the porosity  $Q$  of the SIM backfill from round, square and triangular particles (indicated by the corresponding symbols).

It can be seen that the dependence of porosity on the frequency of vibrations is not unambiguous. There are frequencies at which the porosity is lowest compared to others. That is, we can see the manifestation of certain resonant phenomena that contribute to the compaction of backfills. This effect is particularly noticeable for square particles,

which, when applied to vibrational vibrations of a particular frequency, form a particularly dense backfill, lined into rows or columns, like building bricks in a wall. Instead, these phenomena are less noticeable for round particles, since there are always pores between the packing of spheres.

On the basis of a series of 15 numerical experiments and the least squares method, the following values of unknown parameters were obtained: for round particles –  $Q_{max} = 28.5\%$ ;  $Q_{min} = 18.2\%$ ;  $\alpha = 0.037$ ; for square particles –  $Q_{max} = 24.7\%$ ;  $Q_{min} = 7.39\%$ ;  $\alpha = 0.065$ ; for triangular particles –  $Q_{max} = 20.5\%$ ;  $Q_{min} = 17.2\%$ ;  $\alpha = 0.04$ .

In Fig. 3 porosity dependencies are presented  $Q$  from the ratio of the width of the square mold and the size of the particles  $w$  obtained by approximating (solid curves) of the numerical experiment data.

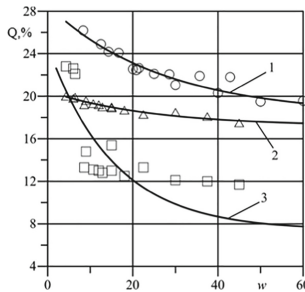


**Fig. 3.** Dependence of porosity  $Q$  from the ratio of the width of the square mold and the size of the particles  $w$ , obtained by approximation (solid curves) of numerical experiment data, where: 1 - round particles; 2 - triangular lobes; 3 - square lobes.

### 4 Results

Based on the obtained results of simulation of the random packing process of different charge particles in a rectangular container (Fig. 1) investigated and substantiated the morphological analysis of the actual entrainment of particles of structurally inhomogeneous materials. Figure 4 presents model shapes of particles of structurally inhomogeneous materials with the factor of shape of backfill. It should be noted that the spherical lobule shape factor is  $FF = 0.71$ , the spheroquadrate lobule shape factor is  $FF = 0.54$ , the triangular lobule shape factor is  $FF = 0.56$ .

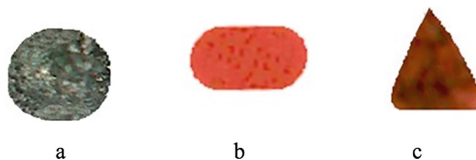


**Fig. 4.** Model forms of natural backfill lobules, where: a - aluminum particles; b - copper particles, c - saponite particles.

From the presented model forms the lobules natural fillings it follows that the physical and structural characteristics of structurally inhomogeneous materials mainly depend on the particle shape, so while the study of these characteristics is necessary to consider the deviation of particle shape from spherical. Therefore, the complete characteristic of the particle shape factor was calculated using the Smart-eye software product. It has been necessary to configure the use of the calibration line before starting, which made it possible to determine in automatic mode with high accuracy the following: the perimeter of the particle (pores), the area fraction (pores), the size and shape of particles, their width and height. In Table 1, the average results of the research of separate areas of the microstructure of particles are given. In turn, the total area of the particles is 4 982 mm<sup>2</sup>, and the calibration coefficient is 0.83 mm × pixel, the porosity ranges from 19 to 24.9%.

**Table 1.** The average results of the study of selected areas microstructure of the particles.

Particle size, mcm	X	Y	Width	Height	R <sub>min</sub>	Perimeter	Area, mcm <sup>2</sup>	FF	Porosity, %
10	0.90	0.74	0.83	34.17	4.450	60.00	4982	0.71	19%
	1.67	0.75	30.83	47.50	9.32	55.04			
	5.83	0.76	11.67	18.33	1.86	55.82			
	8.33	0.78	9.17	7.50	0.83	27.74			
14	12.5	0.79	7.50	7.50	2.36	27.71	4908	0.54	22%
	30.0	0.80	8.33	11.67	1.18	37.69			
	6.67	0.80	61.67	34.17	0.83	50.83			
	4.17	0.83	5.00	15.00	0.83	37.34			
24	9.17	0.83	15.00	12.50	0.90	50.33	3982	0.56	24,9%
	4.17	0.83	10.83	7.50	0.83	33.76			
	7.50	0.83	15.00	11.67	3.44	49.87			
	8.83	0.83	11.67	11.67	2.36	42.93			

$$FF = 1 - (H/D)$$

However, to obtain the necessary in practice, dependency properties, the SIM from the particle size, their shape, size of the hopper and the like have to perform a series of experiments and found and input parameters to build certain functional relationships. The results of computer and full-scale backfilling were processed using the method of least squares.

On the basis of a series of 9 full-scale backfilling and the least squares method, the following values of unknown parameters were obtained: for round particles – Q<sub>max</sub> = 28,7%; Q<sub>min</sub> = 17,8%; α = 0,037; for square particles – Q<sub>max</sub> = 25,2%; Q<sub>min</sub> = 7,76%; α = 0,065; for triangular particles – Q<sub>max</sub> = 20,3%; Q<sub>min</sub> = 11,5%; α = 0,009.

In Fig. 5 porosity dependencies are presented  $Q$  from the ratio of the width of the square mold and the size of the particles  $w$  obtained by approximating (solid curves) of the full-scale backfilling data.

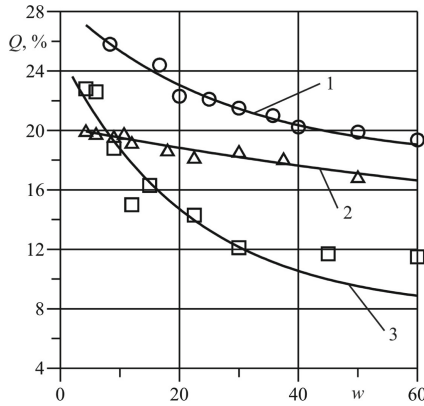


**Fig. 5.** Dependence of porosity  $Q$  from the ratio of the width of the square mold and the size of the particles  $w$ , obtained by approximation (solid curves) of full-scale backfilling data, where: 1 - round particles; 2 - triangular lobes; 3 - square lobes.

It should be noted that the correlation of theoretical and experimental studies used to calculate the porosity of the structurally inhomogeneous materials to optimize the size and shape of the charged particles based on backfilling into a mold for the manufacture of bushings that are used as sliding bearings (Fig. 6).

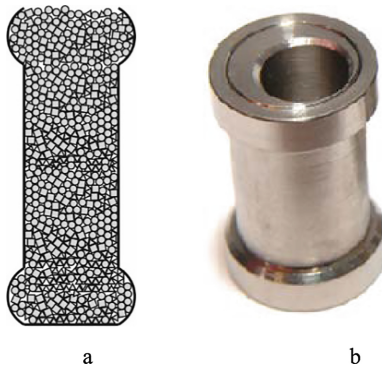


**Fig. 6.** The model of the bearing sleeve for calculating the porosity of the SIM in the window of the developed computer program (a) and the sleeve obtained after pressing and sintering of particles whose composition (size, shape, and the ratio of particles of different sizes) was justified by numerical modeling (b).

By the results of calculations of porosity and coordination number oil permeability of structurally inhomogeneous materials of the sleeve was calculated. The obtained results make it possible to optimize the version of the composition of the charge, which provides an increase in the oil permeability coefficient by 3%, which fully satisfied the technical conditions of operation of the bushings.

Consequently, we can conclude that there is a good coherence of data full-scale backfilling with the data of computer-simulation experiments. This suggests that the results of computer simulation modeling are not stochastic, but subject to specific dependencies, which further confirms the reliability of the results of porosity modeling using the proposed algorithms. On the other hand, the proposed approach makes it possible to obtain easy-to-use engineering formulas that connect the basic physical-mechanical characteristics of structurally inhomogeneous materials (in particular, porosity) with the parameters of the particles of the initial mixes and the size of the technological equipment (molds).

## 5 Conclusions

The algorithms of computer-simulation modeling of nonstationary processes during filling and packing of batches of charge into molds for obtaining structurally inhomogeneous materials are developed. The developed software enables to optimize the porosity of the resulting material to the specific functional properties and technological requirements of particular products, taking into account the shape and size of the particles. Such parameters as temperature, pressure, mold density, contact quality, component content is a prerequisite for creating a two-dimensional problem.

Realization of created computer-simulation models allows to solve structural-imitation tasks in the following directions:

- prediction of the patterns of formation of the structure of materials, taking into account the sizes and shapes (spherical, spherical, triangular) of structural elements of the charge of structurally inhomogeneous materials;
- establishment of correlation relations between components, structure, and properties of structurally inhomogeneous materials.

To obtain more reliable data, we plan to create 3D models. It will enable more accurate results. Besides, it is necessary to increase the number of considered planar geometric shapes, since flat images of the powder material particles are not limited to a circle, square and triangle. It will make it possible to improve the mathematical model and obtain more adequate results.

## References

1. Long, Z., Heng-Wei, Z.: Sintering driving force of  $\text{Al}_2\text{O}_3$  powders at the initial stage of pulse electric current sintering under thermoelastic diffusion. *Int. J. Mech. Mater. Eng.* **13**(9), 2–8 (2018)

2. Apurba Kanti, D., Chatterjee, P.: Study of deformation microstructure of nickel samples at very short milling times: effects of addition of  $\alpha$ -Al<sub>2</sub>O<sub>3</sub> particles. *J. Theor. Appl. Phys.* **13** (3), 63–73 (2019)
3. Leong, K., See, S., Lim, J., Tham, L.: Effect of process variables interaction on simultaneous adsorption of phenol and 4-chlorophenol: statistical modeling and optimization using RSM. *J. Theor. Appl. Phys.* **7**(2), 2009–2020 (2017)
4. Chang, Y., Wang, H., Zhu, Q., Luo, P., Dong, S.: Theoretical calculation and analysis of ZrO<sub>2</sub> spherical nanometer powders. *J. Adv. Ceram.* **2**(1), 21–25 (2014)
5. Sulym, H., Pasternak, I., Pasternak, V.: Boundary element modeling of pyroelectric solids containing 3D rigid shell-like inclusions. *Mech. Mech. Eng.* **22**(3), 727–737 (2018)
6. Shamima, C., Bhuiyan, M., Hoque, S.: Effect of sintering temperature on apparent density and transport properties of NiFe<sub>2</sub>O<sub>4</sub>: synthesized from nanosize powder of NiO and Fe<sub>2</sub>O<sub>3</sub>. *Int. Nano Lett.* **2**(6), 2–5 (2014)
7. Povstyanoy, O., Zabolotnyi, O., Rud, V., Kuzmov, A., Herasymchuk, H.: Modeling of processes for creation new porous permeable materials with adjustable properties. In: Ivanov, V. et al. (eds.) *Advances in Design, Simulation and Manufacturing II. DSMIE 2019. Lecture Notes in Mechanical Engineering*, pp. 456–465. Springer, Cham (2019)
8. Zhang, Q., Lv Si, X., Guo, X.: Improvement of mechanical properties, microscopic structures, and antibacterial activity by Ag/ZnO nanocomposite powder for glaze-decorated ceramic. *J. Adv. Ceram.* **6**(3), 269–278 (2017)
9. Arefpour, A., Soolari, L., Monshi, A.: Improving mold powder through crystallization using calcium fluoride and manganese oxide for continuous casting of steel. *J. Adv. Ceram.* **3**(1), 43–48 (2014)
10. Desalegn Wogaso, W., Davidson, M., Khanra, A.: Prediction of ductile fracture initiation for powder metallurgical aluminum-copper preforms using FEM. *Int. J. Mech. Mater. Eng.* **10** (8), 2–8 (2015)
11. Magnani, G., Galvagno, S., Sico, G., Portofino, S., Freda, C., Burresi, E.: Sintering and mechanical properties of  $\beta$ -SiC powder obtained from waste tires. *J. Adv. Ceram.* **5**(170), 40–46 (2016)

# Author Index

## A

Abramenko, Ivan, [210](#)  
Adamenko, Dmytro, [3](#)  
Akimov, Oleg, [13](#)  
AlGeddawy, Tarek, [336](#)  
Alyokhin, Vitaliy, [13](#)  
Andrushchak, Igor, [562](#)  
Aștilean, Adina, [97](#)  
Avram, Camelia, [97](#)  
Aymen, Albakush, [315](#)

## B

Balaniuk, Anna, [315](#)  
Basova, Yevheniia, [118](#), [380](#)  
Baturin, Yevhen, [75](#)  
Berladir, Kristina, [473](#)  
Berlizeva, Tatyana, [511](#)  
Bezv, Oleh, [452](#)  
Biba, Nikolay, [361](#)  
Bondarenko, Tetiana, [55](#)

## C

Celenta, Giampiero, [108](#)  
Chalyj, Vasyl, [349](#)  
Chocholaty, Ondrej, [532](#)  
Chukhlib, Vitalii, [361](#)  
Cvitić, Ivan, [166](#)

## D

Dašić, Predrag, [147](#)  
Dehtiarov, Ivan, [264](#)  
Denysenko, Yuliia, [23](#)  
Denysiuk, Viktor, [411](#)  
Derevianchenko, Oleksandr, [243](#)  
Dobrotvorskiy, Sergey, [118](#), [380](#)

Dobrovolska, Ludmila, [118](#), [380](#)  
Dolmatov, Anatolii, [401](#)  
Druzhinin, Evgeniy, [156](#)  
Dur, Osman, [552](#)  
Dutchenko, Olena, [23](#)  
Dzhemalyadinov, Ruslan, [462](#)  
Dzhemelinskiy, Vitaliy, [295](#)  
Dzhemilov, Eshreb, [462](#)

## E

Edl, Milan, [137](#)  
Ehring, Dominik, [233](#)

## F

Fomin, Oleksandr, [243](#)

## G

Garashchenko, Yaroslav, [253](#)  
Gasanov, Magomedemin, [371](#)  
Gonçalves, Bruno, [220](#)  
Grabis, Janis, [128](#)  
Grimzin, Igor, [511](#)  
Gubskiy, Serhii, [361](#)  
Guida, Domenico, [108](#)  
Gurey, Volodymyr, [483](#)  
Gusak, Oleksandr, [473](#)  
Gutsalenko, Yuriy, [542](#)

## H

Haidabrus, Bohdan, [128](#), [156](#)  
Havryliuk, Yurii, [85](#)  
Horielyshev, Stanislav, [45](#)  
Hovorun, Tetiana, [473](#)  
Hurey, Ihor, [483](#)  
Hutorov, Andrii, [305](#)



**I**

Ilchuk, Nataliia, 562  
 Ivanov, Vitalii, 264, 315  
 Ivanova, Larysa, 325  
 Ivanova, Maryna, 325  
 Ivanovskiy, Oleksiy, 65

**K**

Kábele, Pavel, 137  
 Karabegović, Isak, 147  
 Karvatskii, Anton, 492  
 Kazantsev, Nikolay, 118  
 Kazlauskaitė, Anastasiia, 210  
 Khavin, Gennadii, 371  
 Khudaybergenov, Djanibek, 473  
 Kiyko, Sergey, 156  
 Klemeshov, Evhen, 361  
 Klochko, Alexander, 65  
 Knyazev, Sergey, 532  
 Kobelev, Vladimir, 315  
 Kondratyuk, Oleg, 285  
 Kononenko, Serhii, 380  
 Kopei, Volodymyr, 432  
 Korotun, Mykola, 23  
 Kosov, Illia, 264  
 Kostyk, Kateryna, 13, 522  
 Kostyuk, Gennadiy, 502, 522  
 Kotliar, Alexey, 325  
 Kozhevnikov, Georgii, 55  
 Kraslawski, Andrzej, 187  
 Krol, Oleg, 35, 75  
 Kulynych, Viktoriia, 442  
 Kunitsyn, Maksym, 390  
 Kunnen, Steffen, 3  
 Kupriyanov, Oleksandr, 285  
 Kurin, Maksym, 401  
 Kusyi, Yaroslav, 276

**L**

Lamnauer, Nataliia, 285  
 Lapchenko, Yurii, 411  
 Larshin, Vasily, 422  
 Leleka, Serhii, 492  
 Lesyk, Dmytro, 295  
 Lishchenko, Natalia, 422  
 Litovchenko, Petro, 45, 325  
 Lukan, Tetiana, 432  
 Lysenko, Tatiana, 511

**M**

Machado, José, 97, 220  
 Mahopets, Sergii, 452  
 Malovana, Nina, 23  
 Martinez, Silvia, 295

Medvid, Iuliia, 432  
 Mikulionok, Ihor, 492  
 Mordyuk, Bohdan, 295  
 Moroz, Sergiy, 349  
 Muzylyov, Dmitriy, 201

**N**

Naboka, Olena, 85, 522  
 Nagarajah, Arun, 3, 233  
 Nechiporenko, Vladimir, 45  
 Nechyporuk, Mykola, 502  
 Nemyrovskiy, Yakiv, 452  
 Nevludova, Viktoriia, 371  
 Novikov, Fedir, 305  
 Nyshnyk, Serhii, 401

**O**

Okun, Anton, 361  
 Onysko, Oleh, 432  
 Orgiyan, Alexandr, 315

**P**

Parmenko, Valeriya, 65  
 Pasternak, Viktoriia, 562  
 Pedash, Oleksii, 295  
 Pedun, Oleksandr, 442  
 Peraković, Dragan, 166  
 Periša, Marko, 166  
 Permyakov, Alexander, 85, 371  
 Pihnastyi, Oleh, 55  
 Pituley, Lolita, 432  
 Pluhnau, Robin, 233  
 Polyansky, Vladimir, 305  
 Ponomarenko, Olga, 511  
 Popov, Viktor, 502, 522  
 Porkuian, Olga, 75  
 Postelnyk, Hanna, 532  
 Prihodko, Olga, 85  
 Prokhorov, Oleksandr, 156  
 Protsenko, Serhiy, 128  
 Prystupa, Stanislav, 349  
 Ptachenchuk, Vitaliy, 349  
 Pupan, Larisa, 542  
 Puzyr, Ruslan, 442

**R**

Rauch, Erwin, 176  
 Ravska, Nataliya, 65  
 Reshetniak, Yaroslav, 473  
 Riabekov, Igor, 305  
 Riabets, Julia, 13  
 Rosenberger, Philipp, 128  
 Rudnev, Aleksandr, 542

**S**

Salenko, Yuliia, [442](#)  
Salo, Valentin, [45](#)  
Saltykov, Leonid, [13](#)  
Salwin, Mariusz, [187](#)  
Savchuk, Volodymyr, [264](#)  
Sevidova, Elena, [542](#)  
Shendryk, Sergii, [210](#)  
Shendryk, Vira, [210](#)  
Shepelenko, Ihor, [452](#)  
Shevchenko, Oleksandr, [442](#)  
Shramenko, Natalya, [201](#)  
Shramenko, Vladyslav, [201](#)  
Skorkin, Anton, [285](#)  
Sobol, Oleg, [532](#)  
Sobol', Oleg, [552](#)  
Sokol, Yevgeny, [118](#)  
Sokolov, Volodymyr, [35](#), [75](#)  
Solovei, Vladyslav, [492](#)  
Stepanov, Mykhaylo, [325](#)  
Stupnytskyi, Vadym, [276](#)  
Svirzhevskiy, Kostiantyn, [562](#)  
Symoniuk, Volodymyr, [411](#)

**T**

Titarenko, Oksana, [542](#)  
Tohidi, Hossein, [336](#)  
Tsekhanov, Yuri, [452](#)

Turmanidze, Raul, [147](#)  
Tymchuk, Sergii, [210](#)  
Tymofeyev, Oleksandr, [502](#), [522](#)

**U**

Uminsky, Sergey, [422](#)  
Usov, Anatoly, [390](#)  
Uysal, Alper, [462](#)

**V**

Varela, Leonilde, [220](#)  
Vaz, José Pedro, [220](#)  
Vovk, Vyacheslav, [65](#)

**Y**

Yakovenko, Ihor, [85](#)  
Yemanov, Vladislav, [45](#)  
Yepifanov, Vitalii, [380](#)  
Yermolenko, Oksana, [305](#)  
Yevsieienkova, Hanna, [502](#)  
Yevtushenko, Nataliia, [511](#)

**Z**

Zablotskyj, Valentyn, [349](#)  
Zabolotnyi, Oleg, [562](#)  
Zaloga, Viliam, [264](#)  
Zorić, Petra, [166](#)  
Zubkova, Nina, [253](#)